UNIVERSITY OF CAMBRIDGE

The role of IFN-γ in cell-autonomous immune responses against *Salmonella* Typhimurium and *Toxoplasma gondii*

Solène C. Rolland

Trinity College

University of Cambridge

MRC Laboratory of Molecular Biology

This dissertation is submitted for the degree of Doctor of Philosophy

March 2020

Summary

The research presented in this thesis investigates the function of interferon gamma in vacuoles, namely *Salmonella enterica* serovar Typhimurium and *Toxoplasma gondii*. IFN-γ is a cytokine that functions in both the innate and the adaptive immune responses. IFN-γ is mainly secreted by T cells and natural killer (NK) cells and activates macrophages, promotes antigen presentation and enhances antiviral and antibacterial immunity.

In the case of bacterial pathogens, such as *S.*Typhimurium, priming with IFN-γ leads to an inflammatory but controlled cell death mechanism known as pyroptosis, following bacterial invasion of the cytosol or experimental lipopolysaccharide (LPS) transfection. LPS is a major component of the outer membrane of Gram-negative bacteria and is sensed in the cytosol by human Caspase-4. The research described in Chapter 2 used a genome-wide CRISPR-Cas9 screen as an unbiased approach to identify new IFN-γ-induced genes that play a role in the cell death pathway. This viability screen enriched for cells resistant to LPS-mediated cell death after IFN-γ priming. Their sequencing generated a list of potential candidate genes including expected genes such as IFN-γ receptors (*Ifngr*) and novel genes such as *Nckap1*, *Fip1l1*, *Srsf10*, *Safb*. However, none of these additional candidates were validated because their deficiency did not provide significant resistance to the cell death phenotype. Overall, these results suggest that, in addition to the Caspase-4-Gasdermin-D axis, the role of IFN-γ-induced genes in the cell death pathway triggered by cytosolic LPS remains to be investigated.

This thesis also examined the role of IFN-γ in response to infection by the eukaryotic parasite *Toxoplasma gondii*, an apicomplexan that actively invades host cells and resides within a unique parasitophorous vacuole. The work presented in Chapter 3 showed that with type II *T.gondii* (PRU strain), IFN-γ inhibits replication in an autophagy-dependent manner. This strain is coated by ubiquitin and by the individual subunits (HOIP, HOIL-1, and Sharpin) of the linear-ubiquitin assembly complex (LUBAC). Autophagy cargo receptors, such as NDP52, p62, and Optineurin, are also recruited to the type II, intracellular parasites. Although all these recruitments were IFN-γ-dependent, the role of LUBAC and the mechanisms for its recruitment remain unknown. This research further showed that PRU changes cytokine expression levels of infected cells: IL-1α, IL-6, and CCL5 expressions are induced upon infection and potentially in a LUBAC-dependent fashion.

Overall, the work presented in this thesis provides new insights into the role of IFN-γ in antibacterial and antiparasitic cell-autonomous innate immunity. Further experiments could validate other candidate genes from the screen or investigate the role of LUBAC in Toxoplasmosis.

Declaration

This thesis is the result of my own work and includes nothing that is the outcome of work done in collaboration, except where specified in the text.

The work in this thesis has not already been submitted before for any degree or for any other qualification.

This thesis does not exceed the word limit of 60,000 words prescribed by the degree committee for the Faculty of Biology.

Solene C. Rolland
Trinity College
University of Cambridge
March 2020

Acknowledgements

I am grateful to my supervisor Felix Randow for allowing me to pursue my PhD under his guidance. I would also like to give thanks for the support I have received from past and current members of the Randow research group both for their help from a scientific perspective as well as for showing sympathy and sharing kind words when experiments were not working. My sincere gratitude goes to the following scientists for their particular impact on my PhD work: Jessica Noad, who trained me when I first joined the lab and provided numerous plasmids and some materials for my projects; Keith Boyle for his encouragement, advice, and honest criticisms on my thesis drafts; Michal Wandel for providing insights to my project and sharing his knowledge about IFN-γ; Claudio Pathe for helping me with microscopy-related experiments and for training me on the high-content microscope. Finally, I wish to thank Conor and Gisela for their kind attitude and for always being in a good mood, trying to cheer me up.

I am grateful to the MRC and the LMB for funding this research and for providing a collaborative environment in which I could pursue and complete my PhD. I also wish to express my gratitude to the staff in the media kitchen for pouring numerous plates, and to the microscopy and flow cytometry teams for their training and maintenance of the microscopes and machines.

I would also like to acknowledge the time that Clara Lloyd spent proof-reading and helping me format my thesis. She has been an important moral support throughout my PhD too.

I am especially thankful to my family, who has been unwavering and constant in their support throughout my PhD. They kept me going and encouraged me during the difficult times.

Table of Contents

Abbreviations

293ET	HEK-293 Human embryonic kidney cells
AIM2	Absent In Melanoma 2
ALG12	Dol-P-Man:Man(7)GlcNAc(2)-PP-Dol-alpha-1,6-mannosyltransferase
ALR	AIM2-Like Receptor
ALS	Amyotrophic Lateral Sclerosis
ANOVA	ANalysis Of Variance
aPKC	atypical Protein Kinase C
ASC	Apoptosis-associated Speck-like protein containing a CARD
ATG	AuTophaGy-related protein
ATP	Adenosine TriPhosphate
β2M	β-2 Microglobulin
BAFF	B-cell-Activating Factor
BCL-2	Beclin-2
BID	BH3-Interacting Domain death agonist
BIN1	Myc Box-dependent-INteracting protein 1
bp	Base pair
CALCOCO2	CALcium-binding and COiled-COil domain-containing protein 2
CARD	CAspase Recruitment Domain
CARM1	Histone-arginine methyltransferase CARM1
CASP4	Caspase-4
CCL4	C-C motif chemokine 4
CCL5	C-C motif chemokine 5
CD14	Monocyte differentiation antigen CD14
CD40	Cluster of Differentiation 40
CDK9	Cyclin Dependent Kinase 9
CHD8	Chromodomain-Helicase-DNA-binding protein 8
cIAP	cellular Inhibitor of Apoptosis Protein
CLIR	LC3C-Interacting Region
Cpdm	Chronic proliferative dermatitis
CRISPR	Clustered Regularly Interspaced Short Palindromic Repeats

CrmA	Serine proteinase inhibitor 2 from Cowpox virus
crRNA	CRISPR RNA
CTNNBL1	Beta-catenin-like protein 1
CXCR4	C-X-C Chemokine Receptor type 4
DAMP	Danger Associated Molecular Pattern
DNA	Deoxyribo-Nucleic Acid
DSB	Double-strand break
DUB	DeUbiquitylating enzyme
E. Coli	*Escherichia Coli*
ELAVL2	ELAV-Like protein 2
EMC6	ER Membrane protein Complex subunit 6
EPEC	Enteropathogenic *E. Coli*
ER	Endoplasmic Reticulum
ERK	Group of MAP kinases
ESCRT	Endosomal Sorting Complex Required for Transport
EXOC2	EXOcyst Complex Component 2
FIP1L1	Pre-mRNA 3'-end-processing factor FIP1
FIP200	Short name for RBCC1: RB1-inducible Coiled-Coil protein 1
GAL	Galectin
GAF	IFN-Gamma Activation Factor
GAS	IFN-Gamma Activation Site/Sequence
GBP	Guanylate-Binding Protein
GFP	Green Fluorescent Protein
GPI	GlycosylPhosphatidylInositol
gRNA	guide RNA
GSDMD	Gasdermin-D
HCT116	Human colon cancer cell line
HeLa	Cervical cancer cell line
HFF	Human Foreskin Fibroblasts
HOIL-1L	Haem-Oxidised Iron-responsive element-binding protein 2 ubiquitin Ligase-1L (RBCK1)

HMBOX1	HoMeoBOX containing 1
HMGB1	High Mobility Group Box 1
HOIP	HOIL-1L Interacting Protein (RNF31)
HSPH1	Heat shock protein 105kDa
ICAM-1	Intercellular adhesion molecule 1
IFN	InterFeroN
IFNGR1	InterFeroN-Gamma Receptor 1
IKK	Inhibitor of NF-KappaB Kinase
IL	InterLeukin
IRG	Immunity-Related GTPase
IRGB10	Immunity-Related GTPase family member B10
IRF	IFN Response Factor
ISG	IFN-Stimulated Gene
ISRE	IFN-Stimulated Response Element
JAK	Janus-Associated Kinase
KD	Knock-down
Kdo	2-Keto-3-deoxy-octonate
KEAP1	Transmembrane 9 superfamily member 2
KO	Knockout
LBP	LPS Binding Protein
LC3	Linear Chain 3
LCORL	Ligand-dependent nuclear receptor CORepressor-Like protein
LIR	LC3-Interacting Region
LPS	LipoPolySaccharide
LUBAC	Linear UBiquitin chain Assembly Complex
MAGE	Multiplex Automated Genome Engineering
MAGeCK	Model-based Analysis of Genome-wide CRISPR-Cas9 Knockout
MAPK	Mitogen-Activated Protein Kinase
MD-2	Lymphocyte antigen 96 (LY96)
MDP	Muramyl DiPeptide
MEF	Mouse Embryonic Fibroblasts

MEK5	Short name for MAP2K5: Dual specificity mitogen-activated protein kinase kinase 5
MHC	Major Histocompatibility Complex
MOI	Multiplicity Of Infection
MV	Membrane Vesicle
NCKAP1	Nck-Associated Protein 1
NDP52	Nuclear Dot Protein 52kDa (also known as CALCOCO2)
NEL	Novel E3 Ligase
NEMO	NF-κB Essential MOdulator
NF-κB	Nuclear Factor kappa-light-chain-enhancer of activated B cells
NGS	Next-Generation Sequencing
NLR	Nucleotide-binding domain and Leucine-rich Repeat-containing protein
NLRC4	NOD-Like Receptor family CARD domain-containing protein 4
NLRP3	NACHT, LRR and PYD domains-containing protein 3
NOD	Nuclear Oligomerisation Domain protein
OMV	Outer-Membrane Vesicle
Optn	Optineurin
OTULIN	Ovarian tumour (OTU) domain-containing deubiquitinase with linear linkage specificity
OVOL3	Putative transcription factor OVO-Like protein 3
p62	other name for Sequestosome-1
PAM	Protospacer Adjacent Motif
PAMP	Pathogen-Associated Molecular Pattern
PB1	Phox and Bemp1P domain
PBS	Phosphate-Buffer Saline
PCR	Polymerase Chain Reaction
PFA	ParaFormAldehyde
PI	Propidium Iodide
PI3P	PhosphatidylInositol-3-Phosphate
PI3PK	PhosphatidylInositol-3-Phosphate Kinase
PIT	Pore-induced Intracellular Trap
PLA	Proximity-Ligation Assay
PPP4R4	Serine/threonine-protein phosphatase 4 regulatory subunit 4

PRR	Pattern Recognition Receptor
P-TEFb	Positive Transcriptional Elongation Factor b
PUB	Peptide:N-glycanase/UBA or UBX-containing proteins
PYD	PYrin Domain
qPCR	quantitative Polymerase Chain Reaction
RAGE	Receptor for Advanced Glycation Endproducts
RANKL	Receptor Activator of Nuclear factor Kappa-B Ligand
RBR	RING-Between-RING / RING-Bcat-Rcat
Rcat	Required for CATalysis
RGEN	RNA-guided engineered nuclease
RING	Really Interesting New Gene
RIP	Receptor-Interacting serine/threonine-Protein
RNA	Ribo-Nucleic Acid
RSA	Redundant siRNA Activity
RUFY4	RUN and FYVE domain-containing protein 4
SAFB	Scaffold attachment factor B
SCV	*Salmonella*-Containing Vacuole
SDS-PAGE	Sodium Dodecyl Sulphate-PolyAcrylamide Gel Electrophoresis
sgRNA	Single guide RNA
Sharpin	SHANK-Associated RH domain-INteracting protein
SINTBAD	other name for TBKBP1: TANK-Binding Kinase 1-Binding Protein 1
siRNA	Small interfering RNA
SKICH	Skeletal muscle and Kidney-enriched Inositol Phosphatase Carboxyl Homology
SLC25A37	Mitoferrin-1
SMAD4	Mothers Against Decapentaplegic homolog 4
SNARE	SyNaptosomal-Associated protein REceptor
SPI	*Salmonella* Pathogenicity Island
SQSTM1	SeQueSTosoMe-1 (also referred as p62)
SRSF10	Serine/arginine-Rich Splicing Factor 10
STAT	Signal Transducer and Activator of Transcription
S.Typhimurium	*Salmonella enterica* serovar Typhimurium

T3SS	Type III Secretion System
TAB	TGF-beta-activated kinase 1 and MAP3K7-binding protein
TAK1	also NR2C2: Nuclear Receptor subfamily 2 group C member 2
TALEN	Transcription Activator-Like Effector Nuclease
TBK1	Serine/threonine-protein kinase TBK1
TGF	Transforming Growth Factor
THP-1	Human monocytic cell line derived from leukaemia patient
TLR	Toll-like receptor
TM9SF2	TransMembrane 9 SuperFamily member 2
TMEM143	TransMEMbrane protein 143s
TNF-α	Tumour Necrosis Factor alpha
TNFR	Tumour Necrosis Factor Receptor
TNFRSF11B	Tumor Necrosis Factor Receptor Superfamily member 11B
tracrRNA	TRans-Activating CRISPR RNA
TRADD	TNF Receptor-Associated Death Domain protein
TRAF	TNF Receptor-Associated Factor
TRIF	TIR domain-containing adapter molecule 1
Ub	Ubiquitin
UBA	UBiquitin-Associated domain
UBAN	Ubiquitin Binding in ABIN and NEMO domain
UBX	Ubiquitin regulatory X
ULK1	Serine/threonine-protein kinase ULK1
VCAM-1	Vascular cell adhesion protein 1
WT	Wild-Type
ZFN	Zinc-Finger Nuclease
ZFP	Zinc-Finger Protein
ZnF	Zinc-Finger domain
ZNF619	Zinc finger protein 619

Chapter 1: Introduction

This thesis presents two separate projects that investigate the role of IFN-γ not in stimulating immune cells but in regulating cell-autonomous pathways in response to pathogen infection. The first part of this introduction focuses on the organisation of the immune system and details cell-autonomous mechanisms that are relevant for the rest of the thesis such as ubiquitylation, inflammasome activation, cell death by pyroptosis and cytokine release. The second section highlights characteristics of the two pathogenic species investigated in this thesis, namely the Gram-negative bacteria *Salmonella enterica* serovar Typhimurium and the eukaryotic parasite *Toxoplasma gondii*. A comparison between the two organisms is made, in terms of the different host responses and the pathogenic strategies established during infection.

1.1 Immune defence mechanisms against pathogens

The immune system is composed of special organs, cells and molecules that constitute a network of multiple interconnected protection mechanisms meant to promote the survival of the host. It relies on a set of circulating and tissue-resident immune cells that survey the body for invading pathogens and damage. It is also crucial for maintaining homeostasis in eukaryotes, as exemplified by the severity of many immunodeficiency disorders and autoimmune diseases (van Dyke, 2011). Primary immunodeficiency disorders (PID) are mostly inherited defects in immune system development and/or function and affect both innate (e.g. phagocytes, NK cells…) and adaptive (e.g. T- and B-cells) immunity (McCusker & Warrington, 2011). The number of people affected by autoimmune diseases, such as type-I diabetes and multiple sclerosis (MS), has dramatically increased in the past decades (Rook, 2011). Patients with systemic lupus erythematosus (SLE) exhibit widespread inflammation and produce autoantibodies; more research is done to investigate the immune mechanisms of tolerance and autoimmunity (Singh et al., 2011).

Vertebrates have adaptive and innate immune systems to protect them against threats such as pathogens (Boehm, 2012), and are based on the distinction between self and

non-self (Chaplin, 2010). The adaptive immune system targets previously recognised microorganisms or antigens. Any pathogen or toxin is recognised, via particular epitopes (antigens) it presents on its cell surface by specific receptors (Schatz & Ji, 2011). These adaptive immune processes are characterised by highly specific mechanisms that require gene rearrangement in T- and B-cells, followed by clonal expansion. Thus, when a host is exposed to a new pathogen, adaptive responses are activated following faster-acting innate immune defence, which constitute the first line of defence against pathogens (Riera Romo et al., 2016) and are essential in the early stages of infection.

The innate immune system, more ancient than the acquired immune response, has developed and evolved to prevent infection, eliminate invading pathogens and activate the adaptive immune system. Innate immunity is composed of physical barriers (skin, mucosa), phagocytes (i.e., neutrophils, monocytes, macrophages), cells that release cytokines and inflammatory mediators (i.e., macrophages, natural-killer cells) and includes recognition mechanisms and microbicidal capabilities.

Cells outside immune lineages, such as the epithelial cells of the intestine, are often the first to encounter invasive pathogens. They have the ability to self-defend by detecting and tackling pathogens. Cell-autonomous immunity refers to any form of defences that do not require any other cells, and includes potent mechanisms inhibiting pathogen replication in the cytosol (Randow et al., 2013). A number of intracellular pathogens (such as *Legionella*, *Salmonella*, Mycobacteria) replicate in specialised vacuoles that provide a more hospitable environment to replicate (Frehel et al., 1986; Kagan and Roy, 2002; Portillo & Finlay, 1995; Steele-Mortimer, 2008) and that keep them isolated from the nutrient-rich cytosolic compartment (Hackstadt et al., 1997; Joshi & Swanson, 2011). Cell-autonomous immunity includes constitutive and IFN-induced processes (MacMicking, 2012; Moretti & Blander, 2017), both of which are involved in microbial clearance (Randow et al., 2013). Cell-autonomous processes regulate innate immune responses to microbes and the production of inflammatory cytokines.

The first part of the introduction shows that the host defence against infections require recognition mechanisms of the threat (see paragraph **1.1.1**), that trigger microbicidal

pathways (see paragraph **1.1.2**) and activate the adaptive immune system by the production and release of effector molecules (see paragraph **1.1.3**). A particular emphasis is made on cell-autonomous immune responses.

1.1.1 Recognition mechanisms

Within both immune and non-immune cells, cytosol-invading pathogens are recognised by the cell-autonomous immune system, which is defined by intrinsic cell-dependent pathways activated in response to threats.

1.1.1.1. Pattern-recognition receptors surveil both extracellular and intracellular compartments

The innate immune system uses germline-encoded pattern recognition receptors (PRRs) in various cellular compartments to detect evolutionary conserved structures specific to pathogens (i.e. components of bacterial cell walls, of secretion systems, or effectors secreted by pathogens); these are known as pathogen-associated molecular patterns (PAMPs) (Janeway, 1989; Mogensen, 2009; Takeuchi et al., 2010). In addition, pathogen entry may cause disruptions in cellular homeostasis (Stuart et al., 2013), such as mislocalised DNA outside of the nuclear or mitochondrial compartments, modified endogenous proteins or membrane damage. These disturbances act as danger-associated molecular patterns (DAMPs), which, through recognition by danger receptors, enable indirect detection of infections (Matzinger, 1994). Sensing of both PAMPs and DAMPs by PRRs trigger multiple effector mechanisms and signalling pathways that interfere with pathogen growth and dissemination. Finally, Toll-like receptors (TLRs) surveil the extracellular compartment and endosomes whereas cytosolic NOD-like receptors (NLRs) are activated during proper infection.

1.1.1.2. Inflammasomes are cell-autonomous sensing mechanisms

Inflammasome activation is not a process exclusive to immune cells such as macrophages (LaRock & Cookson, 2013). It is also present in epithelial cells: NLRC4

canonical inflammasome and Casp11 non-canonical activation can be established during *S.*Typhimurium infection, restricting bacterial replication and spread (Sellin et al., 2014) and enabling shedding of the infected epithelial cells (Knodler et al., 2014a).

Inflammasomes play an essential role for controlling infections; however, aberrant inflammasome signalling results in human autoimmune and autoinflammatory diseases (Guo et al., 2015; Strowig et al., 2012) including neurogenerative diseases (multiple sclerosis, Alzheimer's and Parkinson's diseases) and metabolic disorders (atherosclerosis and type-2 diabetes). In the context of infection, excessive immunoinflammatory dysfunction is responsible for sepsis and causes morbidity (Bordon, 2012; Gao et al., 2018; Winters et al., 2010).

Inflammasomes (**Fig.1**) are key components of cytosolic surveillance and are large multimolecular complexes that assemble in response to PAMP or DAMP detection (Rathinam et al., 2012; Broz & Dixit, 2016) by a subset of NLRs (nucleotide-binding domain and leucine-rich repeat containing proteins) and ALRs (AIM2-like receptors) (Takeuchi & Akira, 2010). Inflammasome activation is mediated by pro-inflammatory caspases and results in cytokine production (IL-1β and IL-18) and cell death by pyroptosis (Lamkanfi & Dixit, 2014).

Canonical inflammasomes recruit human procaspase-1 by its CARD domain and convert it into the catalytically active enzyme (Martinon et al., 2002) mirroring the proximity-induced activation of Caspases-8 and -9 (Riedl & Salvesen, 2007). Canonical inflammasomes are activated in response to a broad range of stimuli including bacterial components (Miao et al., 2006; 2010) because numerous sensing molecules, such as NOD-like receptors (NLRC4, NLRP1, NLRP3) and AIM2 are able to induce CASP1 activation (**Fig.1A**). Both NLRC4 and NLRP1 interact directly with CASP1 via CARD-CARD binding. NLRP1 is activated by anthrax toxins (Chavarría-Smith and Vance, 2013; Hellmich et al., 2012), whereas NLRC4 inflammasome is triggered by flagellin or bacterial T3SS and T4SS effectors (Kofoed & Vance, 2011). By contrast, AIM2 and NLRP3 inflammasomes require the adaptor and scaffold protein ASC, which binds CASP1 CARD by its N-terminal CARD and the sensing protein (AIM2 or NLRP3) by its C-terminal PYD. AIM2 is a Pyrin protein, which is

activated by cytoplasmic DNA (Fernandes-Alnemri et al., 2009; Hornung et al., 2009) and, during *Francisella novicida* infection (Man et al., 2015). AIM2-triggered inflammasome participates in antiviral and antibacterial defence (Rathinam et al., 2010). Unlike the other NLRs, NLRP3 is a PRR that assembles inflammasomes in response to very diverse cues, including toxins and chemicals such as monosodium urate or, more particularly, DAMPs such as potassium efflux (Muñoz-Planillo et al., 2013) or endogenous reactive oxygen species (ROS) (Zhou et al., 2011).

Canonical activation of inflammasomes is driven by oligomerisation of NLR molecules for example, and results in cleavage of pro-caspase-1. By contrast, non-canonical activation of inflammasomes (**Fig.1B**) is directly driven by either murine caspase-11 or human Caspases-4 or -5 themselves (Aachoui et al., 2013a; Kayagaki et al., 2013; Rathinam et al., 2012). Murine Casp11 and human CASP4 directly bind LPS in the cytosol, rendering this LPS activation of non-canonical inflammasome TLR4-independent (Casson et al., 2015; Kayagaki et al., 2013; Shi et al., 2014). Similar to CASP1, CASP4 oligomerises and is activated by autocleavage. Once activated, human Caspases-1 and -4, as well as caspase-11 have the ability to cleave GSDMD (Kayagaki et al., 2015; Qiu et al., 2017; Shi et al., 2015) and to trigger pyroptosis.

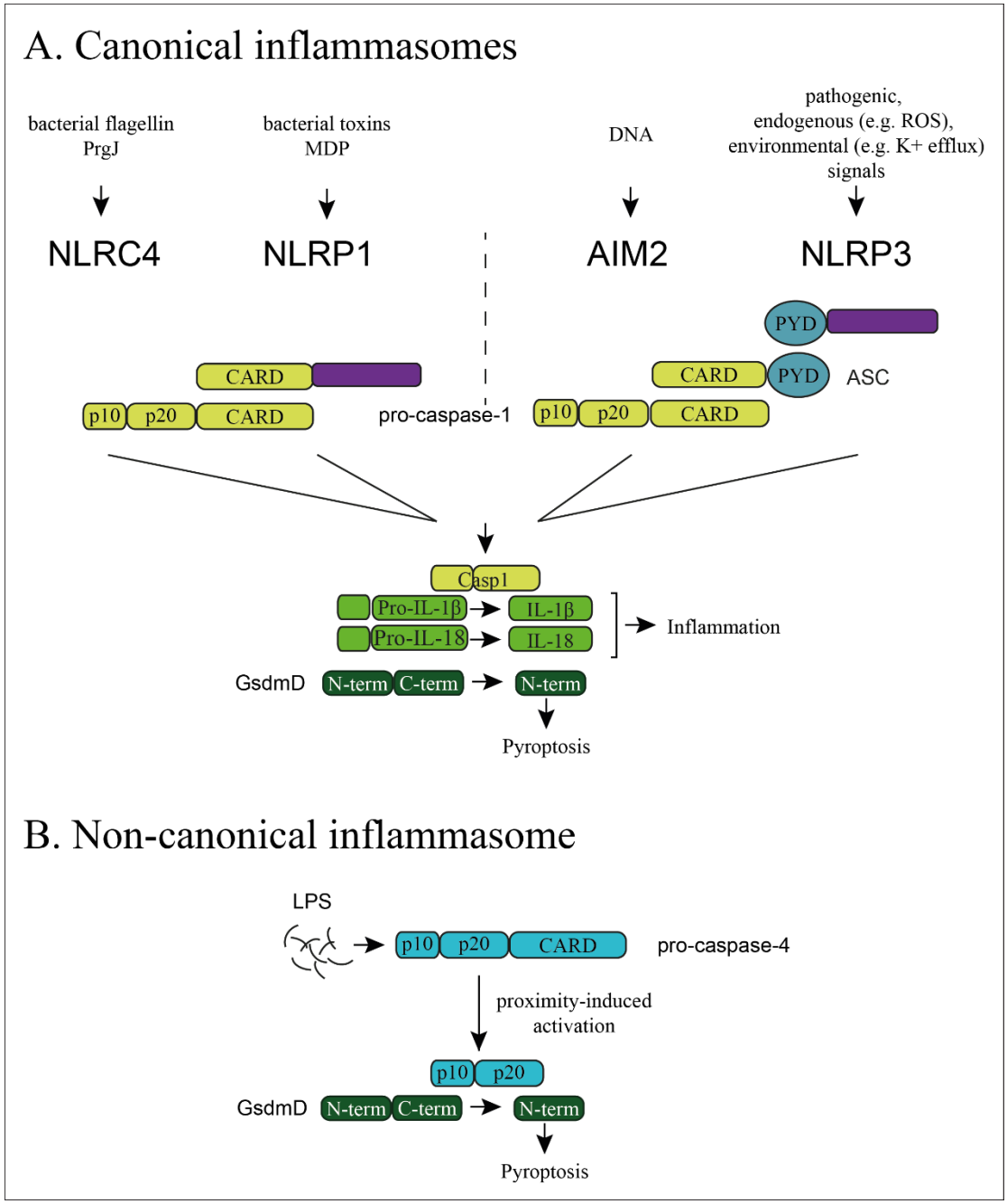

Figure 1: Inflammasomes are activated by various stimuli

Inflammasomes are divided into two categories depending on the inflammatory Caspase that is activated. (A) Canonical inflammasome assembly is triggered by a broad range of stimuli sensed by different inflammasome proteins. NLRC4 and NLRP1 interact directly with pro-caspase 1 via CARD-CARD interaction, whereas AIM2 and NLRP3 require the adaptor ASC, which binds them with their PYD and pro-caspase-1 with its CARD domain. Oligomerisation drives the cleavage of pro-Caspase-1 in a proximity-dependent autoactivation model. Active Caspase-1 processes pro-IL-1β and pro-IL-18 in their mature forms, inducing inflammation. (B) Non-canonical inflammasome assembly is triggered by cytosolic LPS, which directly binds Caspase-4 (caspase-11 in mice) and leads to proximity-induced autoactivation of Caspase-4. Both Caspase-1 and Caspase-4 cleave Gasdermin-D, major effector of pyroptosis. Pyroptosis is an inflammatory form of cell death that occurs as a consequence of inflammasome activation.

1.1.1.3. Other mechanisms of intracellular detection

Further detection occurs both directly, resulting in the deposition of ubiquitin on bacterial surfaces or parasitophorous vacuolar membranes (Lee et al., 2015; Selleck et al. 2015); and indirectly, when exposed glycans from damaged endomembranes are recognised by Galectin-8 (Birmingham et al., 2006; Thurston et al., 2012). Ubiquitin (Ub) and Galectin-8 (GAL8) are intracellular 'eat-me' signals for autophagy cargo receptors; P62, OPTN and NDP52 all bind Ub and NDP52 also binds GAL8 (Boyle & Randow, 2013).

i. Galectins

Cells display complex glycoproteins and glycoplipids on the extracellular leaflet of the plasma membrane, but not on the cytosolic one. Consequently, these glycans are also found on the luminal leaflet of pathogen-containing vacuoles. Upon damage of vacuolar membranes, glycans become exposed to the cytosol where they are sensed by a number of cytosolic receptors known as galectins. Galectins were first found to be implicated in antibacterial autophagy when Galectin-3 was observed to accumulate on membrane remnants generated during cytosolic entry of *Shigella flexneri* (Dupont et al., 2009; Paz et al., 2010). Galectin-3, -8 and -9 are recruited to cytosol-invading bacteria, including *S.*Typhimurium, and bind to glycans exposed in the cytosol upon membrane rupture (Thurston et al., 2012). Galectins are therefore precise indicators of membrane damage and cytosolic entry of *S.*Typhimurium. Moreover, Galectin-8 triggers downstream cell-autonomous immunity by interacting with the autophagy receptor NDP52.

ii. Ubiquitylation

Both cytosolic bacteria and remnants of damaged membranes are ubiquitylated, thereby targeting Ub-bound substrates for proteasomal degradation (Hershko & Ciechanover, 1992) or autophagy. Ubiquitin is a well-conserved regulatory protein and its reversible conjugation to substrates (ubiquitylation) signals primarily for proteasomal degradation. It is also involved in numerous cellular processes such as

cell division and more specifically in intracellular pathogen degradation and immune signalling (Komander & Rape, 2012). Substrate ubiquitylation may be reversed by the action of deubiquitinases (DUBs), which are essential in ensuring cellular homeostasis (**Fig.2**). The ubiquitylation process requires three enzymes. The E1-activating enzyme carries and transfers the Ub molecule to the E2-conjugating enzyme (**Fig.2**). The Ub-loaded E2 interacts with an E3-ligating enzyme. There are three classes of E3s, depending on the mechanism used for the transfer of Ub to the substrate: with the RING E3s, the ubiquitin molecule is directly transferred from the E2 to the substrate (**Fig.2.1**), whereas in both HECT (**Fig.2.2**) and RBR (**Fig.2.3**) E3-ligases, Ub is transferred first to the E3 and subsequently to the substrate.

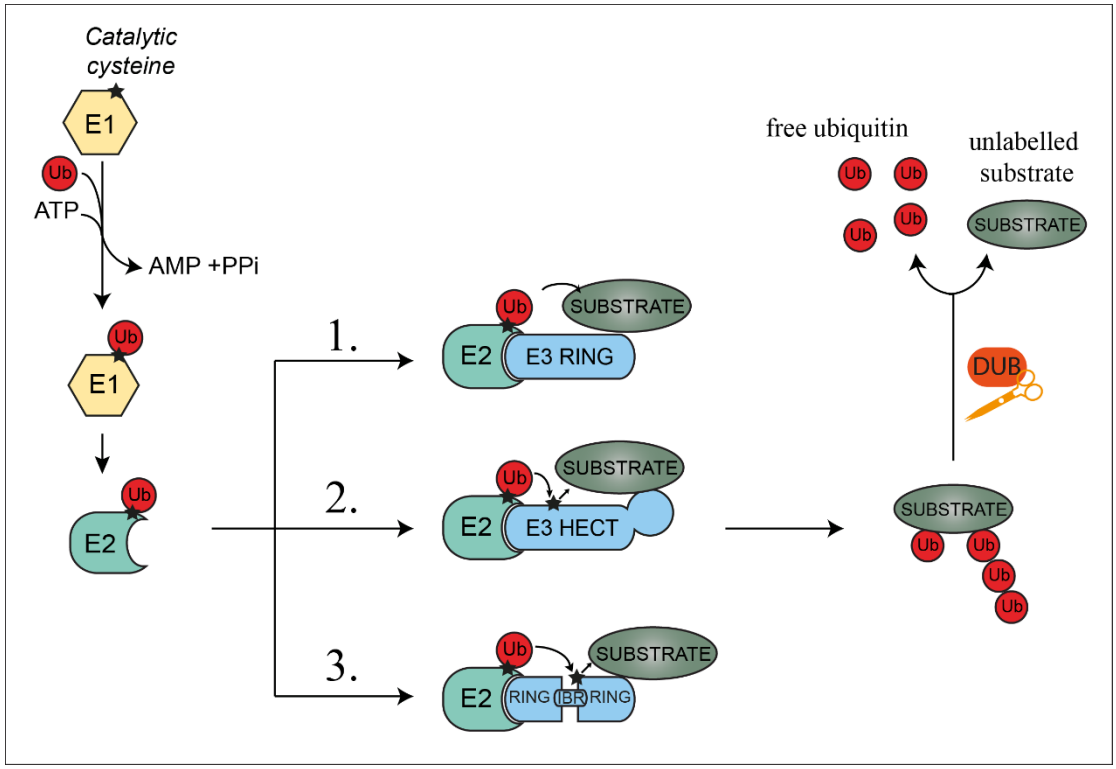

Figure 2: The ubiquitylation cascade

Conjugation of ubiquitin to a substrate takes several steps. Ubiquitin is first loaded on an E1-activating enzyme in an ATP-dependent manner. The ubiquitin molecule is then transferred to an E2 ubiquitin-conjugating enzyme. The E2 then interacts with the E3 ubiquitn-ligating enzyme. E3 ligases are divided into three classes: (1) RING E3 is bound simultaneously to E2 and the substrate and promotes direct transfer of ubiquitin from the E2 to the substrate; (2) HECT E3 helps ubiquitin transfer first from the E2 to the E3 and then from the E3 to the substrate; (3) RBR E3 binds the E2 through the RING1 domain, the substrate via the RING2 (Rcat) domain, and catalyses the HECT-like ubiquitin transfer to the target. Deubiquitinases are cytosolic enzymes that enable release of the Ub-chains from the substrate.

Ubiquitin is covalently attached to the substrate via an isopeptide bond between the C-terminus of the Ub and the substrate's ε amino lysine residue. Mono-ubiquitin already impacts its substrate's functions (Dikic & Dötsch, 2009); however, ubiquitin can be further modified and can form polyubiquitin chains (Hershko & Ciechanover, 1998). Depending on the conjugation site – i.e. the seven internal lysines or the N-terminal methionine of the Ub molecule – the various linkages exhibit different conformations and functions (Dikic et al., 2009). For example, K48-polyubiquitin chains target proteins to the 26S proteasome for degradation (Ciechanover, 2005); K63-linked ubiquitin targets *T.gondii* for endo-lysosomal degradation (Clough et al., 2016); linear (M1) chains play a role in NF-κB signalling (Ikeda et al., 2011).

The linear ubiquitin chain assembly complex (LUBAC) specifically synthesises linear (M1-linked) ubiquitin chains. LUBAC is a multimeric complex composed of three subunits – HOIP, HOIL-1, and Sharpin (Ikeda et al., 2011; Kirisako et al., 2006; Tokunaga et al., 2011) – of which HOIP is the catalytic subunit and acts as an E3 ligase via its RBR domain (Smit et al., 2012). Maximal activity of HOIP requires both Sharpin and HOIL-1; the formation of the complex enhances the stability of each component (Elton et al., 2015; Tokunaga et al., 2011). Autosomal defects in LUBAC are associated with autoinflammation and immunodeficiency in humans, and additional disorders in mice (Boisson et al., 2015; Brazee et al., 2016). HOIL-1 deficiency in mice is associated with increased susceptibility to *Listeria monocytogenes*, *Citrobacter rodentium* and *Toxoplasma gondii* (MacDuff et al., 2015). During bacterial infection, LUBAC – the N-terminal double zinc-finger domain of HOIP – is recruited to cytosolic *S*.Typhimurium via initial ubiquitin deposited by upstream E3 ligases and produces linear ubiquitin chains on the bacterial surface (Noad et al., 2017) and thus amplifies the ubiquitin coat on cytosolic bacteria. This forms a signalling platform by recruiting the NF-κB activator NEMO and the cargo receptor Optineurin, thereby inducing pro-inflammatory signalling and targeting the bacteria to autophagy, respectively (Noad et al., 2017). Physiological effects of linear ubiquitylation are locally modulated and antagonised by the activity of deubiquitylating enzymes (DUBs) such as Ovarian tumor DUB with linear linkage specificity (OTULIN) or cylindromatosis (CYLD) (Takiuchi et al., 2014). OTULIN promotes bacterial proliferation in cells (van Wijk et al., 2017), is a negative regulator

of pro-inflammatory NF-κB signalling in mammals (Fiil et al., 2013; Schaeffer et al., 2014), and critical for the maintenance of homeostasis. A homozygous hypomorphic mutation in human OTULIN, recapitulated in Otulin-deficient mice, is the underlying cause of ORAS (OTULIN-related autoinflammatory syndrome), a life-threatening autoimmune disorder characterised by spontaneous NF-κB activation in myeloid cells and chronic inflammation in multiple tissues (Damgaard et al., 2016). The LUBAC-OTULIN interplay provides an example of the highly regulated balance between pro- and anti-inflammatory signalling necessary for the control of infections and for tissue and cell homeostasis.

iii. Cargo receptors

Ub and GAL8 are intracellular "eat-me" signals because they recruit autophagy cargo receptors in the context of bacterial infection: p62 and Optn only bind to Ub whereas NDP52 binds both Ub and GAL8 (Boyle & Randow, 2013). All three were shown to facilitate restriction of *S.*Typhimurium replication and other intracellular bacteria (Thurston et al., 2009; Wild et al., 2011; Zheng et al., 2009) via LC3 binding on developing autophagophores. Because of their role in antibacterial cell-autonomous defence mechanisms, they were studied in the case of *Toxoplasma gondii* infection. They were found to exhibit the following characteristics:

NDP52 (nuclear dot protein 52)

NDP52 (**Fig.3**) mediates immune defence against *S.*Typhimurium and potentially *T.gondii* (Haldar et al., 2015; Selleck et al., 2015). Its ability to specifically bind to LC3C via its CLIR motif (LC3C-interacting region) leads to recruitment of nascent autophagosomes (von Muhlinen et al., 2012) or other host membranes (Selleck et al., 2015), resulting in the restriction of pathogen growth. NDP52 is recruited to broken vacuolar membrane remnants by binding to GAL8 (**Fig.3**) via a C-terminal region just upstream of the ubiquitin-binding zinc-finger (ZnF) that senses cytosolic bacteria (Thurston et al., 2009 and 2012). The recruitment of NDP52 to *T.gondii* has not yet been characterised.

p62 (sequestosome-1)

p62 has been shown to direct autophagy towards bacterial pathogens (Mostowy et al., 2011) including *S.*Typhimurium (Zheng et al., 2009). In the case of *T.gondii* infection,

IFN-γ induces ubiquitin conjugation and consequent p62 recruitment to the PVs (Lee et al., 2015). p62 recruitment is associated with the escort and deposition of GBPs on the PVs, a mechanism that does not occur in virulent strains (Haldar et al., 2015).

Like NDP52, p62 has the ability to bind both the ubiquitin coat on cytosolic bacteria and LC3 proteins (via its C-terminal UBA and LIR domains, respectively) (**Fig.3**), thereby acting as a bridge between the bacteria and the autophagosomal membrane (Pankiv et al., 2007).

Optn (optineurin)

Optineurin restricts *S.*Typhimurium proliferation both *in vitro* and *in vivo* (Slowicka et al., 2016; Wild et al., 2011). The role and/or recruitment of Optn during *T.gondii* infection have not yet been investigated.

Optn binds the surface of cytosolic bacteria through its UBAN and zinc-finger domains (**Fig.3**). Optn is an effector protein of LUBAC since it binds linear ubiquitin, unlike the other cargo receptors (Noad et al., 2017). Optn binding to LC3 is regulated by TBK1-mediated phosphorylation (Wild et al., 2011), which is an IKK-related kinase.

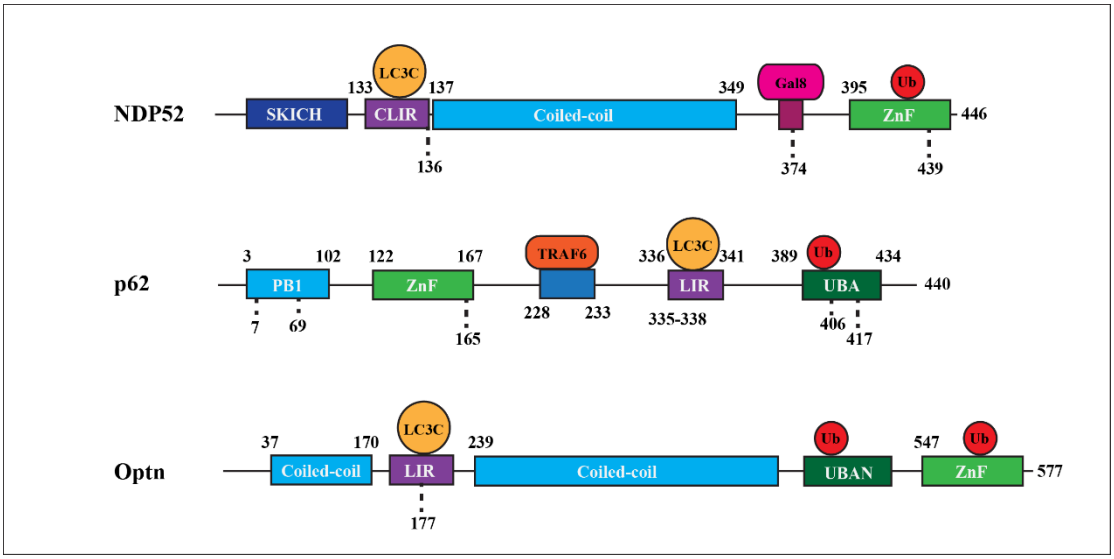

Figure 3: Schematic illustration of the three autophagy cargo receptor proteins

Characterisation of the different domains and binding partners of human NDP52, p62, and Optineurin. (C)LIR, LC3(C)-interacting region; ZnF, zinc-finger; UBA(N), Ub-associated domain (in NEMO).

Moreover, NDP52, Optn, and p62 contribute to autophagic restriction against *S.*Typhimurium in a non-redundant manner. Although NDP52 and Optn binding colocalises, p62 is located on different microdomains on the bacteria, indicating that they recognise distinct ubiquitin linkage types (Cemma et al., 2011). The autophagic cargo receptor protein p62 also plays a role in the presentation of antigens against *Toxoplasma gondii* in an IFN-γ-dependent mechanism (Lee et al., 2015).

Cargo receptors also bind LC3 on developing phagophores via their LIR domains and thus target cytoplasmic bacteria to autophagy (Boyle & Randow, 2013). In addition, cells induce their own death in response to cytoplasmic bacteria, in order to remove the bacteria's replicative niche and expose them to phagocytes in the extracellular environment (Jorgensen et al., 2017).

1.1.2 Microbicidal pathways

One of the major roles of the innate immune system is to preserve the host integrity. When a threat has been identified and localised, not only systemic but also cellular defence mechanisms are triggered to avoid the spread of the infection. Several strategies can be employed by the cells to counteract the attack including autophagy and programmed modes of cell death.

1.1.2.1. Autophagy

Autophagy ("self-eating") is a catabolic process that recycles cells' cytoplasmic content and relies on engulfment of cytosolic cargos into double membrane autophagosomes (**Fig.4**). Nascent autophagosomes are recruited by cargo receptors and target their sequestered materials for lysosomal degradation (Gatica et al., 2018). Autophagy can be either general, for example in response to starvation (Hailey et al., 2010), or selective, with cargo receptors targeting specific cargo such as ubiquitylated proteins and pathogens (Boyle & Randow, 2013; Geisler et al., 2010; Pankiv et al., 2007).

Autophagy is active under normal physiological conditions and maintains cellular homeostasis, regulates nutrient turnover and is induced in response to various stress stimuli (Levine & Kroemer, 2019; Mizushima & Komatsu, 2011; Rabinowitz & White, 2010).

The autophagy process depends on no less than 35 autophagy-related (ATG) proteins, which assemble in several complexes for the initiation and formation of the autophagosome (**Fig.4**) and lysosomal fusion (Bento et al., 2016; Mizushima et al., 2011).

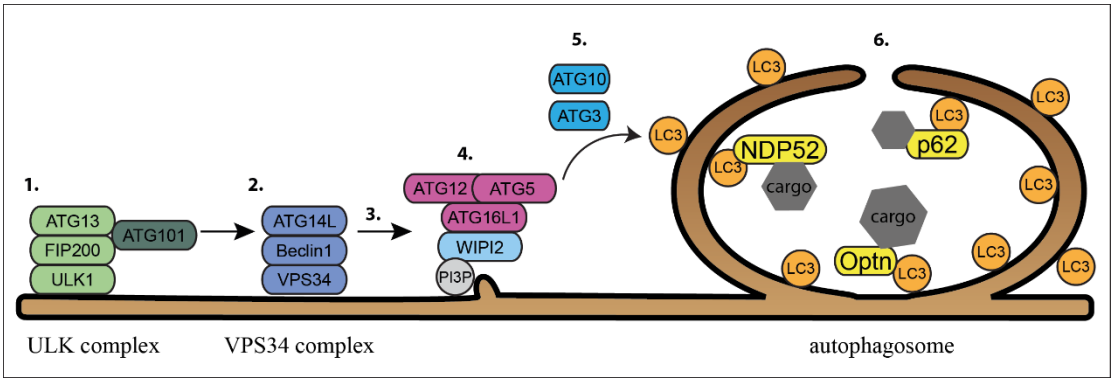

Figure 4: Formation of the autophagosome

The autophagy machinery relies on the establishment of an autophagosome. (1) Translocation of the activated ULK complex to the site of autophagosome initiation enables (2) activation of the VPS34 complex. (3) The class III phosphatidylinositol 3-kinase (PI3K) promotes the accumulation of phosphatidylinositol 3-phosphate (PI3P) on the omegasome, recruiting PI3P-binding proteins (4) such as WIPI2 and the ATG12-ATG5/ATG16L1 complex. Elongation of the membrane proceeds via two conjugation systems. The ATG12-ATG5/ATG16L1 complex dimerises via ATG16, and (5), in concert with ATG3 and ATG10 catalyses conjugation of ATG8/LC3 to phosphatidylethanolamine (PE) present in the isolation membrane. (6) During selective autophagy, the targeting cargo (to be degraded) is associated to the autophagosome by LC3-interacting adaptors such as NDP52, p62 and Optn.

The formation of the phagophore is initiated by the ATG1/ULK complex (**Fig.4.1**), which comprises a serine/threonine kinase ULK1 or ULK2 (uncoordinated 51 like kinase 1 or 2), and the partners ATG13 and FIP200 (focal adhesion kinase family interacting protein of 200kDa) and the scaffold protein ATG101 (**Fig.4.1**). Upon activation, ULK recruits and phosphorylates class III phosphatidylinositol 3 kinase

(VPS34), a main catalytic component of the second complex. This VPS34 complex (**Fig.4.2**) also contains Beclin-1 and ATG14L. Altogether, they participate in the accumulation of phosphatidylinositol-3-phosphate (PI3P) on the nascent omegasome (**Fig.4.4**) and thereby in the establishment of a crescent-shaped double-membrane structure derived from the endoplasmic reticulum (Axe et al., 2008; Obara & Ohsumi, 2008; Simonsen & Tooze, 2009). Localised PI3P production (**Fig.4.3**) enables recruitment of WIPI2 (**Fig.4.4**), which attracts the ATG12-ATG5/ATG16L1 complex (Dooley et al., 2014; Mizushima et al., 2011; Tanida, 2011). The elongation process is driven by two ubiquitin-like conjugation systems based on either ATG12 or ATG8/LC3 (Sugawara et al., 2004). The ATG12-ATG5/ATG16L1 complex acts together with ATG10 and ATG3 (**Fig.4.5**) to catalyse conjugation of ATG8/LC3 to the phagophore membrane by lipidation with phosphatidylethanolamine (PE) (Kabeya et al., 2000). Conjugated LC3 promotes elongation of the autophagosomal membrane (**Fig.4.6**) and cargo selection (Pankiv et al., 2007; Tanida et al., 2004).

The mechanism of closure for the engulfment of cytosolic content or a target substrate is thought to depend on components of the ECSRT (Endosomal Sorting Complex Required for Transport) machinery (Nguyen et al., 2016; Takahashi et al., 2018; Wang et al., 2016). Fusion with lysosomes to form a mature autolysosome allows degradation of the captured content and requires ATG8 and SNARE (SNAP receptors) proteins (Mizushima et al., 2011).

Autophagy is crucial in bacterial restriction in eukaryotes, as demonstrated by mammalian cells deficient in FIP200, ATG5, ATG3, which fail to control intracellular proliferation of *S.*Typhimurium (Birmingham et al., 2006; Shun Kageyama et al., 2011). The autophagy protein ATG5 is also involved in the IFN-γ-mediated parasiticidal effect against *Toxoplasma gondii* (Zhao et al., 2008).

1.1.2.2. Cell death

When pathogens are recognised as foreign and potentially harmful, they can be controlled by autophagy. In some instances, however, infected cells sacrifice themselves by triggering cell death in order to kill the pathogens and/or for the

extracellular exposition and detection of the threat, thereby activating professional immune cells and inducing adaptive immunity mechanisms.

i. Programmed forms of cell death

Cell death is essential for the survival and development of an organism (Fuchs & Steller, 2011; Schwartz, 1991), and there is increasing evidence that programmed cell death mechanisms contribute to immune protection against pathogenic infections as a form of cell-autonomous immunity (Jorgensen et al., 2017). Cell death results in the destruction of the pathogens' replicative niche, exposing them to the extracellular environment where professional immune cells such as phagocytes may in turn target and destroy them.

Apoptosis is a non-inflammatory and programmed mode of cell death. It can be initiated, for example, by DNA damage as a result of chemotherapy; in this case, apoptosis is mediated by the p53 pathway (Kemp et al., 2001). More generally, apoptosis is triggered either by extrinsic cues (death ligands binding to death receptors) or by intrinsic variations (Hengartner, 2000); for example, changes in the mitochondria can lead to the release of cytochrome c in the cytosol and subsequent assembly of the apoptosome and activation of Caspase-9 (Li et al., 1997). Apoptotic caspases initiate (Caspases-2, -8, -9, and -10) and execute (Caspases-3, -6, -7) this cell death mechanism (Cohen, 1997; Degterev et al., 2003); for example, the initiator caspase, Caspase-8 cleaves the effector caspase, Caspase-3, in the CD95 apoptosis pathway (Walczak & Krammer, 2000) (**Fig.5**).

Contrary to pyroptosis and necroptosis, apoptosis is immunologically silent, forming apoptotic bodies that are cleared by efferocytosis. Efferocytosis refers to the engulfment of apoptotic bodies or necrotic debris by professional phagocytes, thereby preserving tissue homeostasis and standing as an antibacterial mechanism (Martin et al., 2012; Poon et al., 2010).

As with apoptosis, pyroptosis results from the activation of caspases, but in this instance, they are inflammatory caspases in contrast to initiator or effector caspases in apoptosis (Fink et al., 2005). The activation of Caspases-4/-1 in humans and caspases-

11/-1 in mice is mediated by the formation of inflammasomes, multimeric signalling platforms that favour proximity-induced auto-proteolysis of pro-caspases (**Fig.1**).

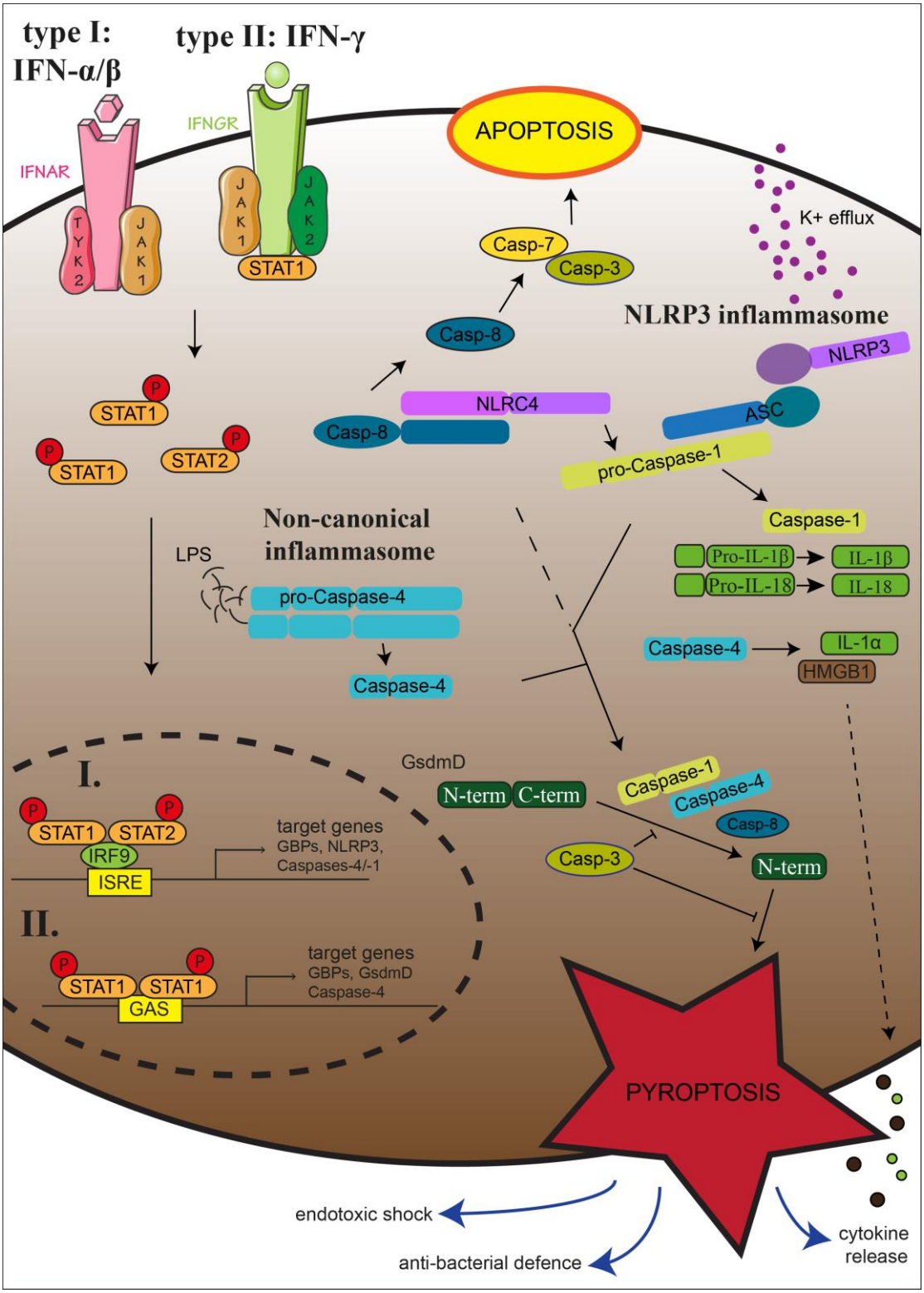

Figure 5: Pyroptosis constitutes one of the multiple lines of defence against microbial infection

In response to a microbial threat, several cell-autonomous defence mechanisms overlap in order to trigger cell death, thereby killing the pathogenic species. Human inflammatory

Caspases-4 and -1 are activated following the establishment of inflammasomes. CASP4 directly binds cytosolic LPS whereas CASP1 is canonically activated in the NLRC4 or NLRP3 inflammasomes for example. Their activation allows maturation of interleukins and cleavage of GSDMD, essential for pyroptosis. Pyroptosis is a lytic form of cell death that triggers inflammation and enables cytokine release. The initiator caspase, CASP8 can also participate in NLRC4 inflammasome activation and is able to cleave GSDMD, although CASP8 is mostly known for its action upon effector Caspases-3 and -7 to trigger apoptosis. Moreover, CASP3 both benefits apoptosis and downregulates the pyroptotic pathway by cleavage of GSDMD in non-active fragments. Microbial infections induce production of type-I or type-II IFNs, which in turn upregulate many genes involved in defence mechanisms; in particular inflammatory caspases.

ii. Pyroptosis

Pyroptosis is a programmed but proinflammatory form of cell death. It was first characterised in macrophages infected with *Shigella flexneri* (Zychlinsky et al., 1992) and later named "pyroptosis" by Cookson & Brennan (2001). It is a non-homeostatic and lytic mode of cell death that requires the enzymatic activity of a dedicated set of cysteine-dependent proteases: Caspases-1, -4, or -5 in humans (Aachoui et al., 2013b; Cookson & Brennan, 2001; Kayagaki et al., 2011). Pyroptosis also occurs in non-immune cells such as epithelial, endothelial and neuronal cells (Adamczak et al., 2014; Cheng et al., 2017; Shi et al., 2014). Pyroptosis is morphologically distinct from apoptosis: cells dying by pyroptosis exhibit swelling, rupture of the plasma membrane and release of the cytoplasmic content, features that are shared with caspase-independent necroptosis (Bergsbaken et al., 2009; Lamkanfi, 2011) but lack the DNA fragmentation characteristic of apoptosis (Jorgensen et al., 2016).

Active inflammatory caspases (Chang & Yang, 2000) can, in turn, cleave the downstream effector Gasdermin-D (GSDMD) releasing the inhibiting C-terminal part from the N-terminal pore-forming domain (Man & Kanneganti, 2015a; Liu et al., 2018). The cytosolic presence of N-terminal GSDMD is sufficient to trigger pyroptotic cell death, even with artificial cleavage in the absence of active caspases (Kayagaki et al., 2015; Shi et al., 2015). N-terminal GSDMD (p30) proteins oligomerise and insert in the plasma membrane to form pore-like structures (Aglietti et al., 2016; Ding et al., 2016). This pore-forming ability is shared across the Gasdermin protein family as, for example, Gasdermin-A and Gasdermin-E form transmembrane pores in lipid membranes (Ding et al., 2016; Feng et al., 2018; Wang

et al., 2017). Overexpression of GSDMD, GSDMA, GSDMB, GSDMC or DFNA5 N-terminal domains is cytotoxic in mammalian cells (Ding et al., 2016). The pore formation process is highly dependent on the membrane lipid composition: phosphatidylinositol (POPI) prevents GSDMD binding and cholesterol reduces GSDMD affinity to the membrane, whereas phosphatidylinositide (PI(4,5)P2) enhances binding and increases formation of slit- and ring-shaped oligomers (Mulvihill et al., 2018). Liposome-floating assays revealed that GSDMD p30 active form colocalises with mitochondria- and plasma membrane-like lipososmes (Chen et al., 2016). The active N-terminal domain of GSDMD can also bind to cardiolipin, a lipid moiety found in bacterial plasma membranes and mitochondrial inner membranes (Ding et al., 2016; Liu et al., 2016).

The pores enable cytosolic contents to leak into the extracellular environment (**Fig.5**). Even though the specificity has not yet been fully characterised, previous work shows that mitochondrial cytochrome c, pro-caspase-3 and lysosomal cathepsin B are released through GSDMD pores (de Vasconcelos et al., 2019). Cytokines such as IL-1β or IL-18 lack the signal peptide for the canonical secretion pathway via the endoplasmic reticulum and the Golgi compartment. They are secreted unconventionally, including passive release through the GSDMD pyroptotic pores (Heilig et al., 2017; Keller et al., 2007; Martín-Sánchez et al., 2016). Release of the inflammatory factor high mobility group box 1 (HMGB1) and IL-1α in the extracellular space (**Fig.5**) sustains the inflammatory and chemotactic responses (Vande Walle & Lamkanfi, 2016).

In the case of pyroptosis, intracellular *S.*Typhimurium are enclosed in pore-induced intracellular traps (PITs) that ensure their destruction (Jorgensen et al., 2016); however recent work with *Pseudomonas aeruginosa* shows that infected macrophages trigger NLRC4 inflammasome-dependent pyroptosis and that *P.aeruginosa* escaped PIT-mediated immunity (Eren et al., 2019).

1.1.2.3. Phagocytosis

Contrary to autophagy, phagocytosis is a cell-mediated "eating" mechanism that protects an organism against foreign particles or organisms. Both phagocytosis and autophagy are highly conserved mechanisms involved in the removal and destruction of extracellular or cytosolic organisms, respectively. These two processes are linked since TLRs and ATG proteins play a role not only in autophagy (see paragraph **1.1.2.1** "Autophagy") but also in phagosome maturation and recruitment (Sanjuan et al., 2007). TLRs are indeed expressed on the surface of specialised cells from the innate immune system such as professional phagocytes (macrophages and neutrophils), which clear infections by phagocytosis of the pathogens (Price & Vance, 2014).

1.1.3 Production and release of effector molecules makes up an integrated immune system

The immune system is a highly connected network. Cytosolic immunity is integrated in organism-wide immune defences that induce inflammation in response to microbial attacks. Inflammatory signalling affects surrounding cells and tissues, promotes the recruitment of immune cells to the site of infection and regulates intrinsic cell-autonomous defences. Some professional immune cells release effectors such as cytokines to signal and induce antimicrobial pathways; for example, helping the intestinal epithelium (Madara & Stafford, 1989) to stand as an efficient barrier against infection.

In response to pathogens, inflammatory signalling can be activated downstream of PRRs (see paragraph **1.1.1.1**). Immune effectors, such as Toll-like receptors (TLRs) survey the extracellular environment, whereas in the cytoplasm, intracellular PRRs such as NOD receptors, recognise opsonised pathogens (Takeuchi & Akira, 2010). Following recognition of a threat, a signal transduction cascade is initiated, thereby activating transcription factors including IFN response factors (such as IRF3) and dimeric nuclear factor kappa-light-chain-enhancer of activated B cells p65/p50 (NF-κB). Once activated, these transcription factors enter the cell nuclei and upregulate

transcription of a large number of genes that induce inflammation (Bouwmeester et al., 2004).
Expression of NF-κB-controlled and/or IFN-induced genes is critical for the immune system to function efficiently and for the cooperation between several pathways linking innate and adaptive immunity (Cooney et al., 2010).

For the immune system to collaborate, a feed-forward loop works through the activation of the NF-κB and IRF signalling pathways that lead to the transcription of key signalling molecules such as cytokines, chemokines, and interferons. They promote immune signalling cascades and are released to activate and recruit professional immune cells; these, in turn, produce additional signalling molecules for further recruitment and activation of pathways to promote the elimination of the threat.

1.1.3.1. NF-κB signalling

The nuclear factor κ-light-chain-enhancer of activated B cells (NF-κB) family contains dimeric transcription factors that bind to specific DNA sequences referred to as κB sites. These regulate a multitude of genes involved in immunity and for example, encode for cytokines and pro-proliferative or anti-apoptotic proteins (Wullaert et al., 2011). Many enteric pathogens, including *S.*Typhimurium and *Shigella flexneri*, are known to interfere with NF-κB signalling and to modulate inflammatory responses to promote bacterial pathogenesis (Kawai & Akira, 2007; Wullaert et al., 2011).

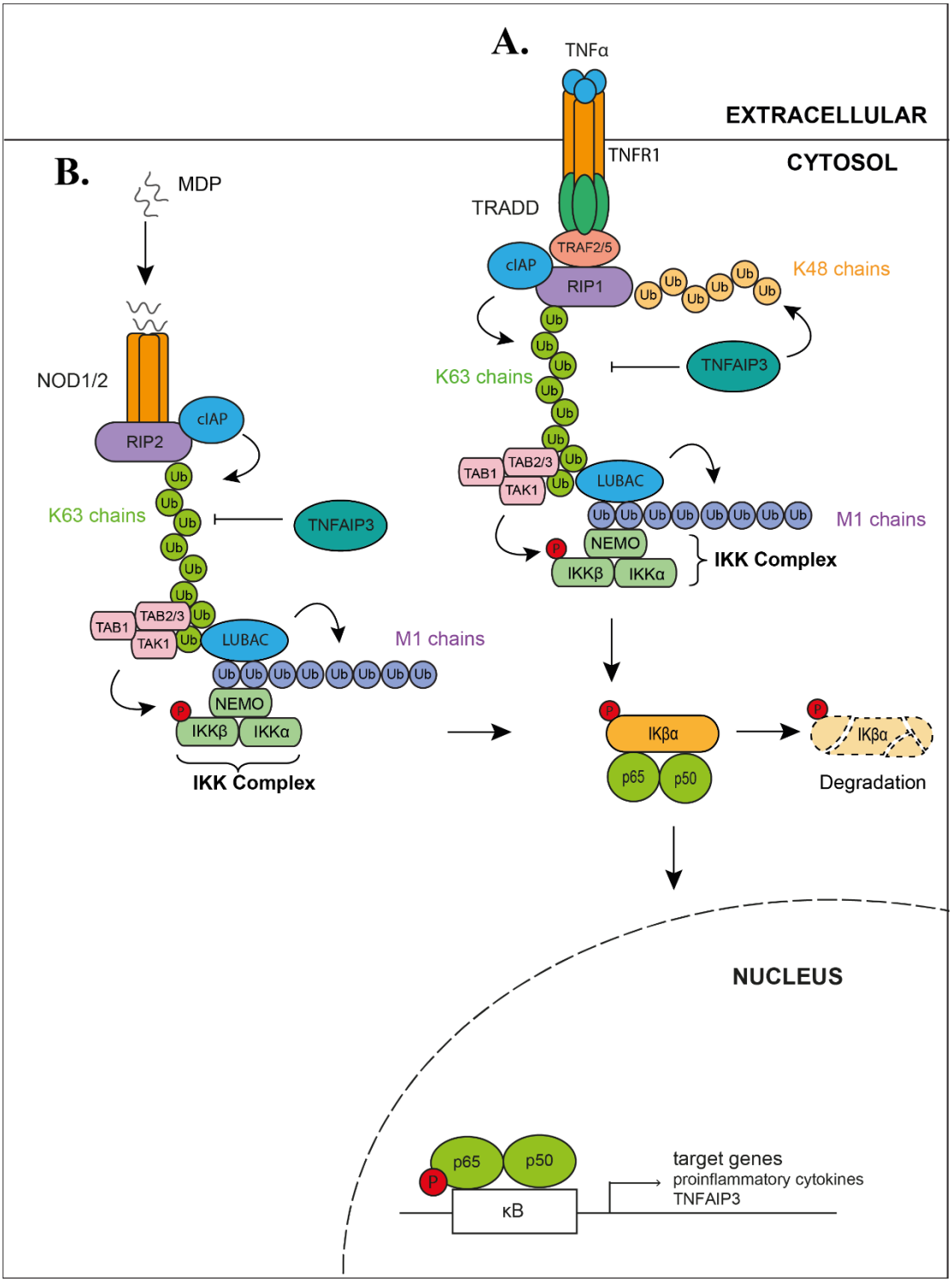

Figure 6: NF-κB signalling

The NF-κB signalling pathway activates target genes, presenting κB sites in their promoter region. The activation can be initiated following one of two pathways. The first pathway (A) is extracellular initiation, where TNF-α binds to TNF receptor 1 (TNFR1) inducing its oligomerisation and subsequent recruitment of TRADD and TRAF proteins. The second pathway (B) is initiated in the cytosol, where peptidoglycans of foreign origin bind to NOD1/2. Both pathways converge in the recruitment of RIP and the E3 ligase cIAP leading to ubiquitylation and recruitment of the kinase TAK1 and the E3 ligase LUBAC that synthesises linear ubiquitin chains and enables recruitment of NEMO and the IKK complex. The IKK

complex is activated by TAK1-mediated phosphorylation leading to removal of the inhibition exerted by Iκβα on the NF-κB dimer (commonly p65/p50), thereby allowing its translocation into the nucleus where it binds κB sites for activation of target genes.

TNF-α binding to TNF-α receptor (TNFR) constitutes the canonical trigger for NF-κB signalling (**Fig.6A**). NF-κB signalling is also triggered by members of the TNF cytokine family, such as CD40 (cluster of differentiation 40), BAFF (B-cell-activating Factor) and lymphotoxin-β via a distinct non-canonical activation pathway (Hayden & Ghosh, 2012).

Although, NF-κB signalling can be activated by multiple stimuli (Ting Liu et al., 2017), the different pathways converge in the ubiquitinylation and subsequent proteasomal degradation of IκBα (**Fig.6**), releasing the inhibition on NF-κB. In resting cells, NF-κB dimers are inhibited by binding of IκB (inhibitor of NF-κB) and are consequently located exclusively in the cytosol (Beg et al., 1992). The degradation of IκBα results in nuclear translocation of NF-κB complexes where they act as transcription factors (**Fig.6**). This common signalling cascade starts with the synthesis of K63 Ub chains (Wertz & Dixit, 2010), which recruit LUBAC and TAB proteins (Besse et al., 2007; Haas et al., 2009; Kanayama et al., 2004). Linear Ub chains (M1-Ub chains) synthesised by LUBAC recruit the IKK complex (Tokunaga & Iwai, 2012), which is activated by TAK1 and thereby activates NF-κB. The IKK complex is composed of NEMO, which is specifically and directly recruited by M1-Ub chains (Fujita et al., 2014; Rahighi et al., 2009), in addition to the two IKKβ and IKKα subunits (Ea et al., 2006). TAB proteins recruit TAK1 for the phosphorylation and activation of the IKK complex (Karin & Delhase, 2000). In particular, the phosphorylation of the IKKβ subunit of the IKK complex mediates the phosphorylation of IκBα leading to its subsequent ubiquitylation (Karin & Ben-Neriah, 2000) and degradation.

RIP and TRAF proteins are involved in signalling upstream of the deposition of K63 ubiquitin chains and independently of the NF-κB receptors (**Fig.6**). Extracellular induction of NF-κB signalling (**Fig.6A**) is canonically triggered by TNF-α (Hayden & Ghosh, 2014). Tumour necrosis factor receptor (TNFR) is activated by binding of TNF-α and oligomerisation, which allows recruitment of TRADD (TNF receptor-

associated death domain protein). TRADD recruits RIP1 via death domain interactions (Ermolaeva et al., 2008; Hayden & Ghosh, 2012; Pobezinskaya et al., 2008) and brings in TNF Receptor-associated factor 2 (TRAF2), which facilitates recruitment of cellular inhibitor of apoptosis proteins (cIAP1 and 2). cIAPs act as E3 ubiquitin ligases and synthesise K63 Ub chains on RIP1 (Mahoney et al., 2008; Varfolomeev et al., 2008), thereby allowing LUBAC recruitment and NF-κB signalling as described above.

In the cytosol (**Fig.6B**), nuclear oligomerisation domain proteins (NOD1 and NOD2) sense peptidoglycans from the bacterial cell wall (such as MDP), activate the transcription factor NF-κB (Girardin et al., 2003a and 2003b) and induce cytokine production in macrophages (Chamaillard et al., 2003). Oligomerisation of NOD receptors allows recruitment of the protein RIP2 (Cooney et al., 2010), which is then ubiquitylated by cIAP, by synthesising K63 chains. These K63 Ub chains are recognised by the TAK1 complex and LUBAC, leading to the downstream activation of the NF-κB dimers mentioned previously.

Among the genes upregulated by NF-κB are pro-IL1β and pro-IL18, inactive forms of inflammatory cytokines, and NLRs such as NLRP3. Therefore, NF-κB activation can serve as the first signal for inflammasome formation.

1.1.3.2. Interferon signalling

Interferons (IFNs) are α-helical proinflammatory cytokines, which are classified into three groups according to the different receptors involved (Sadler & Williams, 2008). First, type-I IFNs, which include IFN-α and IFN-β, bind a receptor consisting of IFN-aR1 and IFN-aR2 (**Fig.7**), which is expressed on all cell types. Second, type-II IFN also referred to as IFN-γ binds to a dimeric receptor made of IFNGR1 and IFNGR2 (**Fig.7**), which is ubiquitously expressed (Platanias, 2005). Third, type-III IFNs include four homologous (IFN-λ1-4) proteins that bind to receptors containing IFNLR1 and IL-10R2 and trigger antiviral responses (Sadler & Williams, 2008; Wack et al., 2015). All interferons impact gene expression but their effect is different owing to their belonging to the three classes (Der et al., 1998).

IFNs are produced in response to viral- or bacterial-induced PRR stimulation. Cytosolic IFN response factors (IRF) are activated by dimerisation upon phosphorylation by TBK1 (Fitzgerald et al., 2003; Sharma et al., 2003). Following nuclear translocation, IRFs bind to IFN-stimulated response elements (ISRE) found in promoter regions of genes upregulated by IRF signalling (Honda & Taniguchi, 2006). IRF target genes that include type-I IFNs (IFN-α/β) and other immunomodulatory cytokines (Honda & Taniguchi, 2006; Sharma et al., 2003). Once produced, type-I IFNs are secreted and can exert autocrine and paracrine effects by binding to IFN receptors on either the producer cell or neighbouring cells, triggering JAK-STAT signal transduction cascades (**Fig.7**) that upregulate hundreds of IFN-stimulated genes (ISGs) (Der et al., 1998; Samarajiwa et al., 2009).

Screens have been performed to identify antiviral ISGs; depending on the study, these screens were designed to investigate virus entry, replication or virion budding. Host restriction effectors such as viperin, ISG20, IFITM2, IFITM3 and PKR were found to inhibit replicons of dengue and West Nile replicon-containing virus-like particles (Jiang et al., 2010). Guanylate-binding protein 1 (GBP1), an IFN-induced GTPase acts as a potent suppressor of classical swine fever virus (Li et al., 2016). Ifit2-deficient mice are more severely infected by rabies virus than their wild-type counterparts (Davis et al., 2017). IFN-α-based drugs are used for the treatment of patients infected with hepatitis C virus and positive outcome is associated with elevated ISG levels in the liver (Sarasin-Filipowicz et al., 2008).

Contrary to type-I IFNs, which are mainly associated with antiviral immunity (Schoggins & Rice, 2011), some proteins upregulated by IFN-γ also contribute to antibacterial immunity (Reljic, 2007; Rottenberg et al., 2002) and include cytosolic pathogen receptors. IFN-γ also plays a role in macrophage activation and immunity against a range of pathogens, including viruses, bacteria and parasites (Nathan et al., 1983; Ohshima et al., 2014; Zhang et al., 2008). For instance, humans with defective type-II IFN signalling are highly susceptible to mycobacterial infections (Zhang et al., 2008).

Both IFN systems are non-redundant; for example, mice that are deficient in type-I IFN signalling are highly susceptible to viral infections but are able to control

bacterial infections such as *L. monocytogenes* (Müller et al., 1994; O'Connell et al., 2004).

IFN-γ requires further discussion for the benefit of this thesis, as it is characterised for its role in antibacterial and antiparasitic defences (Ohshima et al., 2014; Reljic, 2007; Rottenberg et al., 2002). IFN-γ is produced by NK cells, T cells, antigen-presenting cells and macrophages (Carnaud et al., 1999; Frucht et al., 2001; Gessani et al., 1998) and its production is controlled by cytokines such as IL-12 and IL-18 (Farrar and Schreiber, 1993; Fukao et al., 2000; Yoshimoto et al., 1998). IFN-γ antiparallel homodimer signals through the tetrameric receptor (IFGR) consisting of two IFNGR1 chains and two IFNGR2 chains (Fountoulakis et al., 1992), resulting in activation of pre-associated JAK (Janus kinases) tyrosine kinases with the receptor (**Fig.7**). JAKs phosphorylate STAT-1 (signal transducer and activator of transcription 1) enabling STAT-1 to dimerise and form the IFN-γ activation factor (GAF). GAF enters the nucleus, where it binds GAS promoter elements and upregulates expression of IFN-γ-responsive genes (Decker et al., 1997).

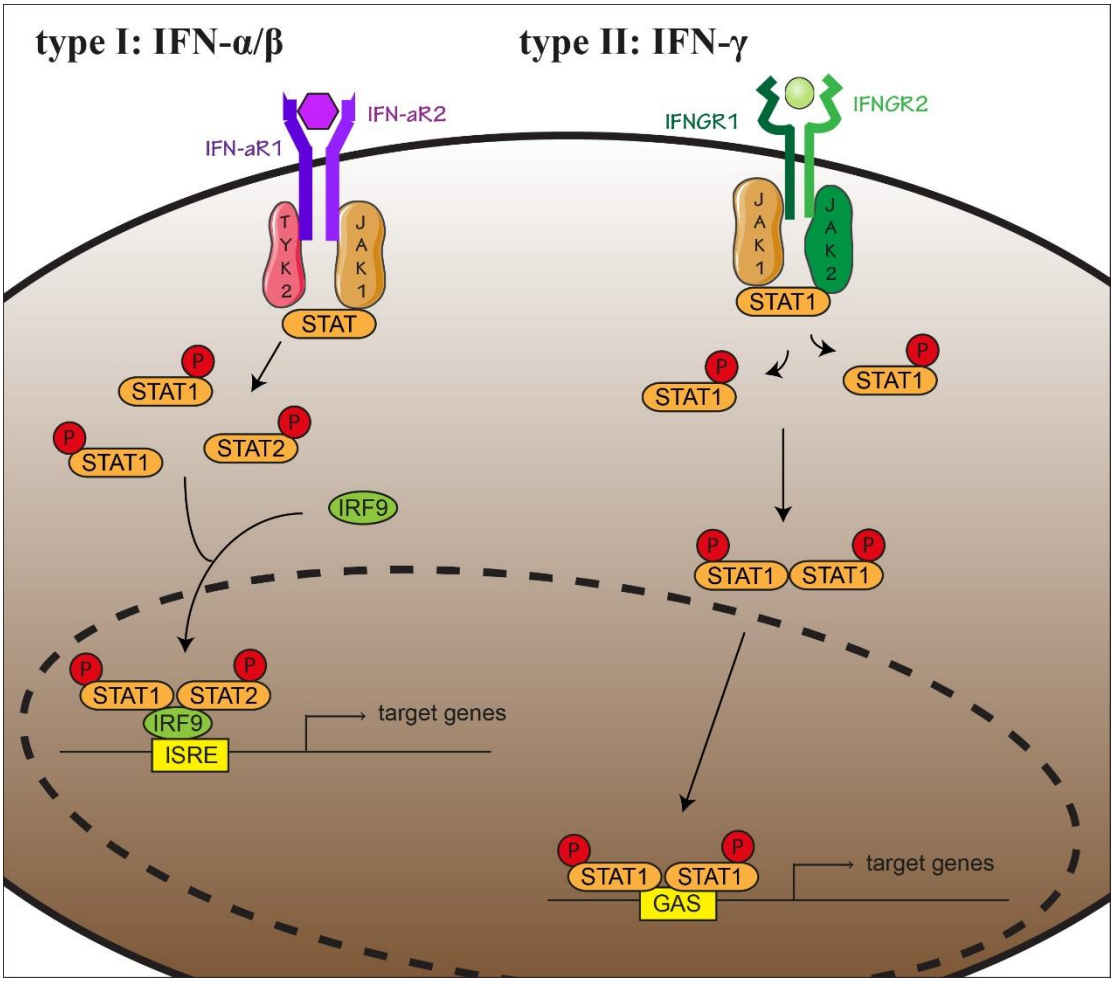

Figure 7: Type-I and type-II interferon signalling

IFNs are sensed by their specific receptors that are then activated and bind (I) TYK2 and JAK1 or (II) JAK1 and JAK2. Both IFN signalling pathways use the JAK-STAT signalling cascade for the phosphorylation of (I) STAT1 and STAT2 or (II) STAT1 only. Type I IFNs induce the formation of the IRF complex composed of STAT1, STAT2 and IRF9. The IRF complex translocates to the nucleus to bind ISRE motif located on promoters of target genes. IFN-γ (type II IFN) leads to the formation of the GAF complex, dimer of phosphorylated STAT1. Nuclear translocation and binding of GAF to GAS induces target gene expression.

IFN-γ induces the Death associated protein (DAP)/DAP-kinase (DAPK) system genes. They are positive mediators of apoptosis and autophagy. Loss of DAPK expression (so far only found within epigenetic mechanisms) has been observed in multiple cancer types (Wei et al., 2010).

Some IFN-γ-induced genes are involved in cell-autonomous immunity (MacMicking, 2012). For example, guanylate-binding proteins (GBPs) are interferon-inducible

(Martens & Howard, 2006) and directly target intracellular bacteria and promote inflammasome activation in response to bacterial infection (Haldar et al., 2015; Man et al., 2017; Santos & Broz, 2018). In addition, certain upregulated proteins, such as nitric oxide synthase, mediate the production of bactericidal reactive oxygen and nitrogen species for the killing of pathogens (Denkers & Gazzinelli, 1998; Haraga et al., 2008).

Interferons are used as treatment against particular disorders; for example, recombinant human IFN-γ (Actinmune – IFN-γ1b) is used in chronic granulomatous disease. It delays the progression in severe malignant osteopetrosis but has been shown to be ineffective and may increase mortality in patients with idiopathic pulmonary fibrosis (Brunton et al., 2011).

1.1.3.3. Cytokine production

Proinflammatory cytokines play an important role during the inflammation process, and they participate in the interactions of the cells involved not only in the innate immune response but also in the establishment of acquired immunity. Proinflammatory cytokines, such as TNF-α, IL-1, and type I IFNs, participate during the activation and effector phases of the innate immune response. Other cytokines also play a role during the establishment of the innate immune response, but the aforementioned ones deserve special attention in the context of this thesis.

i. Interleukins

Interleukins (ILs) are a subgroup of cytokines that are classified into four major families; the classification is based on structural features, since interleukins share little sequence homology as a consequence of constant evolutionary pressure between the host's immune system and infectious agents (Brocker et al., 2010). By binding to high-affinity cell-membrane receptors, interleukins initiate paracrine or autocrine responses to multiple stimuli with a variety of effects, including modulation of cell proliferation, cell activation, or cell differentiation (Commins et al., 2010). The human genome encodes more than 50 interleukins and related proteins, of which three quarters are either characterised or annotated ("Cytokine Tutorial", Univ. of Arizona;

Lippincott, 2007). Only a few interleukins are highlighted here because they are mentioned later in this thesis (see Chapter 3, paragraph **3.3.2**) and include IL-6 and a few members of the IL-1 superfamily such as IL-1α, IL-1β and IL-18. The focus is placed on their role in anti-microbial immunity.

Interleukin 1 has two isoforms, α and β, which both participate in the regulation of immune responses, inflammatory reactions and hematopoiesis (Mochizuki et al., 1987; Sims et al., 1988). IL-1β production is enhanced in response to bacterial infection after detection of the pathogens via PRRs (Brubaker et al., 2015; Takeuchi & Akira, 2010). More generally, in resistance mechanisms against intracellular pathogens, IL-1β is required for IL-12-dependent, NK cell-mediated IFN-γ production (Hunter et al., 1995). Inflammasome activation results in processing of IL-1β and IL-18 by CASP1 and IL-1α by Caspases-11/-4 (Casson et al., 2015; Kayagaki et al., 2011; Martinon et al., 2002) eventually promoting inhibition of S.Typhimurium growth (Thurston et al., 2016). IL-18 belongs to the IL-1 superfamily and is produced by macrophages, but is also constitutively expressed in non-hematopoietic cells such as intestinal epithelial cells. IL-18 was first described to induce the production of IFN-γ (Nakamura et al., 1989), but it has also been characterised to upregulate NK cell activity and to modulate both innate and adaptive immunity (O'Neill et al., 2016; Yoshimoto et al., 1998). Dysregulation of IL-18 is associated with cancer, autoimmune diseases and inflammatory diseases (Fabbi et al., 2014; Yasuda et al., 2019).

IL-6 is a glycosylated soluble mediator that plays a role in inflammation, immune response and hematopoiesis (Kishimoto, 1989). IL-6 expression is highly regulated; for example, in response to IL-1R/TLR stimulation, inhibitor of NF-κB (IκB) kinase (IKK) complex phosphorylates regnase-1 and thereby controls IL-6 mRNA stability (Iwasaki et al., 2011). In hepatocytes, the decreased expression or lack of Homeobox containing 1 (HMBOX1) upregulates the expression of inflammatory factors such as IL-6 and TNF-α (Zhao et al., 2018). However, increased level of IL-6 and TNF-α in cultured HAECs following LPS treatment is independent of HMBOX1 (Ma et al., 2019). IL-6 also has various effects on lymphocytes, as it promotes differentiation of CD4+ T cells and is required for Th17 differentiation in combination with

transforming growth factor (TGF)-β (Bettelli et al., 2006). IL-6 is, therefore, a bridge between innate and adaptive immunity (Tanaka et al., 2014).

ii. TNF-α

TNF-α is a pro-inflammatory cytokine (Carswell et al., 1975) synthesised by macrophages as a membrane-associated 26kDa protein that is cleaved from the membrane in the extracellular domain to produce a mature 17kDa cytokine (Palladino et al., 2003). Both membrane-bound and secreted forms of TNF-α require trimerisation to be active. Along with IL-10, IL-12 and IFN-γ, TNF-α is an important mediator of host survival during primary infection with *Toxoplasma gondii* (Scanga et al., 2002; Sukhumavasi et al., 2008).

iii. Adhesion molecules

Pro-inflammatory cytokines and chemokines all have the ability to induce chemotaxis and cell adhesion molecule (CAM) expression in both endothelium and leucocytes. These CAMs include selectins, integrins, immunoglobuline-like superfamily molecules and cadherins. Expression of these CAMs allows interaction between leukocytes and endothelium and the subsequent leukocyte transmigration at the site of the injury.

1.1.4 Immunity relies on multiple cross-talks to function as a fully integrated system

Various defence mechanisms, including cell death pathways, constitute a multi-layered immunity against invading pathogens. Cross-talk is therefore essential to regulate and produce the most appropriate and efficient response.

Caspases seem to play several roles in diverse immune pathways (Man & Kanneganti, 2015b). Although CASP8 is defined as an apoptotic caspase, it can cleave GSDMD leading to pyroptosis in murine macrophages (Chen et al., 2019; Gram et al., 2019; Orning et al., 2018). A consequence of CASP8-mediated pyroptosis is the activation of the NLRP3 inflammasome (**Fig.5**). In the apoptotic pathway, activated CASP8 cleaves CASP3; however, CASP3 was found to process GSDMD and generate the

p43 and p20 fragments from the full-length protein and not the pore-forming p30 N-terminal fragment (Chen et al., 2019). This suggests that CASP3 inhibits pyroptosis and favours apoptosis (**Fig.5**). In conclusion, several cell death pathways operate, but in a non-exclusive way.

Many inflammatory caspases such as CASP1, CASP4, and Casp11 are upregulated by type-I and/or type-II interferons (Kayagaki et al., 2015; Ramirez & Salvesen, 2018). In addition to inflammatory caspases, NLR proteins and GSDMD are also IFN-induced, promoting inflammasome-mediated activation of CASP1 and pyroptosis, which in turn releases IL-18 (also known as interferon-γ-inducing factor), promoting inflammation (**Fig.5**). GSDMD is a downstream effector of mouse Casp11- and human CASP4-induced pyroptosis; however, pyroptosis following prolonged CASP1 activation is GSDMD-independent (Kayagaki et al., 2015). The absence of GSDMD combined with the absence or prolonged activation of CASP1 results in the activation of CASP8 via ASC specks and consequent apoptosis (Pierini et al., 2012).

Occasionally, cells release IL-1β/18 without lysis and consequent death, meaning that some membrane repair mechanisms might be in play (Jimenez et al., 2014; McNeil & Kirchhausen, 2005). The endosomal sorting complexes required for transport (ESCRT) membrane repair machinery has an anti-inflammatory function by negatively regulating pyroptosis (Rühl et al., 2018).

1.2 Two model organisms to study cell-autonomous immunity: *Salmonella* Typhimurium and *Toxoplasma gondii*

Cell-intrinsic immunity includes self-defence mechanisms that most nucleated cells activate against viruses, bacteria and eukaryotic parasites (Randow et al., 2013).
Although *S.*Typhimurium and *T.gondii* are respectively prokaryotic and eukaryotic pathogens, their life cycle and the clearance or restriction mechanisms established by the infected cells display similarities, which are presented in this section. For instance, both pathogens reside within a vacuole. In rare cases, they become exposed in the

cytosol where sensors and receptors detect the foreign pathogenic elements and can lead to cell death (Jorgensen et al., 2017). Some of these host effectors are IFN-inducible (MacMicking, 2012). For example guanylate-binding protein 1 (GBP1) expression is highly increased in macrophages exposed to IFN-γ. GBP1 is recruited to cytosolic *S.*Typhimurium and is required for the breakage of *T.gondii* parasitophorous vacuole. GBP1 promotes the assembly of supramolecular organising centres, which act as signalling platforms and is required for cell death following *S.*Typhimurium and *T.gondii* infections (Fisch et al., 2019b).

After introducing the pathogenesis and the organisational characteristics of the two organisms, this section focuses not only on host defense mechanisms against *S.*Typhimurium and *T.gondii* but also highlights strategies that these two pathogens use to enter the host cells, spread and use the host cell machinery to establish infection.

1.2.1 Pathogenesis

Both the bacterium *S.*Typhimurium and the parasite *T.gondii* infect humans and can, under different circumstances, be life-threatening.

Bacteria are ancient unicellular organisms that are highly adaptable to changing environments by selection of spontaneous mutants and thereby have evolved traits that make them ubiquitous. Even though they appear simple as they lack a nuclear membrane, they are metabolically active and multiply by a process called binary fission (Davies et al., 1996).

Bacteria are divided into two categories depending on the composition and structure of their cell wall: Gram-positive and Gram-negative; except for *Mycobacteria* (e.g. *M.tuberculosis* or *M.leprae*), whose cell wall has unique properties (Brennan, 2003). Gram-positive bacteria have one thick cell wall composed of a periplasmic space comprised between the cytoplasmic lipid membrane and several peptidoglycan layers (Weidel & Pelzer, 1964). In Gram-negative bacteria, the organisation is more complex: the cell wall, similar to the one in Gram-positive with a thinner single layer of peptidoglycans, is surrounded by an outer membrane. The outer membrane

contains phospholipids and lipopolysaccharides (LPS), respectively on the inner and outer leaflets. **Chapter 2** deals with the immunogenicity of LPS as an endotoxin.

Salmonella enterica are a species of facultative anaerobic Gram-negative bacteria that cause diseases in many organisms, including humans (Haraga et al., 2008). *Salmonella* infections are orally acquired via the consumption of contaminated food or water. The *Salmonella enterica* species consists of several serovars, such as Typhimurium or Typhi. Both strains cause highly inflammatory gastroenteritis, which is associated with water loss, and may be life threatening for the elderly and children under the age of five. Together, they account for three million deaths each year worldwide (Coburn et al., 2007). *S.*Typhi specifically infect humans and cause more severe systemic typhoid fever, whilst in some instances, *S.*Typhimurium may enter the bloodstream and potentially lead to lethal sepsis and meningitis (Feasey et al., 2012) and causes an estimated 155,000 deaths each year (Majowicz et al., 2010).

Toxoplasma gondii is an obligate intracellular protozoan parasite. Humans become infected by the consumption of the oocytes present in contaminated water or food, or by ingestion of the tissue cysts present in undercooked or raw meat (Liu et al., 2015). In comparison to other species from the phylum Apicomplexa, *T.gondii* can infect any nucleated cell (Khan & Grigg, 2017) of warm-blooded animals including humans (Hill & Dubey, 2002), whereas *Plasmodium* spp. and *Cryptosporidium* spp. invade red blood cells and intestine enterocytes respectively (Sibley, 2004).

Members of the Felidae family (cats and relatives) are the definitive hosts of *T.gondii* whereas many birds and mammals – including humans – serve as intermediate hosts (Frenkel, 1973). *T.gondii* infections greatly affect livestock (e.g pigs, sheep, and goats), having a dramatic economic impact on the farming industry and being a sanitary risk by constituting a source of infections for humans (Stelzer et al., 2019).

It is estimated that anywhere from 500 million people worldwide (Denkers & Gazzinelli, 1998) to a third of the world's population are chronically infected (Khan & Grigg, 2017). In most cases, people do not show any symptoms; however, in immune-compromised individuals (Kasper & Buzoni-Gatel, 1998; Furtado et al., 2011), *T.gondii* infections can potentially cause fatal encephalitis, myocarditis,

pneumonitis (Liu et al., 2015), or can lead to severe mental and/or behavioural disorders, such as schizophrenia (Fuglewicz et al., 2017). Congenital toxoplasmosis – that is, infection of pregnant women and transmission to the foetus through the placental barrier (Wujcicka et al., 2018) – can lead to miscarriage or severe neurologic damage in the newborn (Hill & Dubey, 2002).

T.gondii can be found at three different infectious stages that are sporozoites, tachyzoites and bradyzoites (Dubey et al., 1998). The route of contamination common to all intermediate hosts is via sporulated oocysts. Sporozoites are contained in oocysts, whose structure is similar to tachyzoites but which contain increased numbers of effectors such as micronemes and rhoptries (Lycke et al., 1975). Tachyzoites are found as groups or clones and multiply rapidly in any cell of intermediate hosts or all but intestinal cells of the final host. Fast-growing tachyzoites are responsible for the acute phase of the infection and then turn into bradyzoites or tissue cysts in response to host immune defence to become dormant and hence constitute the basis for chronic *T.gondii* infection. (Boyle & Radke, 2009; Sibley, 2011). Bradyzoites grow slowly in tissue cysts that constitute a source of infection for humans and definitive hosts. Intact tissue cysts can persist for the entire life of the host without triggering any inflammatory response.

Tachyzoites and bradyzoites divide by endodyogeny (Ferguson & Hutchison, 1987), which means that the two daughter cells are formed within the mother cell that eventually pops open.

As a eukaryotic single-cell organism, *T.gondii* has common organelles such as nucleus, endoplasmic reticulum, Golgi apparatus, mitochondria. It is also a polarised cell that contains secretory vesicles such as micronemes and the rhoptry bulb, in the apical end (Dubey et al., 1998).

1.2.2 Entry and establishment of the vacuole

Intracellular bacterial pathogens either exploit host membrane trafficking to create protective niches called vacuoles or are cytosol-dwellers, such as *Shigella flexneri* and *Listeria monocytogenes*, which proliferate in the cytosol and often spread to neighbouring cells (Di Russo Case & Samuel, 2016). In the host cell cytosol, both

*S.*Typhimurium and *T.gondii* reside within vacuoles. However, the boundary between these distinct intracellular phenotypes is tenuous and may depend on the timing of infection and on the host cell type. For example, *Listeria monocytogenes* which has long been a model for cytosolic pathogens, now emerges as a bacterium also capable of residing in vacuoles, in a slow/non-growing state (Bierne et al., 2018). On the contrary, the vacuolar membrane surrounding *S.*Typhimurium sometimes breaks open, exposing the bacteria to the cytosolic compartment (Knodler et al., 2014b).

This section presents the mechanisms of cellular entry for both pathogens – i.e. *S.*Typhimurium and *T.gondii* – and the processes involved in the establishment of their vacuole.

Following ingestion, *S.*Typhimurium reach the gut epithelium where they preferentially invade microfold cells (M-cells) in Payer's patches (Jones et al., 1994) before infecting neighbouring epithelial or macrophage cells (Müller et al., 2012) (**Fig.8A** and **8C**). *S.*Typhimurium entry in non-phagocytic host cells (e.g. enterocytes) is mediated by effectors translocated into the cytosol through their type III secretion systems (T3SS). *S.*Typhimurium pathogenicity islands 1 and 2 (SPI1 and SPI2) encode two needle-like (Kubori et al., 1998) T3SSs (Hansen-Wester & Hensel, 2001; Ochman & Groisman, 1996; Shea et al., 1996) that penetrate the cellular membrane and release up to 30 bacterial molecules into the target cell. SPI1 T3SS and SPI2 T3SS are required for biogenesis and maturation (**Fig.8A** and **8B**) of the *Salmonella*-containing vacuole (SCV), respectively (Laughlin et al., 2014). *S.*Typhimurium reside inside SCV within the cytoplasm of host cells and establish a replicative niche. The T3SS-1 effector SopB participates in the rearrangement of the actin cytoskeleton enabling membrane ruffling and bacterial uptake into an SCV (Takeuchi, 1967). Maturation of the SCV is driven by a switch from SPI-1 to SPI-2 T3SS activity allowing the acquisition of lysosomal markers such as RAB7 and LAMP1 to transform the SCV into a late endosome-like compartment permissive to bacterial replication (Madan et al., 2012; Méresse et al., 1999). However, SCVs avoid lysosomal fusion and instead interact with endomembrane compartments and localise in close proximity to the Golgi and its secretory vesicles in order to source nutrients (**Fig.8B**) and additional membrane to enhance bacterial replication (Alix et al., 2011; Kuhle et al., 2006; Salcedo & Holden, 2003).

Occasionally, the SCV membrane is ruptured, resulting in *S.* Typhimurium to enter the nutrient-rich cytosol (Knodler et al., 2014b); this holds true for approximately 10% of intracellular *S.*Typhimurium in tissue culture cells. *In vivo* work on the NAIP/NLRC4 inflammasome claims that SCVs become leaky or rupture and exposed ligands to cytosolic NAIPs (Sellin et al., 2014).

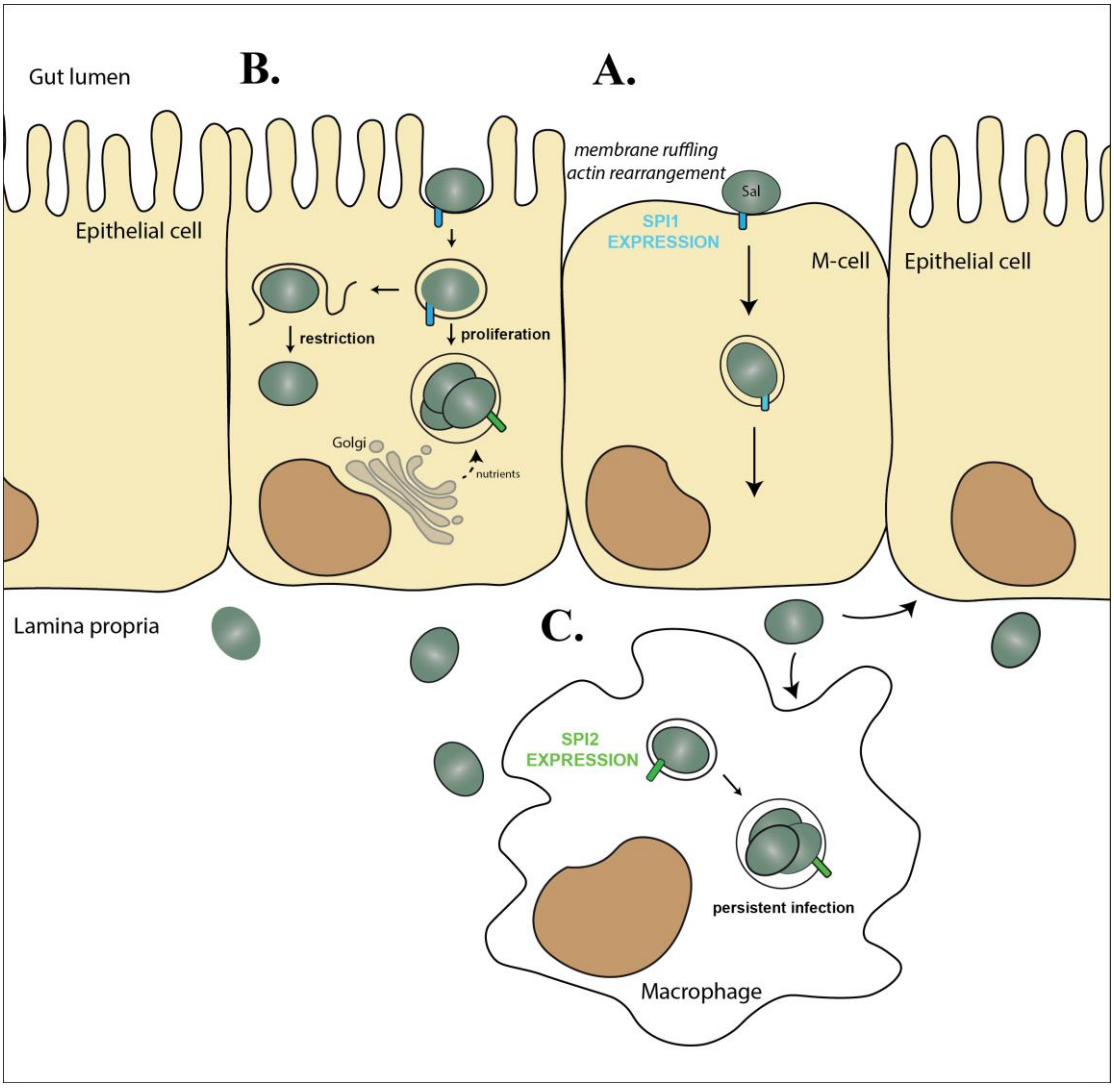

Figure 8: Life cycle of *Salmonella* Typhimurium

(A) *S.*Typhimurium preferentially infect microfold cells (M-cells), which undergo membrane ruffling and actin rearrangement in a SPI1-dependent fashion. *S.*Typhimurium can migrate through the M-cells to reach their basolateral membrane and infect neighbouring epithelial cells. (B) However, epithelial cells are also directly infected at their apical membrane in a SPI1-dependent fashion. *S.*Typhimurium typically reside in vacuoles (SCVs) that become localised in proximity to the Golgi for sourcing nutrients and express SPI2 effectors for maturation. In approximately 10% of the cases, *S.*Typhimurium enter the cytosol where they either proliferate or are restricted by cell-autonomous immune defences. (C) *S.*Typhimurium

also infect macrophages in the lamina propia facilitating bacterial spread and systemic infection. Survival and proliferation in macrophages require SPI2-secreted effectors.

Parasites have evolved various strategies to invade host cells (Sibley, 2004) and establish their replicative niche. In contrast to *S*.Typhimurium entry mechanism, *T.gondii* actively enter host cells relying on the parasite's own cytoskeleton, actomyosin system and calcium-dependent secretory pathway to create a parasitophorous vacuole (Clough & Frickel, 2017).

T.gondii use a unique mode of motility referred to as gliding (Heintzelman, 2015), which is a substrate-dependent locomotion mechanism to penetrate target cells (Sibley, 2004). In order to form the parasitophorous vacuole (PV), which is derived from the host cell membrane but excludes many host proteins (Charron & Sibley, 2004), the parasite membrane enters in contact with the cell membrane and establishes a moving junction (Mordue et al., 1999; Besteiro et al., 2011). The highly regulated secretion of microneme, dense granule proteins and rhoptries, plays a critical role in substrate attachment, host cell invasion and the establishment of the PV. These effector proteins are secreted in a timely fashion at the apical (anterior) tip of the parasite (Carruthers, 1999). *T.gondii* compartimentalises its secretory proteins according to their function.

Microneme proteins include adhesins (e.g. TgMIC2) and escorters (e.g. TgMIC6), are involved in trafficking and storage of ligands (MICs) to be coupled to the gliding motility and host-cell invasion steps (Soldati et al., 2001).

Rhoptry proteins appear to facilitate PV formation and association to host organelles (**Fig.9A**) such as mitochondria, the endoplasmic reticulum or the Golgi (Jones & Hirsch, 1972). The parasitophorous vacuole is also surrounded by host microtubules (Melo et al., 2001) and vimentin-type intermediate filaments (Halonen & Weidner, 1994), structures in close proximity of the host cell nucleus (Boyle & Radke, 2009).

Dense granule proteins may promote intracellular replication by transporting and processing nutrients from the host cell. The Golgi (**Fig.9A**) provides a source of sterols that are taken up by the parasites and used particularly for replication (Boyle & Radke, 2009; Sonda et al., 2001; Yoshifumi et al., 2011). At the tachyzoite stage in

intermediate host cells, *T.gondii* undergo asexual cell division and formation of many parasites (Radke et al., 2001) within the vacuole, is more likely to occur (**Fig.9B**).

The establishment of the PV (**Fig.9A**) is critical for *T.gondii* survival by avoiding both phagocytic engulfment upon entry (Coppens, 2017) and lysosomal destruction, because the PV is rendered nonfusogenic with the host endolysosomal system (Clough & Frickel, 2017).

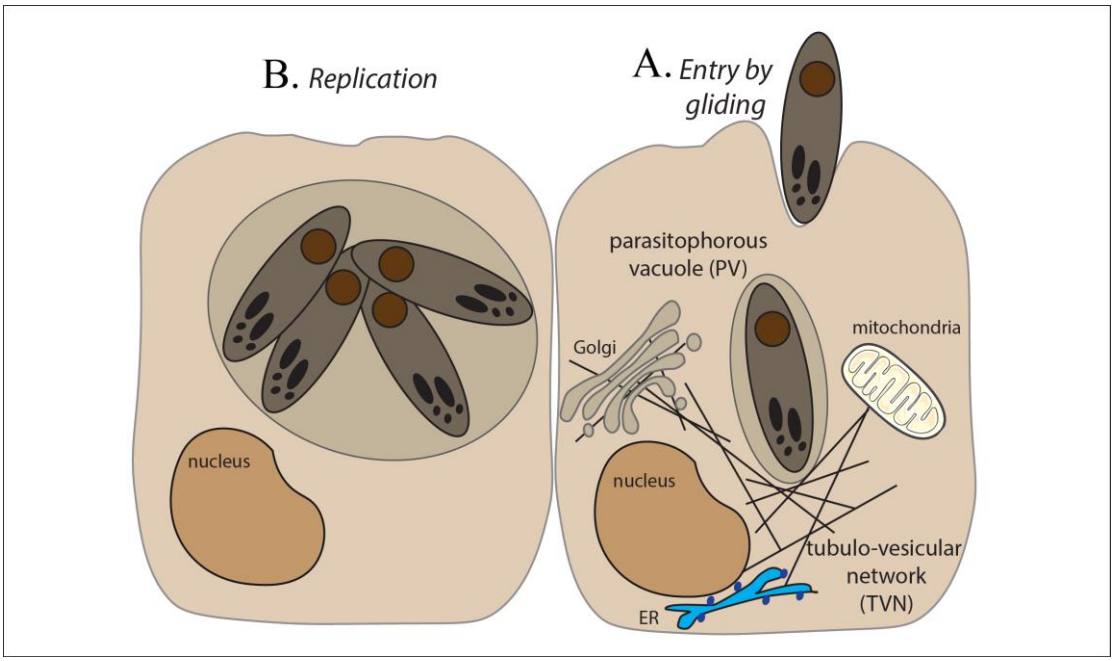

Figure 9: Life cycle of *Toxoplasma gondii*

(A) *T.gondii* infect cells via an active mechanism called gliding that requires effectors and segregation of host membrane proteins out of the forming vacuole. The parasitophorous vacuole containing living parasites interacts with several host organelles (mitochondria, ER, Golgi) for its survival and replication. (B) Asexual replication of *T.gondii* takes place within the vacuoles.

Although cellular entry mechanisms differ between *S.*Typhimurium and *T.gondii* infections, both pathogens establish a vacuole within the host cytosol. In both cases, the formation of this protective environment and its maturation to avoid lysosomal fusion and promote pathogen replication is highly regulated by pathogenic effector proteins. Host organelles, such as the Golgi, are used by the pathogens as a source of nutrients for example.

1.2.3 Host cell-autonomous immunity directed against *S.*Typhimurium and *T.gondii*

Cytosolic *S.*Typhimurium can be targeted by potent intrinsic immune mechanisms, which restrict bacterial proliferation and growth (Birmingham et al., 2006); this makes *S.*Typhimurium a valuable model organism. Cell-autonomous defence mechanisms directed against pathogens have been mostly studied in the case of viral infections, to a smaller extent with bacteria and this thesis (**Chapter 3**) investigates whether similar pathways apply in the case of parasite (e.g. with *Toxoplasma gondii*) infection.

*S.*Typhimurium enter the cell via bacterial-mediated phagocytosis (**Fig.8**) and invade host cells, residing in a SCV. In some instances, the rupture of the SCV enable *S.*Typhimurium to enter the cytosol. Multiple detection mechanisms are present in the cell to counteract infection. For example, autophagy (see paragraph **1.1.2.1** "Autophagy") is mediated by the recruitment of LC3 proteins. After the rupture of the SCV, cytosolic Galectin-8 (GAL8) detects the exposed glycans from the broken vacuole membrane, recruits NDP52, which binds LC3C (**Fig.10.1**), and thereby targets the damaged membrane and associated bacterial cargo to autophagy (Ravenhill et al., 2019; Thurston et al., 2012). Cytosolic bacteria also get ubiquitylated and the ubiquitin deposited on *S.*Typhimurium is detected by NDP52, p62, and Optineurin (**Fig.10.2**). The three autophagy adaptors bind LC3 on the autophagosome to target their ubiquitylated cargo (the bacteria) to autophagy (von Muhlinen et al., 2012; Wild et al., 2011; Zheng et al., 2009). The M1-linkage type specifically synthesised by LUBAC (**Fig.10.3**) is recognised by Optn and also leads to autophagy (Noad et al., 2017).

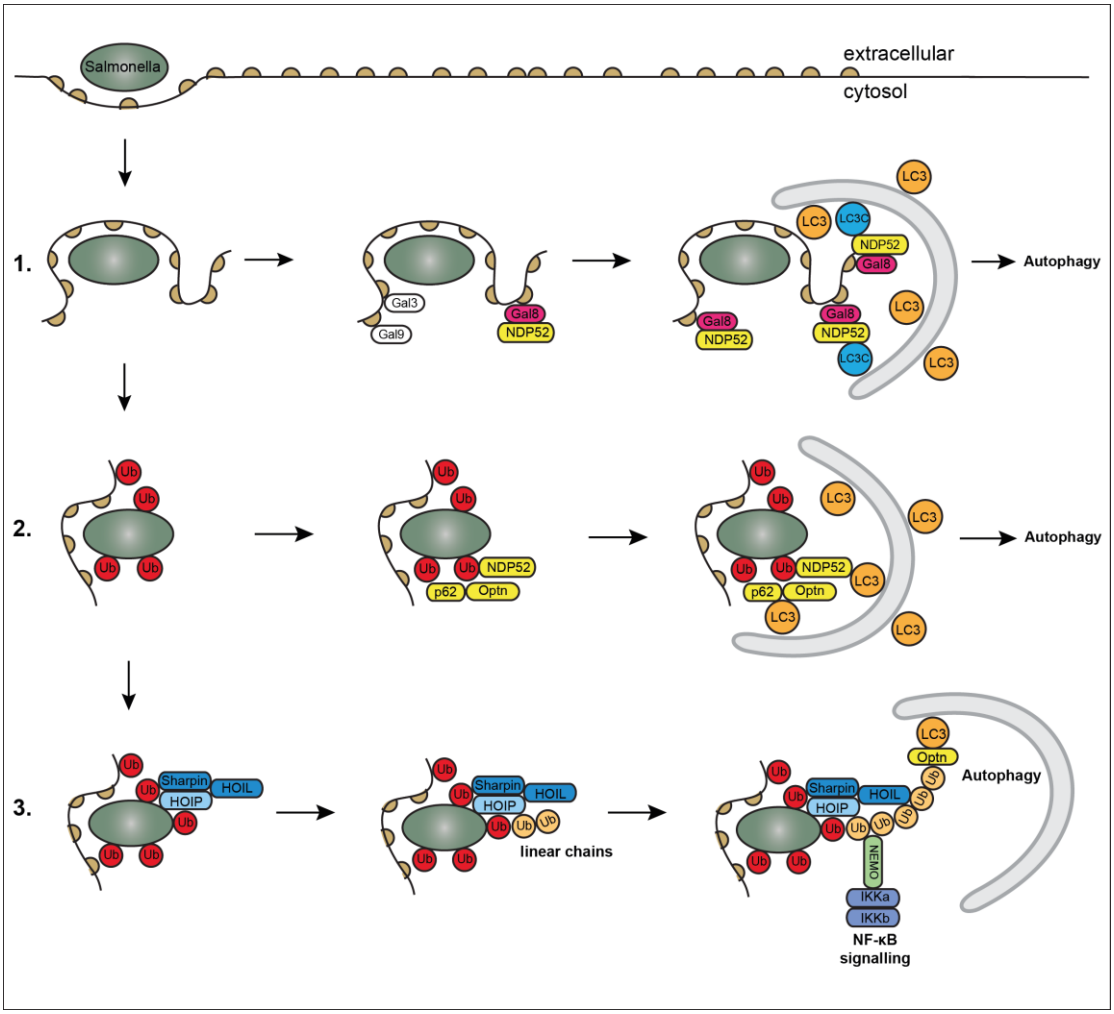

Figure 10: Antibacterial pathways targeting intracellular *Salmonella* Typhimurium

*S.*Typhimurium enter cells in a SPI1-dependent phagocytosis and reside in vacuoles. (1) Galectin-3, -8 and -9 detect glycans exposed on the damaged membrane of the SCV. Galectin-8 recruits NDP52, which interacts specifically with LC3C conjugated to the autophagosomal membrane, targeting the damaged membrane and associated bacterial cargo to autophagy. (2) Ubiquitin deposited on cytosolic *S.*Typhimurium is detected by NDP52, p62 and Optineurin. The three autophagy adaptors bind LC3 on the autophagosome to target their ubiquitylated cargo to autophagy. (3) Ubiquitin deposited on cytosolic *S.*Typhimurium is bound by LUBAC, which synthesises linear ubiquitin chains recruiting the cargo receptor Optn and via interaction with LC3 target the bacteria for autophagy. Alternatively, M1-Ub chains recruit NEMO and trigger the NF-κB signalling.

Despite the multiple strategies by which host cells attempt to contain and clear bacterial infection, a minor fraction of cytosolic *S.*Typhimurium escape autophagy and can replicate extensively. Infected cells also detect the presence of Gram-negative bacteria via lipopolysaccharides (LPS) present on their outer membrane. Gram-

negative bacteria constitutively produce outer-membrane vesicles (OMVs), small spherical bilayered nanostructures (**Fig.11.1**) that reflect the composition of the parental cell membrane and the periplasm (Rüter et al., 2018; Yoon, 2016) and therefore carry LPS, a major constituent of the bacterial outer membrane (Whitfield & Trent, 2014). OMVs are involved in intra- and inter-species communication as well as regulation of inflammation. They act as a delivery system either by direct contact or at a distance (Yoon, 2016) and provide a protected environment for the transport even of hydrophobic components to their target (Bonnington & Kuehn, 2014). OMVs can be taken up into host epithelial cells via clathrin-mediated endocytosis and LPS becomes exposed in the cytosol (Vanaja et al., 2016) likely upon early endosome membrane rupture (**Fig.11.1**), even though the exact mechanism is unknown (Broz, 2016) and consequently activates the non-canonical inflammasome. In the case of uptake of living *S.*Typhimurium (**Fig.11.4**) within the host cell, the SCV may break open and release the bacteria and their associated LPS in the cytosol (Finethy et al., 2017). There is also increasing evidence suggesting that IFN-γ-induced guanylate-binding proteins (GBPs) participate in the lysis of the vacuole (Meunier et al., 2014), control intracellular detection of LPS (Santos et al., 2018) and promote LPS-mediated activation of the non-canonical inflammasome (Pilla et al., 2014) (**Fig.11.4**).

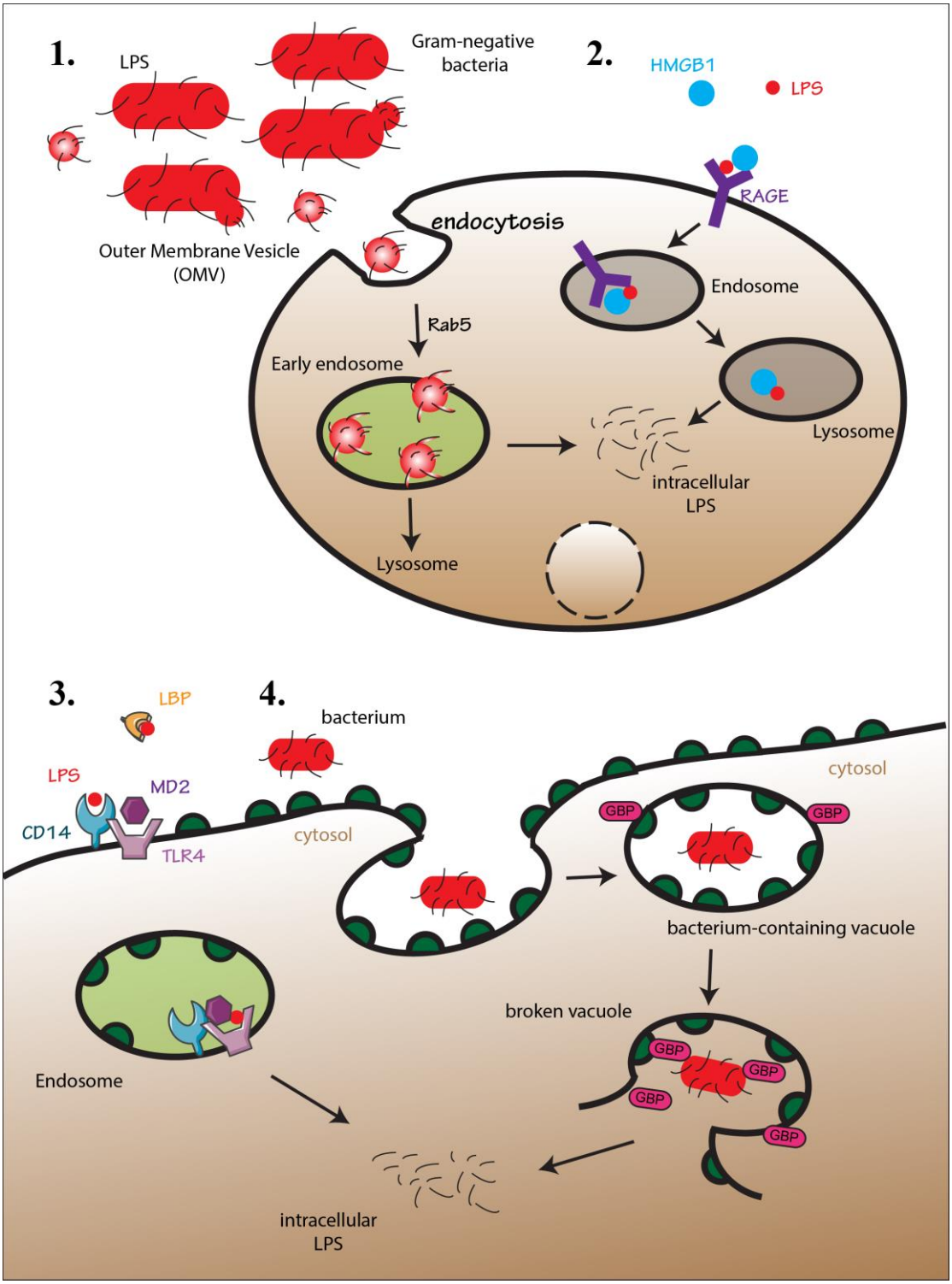

Figure 11: Infection with Gram-negative bacteria results in LPS becoming cytosolic

LPS can access the cytosolic compartment through different mechanisms. (1) Gram-negative bacteria produce outer-membrane vesicles (OMVs) in the extracellular environment and these OMVs can be endocytosed. Free extracellular LPS molecules can either (2) bind to HMGB1, followed by the complex interacting with RAGE or be delivered to CD14 by LBP, promoting the recognition by the MD2-TLR4 complex. In both (2) and (3) the receptors are taken up into endosomes. LPS-containing endosomes (scenario 1, 2 or 3) may release LPS in the cytosol, most likely before fusion with lysosomes and degradation. (4) Gram-negative bacteria also

enter cells and reside in vacuoles, which occasionally break open, exposing the LPS to the cytosol and to GBPs for example.

Extracellular LPS can be internalised following two distinct pathways (**Fig.11.2** and **11.3**). The alarmin HMGB1 released by hepatocytes binds to LPS and triggers its uptake by macrophages via the receptor RAGE (Deng et al., 2018). The complex LPS-HMGB1 destabilises the endosomal membrane leading to the release of LPS in the cytosol (Rathinam et al., 2019) (**Fig.11.2**). Finally, extracellular LPS triggers immune response in a TLR4-dependent fashion (**Fig.11.3**). LPS-binding protein (LBP) is secreted by gastrointestinal tract epithelial cells and its expression is induced upon infection to act as an acute phase serum glycoprotein (Hansen et al., 2009; Vreugdenhil et al., 2000). LBP binds LPS micelles and has the ability to remove LPS molecules from either OMVs or the bacterial surface (Miyake et al., 2006; Steimle et al., 2016). LBP transfers individual LPS molecules to soluble or GPI-anchored CD14 and/or directly to MD2. Both LBP and CD14 act as catalysts for the transfer of LPS to the heterodimeric complex MD2-TLR4 (Fenton & Golenbock, 1998; Ryu et al., 2017; Tsukamoto et al., 2018). Upon delivery of LPS to MD2, two MD2/TLR4 dimers oligomerise to form the active signalling complex. The CD14-LPS-MD2/TLR4 complex is then internalised (Zanoni et al., 2011) and potentially leads to cytosolic release of LPS (**Fig.11.3**). The downstream, LPS-triggered, TLR4-mediated responses may vary between cell types: e.g. induction of cytokine production in intestinal epithelial cells or promotion of T cell adhesion to prevent chemotaxis. LBP also induces NF-κB signalling and cytokine production by enhancing TRIF-TRAF6 association, and inflammatory response by stimulating ERK and p38 MAPK phosphorylation (Kagan & Medzhitov, 2006; Tsukamoto et al., 2018; Yamamoto et al., 2003).

T.gondii are protected in vacuoles which, although they do not display many host proteins to be recognised by the host cell, can still be targeted and initiate host defence mechanisms. TLR signalling pathways provide the first line of defence against pathogens. The TLR adaptor molecule MyD88 (Scanga et al., 2002)

association with TLR11 (Yarovinsky et al., 2005) was shown to be critical for the production of IL-12 following *T.gondii* infection in mouse dendritic cells. Moreover, TLR7 and TLR9 can sense RNA and DNA, respectively, from *T.gondii* in mice (Andrade et al., 2013). Overall, *T.gondii* infection induces the production of many cytokines such as IL-12, IL-6, IL-1, TNF-α (Deckert-Schlüter et al., 1995), resulting in activation of NK and T cells, as well as the subsequent release of IFN-γ (Gazzinelli et al., 1993). Activated human cytotoxic T cells release granulysin to destroy the PVM and pore-forming perforins that allow secretion of granzymes leading to the activation of caspases in infected cells (Krishnamurthy et al., 2017). Additionally, the production of chemokines leads to the migration of neutrophils and monocytes to the location of infection (Biswas et al., 2015).

In addition to eliciting signalling pathways, parasitophorous vacuoles of *T.gondii* also recruit autophagy-related proteins. The TNF-α-dependent conjugation of LC3 enables restriction of *T.gondii* infection *in vitro* and *in vivo* (Choi et al., 2014) and fusion of the PV with lysosomes (Krishnamurthy et al., 2017). The autophagy cargo receptor p62 is also recruited to *T.gondii* by K48-Ub chains. P62 partially participates in TRAF6 and TRIM21 recruitment and is required for the delivery of GBPs to the PV (Haldar et al., 2015; Saeij & Frickel, 2017), promoting host survival (Foltz et al., 2017).

In IFN-γ treated cells, ubiquitylated PVs are engulfed in LC3-decorated bilayered vacuoles (Selleck et al., 2015). IFN-γ-primed MEF cells require IRG proteins and the E3 ligase TRAF6 for the ubiquitylation of the *T.gondii* PVM. In addition, IFN-γ promotes restriction of *T.gondii* replication (Haldar et al., 2015). IRG proteins can directly lyse the PV thereby exposing the parasites into the cytosol to autophagy-mediated clearance (Ling et al., 2006). In human cells, the IFN-γ-dependent K63-linked ubiquitylation results in endo-lysosomal fusion of the PV and impaired *T.gondii* replication (Clough et al., 2016). Furthermore, the IFN-γ- and GBP1-dependent PV lysis in THP-1 cells (**Fig.12.B**) results in loss of integrity of the PVM and potential killing of the pathogen or even cell death (Fisch et al., 2019a; 2019b).

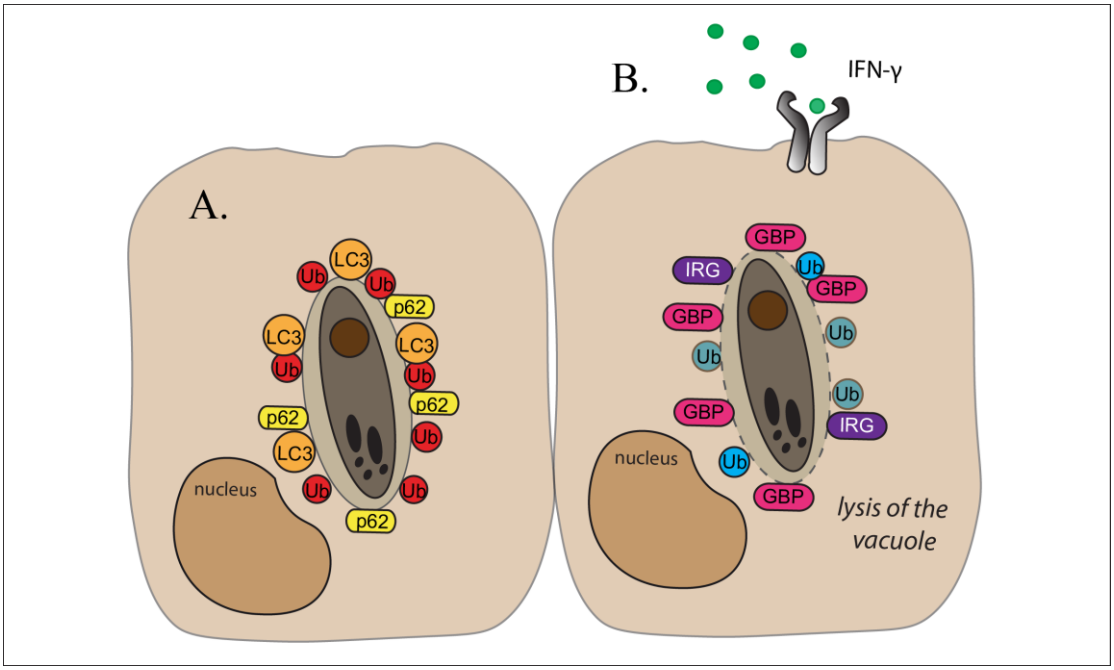

Figure 12: Host immune proteins target *Toxoplasma gondii*

(A) The parasitophorous vacuole can be ubiquitylated and recruits the autophagy cargo receptor p62, as well as LC3 proteins. (B) In IFN-γ primed cells, the vacuole is targeted by GBPs and IRGs, promoting its lysis.

During either *S.*Typhimurium or *T.gondii* infections, host cells trigger multiple processes to restrict proliferation and clear the pathogens. Initially, the pathogenic threat is detected: TLR signalling pathways are activated to promote cytokine production. The TLR4/MD-2 dimer detects the presence of bacterial LPS, whereas *T.gondii* is sensed by TLR11/MyD88 system. Both the SCV and the PVM are targeted by autophagy-related proteins and recruit LC3 proteins and cargo receptors. In both types of infection, the vacuole can be ruptured to expose the pathogen to the host cell cytosol, where additional detection processes and clearance mechanisms take place – e.g. ubiquitylation. Vacuole lysis seems mostly driven by IFN-γ-induced GBPs. IFN-γ, NF-κB and TNF-α signalling pathways are critical to promote microbicidal mechanisms and cytokine production for the recruitment of professional immune cells and activation of adaptive immunity.

Many human immune defence mechanisms against infections can be modelled and studied in mice. However, some drastic interspecies differences can be noticed. For

example, humans cope with *T.gondii* infections and most people are asymptomatic whereas the parasite makes mice lose fear of cats to reach their definitive host.

1.2.4 Microbial effectors for a successful host invasion

Most pathogens secrete effectors not only to enter the host cell but also to subvert host cell mechanisms and to inhibit cell defence mechanisms. This section presents strategies employed by *S.*Typhimurium and *T.gondii* to establish infection.

*S.*Typhimurium do not possess genes that encode for ubiquitin. Nevertheless, they have E3 ligase-like effectors that hijack the host's ubiquitylation machinery to their own advantage. This modulates inflammatory signalling, suggesting that inflammation is an important component of both bacterial pathogenesis and antibacterial immunity. For example, the *S.*Typhimurium effector SopA, a HECT-like E3 ligase (**Fig.2**), modulates host inflammation (Zhang et al., 2006) by ubiquitylating TRIM56 and TRIM65, two host E3 ligases involved in the production of the pro-inflammatory cytokine IFNβ (Fiskin et al., 2017; Kamanova et al., 2016). *S.*Typhimurium also produces novel E3 ligases (NEL), such as SspH1 or SspH2 (Quezada et al., 2009). Their catalytic activity is achieved by a single conserved cysteine residue that is essential for the formation of a HECT-like ubiquitin-E3 intermediate; this is also the case with the *Shigella flexneri* effector IpaH9.8, the SspH1 homolog (Rohde et al., 2007; Singer et al., 2008; Zhu et al., 2008). SspH1 seems to reduce inflammation by inhibiting NF-κB-induced genes, whereas SspH2 activates inflammation via NOD-1 signalling (Bhavsar et al., 2013; Haraga & Miller, 2006). Bacterial pathogenesis is possible by both promoting and dampening pro-inflammatory responses in order to both antagonise and benefit bacterial growth, thereby sparing or hijacking the host. Another effector, SipB, adds to the inflammatory state by activating Caspase-1, thereby inducing production of pro-inflammatory cytokines IL-1β and IL-18 (Hersh et al., 1999).

*S.*Typhimurium pathogenicity islands (SPI) encode needle-like structures that penetrate the cellular membrane and secrete bacterial effector molecules into the host (Kubori et al., 1998), some of which are essential for vacuolar uptake and maturation.

Release of SopB in the cytosol, for example, recruits the Ras-related protein RAB5 that promotes fusion of early endosomes to the SCV (Mallo et al., 2008). Other proteins ensure that SCV maturation down the endolysosomal pathway is stalled (Garcia-Del Portillo & Finlay, 1995; Méresse et al., 1999), to prevent fusion with lysosomes and bacterial degradation (Goren, 1977).

T.gondii also release effectors to build the vacuole and hijack pathways in the host cell. Despite sharing a common organisation and structure, numerous strains of *T.gondii* have been identified and classified into three clonal lineages: type I (e.g. RH or GT-1), type II (e.g PRU of ME-49), and type III (e.g CEP or VEG). They differ genetically by no more than 1% but show substantial differences in terms of virulence – growth rate, migration ability – and variations in their effectors repertoires, which lead to various changes in the host's metabolism as a strategy for *T.gondii* to survive, spread, and/or kill the host cell (Saeij et al., 2005).

Regardless of the strain, *T.gondii* discharge micronemal proteins, such as dense granule proteins (GRAs) and rhoptry proteins (ROPs) from apical secretory organelles in the host cytoplasm. The micronemal proteins play a major role in stimulating immunity (Scorza et al., 2003; Weilhammer & Rasley, 2011) and therefore are considered as vaccine therapies (Rezaei et al., 2019). ROP17, ROP5, and GRA3 (for example), were shown to be implicated in virulence differences in murine infection (Jones et al., 2017). Type I and type III *T.gondii* strains produce ROP16, which can phosphorylate STAT-3 (Yamamoto et al., 2009) and STAT-6 (Ong et al., 2010), thereby inducing IL-4 and IL-6 production, which results in IL-12 inhibition. ROP16 is not the only means by which *T.gondii* avoid host immune defence: infection disrupts IFN-γ signalling via blockade of Stat-1 (Kim et al., 2007) and also prevents cell death in order to preserve the replicative and nutrient-rich environment for the parasite (Hippe et al., 2009).

Aims

This thesis describes a project directed towards the investigation of the molecular basis of cell-autonomous immune response to infection by pathogenic microorganisms and using genetic screens to identify some of the proteins involved. Specifically, the research focuses on the function of interferon gamma (IFN-γ) in mediating the cell-autonomous immune response to two major human pathogens, namely *Salmonella enterica* serovar Typhimurium and *Toxoplasma gondii*.

IFN-γ is a cytokine that regulates multiple signalling pathways for both the innate and the adaptive immune responses and that modulates many genes involved in anti-pathogenic mechanisms. IFN-γ is required for the restriction of *T.gondii* growth and in antibacterial processes, such as upregulation of inflammasome proteins and inflammatory caspases. This project investigates the IFN-γ-induced protein recruitment on *T.gondii* by studying the nature and the function of this recruitment. This thesis also intends to unravel the IFN-γ-dependent cell death mechanism that occurs in the presence of cytosolic *S.*Typhimurium LPS in human cells. The CRISPR-Cas9 technology was employed to this end and is discussed in detail below.

The specific aims of this research project are to:

1. Identify IFN-γ-induced genes required for cell death in response to cytosolic lipopolysaccharide (LPS) using a whole genome CRISPR screen in human HeLa cells.
2. Investigate the recruitment and role of the LUBAC complex and autophagy cargo receptors during *Toxoplasma gondii* infection in IFN-γ-stimulated mouse embryonic fibroblasts.

The results of these two aims are covered in Chapters 2 and 3 respectively. Chapter 4 contains the experimental methodology.

Chapter 2: A genome-wide screen to identify IFN-γ induced genes required for cell death in response to cytosolic LPS

2.1 Introduction

This introductory section presents some background on how an immune response to LPS occurs in both mice and humans and discusses the role of IFN-γ in that response mechanism. This is important because this chapter details a new methodology to investigate the cell death pathway triggered by cytosolic LPS in IFN-γ primed human cells.

2.1.1 Immune responses to cytosolic lipopolysaccharide (LPS)

Cytosolic LPS is recognised by murine caspase-11 and human Caspase-4 and, to a lesser extent by Caspase-5 (Shi et al., 2014). Human Caspase-4 is expressed constitutively (Shi et al., 2014) whereas in most murine cells caspase-11 is induced by proinflammatory signals (Russo et al., 2018); the promoter region of the caspase-11 gene contains NF-κB and STAT1 binding sites (Schauvliege et al., 2002). Depending on whether the species is mouse or human, there are also some differences in terms of binding and cell death activation: for example, CASP4 can bind tetra-acylated LPS, whereas Casp11 cannot (Lagrange et al., 2018). The caspase-11-activating form of LPS is the hexa- or penta-acylated Lipid A (Hagar et al., 2013).

Both Casp11 and CASP4 mediate cell death following transfection or electroporation of LPS, whereas CASP5 only plays a role in infection itself (Shi et al., 2014). Binding of caspases (-11 or -4) to LPS activates the non-canonical inflammasome resulting in cell death by pyroptosis (Kayagaki et al., 2015). Caspases are activated by auto-proteolysis in an induced-proximity model (Salvesen & Dixit, 1999). Oligomerised and active caspases process their target substrates, such as GSDMD leading to pyroptotic cell death.

Casp11 was shown to protect mice against infection but is also responsible with GSDMD for LPS-induced endotoxic shock (Hagar et al., 2013). Both Casp11 and GSDMD are required, respectively for the non-canonical activation of the NLRP3 inflammasome (Kayagaki et al., 2011), and the secretion of mature IL-1β and IL-18 following Caspase-1-mediated cleavage of their pro-IL forms.

2.1.2 The role of IFN-γ

Cell death was observed when murine bone marrow derived macrophages (BMDMs), or human THP-1 or HeLa cells, were incubated with outer membrane vesicles (OMVs) from *E.coli*. OMVs act as LPS transporters from the extracellular compartment to the cytosol (Vanaja et al., 2016). Pyroptosis is triggered by free cytosolic LPS in human and murine macrophages and non-monocytic cells. It seems that IFN-γ potentiates the inflammatory immune response to infection, and somewhat to LPS transfection, at least in macrophages (Shi et al., 2014; Yang et al., 2015).

When human monocyte cell lines such as U937 and THP-1 were electroporated with *E.coli* LPS, cell viability was significantly reduced when compared to non-treated cells or to cells electroporated with bacterial cell wall fragment muramyl dipeptide (MDP). This LPS-triggered cell death was also observed in other human cell lines such as HaCaT or HL60. It was also noticed that priming with IFN-γ in mouse macrophages enhanced cell death upon LPS electroporation (Shi et al., 2014).

Electroporation provides an artificial means of introducing LPS directly into the cytosol. In a more physiological situation, LPS can be exposed in the cytosol following infection with Gram-negative bacteria. LPS is indeed a major component of Gram-negative bacteria's outer membrane. For example, *S.*Typhimurium enter the host cells triggering their own phagocytosis, residing in *Salmonella*-containing vacuoles (SCV), which in some instances break open exposing the bacteria to the cytosol, exhibiting their outer membrane and hence their LPS.
It is not known whether infection with living bacteria lead to activation of the non-canonical inflammasome and eventually to pyroptotic cell death.

It is worth further investigating the requirement of IFN-γ in triggering cell death in the case of either LPS transfection or infection with living *S.*Typhimurium. This chapter will address the role of IFN-γ in the LPS-triggered cell death pathway as it might have been previously overlooked.

2.2 Results: A novel role for IFN-γ in LPS-triggered cell death

This section covers preliminary experiments that led to investigate in more details the IFN-γ-dependent, LPS-triggered cell death pathway in human HeLa cells. Observations and conclusions drawn from these experiments pointed out the incomplete understanding and knowledge about this cell death mechanism.

2.2.1 Cytosolic LPS triggers cell death

This first paragraph focuses on the phenomenon which will become the subject of investigation for the entire chapter, namely LPS-triggered cell death in IFN-γ-primed cells. It shows that studying the impact of cytosolic LPS can be an appropriate model for *S.*Typhimurium infection.

2.2.1.1. *S.*Typhimurium triggers cell death in IFN-γ-primed HeLa cells

Infections with living *S.*Typhimurium rarely leads to cell death because *S.*Typhimurium-triggered cell death requires both IFN-γ and for the *S.*Typhimurium to be cytosolic.

To test whether priming with IFN-γ enhances cell death, HeLa cells were transfected with LPS and bacterial lysate – both from *S.* Typhimurium – or infected with the bacteria (**Fig.1A**). Propidium iodide (PI), a red, membrane-impermeable, DNA intercalating dye (fluorescent upon DNA binding) was used as a marker of cell death because it is only taken up by dead or dying cells. After 5h, the number of dead cells (those with PI-positive nuclei) was counted by microscopy. There was hardly any cell death produced by either bacterial infection or lysate and LPS transfections. However,

in cells primed with IFN-γ overnight, cell death reached 12%, when infected with living *S.* Typhimurium, and 11% and 5% when transfected with lysate and LPS, respectively. Even though percentages of dead cells were lower when transfecting cells with lysate or LPS, it seemed that both *S.* Typhimurium lysate and LPS could reproduce (to a limited degree) the IFN-γ dependent cell death phenotype observed upon *S.* Typhimurium infection.

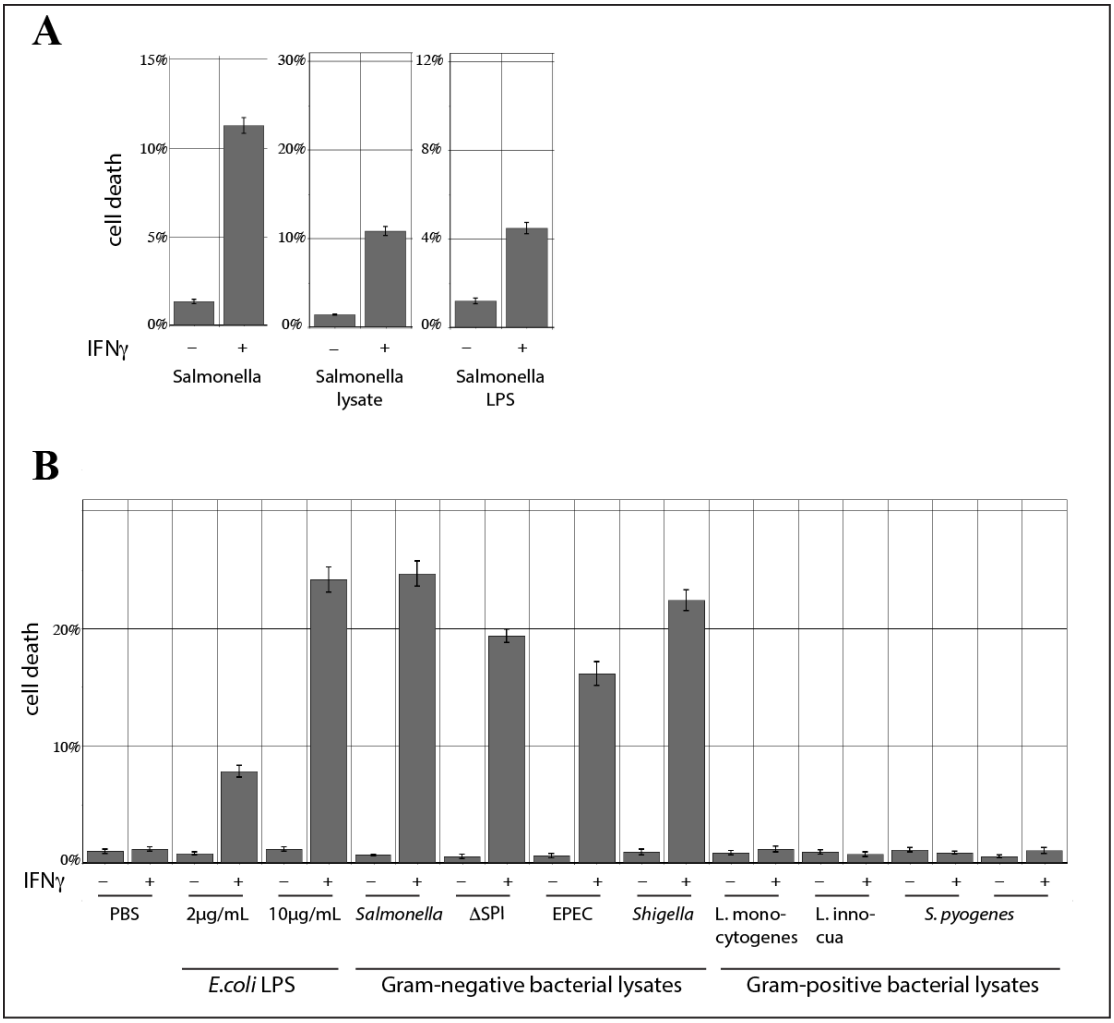

Figure 1: Treatment with *S.* Typhimurium, Gram-negative bacterial lysates or LPS lead to cell death in IFN-γ-primed HeLa cells

HeLa cells were (A) either infected with live *S.* Typhimurium or transfected with either *S.*Typhimurium LPS, or lysate or (B) transfected with commercial *E.coli* LPS, or bacterial lysates from different bacterial strains - including Gram-negative and Gram-positive bacteria. Cell death was measured by microscopy counting of PI-positive nuclei at 5h post-infection/transfection. Data are shown as Mean ± S.E.M of three coverslips and show cells primed overnight with IFN-γ (+) compared to cells grown in standard conditions (-). Experiments shown here were performed by Dr. Michal Wandel.

This experiment indicates that LPS alone could model *S.* Typhimurium infection when investigating the IFN-γ-induced cell death pathway, in contrast to earlier work showing that IFN-γ was not required for cell death upon *E.coli* LPS electroporation (Shi et al., 2014). Certainly, the work using *E.coli* LPS (Shi et al., 2014) employed electroporation (physical method), whereas in this experiment, *S.*Typhimurium lysate or LPS were transfected (requiring the use of chemicals like Lipofectamine). Because the bacterial strains (*E.coli* or *S.*Typhimurium) used were different, the question of bacterial species specificity is addressed in Section 2.2.1.2 with regards to triggering cell death in IFN-γ-primed HeLa cells.

2.2.1.2. Cell death following bacterial lysate transfection is specific to Gram-negative strains

The previous experiment used lysates and LPS from *S.* Typhimurium; however, the cell death phenotype had been reported for other bacterial species such as *E.coli* (Shi et al., 2014). The investigation was therefore extended to include a broader range of bacterial lysates to investigate whether this cell death pathway is specific to *S.*Typhimurium. To test the species specificity of this cell death phenotype, cells were transfected either with LPS from *E.coli* or with lysates from Gram-negative or Gram-positive bacteria (**Fig.1B**). These lysates originated from both invasive bacteria (e.g. *Shigella flexneri, Salmonella enterica,* Listeria monocytogenes, *Streptococcus pyogenes*) and non-invasive bacteria (e.g. ΔSPI *S.*Typhimurium, EPEC, Listeria innocua).

At 5h post-transfection, cells were stained with PI and cell death was assessed, by using microscopy to count the number of PI-positive nuclei (indicative of dead cells) within each sample. In the absence of IFN-γ priming, no cell death was observed (**Fig.1B**). However, when cells were treated overnight with IFN-γ, transfection with *E.coli* LPS or Gram-negative lysates led to a degree of cell death. A dose-response was observed with the two amounts of *E.coli* LPS used: increasing the LPS quantity by 5-fold (from 2μg/mL to 10μg/mL), led to a 3-fold increase (from 8% to 24%) in cell death. All lysates from Gram-negative bacteria showed a cell death phenotype with between 17% and 24% of PI-positive nuclei in cells primed overnight with IFN-

γ. By contrast, none of the cells transfected with lysates from Gram-positive bacterial strains died, even following IFN-γ treatment.

In summary, with either LPS or Gram-negative bacterial lysates, the cell response shows a pronounced cell death phenotype when primed with IFN-γ. However, Gram-positive bacterial lysates did not show a similar effect and cells appeared to be non-responsive to those strains, even when primed with IFN-γ. Because Gram-positive bacteria do not display any LPS on their membrane, this experiment confirms the hypothesis that the trigger is LPS itself, and also shows that IFN-γ priming is required for the cell death to occur.

2.2.1.3. The LPS O-antigen is not necessary to trigger cell death

It is possible that the length of the LPS chains present on bacteria was an important factor in triggering the cell death pathway. LPS is a polymer of sugars bound to Lipid A, and so the number or location of these sugar subunits could be important for recognition and initiation of the cell death pathway.

To explore this further, lysates of *S.*Typhimurium mutants that lacked a range of enzymes required for LPS biosynthesis (and hence expressing LPS of various lengths on their outer membrane) were tested (**Fig.2A**). The LPS chains were truncated in order to identify a minimal fragment sufficient to trigger cell death. HeLa cells were then transfected with the range of bacterial lysates containing different lengths of LPS using Lipofectamine2000.

At 5h post-transfection, cells were trypsinised and stained with propidium iodide. PI-negative cells were counted by flow cytometry to express the percentage of surviving cells after the treatment (**Fig.2B**). In comparison to the control cells (no transfection), commercial LPS and all the lysates triggered significant (p-value < 0.01) cell death when cells were primed with IFN-γ. LPS and lysate from wild-type bacteria resulted in 40% cell death, whereas transfection with the various lysates with LPS having truncated sugar chains led to higher cell death, averaging 60% (p-value < 0.05), when cells were primed with IFN-γ.

No major difference in the cell death was noticed as the LPS chain length decreased from ΔrfaL to ΔrfaF mutants (**Fig.2A**). This suggests that the region of the LPS required for recognition and for triggering the cell death signalling pathway lies within the shortest chain type: namely, that produced by the ΔrfaF mutant strain. It has been shown previously that even Lipid A itself (Kayagaki et al., 2013) is sufficient to bind murine caspase-11 (homologous to human Caspases-4 and -5), which is thought to be the effector of cell death (Yi, 2017).

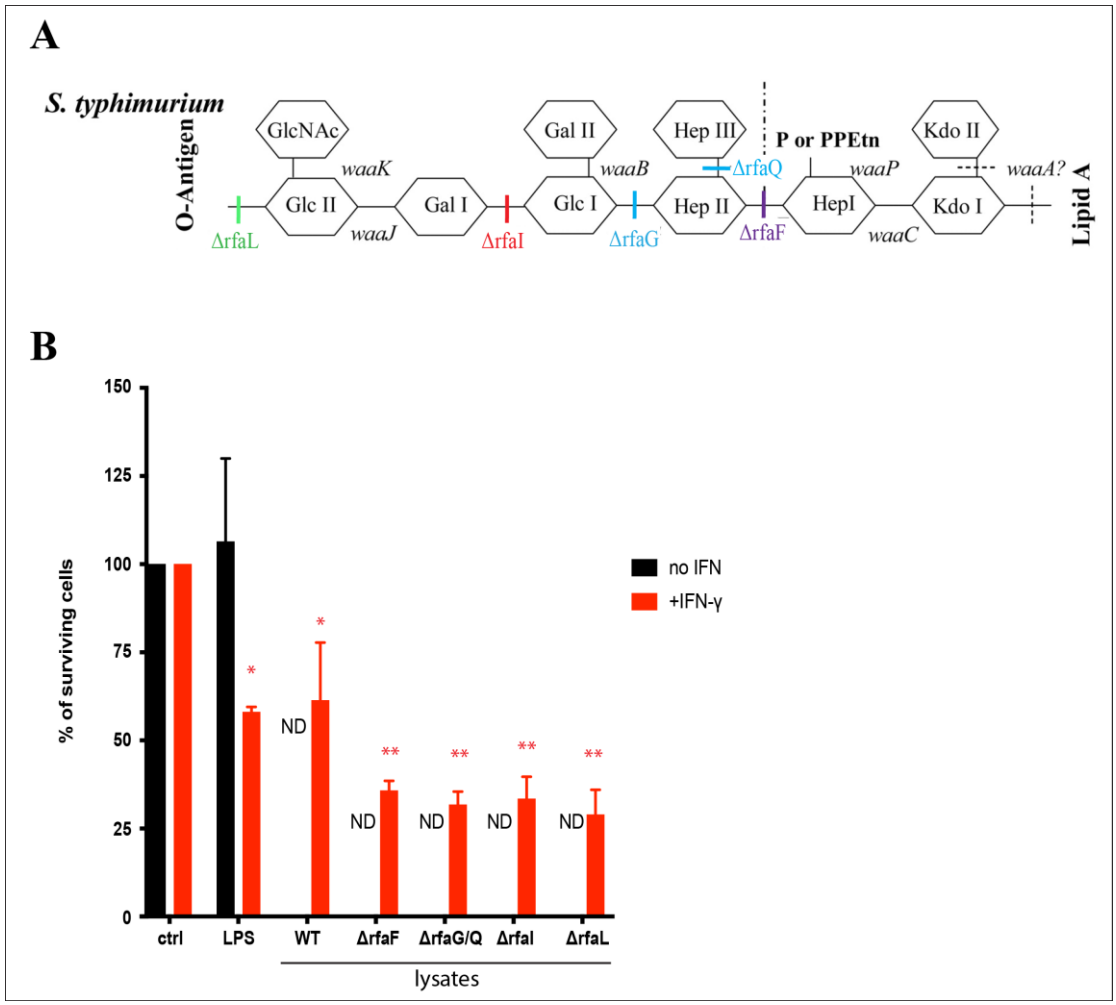

Figure 2: The O-antigen and most of the external sugars of LPS are not required to trigger cell death in IFN-γ-primed HeLa cells

(A) Mutant bacteria lacking the indicated enzymes produce LPS of different lengths, and their lysates were used to transfect HeLa cells. (B) The percentage of surviving cells was calculated based on the number of PI-negative cells detected by flow cytometry at 5h post-transfection. Data are shown as Mean ± S.E.M of two independent experiments each run in duplicates. *P<0.001, **P<0.0001, one-way ANOVA with Dunnett's multiple comparisons test comparing LPS and lysates to control (no infection), following IFN-γ priming. ND, non determined.

In summary, the O-antigen and most of the external sugars of the outer core do not appear to be necessary for IFN-γ-dependent, LPS-triggered, cell death in Hela cells. Instead Lipid A associated with the two keto-deoxyoctulosonate (Kdo) and one heptose (Hep) were sufficient to trigger cell death when transfected into HeLa cells primed with IFN-γ.

2.2.2 Further characterisation of the LPS-triggered cell death phenotype

This section collates additional background observations and exhibits key characteristics of the pathway, essential to understand the project. It emphasises the essential role of IFN-γ priming for the cell death to occur and explains the choice of HeLa cells as the study model.

2.2.2.1. Measuring LPS-triggered cell death

Two different methods were used to assess cell death in the wells. The first one relied on propidium iodide (PI) staining. PI is a DNA stain which binds to double-stranded DNA by intercalating between base pairs without sequence specificity. As it is membrane impermeable, it is normally excluded from viable cells. Counting the number of PI-negative cells in a given population allowed quantification of the percentage of surviving cells. However, this protocol required a lot of handling, pipetting and transfer of cells, which could lead to loss of cells and decreased accuracy in the results. Moreover, conditions were tested in a single 24-well in each experiment, not favouring reproducibility. Because of this lack of reproducibility, another method measuring the number of surviving cells was employed instead.

The second method used CellTiter Glo reagent (Promega), which generates a luminescence signal when reacting with adenosine triphosphate (ATP). The signal is linearly related (**Fig.3A**) to the level of ATP produced – an indicator of metabolically active cells – which allows the percentage of viable cells to be quantified. CellTiter Glo reagent reacts within a few seconds and the luminescence signal produced is

stable for at least 20 minutes. Each condition was performed in triplicate. **Figure 3B** shows the percentage of surviving cells when seeded at different densities and analysed at either 5h post-transfection or on the day following transfection (i.e. overnight). As expected, cell death was observed only in cells treated with both IFN-γ and LPS. Following cell priming with IFN-γ, LPS transfection resulted in 65% or 60% cell death with respectively $0.5x10^3$ or $1.0x10^3$ cells seeded in 96-well plates, when cells were analysed on the day after transfection and using the CellTiter Glo reagent. Result significance was assessed by calculating the p-value using ANOVA: CellTiter Glo detected significant (*$p<0.001$ and **$p<0.0001$) drops in cell survival when cells were primed with IFN-γ overnight and transfected with LPS on the next day.

For the highest cell densities assayed ($10x10^3$ in 96-well plate format), the cell survival increased significantly and LPS transfection was no longer efficient in triggering cell death, even in IFN-γ primed cells. When the concentration of cells in a well was high, the transfection efficiency was likely decreased; additionally, it is unlikely that the IFN-γ priming was homogenous, meaning that not all cells were equally targeted. Because both LPS and IFN-γ are necessary to cause cell death, either of these problems could result in higher cell survival.

Overall, the results obtained favoured the use of the CellTiter Glo reagent as an analysis method in order to obtain the most reproducible results (**Fig.3A**). Moreover, **figure 3B** shows that LPS-triggered cell death is cell density-dependent. For that reason, in future experiments $0.8\text{-}1.0x10^3$ cells were seeded in a 96-well plate and assays carried out in triplicate and analysed using CellTiter Glo.

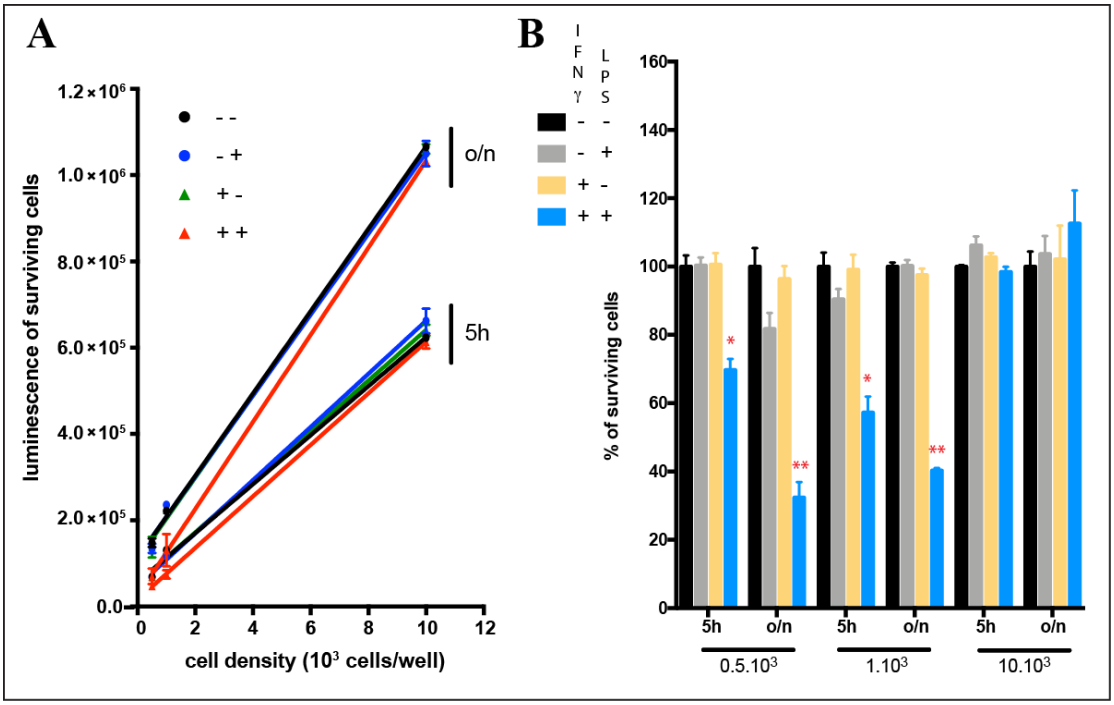

Figure 3: The luminescence signal generated by Cell Titer Glo varied linearly with the number of live cells

Cells were seeded at three different densities in a 96-well plate. Cells were ± primed with IFN-γ overnight followed by ± transfection with LPS the next day. After 5h, cells were either analysed (5h) directly with CellTiter Glo or grown overnight before analysis (o/n). (A) The luminescence signal was recorded for the different conditions and data from a representative experiment performed in triplicates are shown as Mean ± S.D. (B) The percentage of cells surviving after LPS transfection was calculated at 5h or overnight (o/n). Data from one representative experiment performed in triplicate are shown as Mean ± S.D. *P<0.001, **P<0.0001, one-way ANOVA with Dunnett's multiple comparisons test comparing + IFN-γ + LPS (blue) to + IFN-γ no LPS (yellow).

A likely reason for the better reproducibility of the data obtained using the CellTiter Glo reagent (Promega), when compared to using PI staining, is probably a result of the experimental protocol. CellTiter Glo data were acquired based on technical triplicates within one experiment, whereas PI staining was performed with a single sample for each condition. This difference is a result of the large amount of handling and pipetting required for PI staining followed by flow cytometry analysis, which makes reproducibility increasingly difficult as the number of conditions and samples increases. Since the CellTiter Glo kit involved fewer steps of washing and pipetting, and since it could also accommodate internal replicates, the results were more

reproducible. As a result, validation experiments following the screen, were carried out using the CellTiter Glo protocol.

Furthermore, the timing of the analysis impacts the measure of cell death. Using microscopy, at 5h post-transfection, only 5% of the cells transfected with *S.*Typhimurium LPS after overnight priming with IFN-γ and fixed and PI-stained were counted PI-positive (i.e. dead) (**Fig.1A**). By contrast, analysis with CellTiter Glo at 5h post-transfection showed 30% cell death (**Fig.3B**). This difference could be attributed to the timing of the analysis, as equilibrium might not have been reached at 5h post-transfection. It was additionally observed that, independent of the method used to analyse the samples, the percentage of surviving cells was always lower when cells were washed at 5h post-transfection but analysed on the next day (overnight) rather than directly after the 5h-transfection period. For example, when $0.5x10^3$ cells were seeded per well, primed with IFN-γ, transfected with LPS and analysed using CellTiter Glo: 70% of the cells were alive after 5h whereas only 35% survived overnight (**Fig.3B**).

In summary, cell death was highest if measured after overnight incubation and showed more substantial differences with the controls. In addition, the signals obtained with CellTiter Glo were linear with the number of cells seeded initially (**Fig.3A**) and the linearity of the signal was retained after either IFN-γ priming or LPS transfection. In all four experimental conditions and at both analysis time points (5h or overnight), the luminescence intensities were linearly proportional to the number of viable cells in the wells. Consequently, in all the following experiments, cells were washed, and the medium changed at 5h post-transfection with the analysis using CellTiter Glo performed on the following day.

2.2.2.2. Cell death is IFN-γ dependent

Although electroporation of *E.coli* LPS did not require priming with IFN-γ to elicit cell death in macrophages (Shi et al., 2014) in the system investigated in the present study, LPS was introduced into the cytosol by lipid-mediated chemical transfection for entry of LPS in HeLa cells. The role of IFN-γ was therefore addressed with this experimental design. In contrast to the results obtained by electroporation, IFN-γ-

priming was completely required in the case of either LPS transfection or bacterial infection (**Fig.1A**) to trigger cell death and it substantially enhanced cell death following lysates transfection (**Fig.2B**). In these experiments, HeLa cells were transfected with LPS after being primed overnight with IFN-γ (+ +) to ensure the requirement of both IFN-γ and cytosolic LPS for triggering cell death. As controls, cells were treated only with either Lipofectamine2000, either in the absence (- -) or presence (+ -) of IFN-γ priming, or with LPS (- +). The results demonstrate that the effect of LPS on cell survival in HeLa cells is indeed IFN-γ dependent (**Fig.4**). CellTiter Glo was used to assess cell survival after allowing cells to recover overnight after LPS-transfection. At 24h post-transfection, 50% cell death was recorded; by contrast, no cell death was observed in the presence of either IFN-γ alone or LPS alone (**Fig.4**). Only pre-treatment with IFN-γ elicited the LPS-induced cell death in HeLa cells and IFN-γ treatment on its own did not induce lethality (**Fig.4**). Moreover, LPS transfection did not produce a cell death phenotype in HeLa cells that were not primed with IFN-γ. Therefore, Lipofectamine was not the cause of mortality and it can be concluded that cell death was caused by the presence of cytosolic LPS in IFN-γ-primed cells.

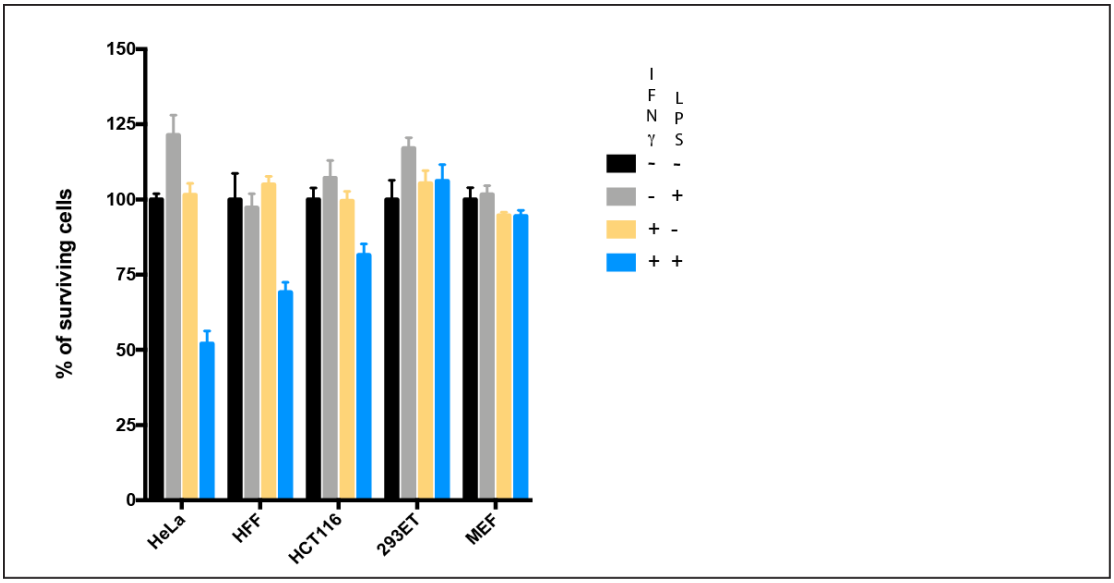

Figure 4: LPS-triggered cell death depends on both IFN-γ and cell line

Human (HeLa, HFF, HCT116, 293ET) and mouse (MEF) cells were seeded in 96-well plates in the presence or absence of IFN-γ (human or mouse, as appropriate for the cell line). Next day, half were transfected with LPS. On the following day, both transfected and non-transfected cells were analysed with CellTiter Glo. Data are shown as Mean ± S.D from a representative experiment run in triplicate for each condition.

2.2.2.3. Cell death occurs only in certain cell lines

Several human and one mouse cell lines were tested to explore whether the IFN-γ-induced, LPS-triggered cell death was indeed cell-type dependent. Infectious bacteria initially encounter skin and mucous, which constitute the first immune barrier against pathogenic threats in susceptible organisms; therefore, HeLa (human cervical cancer cell line), HFF (human foreskin fibroblasts), and HCT116 (human colon cancer cell line) were chosen because they are cell types that make up physical barriers against pathogens and are thus physiologically relevant. 293ET (human embryonic kidney cells) and MEF (mouse embryonic fibroblasts) were also added to the panel for testing to provide insights on tissue- and species-specificity, respectively.

All cells were seeded at similar densities and the same transfection conditions were used in each case. HCT116, HFF and HeLa cells showed an increasing response to LPS transfection with 20%, 30%, and 50% cell death respectively (**Fig.4**) when primed overnight with IFN-γ. However, no cell death was observed with 293ET and MEFs cells and there was no decrease in luminescence signal when cells were transfected with LPS, even after IFN-γ priming. It is important to note that the cultured cell lines originated from different initial stocks and could lose various pathways, including sensing of IFN-γ or LPS and/or certain cell death mechanisms. These differences might explain the observation that IFN-γ induced, LPS-triggered cell death is cell type dependent and that, within the cell lines tested, cell death occurred predominantly in HeLas. Consequently, all further experiments were performed using HeLa cells.

In conclusion, Shao (Shi et al., 2014; Yang et al., 2015) showed cell death upon electroporation of LPS. However, in the experimental system used in the present study, in which LPS was instead transfected using a lipid-based reagent, IFN-γ was required for cell death (thought to be pyroptosis). Electroporation most likely allows transfection of monomeric LPS molecules in the cytosolic compartment, whereas lipid-based transfection creates LPS agglomerates delivering LPS in the cytosol in a less accessible form for recognition and binding of partner proteins.

In addition, *S.*Typhimurium-triggered cell death in IFN-γ-primed cells could be recapitulated by transfecting either Gram-negative bacterial lysates or purified LPS. It was also observed that different cell lines behaved differently in response to cytosolic LPS: IFN-γ-primed 293ET and MEF cells were found to be resistant whereas IFN-γ-primed HCT116, HFF or HeLa exhibited increased cell death following LPS transfection. These results indicate that additional experiments are needed to unravel the mechanism of cell death following the cytosolic presence of LPS. Experiments described in Section 2.2.3 already give an indication on the role of Caspase-4 in the pathway, and Section 2.3 details a genome-wide genetic screening method employed to more completely investigate the LPS-triggered cell death pathway in IFN-γ-primed HeLa cells.

2.2.2.4. LPS-triggered cell death occurs at similar levels in population and clones

As shown earlier, different cell lines respond differently to LPS-transfection when primed with IFN-γ. HeLa cells were chosen because they exhibited most cell death, likely because they are the most sensitive to factors provoking cell death among all the cell lines tested. It was, however, thought prudent to check whether the lab stock of HeLa cells would behave differently than a clonal population that had been derived from a single cell. This was because even maximising the number of cells dying upon the combined treatment of IFN-γ and LPS transfection by optimising cell density, together with the amount of Lipofectamine2000 and LPS added to the well, was still not sufficient to get 100% cell death. This indicated that there was always at least 20% of HeLa cells surviving the treatment.

To investigate whether there was a genetic reason for this resistant population, cells derived from a single HeLa clone were tested (**Fig.5**). HeLa cells are indeed known to bear several copies of particular chromosomes and are polyploid rather than diploid. As a population, HeLa cells are genetically somewhat diverse and individual cells can contain several copies of genes. For that reason, it was thought that it might be more prudent to use a clonal population of cells with the aim of having a more homogenous

IFN-γ induced response to LPS transfection and, more importantly, a cell death greater than 80%.

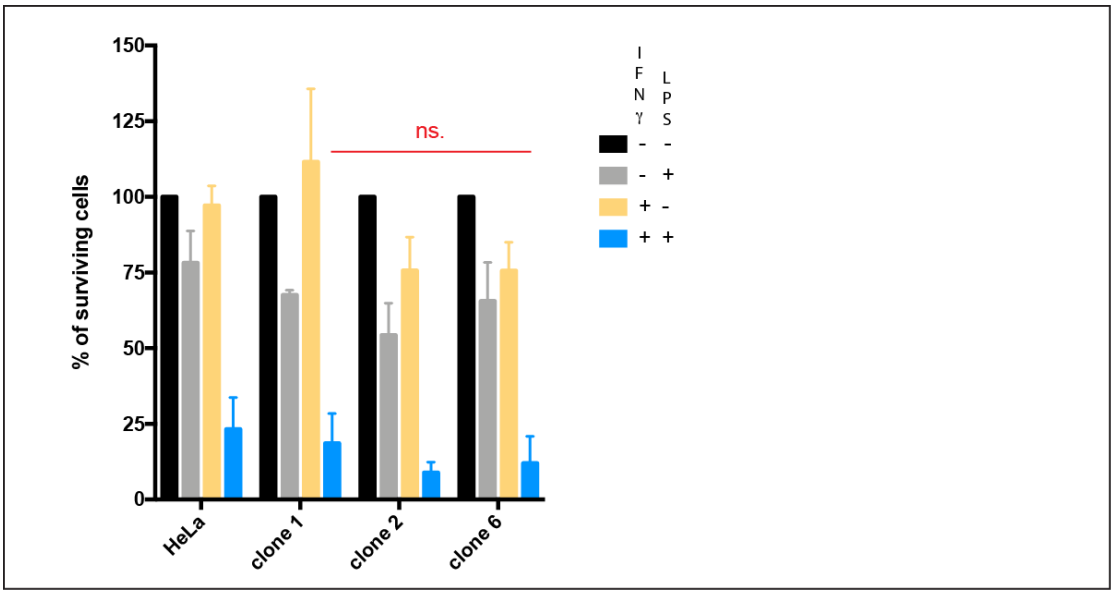

Figure 5: LPS similarly triggers cell death in IFN-γ-primed HeLa clones or population

A population of HeLa cells or cells derived from individual clones were seeded in 96-well plates in the presence or absence of pre-treatment with IFN-γ. The following day, the cells were ± transfected with LPS and then analysed with CellTiter Glo on the next day. Results are shown as Mean ± S.D from a representative experiment run in triplicate for each condition. ns (not significant), using one-way ANOVA with Dunnett's multiple comparisons test comparing cell death following IFN-γ and LPS treatment (+ +) with the population of HeLa cells.

LPS transfection alone led to an average 20% cell death in the HeLa and all the clonal populations. As expected, this phenotype was aggravated by IFN-γ priming which led to 80% cell death, without any significant difference between the four cell lines tested. Only three clones are shown here because they are representative of the initial ten clones tested. All exhibited approximately 20% of surviving cells following IFN-γ priming overnight and LPS transfection. These resisting cells could be explained by insufficient transfection efficiency, which would limit the amount of LPS becoming cytosolic and hence could restrict cell death.

In conclusion, employing a clonal population seemed unnecessary because none of the colonies investigated showed a higher sensitivity to LPS transfection when primed with IFN-γ.

2.2.3 Role of Caspase-4 and Gasdermin-D in the IFN-γ-dependent, LPS-triggered cell death pathway

From previous studies, Caspase-4 (CASP4) and Gasdermin-D (GSDMD) appear to be promising candidates required in the IFN-γ-dependent cell death pathway triggered by LPS. Looking at the LPS-triggered cell death mechanism, F. Shao (Shi et al., 2014; Yang et al., 2015) showed that human CASP4, which is the homolog of murine caspase-11, binds to LPS and is required to generate cell death. V. M. Dixit demonstrated that caspase-11 cleaves GSDMD, leading to pyroptosis (Kayagaki et al., 2015), which is an inflammatory but programmed form of cell death. In the Shao laboratory, characteristic pyroptotic features were indeed recognised in the cell death occurring after LPS treatment.

To determine whether CASP4 and GSDMD were IFN-γ inducible, HeLa cells were grown overnight in the presence or absence of IFN-γ. Cells were then analysed by western-blotting to compare expression at the protein level. **Figure 6** shows blots for CASP4 (**Fig.6A**) and GSDMD (**Fig.6B**). CASP4 expression was increased in cells primed with IFN-γ compared to controls: this is in accordance with previous work (Lin et al., 2000). In the case of GSDMD, the induction by IFN-γ was much more pronounced than was seen with CASP4. Treatment with siRNA was able to knock-down the expression of GSDMD, irrespective of whether cells were primed with IFN-γ or not (**Fig.6B**).

Figure 6: IFN-γ induces both CASP4 and GSDMD

Expression levels of Caspase-4 (A) and Gasdermin-D (B) were assessed by western-blotting comparing expression levels upon IFN-γ priming. For CASP4, untransfected HeLa cells were tested; for GSDMD, HeLa cells transfected with either non-targeting siRNA (siCtrl) or siRNA against GSDMD (siGsdmD) were tested.

CASP4 binds to LPS (Shi et al., 2014) and GSDMD proteins assemble and form pores (Broz & Monack, 2011) in the plasma membrane. This, combined with the fact that they are both induced by IFN-γ treatment, suggested to examine their precise role in the IFN-γ-induced, LPS-triggered cell death pathway.

2.2.3.1. Caspase-4 is necessary for LPS-triggered cell death upon IFN-γ priming

To test whether CASP4 was required in the cell death pathway, it was first knocked-out using three different guides (gRNA 1B-1D) in Cas9-expressing HeLa cells. Since cell death is IFN-γ dependent, the IFN-γ receptor 1 (IFNGR1) was chosen as a positive control because interference with upstream signalling should prevent cell death. IFNGR1 was knocked-out using four different gRNAs (gRNA 5A-5D). The role of GSDMD was also tested at the same time and was knocked-out by four guides (gRNA 3A-3D).

The extent of the knockouts of CASP4 and GSDMD were established using western-blots (**Fig.7A**) and showed variable levels of success depending on the gRNA used. IFNGR1 knockouts were not tested as the specific antibody was not available. Full knockouts (i.e. total absence of protein on the western-blot) were obtained with gRNAs 1B, 1C and 3C for CASP4 and GSDMD, respectively; the GSDMD western-blot indicated that knockout with guides 3A, 3B, 3D were incomplete as shown by the

residual band. All stable Cas9-expressing cell lines treated with gRNAs against CASP4, GSDMD and IFNGR1 were challenged with LPS (+/- IFN-γ priming). Cell death was assessed using the CellTiter Glo reagent and comparing cell survival in knockouts with cells stably expressing Cas9 as a negative control.

In the control population, approximately 38% of the cells survived (**Fig.7B**). By contrast, IFNGR1 knockout cells were substantially more resistant to IFN-γ-induced, LPS-triggered cell death, with 90% of these cells surviving the combined treatment. CASP4 knockout cells (gRNAs 1B and 1C, **Fig.7A**) also showed significant increased survival, with respectively 90% and 70% of IFN-γ-primed cells surviving, following LPS-transfection. For GSDMD, gRNA 3C led to 60% of cells surviving, which was statistically, a non-significant effect.

In conclusion, only CASP4 appeared to be necessary for the IFN-γ-induced, LPS-triggered pyroptotic cell death pathway because the resistance to cell death provided by the two knockouts was significant when compared with the control cells. This is in contrast with GSDMD, for which the knockout did not show a statistically significant reduction in cell death.

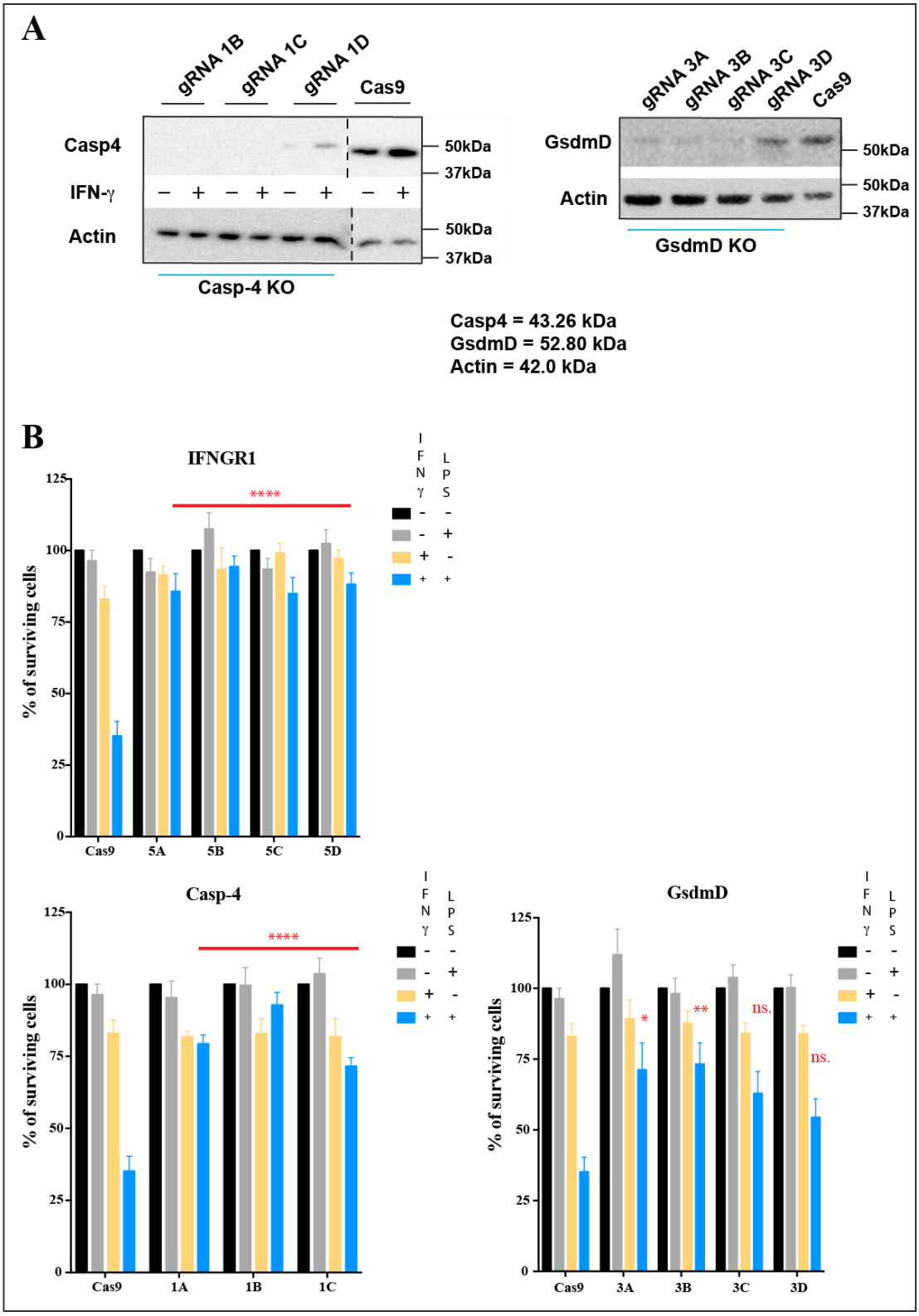

figure continued on next page

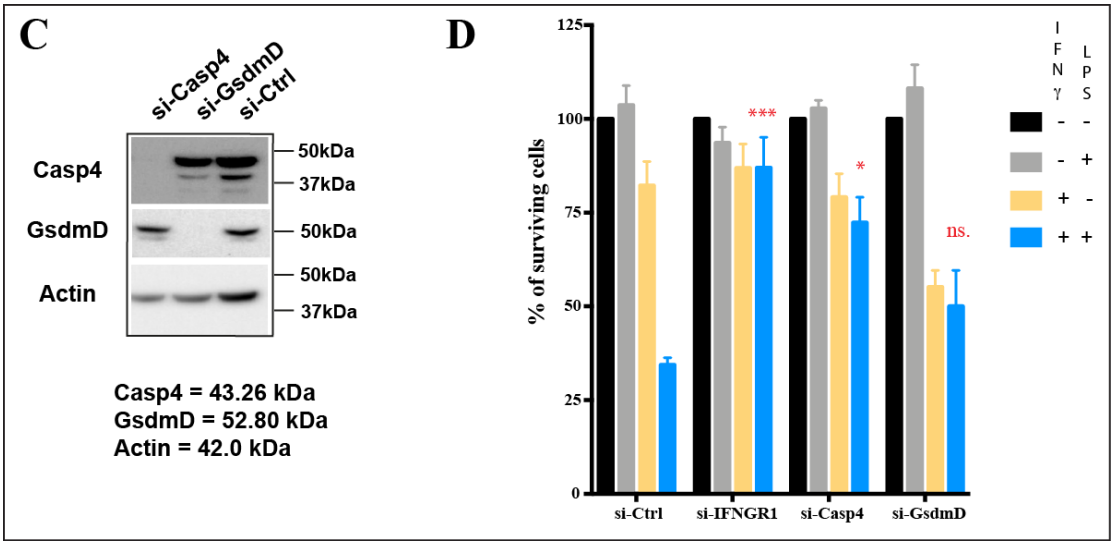

Figure 7: Following priming with IFN-γ, Caspase-4 contributes to LPS-triggered cell death

Three genes – IFNGR1, CASP4 and GSDMD – were either knocked-out using CRISPR-Cas9 and multiple gRNAs or knocked-down using pooled siRNAs. The efficiency of the knockouts (A) and knock-downs in cells treated with IFN-γ overnight (C) were assessed by western-blotting. Knockout (B) and knock-down (D) cells were treated by ± priming with IFN-γ overnight and ± LPS transfection on the next day, and cell survival was assessed with CellTiter Glo on the following day. Results shown are from two experiments, each performed in triplicate, and are shown as Mean ± S.E.M in (B) and (D). *P<0.05, **P<0.005, ***P<0.0002, ****P<0.0001, ns (not significant), one-way ANOVA with Dunnett's multiple comparisons test comparing with the control condition (Cas9-cells for knockouts and non-targeting siRNA for knock-downs).

To complement these results and gain confidence in the results obtained with knockouts, a different method – RNA interference – was used to disrupt protein expression. The same genes, that is, IFNGR1, CASP4 and GSDMD were knocked-down using pooled siRNAs – a mix of four siRNAs targeting a single gene – (Dharmacon). The negative control employed was a non-targeting siRNA, referred to as siControl (siCtrl). The efficacy of the CASP4 and GSDMD knock-downs in cells primed with IFN-γ was checked by western-blotting (**Fig.7C**). The levels of both CASP4 and GSDMD proteins were successfully abbrogated, as shown by the absence of the bands corresponding to these proteins compared with the control cells. With the combined treatment of IFN-γ and LPS, 35% of control cells survived. By contrast, 85%, 75% and 50% survived in the IFNGR1, CASP4 and GSDMD knock-downs, respectively (**Fig.7D**). As expected, the resistance to cell death was more pronounced

in the IFNGR1 than in the CASP4 or GSDMD knock-down cells. CASP4 knock-down showed a 2-fold increased survival ($p<0.05$), whereas GSDMD knock-down did not significantly improve cell survival compared with the non-targeting control. However, GSDMD knock-down cells exhibited death upon IFN-γ treatment alone (yellow bar) and no further increase in cell death was observed when transfecting LPS in these IFN-γ-primed cells. In this regard, the lack of GSDMD seems to have a protective role for the cytosolic LPS-triggered cell death, in IFN-γ-primed HeLa cells.

Taken with the conclusions drawn from **Figure 7A-B**, these results suggest that IFNGR1 and CASP4 are both required for the IFN-γ induced, LPS-triggered cell death in HeLa cells. However, no requirement could be concluded in the case of GSDMD.

2.2.3.2. Neither CASP4 nor GSDMD is sufficient to trigger pyroptosis in response to LPS transfection

CASP4 is necessary for IFN-γ-induced cell death following LPS transfection. To test whether the upregulation of CASP4 or GSDMD would be sufficient to trigger LPS-induced cell death (and hence to replace the IFN-γ induction), HeLa cells overexpressing various constructs for these two proteins were investigated.

HeLa cells were first transduced and then cells were selected for their stable overexpression of three different CASP4 constructs that coded for wild-type (WT), impaired LPS-binding (K19E) and catalytically dead (C258A) CASP4 (Sollberger et al., 2012). These constructs were chosen to enable differentiation between the two main functions of CASP4: namely, LPS binding and catalytic activity. In addition, two different cell lines were constructed that expressed FLAG-tagged GSDMD with the tag located at either the N- or C-terminus of the GSDMD protein. These two constructs were tested to ensure the tag did not alter the protein's behaviour. Because all the CASP4 and GSDMD constructs contained a FLAG tag, the levels of overexpressed proteins were assessed by western-blotting (**Fig.8A**) using a FLAG antibody. All constructs were expressed and the level of the CASP4 constructs on one

hand and the GSDMD constructs on the other hand were similar when normalised to their respective actin expression level.

These five cell lines were tested in the LPS-transfection assay. Fresh medium was added at 5h post-transfection and samples were analysed with CellTiter Glo after overnight incubation. Wild-type HeLa cells were used as a negative control and 25% of the cells survived (**Fig.8B**). Overexpression of neither of the GSDMD constructs, the wild-type CASP4 nor the CASP4 mutant deficient for LPS-binding (K19E) significantly increase cell death in cells primed with IFN-γ when comparing with untransfected cells. The catalytically dead mutant CASP4 (C258A) showed a significant (p-value<0.05) increase in resistance to LPS transfection with 40% of cells surviving compared to only 25% in the control.

In the absence of IFN-γ priming, overexpression of the C-terminal flag-tagged GSDMD led to a significant increase in cell death following LPS transfection, with 40% cell death compared to 20% in the control. This was expected because GSDMD is strongly induced by IFN-γ and overexpressing it in cells essentially recapitulates IFN-γ upregulation. However, this effect on cell death only occurred when the C-terminal tagged protein was overexpressed. In cells, the C-terminal part of GSDMD has an autoinhibitory effect (Ding et al., 2016) and when the protein undergoes cleavage by CASP4, the free N-terminal part oligomerises to form pores (Liu et al., 2016; Chen et al., 2016) in the membrane and that results in pyroptotic cell death (Shi et al., 2015). A tag on the N-terminal part of the protein could therefore prevent oligomerisation and alter GSDMD function in the cell. The catalytically impaired CASP4 mutant (C258A) reproducibly displayed a minor dominant negative effect showing an increase in the percentage of surviving cells compared to the control. This observation is in line with the requirement of the catalytic activity of CASP4 in the IFN-γ-dependent cell death pathway initiated by LPS transfection.

These results indicate that upregulation of CASP4 alone is not sufficient to generate cell death following LPS transfection and is unable to replace IFN-γ priming. GSDMD did not accentuate cell death in the presence of IFN-γ. However, in the absence of IFN-γ priming, overexpression of C-terminal tagged GSDMD was sufficient to induce cell death after transfection with LPS, and in levels comparable to

IFN-γ-primed control cells. This result demonstrates the requirement of GSDMD for LPS-induced pyroptosis. Neither of these two candidates – CASP4 and GSDMD – individually, fully accounts for the requirement of IFN-γ to trigger pyroptosis upon LPS transfection, indicated that, there must be other IFN-γ-induced genes needed in the LPS-triggered cell death pathway.

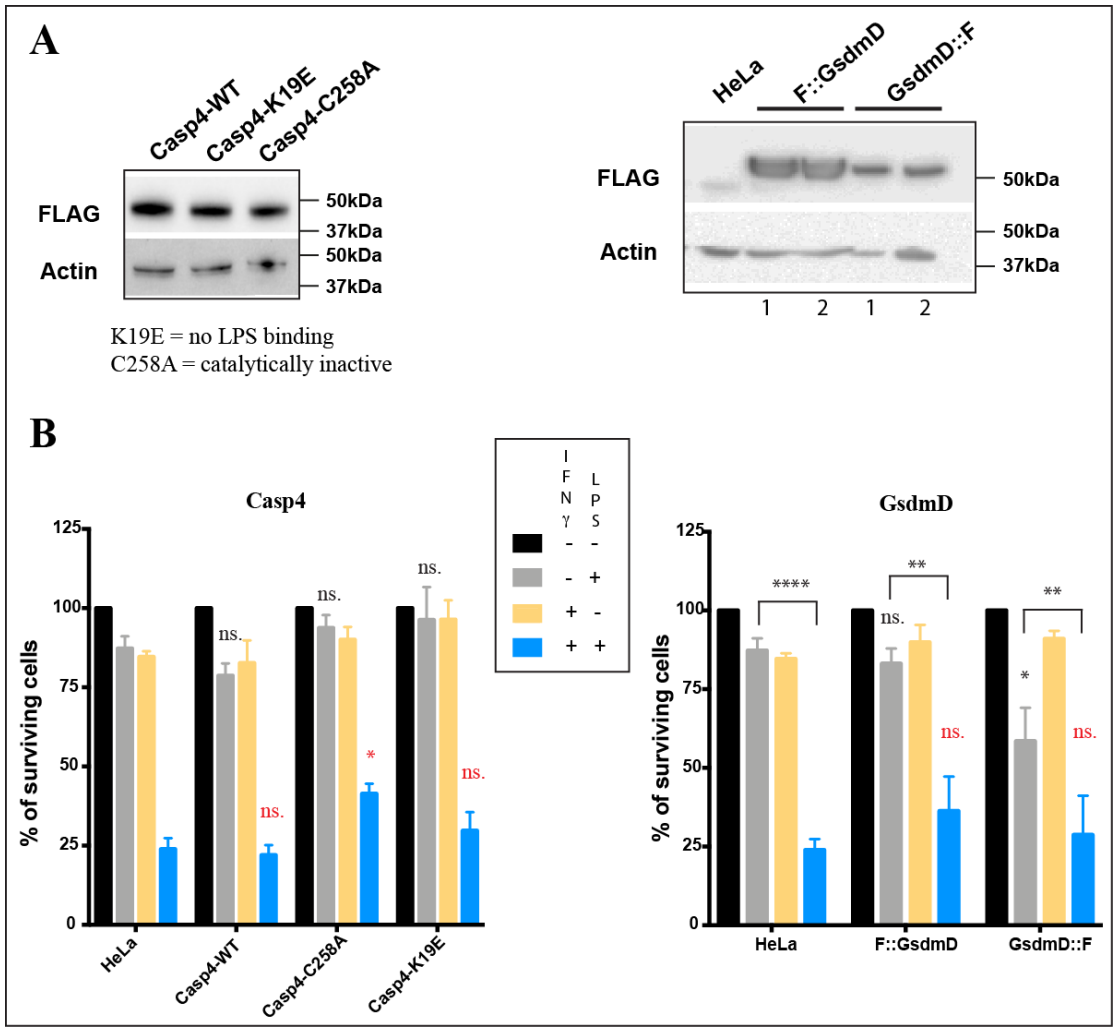

Figure 8: Caspase 4 is not sufficient to trigger cell death following transfection with LPS

A range of Flag-tagged CASP4 (WT - wild-type, C258A - catalytically dead, and K19E - impaired for LPS binding) and Flag-tagged GSDMD (at the N- or C-terminus) constructs, were expressed in HeLa cells. (A) Overexpression of the desired proteins (CASP4 or GSDMD) was confirmed by western-blotting using a Flag antibody. Cells overexpressing either CASP4 or GSDMD were subjected to ± priming with IFN-γ overnight followed by ± LPS transfection on the next day and cell death was assessed with CellTiter Glo at 18h post-transfection; (B) Cell death from three separate experiments performed in triplicate are shown as Mean ± S.E.M. Results compared with the control condition (non-transfected HeLa cells) were evaluated using one-way ANOVA with Dunnett's multiple comparisons test with *P<0.05 and ns (not significant). For each cell line, the effect of LPS transfection on cells (comparison between black and grey bars) and the effect of IFN-γ with LPS transfection (grey

and blue bars) were evaluated using one-way ANOVA with Dunnett's multiple comparisons test with *P<0.05, **P<0.005, ****P<0.0001, ns (not significant).
The three CASP4 constructs were kindly provided by Dr. Michal Wandel.

In summary, CASP4 and GSDMD were investigated as genes required in the IFN-γ-induced, LPS-triggered cell death pathway because CASP4 is a receptor of free cytosolic LPS and GSDMD is an effector in pyroptosis. CASP4 was shown here to be necessary in the IFN-γ-induced, LPS-triggered cell death pathway although its overexpression failed to replace the IFN-γ induction. This was to be expected because both CASP4 knockout and knock-down only showed partial inhibition of pyroptosis. The function of GSDMD was not as straightforward. On the one hand, GSDMD knockout or knock-down displayed a limited effect in the LPS-induced pyroptosis of IFN-γ-primed cells: the increase in survival compared to control cells was not significant compared to effects seen with CASP4 or IFNGR-1 knockouts. On the other hand, LPS transfection in C-terminal FLAG-tagged GSDMD overexpressing-cells resulted in cell death without IFN-γ priming and overexpression of GSDMD replaced the effect of IFN-γ. GSDMD is a known IFN-γ inducible protein (ratio of 1.38 in the microarray performed by M. Wandel, **Table 2**) that is processed and cleaved to separate the N-terminal active region from the C-terminal inhibitory region of the protein (He et al., 2015; Shi et al., 2015); it was indeed observed that overexpression gave different results depending on the location (N- or C-terminal) of the FLAG tag.

This entire section was dedicated to show the limitations of our knowledge about the IFN-γ-dependent, LPS-triggered cell death pathway in human HeLa cells. The next section of this chapter presents a new approach to investigate this mechanism further and try to identify genes involved in the pathway.

2.3 Results: Genetic screen to identify new genes in the IFN-γ dependent, LPS-triggered cell death pathway

In order to investigate the IFN-γ-dependent, LPS-triggered cell death pathway, an unbiased genetic screen was set-up using the CRISPR-Cas9 technology.

Identifying genes that influence a phenotype of interest is frequently achieved through genetic screening, a process by which individuals are tested to find out if they carry mutations in genes associated with a certain known phenotype. Genetic selection refers to a type of genetic screening that is designed so that only the desired mutants survive. Multiple techniques are available, and several strategies can be applied to perform a genetic selection assay, depending on the biological question under investigation (Shemesh et al., 2007; Yamamoto et al., 2009).

Genetic screens are a powerful tool to investigate signalling pathways and understand molecular mechanisms. The immune system is a highly complex and connected network, and an approach that uses a genome-wide forward CRISPR screen permits the study of particular pathways of interest.

2.3.1 Designing a genome-wide CRISPR screen

This section presents the strategy that was used – genome-wide genetic screen - and justifies the technical choices made during the project – CRISPR-Cas9 in human HeLa cells - by comparison with other screening methods. It also shows the rationale of the design and some preliminary optimisations that were essential to check the feasibility of that study.

2.3.1.1. Mutagenesis was achieved using the CRISPR-Cas9 technology

To genetically investigate specific phenotypes, gene expression must be modified. Many techniques are available, and they all present advantages and drawbacks. In this case, the screen required the use of a targeted and highly specific method that could be scaled-up, hence the choice of CRISPR-Cas9.

i. Targeted approaches

In contrast to non-targeted approaches, targeting requires prior knowledge of the target sequence or genomic region. RNA interference (RNAi) offers a sequence-specific, high-throughput knock-down method (Ngo et al., 2006) that could be applied on a genome-wide scale and causes loss-of-function in diploid cells, including human cells (Berns et al., 2004; Zuber et al., 2011). Gene expression is impaired post-transcriptionally targeting mRNAs for degradation. RNAi efficiency is independent of gene copy number and does not create dominant negative mutants. However, the efficiency of a knock-down depends on the timing, the delivery method and the design of the si/shRNA (Maine, 2001); the RNAi technology suffers from high off-target effects and potential incomplete knock-down (Boutros & Ahringer, 2008), which may cause residual protein expression and a low signal-to-noise ratio (Echeverri et al., 2006) making it hard to interpret results.

In order to circumvent the disadvantages of RNAi and ensure protein loss-of-function, knockout methods using programmable nucleases have been developed and have recently undergone a revolution with the discovery of the CRISPR-Cas9 system. Programmable nucleases enable targeted genetic modifications and rely on site-specific DNA double-strand breaks paired with cellular DNA repair mechanisms; consequently, the efficiency of both the homologous recombination (HR) and the non-homologous end-joining (NHEJ) mechanisms is greatly enhanced (Rouet et al., 1994). In the absence of donor DNA, the error-prone NHEJ mechanism is predominant and thus creates site-specific gene disruption, deletion, and chromosomal rearrangements (Kim & Kim, 2014).

ii. Programmable nucleases

Irrespective of their type, programmable nucleases were developed and are now used to disrupt not only protein-coding genes but also non-coding elements. They all create site-specific DNA double-strand breaks (DSBs). Their specificity is based on sequence recognition, mechanism subject to off-target effects.

Zinc-finger nucleases (ZFNs) consist of DNA-binding ZFPs (zinc-finger proteins), which contain a nuclease domain derived from the restriction enzyme FokI (Kim et al., 1996). Their activated dimer form can bind 9-18bp of the targeted gene (**Fig.9.1**),

depending on the number (3-6) of zinc-fingers (Wolfe et al., 2000); but ZFNs have overall a poor targeting density: all 64 combinations of triplet sites are not readily available in zinc-fingers assembly (Kim & Kim, 2014). Moreover, the rules explaining binding to the targeted DNA sequence are still to be resolved; the selection of a library cannot be done *in silico*.

Transcription activator-like effector (TALE) are also DNA-binding proteins and are associated with a FokI-derived nuclease to form TALEN (Miller et al., 2011). TALEs contain amino acid repeats in which a pair of amino acids is responsible for the recognition of a specific nucleotide (**Fig.9.2**). It is possible to design TALENs in order to target specific sequences (Kim et al., 2013), but this becomes very time-consuming. TALENs are the nucleases of choice for targeting small DNA sequences but require a thymine at the 5' end of the target sequence (Lamb et al., 2013) and cannot cleave methylated DNA (Bultmann et al., 2012).

RNA-guided engineered nucleases (RGENs) include, but are not restricted to, the Cas9 protein (**Fig.9.3**). Clustered regularly interspaced small palindromic repeats (CRISPR) are DNA fragments of invading phage or protospacers found integrated in the genome of bacteria or archaea (Barrangou et al., 2007). When armed with the RNA produced from the CRISPRs, RGEN – an essential component of adaptive immunity in these organisms – targets invading DNA. Cas proteins are activated by conformational change following the formation of a complex with cr-RNA and tracr-RNA ((trans-activating) CRISPR RNA). They function as nucleases and the target specificity is carried by 20bp on the cr-RNA. The target sequence (20bp) is followed by the 3bp of the PAM sequence (protospacer adjacent motif), which is recognised by Cas9 itself (Mojica et al., 2009).

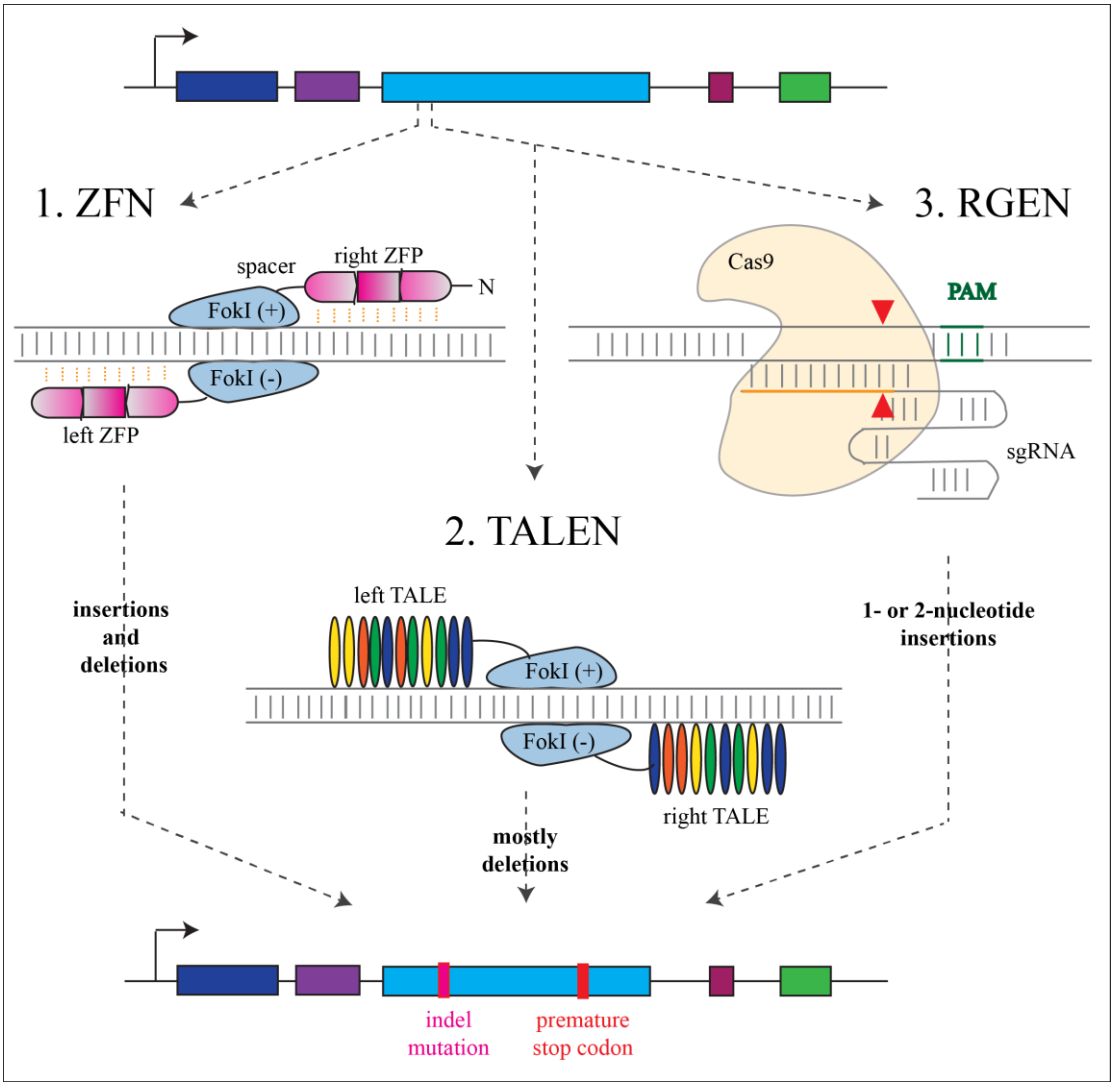

Figure 9: Three types of programmable nucleases

Programmable nucleases are used for genome editing and can target coding or non-coding DNA sequences. Zinc-finger nucleases (1. ZFN) and transcription activator-like effector nucleases (2. TALEN) use the same enzyme FokI but the sequence recognition is mediated by either zinc-finger repeats (ZFP) or amino acid sequences (TALE). RNA-guided engineered nucleases (3. RGEN) require Cas9 and a sgRNA to generate a DNA double-strand break upstream of a PAM sequence.

Generally, TALENs cleave non-methylated DNA regions with almost 100% efficiency in mammalian cells, similar to the success rate obtained with RGENs (Kim & Kim, 2014). However, mutation frequencies are very variable and range overall from 1% to 79% in cultured mammalian cells, with RGENs on the higher side of the window. In terms of specificity, all three methods rely on sequence recognition and are therefore subject to off-target effects (Fu et al., 2013; Mussolino et al., 2011;

Pattanayak et al., 2011). Because ZFNs are activated by dimerisation, they are expected to be more specific. RGENs are the most modular with respect to the variety of potential targets available, since it is easier to synthesise RNA than it is to modulate the number and nature of either ZnF for ZFNs or TALE in the case of TALENs (Kim & Kim, 2014). That is why although ZFNs and TALENs result in targeted mutagenesis at high frequencies, these techniques are not appropriate for genetic screens, lacking versatility and high-throughput in their application.

2.3.1.2. The CRISPR-Cas9 technology

The CRISPR-Cas system is an essential component of adaptive immunity against viruses and plasmids, widespread in bacteria and archaea. Prokaryotes have indeed evolved a small RNA-based detection and silencing mechanism targeting foreign nucleic acids whereby specificity is dictated by the CRISPR spacer content while the resistance is provided by the Cas enzymatic machinery (Barrangou et al., 2007). Following viral and plasmid challenges, short fragments of foreign nucleic acids are integrated in the host genome at one end of a repetitive element known as CRISPR. These repetitive loci provide resistance to subsequent phage infection in a sequence-specific; phage sensitivity is dictated by the CRISPR composition (Wiedenheft et al., 2012).

CRISPR elements are transcribed and processed into a library of short CRISPR RNAs (crRNAs). When the Cas protein is associated with the two-RNA complex containing crRNA and trans-activating crRNA (tracrRNA), it acts as an endonuclease and generates double-strand breaks (DSBs), cleaving foreign nucleic acid sequences and hence protecting the host (Cho et al., 2013). The CRISPR-Cas machinery causes small, frameshifting insertions and deletions around the target sequence by means of error-prone non-homologous end joining (NHEJ) repair of the DSBs.

To apply this system as a targeted mutagenesis tool, the two RNA elements were replaced by a chimeric single guide RNA. Association with the Cas9 protein led to cleavage in vitro (Jinek et al., 2012) and was further used as a sequence-specific genome-editing technique in mouse and human cell lines (Cong et al., 2013; Hart et

al., 2015; Wang et al., 2014) and even in vivo, e.g in bacteria, zebrafish (Jiang et al., 2013; Hwang et al., 2013).

The CRISPR-Cas methodology has been optimised for mammalian genetics and especially to carry out genome-wide screens in human cells (Shalem et al., 2014; Wang et al., 2014) to discover and study genes involved in cell fitness (Hart et al., 2015), proliferation (Wang et al., 2014), viability of cancer or pluripotent stem cells, drug resistance (Shalem et al., 2014) or genes having an influence on the immune response (Parnas et al., 2015).

The design of such a large-scale experiment requires careful planning and essential decision-making about the type of CRISPR single guide RNA (sgRNA) library to use (whole genome vs focused), the format of the screen (pooled or arrayed), the cell line to use to perform the screen (Miles et al., 2016).

i. Pooled vs arrayed screens

To perform a genome-wide screen, the layout preference is for a pooled library, rather than an arrayed library, of sgRNAs. Arrayed screens are run in plates where each well contains one or several guide(s) against a single gene, making the readout high throughput in the case of either positive or negative screens. By contrast, a pooled library allows sequencing of the collected population and is therefore easier to implement for a positive screen, provided the phenotype is selectable. Genome-wide CRISPR screens are theoretically possible with both types of assays (Agrotis & Ketteler, 2015); but in practice, cells are meant to express both Cas9 and one single gRNA at a time, and each gene needs targeting with multiple gRNAs. Consequently, a large number of cells is easier to handle than a large number of wells, rendering pooled libraries preferable. However, when the phenotype is not selectable for, arrayed assays (Kim et al., 2018) will then be used.

ii. Genome-wide library

In order to investigate a specific phenotype in an unbiased manner, a genome-wide pooled library is preferable. It targets the whole coding genome and allows more novel discoveries. A targeted library, by contrast, is narrower and biased by the choice of genes to be mutated. Multiple genome-wide human gRNA libraries have been

developed; these can differ by the number of genes they target, the number of guides targeting each gene, and whether the Cas9 protein is encoded by the same plasmid as the sgRNA. For instance, the sgRNA library described by Wang et al. (2014) includes 73,151 guides targeting 7,114 genes (≈35% of the human protein-coding genome) and 100 non-targeting controls.

To reduce biases due to differences in sequence targeting and mutation efficiency between gRNAs, the library should contain a minimum of four gRNAs per gene. Adding more sgRNAs is primarily beneficial to decrease the off-target effect (Hart et al., 2017) and to gain statistical power when processing the data, resulting in higher p-value. The design of gRNAs is limited by the PAM sequence (NGG or NAG) that is recognised by the nuclease (Cas protein) and is at the 3' end of the 20bp from the targeted sequence. The presence or the addition of a guanine residue at the 5' end of the target sequence in the gRNA increases its transcription because it enhances RNA polymerase III recruitment – the gRNA sequence being under the control of the U6 promoter (Kuscu et al., 2014). More generally, gRNAs are preferentially designed to target early exons in genes for a higher chance of synthesising a non-functional or truncated protein. They are also designed to target the maximum number of isoforms for a higher knockout efficiency (Mohr et al., 2016). Chemical groups can be covalently bound to add variety in the gRNAs, thereby affecting the specificity or the stability of the Cas9-gRNA complex (Moon et al., 2019). Because Cas proteins tolerate mismatches of up to five nucleotides (Hsu et al., 2013), it is possible to alter the sequence to avoid unwanted off-target activity. Modifications in the core of the gRNAs can be made as well: modifying the lengths of the spacer or the scaffold regions can be beneficial and can improve specificity (Cho et al., 2014; Grissa et al., 2007). In order to further improve CRISPR as a genome-editing tool to achieve high on-target specificity, efficiency, and low off-target effects (Cui et al., 2018), the nuclease can be modified. More high-performance effector nucleases such as Cas12a, Cas13a or newly engineered forms of Cas9 are available.

iii. Human HeLa cells as the experimental working model

Over the history of genetics, multiple model organisms have been developed, increasing the level of complexity of the system. The use of yeasts allowed easy manipulations in eukaryotic organisms (Forsburg, 1999) and this work was further

extended with *Caenorhabditis elegans* (Ankeny, 2001; Brenner, 1974) and *Drosophila melanogaster* (Golic & Lindquist, 1989; Rubin & Lewis, 2000) to investigate developmental processes, behavioural changes, neurodegeneration and inheritance. More recently, mouse models have emerged to become the first multi-cellular organism where genes could be targeted by homologous recombination (Thomas & Capecchi, 1986; Thomas et al., 1986). Forward dominant genetic screens were performed, looking at visible phenotypes (Nolan et al., 2000). Furthermore, crossing and study of the offsprings (generations 2 and 3) revealed recessive effects (Nelms & Goodnow, 2001; Simon et al., 2015). Recessive screens are also possible using chromosome engineering approaches (Ramirez-Solis et al., 1995; Zheng et al., 1999) and provide a non-biased way for phenotype-driven genetic screens. As mammals, mice could mimic human diseases and provide a better understanding of human biology. However, the implementation of screens on the organism level in mammals has proven difficult.

Mammalian cultured cells provide a reductionist and simpler model to perform genetic experiments compared to a whole organism. Moreover, many human genes do not have homologs in yeast including in pathways such as apoptosis, or cell differentiation (Goffeau et al., 1996; Grimm, 2004). There are indeed multiple advantages in using cultured mammalian cells: coming from a common source cell lines usually display uniform genetic and phenotypic backgrounds, which are known and help with the consistency of the interpretation. In addition, cells are kept in known and specific growth conditions (e.g. medium composition, temperature are controllable) and are stable (do not differentiate) in the absence of induction. Some cell lines are preferred due to their ease of handling and introducing genetic material, others for their ability to grow in certain conditions or for displaying the phenotype studied (Grimm, 2004; Wang, 2006).

The evolution of CRISPR has made it possible to use this technology in mammalian cells (Jinek et al., 2012) and the development of human CRISPR knockout screens has led to research in many different fields including genomics (Aguirre et al., 2016) as well as identification of biomarkers or cancer vulnerabilities (Hart et al., 2015) and dissection of signalling pathways (Parnas et al., 2015).

For an efficient CRISPR-mediated knockout, it is important to ensure that the cell line used is equipped with DNA repair pathways and, more specifically, the error-prone NHEJ (Jackson & Bartek, 2009). For the implementation of the screen, cells are chosen so that they must be affected by the selection pressure too. **Figure 4** highligted that IFN-γ-primed HeLa cells died the most after transfection with LPS, compared to other cell lines tested.

2.3.2 Justification of the project and rationale of the experiment

2.3.2.1. Optimisation of the cell death assay

The signalling pathway being investigated addresses the impact of cytosolic LPS in IFN-γ-primed HeLa cells. To study the LPS-triggered cell death pathway, cells were transfected with commercially available *S.*Typhimurium LPS purified from bacterial outer membrane. To recapitulate *in vitro* the presence of LPS inside the cells, a transfection protocol was designed and optimised to induce LPS-caused cell death as efficiently as possible in HeLa cells primed with IFN-γ. Both the transfection reagent and the amount of LPS were optimised to reach the highest cell death specifically due to introducing LPS into the cytosol of IFN-γ-primed cells.

The concentration of LPS (7.5μg/mL in a 96-well plate format) was kept constant while a range of reagents for the transfection of LPS was tested (**Fig.10A**). The same volume (0.2μL in a 96-well plate format) of different transfection reagents was added to the reaction to keep total volumes constant (total of 220μL in a 96-well plate format) across conditions, hence the concentrations of these reagents varied. Lipofectamine2000 (Baker et al., 2015) or Fugene (Casson et al., 2015) had already been used to transfect LPS. Liposome-mediated transfection had also been used, although this was mostly for hydrophobic molecules such as Lipid A (Lagrange et al., 2018; Steimle et al., 2016). A broader range of transfection reagents was tested since most of these reagents were available in the lab and straightforward to test in the assay. These transfection reagents were chosen following a literature search (Rahimi et al., 2018; Wang et al., 2018b) and online guides (Hook & Landreman, 2018).

In summary, the choice of reagent for LPS transfection was based on the highest percentage of dying cells obtained in IFN-γ-primed HeLa cells. Conditions were likely not optimal for all the reagents tested because the same volume, hence not the same concentration of reagent was added to the cultured HeLa cells. Only RNAiMax and Lipofectamine2000 generated substantial and detectable cell death. Since only 0.2μL of transfection reagents were diluted in OptiMEM medium, it is possible that there was not a sufficiently high concentration of other reagents to effectively transfect LPS and generate cell death. Oligofectamine (0.6μL) and PEI (0.4μL) were previously tested using PI staining as the readout and both gave 20% cell death. By contrast, 0.2μL of either Lipofectamine2000 or RNAiMax gave 80% and 65% death respectively (data are not shown). Another possible hypothesis is that these reagents simply did not bind or interact with LPS and so the transfection was not effective.

Only the combined treatment of IFN-γ and LPS (**Fig.10A**, blue bar, + +) contributed to any cell death. Neither priming with IFN-γ overnight (yellow bar, + -) nor LPS transfection alone (grey bar, - +) generated an increase in cell death in comparison to control cells that were only treated with the corresponding transfection reagent (black bar, - -). RNAiMax and Lipofectamine2000 respectively generated 50% and 75% cell death, whereas none of the other transfection reagents gave any cell mortality in the conditions tested here. In the case of Lipofectamine2000, the concentration of reagent used was not lethal and no cell death was observed in the presence of the transfection reagent only (in the absence of LPS). Overall, the highest specific cell death due to cytosolic LPS was obtained with Lipofectamine2000 as transfection reagent.

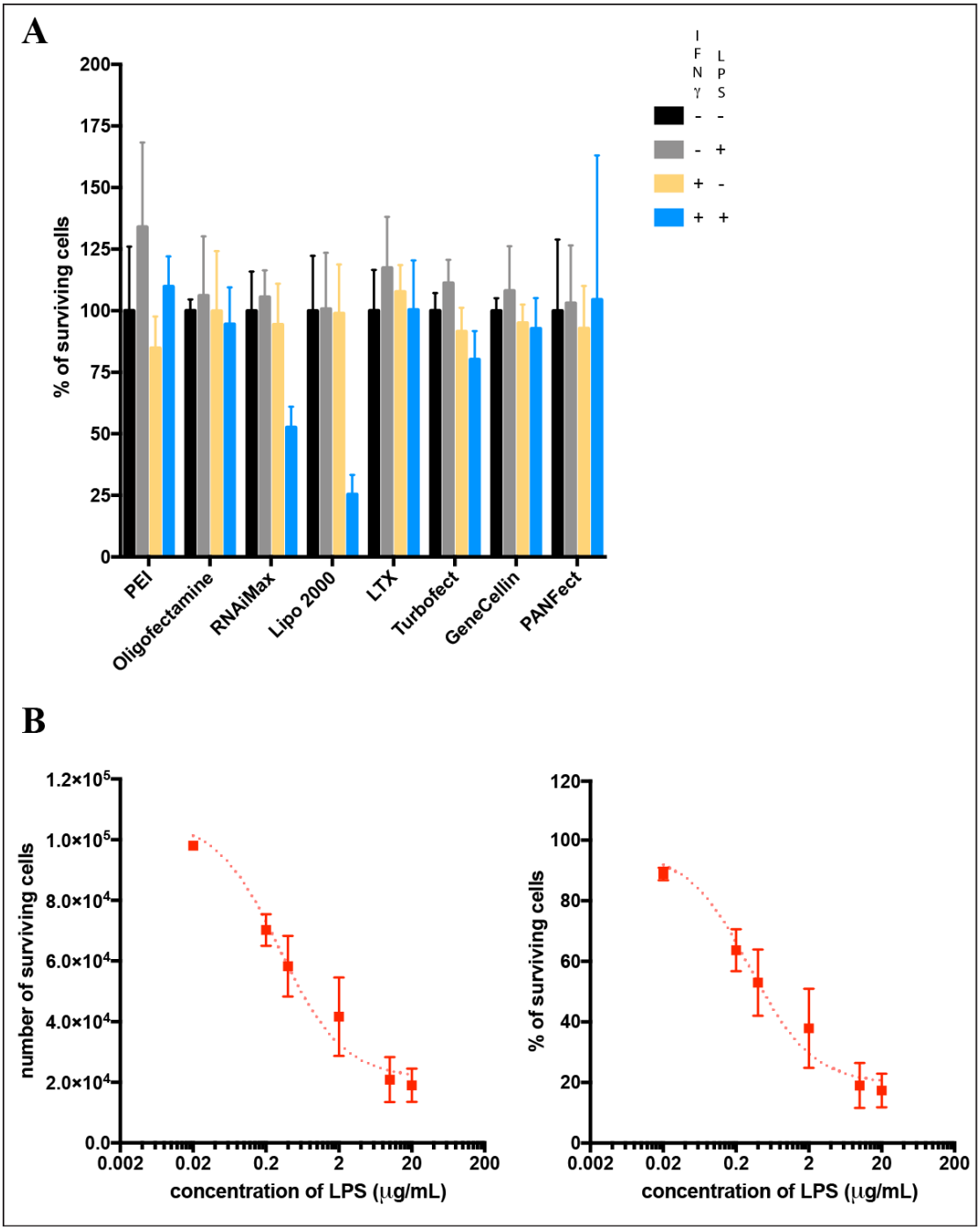

Figure 10: Lipofectamine 2000 was the most efficient LPS transfection reagent to trigger cell death

(A) Following overnight priming of HeLa cells with IFN-γ, eight transfection reagents were evaluated to determine which was able to transfect LPS most efficiently to promote cell death. Results are shown as Mean ± S.E.M for two independent experiments, performed in triplicate, in 96-well plates, using 0.2µL of transfection reagent and 1.5µL of LPS per well. Cell death was assessed using CellTiter Glo. (B) LPS was titrated using 1µL of Lipofectamine 2000 per well for the transfection. Results are shown as Mean ± S.E.M for three independent experiments in 24-well plates, using PI staining to assess cell death.

To further optimise the assay, a titration of LPS was performed using a constant concentration of Lipofectamine2000 as transfection reagent (**Fig.10B**). Based on the results of the previous experiment, 2μg/mL (1μg in a 24-well plate format) of Lipofectamine2000 was used. Increasing the amount of LPS from 10ng to 5μg per well (i.e. 20ng/mL to 10μg/mL) increased cell death from 10% to 85% of the IFN-γ-primed HeLa cells. Adding up to 10μg LPS (20μg/mL) did not further increase cell death; it appeared to have reached a plateau. This was consistent with saturation: for the amount of transfection reagent (Lipofectamine2000) available, no more LPS could be transfected.

Following these tests, 3μg of LPS along with 1μL of Lipofectamine2000 in a total volume of 100μL OptiMEM were added to a 24-well already containing 500μL of medium (final concentrations of 5.0μg/mL of LPS and 1.67μg/mL of Lipofectamine) to transfect LPS into HeLa cells. This ratio was maintained throughout the experimental design and amounts were adjusted appropriately when well sizes were changed.

Future knockout experiments using the CRISPR-Cas9 technology were therefore performed in a population of HeLa cells. Overall, as a result of these studies, the LPS-triggered cell death assay had now been optimised to give a maximum cell death upon IFN-γ priming. This protocol could therefore be used to find IFN-γ-induced genes required in the cell death pathway triggered by the presence of cytosolic LPS.

The cell-death phenotype investigated here naturally leads to the implementation of a loss-of-function screen. Although the inactivation of both copies of a gene in diploid cells (e.g. human cells) has proven difficult, it became possible with the CRISPR-Cas system (Wang et al., 2014). In order to identify genes required in the IFN-γ-induced, LPS-triggered cell death pathway, a genome-wide loss-of-function genetic forward screen was performed, using the CRISPR-Cas9 technology. For the screen to be successful, the selection pressure needs to be sufficiently strong to kill nearly all normal cells, to ensure enrichment of cells specifically carrying genes providing

resistance to IFN-γ-dependent, LPS-triggered cell death, when they are mutated (non-functional). Consequently, it was necessary to optimise transfection conditions and assay readout to ensure that these conditions were fulfilled.

2.3.2.2. Validation of the enrichment strategy

As shown above (**Fig.4**), HeLa cells died upon LPS transfection when they were primed with IFN-γ. IFNGR1 acts as sensor of IFN-γ and thereby is required for the cell death to occur. CASP4 was also shown to be necessary, although not sufficient, in the pathway. There are clearly other players – yet to be identified – required in the IFN-γ-induced, LPS-triggered cell death pathway. In order to perform the genetic screen to identify new genes required in the LPS-triggered, IFN-γ-dependent cell death pathway, the assay had been optimised to give the highest selection pressure possible to select only cells which are resistant to LPS-triggered cell death when primed with IFN-γ. However, for the screen to be successful, the proposed enrichment strategy needed to be validated.

i. CrmA inhibits LPS-induced cell death in IFN-γ-primed HeLa cells

Serine proteinase inhibitor 2 (CrmA) is a cowpox-encoded serpin, which inhibits host caspases, thereby modulating cell death responses to viral infection. CrmA was tested for its ability to inhibit LPS-triggered cell death. A construct was created to overexpress GFP-tagged CrmA in HeLa cells. Expression of the protein was checked by western-blotting (**Fig.11A**) and cells were treated by LPS transfection following IFN-γ priming. On average, 60% of untransfected HeLa cells died under these conditions, whereas none of the HeLa cells overexpressing the GFP-CrmA protein died (**Fig.11B**). This result confirms that CrmA provides resistance to IFN-γ induced, LPS-triggered cell death, and hence CrmA-overexpressing cells mimic the behaviour of cells being mutated, in the future screening process, in genes involved in the LPS-triggered cell death pathway.

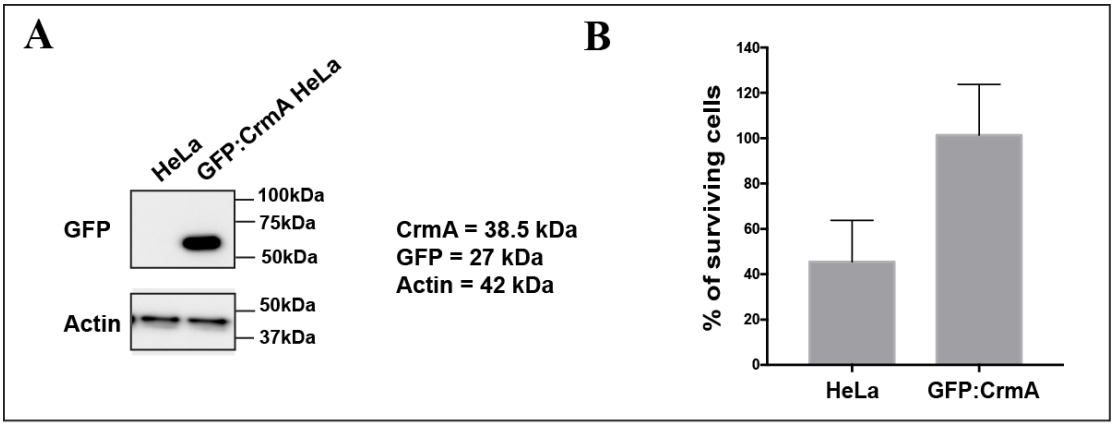

Figure 11: Overexpression of CrmA provides resistance to LPS-triggered cell death

(A) GFP-tagged CrmA was transduced in HeLa cells and expression was assessed by western-blotting. (B) CrmA-expressing cells, together with controls (untransduced), were primed overnight with IFN-γ, and then transfected with LPS. Cell death was assessed using PI staining and flow cytometry to determine the percentage of cells surviving relative to cells that had also been primed with IFN-γ, but which had only been treated with the transfection reagent Lipofectamine 2000 (no LPS).
The GFP:CrmA construct was kindly provided by Dr. Michal Wandel.

ii. Proof of concept using CrmA-overexpressing cells

Overexpression of CrmA was sufficient to give resistance to LPS-triggered cell death in IFN-γ-primed HeLa cells. These cells could therefore be used to test the screening enrichment strategy to see whether a mutant/resistant population would be enriched and then isolated in the screen.

GFP::CrmA-overexpressing HeLa cells were mixed together with HeLa cells in a 1:10,000 ratio. This population was submitted to several rounds of treatment consisting of IFN-γ priming followed by LPS transfection (**Fig.12A**). After each round, surviving cells were analysed for their content in GFP-positive cells. CrmA cells were both resistant to the treatment and expressed GFP, and so their proportion was expected to increase. The enrichment in GFP-positive cells in the surviving population was followed over the course of the successive rounds of selection by flow cytometry (**Fig.12B**). In the input population, 0.01% of cells were GFP-positive. After the first round, 3.5% of cells were found GFP-positive; this percentage continually increased to reach about 75% after the fifth round (**Fig.12C**). The population was therefore substantially enriched in resistant cells. These results indicate that the

selection strategy is successful and could be applied to a pool of cells mutated with the CRISPR-Cas9 technology.

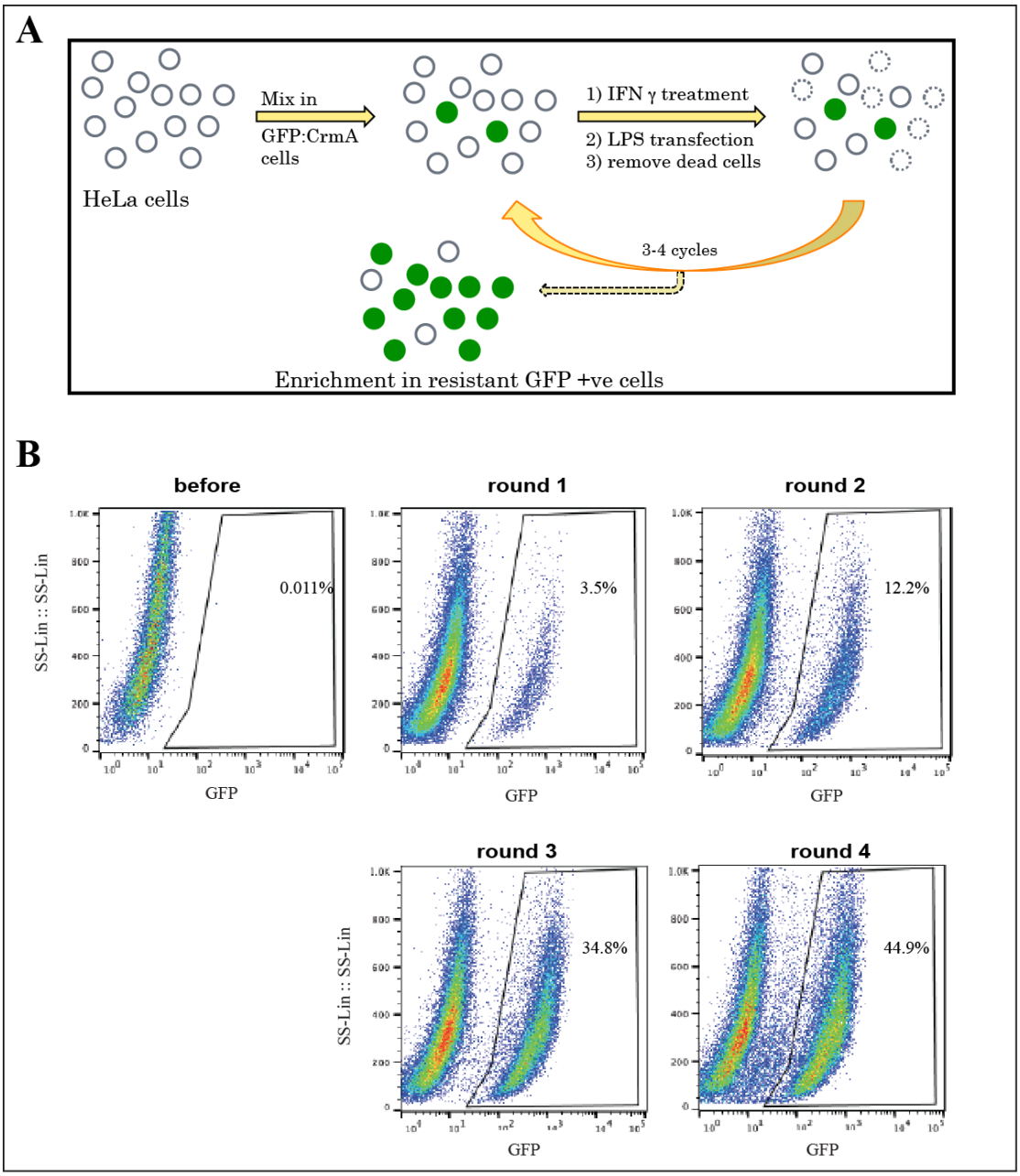

figure continued on next page

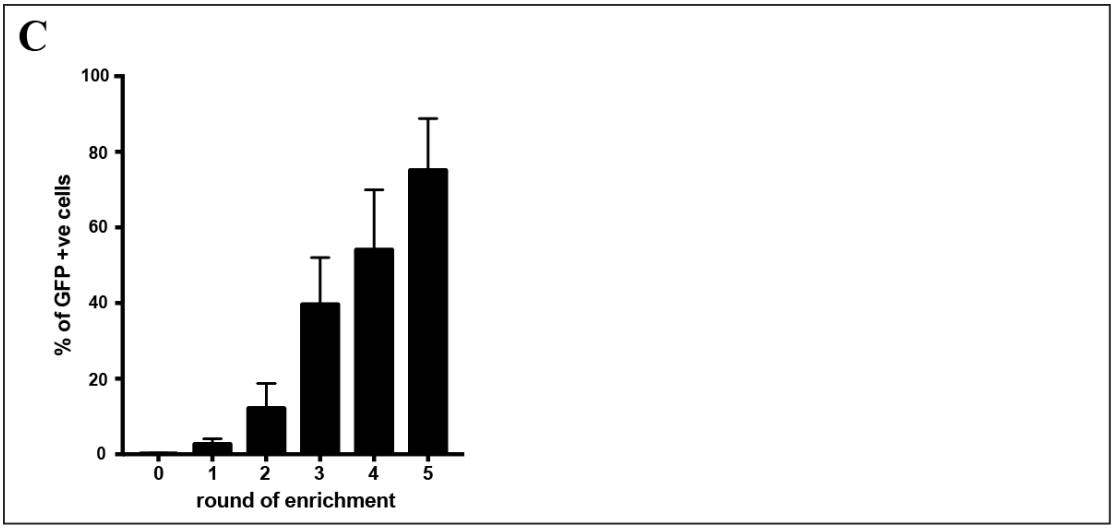

Figure 12: CrmA cells are enriched in a mixed population following LPS transfection

(A) HeLa cells overexpressing GFP::CrmA were mixed with untransduced HeLa cells and the population was subjected to several rounds of treatment (involving IFN-γ priming followed by LPS transfection). The enrichment in GFP-positive cells was assessed by flow cytometry (B) and quantified for each round of enrichment (C). Flow cytometry plots are from one representative experiment, whereas bar graph shows Mean ± S.E.M of three independent experiments.

Since CASP4 and GSDMD are not sufficient to explain the influence of IFN-γ in the LPS-dependent cell death phenotype, the mechanism required more detailed investigation. To do this, a genetic screen was used to identify new genes required in the LPS-triggered, IFN-γ-dependent cell death pathway. In this scenario, IFN-γ priming followed by LPS transfection would provide a selection pressure that would selectively enrich for cells resistant to the treatment.

2.3.3 Implementing a genome-wide CRISPR screen in human cells

Despite variations in screening conditions that depend on the biological question and the strategy implemented, three main steps characterise any CRISPR screen (**Fig.13**): 1) delivery of the components into the cells, 2) the screening process itself, and 3) the data analysis, complemented by the confirmation of the 'hits' from the screen (see

paragraph **2.3.4** "Validation of the hits"), which indicates how trustworthy the results from the screen are.

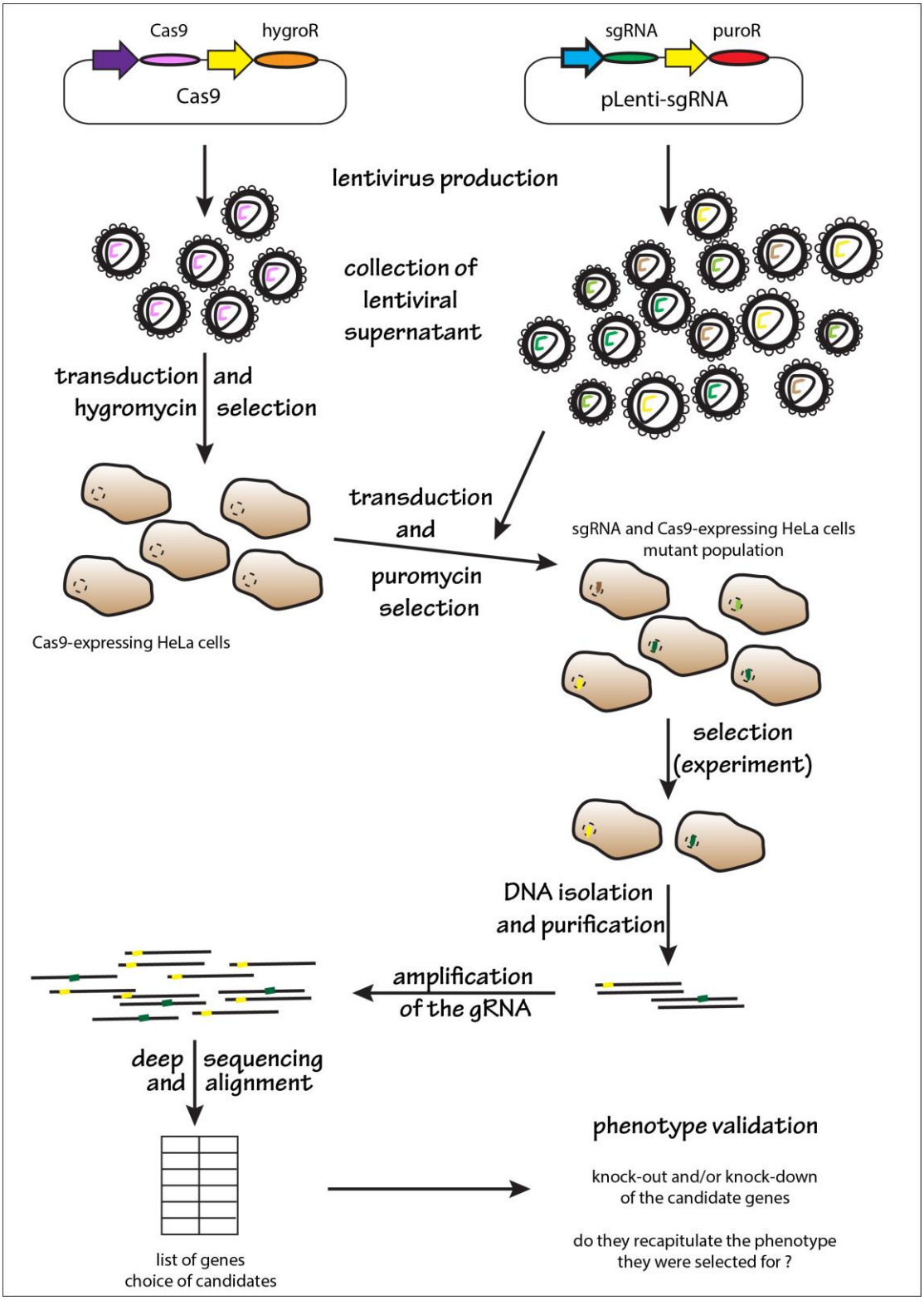

Figure 13: Overview of the workflow for a 2-plasmid CRISPR-Cas9 positive genetic screen

In order to select a mutated population based on a specific phenotype, lentiviruses expressing either the Cas9 or the gRNA library are produced. HeLa cells are then transduced and selected successively for the expression of Cas9 (hygromycin) and the gRNA library (puromycin). Mutated cells are submitted to the selection pressure (here the treatment required IFN-γ priming overnight followed by LPS transfection). In the case of a viability screen, DNA from surviving cells is extracted, purified and amplified before sequencing. Data analysis provides a list of potential 'hits' (candidate genes) that need to be validated.

2.3.3.1. Delivery of the components in the target cells

The CRISPR-Cas9 methodology requires two essential components: a CRISPR-associated endonuclease (Cas protein) and a sgRNA targeting the desired gene to mutate. Having a single vector to deliver Cas9 and a sgRNA into cells allows the simultaneous delivery of both components of the CRISPR system, eliminating the need to generate cell lines expressing Cas9 (Shalem et al., 2014). However, having the nuclease and the sgRNA on two separate plasmids can be advantageous for controlling the level of Cas9 expression. The introduction of Cas9 into cells can be followed by selection of one cell to be expanded in a clonal population. The clone may be chosen for its high expression of the Cas9 protein (within the limit of long-term cytotoxicity). The resulting clonal population would express a homogenous high level of Cas protein ensuring efficient and consistent knockouts. Having the gRNA library on a distinct plasmid also allows determination of the library titre for ensuring delivery of no more than one gRNA per cell (Koike-Yusa et al., 2014; Wang et al., 2014).

The Cas9 protein can be directly delivered into the cytosol and, because proteins are rapidly degraded, this can reduce the off-target effects. Mammalian cells can also be transfected with non-replicating plasmid DNA that will transiently express Cas9 and gRNAs (Cong et al., 2013; Mali et al., 2013) and, although transient expression of Cas9 has shown to be sufficient to perform successful CRISPR in living organisms (Jiang et al., 2014), constitutive expression increases Cas9-mediated knockout efficiency and does not impact the number of off-target cleavages (Koike-Yusa et al., 2014). The use of lentiviral vectors (**Fig.14**) offers the possibility of constitutive expression of both Cas9 and/or gRNAs (Shalem et al., 2014; Wang et al., 2014). Adding enrichment cassettes on the plasmids allows subsequent selection of

transduced cells (Koike-Yusa et al., 2014).

The lentiviral delivery of the CRISPR-Cas9 system (Aregger et al., 2019; Piccioni et al., 2018) is also used in primary cell lines, in cell lines difficult to transfect, or even *in vivo* (Aubrey et al., 2015). It has become a very attractive strategy for gene therapy applications (Chandrasekaran et al., 2018).

In this research project, a 2-plasmid system (Wang et al., 2014) was used (**Fig.14**): this procedure relied on the stable expression of the Cas9 protein being achieved before transducing the cells with the sgRNA pool to generate mutants and hence knockouts by producing DNA double-strand breaks. The sgRNA library targeted the whole human coding genome (18,543 genes) to provide an unbiased approach. The sgRNA library was designed without the Cas9 gene on the coding plasmids; therefore, Cas9 was expressed stably in the cells before they were transduced with the sgRNA library. Having a 2-plasmid system provided two key advantages. First, Cas9 expression and gRNA transduction could be successively selected with hygromycin and puromycin, respectively. Second, lentiviral supernatants generated for the gRNA library were titrated separately. Lentiviral supernatants were used for the transduction of cells and expression of both Cas9 and the gRNA library.

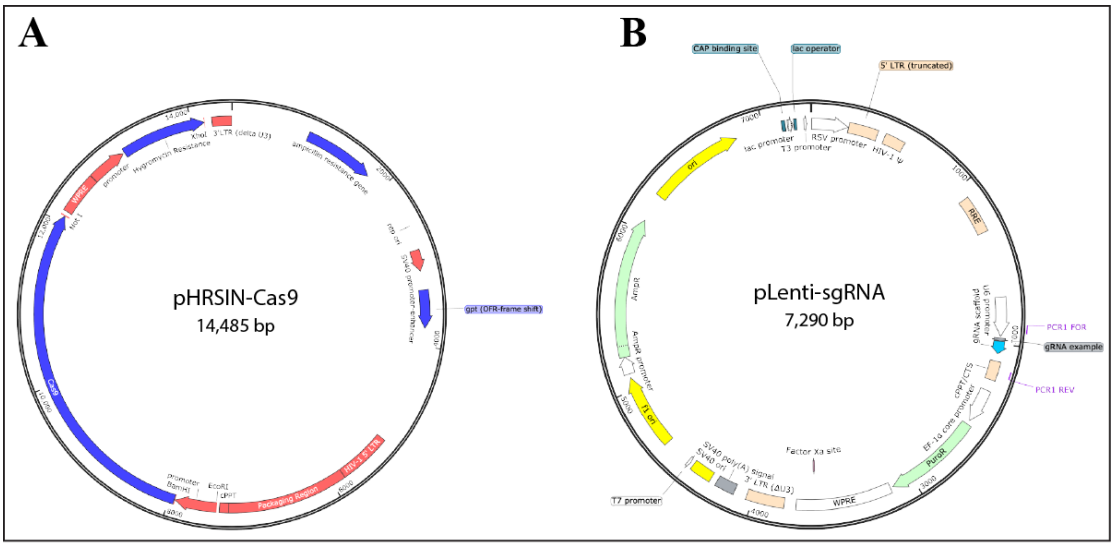

Figure 14: CRISPR screen using a 2-plasmid system

The CRISPR technology is based on two main components: (A) an endonuclease - Cas9- and (B) guide RNAs (gRNAs) that have a common scaffold and a specific sequence targeting the gene of interest.

The Cas9 gene was cloned into the pHRSIN vector by Dr. Jessica Noad and the gRNA library was obtained from Sabatini & Lander.

i. Stable expression of Cas9

HeLa cells were first transduced with lentiviruses expressing Cas9 using a high titre (1:2 dilution of viral supernatant) to ideally transduce all the cells, even with several copies of Cas9. A high level of expression of the Cas9 protein will ensure more efficient knockouts. Notwithstanding the high lentivirus titre, cells were still subjected to selection with hygromycin following transduction, to remove non-transduced cells (cells not expressing Cas9). The expression of the Cas9 protein was evidenced by western-blotting (**Fig.15A**): a specific band was detected at the expected size (MW_{Cas9} = 163.5 kDa) in the transduced and selected population.

To ensure that the expressed protein was functional, a test was performed using a gRNA against β2-microglobulin (**Fig.15B**). This guide was validated by Stuart Bloor (Paul Lehner's lab, Univ. of Cambridge). β2M is a major component of MHC Class I receptors and is required for their expression on the cell surface. Absence of expression or expression of a non-functional β2M would translate into impaired MHC Class I receptors synthesis and hence a decreased number of MHC Class I receptors on the cell surface. Probing for these receptors using a specific antibody (Parham et al., 1979), it was possible to visualise the extent of the β2M knockout. For this assay, Cas9-cells were transduced with the β2M guide and selected with puromycin. They were then stained for MHC I receptors. As expected, cells only expressing Cas9 but not the gRNA (blue curve) were positive for MHC Class I (**Fig.15C**). In addition, there was no background staining – unspecific binding – from the secondary antibody, since cells were negative for MHC I (orange and red curves) in the absence of the primary antibody (Alexa488 only). When Cas9-HeLa cells were treated with the β2M guide, two distinct populations of cells could be seen (green curve). At 5 days post-gRNA-transduction, the majority of the cells had an intermediate level of MHC Class I receptors, between the positive and negative controls. At 10 days post-gRNA-transduction, the main population overlapped with the negative population. The shift was time-dependent, and it appeared that knockout was properly established at 10

days post-gRNA-transduction. Targeting β2-microglobulin (β2M) resulted in progressive loss of this protein's expression. Some proteins have long half-life and, even in the case of an efficient knockout, they might still be present after many days. Although experiments were performed to try to assess the rate of MHC I turnover, the results were inconsistent and durations varied considerably with cell types, activation states, and even isotypes (Prevosto et al., 2016). The kinetics of protein turnover was visualised by the peak (green curve) moving to lower intensities and thus decreased expression of MHC Class I receptors (**Fig.15C**).

Even after 10 days, however, a residual fraction of cells was still MHC-positive. A slow turnover of MHC Class I receptors could not account for the presence of this positive population at 10 days post-gRNA transfection. By contrast, non-targeted cells still expressed MHC Class I receptors and thereby were stained during the experiment and could account for (part of) the residual peak of high intensity. There is also a possibility that the sequence of interest was effectively targeted and mutated but with in-frame indels, generating cells positive for the expression of MHC Class I receptors.

Because these MHC class I-positive cells survived puromycin selection, they should have been successfully transduced with β2M gRNA. However, it was possible that some DNA repair mechanisms were activated and successfully corrected the damage, enabling the protein to be expressed. Another explanation is that the DNA double-strand break created caused a non-deleterious mutation (e.g. in frame indels) and the functional β2M protein was still produced. Alternatively, these cells might not have expressed sufficient Cas9 to generate the targeted DNA double-strand break in the β2M gene. Another possibility is that, since HeLa cells frequently carry multiple copies of genes, the knockout could have only been partial and not target all the copies of the β2M gene present. These cells likely give a partial phenotype, i.e. decreased expression compared to wild-type.
Unfortunately, this resistant population constituted a pool of cells that could not be avoided. A higher number of cells would be necessary during the screen to compensate for this non-targeted population.

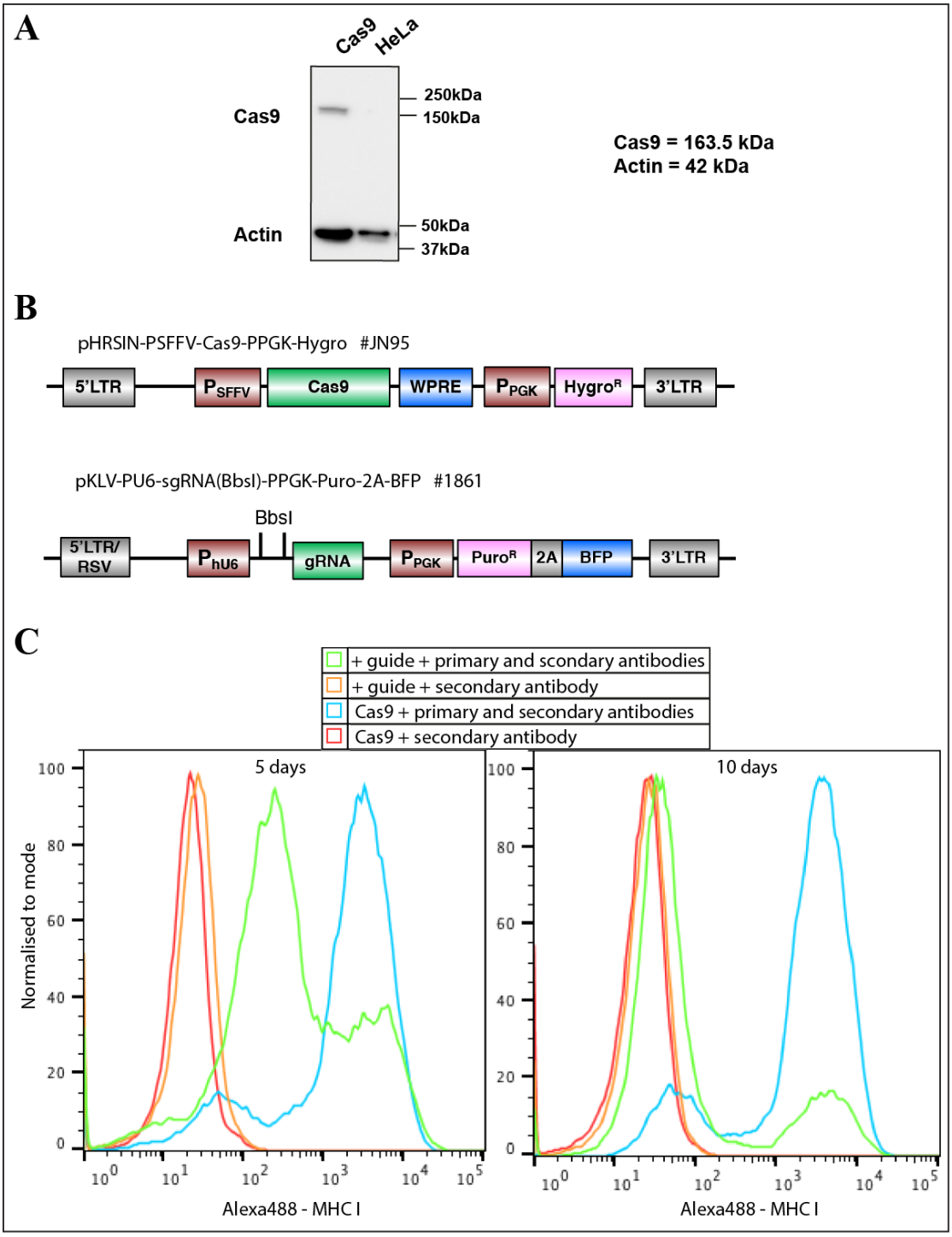

Figure 15: Cas9 was expressed and was functional

(A) The expression of Cas9 was confirmed by western-blotting. (B) Plasmid schematics for the expression of Cas9 and a gRNA targeting β2M. (C) After either 5 or 10 days of gRNA transduction, MHC Class I receptors were immunostained, and the cells analysed by flow cytometry to assess the extent to which the MHC Class I receptors had been removed from the cell surface. Controls (red and orange curves) were cells incubated only with the secondary antibody to measure any non-specific fluorescence signal; cells expressing only Cas9 (cyan curve) were stained by the antibody as they carry MHC Class I receptors on their surface, providing a positive control to compare with; over time, the number of MHC Class I receptors decreased in cells transduced with both the Cas9 protein and the gRNA targeting β2M (green curve).

The Cas9 plasmid was generated by Dr. Jessica Noad and the #1861 gRNA-containing vector was kindly provided by Dr. Stuart Bloor.

Overall, these experiments indicated that the screen, and any other experiment requiring knockouts, should commence at least 10-12 days after transduction with the gRNA library in Cas9-expressing cells in order to allow sufficient time for the knockouts to achieve maximum efficiency. Waiting more than a week was also a way to lose essential genes, thus eliminating cells that carried deleterious mutations that would not survive for this length of time. Accordingly, the background population of cells that was sequenced as reference was sampled at the start of the screen to maximise its being representative of the initial population going into the screening process.

ii. The gRNA library

To knockout cells in a "random" and unbiased way, a genome-wide human gRNA library was used (Park et al., 2016). Because of the 2-plasmid system, the transduction of gRNA was performed into Cas9-expressing cells at a MOI of 0.36, so that cells were targeted by only a single gRNA and so would be mutated in only one gene.

The gRNA library contained a total of 187,536 gRNAs targeting the whole human genome. This corresponds to an average of 10 guides per gene; the number of human protein-coding genes is estimated to be around 20,000 (Wang et al., 2015). The gRNA library was received as three aliquots and was split into three sub-libraries (hL1nC9, hL2nC9, hL3nC9) approximately containing 90,000, 90,000 and 5,000 guides, respectively. These three sub-pools were transformed and expanded separately, and the resulting plasmids were purified. The three sub-pools of purified plasmids were then carefully quantified by qPCR and mixed, based on their individual concentration and the ratio (18:18:1) of the number of guides in each to be sequenced on the MiSeq. Sequences were aligned to the reference provided by the supplier. Overall, 1.025 million reads could be aligned, representing 64% of the total number of reads produced by the analysis (**Fig. 16A**). Among the sequences known to be in the library, 10.16% of them could not be found in the sequenced sample (missing guides). By

contrast, the supplier performed a more comprehensive analysis leading to 4.324 million aligned reads and resulting in only 0.94% of guides missing. The guide distribution in the transformed library was assessed (**Fig.16B**) by looking at the contribution of each gRNA – percentage of representation – to the total gRNA count. The transformed library was not excessively skewed as the initial slope of the curve (**Fig.16B**) was close to the ideal representation (black dashed line), whereby every guide contributes the same to the overall library. In addition, the curve reached a plateau, meaning that some gRNAs were not represented. This was expected given that 10.16% of the guides were missing (**Fig.16A**), which corresponds to a total of 168,482 guides being present (**Fig.16B**).

The overall number of reads per guide was established to be on average 5.7 (**Fig. 16A**) following the sequencing on the MiSeq, compared to 23.1 in the data provided by the supplier, which paralleled the total number of reads (and hence the depth of the analysis). However, increasing the number of reads per guide exponentially decreases the percentage of missing guides in the analysis (**Fig.16C**). Sequencing experiments were performed with three different gRNA libraries. For each library, various numbers of reads were simulated, and, in each case, the randomised results were aligned to the reference and the percentage of missing guides was calculated. For the same sample, the calculated representation of the overall library depended strongly on the number of reads per guide available to assess the percentage of missing guides. For all three libraries tested, increasing the number of reads per guide from 2 to 8 (**Fig.16C**) did, in turn, significantly decrease the percentage of missing guides from 25% to 1%, even though tested samples were identical and only the depth of analysis differed.

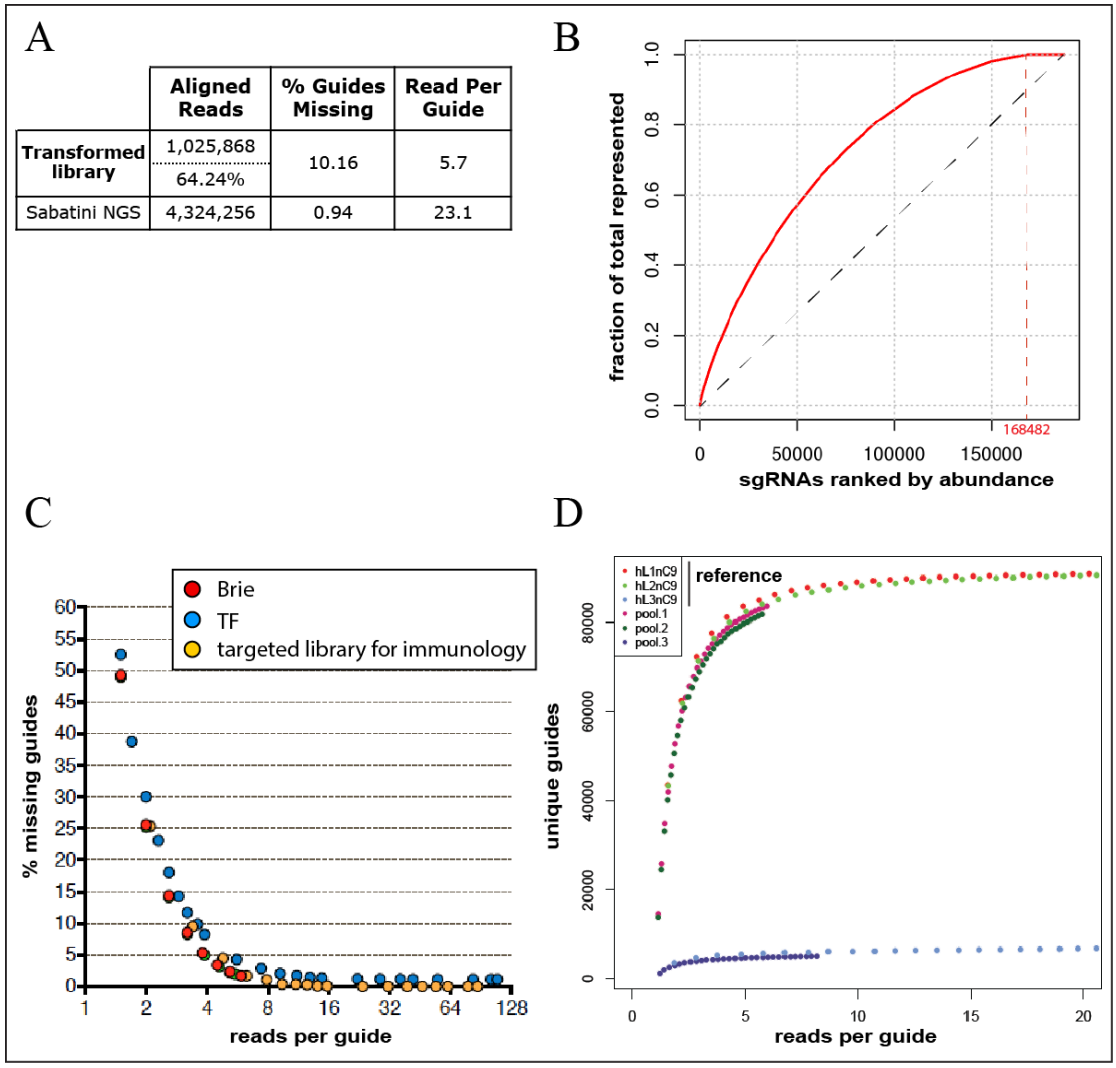

	Aligned Reads	% Guides Missing	Read Per Guide
Transformed library	1,025,868 / 64.24%	10.16	5.7
Sabatini NGS	4,324,256	0.94	23.1

Figure 16: Comparison between the transformed and the reference gRNA libraries

After transformation, the gRNA library was sequenced on the MiSeq. Sequences were demultiplexed (pools 1-3) and aligned to the list given as reference (hL1-3nC9). (A) Comparison of the read counts and proportion of missing guides in the entire library with the NGS data from the supplier. (B) The entire library was plotted on a cumulative curve after ranking all the guides by decreasing abundance. (C) Three other gRNA libraries of various sizes were subjected to high-depth sequencing, and the results were randomly sampled for an increased depth of analysis, looking at a particular number of reads and evaluating the percentage of missing guides in the overall library. For each gRNA library, the same initial samples were used, but the analysis was done differently. For multiple average numbers of reads per guide, the percentage of missing guide in the entire library was calculated based on the comparison to the supplier's data. Experiments performed and data collected by Dr. Patrycja Kozik to generate the data in this panel of the figure (C). (D) The three individual sub-pools (pool1, pool2, pool3) were also plotted to compare them to the reference (hL1nC9, hL2nC9, hL3nC9, respectively).

The sequencing data could also be compared to the supplier's in a sub-library specific manner (**Fig.16D**). It was possible to demultiplex the sequences and identify for each sequence the sub-pool to which it belonged. The three sub-pools (pools 1, 2, 3) were individually compared to the data from the supplier (hL1nC9, hL2nC9, hL3nC9 respectively). To assess the extent to which the distributions matched, multiple numbers of reads per guide were simulated to randomly generate lists of analysed sequences. With only a few counts per guide, the diversity of the selected sequences (and hence the number of unique guides – i.e. newly seen in the analysis) was the greatest. Increasing the number of reads per guide allowed the identification of a few more new guides, but mostly contributed to increase the numbers of guide counts (**Fig.16D)**. Curves for pools 1-3 were much shorter than the curves drawn for the reference, but this was expected and was consistent with the much lower number of reads (1,025,868) obtained compared to the supplier (4,324,256). For each subset, the two curves – from the transformed library and the reference – almost overlapped. The curves from the reference reached plateaus corresponding to the total number of different guides in each sub-pool, 90,000, 90,000 or 5,000 respectively. Curves obtained for the transformed library sub-pools did not reach these plateaus since the numbers of reads per guide generated were not sufficient. However, based on the relationship between number of reads per guide and percentage of missing guides described above (**Fig.16C**), the transformed library was considered to be representative of the initial library and hence suitable for use in future experiments. If the sequencing had been deeper (more total reads) and of better quality (more aligned sequences) leading to a higher number of reads per guide, the percentage of missing guides would decrease in the analysis.

Because the transformed gRNA library was deemed satisfactory in terms of representation and identity to the template, the three sub-pools were then used to create knockouts. 293ET cells were used to produce lentiviruses expressing the gRNA library. The lentiviral supernatant was titrated (**Fig.17A**) in order to establish the dilution to use to transduce the Cas9 cells. It was important that no more than one gRNA entered a single Cas9-expressing cell, since cells used for the screen must be mutated only in one target gene by a single gRNA. Having two or more guides knocking out several genes in one cell would prevent identification of the gene responsible for resistance to IFN-γ-induced, LPS-triggered cell death in the screen.

Also, cells without guides (i.e. non-transduced cells) would be discarded during the puromycin selection. Thus, the transduction should aim for a multiplicity of infection (MOI) of 0.36, which corresponded to 30% infected cells (**Fig.17B**).

The titration was performed by transducing cells with a range of dilutions of lentiviral supernatant, followed by selection with puromycin. Cell death was measured by using PI staining and analysed by flow cytometry. This led to a percentage of surviving cells (PI-negative) compared to non-transduced cells which all died (0%). A MOI = 0.36 would be achieved for 30% of Cas9-expressing cells being transduced with the gRNA library, which translated in 30% puromycin-resistant cells (**Fig.17B**). This proportion was achieved for a 1:500 dilution of the virus (**Fig.17A**). Therefore, the cell population for the screen was transduced with a 1:500 dilution of lentiviral supernatant for the gRNA library. This would enable the generation of mutant cells using the CRISPR-Cas9 technology in which the entire human genome had been targeted. In addition, the strategy of the screen based on the ability of enriching for a population of cells resistant to death upon LPS transfection and after IFN-γ priming was validated with CrmA-expressing cells.

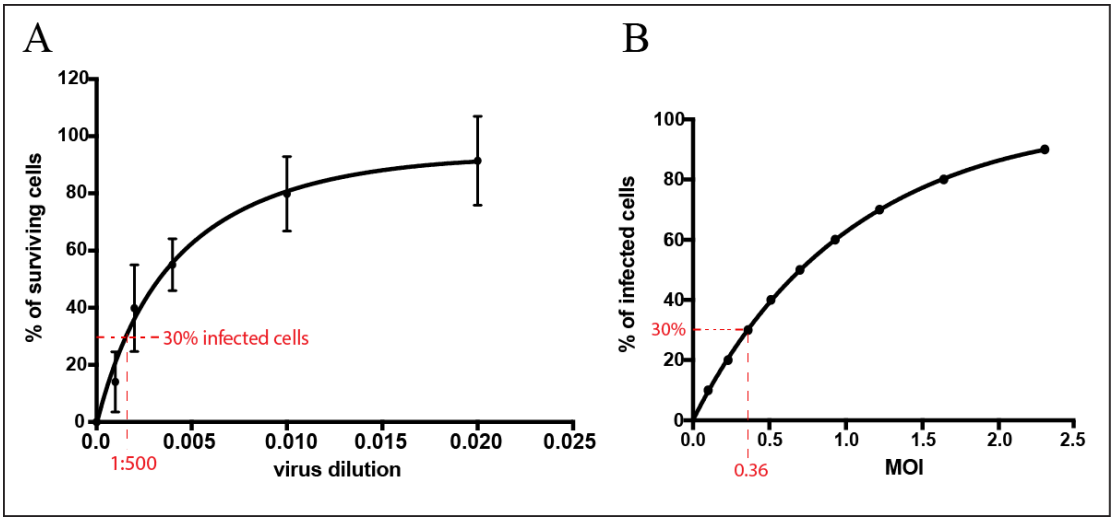

Figure 17: Titration of the guide RNA library

293ET cells had been transfected to generate lentiviral supernatant coding for the gRNA library. Cas9-expressing HeLa cells were then transduced with a range of quantities of lentiviral supernatant. The titer was assessed by looking at cell death following puromycin selection three days after gRNA transduction in HeLa cells. Cell death was analysed by flow cytometry using PI staining. (A) The percentage of surviving (transduced) cells was calculated relative to cells that were not transduced (0%) and cells transduced with non-diluted supernatant (100%). (B) Graph used as a reference for the conversion between infection and multiplicity of infection (MOI).

2.3.3.2. Screening process

This genetic screen aims to unravel the mechanism behind LPS-triggered cell death upon IFN-γ priming, by identifying new genes that are essential in the cell death pathway triggered by cytosolic LPS in IFN-γ-primed cells using CRISPR.

Two IFN-γ inducible genes (CASP4 and GSDMD) that play a role in the LPS-triggered cell death pathway were tested as candidates (see paragraph **2.2.3**. "Role of Caspase-4 and Gasdermin-D in the IFN-γ-dependent, LPS-triggered cell death pathway"), but it was clear that other genes were also involved in this pathway. CASP4 is a homolog of the mouse caspase-11, which has been described to bind directly to LPS and trigger a non-canonical inflammasome resulting in cell death. GSDMD is an effector in pyroptosis, an inflammatory but regulated form of cell death. However, neither CASP4 nor GSDMD was sufficient to account for the IFN-γ-dependent, LPS-triggered cell death pathway. Although IFNGR1, CASP4 and GSDMD are all required in the IFN-γ-induced, LPS-triggered cell death pathway, none of them adequately explain IFN-γ-induced, LPS-triggered cell death.

An unbiased forward genetic screen using the CRISPR-Cas9 technology was used in order to find new genes involved in the IFN-γ dependent cell death pathway triggered by cytosolic LPS. Cells were mutated using a human genome-wide gRNA library and then challenged with the selection pressure; that is priming with IFN-γ followed by transfection with LPS. The objective was to isolate mutants that were resistant to cell death; these cells should carry mutations either in the cell death pathway and thus be required in one of the steps between detection of the LPS as a trigger and the cell dying or in the IFN-γ signalling pathway. DNA sequencing of resistant cells would allow identification of the gRNAs carried by these mutants and that should enable identification of the genes necessary for cell death to occur.

The selection pressure on the cells was provided by LPS transfection after IFN-γ priming overnight. This killing method did not give 100% cell death with the control

cells; therefore, the cells that survive after a single transfection might be interesting mutants, but could conversely contain cells that would have escaped from the selection, i.e. cells that were not affected by the treatment. For that reason, several rounds of LPS transfection were performed with the aim of enriching more stringently for genuinely resistant mutants (**Fig.18**).

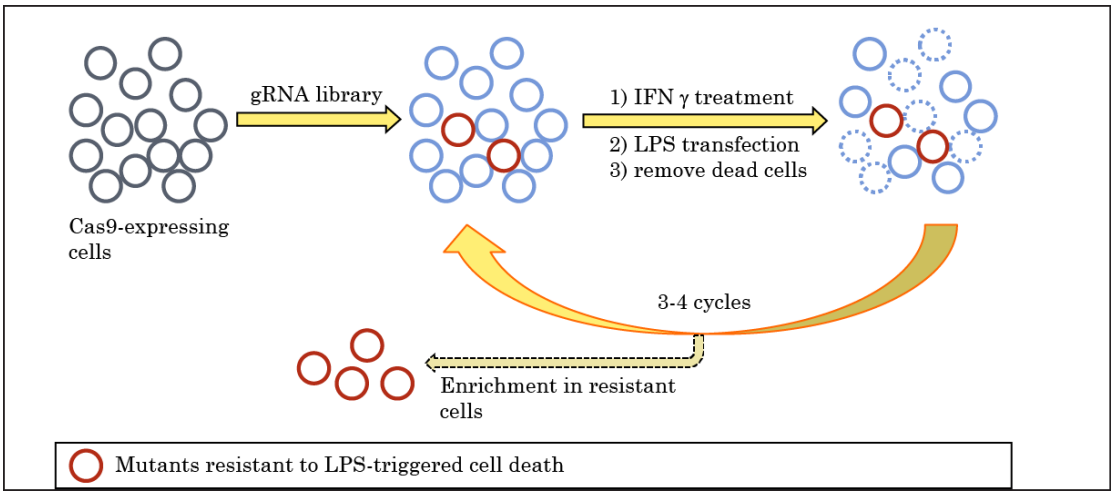

Figure 18: Forward genetic screen based on LPS-transfection

Scheme of the strategy laid out for isolating CRISPR-mutated and IFN-γ-primed cells resistant to LPS-triggered death. Cells were subjected to several rounds of selection, each involving priming overnight with IFN-γ followed by transfection on the next day with LPS.

i. Keeping the gRNA representation

The library representation is defined by the number of molecules of each sgRNA present at any time during the screen: the higher the representation, the more robust the screen (Strezoska et al., 2012). A low library representation results in high background noise and either identification of false positives due to random depletion in the case of negative selection (Schuster et al., 2019), or increased loss of positive 'hits' in positive selection. Certain screen conditions create a natural bottleneck, which is expected in positive screens and leads to decreased library representation. In this case, starting with a library exhibiting a 500-1000-fold representation is necessary (Joung et al., 2017). The library representation is assessed at each step of the screen and is largely dependent on the number of cells used in the screen. When the number of cells to handle becomes problematic, it is advisable to limit the library size rather than compromise on the representation.

In this project, the representation of the library was, at all times, maintained over 500-fold the number of guides; at each step during the screen, a minimum of 10^8 cells were used.

ii. Selection process and timeline

A period of at least a week shall be left after sgRNA transduction before starting the screen to allow time for selection of transduced cells and recovery from selection and cell expansion (see paragraph **2.3.3.1**. "Delivery of the components in the target cells"). The knockout generated using CRISPR-Cas9 has been found to be optimal (most efficient) seven days after gRNA transduction (Joung et al., 2017). In case of constitutive expression of Cas9, one should ensure that the cells tolerate prolonged expression of the nuclease. The duration of viability screens is dictated by the population doubling time because a certain number of mitoses is necessary to observe the phenotype.

In this project, HeLa cells were mutated using the CRISPR technology with a genome-wide human gRNA library. The screen was carried over a time period of a month because a total of five rounds of enrichment were performed (**Fig.19A**). One round of selection consisted of overnight IFN-γ priming followed by LPS transfection, after which surviving cells were carried on to the next round. By the end of this procedure, the population should contain cells that carry a mutation in genes required in the IFN-γ-induced, LPS-triggered cell death pathway.

Throughout the entire process, efforts were made to provide adequate coverage of the entire gRNA library (Hart et al., 2017) and keep the representation throughout the screen by using appropriate numbers of cells (Schuster et al., 2019). It was assumed that initially having 100-fold coverage, that is 100 times more cells than the number of gRNAs in the library, would ensure significant signal over noise during the sequencing analysis. The sgRNA library (Park et al., 2016) contained $1.87x10^5$ gRNAs, indicating that a population of $2x10^7$ cells should be maintained to keep this 100x coverage. However, getting 20 million mutated cells retrospectively meant that at least 60 million cells had to be transduced, since the MOI was chosen to target only 30% of cells with the gRNA library.

In the experiment, 80 million Cas9-expressing cells were transduced with the gRNA library lentiviral supernatant, used at 1:500 dilution according to the titration performed previously (**Fig.17A**). After 48h, cells were submitted to puromycin treatment to select for cells transduced with a gRNA. Cells were grown under puromycin selection for five more days, after which the cells were grown under selection conditions with both hygromycin and puromycin, in order to maintain a population expressing both Cas9 and a gRNA, respectively. Twelve days after gRNA transduction and 15 days after Cas9 transduction, 320 million cells were primed with IFN-γ overnight. Of this total amount, 100 million (500-fold coverage) were treated only with Lipofectamine2000, whereas the other 220 million (1100-fold coverage) were transfected with LPS. On the following day, the control cells (those treated only with transfection reagent) were harvested, pelleted down, and frozen. They constituted the starting point of the screen; thenceforward, their genetic information would serve as the reference ('- cells').

Only 5.4% of the LPS-challenged cells survived the first round (**Fig.19B**), but they were expanded again to 200 million cells. On day 20 after gRNA transduction, they were primed with IFN-γ. On the following day, 120 million (600-fold coverage) were transfected with LPS while the other 80 million ('+ cells') were treated only with Lipofectamine2000.

This time and for the subsequent rounds, the cells treated only with Lipofectamine (but already selected on previous rounds) were grown alongside the selected population. Therefore, at the end of the screen, five different batches of cells ('+ cells' to '5+ cells') were grown at the same time (**Fig.19C**). They came from the successive (1 to 5) rounds of enrichment. They were all pelleted and frozen down at the same time. The pelleted and frozen cells were later used for sequencing.

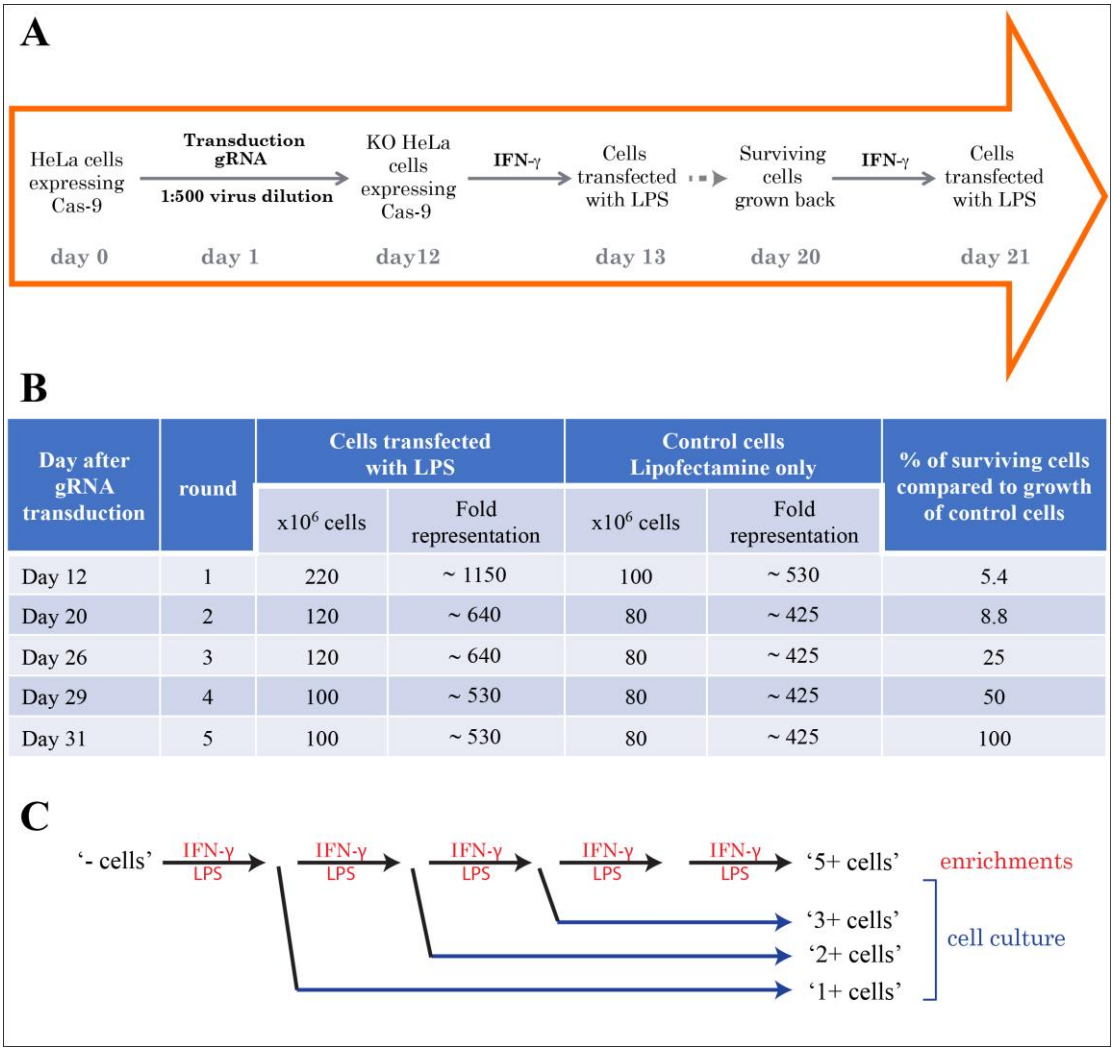

Day after gRNA transduction	round	Cells transfected with LPS		Control cells Lipofectamine only		% of surviving cells compared to growth of control cells
		x10^6 cells	Fold representation	x10^6 cells	Fold representation	
Day 12	1	220	~ 1150	100	~ 530	5.4
Day 20	2	120	~ 640	80	~ 425	8.8
Day 26	3	120	~ 640	80	~ 425	25
Day 29	4	100	~ 530	80	~ 425	50
Day 31	5	100	~ 530	80	~ 425	100

Figure 19: The five rounds of enrichment were performed over a month

(A) A rough timeline showing the first few rounds of enrichment in the screen that lasted 28 days. For each round of selection, the number of cells used was calculated and the amount of cell death was estimated by comparing cell numbers to non-treated cells (B). After each round of enrichment, cells were kept in culture to be frozen at the same time point at the end of the screen (C), no matter which enrichment round there were stopped at.

The initial Cas9- and gRNA-transduced cells were frozen down at the very start of the screen. In this respect, they represented the initial population that was submitted to the first round of selection. They provided a population that could be used to assess the efficiency of the gRNA transduction. Based on the sequencing of that sample, information was obtained concerning the representation of the whole library in the cellular context rather than at the plasmid level (**Fig.16**). Because the sequencing of the '- cells' yielded more reads than the MiSeq data first generated on the transformed

plasmid library, it appeared that only 3.3% of the guides were missing compared to the original plasmid library. This result was obtained from the total percentage of missing guides (13.3%) by subtracting the 10% of sgRNAs in the library that target essential genes. After 10 days, cells mutated in essential genes would have been lost following natural selection.

By contrast, all the populations of cells challenged by one or multiple LPS transfection(s) were kept and maintained throughout the duration of the screen. This was done with the aim of having more comparable samples with cells having had the same life span.

2.3.3.3. Data analysis

Cells are collected and, following DNA amplification for enrichment of the barcodes tagging the gRNAs, the DNA is sequenced using next-generation sequencing (NGS) to identify the gRNAs (**Fig.13**). The readout is based on the relative abundance of the various sgRNA calculated from the number of reads for each guide. To ensure robust analysis, the number of reads must be within the 30-300 window. Analysis software such as MAGeCK (Li et al., 2014) generates a ranking of all the genes and potential 'hits' can then be further validated.

i. Preparation of the samples for sequencing

Cell pellets (see paragraph **2.3.3.2**. "Screening process") were thawed, and the genomic DNA was extracted before being purified. DNA was subjected to several steps of genomic amplification (**Fig.20A**) before analysis by sequencing. Purified DNA was submitted to two amplifications (**Fig.20B**) by PCR (PCR1 and PCR2).

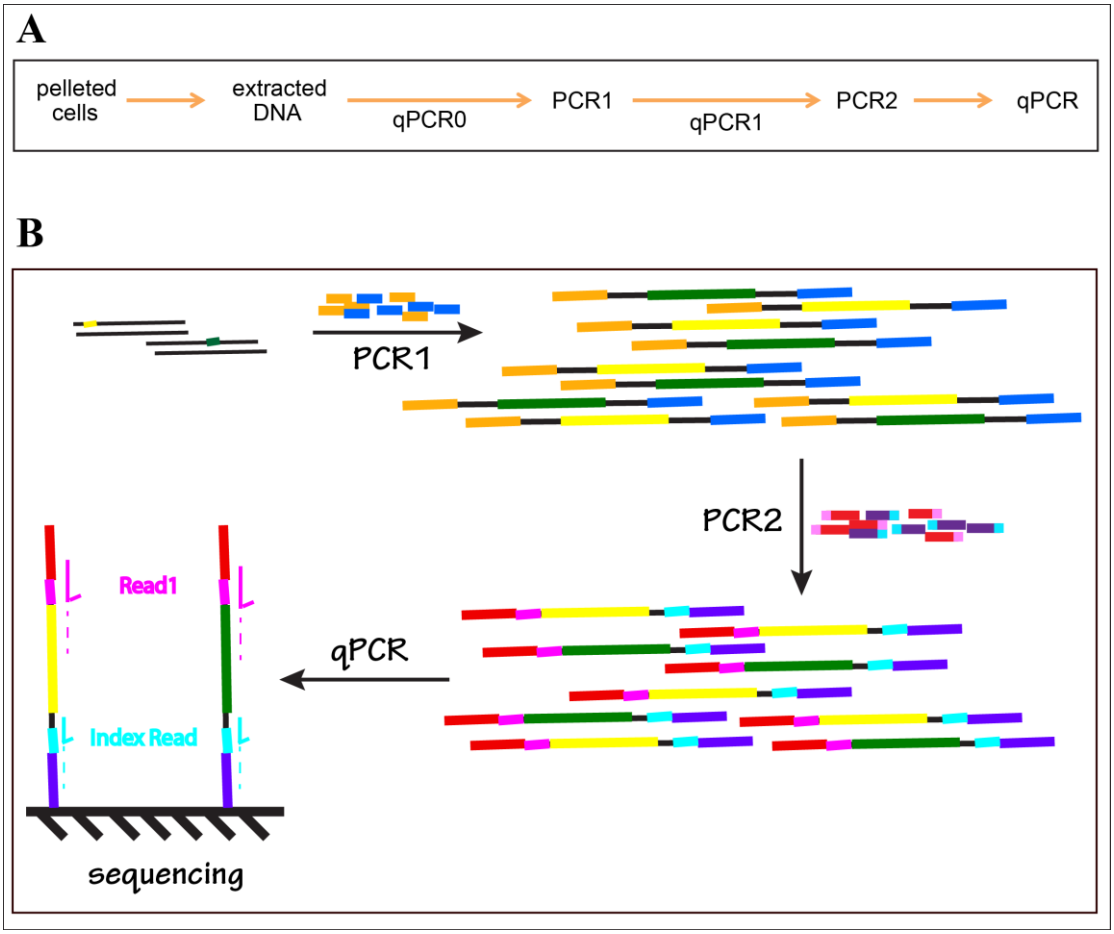

Figure 20: Several PCRs were needed to prepare the samples for sequencing

(A) Scheme of the successive sample preparation steps necessary to perform new-generation sequencing on genomic DNA extracted after the experiment (i.e. from resistant cells to the IFN-γ/LPS transfection treatment): (B) genomic DNA was amplified (PCR1 and PCR2) and gRNA sequences (green and yellow) were flanked, in PCR2, with Illumina adaptors (red and purple) that are necessary for sequencing before precise quantification by qPCR and submission to sequencing.

The full protocol is detailed in **Chapter 4**, paragraph **4.9.2**. "gRNA amplification and sample barcoding". In summary, qPCR0 (see **Chapter 4**, **Fig.2**) was performed to make sure that the primers designed for PCR1 bound and amplified the expected fragment of genomic DNA at the concentration of the purified sample. The primers tested were amplifying as expected and were used in PCR1. Following PCR1, crude products were taken onto qPCR1 in which PCR2 conditions were tested to determine the appropriate number of cycles needed (see **Chapter 4**, **Fig.4**). The PCR2 was therefore run with 20 cycles of amplification. PCR2 products were purified (see **Chapter 4**, **Fig.5**) and then quantified by qPCR (see **Chapter 4**, **Fig.6**). Samples

submitted to sequencing can contain several different cell batches, provided they are individually barcoded in PCR2 and individually quantified in qPCR.

The number of different cell batches in one sample could vary depending on the sequencing depth required. In this case, only two cell batches were submitted in one lane to obtain at least 100x coverage of the entire library that contained ~$2x10^5$ gRNAs. At first, samples from cells frozen before any LPS transfection ('- cells') and cells having been through three rounds of enrichment ('3+ cells') were submitted for sequencing. The second sequencing submission contained cells challenged with one or two LPS transfection(s), '1+ cells' and '2+ cells' respectively.

ii. Sequencing results

The sequences generated by the HiSeq were sorted into two lists: sequences were assigned to the sample from which they originated (demultiplexing), based on the barcode they carried: '- cells' (initial population that had not experienced LPS transfection) or '3+ cells' (cells that had experienced three rounds of selection). The step of demultiplexing was followed by alignment of the trimmed sequences to the reference library. Each gRNA present in the library was attributed the number of copies of their sequences that were found in the analysis. The initial population ('- cells') was treated with IFN-γ overnight and mock transfected with medium containing Lipofectamine2000, although without adding LPS. The sequencing of this population showed the representation of the gRNA library in cells (**Fig.21A,** red curve), as opposed to the previous MiSeq data (**Fig.16B**) performed at the plasmid level.

The curve (**Fig.21A**) shows the representation of the library: it is a cumulative plot for which contributions of each gRNA are added up according to decreasing abundance. The initial slope accounts for the most abundant gRNAs: the steeper the slope, the more enriched the first few gRNAs. Since the screen was designed to enrich genes playing a role in the IFN-γ-induced, LPS-triggered cell death pathway (i.e. gRNAs), it was expected that the most abundant gRNAs contributed progressively more as the number of enrichment rounds increased. Indeed, comparing the library representation

for all four samples (**Fig.21A**), the initial slope grew steeper as an increasing number of enrichments was performed and the top ranked gRNAs significantly outnumbered the other gRNAs. The curve eventually reaches a plateau in all cases, indicating that some gRNAs did not contribute to the representation and hence were depleted from the sample. This plateau was reached earlier as the number of enrichment rounds increased because selection was depleting many gRNAs.
Overall, some gRNAs were depleted while some others became further enriched, validating the selection pressure and the screening process.

The median number of guide counts for each gene was determined and each round of enrichment was plotted to visualise whether some genes were enriched (**Fig.21B**). As expected, non-targeting guides (orange dots) were not enriched over the course of the successive selection rounds. These dot plots, which compare median gRNA counts for each gene, showed that '- cells' already had a significant number of enriched genes known in the IFN-γ signalling pathway such as JAKs 1 and 2, IFNGR1 and STAT-1. This observation makes sense since '- cells' were primed overnight with IFN-γ, even though they were not treated subsequently with LPS. The first round of enrichment ('+ cells') showed further enrichment of CASP8 and also JAK1 and IFNGR1. The second selection round (from '+ cells' to '2+ cells') was the most successful in enriching for genes; all the genes in the IFN-γ signalling pathway (JAK1, STAT-1, IFNGR1, JAK2, IFNGR2) stood out (**Fig.21B**). Other genes, such as CASP4 and GSDMD were also expected to be enriched and were indeed distinct from the majority of the other genes. CASP8 was also isolated in this second round. In the third and final round of enrichment (from '2+ cells' to '3+ cells'), genes for IFNGRs (1 and 2), JAKs (1 and 2), CASP4 and -8, were enriched and were very clearly separated from the rest.

Although GSDMD did not segregate out as a potential 'hit' from the screen, the observation that most genes in the IFN-γ signalling pathway were enriched gave confidence that the screen had worked satisfactorily.

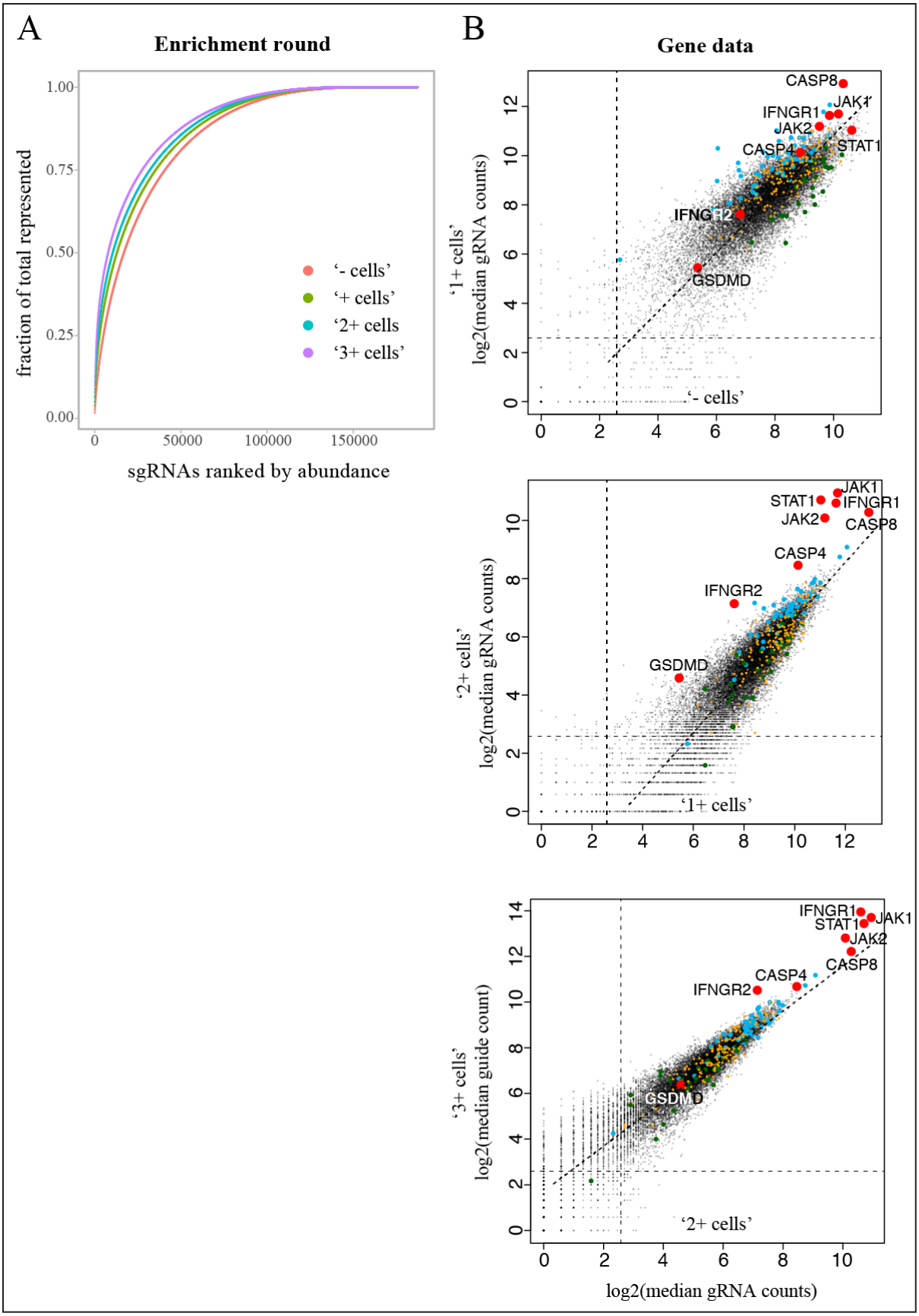

Figure 21: Progressive enrichment for resistant cells during the screen

(A) The gRNA libraries sequenced after the four distinct stages of the screen: before treatment (red) or sampled at each round of enrichment (1:green, 2:blue, 3:purple) were plotted on a cumulative curve after ranking all the guides by decreasing abundance to show progressive depletion in gRNAs and loss of diversity. (B) For the three rounds of enrichment, the median number of gRNA counts for each gene was represented showing whether the genes were enriched or depleted (respectively higher or lower than the diagonal) over the course of the screen.

In all the plots (**Fig.21B**), blue and dark green dots represent enriched and depleted genes (respectively), as calculated by the enrichment fold: that is, the measure of the difference in the representation of a gene and/or gRNA in the selected population compared against a reference population. Since the goal of the screen was to find genes involved in the IFN-γ-induced, LPS-triggered cell death pathway, the genes in the successive rounds of enrichment ('3+', '2+' or '1+ cells') were all compared to their counterpart in the initial population ('- cells', never treated) in order to calculate their enrichment ratios. The sequencing data were processed to score the genes using the MAGeCK algorithm (Li et al., 2014) which considers the library size, the count distribution and the 10 gRNAs available for each gene, generating a ranking of all the genes tested (if found in the sequencing data). After the third round of selection (LPS transfection of IFN-γ primed cells), cell death on a population level had decreased significantly compared to the first two: 25% of surviving cells compared to 5.4% or 8.8%, respectively (**Fig.19B**). The percentage of surviving cells continued to increase in subsequent rounds (50% in round 4); however, resistant cells could be mutated in genes favouring hyperproliferation. This could give them a survival advantage not specific to LPS-triggered cell death and may result in them outnumbering the true 'hits'. '3+ cells' were chosen as a suitable compromise that comprised both a majority of resistant cells and allowed sampling early enough in the screen to avoid false positives.

Table 1 shows the first 50 genes in the 'hit' list comparing the fold enrichment seen in the '3+ cells' compared to '- cells'. Three different analytical methods were used: MAGeCK (Li et al., 2014), RSA (König et al., 2007) and "5th guide" using Fisher's and Wilcoxon tests to calculate p-values (Prabhakaran, S., 2016-2017). The screen identified genes (**Table 1**) potentially playing a role in the IFN-γ induced, LPS-

triggered cell death phenotype. Some highly ranked genes, such as interferon-γ receptors (IFNGR1 and IFNGR2), Janus kinases (JAK1 and JAK2) and STAT-1 were expected because they are major genes in the IFN-γ sensing and signalling pathways. Since the screen identified 'hits' but did not demonstrate directly that they were required in the IFN-γ-induced, LPS-triggered cell death pathway, candidates from the 'hit' list were selected for validation (green). Among the expected 'hits', only IFNGR1 and STAT-1 were carried on to validation experiments to serve as positive controls – i.e. genes necessary for the IFN-γ induced, LPS-triggered cell death to occur.

rank	MagecK	RSA	"5th guide"
1	JAK1	JAK1	JAK1
2	IFNGR2	IFNGR2	STAT1
3	IFNGR1	IFNGR1	IFNGR1
4	JAK2	JAK2	JAK2
5	ELAVL2	STAT1	IFNGR2
6	TMEM143	CASP8	CASP4
7	STAT1	ELAVL2	ECD
8	CASP4	CASP4	TM9SF2
9	SLC25A37	NCKAP1	NCKAP1
10	NCKAP1	FIP1L1	SRSF10
11	HSPH1	CARM1	CASP8
12	QRICH1	CTNNBL1	PLEKHM2
13	LTK	SAFB	GPR148
14	PISD	OVOL3	METAP1D
15	LRIG1	SRSF10	KLRG1
16	TM9SF2	CXCR4	ENTHD1
17	ALG12	C19orf52	SAFB
18	BTF3	HSPH1	CXCR4
19	USP19	BID	CDK9
20	TSNAXIP1	IL17F	HFE
21	CASP8	TM9SF2	EMC2
22	SRSF10	CDH1	GPR61
23	CDK9	SLC25A37	AGAP6
24	HAPLN3	CDK9	DPT
25	MYL6	SNED1	LPA
26	SYN2	ALG12	IL17F
27	TECR	NUTM2F	APBA3
28	NUTM2F	PKN3	ACTR3
29	INCENP	BIN1	ALG12
30	WDFY4	RAB3B	TTN
31	C19orf52	INCENP	SIRT7
32	CDH1	ITGA9	CAPN9
33	PFKP	TGFBR2	SCYL1
34	FAM171B	HAPLN3	AXL
35	DFFB	MYL6	TNFRSF12A
36	POLG	KEAP1	CTNNBL1
37	HOXC13	AXL	NKD2
38	CD1C	C8orf74	FBXW7
39	SAFB	POP4	ZNF556
40	PIP4K2C	SLIT2	MAPKAPK2
41	TLN1	APBA3	KLHL5
42	POP4	CNTNAP3B	NPC1L1
43	DNAH5	HTR6	RAB38
44	DNAJB11	PRB3	POLR2B
45	RNF32	LMOD2	RPL22
46	KRTAP9-9	QRICH1	LMLN
47	PRM2	AKAP2	CEP41
48	SRRM3	AMY1A	C10orf76
49	FAM96A	AMY1B	SLIT2
50	STX1B	AMY1C	HNRNPL

genes involved in IFN-γ signalling

Casp-4 was an expected hit

genes chosen for validation

Table 1: List of the top 50 genes obtained from the sequencing

Sequencing data from the '3+ cells' were compared to '- cells' to calculate the enrichment fold of each gRNA; values that were then used to rank the genes contained in the library. Genes were ranked using three different statistical methods: MAGeCK which was developped with the advent of CRISPR, RSA already used mostly in the case of RNAi screens and "5th guide" which considers the rank of the 5th guide (median) for each gene when all guides are

ranked according to their enrichment fold. In each list, genes in the IFN-γ signalling pathway (red), CASP4 (cyan) as an expected 'hit' and the genes chosen for validation (green) are highlighted.

iii. Interpretation of the data

After the validation experiments, results from either the third round or the first three rounds combined were represented using volcano plots. This gives a graphical visualisation of the genes that were enriched (blue) or depleted (dark green) in the screen. In both plots, 'hits' with the highest confidence (-log p-value > 4) were genes expected because they are key players in the IFN-γ signalling pathway, namely JAKs (1 and 2), IFNGRs (1 and 2), STAT-1. Caspases-4 and -8 were also clearly identified as positive regulators in the IFN-γ-induced, LPS-triggered cell death pathway. Focusing on the third round of enrichment (**Fig.22A**), the candidates chosen for validation (BID, NCKAP1 and SAFB, see paragraph **2.3.4** "Validation of the hits") were also significantly enriched (-log p-value > 3). Additionally, SMAD4, LCORL, EXOC2, and CHD8 showed similar enrichment confidence and should be considered in further validation experiments. SMAD4 (Mothers against decapentaplegic homolog 4) is involved in the transforming growth factor (TGF) signalling pathway in which it acts in conjunction with either DPC4 (Liu et al., 1997), PDK1 (Seong et al., 2007), or FBI-1 (Yang et al., 2015) functioning as negative regulators and making the SMAD4 gene more likely to be a false positive in the screen because its mutation could provide a growth advantage to the cells. Ligand-dependent nuclear receptor co-repressor-like protein (LCORL) has not yet been characterised. Exocyst complex component 2 (EXOC2) is part of the exocyst complex, an octameric protein assembly that controls vesicle trafficking, vesicle fusion and exocytosis (Wu & Guo, 2015; Mei & Guo, 2018). Chromodomain-helicase-DNA-binding protein 8 (CHD8) recruits histone H1 to suppress p53/TP53-mediated apoptosis in early embryogenesis (Nishiyama et al., 2009). CHD8 is also recruited to CTNNB1 responsive genes and negatively regulates them (Thompson et al., 2008). This may be why CTNNBL1 was also identified as a potential candidate.

CXCR4 was also highly enriched in the results of both the third round of enrichment on its own (-log p-value ≈ 5) or the three rounds altogether (-log p-value ≈ 4).

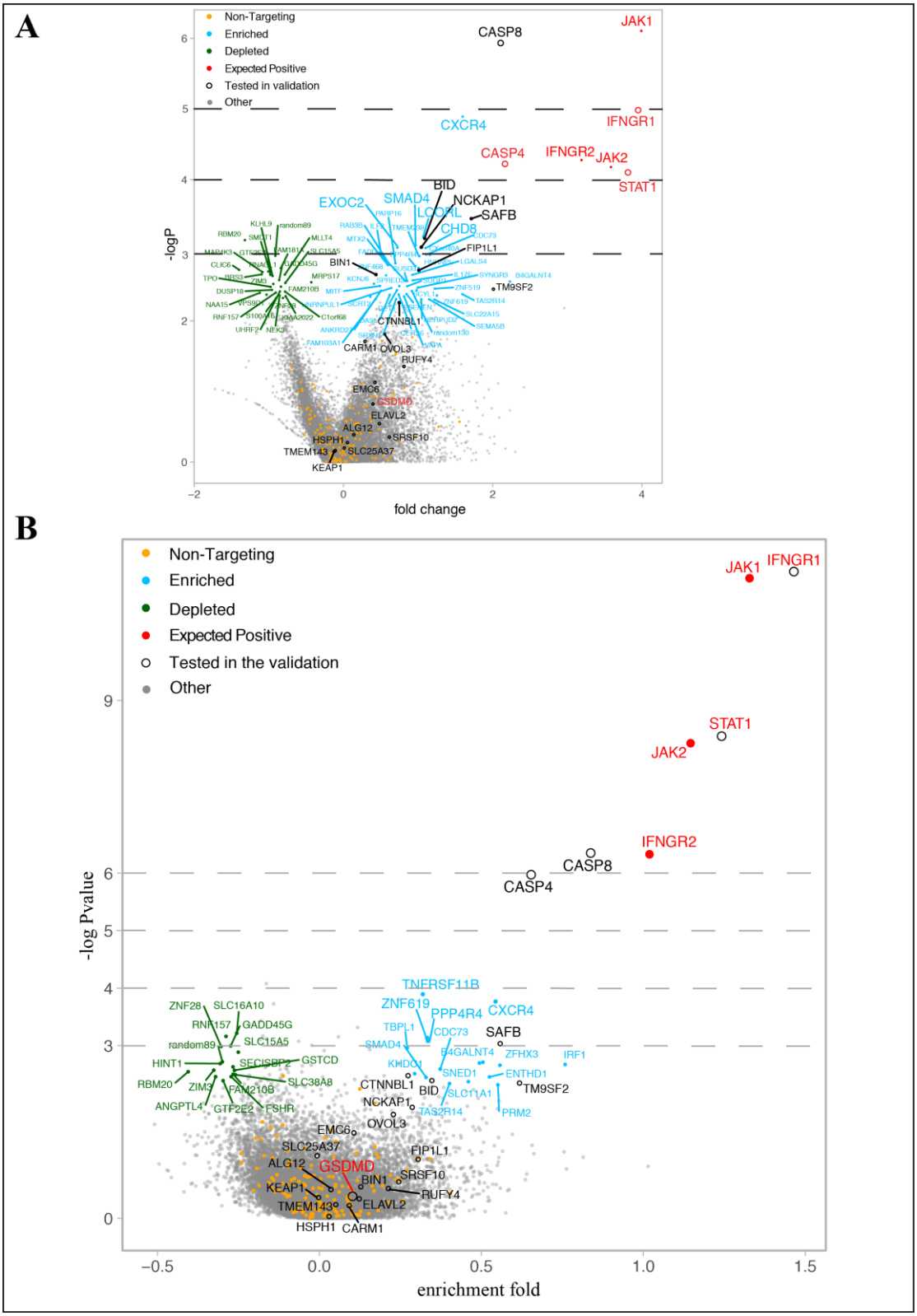

Figure 22: The genes expected as positive controls were significantly enriched during the screen

Volcano plots showing the p-value calculated for the enrichment fold of each gene either for (A) the third enrichment round ('3+ cells') or (B) for the three rounds of enrichment combined ('1+', '2+', and '3+ cells') in comparison to their initial count ('- cells').

Examining the 'hits' (-log p-value > 3) when the sequencing analyses of all three enrichment rounds were combined (**Fig.22B**), SAFB and CXCR4 were present together with TNFRSF11B, ZNF619, PPP4R4. Tumor necrosis factor receptor superfamily member 11B (TNFRSF11B) seems to be mostly associated with osteoclastogenesis and bone homeostasis (Tsuda et al., 1997). More recently, polymorphisms in TNFRSF11A and TNFRSF11B genes have been studied in the context of infections (Jingjing et al., 2019). TNFRSF11B also acts as a receptor for RANKL (receptor activator of nuclear factor kappa-B ligand), the expression of which is substantially changed during *Porphyromonas gingivalis* infection (Yamaguchi et al., 2017). By contrast, Zinc finger protein 619 (ZNF619) and Serine/threonine-protein phosphatase 4 regulatory subunit 4 (PPP4R4) have not been studied extensively to date.
As mentioned, these graphs (**Fig.22**) were generated only after the validation experiments were done and therefore these latter considerations were not taken into account in the choice of candidates to validate.

RNA-seq data (**Table 2**) comparing RNA levels in cells either with or without priming with IFN-γ, were used to provide additional information about whether the high ranked genes were IFN-γ inducible. Known functions of the candidate genes were also considered.
Candidates to follow-up in validation experiments were high ranked in the '3+ cells' sample with higher confidence (-log p-value > 3). Most of these were subsequently found to be also highly ranked in the '2+ cells' sample. However, amongst the IFN-γ inducible genes and highly ranked in the screen (**Table 2**), only CTNNBL1 stood out as new (non-expected as a positive control); STAT-1 is a direct downstream effector of the IFN-γ signalling pathway; CASP4 and IFNGR1 were shown to be necessary for the IFN-γ induced, LPS-triggered cell death; CASP8 is known as an essential component of inflammasomes, inducing cell death upon infection.

siRNA	IFN-γ enrichment (RNA seq)
ALG12	0.953
BID	0.961
BIN1	1.09
CARM1	1.00
CASP4	3.53
CASP8	1.74
CTNNBL1	1.25
ELAVL2	1.06
EMC6	N/A
FIP1L1	0.964
GSDMD	1.38
HSPH1	0.985
IFNGR1	1.08
KEAP1	1.02
NCKAP1	0.966
OVOL3	N/A
RUFY4	0.977
SAFB	1.02
SLC25A37	1.04
SRSF10	N/A
STAT1	4.57
TM9SF2	0.949
TMEM143	0.985

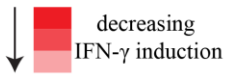

>1: IFN-γ inducible gene

Table 2: Enrichment ratio upon IFN-γ treatment for the genes chosen for validation

Genes were partly chosen based on their expression being IFN-γ inducible; RNA-seq was performed by M. Wandel by treating HeLa cells with IFN-γ and measuring mRNA levels in both the primed and unprimed cells. The enrichment ratio of mRNA level upon IFN-γ treatment was calculated for each gene. Genes are ranked by alphabetical order. N/A: non-available, which means either that the gene was not tested, or that mRNA levels could not be measured.

2.3.4 Validation of the 'hits'

Candidates selected from the screen results (**Table 3**) were validated using genetic techniques – CRISPR-Cas9 (knockouts) and/or RNA interference (knock-downs) – in follow-up experiments. Because the gene list was generated in a screen experiment, it was important to try to reproduce the observed phenotype (resistance to IFN-γ-induced, LPS-triggered cell death) on an individual basis. It was expected that, following mutation of one of the genes in the list of candidates, fewer (or no) cells would die following the challenge of IFN-γ priming and LPS transfection relative to the control cells.

Gene name	Protein	Function	Location
STAT1	Signal transducer and activator of transcription 1-alpha/beta	Signal transducer and transcription activator that binds to ISRE and GAS to activate target genes and mediate cellular responses to type-I and type-II interferons (IFNs), respectively.	nucleus
IFNGR1	Interferon gamma receptor 1	Associates with IFNGR2 to form the transmembrane receptor for IFN-γ.	plasma membrane
CASP4	Caspase-4	Inflammatory caspase essential in the non-canonical activation of NLRP3 inflammasome. Can be activated by cytosolic LPS. Its activation results in pyroptotic cell death via cleavage of GSDMD.	cytosol
CASP8	Caspase-8	Most upstream protease in the apoptotic cell death pathway. Likely target for the cowpox virus protease CrmA.	cytosol
GSDMD	Gasdermin-D	Forms membrane pores by homooligomerisation after cleavage/activation by caspases. Promotes pyroptosis and exhibits bactericidal activity.	cytosol
ELAVL2	ELAV-like protein 2	RNA-binding protein recognising a GAAA motif on the 3'UTR of target mRNAs.	nucleus
NCKAP1	Nck-associated protein 1	Part of the WAVE complex that regulates actin filament reorganisation. Involved in lamellipodia formation and endocytic trafficking.	plasma membrane
FIP1L1	Pre-mRNA 3'-end-processing factor FIP1	Part of the cleavage and polyadenylation specificity factor (CPSF) complex: promotes poly(A) addition at the 3' end of pre-mRNAs.	nucleus
TMEM143	Transmembrane protein 143	not known.	plasma membrane
SLC25A37	Mitoferrin-1	Plays a role in heme biosynthesis by specifically mediating iron uptake in developing erythroid cells.	mitochondrion
SRSF10	Serine/arginine-rich splicing factor 10	Splicing factor that promotes exon skipping in alternative splicing and, in its dephosphorylated form, represses pre-mRNA splicing.	nucleus
ALG12	Dol-P-Man: Man(7)GlcNAc (2)-PP-Dol alpha-1,6-mannosyltransferase	Adds the eighth mannose residue onto the dolichol-PP-oligosaccharide precursor required for protein glycosylation.	endoplasmic reticulum
TM9SF2	Transmembrane 9 superfamily member 2	May have a function of channel or transporter in the intracellular compartment.	endosomes and Golgi apparatus

table continued on next page

Gene name	Protein	Function	Location
EMC6	ER membrane protein complex subunit 6	not known.	endoplasmic reticulum
OVOL3	Putative transcription factor ovo-like protein 3	not known.	nucleus
SAFB	Scaffold attachment factor B1	Allows the formation of a 'transcriptosomal' complex that couples transcription and RNA processing, by binding to the specific DNA regions (S/MAR).	nucleus
CTNNBL1	Beta-catenin-like protein 1	Part of the spliceosome complex required for activating pre-mRNA splicing. May induce apoptosis.	nucleus
BIN1	Myc box-dependent-interacting protein 1	Controls the plasma membrane shape. Regulates endocytosis, intracellular vesicules sorting and actin bundling.	nucleus and endosomes
RUFY4	RUN and FYVE domain-containing protein 4	Binds to phosphatidylinositol 3-phosphate and thereby positively regulates autophagosome formation and their fusion with lysosomes.	autophagosomes and cytoplasmic vesicles
CARM1	Histone-arginine methyltransferase CARM1	Methylates proteins involved in DNA packaging, transcription regulation, pre-mRNA splicing, and mRNA stability (for example, the RNA-binding protein ELAVL1). Can act with CTNNB1/beta-catenin to activate transcription. During inflammation, acts as a coactivator of NF-κB in monocytes.	nucleus
BID	BH3-interacting domain death agonist	The proteolytic product p15 allows release of cytochrome c. Counters the protective effect of Bcl-2.	mitochondrion
HSPH1	Heat shock protein 105 kDa	Acts as a nucleotide-exchange factor (NEF) for chaperone proteins HSPA1A and HSPA1B. Prevents the aggregation of denatured proteins in cells under stress conditions.	cytosol
KEAP1	Kelch-like ECH-associated protein 1	Key sensor that regulates the response to oxidative and electrophilic stress. In selective autophagy, interacts with p62 in inclusion bodies, increasing p62 sequestering activity and degradation.	nucleus

Table 3: Characterisation of the genes chosen from the screen results

Genes chosen for validation were searched mostly using UniProt in order to indicate along with the gene name, the full name of the coded protein, their main known functions and the protein's location within cells (subcellular compartment if relevant).

2.3.4.1. Validation using knockouts

Cas9-expressing cells were transduced with gRNAs targeting 12 genes selected from the list of potential 'hits', including positive (CASP4, STAT-1, IFNGR1) and negative (Cas9-expressing cells ± β2M-transduced) controls. Each gene was tested using three or four different targeting gRNAs (**Fig.23A**); for each gene, two of the guides were selected from the original library for their high enrichment ratio whereas the other guides were newly designed. As expected, cells mutated in CASP4, STAT-1

or IFNGR1 showed significant resistance to LPS transfection: cell death occurred in respectively 20%, 10% and 12% of IFN-γ-primed cells, compared to 65% in cells transduced with the β2M guide (**Fig.24B**). These percentages were determined on a gene level by combining the results generated by all the different gRNAs used for each gene, albeit similar observations were obtained for individual guides (**Fig.24A**). In the cases of GSDMD and CASP8, the resistance phenotype was more partial (35% cell death) and significant only in the case of GSDMD. In the case of CASP8, there was greater variability between the different guides (**Fig.24A**): guides 2A and 2B gave respectively 40% and 65% cell death whereas 2C and 2D showed 30% and 25% cell death, respectively.

A

gene	ID	number
Caspase-4	1	3 (B-D)
Caspase-8	2	4 (A-D)
Gasdermin-D	3	4 (A-D)
STAT-1	4	3 (A,B,D)
IFNGR1	5	4 (A-D)
NCKAP1	6	3 (A,B,D)
SRSF10	7	4 (A-D)
ALG12	9	4 (A-D)
FIP1L1	10	4 (A-D)
SLC25A37	11	3 (A-C)
TM9SF2	12	4 (A-D)
SAFB	8	4 (A-D)

B

siRNA	
A2	STAT1
A3	IFNGR1
A4	CASP4
A5	CASP8
A6	GSDMD
A7	ELAVL2
A8	NCKAP1
A9	FIP1L1
A10	TMEM143
A11	SLC25A37
B2	SRSF10
B3	ALG12
B4	TM9SF2
B5	EMC6
B6	OVOL3
B7	SAFB
B8	CTNNBL1
B9	BIN1
B10	RUFY4
B11	CARM1
C2	BID
C3	HSPH1
C4	KEAP1

Figure 23: Knockout and knock-down experiments were performed to validate the 'hits' obtained

To perform validation experiments for genes chosen among the 'hits' identified in **Table1** and further characterised in **Table3**, (A) three or four gRNAs were synthesised to target 12 of them and (B) pooled siRNAs were ordered to target 23 genes. All genes for which gRNAs were designed were also tested in the knock-down experiment (siRNA pool ordered).

Looking at the other seven candidates, none of the guides (**Fig.24A**, lower panel) showed a significant reduction in cell death for any of the genes tested, when compared with Cas9-cells (negative control). Even when averaging the different guides for one gene (**Fig.24B**), no candidate stood out as successfully able to reproduce the phenotype for which they were selected: i.e. resistance to cell death triggered by LPS upon IFN-γ priming.

The observation that not a single new gene could be validated was surprising; especially because positive controls (IFNGR1, STAT-1) convincingly exhibited the desired result, showing hardly any cell death in IFN-γ-primed cells following LPS transfection. Further validation was therefore undertaken.

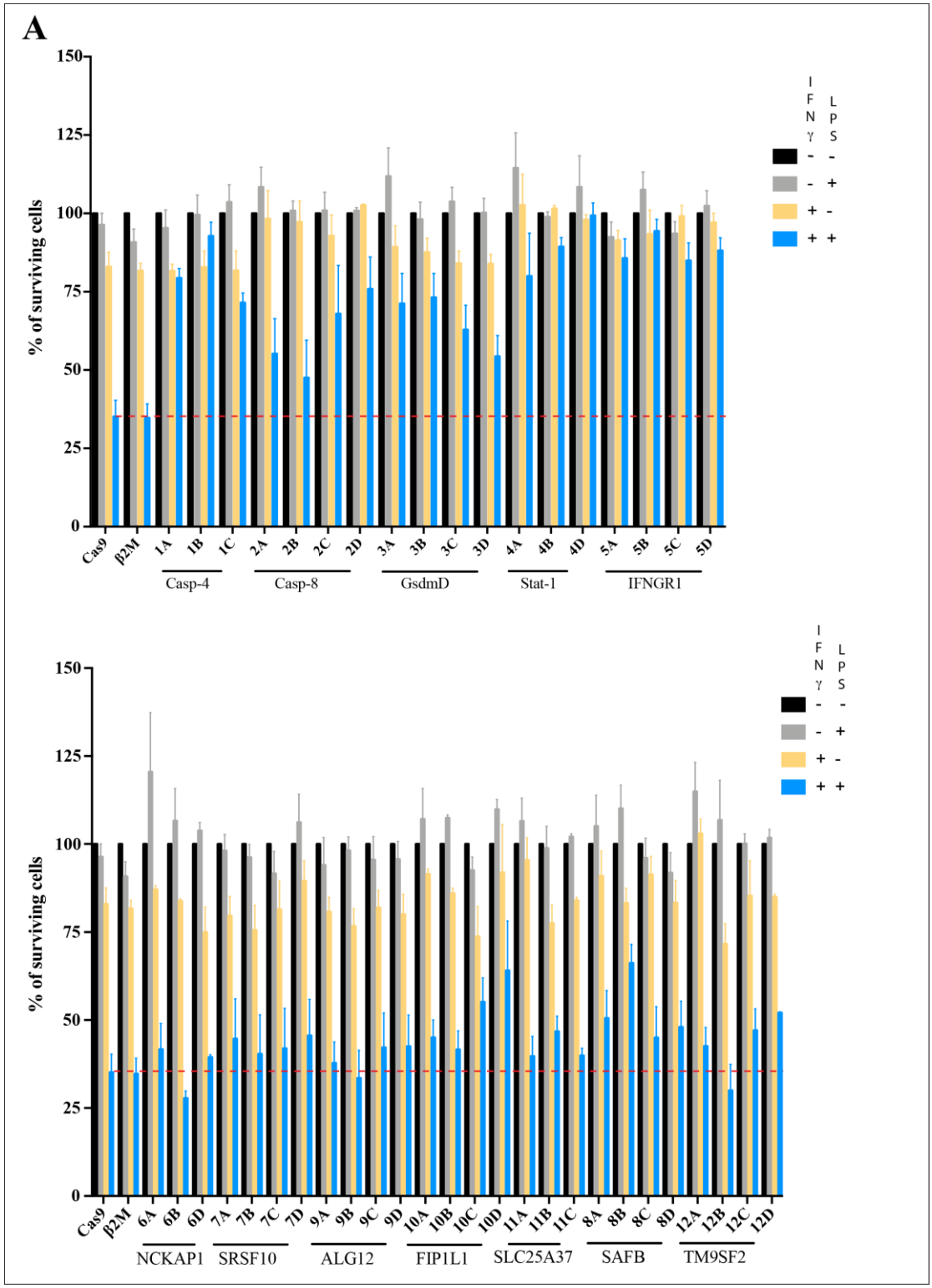

figure continued on next page

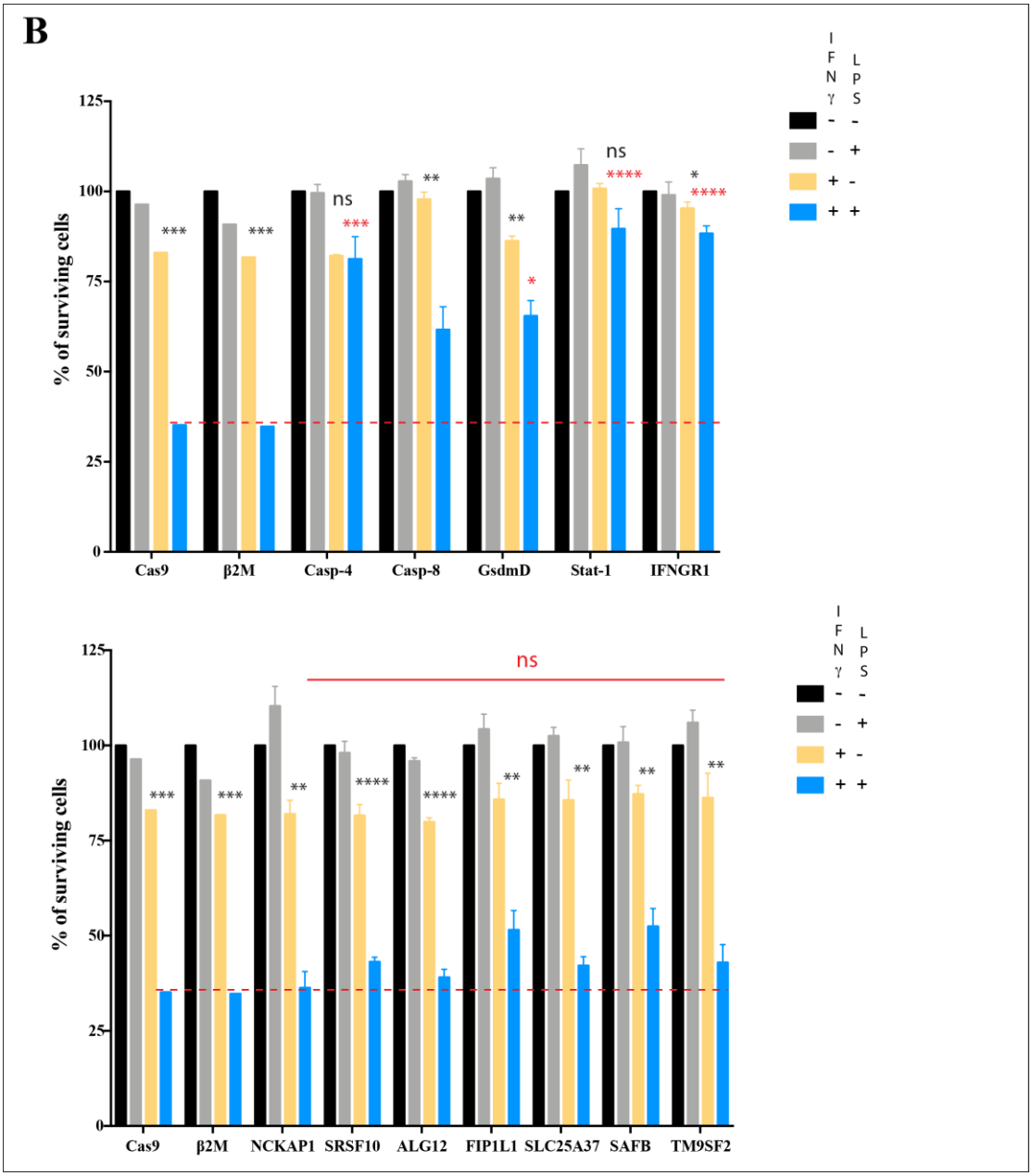

Figure 24: Knockout experiment for the validation of potential 'hits'

Cas9-expressing HeLa cells were transduced with gRNAs directed against specific genes (**Fig.23A**) and selected accordingly (hygromycin for Cas9 and puromycin for the gRNAs). On day 6 after gRNA transduction, cells were primed with IFN-γ overnight and transfected with LPS on the next day (blue). For each knockout cell line, controls were carried out: no treatment (black); transfection with LPS without priming with IFN-γ (grey), priming with IFN-γ but no transfection (yellow), meaning that a total of four conditions were set-up. Cells were analysed with CellTiter Glo on the day after LPS transfection to measure the number of live cells in each condition. The percentages of survival were calculated for each gRNA (A) for the 12 genes tested taking the unprimed and untransfected cells (black) as reference (100%). (B) shows the averages of guides for each gene. Upper graphs show genes for which resistance to cell death was expected, whereas the lower panel investigated new candidates. Results from seven independent experiments, all performed in triplicate, are shown as Mean ± S.E.M. Statistics were calculated for each gene knockout cell line (B) on the one hand, cell death following combined treatement by both IFN-γ and LPS (blue bar) was compared to the control cells (Cas9-expressing cells or cells transduced with β2M guide) and evaluated using

one-way ANOVA with Dunnett's multiple comparisons test: *P<0.05, **P<0.005, ***P<0.0002, ****P<0.0001, ns (not significant); on the other hand, the effect of LPS transfection was evaluated in cells primed with IFN-γ (yellow and blue bars) using unpaired t test, without assuming a consistent SD: *P<0.05, **P<0.005, ***P<0.0002, ****P<0.0001, ns (not significant).

2.3.4.2. Use of RNA interference as an alternative validation method

An alternative method of validation was provided in case the candidate genes had not been successfully knocked-out in the previously described method. In this alternative method, the same genes and others chosen from the top-ranked in the screen list were knocked-down using RNA interference. HeLa cells were transfected with pooled siRNAs (a mix of four siRNAs for each gene) against 23 genes (**Fig.23B**), including all the genes previously tested in the gRNA experiment. The additional candidate genes were chosen for being highly ranked with the MAGeCK algorithm (**Table 1**), having a p-value higher than 3 and picked amongst the more IFN-γ inducible genes (**Table 2**).

Two different siRNA controls were used as reference (negative controls) in order to compare the amount of cell death with the knock-downs. Pooled siRNAs targeting CASP4, STAT-1, and IFNGR1 were used as positive controls. Cells knocked-down for each of the three, showed significant resistance to cell death after IFN-γ priming followed by LPS transfection. Control cells died by 70%, whereas only 15% and 10% of cells died when knocked-down for IFNGR1 and STAT-1, respectively. CASP4 showed a milder phenotype with 25% of cells dying (**Fig.25**, upper graph).

Amongst all the candidates tested (**Fig.25**), only SAFB knock-down cells demonstrated a significant increase in survival (p=0.03). SAFB was not noticed as an IFN-γ inducible gene and is a member of the family of RNA-/DNA-binding proteins. SAF proteins are multifunctional (Norman et al., 2016) and are implicated in cell growth and death processes and are characterised as tumour suppressors via their mechanism of transcription repression (Hong et al., 2012).

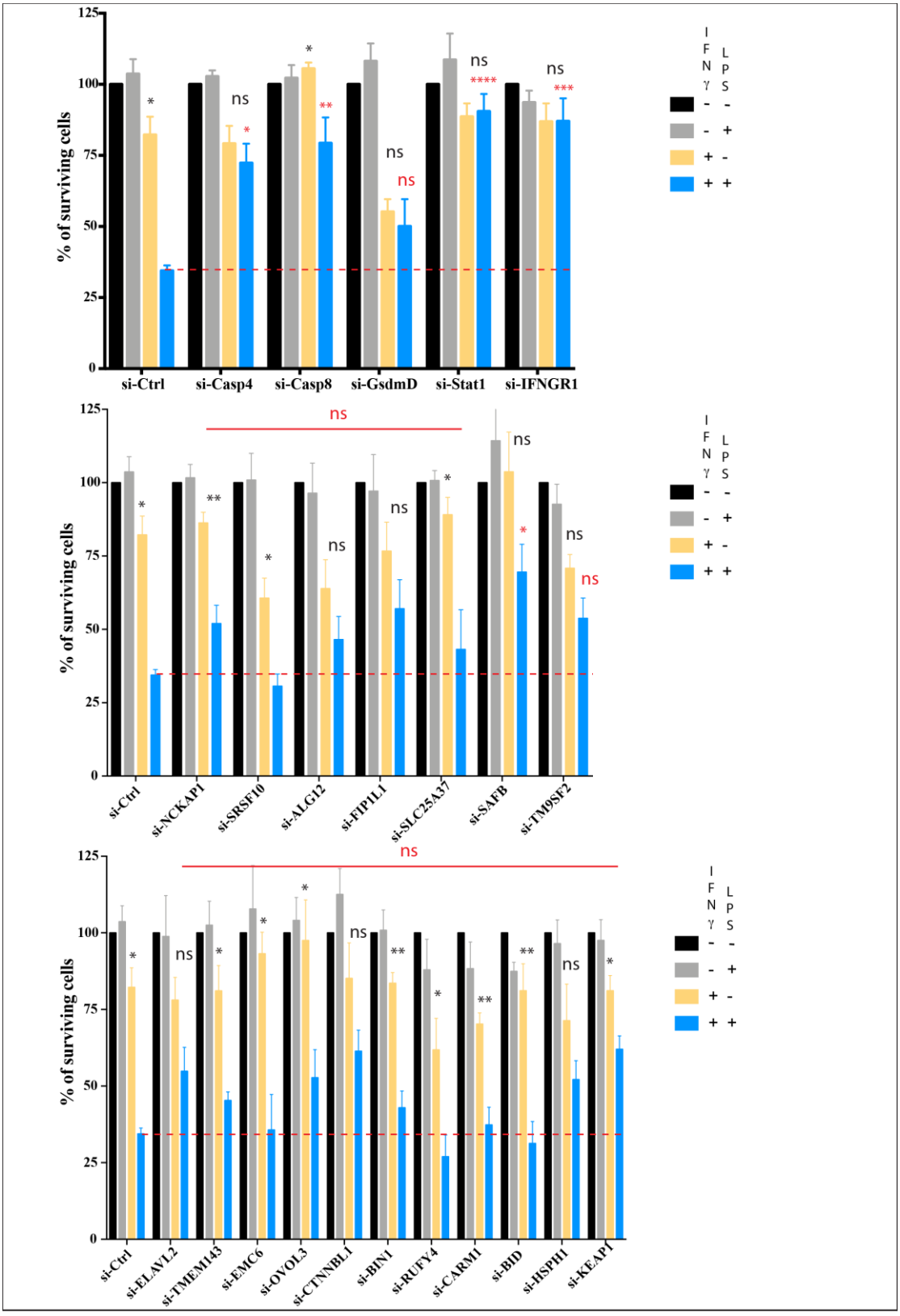

Figure 25: Knock-down experiments for the validation of potential 'hits'

Pooled siRNAs against 23 genes (**Fig.23B**) were transfected into HeLa cells to generate 23 knock-down cell lines. At 48h post-siRNA transfection, the 23 cell lines were primed with IFN-γ overnight before transfection with LPS (blue). For each knock-down cell line, controls were carried out: no treatment (black); transfection with LPS without priming with IFN-γ

(grey), priming with IFN-γ but no transfection (yellow), meaning that a total of four conditions were set-up. Cells were analysed with CellTiter Glo on the day after LPS transfection to measure the number of live cells in each condition. The percentages of survival were calculated for each gene tested taking the unprimed and untransfected cells (black) as reference (100%). Experimental conditions were tested in triplicates. Data are shown as Mean ± S.E.M from the triplicates of four independent experiments. For each gene knock-down, cell survival following combined treatement by both IFN-γ and LPS (blue bar) was compared to the control cell line (cells transfected with non-target siRNA: si-ctrl) and evaluated using one-way ANOVA with Dunnett's multiple comparisons test: *P<0.05, **P<0.005, ***P<0.0002, ****P<0.0001, ns (not significant). In each gene knock-down, the effect of LPS transfection was evaluated in cells primed with IFN-γ (yellow and blue bars) using unpaired t test, without assuming a consistent SD: *P<0.05, **P<0.005, ns (not significant).

In summary, when mutated using CRISPR and silenced by siRNA, none of the new genes identified in the screen gave a significant reduction in cell death when IFN-γ treated cells were transfected with LPS. None of the putative target genes were able to reproduce the resistance phenotype to LPS transfection upon IFN-γ-priming, for which they were initially selected. Consequently, no new gene could be validated and qualified as being involved in the IFN-γ-induced, LPS-triggered cell death pathway studied here.

2.4 Discussion

The work in this chapter used the CRISPR technology to establish a novel strategy to identify additional components in the IFN-γ-induced, LPS-triggered cell death pathway. This strategy was based on using an unbiased genetic screen to identify genes that play a role in the pathway.

The presence of LPS in the cytosol leads to cell death in IFN-γ-primed HeLa cells. This is a mechanism by which the host protects against pathogenic infections, through restricting bacterial proliferation and potential spread to neighbouring cells. In human cells, cytosolic LPS is recognised by CASP4, which is activated in a proximity-induced fashion. The active form of CASP4 cleaves GSDMD, the main effector of pyroptosis, which is a programmed but pro-inflammatory form of cell death (**Fig.26**). Expression of both CASP4 and GSDMD is induced by IFN-γ. However,

overexpression of neither CASP4 nor GSDMD individually was sufficient to recapitulate the effect of IFN-γ on cell death triggered by cytosolic LPS (**Fig.8**).

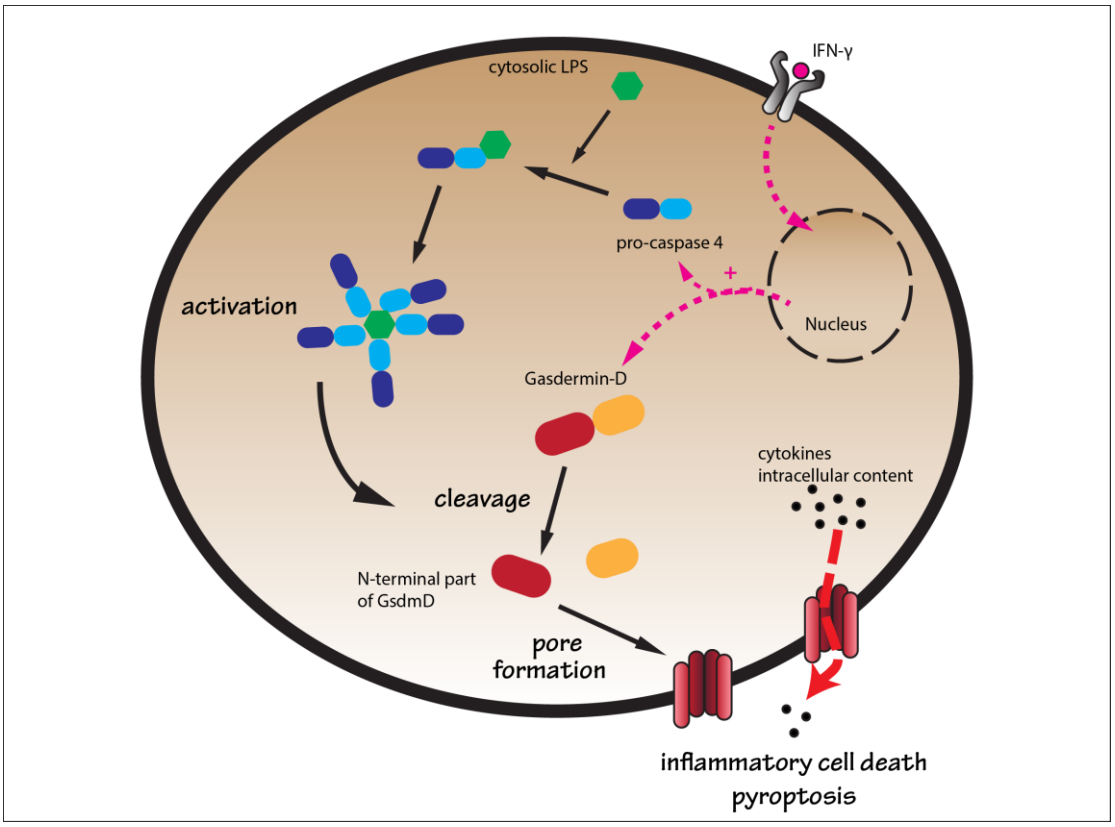

Figure 27: Schematic illustration of how cytosolic sensing of LPS triggers pyroptotic cell death

Cytosolic LPS is bound by CASP4 that is then activated by proximity-induced proteolysis. Active CASP4 cleaves GSDMD to release the inhibitory C-terminal part and to enable N-terminal GSDMD to oligomerise and form pores in the plasma membrane. These pores not only allow the release of signalling molecules such as interleukins, but also result in pyroptotic cell death.

This project would require further optimisation before performing at least one additional screen repeat to make sure that the results are reproducible and to gain deeper understanding of the multiple redundant mechanisms at stake. In order to follow up on results that challenge the current published views on the topic, the role of IFN-γ in triggering cell death is also discussed.

2.4.1 Repeating the screen to achieve reproducibility

The screen was undertaken based on the observation that CASP4 and GSDMD only had partial effects on the IFN-γ-induced, LPS-triggered cell death in HeLa cells: neither of these two candidates were able to explain completely the mechanism by which LPS promoted cell death in cells treated with IFN-γ (**Fig.8**). It was therefore reassuring to find CASP4 highly enriched by the successive rounds of selection (**Fig.21**). However, GSDMD was not identified in the first 100 genes in the 'hit' list. This means either that the screen design was not completely suitable or that other cell death mechanisms are redundant with the GSDMD-driven pyroptosis pathway.

Using the CRISPR-Cas system as the genetic screening technique for the project detailed in this chapter was novel and came with a number of challenges. Several methodological points warrant discussion and would need to be improved for future implementations to be successful; in particular, the choice of cell line and the design of the gRNA library are crucial for the implementation of such a screen. Robust data analysis is also required and clear definition of criteria to select genes to be validated are also essential.

To gain confidence in the results previously generated, repeating the screen is necessary. The same methodology could be applied again; alternatively, changes could be implemented to make the screen more robust. The time points for sampling the selected cells and the number of enrichment rounds to perform are discussed in paragraph **2.4.1.1**. ("Loss of essential genes and slow-growing mutants"). The data analysis pipeline could also be improved in terms of choice of enrichment rounds to consider, the processing of the data (as multiple programmes are available), and the ways of representing the results to show clearly the potential 'hits' to be validated.

2.4.1.1. Loss of essential genes and slow-growing mutants

To ensure protein depletion (i.e. knockout), Cas9-expressing HeLa cells were expanded for 10 days after gRNA transduction before starting the screen. Although cells knocked-out in essential genes (i.e. regulating cell cycle, replication, metabolism) died during this waiting time, the loss of essential genes is not critical for

the result of the screen. The analysis did not consider genes that were lost but rather identified genes that were enriched over time.

The successive enrichment rounds were compared to the reference ('- cells'): HeLa cells that had undergone overnight priming with IFN-γ. IFN-γ-regulated genes providing a survival advantage would be present in the starting pool and selected for by this first incubation. This was a deliberate choice for the reference, to avoid generating false positives. Consequently, when calculating gene enrichment ratios after the different enrichment round(s), these genes would not show any positive enrichment as the screen selected for genes involved in the cell death mechanism triggered specifically by cytosolic LPS. Therefore, if any essential gene were to be involved in the IFN-γ-induced, LPS-triggered cell death pathway, the method used was not relevant to identify such a gene.

Two different strategies could be applied to determine the sampling time points for cells from each enrichment round. The first strategy, which was implemented for the screen detailed in this thesis, assumes that cells are more genetically comparable if they are grown for the same duration. Therefore, cells of the different enrichment rounds were kept in culture for the entire duration of the experiment and eventually individually pelleted and frozen. This approach favours fast-growing clones, which will outgrow slow-growing mutants, thereby introducing a bias in the analysis. The second strategy would be based on the possibility that some genes, enriched in the early rounds, could be lost at later time points if they were detrimental to cell viability in the long-term. However, by isolating and saving the cells immediately after each enrichment round, these short-lived and enriched mutants resistant to IFN-γ-induced, LPS-triggered cell death could be identified.

The screen described here was carried over five rounds of selection (i.e priming with IFN-γ followed by LPS transfection) and DNA from the cells isolated after the first three rounds was sequenced. Because the treatment after the fifth round did not seem to produce any additional cell death (**Fig.19**), it might prove insightful to consider the cells isolated after this stage of enrichment ('5+ cells'). However, this last batch of cells was initially disregarded because it would contain hyperproliferative mutants that might not be specific to the selection pressure – IFN-γ priming followed by LPS

transfection – to which they had been exposed. To build a dataset that can be trusted and avoid the identification of false-positives, sequencing the '4+' and '5+ cells' batches would allow combining data from all five enrichment rounds and get additional information.

To follow-up on this project, the screen needs to be repeated, ideally sampling the cells directly after each round of selection and then sequencing them, allowing dataset combinations as desired.

2.4.1.2. Using a robust pipeline for the result analysis

Irrespective of the computational algorithm used to rank the genes, the enrichment fold for each gRNA was calculated. Data processing methods differed in the way they rank the genes based on the information from each individual gRNA.

Despite the absence of GSDMD in the top ranked genes, the screen seemed to have functioned effectively because the genes of the entire IFN-γ signalling pathway: IFN-γ receptors (IFNGR1 and 2), STAT-1, JAKs (1 and 2) knockout cells were strongly (high enrichment fold) and robustly (high -log p-value) enriched in the screen, as expected. However, none of the new genes identified by the screen and chosen for validation showed even partial resistance to LPS-triggered cell death upon IFN-γ priming when knockout and/or knock-down individually.

The candidates selected for validation were chosen based on the rankings obtained with the MAGeCK algorithm for the successive rounds of enrichment. Two other algorithms were used to rank the genes after the screen: RSA and "5th guide". A more robust approach would consider genes highly ranked in the three different analysis methods (MAGeCK, RSA and "5th guide") for selecting candidates to validate. The rankings shown in **Table1** were generated from the '3+ cells' batch. For example, SAFB was ranked 39, 13 and 17 with MAGeCK, RSA and "5th guide" analysis methods, respectively. Although no more time was allocated to undertake additional experiments, other 'hits' with a similar or higher ranking should be considered. This would include QRICH, LTK, PISD, LRIG1, and ECD. Chemokine receptor 4

(CXCR4) has been identified as a mediator of LPS-initiated inflammatory response (Triantafilou et al., 2001) and was ranked 16 and 18 using RSA and "5th guide" methods, respectively, suggesting that it would be a promising candidate to test too. Unlike other CDKs, cyclin-dependent kinase 9 (CDK9), which was ranked 23, 24, and 19 acts as a regulator of transcription and not of the cell cycle. CDK9 heterodimerises with CyclinT1 to form the positive transcriptional elongation factor b (P-TEFb), complex shown to play a key role in signalling cascades (Brasier, 2008) such as TNF-inducible NK-κB activation (Nowak et al., 2008) and IL-6-inducible STAT3 (Hou et al. 2007) and so could be a potential target for anti-inflammatory therapy (Wang & Fischer, 2008).

In addition to using the three algorithms, it would be interesting to consider other enrichment rounds individually or to combine the data of several stages. For example, to check whether top-ranked genes overlap between enrichment rounds and whether 'hits' specific to '1+ cells' or '2+ cells' could be validated. That will potentially lead to the identification of both stage-specific and common 'hits'; the latter definitely constituting a pool of candidates for validation.
In order to make such analysis easier, the genes' enrichment fold were represented on volcano plots (**Fig.22**), which provide a clearer view of the enriched genes in the screen, and a way of comparing either individual enrichment rounds (e.g. '3+ cells', **Fig.22A**) or combined results from the three sequenced samples (**Fig.22B**).

Criteria could be defined to select genes for validation experiments using volcano plots displaying data from the screen. Results from either the screen already performed and/or new repeats and processed by the three different ranking methods could be compared. Furthermore, candidates for validation could be chosen considering one or multiple enrichment rounds. In addition, the cut-off in terms of confidence was set to -log p value > 3.

More comprehensive analysis of the results generated by the screen have identified several additional candidates (CXCR4, CDK9, LCORL, EXOC2, CHD8, TNFRSF11B, ZNF619 and PPP4R4) as putative members of the IFN-γ-induced, LPS-triggered cell death pathway and so would be attractive targets for future validation studies. These new genes were identified based on their p-value (confidence in the

enrichment fold comparing to the initial population) in analysis done considering only the '3+ cells' or the three enrichment rounds together ('1+', '2+' and '3+ cells').

2.4.1.3. A more systematic approach for validation of the candidates

Once chosen, candidates are tested in validation experiments and it is usually preferable to follow-up a CRISPR screen by again using CRISPR in the validation procedure. In this way, if the potential candidate does not pass the test, it is assumed that it was a false positive in the 'hit' list. As discussed above, the knockouts in the validation experiments performed might not have been complete and this would likely be due to intrinsic redundancy in HeLa cells, which usually carry multiple copies of the same gene and often have more than two alleles. In the future, the absence of the target proteins should be checked by western-blotting.
However, even if the phenotype is reproduced on an individual basis using knockouts, the candidate gene still needs to go through further confirmations, characterisations, and functional experiments to demonstrate that it is required in the pathway.

In addition to knockouts, alternative validation techniques such as knock-downs using siRNAs could generate more information on potential candidates. Reproducing the resistance phenotype in these experiments validates further the genes as true positives. However, when the knock-down cells did not show any phenotype, it was hard to know whether the knock-downs were incomplete or whether the tested genes were simply false positives. It would thus be worth following up the work on SAFB since it was the only gene to produce a significant resistance to cell death (**Fig.25**). During the screen, cells were selected following multiple rounds of LPS transfection: because of this, cells mutated in a single gene might not show a difference in survival with only a single round of applying the selection pressure. Therefore, it might be useful to test again the knockout / knock-down cells, assessing their survival after multiple selections. In addition to the number of selection rounds to apply, the timing of analysis (measure of cell death) might play a role in the validation of a candidate gene: analysing cells, even when using the same technique, showed increased cell death over time (**Fig.3B**). This might be explained by the existence of concomitant cell death pathways being activated but triggered or responding to the LPS challenge at various time points after the treatment. Whether the response is produced directly

by IFN-γ or, alternatively, by LPS and the nature of the proteins involved, will dictate the time required for the cell to die. It has been shown that GSDMD-dependent pyroptosis is generally a faster process than apoptosis (Bergsbaken et al., 2009). This may account for both Caspases-4 and -8 becoming enriched during the screen as a consequence of their representing the pyroptotic and the apoptotic cell death pathways, respectively. A delay in cell death might also be due to membrane repair mechanisms led by the ESCRT complex (Rühl et al., 2018).

In order to test these hypotheses and also because of the absence of candidates from the screen that could be validated in subsequent experiments, a focused screening approach might be best.

2.4.1.4. Focusing the screen to investigate beyond redundancy

The screen can be biased in different ways: either by limiting the gRNA library or by performing it in knockout cell lines.

Repeating the screen using a focused sgRNA library might help identify true candidates for further validation, in addition to the positive controls (IFNGRs, STAT-1, JAKs). Using a genome-wide library in a CRISPR screen allows for an unbiased approach when it comes to a biological question. However, it may be worth introducing a bias by using a targeted screen (Wang et al., 2014). To investigate the IFN-γ-dependent and LPS-triggered cell death pathway, libraries specifically targeting subsets of genes known to be either IFN-γ-regulated or known for their involvement in cell death pathways or LPS sensing would be appropriate choices (https://www.synthego.com/crispr-libraries); a library designed based on the results of the first genome-wide screen and targeting, for example, the first 1000 ‘hits’ found could be another option.

CASP4 and GSDMD were expected to be in the ‘hit’ list generated by the screen because CASP4 acts as a direct receptor for cytosolic LPS (Shi et al., 2014) and GSDMD is the principal effector in pyroptosis (Rühl & Broz, 2016). The requirement of these two proteins in the IFN-γ-induced, LPS-triggered cell death pathway was tested: the absence of CASP4 resulted in decrease of cell death, whereas

overexpression of GSDMD partially induced cell death in the absence of IFN-γ priming. However, the combined effect of CASP4 and GSDMD was not addressed. It would be interesting to look at double knockout or knock-down HeLa cells to see whether the absence of both proteins completely abrogates LPS-triggered cell death upon IFN-γ priming. Similarly, simultaneous overexpression of CASP4 and GSDMD could recapitulate the effect of IFN-γ priming; i.e. the cell death observed when transfecting LPS would be the same in the absence or presence of IFN-γ.

Working in CASP4-deficient cells could allow deeper understanding in the cell death pathway and overcome possible pathway redundancy. CASP4 knockdown in human MDMs (monocyte-derived macrophages) or in intestinal epithelial cells showed decreased level of IL-1α processing after infection with *L.pneumophila* (Casson et al., 2015) and IL-18 secretion as well as increased bacterial load upon infection with enteropathogenic *E.coli* or *S.*Typhimurium (Knodler at al., 2014). These findings also suggested involvement of CASP1, which could be investigated in CASP4-deficient cells. Such a cell line could be generated by using CRISPR-Cas9 to knockout CASP4 in HeLa, hence providing a different genetic background for a new screen.

In the case of *S.*Typhimurium infection, the autophagy machinery is recruited to cytosolic bacteria for the degradation of the pathogen (Boyle & Randow , 2013). Projects in the Randow laboratory have demonstrated the ubiquitylation of LPS chains on cytosolic bacteria following infection and rupture of the SCV membrane. Ubiquitin constitutes a signal for the recruitment of the autophagy machinery. Therefore, autophagy might also play a role when cells are transfected with LPS. To address the possible redundancy of cell death pathways, it would be best to silence (e.g. use of ATG5-knockout cells) or inhibit the autophagy pathway (e.g. with small molecules inhibitors such as wortmannin, bafilomycin, chloroquine or MG-132) during the screen. This might impact the percentage of cell death by changing the way LPS is sensed in the cytoplasm.

Inflammasomes, autophagy, and cell death are innate immune defence mechanisms that the host set up to control pathogenic infections. All three interact with each other to preserve host viability by pathogen clearance (Krakauer, 2019). The autophagy protein family Beclin-2 (BCL-2) contains several members known to control

mitochondrial membrane integrity (Chipuk et al., 2010) and to regulate the release of cytochrome c in the cytosol. Cytochrome c indirectly promotes caspase-9 activation and subsequent apoptosis by cleavage of caspases-3 and-7 (Riedl & Salvesen, 2007). Hence autophagy and apoptosis are closely linked. Similarly, necroptosis (believed to actually be pyroptosis) is negatively related to autophagy. Under starvation condition, autophagy is activated in order to prevent necrosis (Bell et al., 2008; Farkas et al., 2011).

Because of these interconnections between pathways, it would also make sense to prevent apoptosis from happening (either by using caspase inhibitors or by making knockout cell lines) and assess the impact on the IFN-γ-dependent, LPS-triggered cell death. This cell death mechanism was hypothesised to be pyroptosis (Jorgensen & Miao, 2015), but a decrease in the percentage of non-apoptotic cells dying following the treatment would suggest that part of the cell death is due to apoptosis. Such a result would also explain why GSDMD was not part of the top 'hits' in the list resulting from the screen.

2.4.2 Role of IFN-γ in LPS sensing

The sensing mechanisms, and thereby downstream effects, are impacted differently depending on whether LPS is attached to the bacteria or displayed as a free molecule in the cytoplasm. Introducing LPS into cells by electroporation or cationic chemical transfection leads to different phenotypes regarding cell death and could explain the extent to which IFN-γ is required. Variations between species (mouse vs human) and cell lines (macrophage-derived vs non-immune) will also be discussed in the following sections.

2.4.2.1. Impact of the delivery method for LPS

It was shown that LPS from Gram-negative bacteria delivered to the cytosol by transfection or electroporation is sufficient to induce caspase-11 activation (Hagar et al., 2013; Kayagaki et al., 2013). However, depending on the technique used, LPS

molecules are most likely sensed differently by the cell. Electroporation or chemical transfection are usually used for introducing nucleic acids (DNA or RNA) into cells.
Electroporation is a direct physical method based on the induction of pore formation by applying an electric field. The hydrophilic pores are lined by phospholipid headgroups, facilitating the introduction of polar and charged molecules in cells (Tieleman, 2004). Two distinct models try to explain the mechanism by which the electroporated substrate gets into the cell. One suggests the formation of large stable pores in the plasma membrane allowing transport through it without much interaction (Smith et al., 2004). The other claims that small pores provide flexibility to the plasma membrane allowing structural modifications for the translocation of the payload (Sukharev et al., 1992).
Because this method is a direct transfer, LPS molecules would most likely not be affected and would instead remain aggregated in micelles or vesicles, since they are naturally in aqueous solution.

Transfection is a chemical method relying on successive interactions to deliver the desired molecule into cells. The transfection reagent Lipofectamine2000 is a mixture of lipid subunits that assemble as liposomes in aqueous environment and entrap the transfection payload, that is, LPS in the experiments described in this chapter. Two major uptake mechanisms are involved: clathrin-dependent endocytosis and/or transmembrane transport of lipoplexes by a caveolae-dependent pathway into the cell membrane channels. A correlation between clathrin-mediated or caveolae-dependent endocytosis and lipoplexes transfection was convincingly supported by several pieces of evidence, including the use of inhibitors of endocytosis, co-localization with pathway-specific markers and defective in clathrin-mediated endocytosis (Cui et al., 2012). The uptake of lipoplexes in HEp-2 cells was mediated via both the clathrin- and the caveolae-dependent pathways, although it is not definite which is the main mechanism.

Lipofectamine, contrary to alternative formulations, is able to efficiently avoid active intracellular transport along microtubules and the subsequent entrapment and degradation of the payload within acidic/digestive lysosomal compartments. This result is achieved by random Brownian motion of Lipofectamine-containing vesicles

within the cytoplasm (Cardarelli et al., 2016). In this way, LPS is released in the cytoplasm upon vesicle membrane rupture or fusion.

The introduction of LPS into the cell cytoplasm via either electroporation of chemical transfection influences the shape and the aggregation or assembly of LPS molecules. Therefore, there is a chance that cells recognise cytoplasmic LPS through different pathways depending on the transfection mechanism. Furthermore, similar considerations apply regarding LPS being either bound at the surface of Gram-negative bacteria (alive or in lysates) or free in solution. It was indeed shown (**Fig. 1A**) that infection with living *S*.Typhimurium produces more cell death compared to infection with *S*.Typhimurium lysates or transfection with *S*.Typhimurium LPS in IFN-γ-primed HeLa cells. In the absence of IFN-γ, the delivery of LPS into cells by cationic lipids using Lipofectamine2000 transfection reagent (**Fig.3**) has no effect on the viability of cells (Eldstrom et al., 2000), and provided an appropriate way of investigating acute actions of LPS in the intracellular compartment of human cells.

In addition, responses to the presence of cytosolic LPS may differ between cell types, especially comparing with professional immune cells. The extent to which IFN-γ is required for the detection and sensing of LPS, and for cell death to occur depends on the cell lines used.

2.4.2.2. Differences between cell lines

When infected by Gram-negative bacteria, epithelial cells in the lungs, the intestinal or urinary tracts are the first line of defence against the pathogenic threat. Both murine (Hornef et al., 2002; Knodler et al., 2014a) and human intestinal epithelial cells are responsive to LPS. The activation of immune responses is generally mediated by the binding of extracellular LPS to the cell surface receptor TLR4. However, it was also shown that the recognition of intracellular LPS is enhanced by IFN-γ in human intestinal epithelial cells (Suzuki et al., 2003).

In this project, HeLa cells derived from a cervical cancer specimen were used as a model to investigate the IFN-γ-induced, LPS-triggered cell death pathway, which is a cell line dependent mechanism. IFN-γ-primed embryonic cells (293ET and MEF) did

not die following transfection with LPS whereas 50% of HeLa cells died in the same conditions (**Fig.4**). This particular cell death process was also noticed in HFF and HCT116 cells (**Fig.4**), albeit to a lesser degree than in HeLa cells. This could be because the same conditions (i.e. amounts of Lipofectamine2000 and LPS) – that had been optimised to produce the greater percentage of cell death in HeLa cells – were used to transfect LPS across the different cell lines and transfection efficiency can significantly vary between different cell types (Chu et al., 1987; Yamano et al., 2010). In addition, there was always a pool of HeLa cells resistant to the treatment: around 20% of the cells did not die. The percentage of resistant cells in the population was not reduced when cells cloned from a single starter cell were employed to attempt to obtain a more homogenous population. One way forward could be to put greater effort in obtaining a population in which complete cell death (100%) was achieved following LPS transfection, as this would have the potential to generate a considerably more robust selection pressure for the screen. Lipofectamine2000 was chosen as the transfection reagent because it led to the highest cell death among the transfection reagents tested (**Fig.10A**). It is possible that an increased amount of Lipofectamine or other transfection reagents could increase the percentage of cell death, but this hypothesis was not thoroughly investigated. The titration of LPS indeed showed saturation of the transfection capacity (**Fig.10B**) indicating that this variable could be further optimised. As performed in earlier experimentation, any future optimisation experiments will include conditions without adding LPS and/or IFN-γ to control for the absence of cytotoxicity originating from either the transfection reagent or IFN-γ: the screen selection relies on cell death triggered specifically by LPS.

HeLa cells were used for primarily technical reasons: they are relatively easy to transduce and have a relatively fast doubling time, thereby shortening the overall duration of the screen. More importantly, HeLa cells displayed the phenotype being studied: that is, LPS-triggered cell death upon IFN-γ priming. HeLa cells respond to IFN-γ priming as shown by RNA-Seq (experiments performed by M. Wandel) by inducing many genes and hence protein expression. According to the Protein Atlas Database (available at http://www.proteinatlas.org, Uhlen et al., 2015), HeLa cells express both CASP4 and GSDMD in contrast to, HEK293 (293ET) cells, for example. However, higher mRNA levels for both CASP4 and GSDMD were found in

THP-1 cells, a myeloid cell type. This leads to a consideration of the role of macrophages during infection and their relevance in the experimental system employed. Most of the earlier studies showing pyroptosis resulting from the presence of cytosolic LPS and which identified caspase-11 as a direct LPS binding partner (Demon et al., 2014; Shi et al., 2014) were performed in macrophages. Macrophages and monocytes are highly sensitive to IFN-γ because they display a high concentration of IFN-γ receptors on their surface (Valente et al., 1992). The TLR4-independent activation of the non-canonical inflammasome by intracellular LPS was originally showed in macrophages (Kayagaki et al., 2013). This one-step non-canonical inflammasome was similarly activated in response to LPS in human monocytes (Viganò et al., 2015) requiring Caspases-4 and -5. These experiments were carried out in BMDM (bone-marrow derived macrophages) isolated from mice, which were knocked-out in crucial genes such as caspase-11, TLR4, or GSDMD.

Repeating the selection process in a different cell line such as immortalised macrophages might be more effective in giving further insight in the IFN-γ-induced, LPS-triggered cell death pathway. New optimisation experiments would need to be performed to address any limitation in the ability of these cells to 1) sense IFN-γ, 2) be transfected with LPS, and 3) trigger cell death in response to cytosolic LPS when primed with IFN-γ. Additional experiments will be necessary to identify conditions that could be used to produce a suitable selection pressure in a viability assay. Using macrophages would also have the potential to direct the focus away from innate immunity in non-immune cells to that in dedicated phagocytes.

Finally, the choice of the model cell line for the experiment considers the species-specific differences. As mentioned earlier, MEF cells did not die when transfected with LPS, even when primed with murine IFN-γ. *In vivo* data suggest that rodents such as mice and rats are less susceptible to sepsis when receiving a LPS dose, compared to chimpanzees or even humans. Physiological changes were noticed with a dose of 1-5ng/kg in humans whereas similar effects were observed in mice with a 105-fold higher dose of 0.5mg/kg (Vaure & Liu, 2014). This study was consistent with the results obtained here and, to some extent explains the absence of cell death in MEFs compared to 50% in HeLas (**Fig.4**).

In conclusion, the CRISPR screen successfully performed and described in this chapter, did not allow the robust identification of novel regulators or mediators in the cell death pathway following LPS challenge and enhanced by IFN-γ. However, several technical changes would be implemented in future repeats of the screen. In addition, multiple hypotheses were discussed: investigating possible redundancy between cell death pathways or cell line-specific LPS sensing mechanisms and downstream responses. Further experimental work would be necessary to address these new questions.

Chapter 3: Host responses to *Toxoplasma gondii*: Recruitment of host immune proteins and production of cytokines in an IFN-γ dependent manner

3.1 Introduction

This chapter investigates the innate immune defence against pathogens in non-immune cells; more specifically, the cell-autonomous defence against the parasite *Toxoplasma gondii*. This work complements work done in the Randow laboratory on cytosol-invading pathogens such as *Shigella flexneri* or *Salmonella enterica* serovar Typhimurium.

3.1.1 The restriction of pathogens

3.1.1.1. Role of ubiquitylation

Ubiquitylation is a versatile post-translational modification that has various effects depending on the length and the linkage types of the synthesised polyubiquitin chains (Kulathu & Komander, 2012). Ubiquitin conjugation acts as an immune signal in the case of infections. For example, K63-linked ubiquitin chains drive IFN-γ-dependent endo-lysosomal fusion of the parasitophorous vacuole (PV) that mediates killing of *T.gondii* in HeLa cells (Clough et al., 2016). In IFN-γ-primed cells, the deposition of ubiquitin chains on the parasitophorous vacuole membrane (PVM) is essential for the recruitment of sequestosome-1 (p62) that transports guanylate-binding proteins (GBPs) in proximity of the PVM. In mouse cells, GKS proteins (subfamily of IRGs, including Irga6, Irgb6) target the PVM (Haldar et al., 2013; Hunn et al., 2008) and facilitate GBP coating on the PV, but hypervirulent strains of *T.gondii* (type I) produce ROP18, which can inhibit GKS proteins by phosphorylating them (Steinfeldt et al., 2010).

During *S.*Typhimurium infection, M1-linked Ub is required for the restriction of *S.*Typhimurium proliferation (Noad et al., 2017; van Wijk et al., 2017). M1-linkage type recruits the NF-κB essential modulator (NEMO) leading to NF-κB activation

(Noad et al., 2017). However, it is currently unknown whether or not M1-linked polyubiquitin coats *T.gondii* in MEF cells. This chapter will therefore investigate the presence of linear polyubiquitin chains on *T.gondii* and the recruitment mechanism of LUBAC and its three constitutive subunits (HOIP, HOIL-1, Sharpin), because it specifically synthesises linear ubiquitin chains (M1-linkage type).

3.1.1.2. Cargo receptors are the link to autophagosome

The ubiquitin coat on bacteria acts as a recruitment platform for cargo receptors such as NDP52, p62 and Optn, ultimately leading to the recruitment of the autophagy machinery for degradation of the ubiquitylated substrate (Cemma et al., 2011; Thurston et al., 2009; Wild et al., 2011; van Wijk et al., 2017; von Muhlinen et al., 2012; Yoshikawa et al., 2009). Both NDP52 and p62 were also shown to be recruited to *T.gondii* or its PVM in IFN-γ-primed human cells (Selleck et al., 2015). However little is known about the mechanisms by which they are recruited and whether they are recruited in mouse cells. Therefore, the requirement of IFN-γ will be addressed in this chapter, together with *T.gondii* strain specificity.

3.1.2 Immune signalling during *T.gondii* infection

3.1.2.1. The protective role of IFN-γ

IFN-γ plays an essential role in defence against *T.gondii* infection. Following *T.gondii* infection with non-virulent strains, mice devoid of IFN-γ died of Toxoplasmosis whereas wild-type mice developed chronic *T. gondii* infection (Suzuki et al., 1988). IFN-γ was also shown to restrict *T.gondii* growth (Selleck et al., 2015) and, in some instances, to kill the pathogens (Zhao et al., 2008; Sasai et al., 2018). In human fibroblasts, IFN-γ triggers cell death upon *T. gondii* infection, thereby limiting replication and preventing spread of the infection (Niedelman et al., 2013).

3.1.2.2. *T.gondii* infection induces chemokine production

T. gondii infection *in vivo* triggers IFN-γ production by NK cells as a result of IL-12, TNF-α, and IL-1β production in macrophages. Furthermore, IFN-γ is also regulated by IL-10 (Hunter et al., 1994; Hunter et al., 1995; Gazzinelli et al., 1996). An extensive study (Aviles et al., 2008) characterised the variations in chemokine and cytokine levels during *T.gondii* infection, to show that proinflammatory cytokines and their receptors induce *T.gondii* tachyzoites conversion to bradyzoites preventing replication and protecting the host. Furthermore, the NF-κB signalling is activated by the *T.gondii* effector GRA15 (Sangaré et al., 2019); and NF-κB activation is known to induce the production of, for example, IL-6 in macrophages (Liu et al., 2017) or upon LPS activation (Yamamoto et al., 2004) and of IL-8 (Keusekotten et al., 2013).

In order to understand the immune response against *T.gondii* in greater detail, the role played by IFN-γ was investigated using a targeted approach that considered proteins related to autophagy such as the linear ubiquitin-binding assembly complex (LUBAC) and cargo receptors such as NDP52, Sequestosome-1 (p62) and Optineurin (Optn). The recruitment mechanisms of these proteins to the parasite were investigated using microscopy (see paragraph **3.2**). The potential relationship of LUBAC with the production of signalling molecules such as cytokines was also investigated (see paragraph **3.3**).

3.2 Results: Protein recruitment to *T.gondii*

One of the principal goals of this study was to investigate the recruitment of proteins to the vicinity of *T.gondii*, i.e. either to the parasitophorous membrane or to the parasite itself, that might be associated to the cellular immune response to this pathogen. Following infection, cytosolic *S.*Typhimurium are targeted by host proteins of the autophagy machinery, resulting in either degradation of the pathogens or restriction of their replication (Wang et al., 2018a). Similarly to cytosolic bacteria and even though *T.gondii* is a eukaryotic parasite, it (or its parasitophorous vacuole membrane – PVM) has been shown to be coated by ubiquitin (Coers & Haldar, 2015). In order to investigate whether either *T.gondii* or its PVM behaves as an immune signalling platform, MEF cells were infected with the parasite. Because the precise

location of the recruitment was not addressed in this study, the word *T.gondii*, as used throughout the chapter, probably refers to the PVM since it is the likely target of such host proteins.
In case there was a difference between *T.gondii* strains, two different strains were used: type I – RH – which is more virulent than type II – PRU (Zajdenweber et al., 2007). Both strains were engineered to express Td-tomato fluorophore and could therefore be used in microscopy and imaging experiments.

3.2.1 Type II *T.gondii* is targeted by host proteins

3.2.1.1. Cytosolic exposure of type II *T.gondii* is IFN-γ-independent

Galectin-8 (GAL8) is an early marker of cytosolic entry of *S.*Typhimurium because it binds exposed intravesicular glycans, hence colocalising with membrane remnants of the broken vacuoles (Randow et al., 2013). GAL8 recruits cargo receptors such as NDP52 (Li et al., 2013), which associates with "eat-me" signals (Randow & Youle, 2014) for the targeting of bacteria to xenophagy (Thurston et al., 2012).

To determine whether GAL8 was recruited to *T.gondii*, MEF cells seeded on coverslips were infected with type II (PRU) *T.gondii* for 1h, before being fixed with PFA and later immunostained with the GAL8 antibody. Although the fluorescence levels were low and therefore recruitment events challenging to detect (**Fig.1A**), 34% of intracellular *T.gondii* were counted positive for GAL8 in the absence of IFN-γ, whereas 22% were positive following IFN-γ priming (**Fig.1B**). However, this difference was not considered to be statistically significant ($p > 0.05$).

This experiment demonstrated that IFN-γ priming did not induce a difference in the recruitment of GAL8, shortly after active invasion of type II *T.gondii* parasites. This result suggested an IFN-γ-independent entry mechanism of *T.gondii* in the cytosol of the host cells. This is an unexpected result and may possibly be the result of non-specific antibody binding.

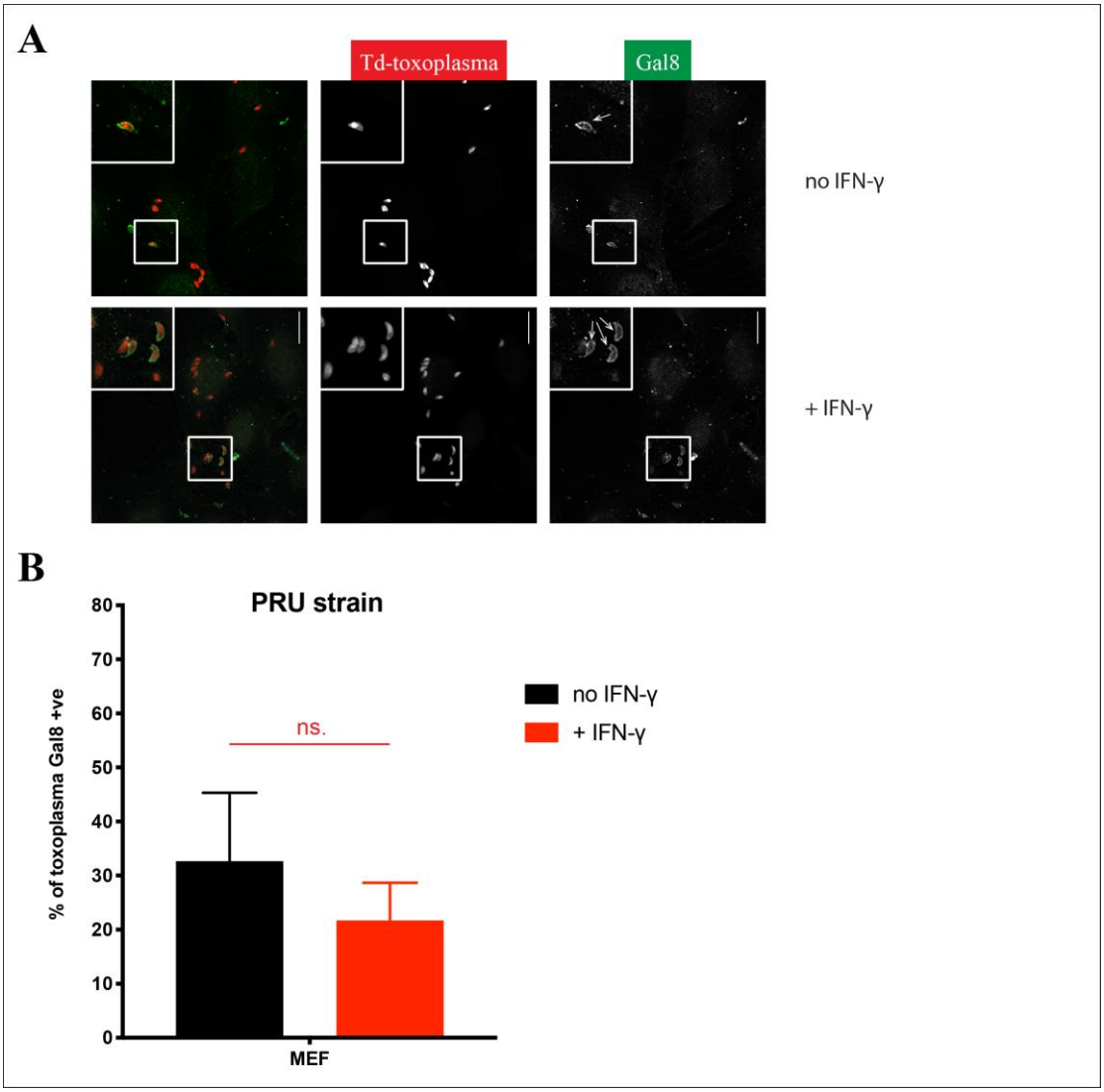

Figure 1: Galectin-8 is localised to type II *T.gondii*

MEF cells were infected with type II (PRU) *Toxoplasma gondii* strain in 4:1 ratio compared to the number of cells seeded on coverslips. Cells were incubated with IFN-γ overnight before infection. At 1h post-infection, cells were washed and fixed with 4% PFA. Coverslips were stained using Galectin-8 as primary antibody followed by Alexa488 as secondary antibody. (A) Images of PRU-infected cells were taken on a Zeiss-780 microscope using a 63x oil-immersion objective. Scale bar is 20μm. (B) At least 100 *T.gondii* were counted for each coverslip and the number of GAL8-positive *T.gondii* was recorded. Data are shown as Mean ± S.E.M from four independent experiments, all performed in duplicate. ns (not significant), unpaired t test without assuming a consistent SD scoring for the difference of GAL8-coating in the presence or absence of IFN-γ priming.

It was indeed noticed that the antibody stained a few extracellular *T.gondii*. Even though only intracellular parasites were counted, it is possible that the GAL8 antibody recognises *T.gondii* irrespective of their location. An alternative method relying on the overexpression of GFP-tagged GAL8 in MEFs could be used to validate this

interpretation. GFP-GAL8-overexpressing MEFs would then be infected with *T.gondii* to look at GAL8 specific recruitment to intracellular *T.gondii*. In this way, the requirement of IFN-γ or its effect on inducing *T.gondii* cytosolic entry would be addressed.

Following cytosolic entry and escape from the SCV, *S*.Typhimurium is ubiquitinylated by multiple E3 ligases, including LUBAC (Noad et al., 2017). Ubiquitin chains act as anchors for autophagy cargo receptors (von Muhlinen et al., 2012; Wild et al., 2011; Zheng et al., 2009). To establish whether similar events happen in the case of *T.gondii* infections, other microscopy-based experiments were performed and are detailed in the next paragraphs.

3.2.1.2. Ubiquitin coats *T.gondii* in MEFs

Initially, MEF cells seeded on coverslips were infected with either type I (RH) or type II (PRU) *T.gondii* for 1h, before being fixed with PFA and later immunostained with the FK2 antibody, which recognises all ubiquitin chains. FK2-positive parasites were counted among the infectious *T.gondii*, defined as intracellular parasites, which were typically located close to the nucleus (Denkers et al., 2004).

Very few events (3%) were recorded with the type I (RH) *T.gondii* strain; whereas, in cells infected with the PRU (type II) strain, 12% of *T.gondii* were FK2-positive in the absence of IFN-γ priming (**Fig.2A**). Moreover, ubiquitin conjugation was greatly enhanced, increasing from 12% to 56% of the parasites, when cells were primed overnight with murine IFN-γ (**Fig.2B**). This indicates that ubiquitin was primarily attached to type II *T.gondii* and was significantly ($p<0.0001$) induced by priming with IFN-γ.

The presence of Ub chains in the vicinity of *T.gondii* suggests the recruitments of one or multiple E3-ligase(s) for the synthesis of these chains and of downstream effectors such as autophagy cargo receptors. Both questions were subsequently addressed studying the role of LUBAC and of NDP52, p62 and Optn, specifically.

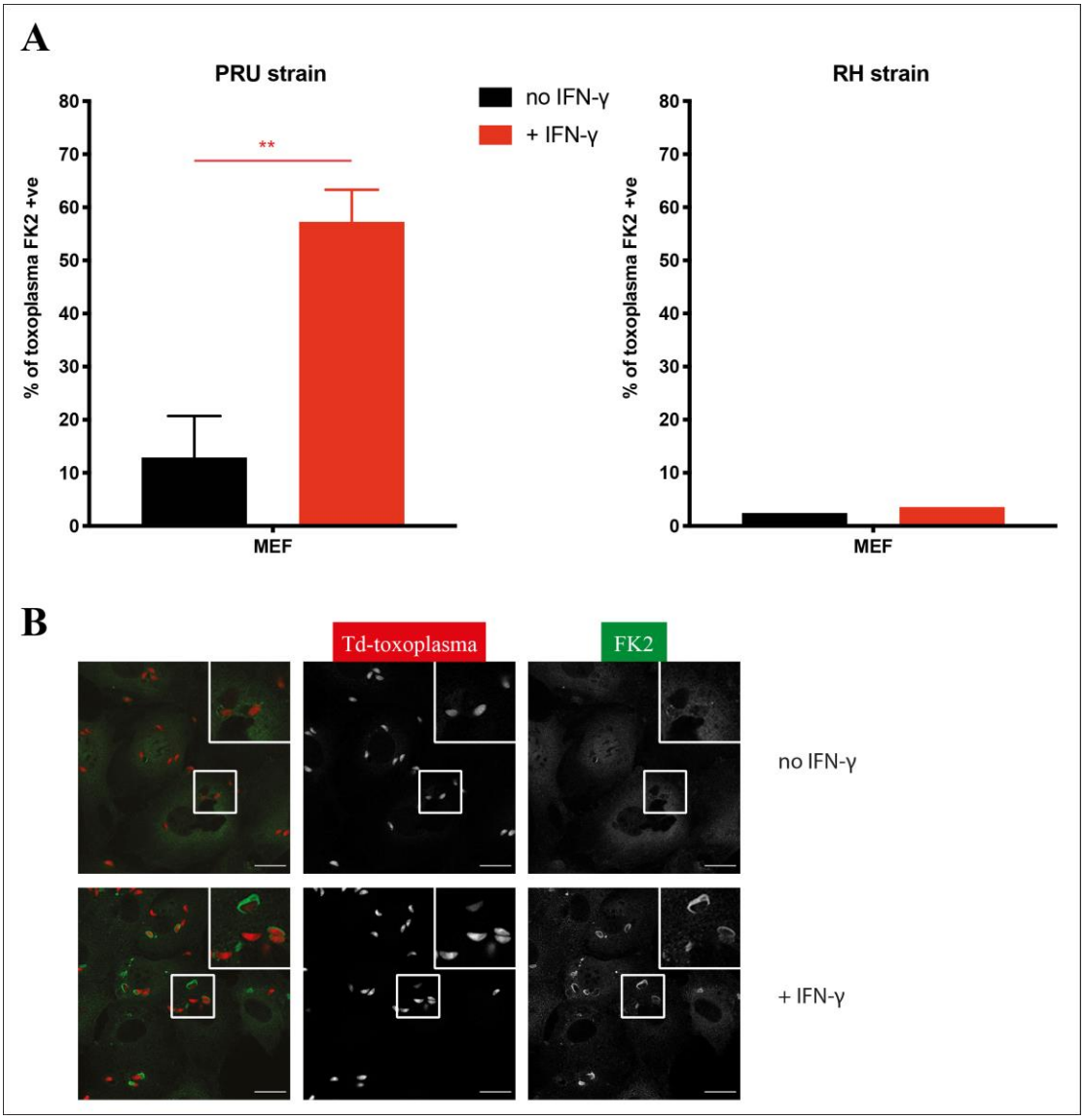

Figure 2: Ubiquitin is conjugated to type II *T.gondii* parasites

MEF cells were infected with type II (PRU) or type I (RH) *T. gondii* strains in 4:1 ratio compared to the number of cells seeded on coverslips (MOI of 4:1). Cells had been incubated with IFN-γ overnight before the infection. At 1h post-infection, cells were washed with PBS and fixed with 4% PFA. Coverslips were immunostained for ubiquitin chains with the FK2 antibody, followed by Alexa488. At least 100 parasites were counted for each coverslip and the number of FK2-positive *T.gondii* was recorded (A), data are shown as Mean ± S.E.M from five independent experiments, all performed in duplicate. **P<0.0001, unpaired t test without assuming a consistent SD scoring for the difference of Ub-coating in the presence or absence of IFN-γ priming. (B) Images of PRU-infected cells were taken on a Zeiss-780, microscope using a 63x oil-immersion objective. Scale bar is 20μm.

3.2.2 LUBAC colocalises with type II *T.gondii*

The linear ubiquitin assembly complex (LUBAC) acts as an E3-ligase that specifically synthesises linear (M1-linked) ubiquitin chains (Kirisako et al., 2006). Linear ubiquitin chains are detected by FK2 staining, as would K63, K48, and all the other ubiquitin linkage types (except for K6) without distinction (Noad et al., 2017; Wandel et al., 2017; Zheng et al., 2009). Because ubiquitin coats type II *T.gondii*, the presence and role of LUBAC were assessed during *T.gondii* infection.

3.2.2.1. LUBAC is recruited to the PRU in an IFN-γ-dependent manner

LUBAC is a heteromultimeric complex containing the proteins HOIP, HOIL-1, and Sharpin. It induces NF-κB signalling and thereby promotes inflammation and inhibits apoptosis (Brummelkamp et al., 2003; Gerlach et al., 2011; Ikeda et al., 2011; Tokunaga et al., 2011). Since ubiquitin was conjugated with type II *T.gondii* (**Fig.1**), GFP-tagged human HOIP, HOIL-1, and Sharpin were overexpressed in MEF cells (**Fig.3A**) to investigate their recruitment to both strains of *T.gondii*. Both strains of *T.gondii*, engineered to express the Td-tomato fluorophore, were used to infect IFN-γ-primed MEFs. Cells were imaged using microscopy, (**Fig.3B**) and recruitment of each individual LUBAC subunit was counted manually.

At 1h post-infection, MEFs infected with RH (type I strain) did not show recruitment of any of the LUBAC subunits (**Fig.3C**, right graph). By contrast, infection with PRU led to recruitment of all three LUBAC subunits in an IFN-γ-dependent manner. HOIP, HOIL-1, and Sharpin were recruited to less than 10% of the parasites without IFN-γ, but colocalisation was significantly ($p<0.05$, $p<0.05$ and $p<0.0001$ respectively) increased when cells were primed overnight with IFN-γ to reach respectively 25%, 21%, 42% of intracellular *T.gondii* (**Fig.3C**, left graph). This 2-fold difference in recruitment between HOIP, HOIL-1 on the one hand (~ 20%) and Sharpin on the other hand (~ 40%) might be explained by Sharpin being recruited by both HOIP and HOIL-1; and also by HOIL-1 and HOIP recruitments being exclusive.
This experiment demonstrated that only the PRU strain was targeted by HOIP, HOIL-1, and Sharpin, and that recruitment of these proteins was significantly induced by IFN-γ.

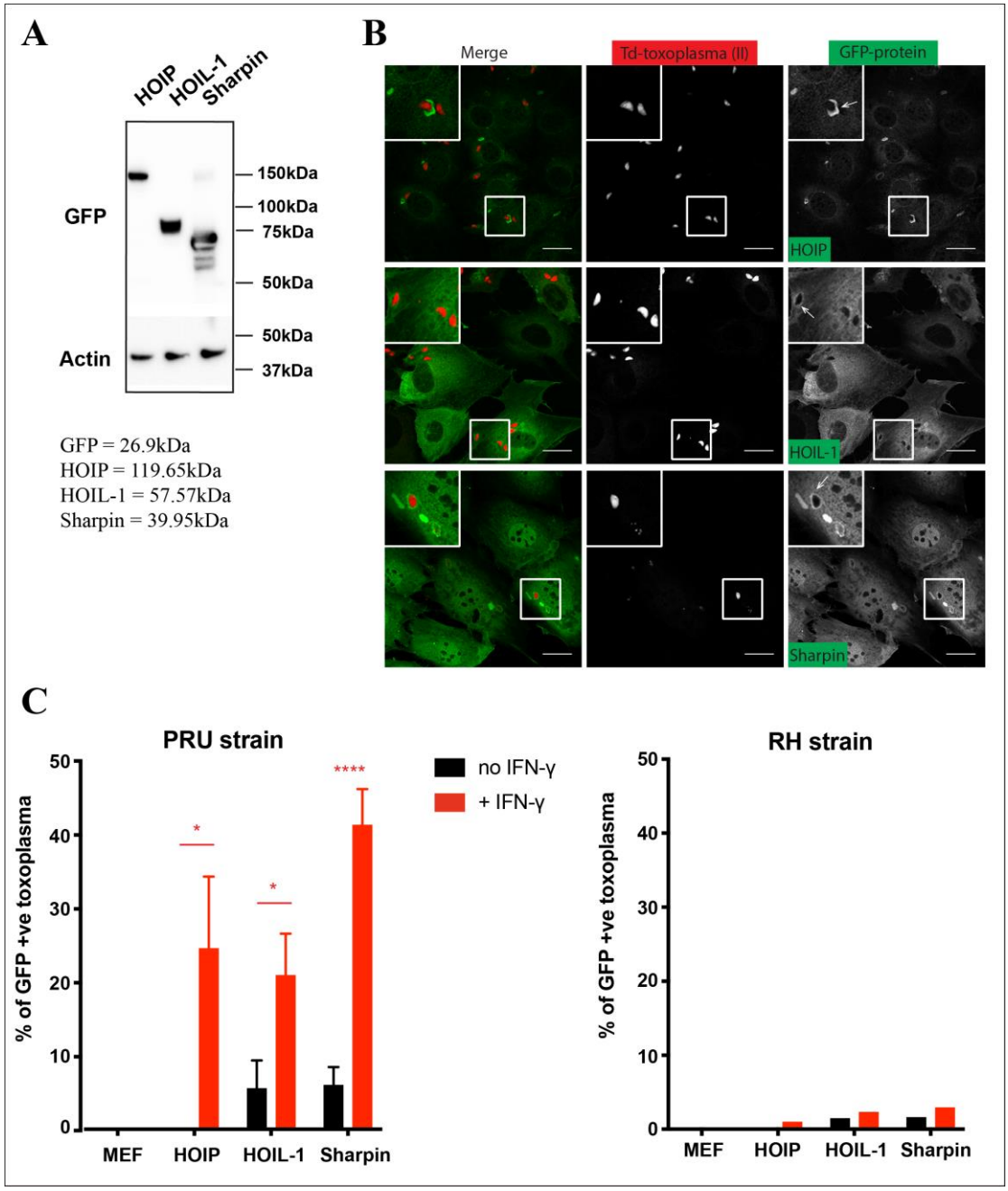

Figure 3: LUBAC subunits are recruited to PRU *T.gondii* parasites in an IFN-γ-dependent manner

MEF cells overexpressing GFP-tagged human LUBAC subunits (HOIP, HOIL-1, Sharpin) were infected with type II (PRU) or type I (RH) *Toxoplasma gondii* strains (MOI of 4:1). Cells were incubated with IFN-γ overnight before the infection. (A) Expression levels of all three LUBAC subunits were assessed by western-blotting probing for GFP. (B) At 1h post-infection, cells were washed with PBS and fixed with 4% PFA. Images of PRU-infected cells were taken on a Zeiss-780 microscope, using a 63x oil-immersion objective. Scale bar is 20µm. (C) At least 100 *T.gondii* were counted for each coverslip and the number of GFP-positive *T.gondii* was recorded. Results from three independent experiments, all performed in duplicate, are shown as Mean ± S.E.M. *P<0.05, ****P<0.0001, multiple unpaired t-test without assuming a consistent SD scoring the difference of protein recruitment in the presence or absence of IFN-γ priming.

Constructs for the expression of GFP-tagged wild-type HOIP, HOIL or Sharpin were generated by Dr. Felix Randow.

The next experiments will address the requirement of each individual LUBAC subunit for the recruitment of the others.

3.2.2.2. Kinetic analysis of the recruitment of HOIP, HOIL-1 and Sharpin

In the previous experiment, infected cells were fixed at 1h post-infection. Analysis by microscopy showed that: first, all three proteins (HOIP, HOIL-1, Sharpin) were recruited specifically to the PRU strain; and second, their recruitment was enhanced when cells were treated with IFN-γ overnight before infection. To see whether recruitment of the different proteins changed over time, IFN-γ-primed MEF cells overexpressing GFP-tagged wild-type HOIP, HOIL-1, and Sharpin were infected with type II *T.gondii* (PRU strain). Cells were then fixed not only at 1h post-infection but also at 2h and 6h post-infection.

The recruitment kinetics of these three proteins was different. HOIL-1 did not show a significant change in recruitment over these three time points, as 18% at 1h and ~13% at both 2h and 6h of the intracellular *T.gondii* parasites were counted positive. However, HOIP and Sharpin showed the highest percentages of recruitment at 1h post-infection, after which their recruitment to type II *T.gondii* was reduced over time (**Fig.4**). For example, Sharpin was recruited to 37% of *T.gondii* at 1h, but then only to 27% at 2h and to 20% at 6h post-infection. This decrease could be due to parasites dying over time. Using a vacuole marker, for instance, will help addressing this question assuming that opened and broken parasitic vacuoles account for dead parasites. An alternative strategy will be to employ death dyes that could be incorporated in the cell cytoplasm and stain dead parasites.

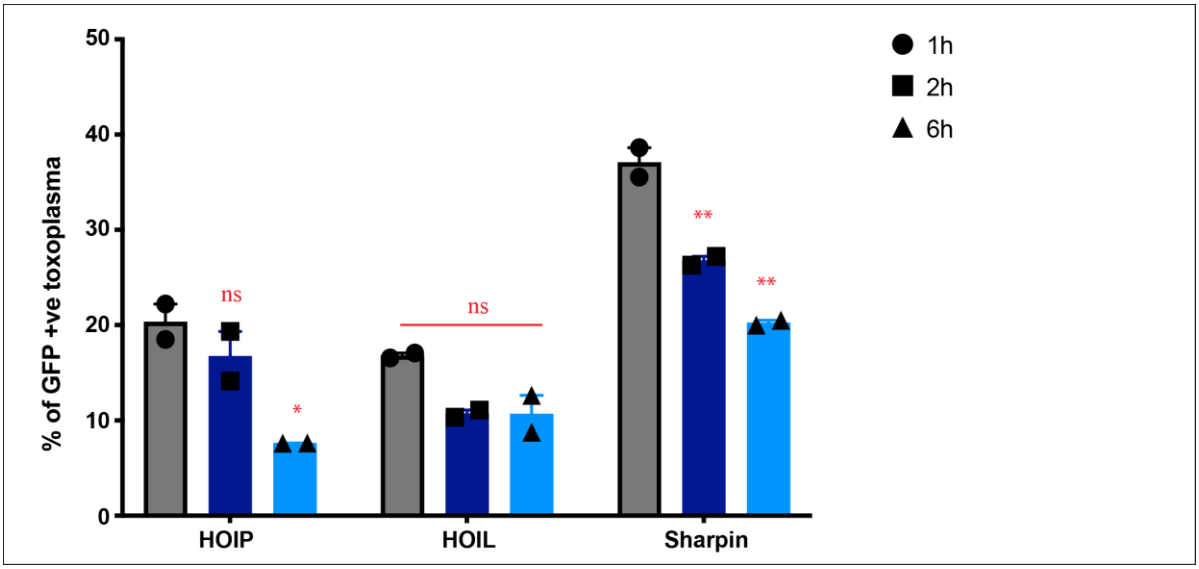

Figure 4: Kinetics of recruitment of LUBAC subunits to PRU

MEF cells overexpressing GFP-tagged human LUBAC subunits (HOIP, HOIL-1, Sharpin) were infected with type II (PRU) *Toxoplasma gondii* strain (MOI of 4:1). Cells were incubated with IFN-γ overnight before the infection. At 1h post-infection, cells were washed with PBS and fixed with 4% PFA. At least 100 *T.gondii* were counted for each coverslip and the number of GFP-positive *T.gondii* was recorded. Results from three independent experiments, all performed in duplicate, are shown as Mean ± S.E.M. *P<0.05, **P<0.005, ns (not significant), unpaired t test without assuming a consistent SD, scoring for the difference of recruitment at 2h and 6h compared to the 1h time point, for each construct.
Constructs for the expression of GFP-tagged wild-type HOIP, HOIL or Sharpin were generated by Dr. Felix Randow.

Of the time points tested, 1h post-infection appeared to produce the highest levels of protein recruitment to type II *T.gondii*. Consequently, all subsequent experiments were performed using only the PRU strain, priming cells overnight with IFN-γ and fixing cells at 1h post-infection. However, it is worth bearing in mind that other proteins may have different (slower or faster) kinetics.

3.2.2.3. HOIP, HOIL-1, and Sharpin are recruited independently from each other

In the case of *S.*Typhimurium, LUBAC recruitment is HOIP-dependent. HOIL-1 and Sharpin both require the presence of the HOIP subunit to be recruited to these bacteria (Noad et al., 2017). In order to determine whether the same recruitment mechanism

takes place with *T.gondii*, GFP-HOIP, -HOIL-1, and -Sharpin were overexpressed in MEFs. These cells were transfected with siRNA to knock-down the expression of the other two LUBAC subunits (**Fig.5A**); e.g. in GFP::HOIP-overexpressing MEFs, HOIL-1 and Sharpin were knocked down. These cells were infected with type II *T.gondii* (PRU strain) after overnight priming with IFN-γ. HOIP, HOIL-1 and Sharpin were respectively counted on 35%, 20% and 30% of *T.gondii*, in both the control and the double knock-downs cell lines (**Fig.5B**).

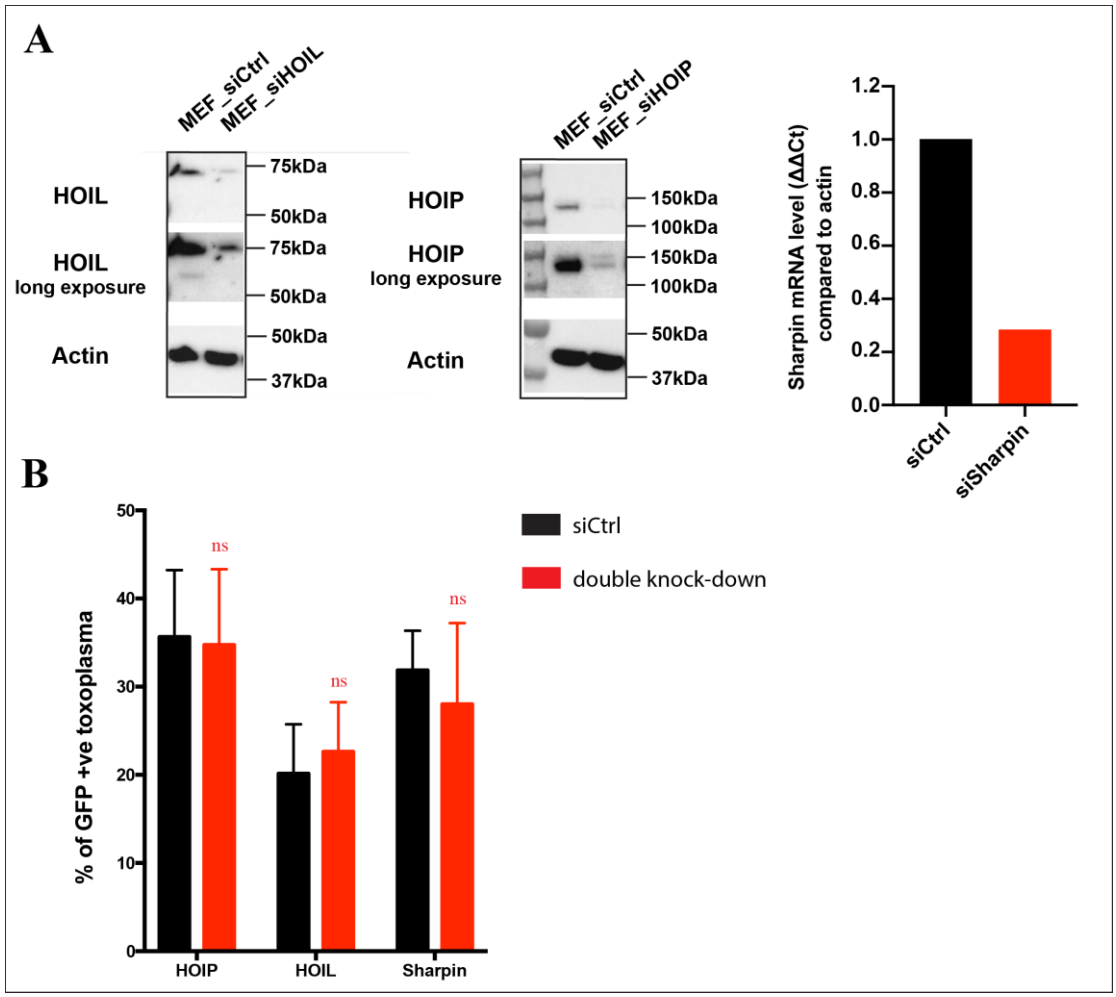

Figure 5: The LUBAC subunits are recruited independently of each other

MEF cells overexpressing GFP-tagged human subunits of LUBAC (i.e HOIP, HOIL-1 and Sharpin) were transfected with either control siRNA (siCtrl) or with a combination of both siRNAs targeted the other two subunits of the complex. For example, GFP-HOIP overexpressing MEFs were transfected with siRNAs against HOIL-1 and Sharpin. (A) Efficiency of the individual knock-downs was assessed by western-blotting for HOIP and HOIL-1 and by qPCR for Sharpin. (B) At 48h after siRNA treatment, cells were primed with IFN-γ overnight before infection with type II (PRU) *Toxoplasma gondii* strain (MOI of 4:1). At 1h post-infection, cells were washed and fixed with 4% PFA. At least 100 *T.gondii* were counted for each coverslip and the number of GFP-positive *T.gondii* was recorded. Results from three independent experiments, all performed in duplicates are shown as Mean ± S.E.M.

ns (not significant), one-way ANOVA with Dunnett's multiple comparisons test comparing with the control condition (siCtrl).
Constructs for the expression of GFP-tagged wild-type HOIP, HOIL or Sharpin were generated by Dr. Felix Randow.

This experiment suggests that the three LUBAC subunits bind independently to *T.gondii*. The residual expression of the different LUBAC subunits in the case of the double knock-downs might be sufficient for the recruitment of the other subunit. To test that hypothesis, the same experiment would need to be performed in knockout cells, ensuring the complete absence of the proteins.

To explore whether the three subunits each recognise different ligands or bind the same ligand but using three distinct binding modes, experiments were performed to understand the recruitment mechanism of HOIP (see paragraph **3.2.2.4** "HOIP is recruited via two distinct mechanisms").

3.2.2.4. HOIP is recruited via two distinct mechanisms

In order to further investigate the recruitment mechanism of LUBAC, a range of constructs expressing GFP-tagged truncations or mutated versions of human HOIP (**Fig.6A**) were tested for recruitment to type II *T.gondii* in IFN-γ primed MEFs. Expression of each construct was confirmed by western-blotting with a GFP antibody (**Fig.6B**).

To determine whether some specific domains were necessary and/or sufficient for HOIP recruitment, protein truncations were used. Both N-terminal fragments containing the PUB domain either alone (residues 1-294; N294) or also containing the triple zinc-finger (residues 1-438; N438) were recruited to a level similar to that observed for the wild-type protein. Threonine360 and Arginine375 are essential for binding to Ub chains and recruiting NEMO respectively (Fujita et al., 2014). Additionally, mutating the second zinc-finger at these two residues (T360A or R375A) in the N-terminal fragment (N438) did not alter the recruitment compared to wild-type (**Fig.6C**). This indicates that the PUB domain is sufficient to bind to type II *T.gondii* in IFN-γ-primed cells and that the recruitment of N-terminal part of HOIP is

independent of Ub and NEMO. To support this hypothesis, C-terminal truncations lacking the PUB domain: ΔN294, ΔN438, and ΔN527 were observed to be impaired in their recruitments and respectively colocalised with 13%, 7% and 3% of *T.gondii* compared to 25% for the wild-type. Further investigation into the recruitment mechanism showed that, by contrast, the UBA domain was not required for binding because overexpression led to significant drop in recruitment (5%), similar to other C-terminal constructs (**Fig.6C**). However, the UBA domain is required for the interaction with endogenous HOIL-1 and together with the RBR domain, has been shown to be essential for recruitment of HOIP to *S.*Typhimurium (Noad et al., 2017). In summary, these experiments indicate that neither the catalytic activity (RBR domain) nor HOIL-1 is required for HOIP binding to *T.gondii* (PRU strain).

Interestingly, the full-length protein mutated in the ubiquitin-binding residue (T360A) showed a significant ($p<0.0001$) decrease in its ability to recruit to *T.gondii*. Only 8% of intracellular *T.gondii* recruited the mutated protein compared to 25% for the wild-type protein. This suggests that in the context of the full-length protein, Zn finger 2 is necessary for recruitment. Following up on this observation, constructs expressing the individual Zn fingers and combinations of the three ZnFs were used to study the extent to which they were required for HOIP recruitment. All the individual ZnF domains on their own, as well as the triple ZnF fragment, were recruited to *T.gondii* to similar levels as those seen with wild-type HOIP. This indicated that, in addition to the PUB domain, any zinc-finger domain in HOIP was sufficient to bind to *T.gondii*. Overexpression of a pair of successive ZnF – i.e. ZnF1+ZnF2 or ZnF2+ZnF3 – showed increased recruitment (42% and 48%, respectively) compared to wild-type (25%).

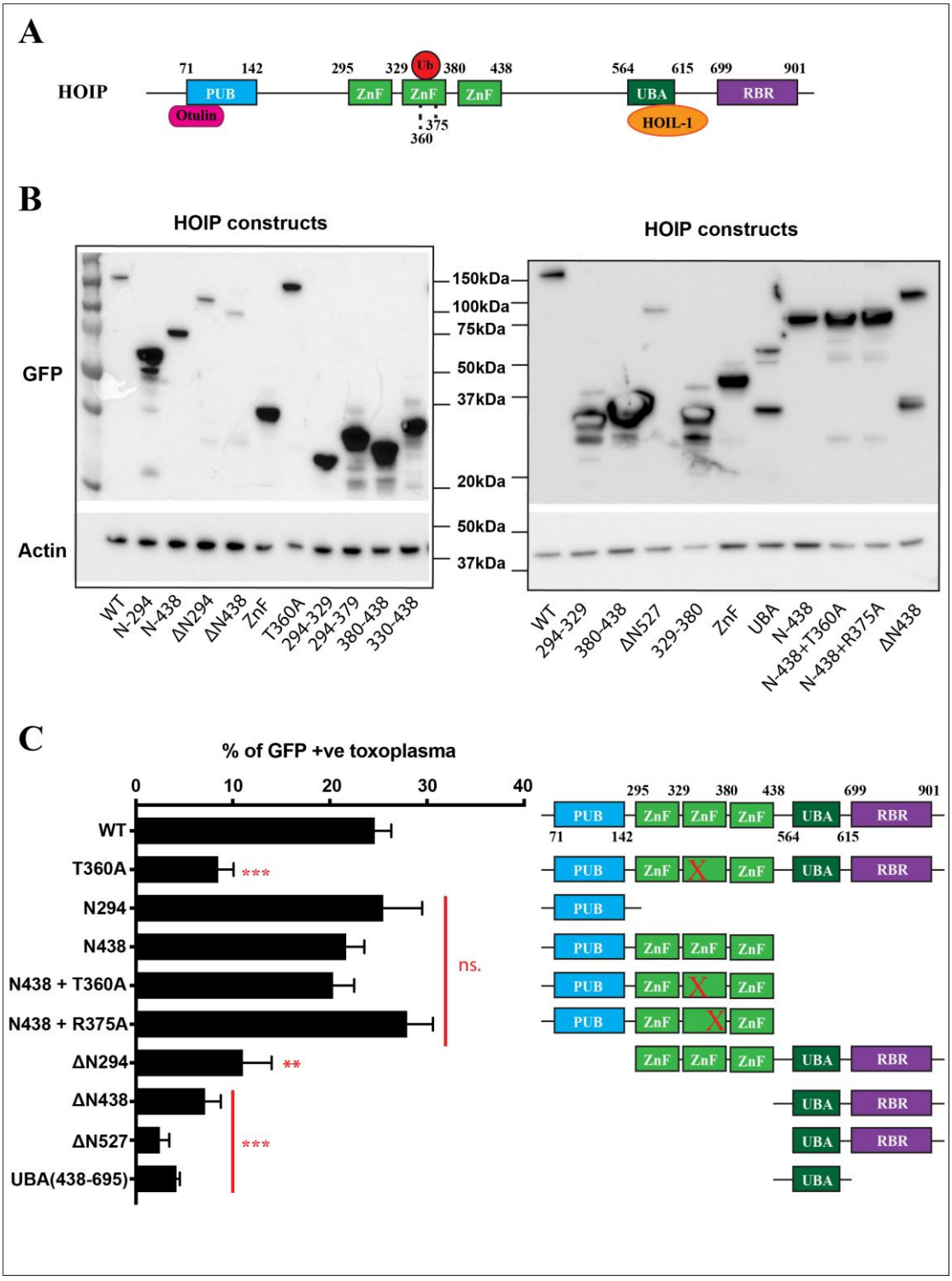

figure continued on next page

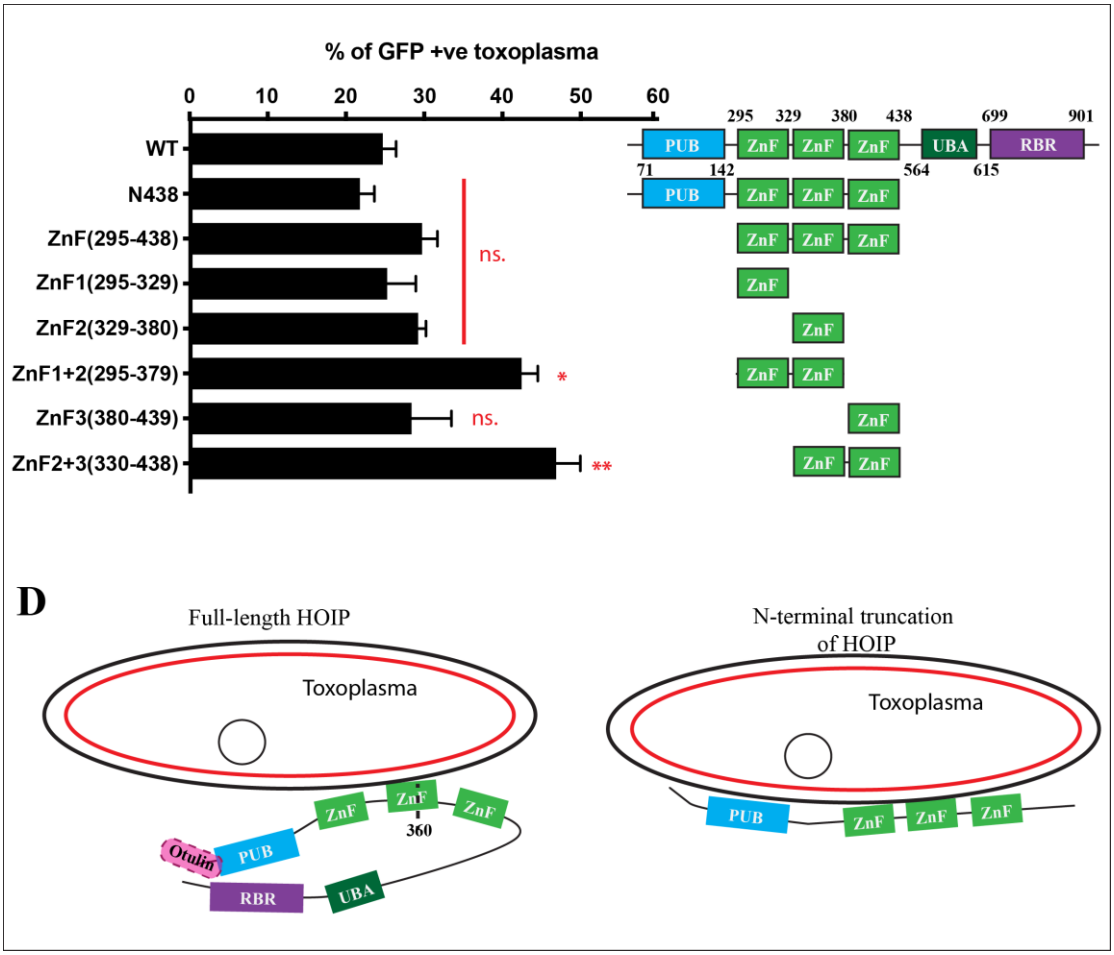

Figure 6: The 2-mode recruitment mechanism of HOIP

(A) Schematic of human HOIP with the various domains and mutated sites. MEF cells overexpressing GFP-tagged constructs of mutated and truncated forms of human HOIP were primed with IFN-γ overnight before infection with type II (PRU) *Toxoplasma gondii* strain (MOI of 4:1). (B) Overexpression of the constructs was checked by western-blot probing for GFP. (C) At 1h post-infection, cells were washed and fixed with 4% PFA. At least 100 *T.gondii* were counted for each coverslip and the number of GFP-positive *T.gondii* recorded. Results from three independent experiments, all performed in duplicate, are shown as Mean ± S.E.M. *P<0.005, **P<0.0002, ***P<0.0001, ns (not significant), one-way ANOVA with Dunnett's multiple comparisons test comparing with the wild-type. (D) Schematic of the hypothetical recruitment mechanisms of HOIP to *T.gondii*. The full-length protein is mostly bound through the triple zinc-finger domain; by contrast, the N-terminal part can also bind via the PUB domain, freed from the inhibition exerted by the C-terminal part of HOIP.
Constructs for the expression of GFP-tagged mutated or truncated HOIP were generated by Dr. Jessica Noad.

In conclusion, HOIP appears to be recruited to type II *T.gondii* in IFN-γ-primed MEFs through two distinct mechanisms (**Fig.6D**). First, in the full-length protein, the UBA and/or RBR domain(s) exert(s) an inhibitory effect on the PUB domain. Binding

to *T.gondii* is then mediated by the zinc-finger domain, especially ZnF2. Such a scenario is not surprising because HOIP exists in an auto-inhibited form, where the UBA domain represses the catalytic activity by blocking the RBR domain (Kirisako et al., 2006; Smit et al., 2012). The requirement of the catalytic activity should be addressed in future experiments. Second, the recruitment of N-terminal HOIP is mainly driven by the PUB domain.

Through its binding to NEMO (Arg375), Ub (T354/F355) (Fujita et al., 2014) and OTULIN via the PUB domain (Elliott et al., 2014; Schaeffer et al., 2014), HOIP is essential for the activation of NF-κB signalling: for example, it regulates immune and inflammatory responses in response to PAMPs. During apoptosis, HOIP can undergo cleavage by effector caspases at Asp390 (Joo et al., 2016) releasing the N- and C-terminal fragments separately, consequently separating HOIP's functions. Although the C-terminal part retains its catalytic activity, linear ubiquitylation of the substrate NEMO is decreased (Goto & Tokunaga, 2017). Moreover, phosphorylated OTULIN (at Tyr56) bound to HOIP's PUB domain negatively regulates HOIP ubiquitylation (Elliott et al., 2014; Schaeffer et al., 2014). This latter role of OTULIN could explain the double recruitment mechanism of HOIP to *T.gondii*: the presence of the catalytic domain (hence the full-length model) provides substrates to OTULIN requiring the PUB domain to be available for binding, and thus HOIP recruitment is mediated by the zinc-finger. In the cleaved form of HOIP, PUB recruitment to *T.gondii* is then favoured.

Future experiments should also investigate the recruitment mechanisms of HOIL-1 and Sharpin to determine whether, for example ubiquitin binding is required.
Within the scope of this project and because *T.gondii* is ubiquitinylated and recruits LUBAC, the recruitment of autophagy cargo receptors was addressed next (see section **3.2.3** "Recruitment of autophagy cargo receptors"), following the comparison with cell-autonomous defence mechanisms during *S.*Typhimurium infection.

3.2.3 Recruitment of autophagy cargo receptors

Cargo receptors act as intermediates between cargo proteins and autophagosomal membranes. They are recruited to their partners by binding to their Ub coats or other 'eat-me' signals (Birgisdottir et al., 2013; Boyle & Randow, 2013; Stolz et al., 2014; Thurston et al., 2012). These receptors include Calcium-binding and coiled-coil domain-containing protein 2 (NDP52), Sequestosome-1 (p62) and Optineurin (Optn) (see **Chapter 1, Fig.4**), factors that are known to bind the ubiquitin coat of cytosolic bacteria and to play a role in restricting bacterial proliferation (Thurston et al., 2009; Wild et al., 2011) and to be essential for targeting bacteria to autophagy (Zheng et al., 2009; Mostowy et al., 2011). Because NDP52 (Xie et al., 2015), p62 (Seibenhener et al., 2004) and Optn (Wild et al., 2011) can bind ubiquitin, together with the fact that type II *T.gondii* was coated with ubiquitin (**Fig.2**), the recruitment of NDP52, p62 and Optn to PRU was investigated further in IFN-γ-primed MEF cells.

3.2.3.1. NDP52, p62 and Optn recruitment to type II *T.gondii* is IFN-γ-dependent

MEF cells overexpressing GFP-tagged wild-type human NDP52, p62 or Optn (**Fig.7A**) that had been primed with IFN-γ overnight were infected with both strains of *T.gondii*. Coverslips were then imaged (**Fig.7B**) and the extent to which each cargo receptor protein was recruited, was manually counted on the microscope.

Infection with the type II strain (PRU) resulted in all three cargo receptor proteins being recruited, although only in cells that had been primed overnight with IFN-γ. Thus, NDP52, p62, and Optn were recruited to less than 2% of the parasites in cells grown in standard conditions. NDP52, p62 and Optn colocalisation was significantly ($p<0.05$, $p<0.0001$, $p<0.0002$, respectively) increased when cells were primed overnight with IFN-γ to reach respectively 15%, 36%, and 28% of intracellular *T.gondii* (**Fig.7C**, left graph). By contrast, none of these proteins were recruited to RH (type I strain) in MEFs (**Fig.7C**, right graph). This experiment demonstrated that NDP52, p62, and Optn target only the PRU strain and that IFN-γ priming is required for efficient recruitment of these proteins.

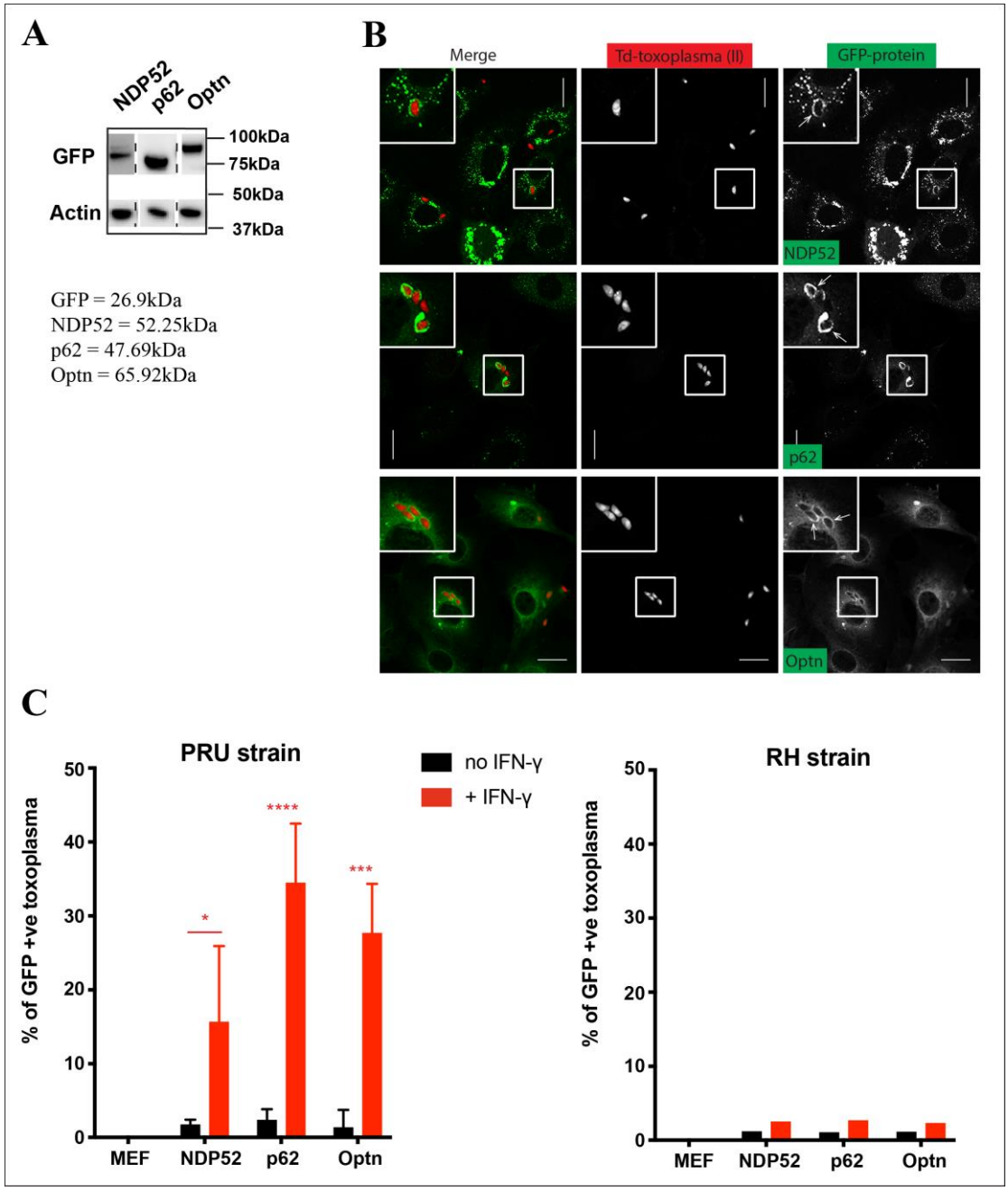

Figure 7: Cargo receptors are recruited to PRU parasites in an IFN-γ-dependent manner

MEF cells overexpressing GFP-tagged human cargo receptor proteins (NDP52, p62, Optn) were infected with type II (PRU) or type I (RH) *Toxoplasma gondii* strains (MOI of 4:1). (A) Expression levels of these three overexpressed proteins were assessed by western-blotting. Cells were incubated with IFN-γ overnight before infection. At 1h post-infection, cells were washed and fixed with 4% PFA. (B) Images of PRU-infected cells were taken on a Zeiss-780 microscope, using a 63x oil-immersion objective. Scale bar is 20μm. (C) At least 100 *T.gondii* were counted for each coverslip and the number of GFP-positive *T.gondii* was recorded. Results from three independent experiments, all performed in duplicates are shown as Mean ± S.E.M. *P<0.05, ***P<0.0002, ****P<0.0001, multiple unpaired t-test without assuming a consistent SD scoring the difference in protein recruitment in the presence or absence of IFN-γ priming.

Constructs for the expression of GFP-tagged wild-type Optn and p62 were generated by Dr. Ben Ravenhill; the GFP-tagged wild-type NDP52 by Dr. Jessica Noad.

The recruitment of these three cargo receptors was initially investigated because they bind to ubiquitin. This hypothesis could be tested in follow-up experiments targeting ubiquitin chains for degradation using deubiquitinases (DUBs), after which recruitment events would again be counted. This protocol could be used to assess whether M1-ubiquitin linkages are necessary for NDP52, p62 or Optn recruitment by overexpressing OTULIN – a DUB specific for linear ubiquitin chains (Keusekotten et al., 2013) – and hence removing specifically LUBAC-synthesised ubiquitin chains. Because overexpression of deubiquitinases could be detrimental for the cells, the overexpression of autophagy cargo receptors deficient in Ub-binding would be preferred.

Next, in order to investigate NDP52, p62, and Optn recruitment mechanisms to type II *T.gondii*, GFP-tagged truncations or mutants of these three cargo receptors were expressed in MEFs. The experiments are detailed and the results explained in paragraphs **3.2.3.2** for NDP52, **3.2.3.3** for p62 and **3.2.3.4** for Optn.

3.2.3.2. NDP52 recruitment is independent of GAL8-binding

NDP52 (**Fig.8A**) is an essential protein in the autophagy targeting *S.*Typhimurium. It is recruited to broken SCVs via GAL8 (Thurston et al., 2009, 2012) and leads to autophagophore formation via binding to LC3 (Slobodkin & Elazar, 2013). In more recent research, there has been evidence for NDP52 forming a heterotrimer by binding both FIP200 and SINTBAD/NAP1 via its SKICH domain and through them, recruiting respectively the ULK and TBK1 complexes that are crucial in the first steps of autophagosome formation (Ravenhill et al., 2019). The role and, more specifically, the recruitment mechanism of NDP52 were therefore investigated in this project.

First, three GFP-tagged full-length mutants were overexpressed in MEFs (**Fig.8B**). Their overexpression was checked by western-blotting using a GFP antibody. Only the D439K mutant in the ZnF domain showed a band higher than expected (79.2kDa).

The sample did not migrate in a fashion similar to that observed with the wild-type and the other mutants: this could be due to protein aggregation. Sequencing the construct confirmed that there was only the D439K missense point mutation. If analysis had been performed by western-blotting with a NDP52 antibody, this might have excluded the possibility that this band represented the expression of a different protein. To avoid misinterpretation, D439K mutant-expressing cells were not considered during the analysis. However, this mutant is worth investigating because it prevents NDP52 binding to Ub and cytosolic *S.*Typhimurium recognition is abrogated with D439R mutation (Xie et al., 2015).

The L374A single point mutant – which eliminates the ability of binding to GAL8 – was recruited to 13% of type II *T.gondii*; this is a result very similar to the 16% obtained with the wild-type protein (**Fig.8C**). This suggests that NDP52 recruitment to PRU is GAL8-independent. The inability of NDP52 to bind LC3C, as a consequence of the V136S mutation, significantly ($p<0.05$) increased recruitment of mutated NDP52 to 32% of *T.gondii* compared to 16% with the wild-type protein. LC3C interaction might hinder NDP52 binding to *T.gondii*.

Two additional mutants located in the shorter ΔSKICH version of NDP52 (**Fig.8A**) were used and their overexpression was checked by western-blotting (**Fig.8B**). The ΔSKICH truncations of NDP52 did not form aggregates, therefore giving a more diffuse cytosolic GFP staining than with the full-length (**Appendix1**). In the absence of the SKICH domain, binding to FIP200 and SINTBAD/NAP1 was also impaired. Deletion of the SKICH domain (ΔSKICH), even with an additional L374A mutation, did not significantly change the recruitment of the V136S mutant (respectively 43% and 38% of *T.gondii* compared to 32% for the V136S NDP52 construct.

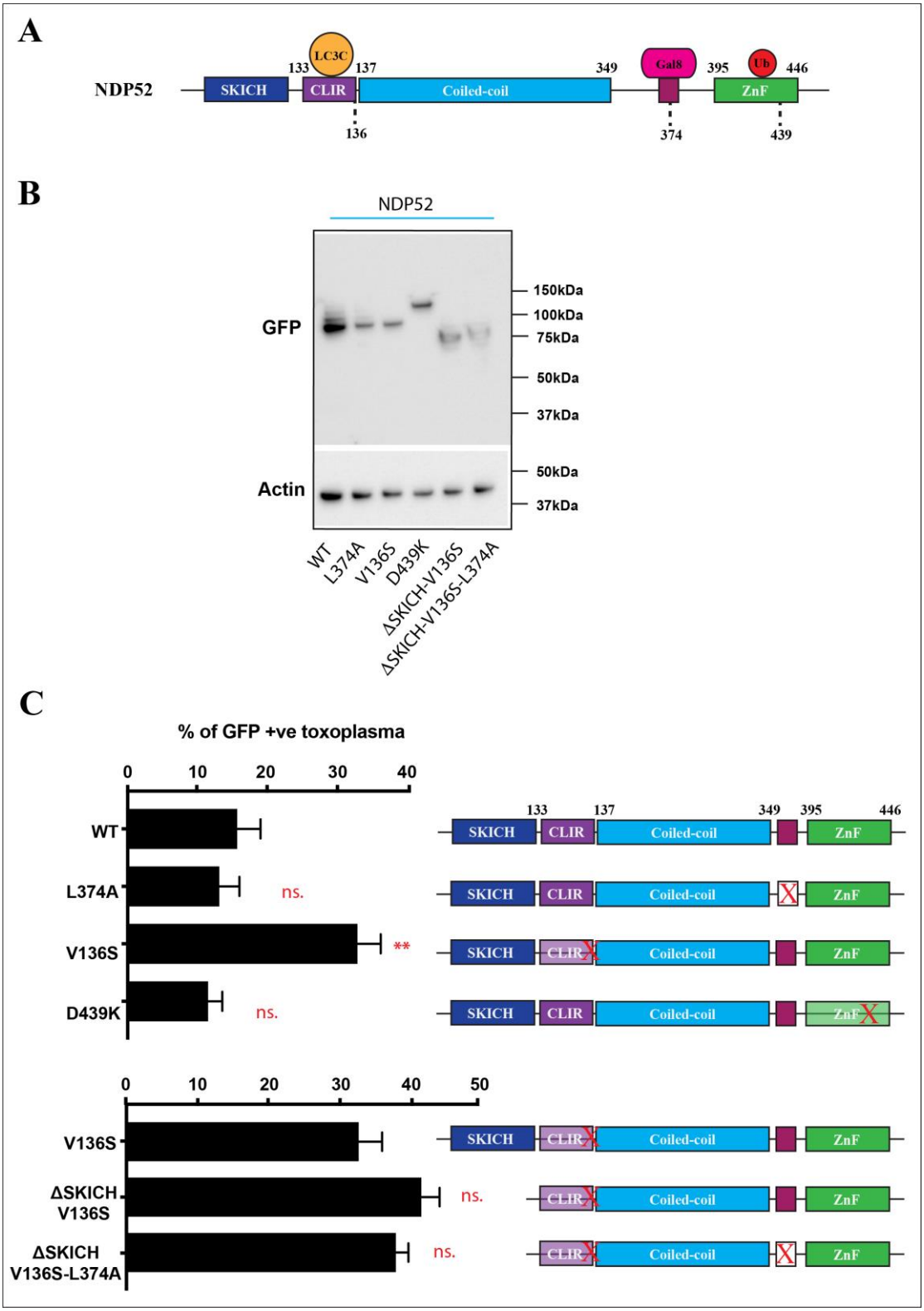

figure continued on next page

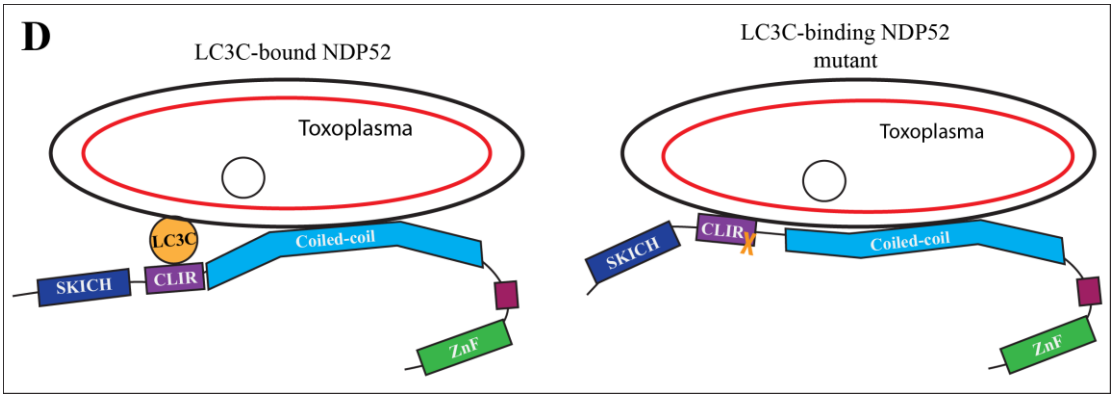

Figure 8: Gal-8 binding is not required for NDP52 recruitment

(A) Schematic of human NDP52 with the various domains and mutated sites. MEF cells overexpressing GFP-tagged constructs of mutated and truncated forms of human NDP52 were primed with IFN-γ overnight before infection with type II (PRU) *Toxoplasma gondii* strain in 4:1 ratio compared to the number of cells seeded on coverslips. (B) Overexpression of the constructs was checked by western-blot probing for GFP. (C) At 1h post-infection, cells were washed and fixed with 4% PFA. At least 100 *T.gondii* were counted for each coverslip and the number of GFP-positive *T.gondii* recorded. Results from three independent experiments, all performed in duplicate, are shown as Mean ± S.E.M. **P<0.005, ns (not significant), one-way ANOVA with Dunnett's multiple comparisons test compared with the wild-type. (D) Schematic of the potential recruitment modes of NDP52 whether it is bound or not to LC3C. Constructs for the expression of GFP-tagged wild-type, truncated or mutated NDP52 were generated by Dr. Jessica Noad.

In summary, NDP52 binding to GAL8 is not required for colocalisation to *T.gondii* (**Fig.8D**). Testing NDP52 mutant for Ub-binding (D439K) would help determine whether the recruitment mechanism is similar to *S.*Typhimurium infection. However, LC3C binding seems to impair recruitment to *T.gondii*, as CLIR-mutated NDP52 (V136S) showed enhanced recruitment. In conclusion, these experiments show NDP52 exhibiting a new recruitment mechanism that requires either Ub or an unknown ligand on *T.gondii*. To address the hypothesis that NDP52 could be recruited by both GAL8 and ubiquitin in a redundant fashion, the L374A+D439K double mutant should be used.

3.2.3.3. PB1 and UBA domains are required for p62 recruitment to *T.gondii*

The recruitment of p62 (**Fig.9A**) to *T.gondii* was further investigated, using the same strategy as for NDP52, because Sequestosome-1 (p62) promotes NF-κB activation (Sanz et al., 2000) and facilitates proteasomal degradation of ubiquitylated substrates (Pankiv et al., 2007; Seinbenhener et al., 2004).

Several GFP-tagged mutants and truncations (**Fig.9B**) of p62 were tested for their colocalisation with type II *T.gondii* in MEFs primed overnight with IFN-γ. The objective of these experiments is, for example, to determine whether ubiquitin binding was required for p62 recruitment.

P62 preferentially binds to K63-polyubiquitin chains and the two lysine residues K406 and K417 in the UBA domain have been shown to be essential for this binding (Seinbenhener et al., 2004). However, individual (K406V and K417V) and double mutations (K406V+K417V) to valine did not influence the recruitment of p62 to *T.gondii* (**Fig.9C**) compared to wild-type. LC3 family members also bind the p62 LIR motif (residues 336-341) (Pankiv et al., 2007) linking p62 to the autophagy machinery. Two constructs mutated in the KIR domain were tested but neither showed a difference in recruitment to *T.gondii* (34%, 31%) compared to wild-type (35%). Neither LC3 nor Ub binding seemed to be required for p62 recruitment to type II *T.gondii*. This hypothesis was further validated using the N-terminal fragment (N165) of p62 which, despite the absence of both the UBA and the LIR domains, was recruited to *T.gondii* (29%) in similar levels to the wild-type (35%).

The PB1 domain has been shown to interact with the proteasome (Seinbenhener et al., 2004), but the K7A/D69A double mutation specifically prevented p62 polymerisation (Lamark et al., 2003). Recruitment of the double mutant (K7A+D69A) to *T.gondii* (37%) was, however, indistinguishable from the wild-type protein (**Fig.9C**). The truncation mutant (ΔN165) lacking PB1 and ZnF further demonstrated the dispensability of PB1 domain for recruitment to *T.gondii*.

Removing both the N-terminal PB1 and the C-terminal UBA domain decreased the extent to which p62 was recruited to *T.gondii*. Only 22% of these *T.gondii* were positive, compared with 35% in the wild-type. This result suggests that PB1 and UBA

are redundant in driving the recruitment of p62 to *T.gondii*. However, since removing both of them did not completely abrogate the binding, there must be another binding site which remains to be characterised. Further experiments could address this question by overexpressing individual domains and looking at recruitment to see whether any of them was sufficient. Alternatively, the mutations in the UBA domain could be transferred in the ΔN165 fragment to see whether it recapitulates the loss of recruitment seen for ΔUBA+ΔPB1 construct.

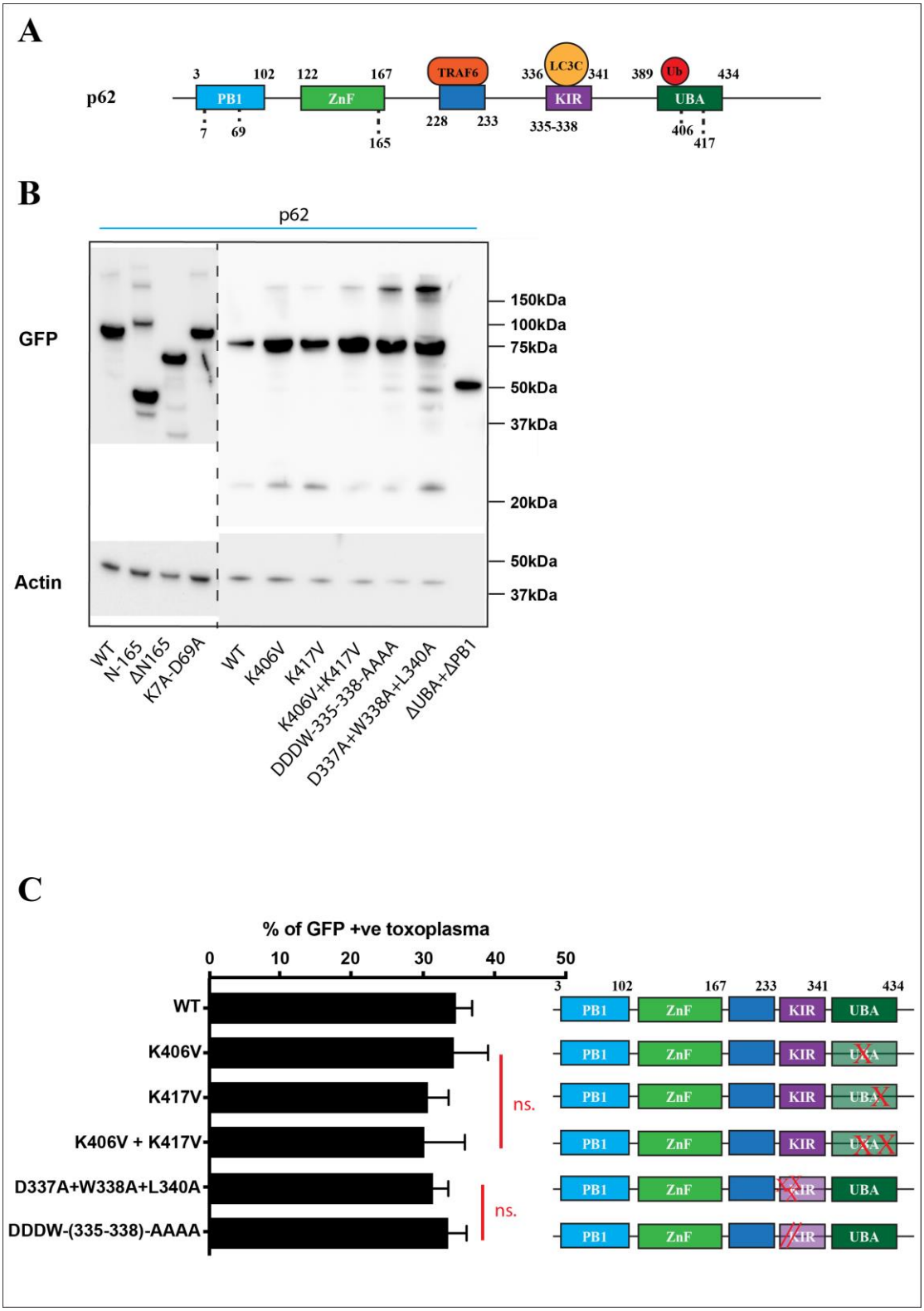

figure continued on next page

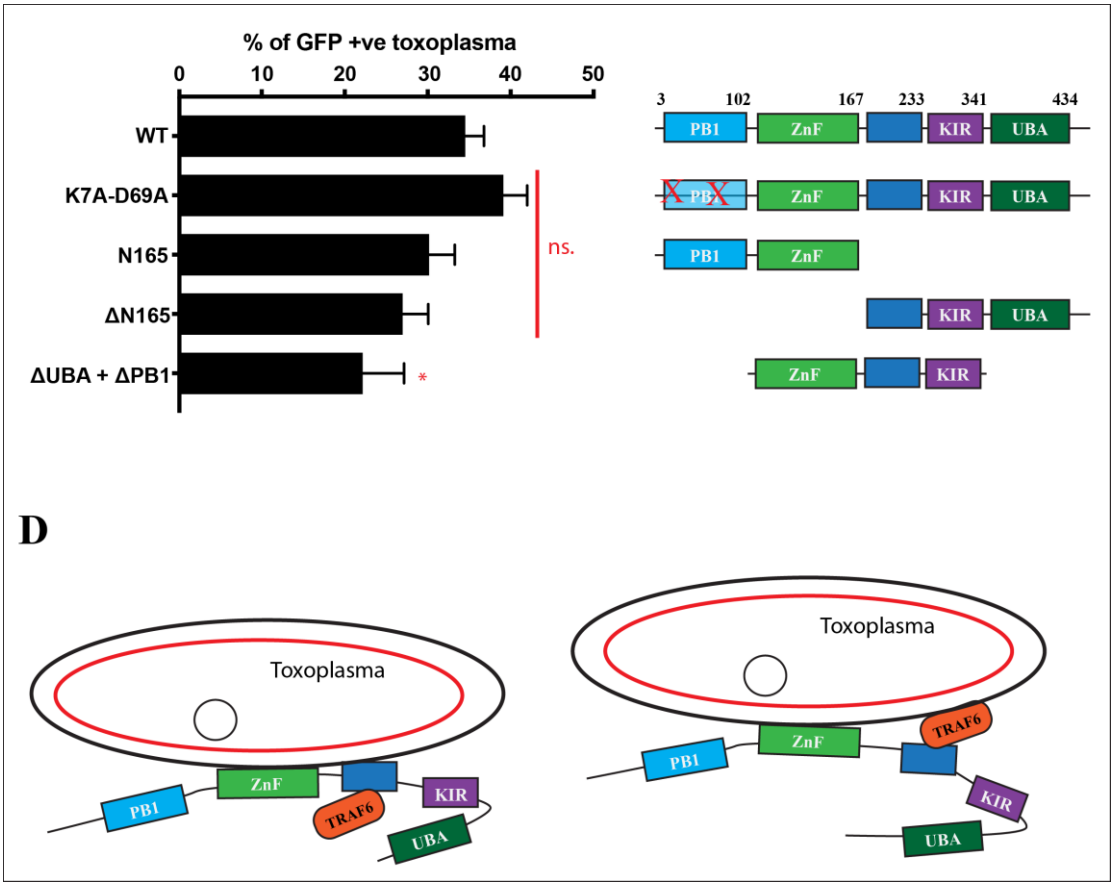

Figure 9: The PB1 and UBA domains of p62 are required for recruitment

(A) Schematic of human p62 with the various domains and mutated sites. MEF cells overexpressing GFP-tagged constructs of mutated and truncated forms of human p62 were primed with IFN-γ overnight before infection with type II (PRU) *Toxoplasma gondii* strain in 4:1 ratio compared to the number of cells seeded on coverslips. (B) Overexpression of the constructs was checked by western-blot probing for GFP. (C) At 1h post-infection, cells were washed and fixed with 4% PFA. At least 100 *T.gondii* were counted for each coverslip and the number of GFP-positive *T.gondii* recorded. Results from three independent experiments, all performed in duplicate, are shown as Mean ± S.E.M. ns (not significant), *P<0.05 one-way ANOVA with Dunnett's multiple comparisons test compared with the wild-type. (D) Schematic of the potential recruitment mechanism of p62 via the zinc finger and the TRAF6-binding domain.
Constructs for the expression of GFP-tagged wild-type, truncated or mutated p62 were generated by Dr. Ben Ravenhill.

3.2.3.4. The recruitment of Optineurin

Optineurin interacts with ubiquitin and LC3 to induce autophagy in response to bacterial infection, for example (Gomes & Dikic, 2014). To investigate the recruitment mechanism of Optineurin (**Fig.10A**), full-length mutants and truncations

of the protein were overexpressed (**Fig.10B**) and their recruitment to *T.gondii* was compared to that observed with overexpressed GFP-wild-type Optn.
The N-terminal fragment (residues 1-555; N555) that lacks the ZnF domain showed recruitment comparable to wild-type, suggesting that the ZnF domain of Optn is not required for binding.

Optn binds to linear ubiquitin chains via its UBAN domain (Wagner et al., 2008). The D474N mutant has been characterised by its failing to recruit to ubiquitylated *S.*Typhimurium (Noad et al., 2017). By contrast, this mutant protein accumulated on 22% of *T.gondii* (**Fig.10C**), a non-significant decrease compared to the 27% observed for the wild-type protein. Another mutant in the UBAN domain, the natural variant E478G that has been shown to be implicated in ALS (Amyotrophic Lateral Sclerosis) pathogenesis and to activate NF-κB signalling (Maruyama et al., 2010), was also investigated. In this case, the mutant's limited reduction in recruitment to *T.gondii* was calculated to be statistically significant ($p<0.05$), suggesting that this glutamic acid residue is necessary for binding.

Phosphorylation by TBK1 on S473 enhances LC3B affinity for Optn (Wild et al., 2011; Rogov et al., 2013). Mutating the serine residue (S473A) disrupts TBK1-mediated phosphorylation and hence prevents enhanced recruitment of the autophagy machinery. The S473A mutant was recruited to 18% of *T.gondii* (**Fig.10C**), which gave a similar level of recruitment (27%, a non-significant decrease) to that observed with the wild-type.

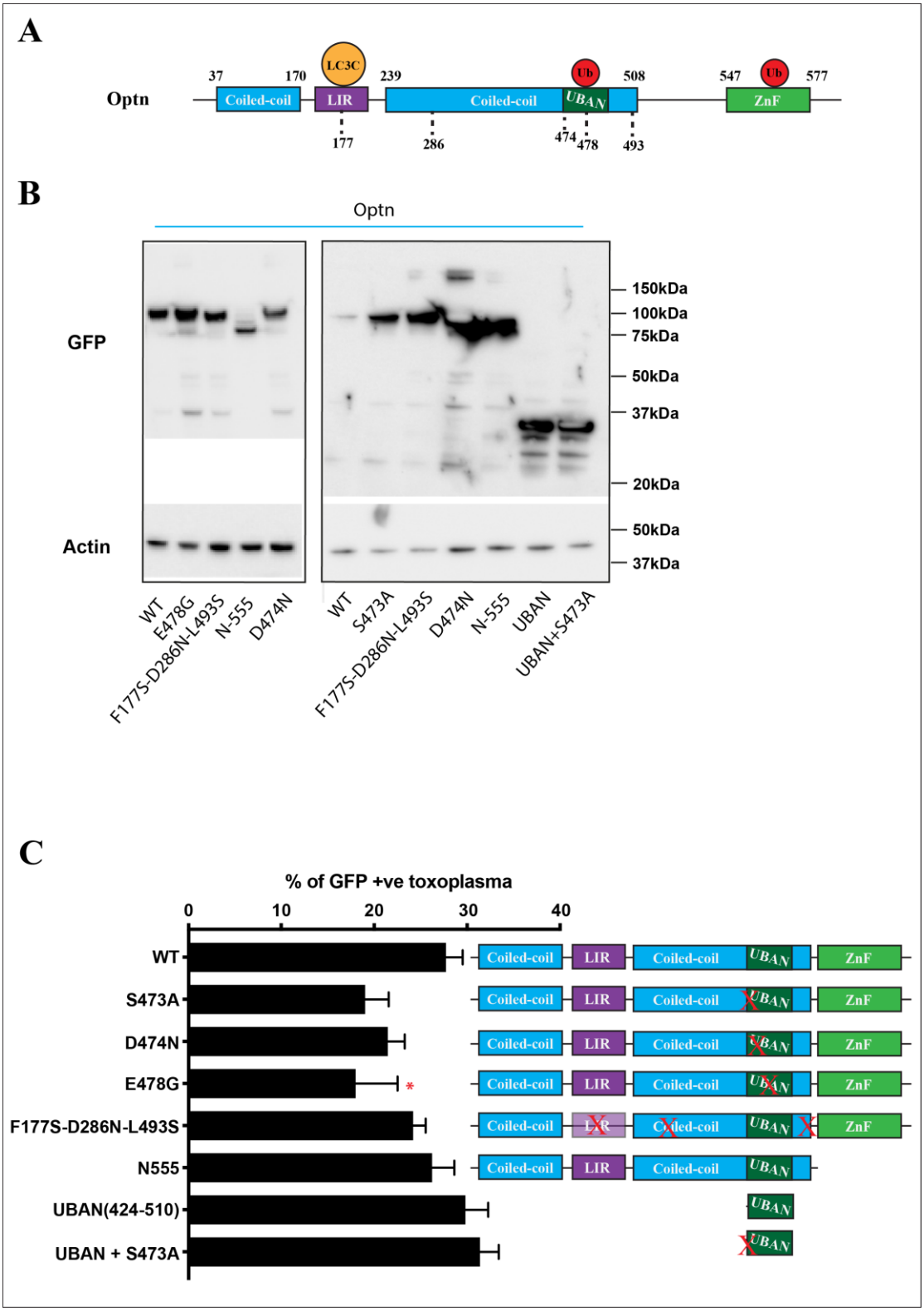

Figure 10: Optn recruitment is mediated by ubiquitin

(A) Schematic of human Optn with the various domains and mutated sites. MEF cells overexpressing GFP-tagged constructs of mutated and truncated forms of human Optn were primed with IFN-γ overnight before infection with type II (PRU) *Toxoplasma gondii* strain (MOI of 4:1). (B) Overexpression of the constructs was checked by western-blot probing for GFP. (C) At 1h post-infection, cells were washed and fixed with 4% PFA. At least 100 *T.gondii* were counted for each coverslip and the number of GFP-positive *T.gondii* was

recorded. Results from three independent experiments, all performed in duplicate, are shown as Mean ± S.E.M. *P<0.05, one-way ANOVA with Dunnett's multiple comparisons test compared with the wild-type.
Constructs for the expression of GFP-tagged wild-type and E478-mutated Optn were generated by Dr. Ben Ravenhill; the other truncations and mutants used here were made by Dr. Jessica Noad.

Overexpression of the UBAN domain was sufficient for it to be recruited to *T.gondii* and altering the nearby phosphorylation site did not influence this recruitment. This observation strongly suggests that Optn recruitment is driven by ubiquitin via the UBAN domain, and that it is M1-linked ubiquitin independent as the D474N mutant is recruited fine. However additional experiments testing a shorter N-terminal fragment lacking the UBAN domain (N473) and UBAN constructs mutated at residues 474 and 478 would be required to confirm this hypothesis, particularly since full-length D474N recruitment was not reduced compared to wild-type. Based on the observation that LC3 can also bind Optn at the LIR domain (Birgisdottir et al., 2013) and mutation at residue 177 inactivates LC3 binding (Noad et al., 2017), the triple F177S+D286N+L493S mutant in which LC3C binding is impaired, was expressed and was also recruited (25%) similar to wild-type Optn. This was expected if there was redundancy. Future work studying recruitment of the N473-LIR mutant would be useful to determine whether there are redundant binding mechanisms of Optn to *T.gondii*.

3.2.4 Interpretation of the microscopy experiments

A few remarks need to be made concerning the microscopy experiments carried out in this thesis. Further discussion will follow (see section **3.4** "Discussion") but these technical disclaimers need to be clarified.

Firstly, all quantitation was performed manually and in a blinded fashion to avoid bias based on the knowledge of the protein and the particular mutant or truncation considered. Positive events – recruitment of the GFP-protein to *T.gondii* – were counted based on internal controls: a first positive event compared to background was

defined; and subsequently, other events with similar intensity were counted as positives. The intensity threshold for counting positive events was therefore variable between constructs. Secondly, no construct expressing the GFP protein on its own was used as negative control for recruitment. It might be prudent to include this in future experiments to ensure that recruitment is specific to the protein of interest and not due to the GFP-tag.

In addition, one coverslip for each construct was counted on the same day, ensuring standardised criteria for judging positive events. Experiments were repeated three times and always performed in duplicate so that six coverslips were examined for each construct to assess the reproducibility of the data. However, because of the great number of constructs used in these experiments and given the somewhat surprising results, the question of using automated counting as opposed to manual counting should be considered for future work. Automated counting appears to be a more impartial way of determining positive events based on computationally calculated intensity levels, and can help avoid human errors (Fisch et al., 2019c).

Finally, in the case of Optn, background fluorescence was relatively high, making it harder to distinguish between noise and true positives. In order to obtain better results and reduce the level of background fluorescence, cells could be permeabilised with saponin to leak out the cytosol and remove all cytosolic proteins not bound to *T.gondii*. Cells could then be fixed to preserve binding and allow imaging and counting.

3.3 Results: IFN-γ restricts type II *T.gondii* replication and induces cytokine production upon *T.gondii* infection

According to the recruitment experiments previously described, overnight IFN-γ priming is required for the significant recruitment of any of the LUBAC subunits or cargo receptors such as p62, NDP52 or Optn in MEFs infected with type II *T.gondii*. In the following experiments performed using IFN-γ-primed MEF cells, immune

responses in terms of *T.gondii* killing are addressed with both type I and type II strains, whereas cytokine production is investigated only with the PRU strain, because the role of LUBAC – recruited only to type II *T.gondii* parasites – is also considered.

3.3.1 IFN-γ antagonises type II *T.gondii*

3.3.1.1. Restriction of *T.gondii* infectivity

The results presented above (**Fig.3** and **7**) showed that proteins were recruited to *T.gondii* when cells were primed with IFN-γ. Consequently, the impact of IFN-γ on parasite entry in cells was studied.

MEF cells – either primed overnight with IFN-γ or not – were infected with type I (RH) or type II (PRU) strains of Td-tomato-expressing *T.gondii*. At 1h post-infection, cells were washed and fresh medium was dispensed in the wells, keeping IFN-γ treatment in the wells originally primed. At 2h, the cells were fixed, and all samples were analysed at the same time using flow cytometry. Cells harbouring *T.gondii* were visible by flow cytometry (**Fig.11**) as the parasites express the fluorescent protein Td-tomato. Cells were individually measured for their brightness, which provided a measurement of the cell burden in *T.gondii* (assuming that all parasites were expressing similar levels of the fluorophore). Several gates were set up to analyse the samples, and this workflow could be applied systematically in future experiments to facilitate reproducibility. The first gate was designed in order to leave the debris out of the analysis (**Fig.11**, left column) and this population was further selected to keep only single cells (**Fig.11**, middle column). On this single-cell population, the next gate was drawn to analyse the *T.gondii*-positive cells; that is infected cells (**Fig.11**, right column). The same gating was used for all samples run on the same day. In term of fluorescence, the addition of IFN-γ did not alter uninfected cells. However, in the presence of IFN-γ, fewer cells were infected as 25.8% of IFN-γ-primed cells were *T.gondii* positive compared to 40.5% of control cells for a same dose of parasite added to the cells.

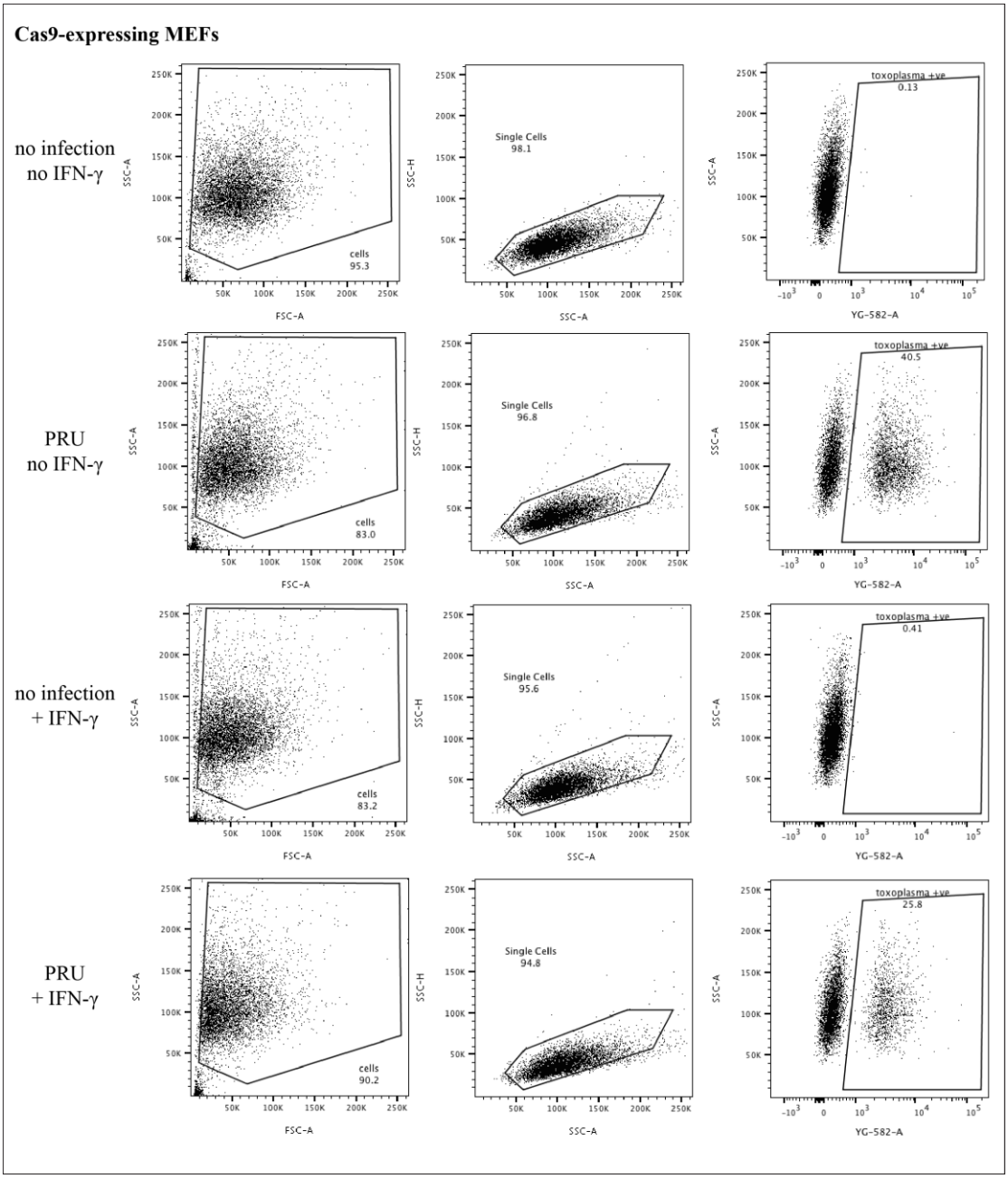

Figure 11: Infected cells are detected as a separate population by flow cytometry

MEF cells were infected with type II (PRU) Td-Tomato-expressing *Toxoplasma gondii* strain in 1:1 ratio compared to the number of cells seeded in wells. Cells were incubated with IFN-γ overnight before the infection. At 1h post-infection, cells were washed, and fresh medium was added, keeping IFN-γ if required. At 2h cells were analysed by flow cytometry. Representative plots are shown for uninfected and infected cells and whether they were primed with IFN-γ or not.
From left to right, gate on cells to remove debris from the analysis (side scatter vs forward scatter); gate on the cell population for single cells (side scatter horizontal vs side scatter); plot of the single cell (side scatter vs Tomato-*T.gondii*) for their parasite burden, the gate is drawn on infected *T.gondii*-positive cells.

To summarise, IFN-γ priming decreases susceptibility and hence protects MEF cells against type II *T.gondii* infection; it could also be that parasites invaded the cells but were killed soon after entry.

Indeed, IFN-γ has been shown to inhibit *T.gondii* growth in human fibroblasts (Pfefferkron & Guyre, 1984) and even to kill the parasites in haematopoietic and non-haematopoietic cells (Clough et al., 2016).

3.3.1.2. IFN-γ-primed cells restrict PRU replication

To determine whether IFN-γ promotes immune defence mechanisms against *T.gondii*, parasite replication was followed over time. Cells were infected either with PRU or RH strain and samples were fixed at the three different time points of 2h, 24h, and 48h. These time points were chosen to ensure that *T.gondii* had time to replicate, since a replication cycle lasts between 6h and 12h. The 2h time point was used as the control condition for entry level, i.e. infectivity in the different conditions. In all conditions, cells were infected with the same concentration of parasites and the gating on the flow cytometry plots was applied to all samples from the same experiment. In control cells, type II *T.gondii* replicate over time. The infected population shifted to higher fluorescence intensities (**Fig.12A**), which was expected: as the parasitic burden increased over time, vacuoles contained more parasites and thus cells were detected as brighter overall. By contrast, IFN-γ-primed cells did not exhibit this shift (**Fig.12A**). IFN-γ most likely prevents *T.gondii* from replicating in cells.

The absence of a shift in IFN-γ-primed cells was well captured by chromatograms showing the intensity distribution of the population of infected cells (**Fig.12B**). These curves clearly demonstrate that restriction of replication is IFN-γ-dependent and occurs only with the type II strain (PRU). In the case of infection with the RH (type I) strain, curves in the presence (cyan) or absence (red) of IFN-γ overlap (**Fig.12B**) for the three time points indicating that IFN-γ did not induce restriction of *T.gondii* replication in this strain. Both curves shifted towards higher fluorescence intensities indicating normal replication and growth of the parasites.

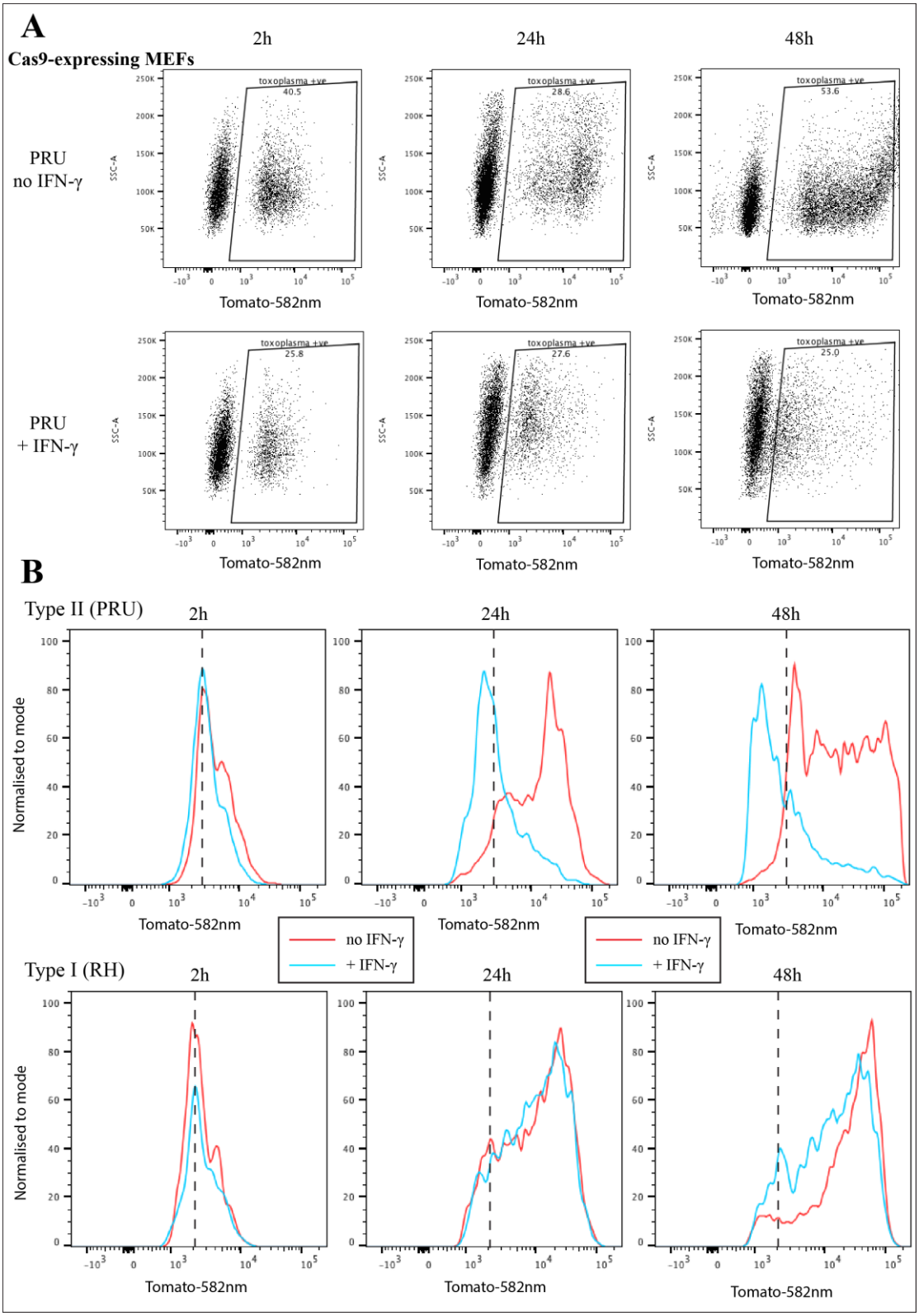

figure continued on next page

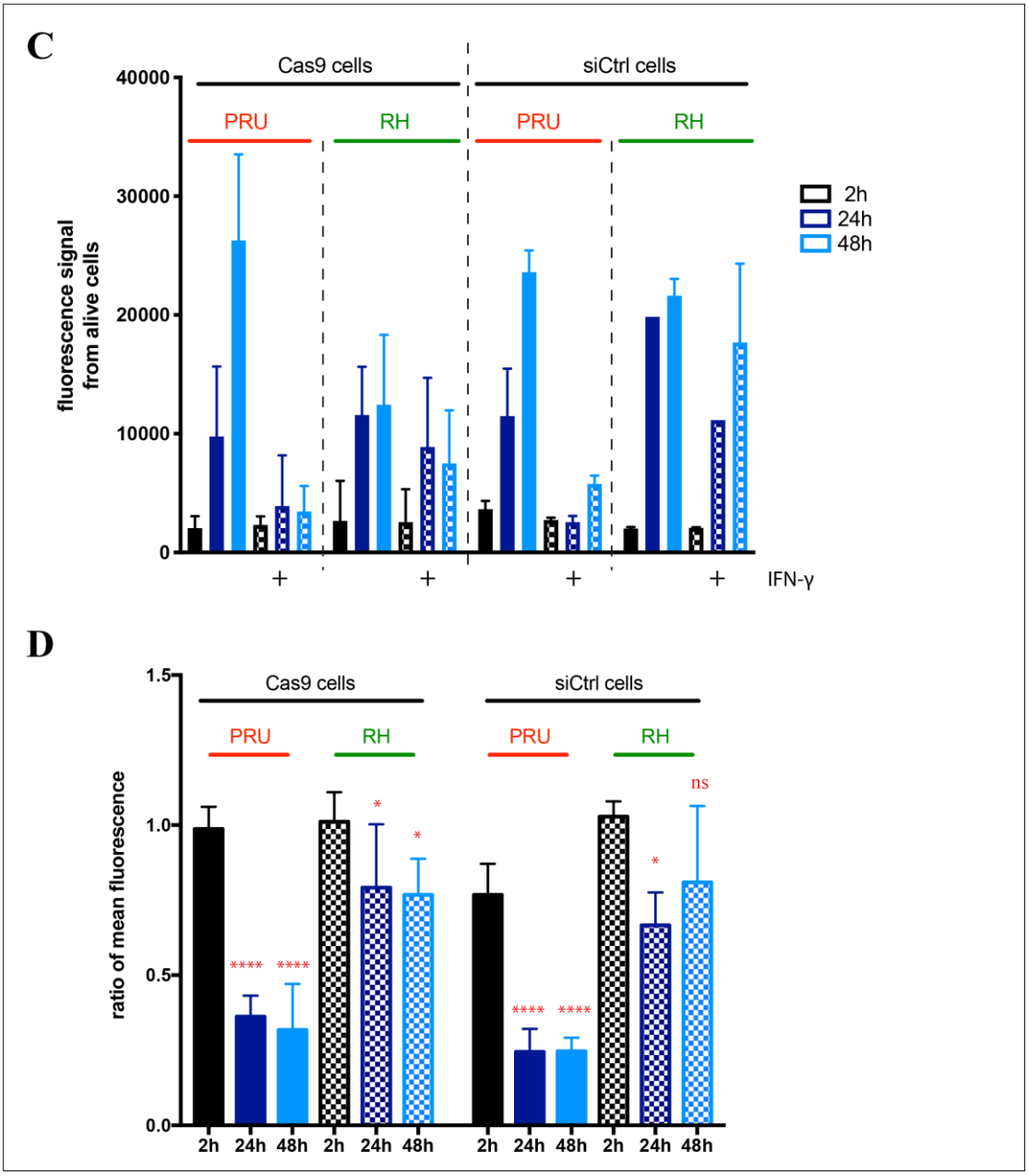

Figure 12: IFN-γ prevents type II *T.gondii* from replicating

MEF cells were infected with type II (PRU) or type I (RH) Tomato-*Toxoplasma gondii* strains in 1:1 ratio compared to the number of cells seeded in wells. Cells were incubated with IFN-γ overnight before the infection. At 1h post-infection, cells were washed with PBS and fresh medium was added. At 2h, 24h and 48h post-infection, cells were fixed with 4% PFA and cells harvested at the three different time points were analysed by flow cytometry at the same time. (A) shows representative scatter plots of PRU-infected Cas9-MEFs primed or not with IFN-γ. (B) shows chromatograms of PRU- or RH-infected Cas9-expressing MEFs, primed (cyan) or not (red) with IFN-γ. (C) Mean intensities of the red signal (measure for the abundance of *T.gondii* parasites) in the infected population were calculated and (D) the ratios between cells primed or not with IFN-γ were calculated for each sample. Data are shown as Mean ± S.E.M from three independent experiments, all performed in duplicate. *P<0.05, ****P<0.0001, ns. (not significant) one-way ANOVA with Dunnett's multiple comparisons test compared to the 2h-time point in each case.

In order to quantify and visualise changes in cell intensity due to modifications in *T.gondii* infectivity and/or replication, means of intensity were calculated and plotted as histograms. Even though the distribution is not a Gaussian, the variations observed with mean intensities were significant and representative of what was seen on the curves.

For example, the fluorescence signal in siCtrl cells is measured to be 4,000 at 2h post-infection, 11,000 after 24h and then 23,000 at 48h post-infection in unprimed cells; this is in contrast with levels of 3,000, 3,000 and 7,000 at 2h, 24h and 48h respectively, in IFN-γ-primed MEF cells (**Fig.12C**). In the absence of IFN-γ, *T.gondii* replicated over time and to a greater extent with the PRU strain (**Fig.12C**). In the presence of IFN-γ, the PRU strain was prevented from replicating and, in both the cell lines tested the mean signal intensity did not increase significantly over time. By contrast, infection with type I strain (RH) still showed increased mean signal intensity of the infected population, even in cells primed with IFN-γ (**Fig.12C**). To better visualise the effect of IFN-γ on the mean intensity of infected cells and hence on the replication of *T.gondii*, mean signal intensities of infected cells primed with IFN-γ were normalised to infected cells not treated with IFN-γ (**Fig.12D**) for each time point. At 2h, ratios were therefore close to 1.0 because there was little difference in terms of parasite burden between conditions. Changes were therefore expected to be seen at later time points. In the case of PRU, for both cell lines tested, there was a significant reduction ($p<0.0001$) in the intensity ratio from 1.0, at 2h down to 0.4, at 24h, and this ratio was maintained at the 48h time point. This reduction indicated either prevention of *T.gondii* replication or death of some of the parasites. In the case of RH, there was a significant ($p<0.05$) reduction from 1.0, at 24h, down to 0.8, at 48h, for the Cas9-expressing cells. The reduction was also observed with cells transfected with siRNA control (**Fig.12D**) for which the ratio was decreased to 0.7, at 24h, although it was not maintained at the 48h time point.

In summary, the PRU (type II) strain was more sensitive to IFN-γ treatment than the more virulent RH (type I) strain, as priming with IFN-γ prevented type II *T.gondii* replication and/or promoted killing.

3.3.1.3. Atg5 is required for *T.gondii* restriction

Next, the potential role of autophagy in this restriction process was investigated. Atg5 is a key protein in the defence against pathogens (Chen et al., 2012) either functioning in the autophagy pathway or more generally in innate immunity (Zhao et al., 2008; Sibley, 2011). Atg5 was shown to have an impact on resistance to *T.gondii* (Niedelman et al., 2013; Choi et al., 2014) and so was tested as a positive control in the restriction of *T.gondii*. It was expected that the absence (by knock-down or knockout) of Atg5 would show higher ratios of mean intensity at 24h and 48h compared to the control. MEFs were successfully knocked out for Atg5 as shown by western-blotting (**Fig.13**).

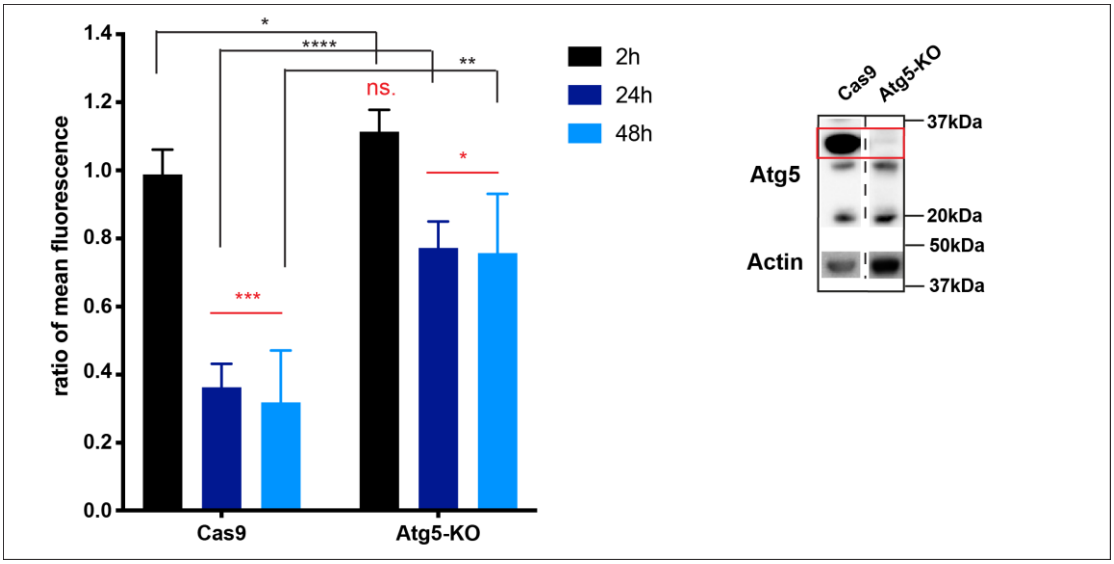

Figure 13: Atg5 is required in the IFN-γ-dependent restriction of PRU

MEF cells expressing Cas9 and knockout for Atg5 (western-blot) were infected with type II (PRU) or type I (RH) Tomato-*Toxoplasma gondii* strains in 1:1 ratio compared to the number of cells seeded in wells. Cells were incubated with IFN-γ overnight before infection. At 1h post-infection, cells were washed with PBS and fresh medium was added. At 2h, 24h and 48h post-infection, cells were fixed with 4% PFA and later analysed by flow cytometry. Mean intensities of the *T.gondii* signal were measured and the ratios between cells primed or not with IFN-γ were calculated for each sample. Data are shown as Mean ± S.E.M from three independent experiments, all performed in duplicate. *P<0.005, ***P<0.0001, ns (not significant) one-way ANOVA with Dunnett's multiple comparisons test comparing to the 2h-time point of Cas9 cells. *P<0.05, **P<0.005, ****P<0.0001, unpaired t test without assuming a consistent SD, comparing ratios between control cells and Atg5-KO cells at a given time point.

Cas9-expressing cells (control) or knockout for Atg5 (Atg5-KO) were infected with type II *T.gondii* (PRU) and ratios of the mean intensity (**Appendix2**) of the infected population were calculated comparing cells primed with IFN-γ with non-primed cells. Atg5-KO cells showed a statistically significant ($p<0.005$) reduction of the intensity ratios at 24h and 48h with values of 0.78 and 0.76, respectively compared with 1.1 at 2h (**Fig.13**). These decreases, however, were not as pronounced ($p<0.0001$) as the ones obtained with Cas9-expressing MEFs, where the ratios were 0.99, 0.36, and 0.32 at 2h, 24h, and 48h respectively. Indeed, statistics comparing Cas9-MEFs to Atg5-KO MEFs showed that ratios at both 24h and 48h were significantly ($p<0.0001$ at 24h and $p<0.005$ at 48h) different between the two cell lines. This means that the Atg5 knockout counteracted the effect of IFN-γ priming in the resistance to type II *T.gondii* infections. These results highlight the role of Atg5 in restricting *T.gondii* upon IFN-γ priming and suggest that Atg5 plays a major role downstream of IFN-γ. However, the knockout of Atg5 did not completely abrogate resistance to *T.gondii* and therefore it can be concluded that there must be an additional pathway to autophagy acting in the IFN-γ-dependent restriction of *T.gondii* replication.

On the one hand, Atg5 is a major protein in the autophagy machinery. On the other hand, LUBAC has been shown to play a role in autophagy: by ubiquitinating substrates it indirectly signals for proteasome degradation and mediates the recruitment of the autophagy machinery (Ji & Kwon, 2017).

3.3.1.4. Restriction of *T.gondii* replication is LUBAC-independent

Next, the role of LUBAC in resistance to *T.gondii* in IFN-γ-primed cells was investigated. Although it was shown above that LUBAC (**Fig.3**) and cargo receptors such as NDP52, p62, and Optn (**Fig.7**) are recruited to type II *T.gondii* in the presence of IFN-γ, their precise role remains unclear and their functions have not been characterised.

By synthesising linear ubiquitin chains, LUBAC is likely to induce recruitment of other proteins. Cargo receptors usually contribute to the cellular defence machinery by targeting substrates for autophagy or proteasomal degradation (Ji & Kwon, 2017).

They are therefore expected to either recruit other proteins, directly signal for the destruction of the parasites or, for the release of signalling molecules such as cytokines, inducing downstream events on the *T.gondii*. The results presented above confirmed that Atg5 plays a role in the IFN-γ-dependent resistance to *T.gondii*. Since LUBAC is another autophagy-related protein complex, its role in restricting type II *T.gondii* replication in IFN-γ-primed cells was also investigated.

MEF cells in which HOIP or HOIL-1 had been knocked-out or which were deficient in Sharpin (**Fig.14A** and **B**) together with their wild-type control were generated and kindly provided by Henning Walczak. These cells were infected with type II *T.gondii* (PRU). Knockouts of HOIP and HOIL-1 were assessed by western-blotting (**Fig.14A**): cells knocked-out for HOIL-1 and HOIP exhibited a strong reduction in protein expression (HOIL-1 and HOIP, respectively), similar to the knock-downs obtained with siRNAs. However, despite repeating the experiment multiple times, it was not possible to account for full knockouts and complete absence of the desired proteins. Discussion with Dr. Walczak led to the hypothesis that either the antibody used is not as specific as the in-house one they use, or that the cells were cultured for too long, explaining genetic instability.

The deficiency for Sharpin was determined at the transcriptional level by measuring relative amounts of mRNA using qPCR. The ΔΔCt method was used to analyse these data, using actin as the reference gene. Levels of HOIP, HOIL-1, and Sharpin were compared between wild-type (black bars) and deficient cell lines (red bars). Atg5-KO MEFs were compared to Cas9 MEFs and as expected, transcriptional levels of all three LUBAC subunits were similar in both cell lines (**Fig.14B**). Sharpin-deficient MEFs (cpdm) exhibited reduced levels of Sharpin as expected but also showed reduced levels of both HOIP, HOIL-1, suggesting some sort of stabilisation mediated by Sharpin for the expression – or at least transcription – of HOIL-1 and HOIP.

For each cell line, ratios of mean intensity were calculated as intensity of IFN-γ-primed cells over intensity of unprimed cells (**Fig.14C**). Cas9-expressing MEFs were used as a negative control. IFN-γ induced restriction of *T.gondii* replication (**Fig.12**); by contrast, Atg5-KO cells partially lost this ability, and the ratio was increased to 0.78, at 24h or 48h, compared to 0.37 in the Cas9-cells. None of the other wild-type

cell lines – HOIP-WT, HOIL-1-WT, Sharpin – showed a phenotype similar to the control. These cells do not seem to be sensitive to IFN-γ treatment. The knockout and deficient cell lines did not exhibit any difference from their respective wild-type (**Fig.14C**). Because the wild-type did not show any response to IFN-γ priming during *T.gondii* infection, no conclusion could be drawn from this experiment. In addition, it would have been hard to make sense of the data as the knockouts could not be confirmed either. The use of these HOIP or HOIL or Sharpin deficient cell lines was not fruitful.

To address the role of LUBAC in *T.gondii* resistance, MEF cells were knocked-down for the individual LUBAC subunits using siRNA. Single knock-downs were not confirmed by western-blotting (**Fig.14A**) as a residual band was visible after long exposure of the membrane. These "knock-down" MEFs for either one, two or all three LUBAC subunits were infected with the PRU strain. Ratios of mean intensity were calculated (**Fig.14D**) and for each cell line the 2h time point was compared with both 24h and 48h time points. MEFs transfected with siCtrl showed a substantial decrease ($p<0.0001$) from 0.78, at 2h down to 0.25, at 24h and 48h. In the single "knock-downs", ratios also dropped significantly ($p<0.0001$) and ratios, at 24h and 48h, were similar to the control except for the 48h time point of the HOIL-1 "knock-down", for which the drop was accentuated at a ratio of 0.13. In the double or triple "knock-downs", the drops were less substantial ($p<0.005$), especially for the 24h time point where the ratio was 0.45 (compared to 0.25 for the control). Moreover, in the HOIP+Sharpin double "knock-down", the 24h and 48h ratios reached 0.43 and 0.37 respectively, a non-significant decrease from the 0.72 ratio at 2h. This behaviour was not, however, replicated in the triple (entire LUBAC) "knock-down" and a significant difference was not observed relative to the control cells or any of the "knock-down" cells. Nonetheless, decreases in intensity ratio were lower in the cases of double (two out of the three LUBAC subunits) or triple knock-downs (the entire LUBAC).

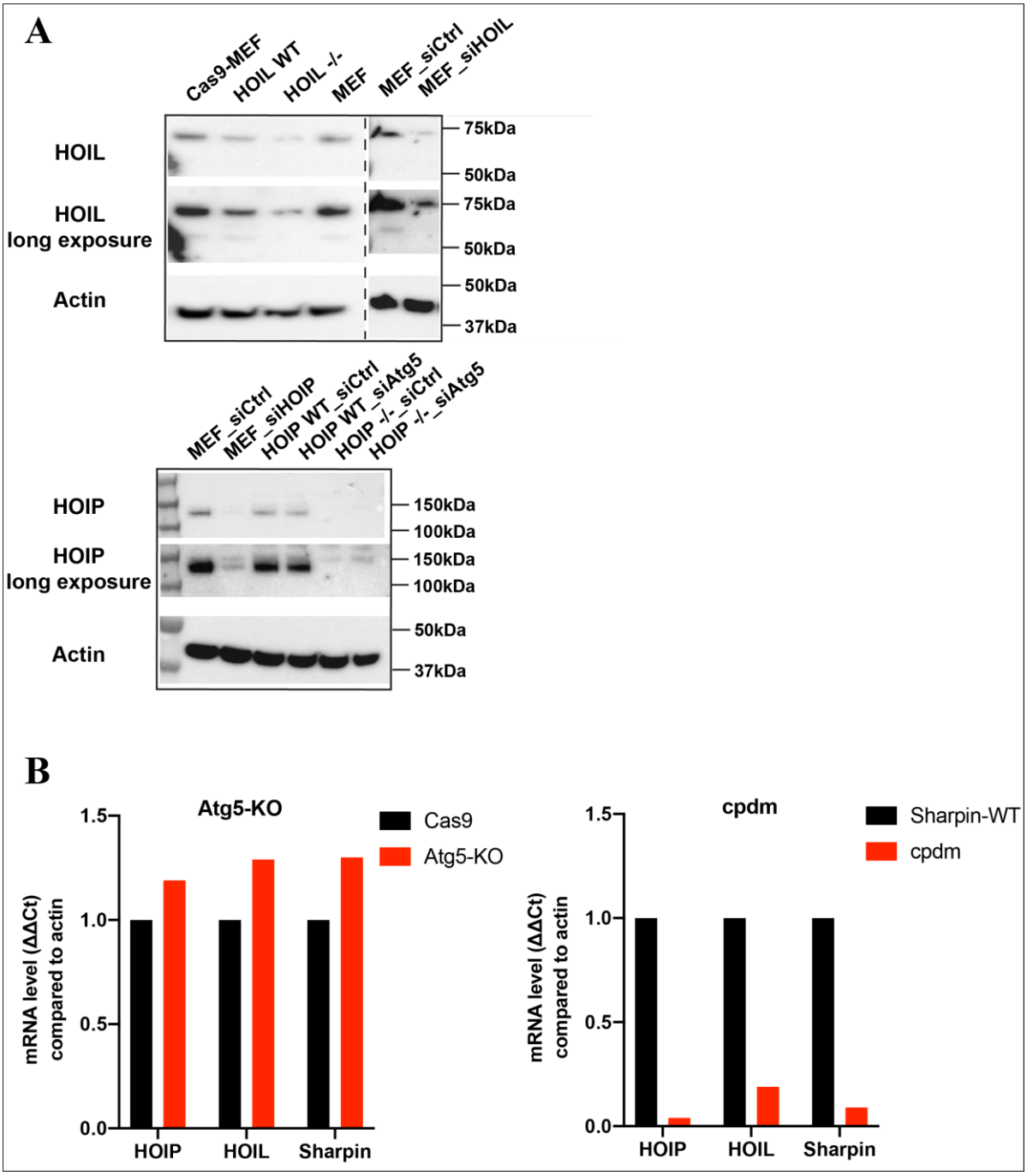

figure continued on next page

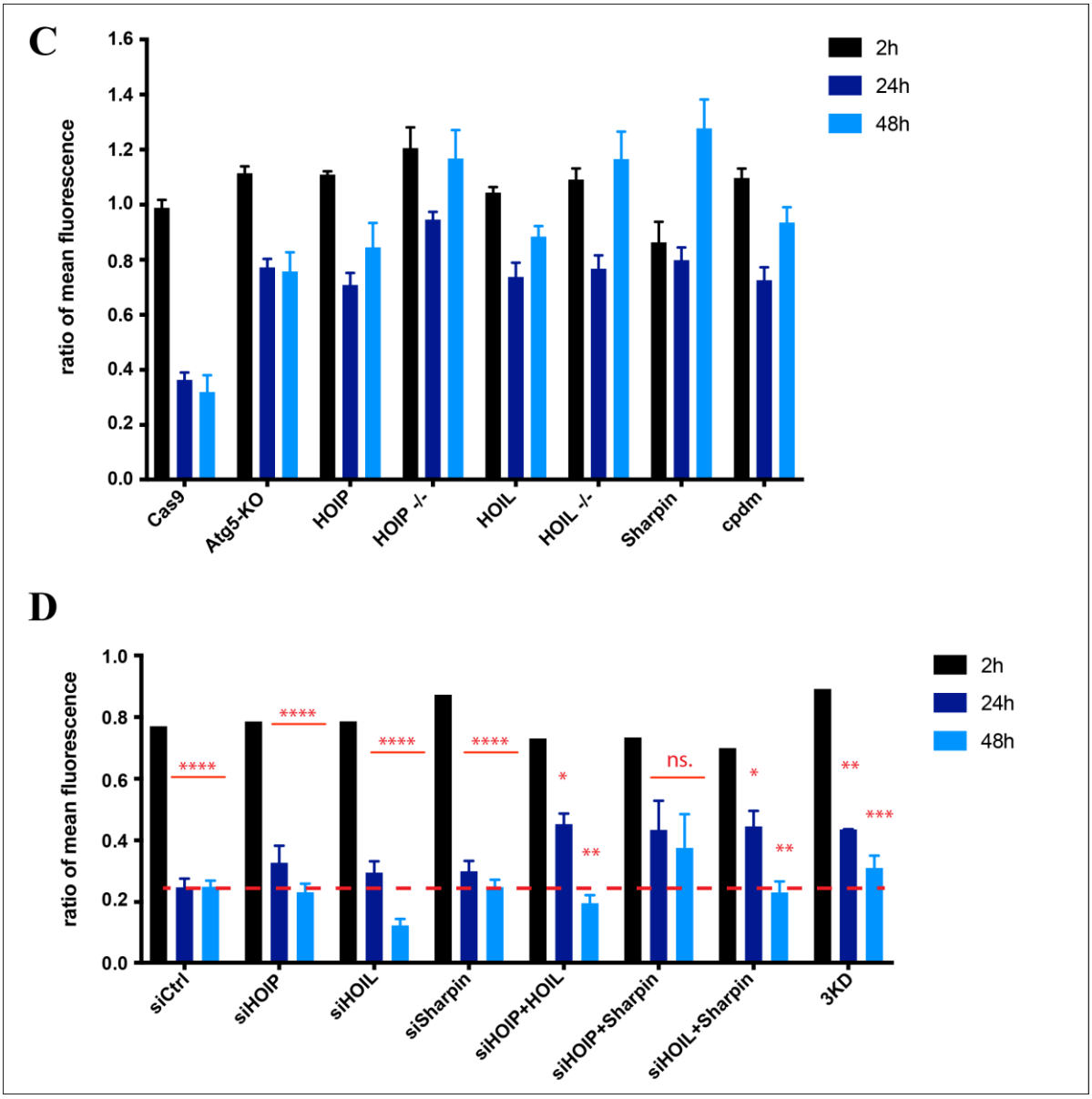

Figure 14: None of the LUBAC subunits is individually required for *T.gondii* restriction

MEFs either knockout or knock-down for HOIP, HOIL-1 or Sharpin or Atg5-KO along with their individual controls (respectively wild-type for the knockouts and siCtrl for the knock-downs) were infected with type II (PRU) Tomato-*Toxoplasma gondii* strain (MOI 1:1). Cells were incubated with IFN-γ overnight before infection. At 1h post-infection, cells were washed with PBS and fresh medium was added. At 2h, 24h and 48h post-infection, cells were fixed with 4% PFA to be then analysed by flow cytometry. (A) Knock-downs were validated by western-blotting, whereas knockouts were checked both by western-blotting (A) and qPCR (B). Mean intensities of the *T.gondii* signal were measured and the ratios between cells primed or not with IFN-γ were calculated for each sample (C and D). Data are shown as Mean ± S.E.M from three independent experiments, all performed in duplicate. *P<0.05, **P<0.005, ***P<0.0002, ****P<0.0001, ns (not significant) one-way ANOVA with Dunnett's multiple comparisons test compared to the 2h-time point for each cell line.

In conclusion, LUBAC appeared at best, to play only a minor role and/or to be part of redundant pathways in restricting *T.gondii* replication in IFN-γ-primed MEFs. These results should be considered with care because knock-downs were incomplete and residual protein expression might be enough to drive the effect, thereby explaining the absence of any major and reproducible changes between the different cell lines.

The recruitment of LUBAC to type II *T.gondii* in IFN-γ-primed MEF cells could not directly be linked to restriction of parasite replication or growth. However, LUBAC could signal directly or act as upstream effector for the release of signalling molecules such as cytokines, inducing downstream events on the *T.gondii*.

3.3.2 *T.gondii* infection induces production of cytokines and adhesion proteins

As an obligate parasite, *T.gondii* establishes a niche to develop, replicate, and spread in the form of tachyzoites (Radke et al., 2001). Differentiation into bradyzoites, which form latent cysts (Radke et al., 2003), is a mechanism thought to enable the parasite to evade host cell defence mechanisms (Hunter & Sibley, 2012); however, more recent work showed that bradyzoites are not entirely quiescent: the cyst burden is also controlled by the host immune system (Watts et al., 2015). In order to grow, *T.gondii* induces changes in the host cell metabolism (Hargrave et al., 2019) to increase its survival by reprogramming key metabolic pathways such as glycolysis or lipid and sterol metabolism (Nelson et al., 2008). Cells have several mechanisms to counteract infections, however: for example, IFN-γ prevents *T.gondii* growth (Suzuki et al. 1988) and favours the degradation of tryptophan (Pfefferkorn, 1984), an essential amino acid for *T.gondii*. In response to *T.gondii* effectors, namely rhoptries and dense granule proteins (Sibley, 2004), host cells produce pro-inflammatory cytokines such as IL-12 (Denkers, 2003) and TNF-α or activate the NF-κB signalling pathway (Sangaré et al., 2019).

3.3.2.1. The expression profile of signalling molecules is modified following *T.gondii* infection

Cells rely not only on intracellular proteic adaptors to recognise and bind pathogens or danger factors but also on signalling molecules (Meissner et al., 2013) to activate an immune response either intrinsically or in the neighbouring cells (respectively autocrine and paracrine effects). These somewhat redundant mechanisms provide a multi-layered cell defence against pathogens (Randow et al., 2013).

To determine whether infection with PRU of IFN-γ-primed MEFs was changing expression levels of signalling molecules, qPCR was performed with primers amplifying interleukin-1alpha (IL-1α), interleukin-6 (IL-6), C-C motif chemokine ligand 4 (CCL4) and 5 (CCL5), tumour necrosis factor (TNF-α), vascular cell adhesion protein-1 (VCAM-1), intercellular adhesion molecule-1 (ICAM-1) as potential signalling molecules involved in inflammation and/or immune response. GAPDH and actin were used as control genes. The pro-inflammatory cytokines IL-1α, IL-6, and TNF-α were shown to have their expression greatly modified to establish immune responses upon *T.gondii* infection in pregnant women (Wujcicka et al., 2018), but also in some cell lines such as astrocytoma cells (Pelloux et al., 1994). A study in cats (Levy et al., 2004) linked the decreased levels of IL-12, IL-6, IL-2, and IFN-γ with an increase susceptibility to *T.gondii* infection and replication. Chemokines CCL4 and CCL5, among others, activate chemokine receptors to build an immune response. Both secreted CCLs in the plasma of mice and mRNA expression in the brain were measured overtime and showed increased levels following infection with a mild-infectious strain (ME49) of *T.gondii* (Aviles et al., 2008). Cell adhesion proteins VCAM-1 and ICAM-1 are both NF-κB-dependent (Nowak et al., 2008) and their surface expression is enhanced by TNF-α (Li et al., 2000). ICAM-1 expression is increased following ME49 *T.gondii* infection in rats (Pastre et al., 2019). VCAM-1 also indirectly induces IFN-γ production in mice infected with *T.gondii* (Suzuki et al., 2011). VCAM-1 is indeed known to bind the α4β1 integrin on CD8+ T cells, hence driving the recruitment of the T cells into the brain during the chronic stage of *T.gondii* infection (Wang et al., 2007; Silva et al., 2010). VCAM-1 and ICAM-1 promote cell-cell recognition and adhesion for the recruitment of monocytes and lymphocytes to the site of inflammation (Carman & Springer, 2004; Reijerkerk et al., 2006).

For these experiments, all cells were primed overnight with IFN-γ and half the wells were then infected (MOI 4:1) with the PRU (type II) strain. At 1h post-infection, cells were washed and at 24h post-infection, cells were lysed, and their RNA purified. The ΔΔCt analysis method was used to normalise mRNA levels to the endogenous gene GAPDH. Expression levels of signalling molecules were compared between uninfected (black) and PRU-infected MEFs (**Fig.15**). Actin levels were unchanged by the infection (data not shown), which was expected because actin is usually also used as control gene. By contrast, levels of IL-6 ($p<0.0001$), CCL4 ($p<0.05$), CCL5, and ICAM-1 ($p<0.005$) were significantly increased by 90-, 2-, 5- and 5-fold, respectively, following infection with *T.gondii* (**Fig.15**). IL-1α was not detected in the uninfected samples, but it was measured at reasonable levels in infected cells.

In summary, infection with *T.gondii* in IFN-γ-primed MEFs induced transcription of IL-1α, IL-6, CCL4, CCL5, and ICAM-1.

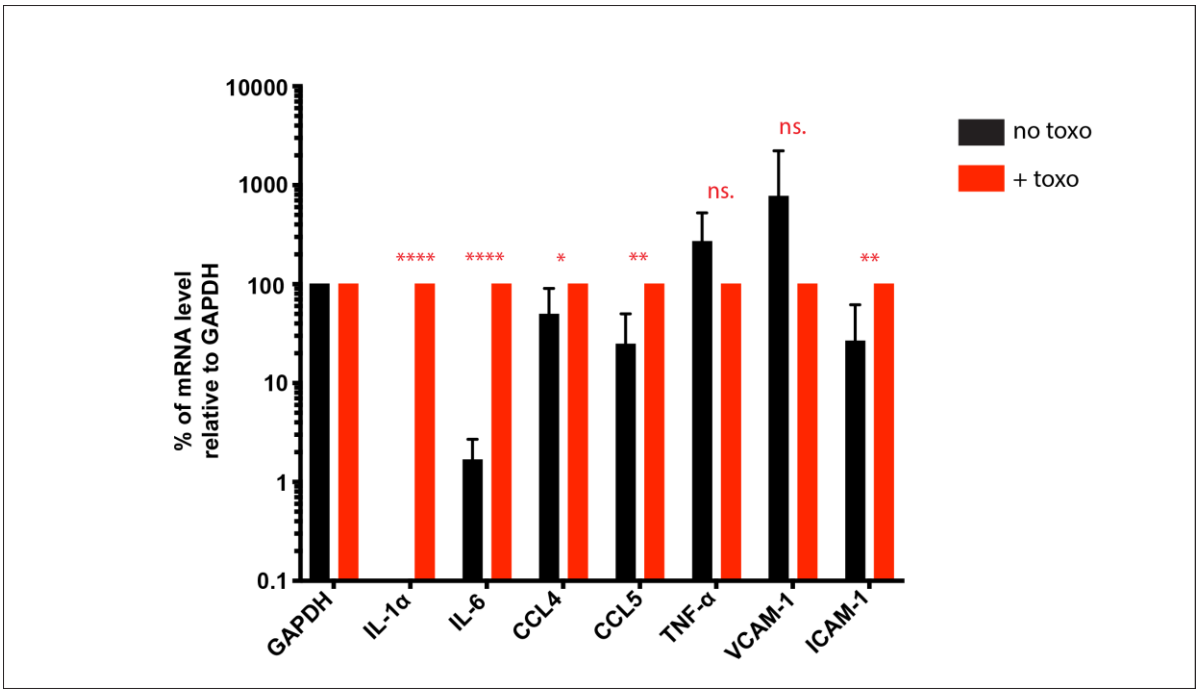

Figure 15: *T.gondii* induces cytokine expression in MEF cells

MEFs were all primed with IFN-γ and on the next day, cells were infected or not with type II (PRU) Tomato-*Toxoplasma gondii* strain (MOI of 4:1). At 1h post-infection, cells were washed with PBS and fresh medium was added. At 24h post-infection, cells were collected, lysed and their RNA was purified. Following reverse transcription, mRNA levels were quantified by qPCR and analysed using the ΔΔCt method with GAPDH as the reference gene. Data are shown as Mean ± S.E.M from three independent experiments, all performed in triplicate. *P<0.05, **P<0.005, ****P<0.0001, ns (not significant), unpaired t test without assuming a consistent SD, showing the effect of *T.gondii* infection for each cytokine.

3.3.2.2. Cytokine expression is regulated by LUBAC

ICAM-1 expression (Nowak et al., 2008) and pro-inflammatory cytokine synthesis (Merline et al., 2011; Bryant et al., 2015) are NK-κB-dependent. LUBAC induces NF-κB signalling (Tokunaga et al., 2011), thereby controlling apoptosis (Ikeda et al., 2011) and activating the autophagy machinery to restrict cytosol-invading bacteria (Noad et al., 2017). LUBAC was recruited to *T.gondii* in IFN-γ-primed cells (**Fig.3**). Consequently, the role of LUBAC in the increased production of immune-related molecules (**Fig.15**) was addressed.

The function of LUBAC in generating signalling molecules was examined in cells transfected with siRNA targeting one of the LUBAC subunits or the entire complex (triple knock-down). Knock-downs of HOIP, HOIL-1, and Sharpin were individually tested by western-blotting (**Fig.16A**) for the single knock-down cell lines and for the LUBAC (triple) knock-down; however levels of expression were decreased but not completely abrogated by any of the siRNA. Cells transfected with siHOIP especially showed protein, even though the triple knock-down was clear of any HOIP. Given this result, further interpretation about the cytokine levels will be closely paired with the observations from the western-blot.

Results from the qPCR (i.e. cytokine transcript levels) were normalised to GAPDH. The graph featuring actin (**Fig.16B**) is shown as an additional internal control: actin levels were similar across all the knock-down cell lines and to the control, validating direct comparisons between cell lines. Each signalling molecule, which previously showed induction upon *T.gondii* infection (**Fig.15**) was analysed individually (**Fig.16B**) and expression levels were compared across cell lines primed with IFN-γ and infected with type II *T.gondii*. In all the cell lines tested, IL-1α expression was dramatically increased following *T.gondii* infection. The increase in IL-1α expression was lower when either HOIP or the whole LUBAC complex were knocked-down; however this variation should be disregarded as the knock-down was not achieved (**Fig.16A**).

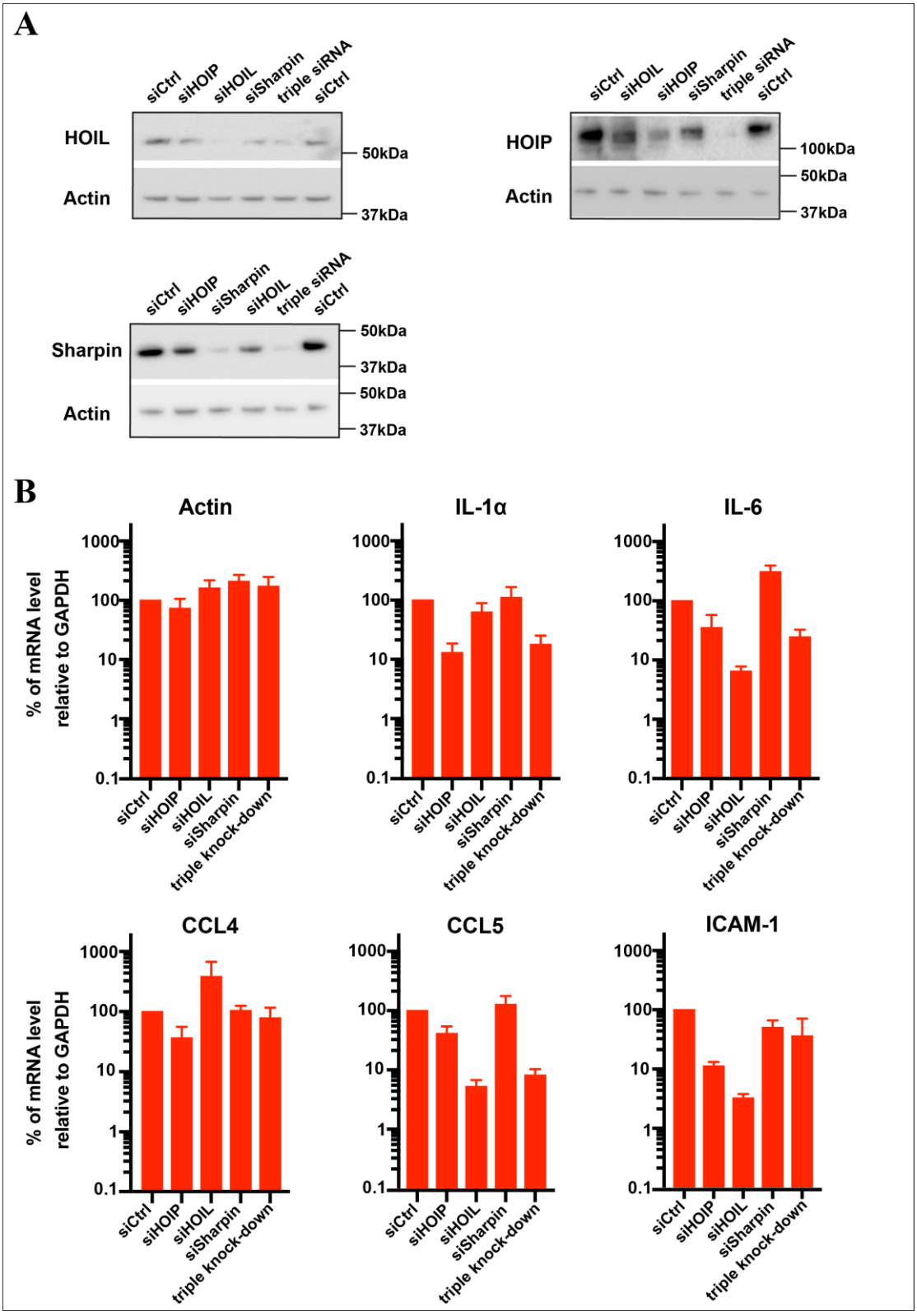

Figure 16: HOIL-1 is required for IL-6 and CCL5 induction upon *T.gondii* infection

MEFs were transfected with siRNA either control, or targeting one of the three LUBAC subunits (HOIP, HOIL-1 or Sharpin), or the entire complex (triple knock-down). 48h after siRNA transfection, cells were all primed with IFN-γ overnight and on the next day, cells were infected with type II (PRU) Tomato-*Toxoplasma gondii* strain in 4:1 ratio compared to

the number of cells seeded in wells. Samples from the different knock-down cell lines produced were isolated and later analysed by western-blotting (A) to assess the expression levels of the three targeted proteins (HOIP, HOIL-1, Sharpin). At 1h post-infection, cells were washed with PBS and fresh medium was added. At 24h post-infection, cells were collected, lysed and their RNA purified. After reverse transcription, mRNA levels were quantified by qPCR and analysed using the ΔΔCt method (B) with GAPDH as the reference gene. Data are shown as Mean ± S.E.M from three independent experiments, all performed in triplicate.

IL-6 induction following *T.gondii* infection was reduced in the HOIL-1 knock-down and to a smaller extent in the LUBAC knock-down. Regarding CCL4, induction by *T.gondii* was significant (p-value < 0.05) (**Fig.15**) and no major change was observed in any of the knock-downs (**Fig.16B**). mRNA levels of CCL5 were significantly reduced with cells knocked-down for HOIL-1 and reduced to a similar level in the triple knock-down. Finally, ICAM-1 levels were increased during *T.gondii* infection (similar to CCL5 induction, p-value < 0.005) in the control, but ICAM-1 transcripts were induced to lower levels in the absence of HOIL-1. However, this decrease in mRNA level was not recapitulated by the triple knock-down.

In summary, HOIL-1 seems required for the induction of IL-6 and CCL5 upon *T.gondii* infection whereas IL-1α induction might be partly HOIP-dependent. On the contrary, CCL4 and ICAM-1 levels are infection-dependent (**Fig.15**) but LUBAC-independent (**Fig.16**).

3.4 Discussion

There is increasing literature about the balance that *T.gondii* initiate to settle in cells, making use of cellular resources but evading immune responses in order to replicate and grow. *T.gondii* releases a number of effectors that impact the cell metabolism and signalling. Some of those changes were considered in this chapter and more particularly in relationship with IFN-γ. However, hosts have multiple mechanisms of defence to fight against infections, including cell-autonomous pathways such as autophagy. In the case of *S*.Typhimurium, the host response is multi-layered but requires autophagy to restrict bacterial growth and eventually destroy the pathogens

(Randow et al., 2013). In order to potentially draw a parallel with *T.gondii* infection, this chapter investigated the role of autophagy and, more particularly the roles of LUBAC and cargo receptors.

3.4.1 Role of autophagy in *T.gondii* clearance

The role of LUBAC and the autophagy receptors in the case of *T.gondii* infection was considered based on the comparison with cell-autonomous defence mechanisms exhibited against *S.*Typhimurium (see **Chapter 1**, **Fig.10**).

The results obtained showed that all LUBAC subunits and three major cargo receptors (NDP52, p62, and Optn) were recruited to type II *T.gondii* in IFN-γ-primed MEF cells. These results also suggest a range of experiments that could be employed in the future to obtain additional information about this process.

3.4.1.1. Is LUBAC involved in the restriction of the parasite?

Although LUBAC components are constitutively expressed, the complex is recruited to *T.gondii* in an IFN-γ-dependent manner, which suggests upstream IFN-γ-induced recruitment machinery that requires further experiments to be identified.

All LUBAC subunits, namely HOIP, HOIL-1 and Sharpin were recruited individually and independently of the other LUBAC subunits. This contrasts with the results obtained from bacterial infections where, in the case of *S.*Typhimurium, endogenous levels of HOIL-1 enable HOIP to be recruited, and, in a feed-forward loop, recruit HOIL-1 and Sharpin to the ubiquitylated cytosolic bacteria (Noad et al., 2017). Moreover, the two distinct mechanisms of HOIP recruitment (**Fig.6D**) to *T.gondii* are novel but require further experiments to identify the precise ligands involved.

To identify ligands more precisely, *in vitro* binding assays could be performed with purified *T.gondii* and cell lysates containing the tagged protein of interest. Lysates from cells either primed or not with IFN-γ overnight could be compared for their ability to bind to *T.gondii*. Both strains of *T.gondii* (RH and PRU) should also be used. The isolation of the parasite from HFF cells, in which they replicate within vacuoles would be critical to obtain either naked or vacuolar *T.gondii*, thereby

influencing the results of the pull-down assay. The proteins identified would belong either to the parasite membrane or to the PVM, respectively.

Further investigation of the recruitment mechanisms would have the potential to identify ligands and discriminate between the parasitophorous vacuolar membrane (PVM) and the parasite itself as the target (Jones & Hirsch, 1972; Kimata & Tanabe, 1987; Bradley et al., 2002). Using confocal microscopy was sufficient to count recruitment events; however, using super-resolution microscopy would enable a more detailed picture to be developed and might reveal whether recruitment is to the PVM or onto the parasite itself. Also, looking at intensity profiles across an image would have the potential to see to what extent the fluorescence signals overlap and hence identify colocalisation of tagged-proteins with *T.gondii*.

To investigate further the recruitment mechanisms and test whether LUBAC subunits are bound directly to *T.gondii,* an *in situ* proximal biotinylation could be employed. The ascorbate peroxidise enzyme APEX fused to a resident protein, in this case the LUBAC subunits (HOIP, HOIL-1 and Sharpin), allows proximity-dependent biotinylation in cells pretreated for 30 minutes with 500µM biotin-phenol to enable sufficient uptake as biotin-phenol has poor membrane permeability. The addition of 1mM H_2O_2 enables the production of phenoxyl radicals which biotinylate proximal proteins on electron rich amino acids, in particular tyrosine. APEX has been used to identify resident proteins in the mitochondrial matrix or to specifically label resident proteins in the mitochondrial intermembrane space (IMS), despite it being connected to the cytoplasm (Hung et al., 2016; Rhee et al., 2013). Since the half-life of phenoxyl radicals is very short (<10ms), this approach preferentially labels proteins located in close proximity (radius of 20nm) to the APEX-fused protein (Lam et al., 2015) for subsequent identification by TMT mass spectrometry. For the follow-up experiment, different infection conditions will be compared, that is: no infection, or infection with either type I (RH) or type II (PRU) *T.gondii*. In addition, for each of these infection conditions, cells primed or not with IFN-γ overnight would be used. Results obtained from cells primed with IFN-γ overnight and infected with the PRU *T.gondii* strain should facilitate identification of true binding partners. This experimental method should help identify binding partners, which could be host molecules or targets on

either the parasite or the PVM segregating binders of the *T.gondii* itself, or the parasitophorous membrane.

LUBAC constitutively restrict bacterial proliferation (Noad et al., 2017). Moreover, its action is not known to be antagonised by any *S.*Typhimurium effectors but is regulated by the deubiquitinase (DUB) OTULIN (Fill et al., 2013; Keusekotten et al., 2013). More specifically, because LUBAC synthesises linear ubiquitin chains, using the deubiquitinase OTULIN would help determine the extent to which LUBAC is (indirectly) required for the recruitment of cargo receptors such as NDP52, p62 and Optn to type II *T.gondii* in IFN-γ-primed cells (Keusekotten et al., 2013; Fiil et al., 2013).

3.4.1.2. How and why are autophagy cargo receptors recruited to the parasite?

The proximal biotinylation strategy described above would be applicable to studying NDP52, p62, and Optn in order to determine whether binding to *T.gondii* requires partners and/or complex formation. For instance, the PB1 domain of p62 was shown to be necessary for recruitment (**Fig.9C**) and is known to interact with the proteasome (Haldar et al., 2015; Seibenhener et al., 2004), the atypical protein kinase C (aPKC), and the dual specificity mitogen-activated protein kinase kinase 5 (MEK5) (Moscat & Diaz-Meco, 2000). Any of these could act either as downstream effectors or upstream baits of p62. Additionally, p62 has been shown to participate in the immune response against *T.gondii*: in conjunction with IFN-γ stimulation, p62 activates CD8+ T cells that recognise *T.gondii*-derived antigens originally present in the parasitophorous vacuole (Lee et al., 2015).

Both p62 and Optn required functional ubiquitin-binding domains (UBA and UBAN) to be recruited efficiently (**Fig.9** and **10**). Overexpressing a range of DUBs would provide an additional method for testing the precise way in which ubiquitin chains facilitate the recruitment of p62 and Optn to *T.gondii*. By removing ubiquitin from multiple host and external parasitic targets, it is to be expected that the recruitment of p62 and Optn would be reduced.

Live imaging (Niedelman et al., 2013) would be useful to determine the extent to which there is a time-sequence for the protein recruitment events on *T.gondii*. In the present study, patterns of proteins around the parasite – or its vacuole – were observed. Depending on the constructs, the shapes of recruitment events differed, even within one coverslip. In some instances, the GFP coat was observed to be either fully or partially surrounding the parasite; whereas, in other instances, a "tail" could be observed, as if the recruitment was onto the broken vacuole, with the *T.gondii* escaping or moving away from the membrane remnants. Live microscopy could help enrich the understanding of the time course of these recruitment events and would help establish whether recruitment is progressive and how sudden or stable it is. In addition, investigating the timeline will lead to know how early proteins are recruited after infection.

In summary, live imaging would provide further insight on the sequence of recruitment events, potentially revealing the necessary presence and/or function of LUBAC for the downstream recruitment of cargo receptors. Furthermore, looking at both host proteins and parasite effectors during infection will increase the knowledge of how the balance between host resistance and parasite virulence is established.

3.4.2 Host signalling could be silenced by *T.gondii* effectors

T.gondii has evolved mechanisms to antagonise host cell signalling pathways to avoid destruction (Zhao et al., 2009). For example, the effector ROP18 – present in virulent strains – phosphorylates IRGs, inhibiting their association with the PV and thereby protecting the parasite against clearance (Fentress et al., 2010; Steinfeldt et al., 2010).

3.4.2.1. Impacts of IFN-γ on the cell response

IFN-γ seems to play a role at the different stages of the infection process, namely cell entry, PVM rupture and parasite replication.

Flow cytometry experiments (**Fig.11**) showed that IFN-γ reduced the infectivity of type II *T.gondii* by almost half. Priming cells with IFN-γ seems to protect them against parasite infection.

Following *T.gondii* infection, members of the immunity-related GTPase (IRG) and guanylate-binding protein (GBP) families, which are IFN-γ inducible (Martens & Howard, 2006) adhere specifically to the parasitophorous vacuole (PV). GBPs recruit antimicrobial protein complexes that include the inflammasome and the autophagy machinery (MacMicking, 2012), whereas IRG proteins have the ability to lyse the PV membrane, exposing the parasites to the cytosol for targeting by autophagy (Ling et al., 2006).

As a marker of cytosolic entry for *S*. Typhimurium (Thurston et al., 2012), the presence of GAL8, following *T.gondii* infection, was assessed using antibody staining (**Fig.1**). Microscopy experiments need to be repeated using overexpressed fluorescently-labelled GAL8 to avoid unspecific staining. In addition, because *T.gondii* makes its own vacuole by releasing rhoptries and using lipids from the plasma membrane, the PVM content is species-specific. Moreover, upon rupture, the PVM might not expose any ligand being recognised as extracellular or foreign and therefore not targeted by GAL8.

Parasite replication was also assessed by flow cytometry looking at mean intensity in cells infected with fluorescent *T.gondii*. As mentioned, the mean intensity was used to measure either *T.gondii* growth or restriction of replication. However, curves showing the different cell populations based on the single cells' intensity (i.e. *T.gondii* load) are more bimodal than Gaussian, making the use of mean of intensity questionable for the data analysis. Performing plaque assays to more precisely count the number of parasites per cell and even looking at the distribution of the number of *T.gondii* per vacuole would provide a clearer picture of the mechanism and would discriminate between restriction of replication and/or killing of *T.gondii*.

The results presented in this chapter have demonstrated that IFN-γ drives restriction of type II *T.gondii* in MEFs (**Fig.12**), thereby confirming previous observations (Selleck at el., 2015). Priming with IFN-γ has also been shown to be required for the

recruitment of LUBAC and the autophagy cargo receptors NDP52, p62 and Optn to type II *T.gondii* (most likely to the PVM). No connection was made so far between their recruitment and the restriction of replication or killing of the parasites. Because *T.gondii* restriction may be promoted or activated by the production of cytokines (e.g. IL-1α, IL-6) and the upregulation of certain adhesion proteins (e.g. VCAM-1 or ICAM-1), several candidates were tested and their mRNA level was assessed by qPCR showing that indeed, IFN-γ-primed cells produced increased levels of IL-1α, IL-6 and CCL5, in a potentially HOIP, HOIL-1 and HOIL-1 dependent manner, respectively.

Analysing the changes in the synthesis and production of both adhesion and signalling proteins, either individually or together, would give a better understanding of their relationship with IFN-γ. Inhibiting or inducing some of them to try to recapitulate effects on infectivity, parasite replication and cell death, will shed light on the mechanisms by which IFN-γ impacts the cell response to *T.gondii* infections.

3.4.2.2. Signalling conflicts between host cytokines and parasite effectors

During an infection, the parasites deliver a set of effectors to invade the host cells, replicate, and establish tissue cysts. Even though the parasites try to use the host cell resources, some defence mechanisms are also set-up by the hosts on a cellular level to fight against the infection.

As shown by the qPCR experiments, infection with *T.gondii* alters cytokine levels such as IL-1α or IL-6 (**Fig.15**). It would be interesting to broaden the spectrum of signalling molecules tested in order to see whether more are affected upon *T.gondii* infection. For example, interleukin-12 (IL-12) was shown to play a critical role in controlling *T.gondii* growth in cells (Suzuki et al., 2011; Hargrave et al., 2019). The cytokine IL-10 was shown to be anti-inflammatory (Wujcicka et al., 2018) and increased levels of IL-10 were observed in enhanced *T.gondii* infection and replication (Levy et al., 2004). IL-10 protects mice against *T.gondii* (Gazzinelli et al., 1996) by controlling the inflammatory immune response.

All transcript analyses were initially performed with IFN-γ-primed MEF cells; using unprimed cells might reveal different cytokine profile changes. Additionally, type I and III *T.gondii* were shown to antagonise IL-12 by activating signal transducer and activator of transcription 3 and 6 (STAT3 and STAT6) (Boyle & Radke, 2009) via the release of rhoptry protein 16 (ROP16) (Ong et al., 2010). Experiments investigating modifications in mRNA levels could be performed again using the type I *T.gondii* strain (RH), because changes in transcription levels of signalling molecules might be different than those seen with the PRU (type II) strain and perhaps explained by the differences between the effector molecules released by the two distinct strains, linking it to virulence.

By synthesising linear ubiquitin chains, LUBAC activates NF-κB signalling to restrict cytosolic bacteria (Noad et al., 2017). High content microscopy was used to measure p65 nuclear translocation upon *T.gondii* infection. As a positive control, cells were treated with TNF-α (Hayden & Ghosh, 2014). As a negative control, the supernatant from the pelleted *T.gondii* after harvest and cell lysis was added to the cells. Automated analysis did not allow segregation between the different treatment conditions: levels of p65 nuclear translocation were already high in the negative control and even the addition of TNF-α did not show a significantly higher number of p65 translocation events. Thus, the effect of *T.gondii* infection on NF-κB signalling could not be addressed. This assay needs further optimisation and/or development of alternative methods such as ELISA, to measure NF-κB activation upon *T.gondii* infection.

T.gondii also subverts the host cell metabolism. Arginine metabolism was identified to be reprogrammed in the case of *T.gondii* infection (Hargrave et al., 2019). Arginine is converted in ornithine or proline rather than in toxic nitric oxide species (NOS) (Adams et al., 1990). *T.gondii* also affects host glycolysis by modulating seven enzymes (Nelson et al., 2008) resulting in up-regulation of the anabolic pathway. This increase translates to higher production of ATP providing energy and, more importantly, pyruvate that generates even more ATP by entering the oxidative phosphorylation route (Ainscow & Brand, 1999). Other metabolic cascades are probably modified (Blader et al., 2001) by *T.gondii* infection, whether it serves the *T.gondii* directly for growth or by silencing immune responses to protect *T.gondii* for

survival. Experiments testing whether LUBAC subunits or other cargo receptors (p62, Nemo, NDP52) are involved in directing the modifications in these pathways could be performed to get a better understanding of these mechanisms.

Although some work has also been done in human or mouse macrophages (Ling et al., 2006; Zhao et al. 2008; Clough & Frickel, 2017), it might be worth looking at other human epithelial or intestinal cell lines, which would be more physiologically relevant. Humans get infected most commonly through contaminated food or water (Hoffmann et al., 2012) before the infection migrates to the brain where bradyzoites establish cysts (Denkers & Gazzinelli, 1998). Since the human immune system is more efficient in fighting *T.gondii* infections than the murine one, the pathogenicity is indeed much lower in humans.

Appendices

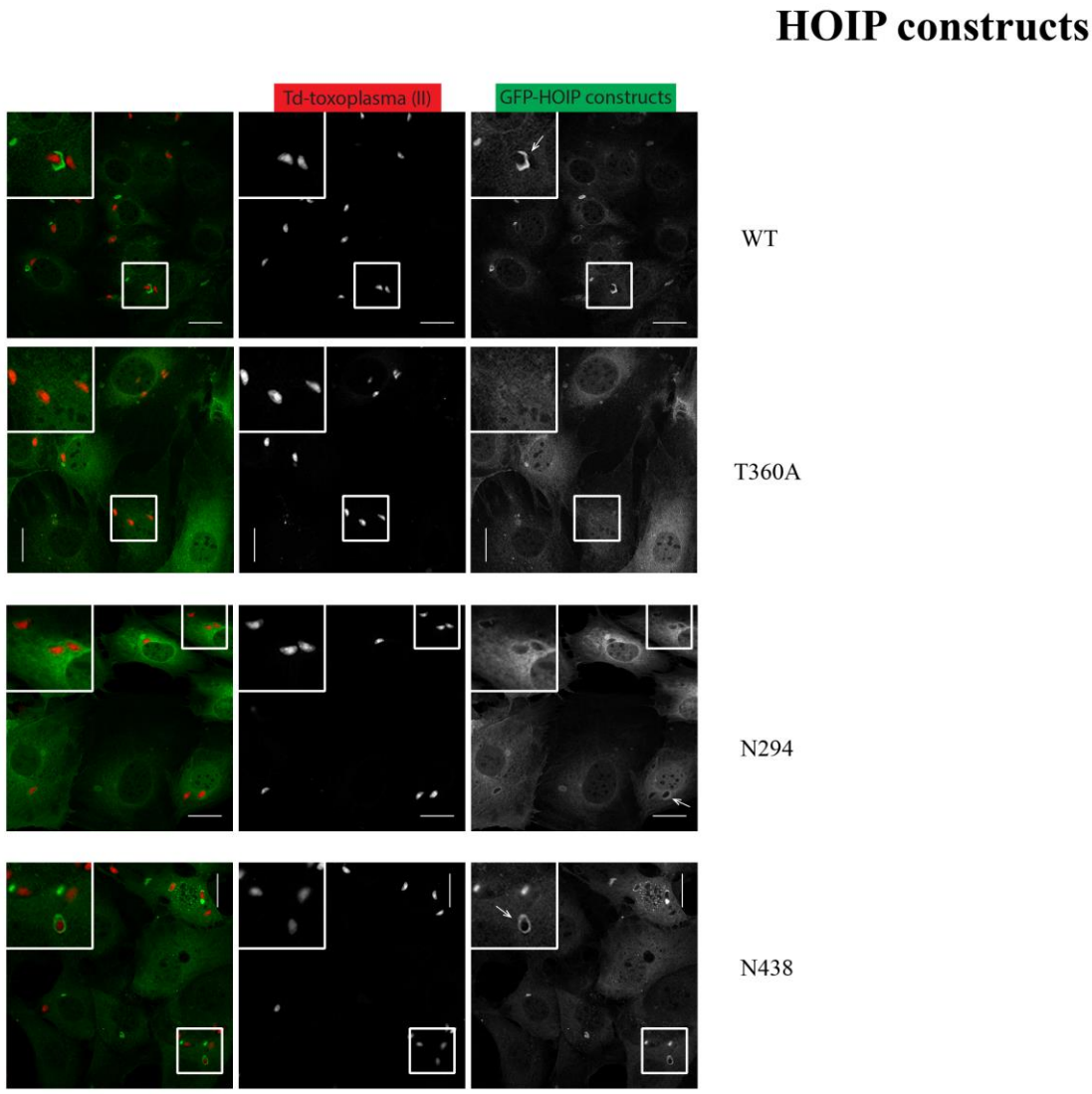

All the plasmids for the expression of GFP-tagged proteins were already made; more specifically the WT was provided by Dr.Felix Randow and the three others by Dr.Jessica Noad.

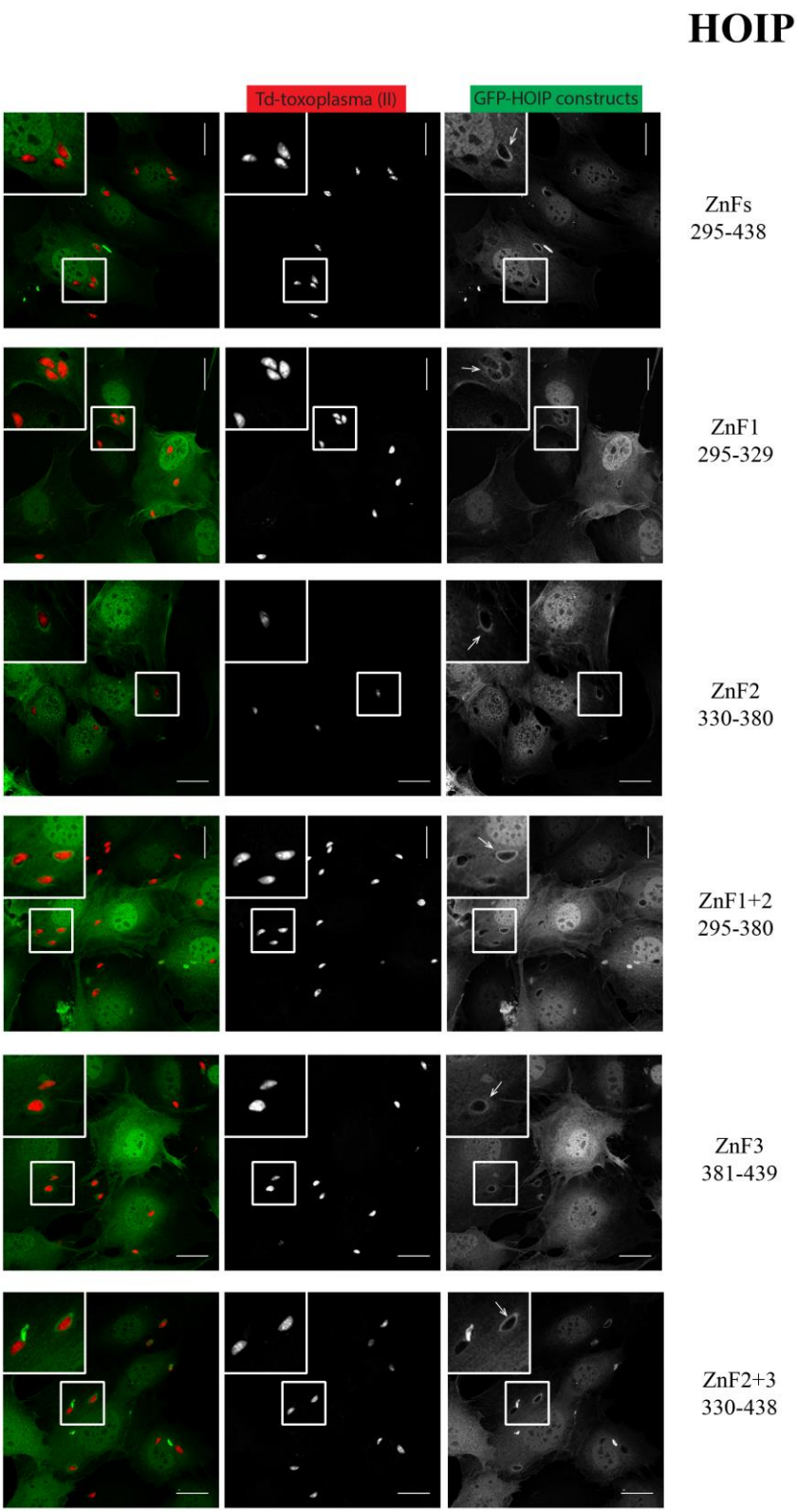

All the plasmids for the expression of GFP-tagged proteins were already made; more specifically on this page, they were all provided by Dr.Jessica Noad.

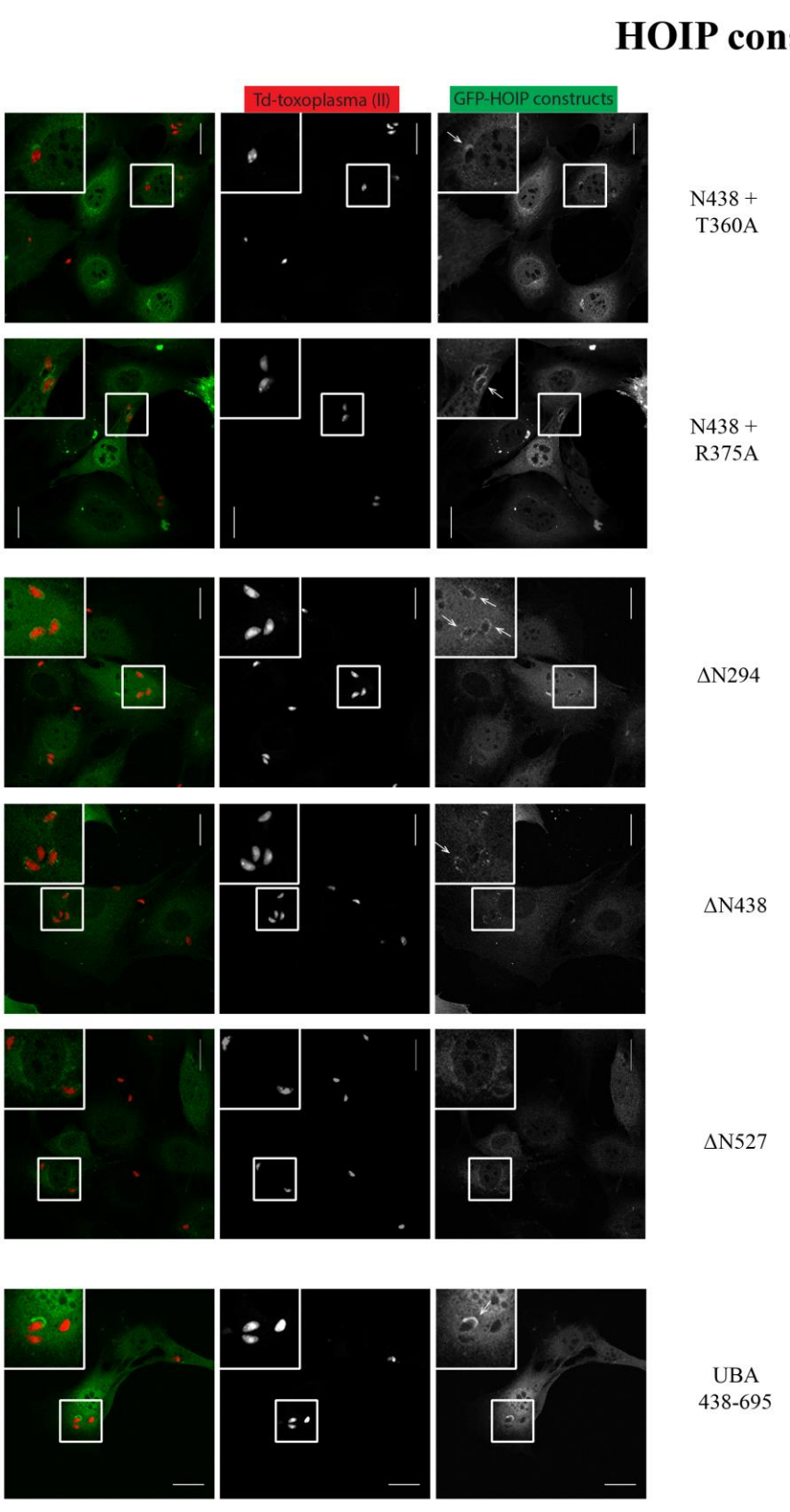

All the plasmids for the expression of GFP-tagged proteins were already made; more specifically on this page, they were all provided by Dr.Jessica Noad.

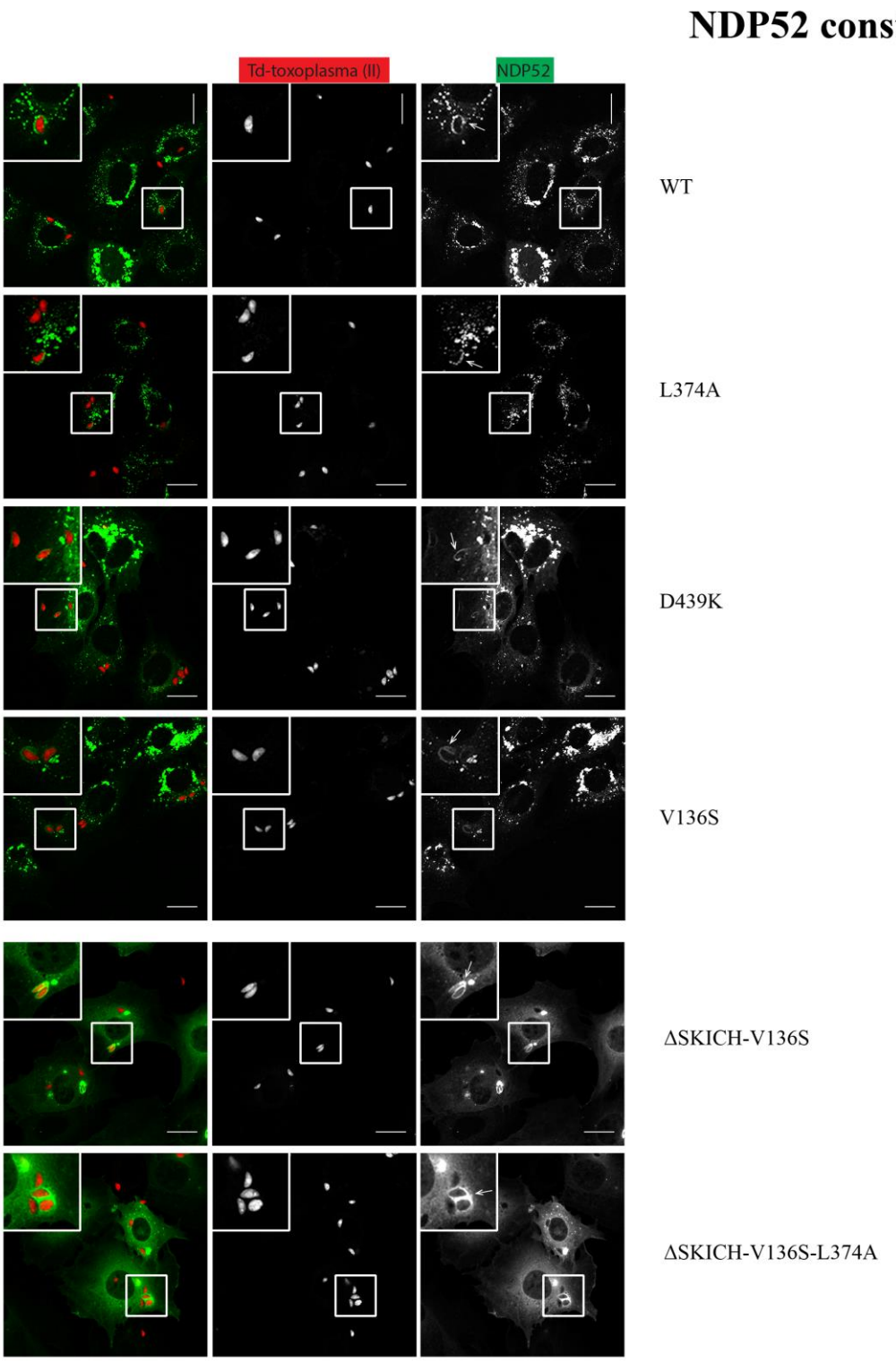

All the plasmids for the expression of GFP-tagged proteins were already made; more specifically on this page, they were all provided by Dr.Jessica Noad.

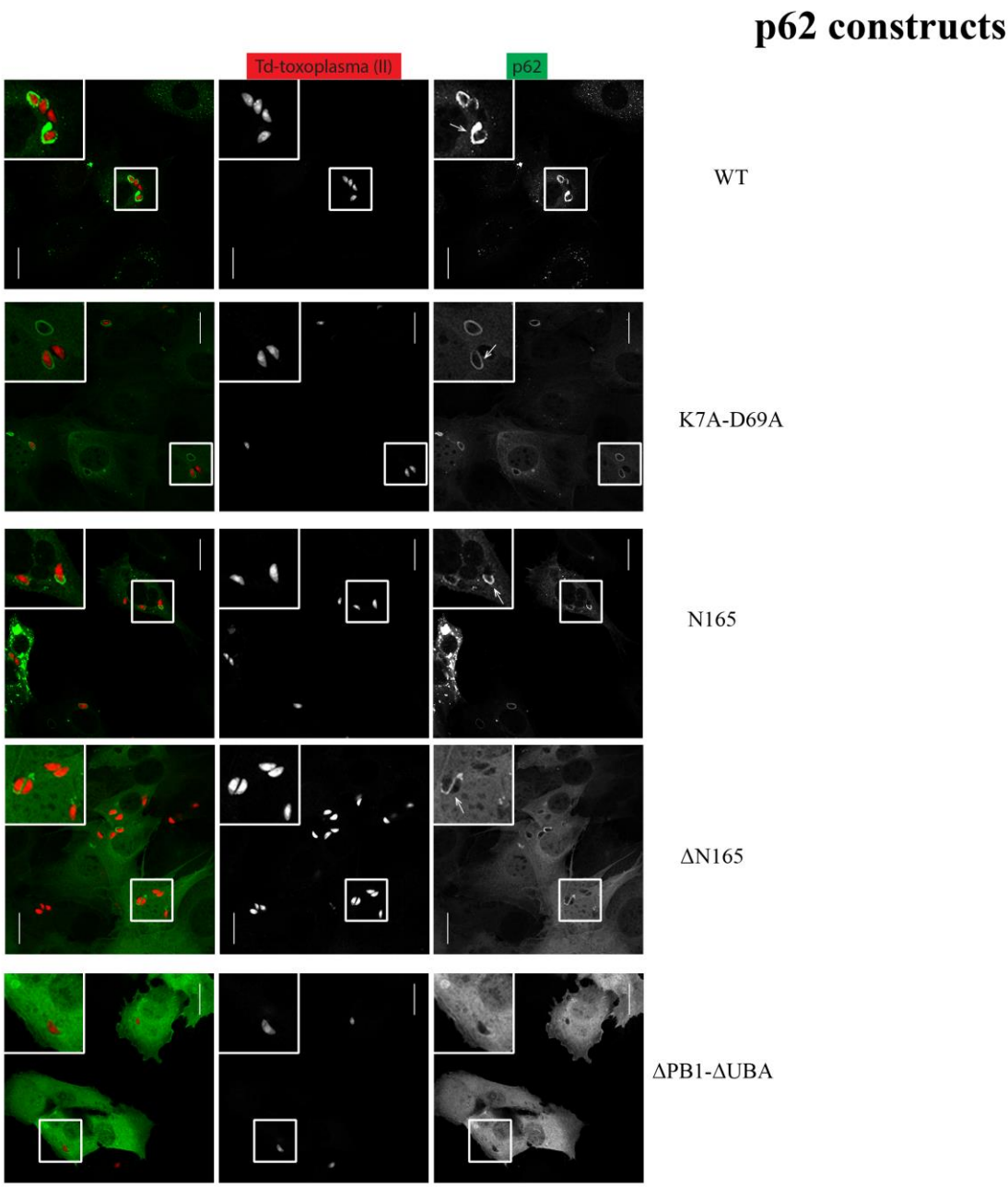

All the plasmids for the expression of GFP-tagged proteins were already made; more specifically on this page, all the truncations and the WT were provided by Dr.Ben Ravenhill, whereas the point mutation was developed by Dr.Jessica Noad.

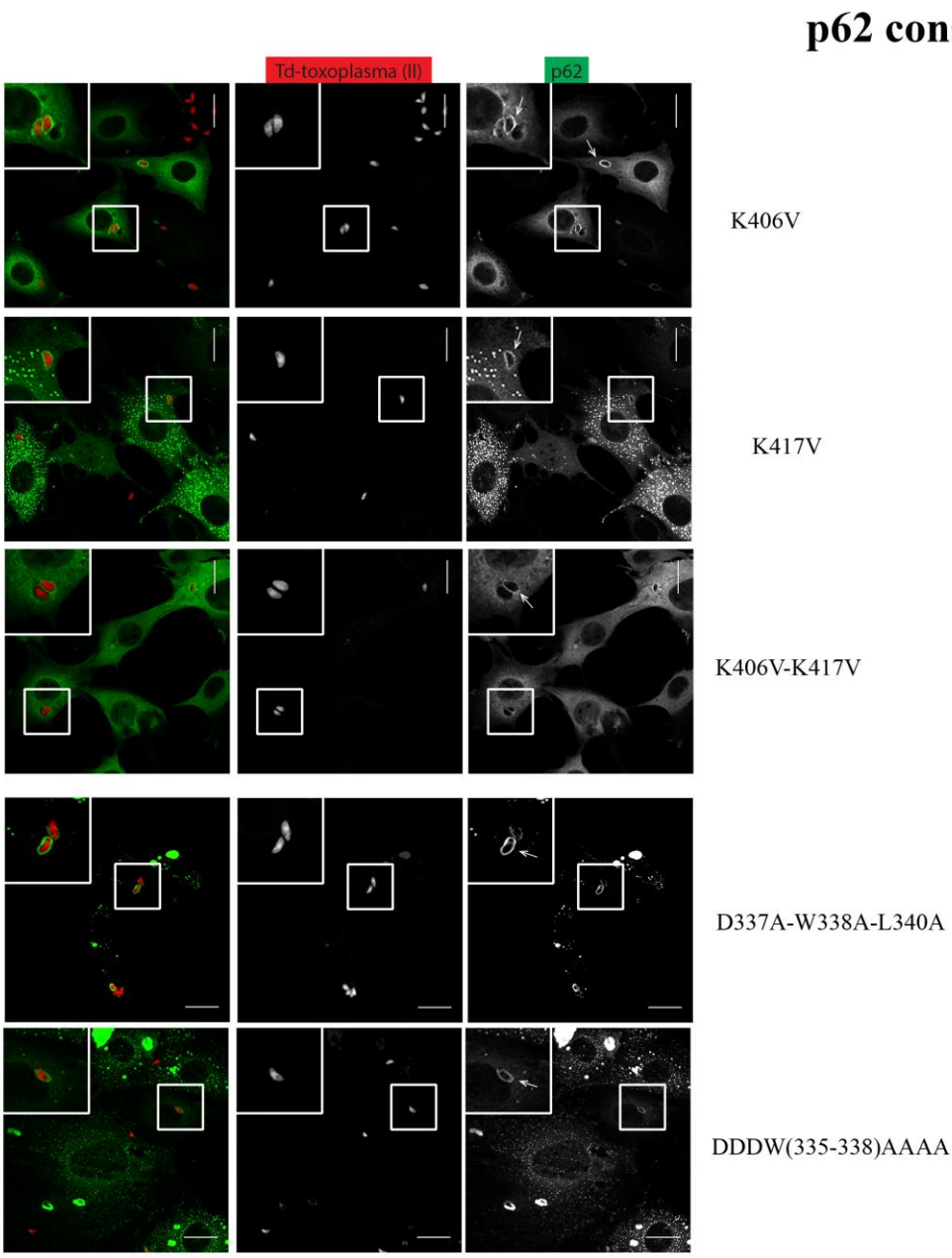

All the plasmids for the expression of GFP-tagged proteins were already made; more specifically on this page, they were all provided by Dr.Ben Ravenhill.

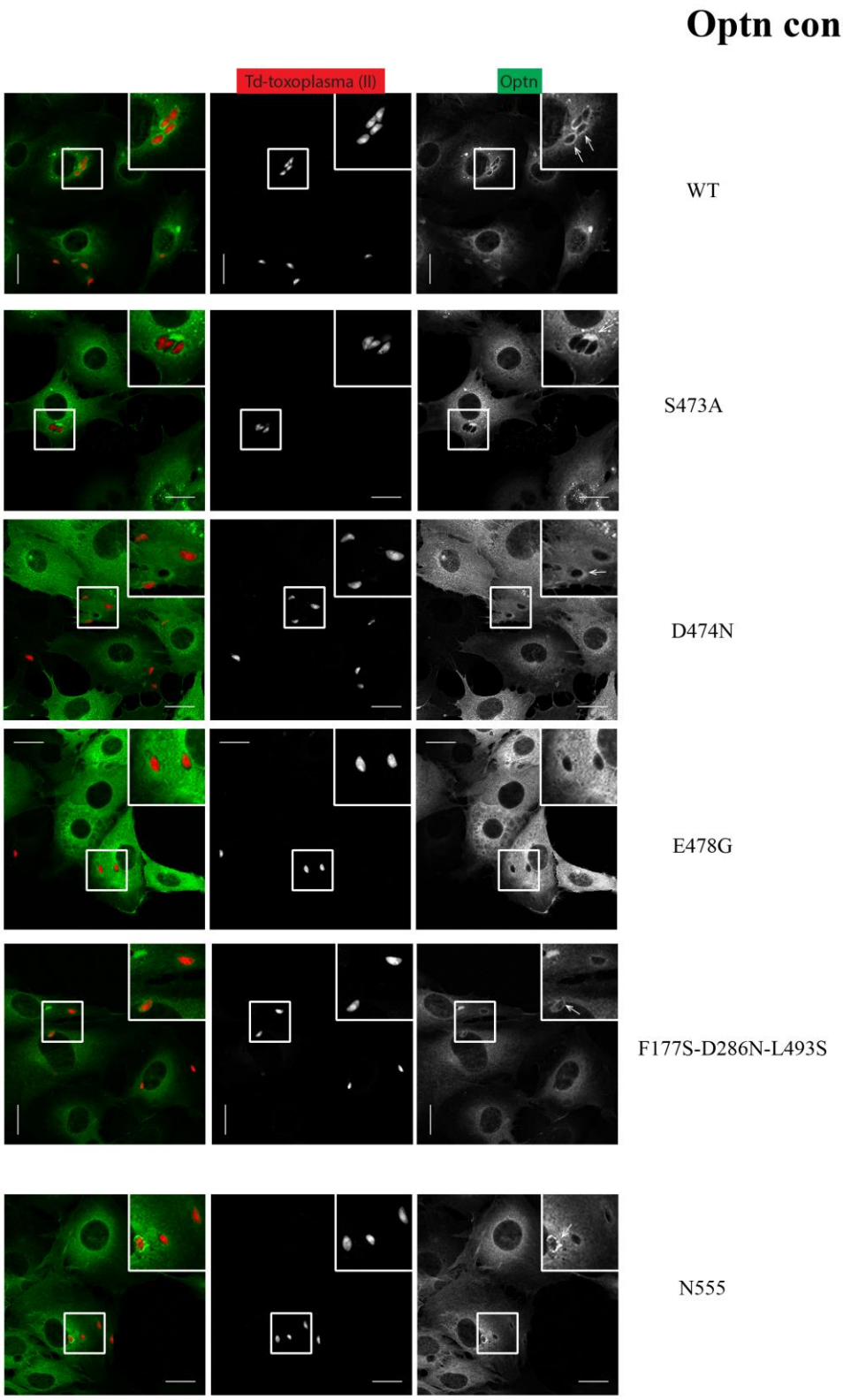

All the plasmids for the expression of GFP-tagged proteins were already made; more specifically on this page, the WT and E478G were provided by Dr.Ben Ravenhill and the others by Dr.Jessica Noad.

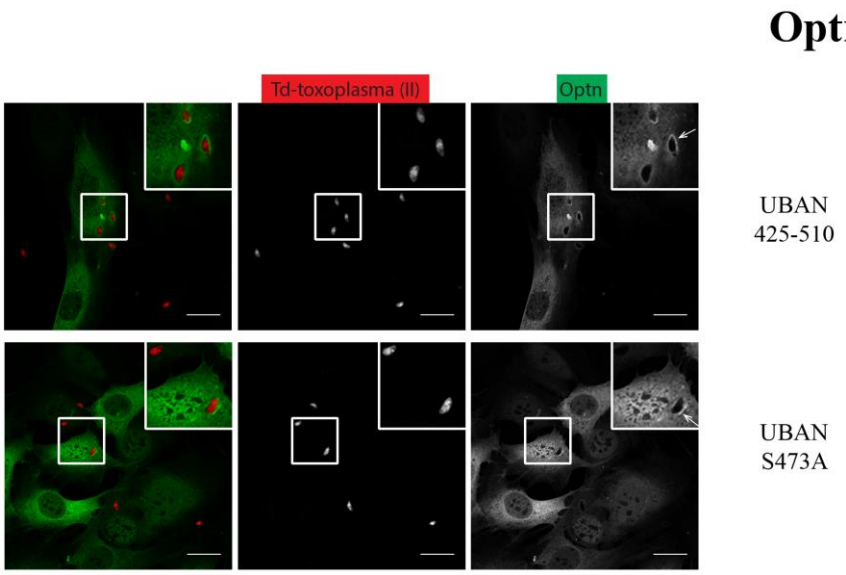

All the plasmids for the expression of GFP-tagged proteins were already made; more specifically on this page, they were both provided by Dr.Jessica Noad.

Appendix 1: Recruitment of HOIP, NDP52, p62 and Optn constructs to type II *T.gondii*

MEF cells overexpressing GFP-tagged constructs were primed overnight with IFN-γ and infected with type II *T.gondii* (PRU), in a 4:1 ratio compared to the number of cells seeded on the coverslips. At 1h post-infection, cells were washed with PBS and fixed with 4% PFA. Images were taken on a Zeiss-780, with 63x oil objective. Scale bar is 20μm.

Type I strain (RH)

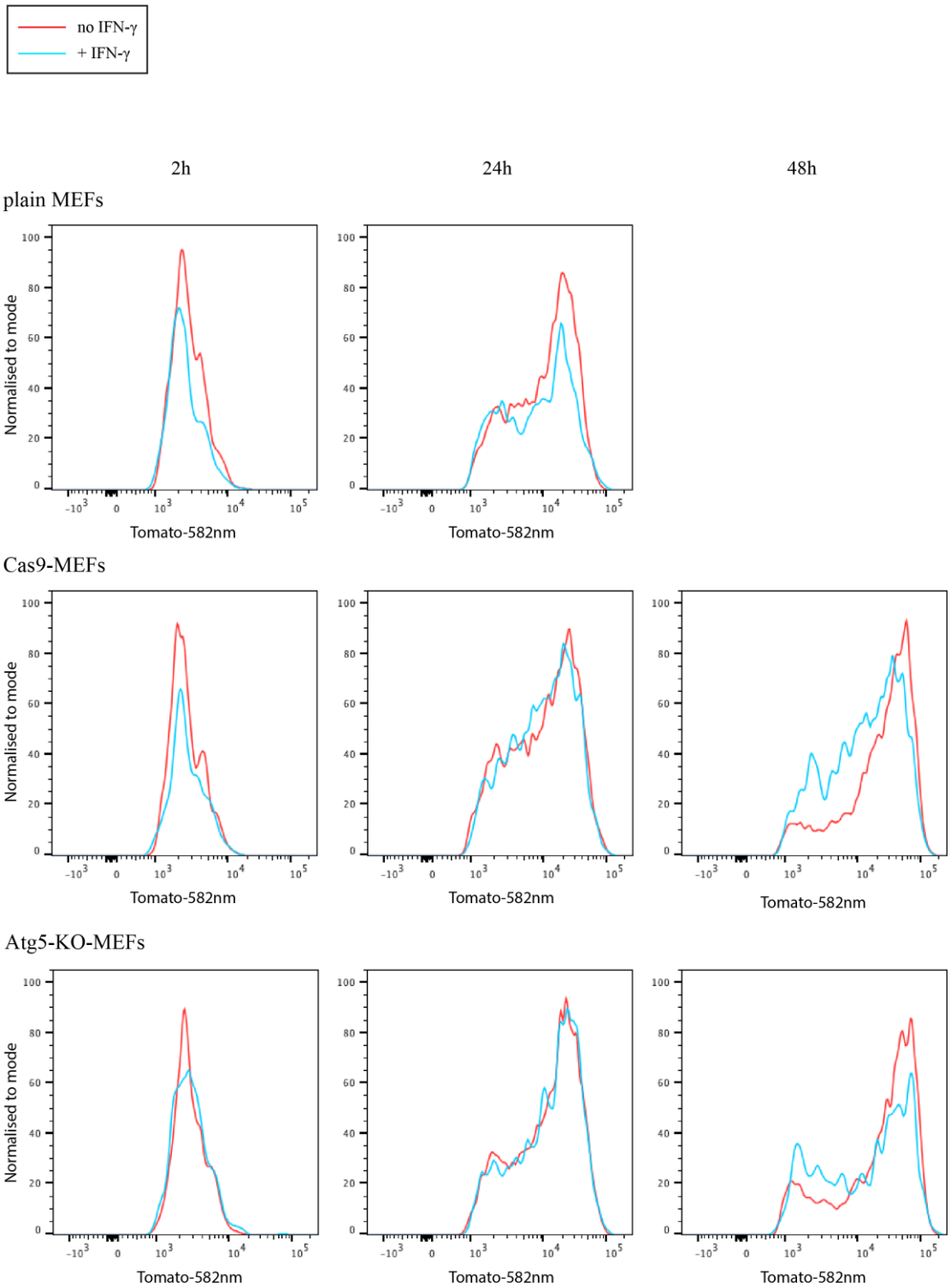

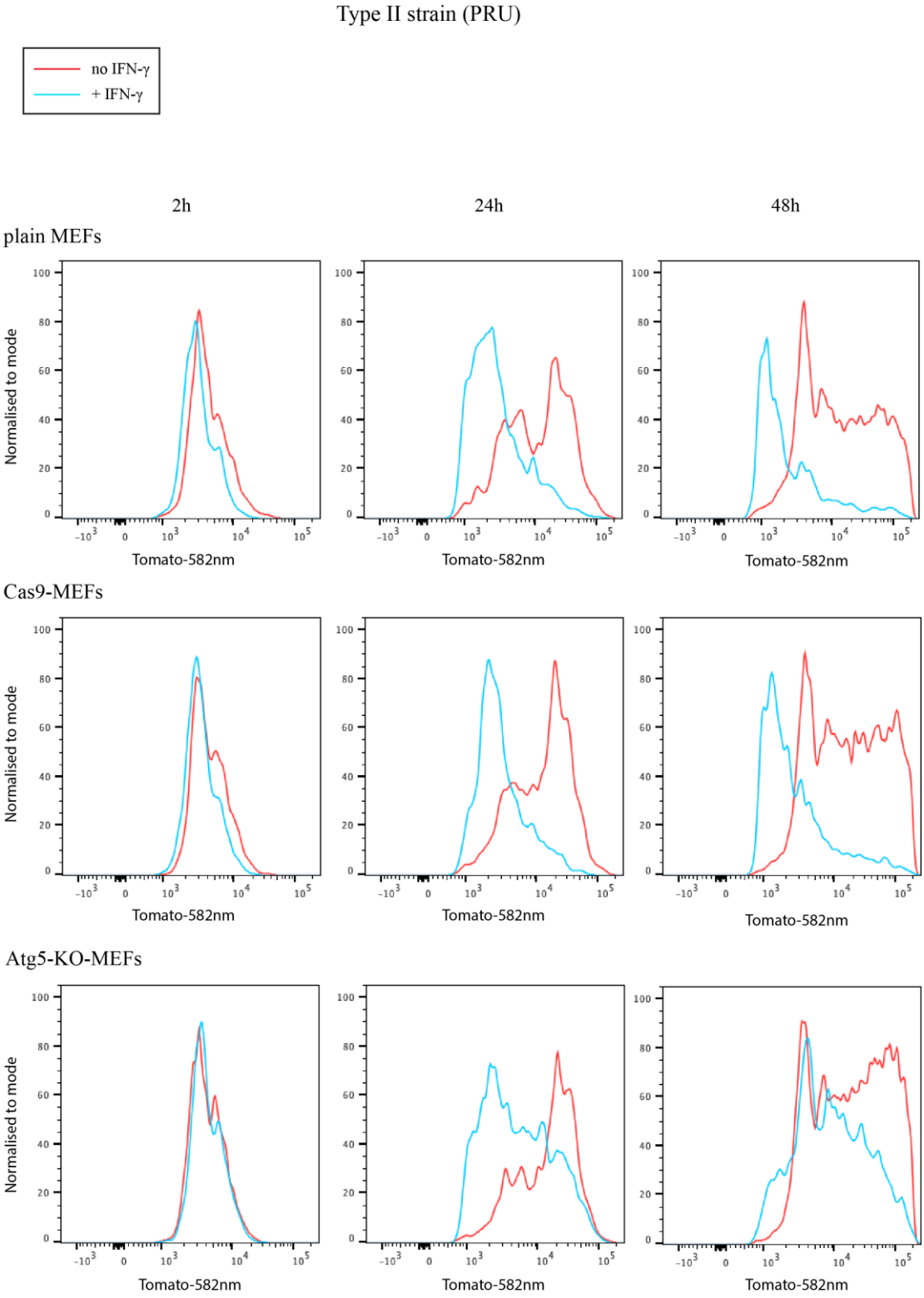

Appendix 2: Chromatograms showing the *T.gondii*-infected population

Wild-type, Cas9-overexpressing and Atg5-KO-MEF cells were incubated with IFN-γ overnight before infection with type I (RH) or type II (PRU) Tomato-*Toxoplasma gondii* strains in 1:1 ratio compared to the number of cells seeded in wells. At 1h post-infection, cells

were washed with PBS and fresh medium was added. At 2h, 24h and 48h post-infection, cells were fixed with 4% PFA and cells collected at all time points were analysed by flow cytometry at the same time. Data analysis using FlowJO enables the visualisation of chromatograms for the three cell lines infected with both the RH and PRU strains, and either primed (cyan) or not (red) with IFN-γ.

Chapter 4: Materials and methods

PART I - MATERIALS

4.1 Reagents

4.1.1 Chemicals

Reagents		**Source**
Restriction enzymes	all	New England Biolabs (NEB)
Selection reagents	Ampicillin	Melford
	Blasticidin	Invitrogen
	Gentamycin	Gibco
	Histidinol dihydrochloride	Sigma
	Hygromycin	A&E Scientific (PAA)
	Kanamycin	Merck
	Puromycin	Invitrogen
Protease inhibitors	Leupeptin, aprotinin, benzamidine and phenylmethylsulfonyl fluoride (PMSF)	Sigma
Interferon-gamma (IFN-γ)	Human and murine	BD Pharmingen
PCR grade water	Distilled water	Life Technologies
Propidium iodide	Cell death assays	Sigma
Cell Titer Glo 2.0		Promega
Primers	All sequences	Sigma
Sequencing	For plasmids	GATC (Eurofins)
	For gRNA library	MiSeq in the LMB
	For the screen	HiSeq at the CRUK

4.1.2 Antibodies

4.1.2.1. Primary antibodies

Antibody	**Cat. no**	**Source**	**Application**
Mouse monoclonal α-Flag M2	F1084	Sigma	WB (1:2000)
Mouse α-GFP (JL8)	632381	Clontech	WB (1:2500)
Rabbit α-□βActin	ab8227	Abcam	WB (1:5000)
Mouse α-MHC class I (W6/32)	sc-32235	Santa Cruz	FC (1:50)
Mouse monoclonal α-CRISPR-Cas9	ab191468	Abcam	WB (1:1000)
Mouse α-CASP4	M029-3	MBL	WB (1:1000)
Mouse α-CASP8	9746	CST	WB (1:1000)
Rabbit α-GSDMD	NBP2-33422	Novus Bio	WB (1:500)
Mouse monoclonal α-HOIP	MAB8039	R&D Systems	WB (1:500)
Goat polyclonal α-HOIL	sc-49718	Santa Cruz	WB (1:1000)
Rabbit polyclonal α-Otulin	ab151117	Abcam	WB (1:1000)
Mouse monoclonal α-Ubiquitin FK2	BML-PW8810-0500	Enzo	IF (1:400)
Goat polyclonal α-Galectin8	AF1305	R&D Systems	IF (1:100)
Rabbit polyclonal α-NF-κB p65 (C-20)	sc-372	Santa Cruz	IF (1:1000)
Mouse monoclonal α-LPS (S.Typhimurium)	8210-0407	Bio-Rad	IF (1:1000)

WB: western-blot; IF: Immunofluorescence; FC: Flow cytometry

4.1.2.2. Secondary antibodies

Technology	**Species**	**Source**	**Application**
AlexFluor-conjugated	α-mouse, α-goat, α-rabbit	Invitrogen	FC (1:500) IF (1:400)
HRP-conjugated	α-mouse, α-rabbit, α-goat	Dako	WB (1:5000) WB (1:2500)

4.2 Primers

4.2.1 Primers used for sequencing

Vector	ID	Sequence	Ori
M6P	Flx 190	5’-TAGACGGCATCGCAGCTTGGA-3’	F
	Trx 109	5’-TCAAGATCCGCCACAACATCG-3’	F
	Flx 561	5’-ACGCACACCGGCCTTATTCCA-3’	R
	Flx 211	5’-CTGGTGATATTGTTGAGTCA-3’	R
pET-11	T7	5’-TAATACGACTCACTATAGGG-3’	F
	pET-RP	5’-CTAGTTATTGCTCAGCGG-3’	R
gRNA library	PCR2	5’-TTAGCTCACTCATTAGG-3’	
	M13FP	5’-TGTAAAACGACGGCCAGT-3’	F
	scr15	5’-GTTTTAGAGCTAGAAATAGCAAGTTAAAATAAGGCTAG-3’	F
	scr16	5’-GGTGTTTCGTCCTTTCCACAAGATATATAAAGCC-3’	R

ID: primer identification reference; Ori: orientation; F: forward; R: reverse

In all the subsequent tables, sequences are all written in their 5’ → 3’ orientation.

4.2.2 Primers for Illumina sequencing – samples from the screen

Use	ID	Sequence	Ori
PCR1 of screen samples	PCR1-FOR	AATGGACTATCATATGCTTACCGTAACTTGAAAGTATTTCG	F
	PCR1-REV	CTTTAGTTTGTATGTCTGTTGCTATTATGTCTACTATTCTTTCC	R
PCR2 of screen samples	FS-mix	Mix of 8-staggered PCR primers: P5_XPR/LKO1_1-8	F
	pkREbar N701	CAAGCAGAAGACGGCATACGAGATTCGCCTTAGTGACTGGAGTTCAGACGTGTGCTCTTCCGATCTTTCTACTATTCTTTCCCCTGCACTGT	R
	pkREbar N702	CAAGCAGAAGACGGCATACGAGATCTAGTACGGTGACTGGAGTTCAGACGTGTGCTCTTCCGATCTATTCTACTATTCTTTCCCCTGCACTGT	R

4.2.3 Primers used for qPCR

Gene	Species	ID	Sequence	Ori
CASP4	Human	scr140	TGGAATCCCTGGGCAAAGAT	F
		scr141	GGTCCAGCCTCCATATTCGG	R
CASP8	Human	scr146	AGGAGCTGCTCTTCCGAATT	F
		scr147	ACCTCAATTCTGATCTGCTCAC	R
GSDMD	Human	scr156	CCAGAAGAAGACGGTCACCA	F
		scr157	CCTCTGCTTCTTATCCGGGA	R
STAT-1	Human	scr164	TGATCTCCAACGTCAGCCAG	F
		scr165	CCAACATGTTCAGCTGGTCC	R
IFNGR1	Human	scr166	TACCAGATCATGCCACAGGT	F
		scr167	CCTGGCTTTAACTCTGACCC	R
NCKAP1	Human	scr172	ACTGCTGTCTCGAATTGAAGA	F
		scr173	GCTATGGGGTACAAATTCTTCCA	R
SRSF10	Human	scr180	AAGACTTGCGGCGTGAATTT	F
		scr181	GCCGTCCACAAATCCACTTT	R
ALG12	Human	scr186	GGTCATCTGTCCCTACACCA	F
		scr187	GAGAACACTGCGATCACCAC	R
FIP1L1	Human	scr196	TGGTTATGATAGTCGTTCTGCAC	F
		scr197	CTCTCTCTCTCTCTGGTGCG	R
SLC25A37	Human	scr202	ATAGCTGGGAGTATGGCCAC	F
		scr203	GTGGTGTAGCTCCGGTAGAA	R
SAF-B	Human	scr206	TAACGGGCTGGAGGAAAACT	F
		scr207	CATGTTCCTGAAGCTGCTCC	R
TM9SF2	Human	scr216	TTGAAACTGGGTCCATGGGA	F
		scr217	TCCCCAGAAGCCTTGTTACT	R
β-actin	Human	G345	CCTGG CACCC AGCAC AAT	F
		G346	GCCGA TCCAC ACGGA GTACT	R
HOIP=rnf31	Mouse	scr244	GTGGCCGGGATGTACTACG	F
		scr245	CTCTCTTAGCAGCTGGTCCA	R
HOIL=rbck-1	Mouse	scr248	CGGAGATGAACAGGCTGCTA	F
		scr249	CTTAAGGGAGGCCACTGTCA	R

Sharpin	Mouse	scr256	TGCCCCATTTCTCCACCAT	F
		scr257	CTGCTTTCTCATCCCCACCT	R
β-actin	Mouse	G360	TGACAGCATTGCTTCTGTGTAAATT	F
		G361	ATTGGTCTCAAGTCAGTGTACAGGC	R
IL-1α	Mouse	scr260	CAAGATGGCCAAAGTTCGTGAC	F
		scr261	GTCTCATGAAGTGAGCCATAGC	R
IL-6	Mouse	scr264	AGGATACCACTCCCAACAGACCT	F
		scr265	CAAGTGCATCATCGTTGTTCATAC	R
CCL4	Mouse	scr276	CAACACCATGAAGCTCTGCG	F
		scr277	GCCACGAGCAAGAGGAGAGA	R
CCL5	Mouse	scr272	CCAATCTTGCAGTCGTGTTTGT	F
		scr273	CATCTCCAAATAGTTGATGTATTCTTGAAC	R
ICAM-1	Mouse	scr268	GGCATTGTTCTCTAATGTCTCCG	F
		scr269	CCGCTCAGAAGAACCACCTTGG	R
VCAM-1	Mouse	scr270	TACTCCCGTCATTGAGGATATTGG	F
		scr271	CTCCTTCACACACATAGACTCC	R
TNF-α	Mouse	scr274	GGCAGGTCTACTTTGGAGTCATTGC	F
		scr275	ACATTCGAGGCTCCAGTGAA	R
GAPDH	Mouse	scr278	TGTGTCCGTCGTGGATCTGA	F
		scr279	CCTGCTTCACCACCTTGTTGAT	R

ID: primer identification reference with “G” designed by Grigory Ryzhakov and “scr” by Solene Rolland; Ori: orientation; F: forward; R: reverse

4.2.4 Primers for amplification of open reading frames (ORFs)

Gene	**ID**	**Sequence**	**RE**	**Ori**
ALG12	scr109	GGCCGGACATGTCAGCTGGAAAGGGGTCATCAG	PciI	F
	scr110	GGCCGGGCGGCCGCTCAGGACGGCCGGGGGAGC	NotI	R
EMC6	scr111	GGCCGGACATGTCAGCCGCGGTGGTGGCCAAGC	PciI	F
	scr112	GGCCGGGCGGCCGCTCAGTAGACGTGCACCATG	NotI	R
TM9SF2	scr113	GGCCGGCGTCTC/ACATGTCAGCGAGGCTGCCGGTGTTG	BsmBI+PciI	F
	scr114	GGCCGGGCGGCCGCTCAGTCAACCTTCACCACA	NotI	R

GSDMD	scr115	GGCCGGACATGTCAGGGTCGGCCTTTGAGCGGG	PciI	F
	scr116	GGCCGGGCGGCCGCCTAGTGGGGCTCCTGGCTC	NotI	R
FIP1L1	scr117	GGCCGGACATGTCGGCCGGCGAGGTCGAGCGCC	PciI	F
	scr118	GGCCGGGCGGCCGCCTATTCTGCAGGTGTAGCT	NotI	R
SRSF10	scr119	GGCCGGACATGTCCCGCTACCTGCGTCCCCCCA	PciI	F
	scr122	GGCCGGGCGGCCGCTCAGTGGCCACTGGACTTA	NotI	R
CASP4	scr123	GGCCGGACATGTCAGCAGACTCTATGCAAGAGA	PciI	F
	scr124	GGCCGGGCGGCCGCTCAATTGCCAGGAAAGAGG	NotI	R
CASP8	scr128	GGCCGGACATGTCAGACTTCAGCAGAAATCTTT	PciI	F
	scr127	GGCCGGGCGGCCGCTCAATCAGAAGGGAAGACA	NotI	R
SAF-B	scr130	GGCCGGACATGTCAGCGGAGACTCTGTCAGGCC	PciI	F
	scr131	GGCCGGGCGGCCGGAGACGTCAGTAGCGGCGAGTGAAG	BsmBI+NotI	R

ID: primer identification reference; RE: restriction enzyme for which the restriction site is underlined; Ori: orientation; F: forward; R: reverse

4.2.5 Primers for generating sgRNAs

Gene	**ID**	**Sequence**	**Ref**	**Ori**
CASP4	scr21	CACCGTATGCAAGAGAAGCAACGTA	~~1A~~	F
	scr22	AAACTACGTTGCTTCTCTTGCATAC		R
	scr23	CACCGAGAAACAACCGCACACGCC	1B	F
	scr24	AAACGGCGTGTGCGGTTGTTTCTC		R
	scr25	CACCGGGATGAAGGAGCTACTTGA	1C	F
	scr26	AAACTCAAGTAGCTCCTTCATCCC		R
	scr27	CACCGAGGATATGGAGTCAGCGCTG	1D	F
	scr28	AAACCAGCGCTGACTCCATATCCTC		R
CASP8	scr29	CACCGCCTGGACTACATTCCGCAA	2A	F
	scr30	AAACTTGCGGAATGTAGTCCAGGC		R
	scr31	CACCGTCTGATAGAGCATGACCCTG	2B	F
	scr32	AAACCAGGGTCATGCTCTATCAGAC		R
	scr33	CACCGATGATCAGACAGTATCCCCG	2C	F
	scr34	AAACCGGGGATACTGTCTGATCATC		R

	scr35	CACCGCTACCTAAACACTAGAAAGG	2D	F
	scr36	AAACCCTTTCTAGTGTTTAGGTAGC		R
GSDMD	scr37	CACCGGACAGGCAAAGATCGCAGG	3A	F
	scr38	AAACCCTGCGATCTTTGCCTGTCC		R
	scr39	CACCGTCAGAGTCAATAACCAGCT	3B	F
	scr40	AAACAGCTGGTTATTGACTCTGAC		R
	scr41	CACCGCACCTGCTGGACCGTCCAG	3C	F
	scr42	AAACCTGGACGGTCCAGCAGGTGC		R
	scr43	CACCGGAGGCACCTCATCATGGAG	3D	F
	scr44	AAACCTCCATGATGAGGTGCCTCC		R
STAT-1	scr45	CACCGTCCCATTACAGGCTCAGTCG	4A	F
	scr46	AAACCGACTGAGCCTGTAATGGGAC		R
	scr47	CACCGAGGTCATGAAAACGGATGG	4B	F
	scr48	AAACCCATCCGTTTTCATGACCTC		R
	scr49	CACCGTGACTCCACCATGTGCACGA	~~4C~~	F
	scr50	AAACTCGTGCACATGGTGGAGTCAC		R
	scr51	CACCGTGGAGCGGTCCCAGAACGG	4D	F
	scr52	AAACCCGTTCTGGGACCGCTCCAC		R
IFNGR1	scr53	CACCGGTACTCCCAATATACGATA	5A	F
	scr54	AAACTATCGTATATTGGGAGTACC		R
	scr55	CACCGGTCCCTGTTTTTACCGTAG	5B	F
	scr56	AAACCTACGGTAAAAACAGGGACC		R
	scr57	CACCGACAGTACTGAGAATTCAGTG	5C	F
	scr58	AAACCACTGAATTCTCAGTACTGTC		R
	scr59	CACCGGAGTACCAGATCATGCCAC	5D	F
	scr60	AAACGTGGCATGATCTGGTACTCC		R
NCKAP1	scr61	CACCGTATGCCCATGAAATGACTCA	6A	F
	scr62	AAACTGAGTCATTTCATGGGCATAC		R
	scr63	CACCGGCATATACTAGTGTCTCAA	6B	F
	scr64	AAACTTGAGACACTAGTATATGCC		R
	scr65	CACCGGGTGAGCATGCCGACGCCC	~~6C~~	F
	scr66	AAACGGGCGTCGGCATGCTCACCC		R

	scr67	CACCGAGAATTTGTACCCCATAGCA	6D	F
	scr68	AAACTGCTATGGGGTACAAATTCTC		R
SRSF10	scr69	CACCGTCTCTGTTCGTCAGGAACG	7A	F
	scr70	AAACCGTTCCTGACGAACAGAGAC		R
	scr71	CACCGTTTTAGGTCTGAAGACTTG	7B	F
	scr72	AAACCAAGTCTTCAGACCTAAAAC		R
	scr73	CACCGAAGCCGAAGTTATGAAAGG	7C	F
	scr74	AAACCCTTTCATAACTTCGGCTTC		R
	scr75	CACCGGGACGCAGGTAGCGGGACA	7D	F
	scr76	AAACTGTCCCGCTACCTGCGTCCC		R
ALG12	scr85	CACCGCGAAAGCACGTAAACCGCG	9A	F
	scr86	AAACCGCGGTTTACGTGCTTTCGC		R
	scr87	CACCGGAAGTGAGACGGCACTTCG	9B	F
	scr88	AAACCGAAGTGCCGTCTCACTTCC		R
	scr89	CACCGCGTGATGTTGAGCATGGGGA	9C	F
	scr90	AAACTCCCCATGCTCAACATCACGC		R
	scr91	CACCGCAGCTACGTACCTACAGGC	9D	F
	scr92	AAACGCCTGTAGGTACGTAGCTGC		R
FIP1L1	scr93	CACCGGATGTGCTTATAGGCCCAT	10A	F
	scr94	AAACATGGGCCTATAAGCACATCC		R
	scr95	CACCGAGGAAGAGTGGCTCTATGG	10B	F
	scr96	AAACCCATAGAGCCACTCTTCCTC		R
	scr97	CACCGTGAGTGGGAGGAGCTCCTGG	10C	F
	scr98	AAACCCAGGAGCTCCTCCCACTCAC		R
	scr99	CACCGCCGAGTAGAAGGCAGGCGA	10D	F
	scr100	AAACTCGCCTGCCTTCTACTCGGC		R
SLC25A37	scr101	CACCGGTCATGTACCCGGTGGACT	11A	F
	scr102	AAACAGTCCACCGGGTACATGACC		R
	scr103	CACCGGCGTCAACGTCATGATCAT	11B	F
	scr104	AAACATGATCATGACGTTGACGCC		R
	scr105	CACCGCACTCGGTCATGTACCCGG	11C	F
	scr106	AAACCCGGGTACATGACCGAGTGC		R

	scr107	CACCGCAAAATACATGGCATGGGC	11D	F
	scr108	AAACGCCCATGCCATGTATTTTGC		R
TM9SF2	scr77	CACCGTCTTGGTCAGGTACTATTCG	12A	F
	scr78	AAACCGAATAGTACCTGACCAAGAC		R
	scr79	CACCGAAAGAGCGACGAGTGCAAGG	12B	F
	scr80	AAACCCTTGCACTCGTCGCTCTTTC		R
	scr81	CACCGACGATGTTGAAGATGGTCAG	12C	F
	scr82	AAACCTGACCATCTTCAACATCGTC		R
	scr83	CACCGCTGAAGATCCTTCTCCCCAG	12D	F
	scr84	AAACCTGGGGAGAAGGATCTTCAGC		R
SAF-B	scr132	CACCGAAATTGAAATTACCTCCGA	8A	F
	scr133	AAACTCGGAGGTAATTTCAATTTC		R
	scr134	CACCGCGAGTGATCGATCTGCGGG	8B	F
	scr135	AAACCCCGCAGATCGATCACTCGC		R
	scr136	CACCGTAGGCAATTGAAGATGAAGG	8C	F
	scr137	AAACCCTTCATCTTCAATTGCCTAC		R
	scr138	CACCGGAGGATGTTGAGACCAGTC	8D	F
	scr139	AAACGACTGGTCTCAACATCCTCC		R

ID: primer identification reference; Ref: symbol by which they were referred as during experiments, if they are strikethrough, it means that the plasmid failed transformation and therefore was not used in validation experiment; Ori: orientation; F: forward; R: reverse

The amplified fragments from human cDNA were then digested with restriction enzymes in order to create overhangs and were ligated into the backbone:

ID	**RE backbone**	**Plasmid description**	**RE insert**	**Resistance**
1862	BbsI/BbsI	pKLV-P_{hU6}-sgRNA-P_{PGK}-Puro-2A-BFP	BbsI/BbsI	puromycin

ID: primer identification reference; RE: restriction enzyme used to cut and create overhangs.

4.3 Plasmids

ID	Plasmid description	Resistance
SR08	M6P.Blast.NtermFLAG.GSDMD	blasticidin
SR09	M6P.Blast.GSDMD.CtermFLAG	blasticidin
MW724	M6P.pac.NtermFLAG.CASP4-WT	puromycin
MW738	M6P.pac.NtermFLAG.CASP4-K19E	puromycin
MW739	M6P.pac.NtermFLAG.CASP4-C258A	puromycin
SR10	M6P.Blast.NtermGFP.ALG12	blasticidin
SR11	M6P.Blast.NtermGFP.GSDMD	blasticidin
SR12	M6P.Blast.NtermGFP.TM9SF2	blasticidin
SR13	M6P.Blast.NtermGFP.CASP8	blasticidin
SR15	M6P.Blast.NtermGFP.SRSF10	blasticidin
SR17	M6P.Blast.NtermGFP.EMC6	blasticidin
SR18	M6P.Blast.NtermGFP.CASP4	blasticidin
SR21	M6P.Blast.NtermGFP.SAFB	blasticidin
JN141	M6P.pac.Otulin-WT	puromycin
JN145	M6P.Blast.NtermGFP.Otulin-WT	blasticidin
CE009	M6P.Blast.NtermGFP.Lysenin-W20A	blasticidin
F1032	M6P.Blast.NtermGFP.HOIL-WT	blasticidin
F1035	M6P.Blast.NtermGFP.Sharpin-WT	blasticidin
F1034	M6P.Blast.NtermGFP.HOIP-WT	blasticidin
JN110	M6P.Blast.NtermGFP.HOIP-T360A	blasticidin
JN70	M6P.Blast.NtermGFP.HOIP-N294	blasticidin
JN71	M6P.Blast.NtermGFP.HOIP-N438	blasticidin
JN164	M6P.Blast.NtermGFP.HOIP-N438-R375A	blasticidin
JN136	M6P.Blast.NtermGFP.HOIP-N438-T360A	blasticidin
JN73	M6P.Blast.NtermGFP.HOIP-ΔN294	blasticidin
JN74	M6P.Blast.NtermGFP.HOIP-ΔN438	blasticidin
JN85	M6P.Blast.NtermGFP.HOIP-ΔN527-R646W	blasticidin
JN78	M6P.Blast.NtermGFP.HOIP-ZnF	blasticidin
JN79	M6P.Blast.NtermGFP.HOIP-UBA	blasticidin
JN81	M6P.Blast.NtermGFP.HOIP-ZnF1	blasticidin

JN89	M6P.Blast.NtermGFP.HOIP-ZnF2	blasticidin
JN82	M6P.Blast.NtermGFP.HOIP-ZnF1+2	blasticidin
JN83	M6P.Blast.NtermGFP.HOIP-ZnF3	blasticidin
JN84	M6P.Blast.NtermGFP.HOIP-ZnF2+3	blasticidin
JN57	M6P.Blast.NtermGFP.Nemo	blasticidin
BR295	M6P.Blast.NtermGFP.Optineurin-WT	blasticidin
BR294	M6P.Blast.NtermGFP.Optineurin-E478G	blasticidin
JN158	M6P.Blast.NtermGFP.Optineurin-N555	blasticidin
JN138	M6P.Blast.NtermGFP.Optineurin-F177S-D286N-L493S	blasticidin
JN139	M6P.Blast.NtermGFP.Optineurin-D474N	blasticidin
JN167	M6P.Blast.NtermGFP.Optineurin-N522-S473A-L494S	blasticidin
JN130	M6P.Blast.NtermGFP.Optineurin-(424-510)	blasticidin
JN159	M6P.Blast.NtermGFP.Optineurin-(424-510)- S473A	blasticidin
BR256	M6P.Blast.NtermGFP.p62-WT	blasticidin
BR274	M6P.Blast.NtermGFP.p62-N166	blasticidin
BR280	M6P.Blast.NtermGFP.p62-ΔN165	blasticidin
JN183	M6P.Blast.NtermGFP.p62-K7A-D69A	blasticidin
BR385	M6P.Blast.NtermGFP.p62-D337A-W338A-L341A	blasticidin
BR262	M6P.Blast.NtermGFP.p62-DDDW335-338AAAA	blasticidin
BR260	M6P.Blast.NtermGFP.p62-F406V	blasticidin
BR261	M6P.Blast.NtermGFP.p62-L417V	blasticidin
BR299	M6P.Blast.NtermGFP.p62-F406V-L417V	blasticidin
BR298	M6P.Blast.NtermGFP.p62-PB1+LIR	blasticidin
BR296	M6P.Blast.NtermGFP.p62-ΔPB1-ΔUBA	blasticidin
JN64	M6P.Blast.NtermGFP.NDP52-WT	blasticidin
JN65	M6P.Blast.NtermGFP.NDP52-L374A	blasticidin
JN68	M6P.Blast.NtermGFP.NDP52-D439K	blasticidin
JN69	M6P.Blast.NtermGFP.NDP52-V136S	blasticidin
JN170	M6P.Blast.NtermGFP.NDP52-ΔSKICH -V136S	blasticidin
JN171	M6P.Blast.NtermGFP.NDP52-ΔSKICH -V136S-L374A	blasticidin

ID: plasmid identification reference with BR=Ben Ravenhill, CE=Cara Ellison, JN=Jessica Noad, MW=Michal Wandel, SR=Solene Rolland; RE: restriction enzyme; WT: wild-type; ZnF: zinc-finger.

Apart from Lysenin, all the above plasmids code for the expression of human proteins.

These proteins were all ligated into the same plasmid backbone: M6P (**Fig.1**).

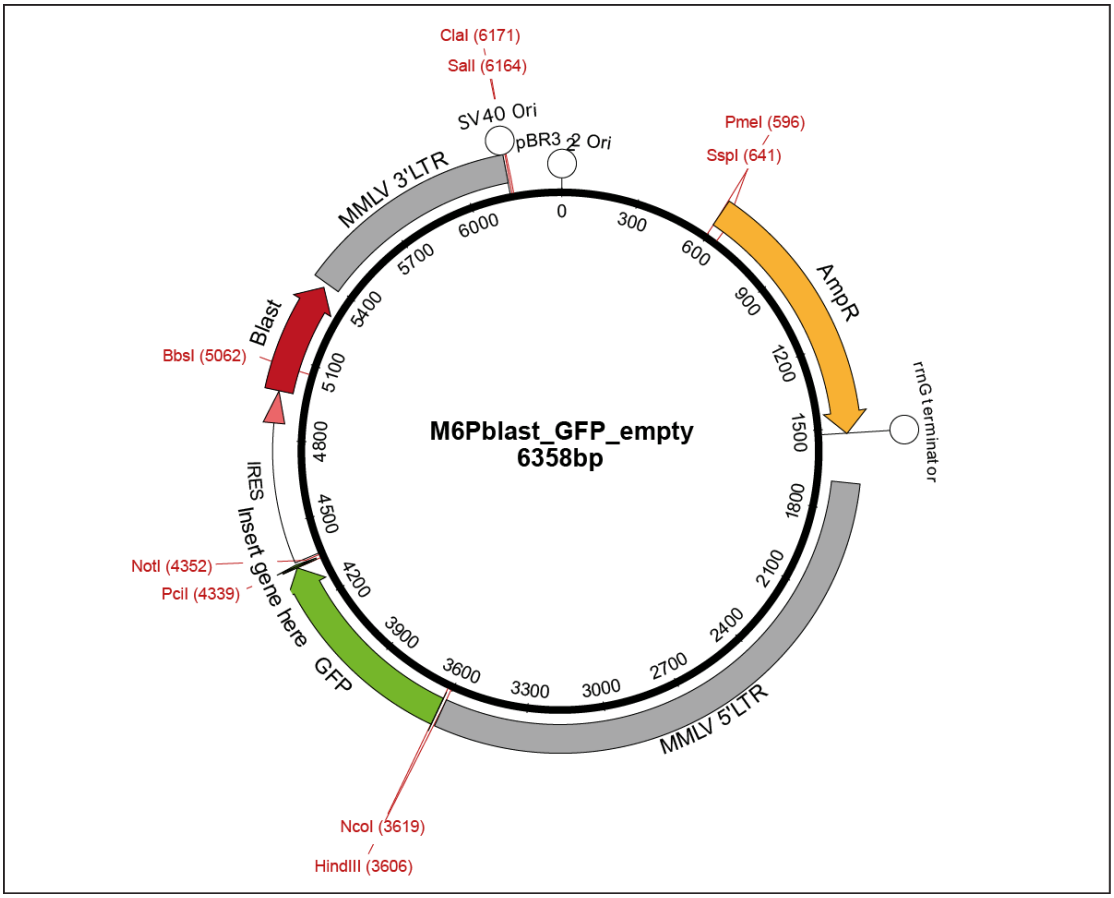

Figure 1: M6Pblast-GFP vector plasmid map

MMLV long terminal repeats (LTRs) enable integration of the plasmid sequence into the host cell genome. The gene of interest is inserted between PciI and NotI (all single restriction sites are labelled in red). AmpR – Ampicillin resistance, Blast – Blasticidin resistance, Ori – origin of replication, IRES – Internal ribosome entry site, GFP – Green fluorescent protein.

Even though most of them show N-terminal tag GFP and blasticidin as antibiotic resistance, other variations were made to allow Flag tags and/or puromycin resistance for selection.

ID	**RE backbone**	**Plasmid description**	**RE insert**	**Resistance**
JN95	SalI/BamHI and	pHRSIN-P_{SFFV}-Cas9-P_{PGK}-Hygro	BamH1/ApaI	hygromycin

	ApaI/SalI			
#1861	BbsI	pKLV-P_{hU6}-sgRNA(β2M)-P_{PGK}-Puro-2A-BFP	BbsI	puromycin
#1862	BbsI/BbsI	pKLV-P_{hU6}-sgRNA-P_{PGK}-Puro-2A-BFP	BbsI/BbsI	puromycin

ID: plasmid identification reference with JN=Jessica Noad; RE: restriction enzyme

4.4 siRNAs

4.4.1 Dharmacon pools

They were used for the validation of some candidates form the screen (pools of 4 human siRNAs from Dharmacon).

All sequences are given in the table below in the sense (5' → 3') orientation

Target gene	**Sequence (5' → 3')**	**Target gene**	**Sequence (5' → 3')**
STAT-1	AGAAAGAGCUUGACAGUAA UAAAGGAACUGGAUAUAUC GAGCUUCACUCCCUUAGUU GAACCUGACUUCCAUGCGG	ALG12	GUACGACCAUCUUGAGUUC GCAGGGAUCCUCUGUUUAG UCACUUGGCCGGAAGGAAA GCGCCUGGAGGUACGACAA
IFNGR1	GAAGUGAGAUCCAGUAUAA CCGUAGAGGUAAAGAACUA CGAAACUACCUGUUACAUU ACAUGAACCCUAUCGUAUA	TM9SF2	GAAUUUGGCUGGAAACUUG GCACAAAGAUAUUGCUAGA CCUAUUGGCUGUUACAUUA GGAAAGCGCCCAUCUGAAA
CASP4	GGACUAUAGUGUAGAUGUA GAGACUAUGUAAAGAAAGA GAGGGAAUCUGCGGAACUG UAGAGGAAGUAUUUCGGAA	EMC6	GGAGGUGGAACAAAUAUUU GGACGUUCCUCUACGGCAU CCGCCGUCCUGGAUUAUUG UCACCGGCCUCUACGGCUU
CASP8	GGACAAAGUUUACCAAAUG CAACGACUAUGAAGAAUUC GCAAGAACCCAUCAAGGAU GAAGAUAAUCAACGACUAU	OVOL3	UUGCUAAGGUGCAUGGACA CCUUCGAUCUCAAGCGCCA CGAGGCAAAUAAACACAGA CCAGCUACGCUUACCGUGA

GSDMD	GCACCUCAAUGAAUGUGUA CCUACUGCCUGGUGGUUAG CAAUAAAGGUGGCAUACGA CGACAGGCCACAAGCGUUC	SAF-B	GGACCAAGAUGAUCAGAAA GGAAGAGGGUGAUUUAGAU GGACUGUAGUAAUGGAUAA UCAAAGAGGUCUAGCAAAG
ELAVL2	CAAUAUGGCUUAUGGAGUA GGUGUAGGGUUUAUUCGAU GCGAAUUGAGGCAGAAGAA GAGUUAACCUUCUGCGUUU	CTNNBL1	GAGGAGAGAUCAUCGACAA AACCAAGAAUUGCGGAUUA GCAGAUUAUUGACAGAGAU GUCCAUAGCUGUGGUCGAU
NCKAP1	GCACAUUGCUGAAUUAAUA GCAGAAGACUUAUUUGUAA GCAGACGACUUUAUAGAUA GAAAUACGCUUUACCAAGU	BIN1	CAAACAAGAUCGCAGAGAA GCUCAAGGCUGGUGAUGUG GACAUCAAGUCACGCAUUG GAACAGCCGCGUAGGUUUC
Fip1L1	CAACAGCGAUGAAGAACGA GCAAAGGACCUAGAUGAAA GGACUAUUAUGCCAGAAGA GGUCAGACUAUAACUAUCA	RUFY4	GGAAAGAGCCCCAUGGAUU GCAUAUGGAGGGCCUGAAA CAACAAAGGAAGACUCUAC GAUCAAGAGCCUCAGACUU
TMEM143	GCGGAGAGGAGAUACUUUA CAGUAAAUUUGGAUCAGUA GAUCAGCCAUCACUAACGG CCUCCAAGAUGUUCGGGCA	CARM1	GGACAUGUCUGCUUAUUGC UCAGGGACAUGUCUGCUUA ACAACAACCUGAUUCCUUU AGACAGAGCUACGACAUCA
SLC25A37	AAAUCGAGCUCCAUACUAA AGACACGAAUGCAGAGUUU CAGCAGAAGUGGUGAAGCA GUAAGACCCUUCUGAACAC	BID	GCACCUACGUGAGGAGCUU GAGUAAGGGCACUGACGGA GCCAGAAGCUACUGCGAUG UGCAAUACAUACCACGCUA

SRSF10	GCUGAAGACGCUUUACAUA GAUCGAAAGACACCAAAUC GUUAUGGUCCUAUAGUUGA CAACUAUAGAAGAUCGUAU	HSPH1	GGAACAAACUCAUCUCAAA GACAGAGGCUGCAGCAUUA GAACAGGUCACAAUUUGAA CAAUAUCUCUGAUCUGGAA
Non-targeting control 1	UAGCGACUAAACACAUCAA UAAGGCUAUGAAGAGAUAC AUGUAUUGGCCUGUAUUAG AUGAACGUGAAUUGCUCAA	KEAP1	GGACAAACCGCCUUAAUUC CAGCAGAACUGUACCUGUU GGGCGUGGCUGUCCUCAAU CGAAUGAUCACAGCAAUGA

Non-targeting control 2	UAAGGCUAUGAAGAGAUAC AUGUAUUGGCCUGUAUUAG AUGAACGUGAAUUGCUCAA UGGUUUACAUGUCGACUAA		

4.4.2 Other siRNAs

Target	**Species**	**Sequence**
HOIP	Mu	5’-GACCCUAACUGCAAGGUGA-3’
HOIL	Mu	5′-ACACGUCACUCAACCCACA-3’
Sharpin	Mu	5′-CUUUCAUCAAUGCCUCAAA-3’
Atg5	Mu	#4390771, s62452

Mu: murine

PART II - METHODS

4.5 Cell lines and pathogenic strains

In the experiments undertaken in this thesis, the following cell lines and pathogens (bacteria or parasites) were used in a containment level 2 laboratory.

4.5.1 Cell lines

*MEF, fibroblast cell line derived from mouse embryonic tissue, kindly provided by C. Sasakawa.

*HeLa, epithelial cell line derived from human cervical carcinoma cells; obtained from European Collection of Authenticated Cell Cultures.

*HCT116, epithelial cell line derived from human colon cells; obtained from European Collection of Authenticated Cell Cultures. Used as an alternative non-phagocytic human epithelial cell line to HeLa cells.

*HEK-293ET, epithelial cell line derived from human embryonic kidney cells; obtained from European Collection of Authenticated Cell Cultures. Used for viral production (retroviruses and lentiviruses) and often referred to as “293ET” only.

*Sharpin-cpdm and corresponding WT MEFs, mouse embryonic fibroblast cell line encoding spontaneous frameshift mutation in the Sharpin gene and wild-type littermates, kindly provided by H. Walczak.

*HOIL (-/- and corresponding WT) MEFs, mouse embryonic fibroblast cell line knockout in the RBCK1 gene using the CRISPR-Cas9 technology and its corresponding wild-type control, kindly provided by H. Walczak.

*HOIP (-/- and corresponding WT) MEFs, mouse embryonic fibroblast cell line knockout in the RNF31 gene using the CRISPR-Cas9 technology and its corresponding wild-type control, kindly provided by H. Walczak.

*HFF, fibroblast cell line derived from human foreskin cells; obtained from ATCC (ATCC® SCRC-1041™). Used for growth and culture of *Toxoplasma gondii* and also in a few experiments as an alternative non-phagocytic human epithelial cell line to HeLa cells.

4.5.2 Bacterial strains

**Salmonella enterica* serovar Typhimurium (*S.*Typhimurium), strain 12023, provided by Dr David Holden, Imperial College London. Wild-type non-fluorescent or stably expressing BFP, GFP, mCherry were used for infection of non-phagocytic cells (HeLa and MEF cells, mostly).

**Escherichia coli* (*E.coli*), strain MC1061: used for plasmid production.

**Escherichia coli* (*E.coli*), strain BL21: used for protein expression.

4.5.3 Parasitic strains

Toxoplasma gondii, type I (RH) and type II (PRU), kindly given by Eva Frickel, Francis Crick Institute London. Both strains stably expressing Td-tomato were used for infection of non-phagocytic cells, mostly MEFs.

4.6 Molecular cloning techniques

4.6.1 RNA extraction

The monolayer of HeLa or MEF cells was lysed using the RLT Plus buffer complemented with 2-β-mercaptoethanol (Merck, M6250) in proportion of 10µL for 1mL of buffer. RNA was then extracted from the cells using the RNeasy Plus Mini Kit (Qiagen), following the manufacturer's instructions. RNA concentration was measured on a NanoDrop (Thermo) and the RNA was used to make cDNA either directly or was frozen at -80°C for subsequent use.

4.6.2 Making cDNA

cDNA libraries or cDNA samples were synthesised from RNA extracted from HeLa and MEF cells (wild-type, knockout or knock-down) using the SuperScript III Reverse Transcriptase Kit (Invitrogen) and Oligo(dT) from New England Biolabs (NEB). Reaction mix 1 which contained 500ng of RNA, 1µL of 50µM Oligo(dT), 5µL of 2mM dNTPs, and 2µL of distilled water was incubated at 65°C for 5 minutes in a Veriti™ 96-Well Thermal Cycler (Applied Biosystems) for denaturation. The mixture was then snap-cooled on ice. Reaction mix 2 contained 0.5µL of the SuperScript Reverse Transcriptase, 4µL of buffer, 1µL of DTT (all three reagents provided in the kit) and 1.5µL of distilled water. Reaction mix 2 was added to the cooled mix 1 and the mixture was incubated in the thermal cycler, first at 50°C for 60 minutes for reverse transcription, and then at 75°C for 10 minutes for heat inactivation of the enzyme before holding at 4°C.

The cDNA generated from particular cell lines was used to assess the mRNA level by qPCR (using a 1:15 dilution of cDNA) and stored at -20^{o}C. The resulting cDNA libraries were stored at -80^{o}C and carried on into PCRs to generate DNA fragments of the genes of interest.

4.6.3 Polymerase Chain Reaction (PCR)

The reactions were carried out either in tubes (200µL-PCR tubes, eppendorf, CAT # 0030124332) closed with lids or in 96-well plates (96-Well PCR Plate_Semi-Skirted, STARLAB, CAT # I1402-9710) sealed with adhesive PCR plate foil (ThermoFisher Scientific, CAT # AB0626).
The runs were programmed, set up and performed on a Veriti™ 96-Well Thermal Cycler (Applied Biosystems) or a Techne Prime Thermal cycler.

PCR was used to amplify genes of interest from existing plasmids or from cDNA. Primer pairs (see paragraph **4.2** "Primers") were designed to include appropriate flanking sequences containing the desired DNA restriction enzyme sites directly adjacent to 15-20 complementary nucleotides to the 5' (Forward) or 3' (Reverse) end of the gene of interest. DNA restriction sites were added to enable cloning of the amplified gene in a mammalian or bacterial expression vector.
PCR fragments were synthesised using KOD Hot Start polymerase kit (Merck Millipore). A 50µL-reaction contained 1X buffer for KOD polymerase, 0.2mM of each deoxynucleoside triphosphate (dNTP), 1.5mM MgSO4, 100pM each of forward and reverse primers, template DNA (50ng of plasmid or 1:15 dilution of cDNA) and 0.02U of KOD polymerase. Sometimes, particularly for more difficult reactions, 5% DMSO were added to the reaction mix. Standard cycling conditions were as follows: initial DNA denaturation and polymerase activation for 2min at 94°C followed by cyclical DNA denaturation (94°C, 20s), primer annealing (55-60°C, 10s) and extension (70°C, 30s/kb of DNA). These cycles were repeated 18 times for plasmid DNA before a final extension period of 7min at 70°C and final cooling to 4°C.

Following the reaction, all PCR products were purified using the QIAquick PCR purification kit (Qiagen) according to the manufacturer's protocol.

Several PCRs were also necessary to amplify and generate samples for sequencing from DNA extracted from samples isolated during the screen (see paragraph **4.9** "Samples for the screen"). In this case, primers were designed differently (see paragraph **4.2.2** "Primers for Illumina sequencing-samples from the screen").

4.6.4 DNA digestion and ligation

4.6.4.1. DNA digestion

Restriction enzymes from NEB were used to digest PCR products and plasmids to generate overhangs for ligation. Digest reactions contained 0.5µL of each restriction enzyme, 2µL of appropriate 10X NEBuffer (NEB) and approximately 1µg of DNA. The total reaction volume was made up to 20µL by adding distilled water. Digest reactions of PCR products were incubated at 37°C for 1h30min. Backbone vectors – where the insert will be cloned into – were incubated at 37°C for 1h for digestion and were then dephosphorylated by adding 1.5µL of alkaline phosphatase (1000U/mL, Roche) and by incubating for an additional 30min at 37°C. The dephosphorylation removes the phosphate groups at the 5' end of the backbone preventing its self-ligation. Incubation were performed by putting samples in a 37°C-waterbath.
5µL of loading buffer (10mM EDTA, 30% glycerol, 0.05% Orange G (Sigma)) were added to each digestion product. The digestion products were then run at 85V for 20min in TAE buffer (20mM acetic acid, 1mM EDTA, 40mM Tris (pH 7.6)) on a 1.5% (w/v) low melting point agarose gel (Nusieve GTG, Lonza or UltraPure agarose, Invitrogen) containing SYBR Safe (Life Technologies) for DNA visualisation. DNA bands were visualised using a blue light transilluminator. Bands observed at the desired size were excised and incubated at 70°C for the time required for the agarose to melt, before ligation.

For the generation of sgRNA to validate some of the genes in the 'hit' list from the screen, 2.5µg of the gRNA backbone (#1862) were digested for 2h at 37°C with 1.5µL of enzyme BbsI and 3µL of NEB Buffer 2.1 in a 30µL reaction. The linearised product was purified using Qiagen purification kit and eluted in 40µL. 1.5µL of BbsI and 4µL of NEB Buffer 2.1 were added and the second digestion reaction was carried on for 2h at 37°C, before adding 4µL of alkaline phosphatase (1000U/ml, Roche). The reaction was incubated for an extra hour at 37°C before gel purification.

4.6.4.2. Ligation of DNA fragments

To create new plasmids, digested DNA fragments (both insert and dephosphorylated backbone vector) with compatible overhangs were ligated. A 25µL ligation reaction contained 1µL of digested and dephosphorylated backbone vector and 4µL of digested DNA insert from the melted agarose samples along with 2.5µL of 10X T4 DNA ligase buffer (NEB), 2.5µL of ligation additives (1mM ATP, 10mM DTT), 0.5µL of 20mg/mL BSA (NEB), and 0.5µL of T4 DNA ligase (400000U/mL, NEB) in 14µL of distilled water. Reactions were incubated at room temperature for at least 2h before the ligated products were transformed into competent bacteria.

For the generation of sgRNA plasmids, sense and antisense oligos for each gene were designed to exhibit the overhangs for the ligation already. First, 0.5µL of each oligo was incubated separately for 1h at 37°C with 2.5µL of NEB Buffer 4, 2.5µL of ligation additives (1mM ATP, 10mM DTT), 0.5µL of BSA and 2.5µL of T4 polynucleotide kinase (PNK) in 17µL of water. For each gene, the two reactions corresponding to the sense and antisense oligos were then combined and incubated for 5min at 95°C. The paired oligo mixtures were slowly cooled to room temperature.
In 16µL of water, 1µL of purified, digested and dephosphorylated backbone (#1862), 2.5µL of 10X ligation buffer, 2.5µL of ligation additives, 0.5µL of BSA and 0.5µL of T4 DNA ligase were added to 2µL of the cooled annealed oligo pair. The ligation mixture was left overnight at room temperature before being transformed into competent bacteria.

4.6.5 Transformation into competent bacteria

E.coli (MC1061)

For a freshly ligated plasmid, 50µL of *E.coli* strain MC1061 was added to 4.5µL of ligation mixture. The bacterial mix was incubated on ice for 30min followed by heat-chock for 5min in a water bath at 37°C.
In the case of a plasmid rescue, 0.5µL of the plasmid to be rescued were mixed with 10µL of *E.coli* strain MC1061. The bacterial mix was incubated on ice for 5min and was followed by heat-chock (5min in the 37°C-water bath), before adding 100µL of PBS.

In both cases, 50µL of the bacterial solution were then plated on agar, supplemented with either ampicillin (TYE+AMP) or the appropriate antibiotic, and the plates were incubated overnight at 37°C to obtain single resistant colonies.

4.6.6 Plasmid purification

Depending on the scale of the bacterial culture and the expected growth and purification yields, two different methods were used to purify plasmids.

4.6.6.1. Qiagen kit

Single colonies of transformed resistant bacteria were grown overnight in a shaking incubator (220rpm at 37°C), in 5mL of LB medium supplemented with either ampicillin (100µg/mL) or the appropriate antibiotic. Plasmids from the 5mL of bacterial culture were purified using the QIAprep spin miniprep kit (Qiagen) according to the manufacturer's protocol. Plasmid concentrations were measured on NanoDrop (Thermo) and plasmids sequences were verified by sequencing using GATC services.

4.6.6.2. Cesium Chloride (CsCl) maxi-prep

Packaging (pCMV delta R8.2 – lentiviral or pMD-OGP – retroviral) and envelope (pMD- VSV-G) plasmids were needed in large quantities (several µg), as they were necessary to produce viruses. Hence the need to scale-up the production and purification of these three plasmids.

Three solutions were prepared for this protocol:

Maxi1 was a 2L solution of 10mM EDTA, pH8 (40mL of 0.5M EDTA in water);

Maxi2 was always prepared fresh and was a solution of 0.2M NaOH, 1%SDS (180mL of water with 10mL of 4M NaOH and 10mL of 20%SDS);

Maxi3 was a solution of 5M KOAc, pH4.7 (500g of KOAc with 300mL glacial HOAc topped up with water to 2L).

Single colonies of transformed resistant bacteria were grown overnight in a shaking incubator (220rpm at 37°C), in 2mL of LB medium supplemented with ampicillin

(100µg/mL). The next day, these 2 mL were transferred into a 1L flask of LB complemented with ampicillin (100µg/mL). Bacteria were grown overnight to reach saturation. The bacterial suspension was then spun down for 30min at 5krpm at 4°C to pellet the cells. The cell pellet was resuspended in 40mL of Maxi1, before adding 80mL of Maxi2 followed by 40mL of Maxi3 to lyse the cells. The sample was spun down for 10min at 5krpm at 4°C to pellet the debris. The supernatant (150mL) was poured into a 250mL bottle, which was then filled with isopropanol to precipitate DNA. The precipitate was pelleted by centrifugation for 5min at 5krpm and 4°C. The bottle was carefully drained, and its walls were rinsed gently with 70% ethanol to dry them out. The DNA pellet was re-suspended in 4mL 10mM EDTA, before adding 5.5g of CsCl followed by 0.1mL of 1% Triton X-100. After the salt dissolved, 0.5mL of 10mg/mL ethidium bromide was added. This new solution was spun down for 10min at 10krpm. The supernatant was transferred into sealed tubes and centrifuged overnight at 60krpm.

After centrifugation, the solution featured three bands between the pellet (RNA) and the supernatant (proteins). The middle band was taken out using a syringe equipped with a needle since the top band contained genomic DNA and the lower band contained plasmid DNA. To extract the content of the isolated middle band, 10mL of n-butanol saturated with 1M NaCl were added to the isolated band. Butanol was aspirated in a trap containing NaOH in order to destroy ethidium. After extraction, 10mL of 5M ammonium acetate and 20mL of 95% ethanol were added before centrifugation for 10min at 10krpm. The pellet was washed with 70% ethanol and let to dry before it was re-suspended in TE buffer.

4.7 Nucleic acids quantification and analysis

4.7.1 Quantitative PCR (q-PCR)

qPCR reactions were run in a 96- or 384-well plate format. In both cases, the ViiA 7 Real-Time PCR System (ThermoFisher Scientific) was used to perform the quantifications. The parameters were set on Comparative and Fast Analysis using SYBR Green Standard Reagents and included a Melt Curve. Wells were assigned based on which primer sets (Target) and sample type (Sample) they were. Usually,

conditions were as follows: the initial denaturation (95°C, 5min), was followed by 35 cycles of denaturation (95°C, 30s) and extension (60°C, 45s). The Melt Curve analysis was done between 65°C and 95°C.

4.7.1.1. Analysis of mRNA levels

Total RNA from cells was isolated and purified using the RNeasy Plus Mini Kit (Qiagen). This extracted RNA was then converted into cDNA using the SuperScript III reverse transcriptase kit (Invitrogen) (see paragraph **4.6.2** "Making cDNA"). Gene expression was quantified using 6µL of cDNA (1:15 dilution in distilled water), 2µL of each primer at 2µM concentration, and 10µL of SYBR Green Reagent (Applied Biosystems). Primer pairs were designed to amplify the gene of interest (see paragraph **4.2.3** "Primers used for qPCR") and selected based on a few trials in a previous experiment testing amplification. Primers were chosen so that the Ct value was as low as possible and so that the melting curve showed only one discreet peak (specific amplification). Each sample was amplified with primers for the gene of interest and for β-actin and/or GAPDH as control genes. All samples were run in duplicates. Relative amounts of cDNA were calculated using the ΔΔCt method, which normalises cDNA levels to the gene chosen as reference (β-actin or GAPDH) and makes it possible to compare gene expression in between cell lines.

4.7.1.2. Precise quantification of amplified DNA sequences

Before submitting samples to sequencing, the concentration of amplified sequences from DNA extracted from cells was determined using qPCR. The Kapa SYBR Fast kit was used; ROX and primer mixes were added to the Master Mix to prepare the new Master Mix, according to the manufacturer's recommendation. A 20µL reaction contained 4µL of sample, 10µL of Master Mix, 2µL of primer mix and 0.4µL of ROX (or 12.4µL of the new Master Mix) with 3.6µL of distilled water. Along with standards and water, samples were run in triplicates and at five different dilutions: 1:100 / 1:10,000 / 1:50,000 / 1:100,000 / 1:1,000,000.

Results were analysed using averaged Ct values from the three replicates. Standards were used to draw a calibration curve, allowing the sample concentrations to be calculated.

4.7.2 Sequencing

After quantification, DNA samples were submitted to sequencing analysis in order to identify the sequences present and to get a measure of their representation.

The gRNA library was sequenced within the LMB using a MiSeq. The three sub-libraries were mixed in a 18:18:1 ratio as they supposedly contained 90,000, 90,000 and 5,000 guides respectively, making up a sample with a final concentration of 4nM. Sample preparation was then carried out following several Illumina preparation guides before analysis (see paragraph **4.8.2.3** "MiSeq sequencing and analysis").

The samples isolated from the screen were however sent to the Genomics Facility in the CRUK, Cambridge for analysis on a HiSeq, not available at the LMB. Because samples isolated from different batches of screened cells were barcoded (see paragraph **4.9.2** "gRNA amplification and sample barcoding"), two samples were submitted at the same time to be analysed in one lane. They were mixed to get to a final concentration of 4nM with equal representation of the two samples (see paragraph **4.9.3** "Quantification and submission for sequencing").

4.8 The gRNA library

Human Two Plasmid Activity-Optimized CRISPR Knockout Library was made available by David Sabatini and Eric Lander (Addgene # 1000000095) and was delivered as three sub-pools (hL1nC9, hL2nC9 and hL3nC9) containing approximately 90x, 90x, and 5x 10^3, respectively.

4.8.1 Transformation and purification

4.8.1.1. Transformation in Ultra electrocompetent *E.coli*

This protocol was adapted from the EnduraTM Comptetent Cells "Transformation protocol" (Lucigen, MA133) and the Broad Institute "Amplification of pDNA libraries".

Each sub-pool from the gRNA library was transformed and purified individually. For each sub-pool, 1µL of plasmid DNA was mixed with 25µL of electrocompetent cells in an electroporation cuvette (0.1cm gap, Flowgen Bioscience) on ice. The electroporation was carried out at 1.8kV for 5ms. Immediately after the pulse, 975µL of warmed Recovery Medium (provided with the electrocompetent cells) were added to the cuvette to resuspend the cells. This 1mL-mixture was then transferred to a culture tube and placed in a shaking incubator (220rpm, 37°C) for 1h.

For each sub-library, 10 bioassay plates (Nunc™ Square BioAssay Dishes, ThermoFisher) had been prepared with LB agar complemented with ampicillin. They were pre-warmed at 30°C for about 30min. The incubated mix was diluted by adding 9mL of LB medium. 100µL were taken out, of which 50µL were directly spread onto a small LB+AMP agar plate, while the remaining 50µL were used to make three serial 1:10 dilutions, which were also plated. Then, around 1mL of the initial mix was spread on each of the 10 agar plates. The 10 culture and 4 counting plates were put overnight in an incubator at 30°C.
Plated serial dilutions were used to estimate the number of total colonies grown on the 10 bioassay plates. For example, counting 50 colonies on dilution plate IV would translate to 10^7 colonies in total for the whole culture (after accounting for all the dilution steps (4) and the total number of plates (10)). The transformation gave the following numbers of colonies for each sub-pool:

Sub-library	**Number of colonies**	**Number of guides**	**Fold coverage**
hL1nC9	$1.6x10^8$	$90x10^3$	1778
hL2nC9	$1.8x10^8$	$90x10^3$	2000
hL3nC9	$7.0x10^6$	$5x10^3$	1400

A 1000-fold coverage is commonly referred to as the minimum acceptable threshold for the purification and use of the library without the risk of losing diversity and representation. Therefore, each bioassay plate was washed, and colonies harvested with 30mL of LB medium.

4.8.1.2. Plasmid purification

For each bioassay plate, the 30mL bacterial solution was pelleted down by centrifugation. Plasmids were purified using a column from the HiSpeed MaxiPrep kit (Qiagen) following the manufacturer's protocol.

4.8.2 Verifications

4.8.2.1. Single digests

Purified plasmids were digested with either BamHI, MluI or PciI, all single cutters in the plasmid map. 10µL-digestion reactions were set-up as follow: 2.5µL of purified plasmid was mixed with 1µL of NEB Buffer 3.1, 6µL of distilled water and 0.5µL of the desired restriction enzyme (BamHI, MluI or PciI). Samples were incubated for 1h at 37°C before being loaded on a 1% agarose gel containing 1:10000 SYBR Safe DNA gel stain. The gel was run at 85V for 25min. Bands were revealed using a blue light transilluminator. Bands were observed at the size expected for the linearised form of the plasmid.

4.8.2.2. GATC sequencing

Samples from the purified sub-pools were sent to GATC for sequencing with primers designed to amplify sequences in the backbone (PCR2, M13FP and scr16 (in the U6 promoter)). Primer scr15, however, was designed to amplify the gRNA sequence as it complemented the beginning of the gRNA scaffold. Sequencing with scr15 did not yield a result; this is as expected since gRNA sequences are variable within the library.

4.8.2.3. MiSeq sequencing and analysis

The purified sub-libraries were sequenced using the MiSeq available at the LMB to check for coverage and compare the gRNA distribution to the reference (sequencing data from the initial pool, provided by the supplier). First, purified plasmids were

amplified by PCR; primers were designed to flank sequences with specific Illumina adapters (both forward and reverse primers) and a specific barcode (contained in the reverse primers) allowing the identification of each sub-library, because the three sub-libraries were mixed and run as a single sample. After PCR, individual amplified sub-libraries were loaded on a 2% low melting point agarose gel for 1h30 at 85V. Bands of the desired size were melted and purified using QIAquick Gel Extraction Kit (Qiagen) according to the manufacturer's protocol except for the melting step which was performed without QB Buffer. Following purification, samples were quantified by quantitative polymerase chain reaction (qPCR). The Kapa SYBR Fast kit was used; ROX and primer mixes were added to the Master Mix. A 20µL reaction contained 4µL of sample, 12.4µL of the complemented Master Mix and 3.6µL of distilled water. Along with standards and water, samples were run in triplicates and at 4 different dilutions: 1:10,000 / 1:50,000 / 1:100,000 / 1:1,000,000.

Sub-library	Concentration (nM)	95%-confidence interval
hL1nC9	28.8	1.6
hL2nC9	18.3	1.3
hL3nC9	16.1	1.2

After analysis using Microsoft Excel, the sub-library concentrations were determined using the standard curve:

To respect the ratio in terms of numbers of gRNAs in the different sub-libraries, samples were mixed 18:18:1 respectively to get a final sample at 4nM. This mix was then prepared for sequencing following the "MiSeq Reagent Kit Reagent Preparation Guide", the "MiSeq System Denature and Dilute Libraries Guide" and the "MiSeq System Guide" (documents 15034097 Rev.B, 15039740 v01 and 15027617 v01, from Illumina). The mixture was denatured, diluted further to 10pM and 15% PhiX at 12.5pM were spiked in for the analysis. PhiX is a well-characterised library derived

from the small genome of the bacteriophage PhiX. It helps mitigate sequencing in the case of unbalanced and/or low-diversity libraries.
The sample was run on the MiSeq (available at the LMB) using the information from the sample sheet:

Date	10/01/2018
Workflow	Generate FASTQ
Application	MiSeq FASTQ Only
Assay	Custom Library Prep Kit
Description	gRNAlib_Sabatini
Reads	75

Sample_ID	**Sample_Name**	**I7_Index_ID**	**index**
lib1	hL1nC9	op19	TTAATCAG
lib2	hL2nC9	op7	CATGCTTA
lib3	hL3nC9	op17	TCCTTGGT

The three sub-libraries were deconvoluted from the PhiX and demultiplexed (segregation of the sequences based on their barcode to recreate the sub-libraries) to be analysed separately if needed. Consequently, three files containing all sequences present in the three sub-pools, were generated from BaseSpace. Sequences were trimmed according to the expected gRNA size, selected following readability criteria, counted and finally aligned to the reference list using programming in R.

4.8.3 gRNA design

To validate some of the candidate genes in the ‘hit’ list from the screen, additional gRNAs were generated. gRNA sequences were designed using the online tool CHOP CHOP (http://chopchop.cbu.uib.no/) to target early exons in the gene of interest considering the different isoforms. BbsI overhang sequences were added to both the sense and antisense strands. The gRNA backbone did not contain the Cas9 protein and the insert site was located between two BbsI restriction sites.

First, 2.5µg of the gRNA backbone (#1862) were digested for 2h at 37°C with 1.5µL of enzyme BbsI and 3µL of NEB Buffer 2.1 in a 30µL reaction in distilled water. The linearised product was purified using Qiagen purification kit and eluted in 40µL. 1.5µL of BbsI and 4µL of NEB Buffer 2.1 were added and the second digestion reaction was carried on for 2h at 37°C, before adding 4µL of alkaline phosphatase ((1000U/ml), Roche). The reaction was incubated for another hour at 37°C before gel purification.

Sense and antisense oligos for each gene were designed to exhibit the overhangs ready for the ligation. First, 0.5µL of each oligo was incubated separately for 1h at 37°C with 2.5µL of NEB Buffer 4, 2.5µL of ligation additives (1mM ATP, 10mM DTT), 0.5µL of BSA and 2.5µL of T4 polynucleotide kinase (PNK) in 17µL of water. For each gene, the two reactions corresponding to the sense and antisense oligos were then combined and incubated for 5min at 95°C. The paired oligo mixtures were slowly cooled to room temperature. Finally, 1µL of purified, digested and dephosphorylated backbone (#1862), 2.5µL of 10X ligation buffer, 2.5µL of LA, 0.5µL of BSA and 0.5µL of T4 ligase in 16µL of water were added to 2µL of the cooled annealed oligo pair. The ligation mixture was left overnight at room temperature before being transformed into competent bacteria.

4.9 Samples for the screen

After each round of selection in the genetic screen, some cells were set apart and grown alongside the others which were carried over to the next round. The selected cells were grown and, at various stages in the selection process, they were trypsinised, pelleted and frozen.

4.9.1 DNA extraction and purification

Frozen pellets were thawed, and DNA extraction was carried out using the DNeasy Blood & Tissue Kit (Qiagen, CAT #69506), following manufacturer's instructions apart for the final elution which was done using distilled water instead of Buffer AE.

4.9.2 gRNA amplification and sample barcoding

The extracted DNA was processed following a series of PCRs in order to prepare the sample for sequencing analysis.

4.9.2.1. qPCR0: checking for primer binding

The first step was run on a qPCR machine but was not intended as a sample quantification as such. qPCR0 was performed to test and to ensure that the chosen primers for PCR1 in fact bind and amplify sequences in the purified DNA. In the case of inhibition of amplification, primer pairs would be changed and tested again. This preliminary experiment also indicated whether a diluted sample was needed or if the initial concentration were sufficient; if any saturation were noticed, samples would be diluted in order to be able to amplify the sequences.

A 20µL qPCR0 included 9.8µL of (diluted) DNA, 0.1µL of each primer (reverse and forward) at a concentration of 100µM and 10µL of SYBR Green Master Mix (Applied Biosystems). Each sample (purified DNA at decreasing concentrations) was run in duplicate along with some negative controls, which contained water instead of DNA. On the amplification plot, all samples showed products being synthesised in a time-dependent fashion. The melt curve appeared less clean as in the control samples and a low melting point product was initially detected; however, it was subsequently shown that this was an artefact originating from the Master Mix used. All the actual samples had a clear and single peak on the melt curve, suggesting that fragments were being amplified and that those amplification products were pure.

The melt curve was recorded to assess the amplification and purity of the samples. All samples were amplified and the melt curve (**Fig.2,** blue lines) showed a single peak at 79°C for the different sample concentrations, meaning that the amplified products were identical in sequence length and were not contaminated; the presence of a contaminant would show another peak on the melt curve.

In this example (**Fig.2**), control samples (water, in red) also provided a peak on the melt curve. There was some sample contamination such as traces of DNA that had been amplified or primers that reacted or oligomerised. However, this peak for the

water samples was at 73°C and was very distinct from the 79°C peak for the samples. A replicate experiment was conducted following the same protocol, this time using an unopened water bottle; it was found that this also provided a peak at 73°C. Interestingly, Paul Monis published a comparison of SYT09 and SYBR Green (Monis et al., 2005) finding SYT09 less inhibitory to PCR and more reproducible for DNA melting curves than SYBR Green. It was therefore thought that the SYBR Green Master Mix was the source of this extra feature. A comparison experiment was done in P. Kozik's laboratory with EvaGreen (Biotium) and then the peak at 73°C was not observed, demonstrating that SYBR Green caused the presence of the extra peak at 73°C.

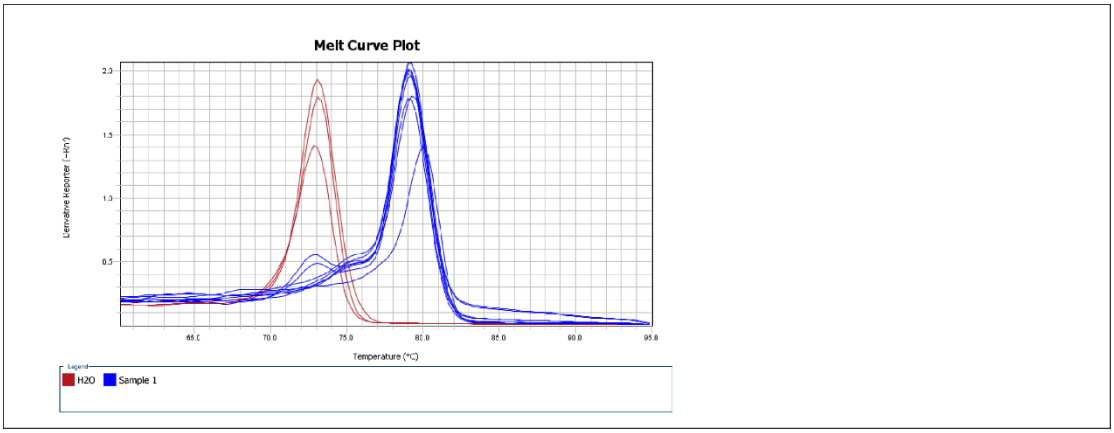

Figure 2: qPCR0 as a test for the use of PCR1 primers

The melt curve shows the different samples tested (in blue) and the water (in red).

The observation that the samples, primers, and conditions tested all produced a single product validated the use of the primers for PCR1.

4.9.2.2. PCR1: first amplification

The goal in this reaction was to amplify gRNA sequences above the rest of the genomic DNA, which constitute only background noise in the analysis. Only a limited number of cycles was performed, since PCR2 also further amplified the desired

gRNA sequences. PCR1 primers were designed to bind to common part from the gRNA backbone on each side of the desired sequence (**Fig.3A**).

To preserve the diversity and the distribution of gRNA in the samples, a large number of reactions were run:

Enrichment stage	**DNA concentration (ng/µL)**	**Volume (mL)**	**Total amount (g)**	**Number of PCRs**	**DNA / well**
0	370	6.0	2.22	288	5µg
3	340	3.5	1.19	266	5µg
1	349	3.1	1.08	288	4µg
2	230	1.5	0.345	192	4µg

Reducing the amount of DNA going through amplification significantly increases the risk of losing some sequences, consequently introducing a random bias on both the representation and the distribution of the gRNA sequences in the sample.

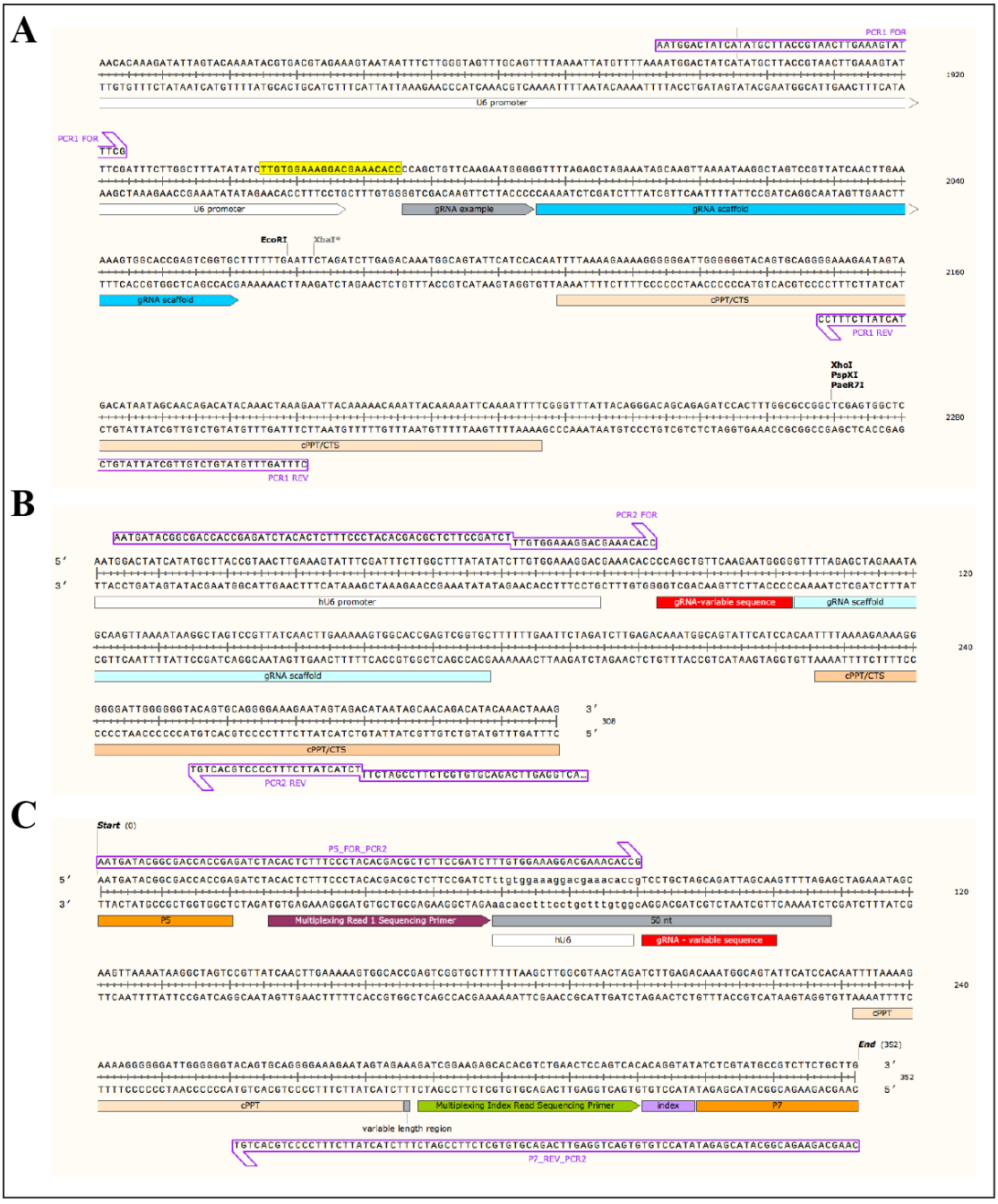

Figure 3: amplifications of DNA fragments for sequencing of the gRNAs

(A) PCR1 primers bind to the U6 promoter (forward) and the cPPT/CTS sequence (reverse) which are quite distant from the gRNA sequence itself; but PCR2 primers (B) bind right before the variable part of the gRNA sequence (forward) and still in cPPT sequence but closer to the gRNA. Primers for PCR1 and PCR2 do not overlap. The amplified fragment after PCR2 (C) contains the whole gRNA sequence flanked by P5 and P7 Illumina adapters, necessary for the sequencing.

PCR1 reactions were set-up in 100µL (total) in order to reduce the number of plates to run. Each well contained 5mg of genomic DNA diluted in 76µL of water, 1µL of dNTP mix (25mM each, from 100mM individual dNTPs solution, Sigma-Aldrich, CAT # DNTP100-1KT), 0.5µL of each primer at 100µM concentration, 20µL of Herculase Buffer and 1µL of Herculase (Herculase II Fusion DNA Polymerase, Agilent Technologies, CAT # 600675).
Master mixes of Herculase Buffer, dNTP and primers were prepared and dispensed accordingly. Samples were put in the block at 95°C and the cycling conditions were as follows: initial DNA denaturation and polymerase activation for 1min at 95°C followed by cyclical DNA denaturation (95°C, 30s), primer annealing (55°C, 30s), and extension (70°C, 30s). These cycles were repeated 18 times before a final extension period of 10min at 72°C and cooling to 4°C.

In order to keep the diversity of the gRNA represented in the samples, 90µL were taken out of each well and were combined together by sample. This was based on the assumption that PCRs amplified all sequences with the same efficiency and in a proportional manner.

4.9.2.3. qPCR1: determination of the number of cycles for PCR2

The qPCR1 reaction was not a quantification but was used to determine the number of cycles needed in PCR2. Each sample was run at three different concentrations: non-diluted sample, 1:5 and 1:25 dilutions. Water samples were run alongside as controls. All samples were run in triplicates. 20µL reactions contained 2µL of (diluted) PCR1 product, 0.5µL of each PCR2 primer and 17µL of SYBR Green Master Mix.
The threshold cycle – Ct value – (now standardized by the MIQE guidelines as quantification cycle (C_q)) of the least concentrated sample gave the number of cycles for PCR2, if below 20.

The melt curve (**Fig.4**) showed a single peak for all the concentrations and in both samples tested, which demonstrated the purity of the amplified fragments in comparison with the water control where no product was detected. The amplification plot and, more particularly, the cycle threshold (Ct) values (the number of cycles

necessary for the fluorescent signal to exceed background, i.e. where exponential amplification can be reliably detected) were studied carefully. The Ct value of the PCR1 products were similar between sample dilutions, which is counterintuitive as a drop of Ct value is expected with less diluted samples; this result suggests qPCR saturation or inhibition. However, Ct values were significantly lower than the Ct value of the water sample (set by default at the maximum number of cycles run during the experiment, which was 40). For both cell batches – '- cells' and '3+ cells' – the Ct values were evaluated to be around 32. This was considered too high compared to regular values (Aird et al., 2011; Kebschull & Zador, 2015; Bevan et al., 1992); either samples might be too diluted or the qPCR might not be working.

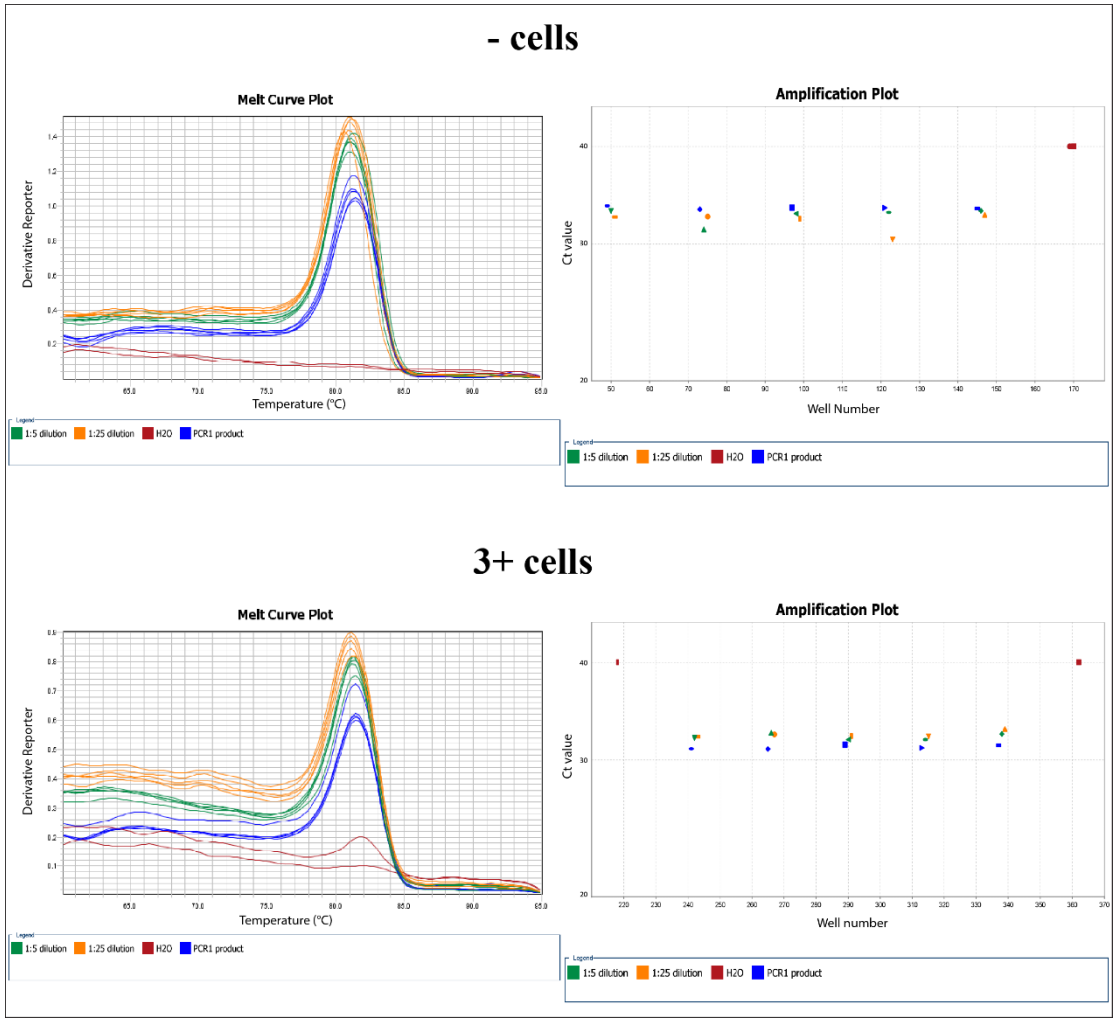

Figure 4: qPCR1 was used to mimic PCR2 conditions to determine the number of PCR2 cycles required

Melt curves (left panel) and amplification plots (right panel) of samples from '- cells' and '3+ cells' (cells submitted to none or three rounds of enrichment respectively) are shown here as examples of the types of results given by qPCR1.

qPCR1 was set up to mimic PCR2 cycling conditions and the number of cycles was set up to 40 for qPCR1. Ct values obtained for the different samples were relatively high (~30) compared to those one can expect (~20) in such experiment. Two test PCR2 reactions were run side-by-side, set for either 20 or 30 amplification cycles. PCR2 products of those two test experiments were run on a gel. In both conditions, products were synthesised and bands on the gel were at the expected size (~350bp) for the fragment.

The amount of cycles performed in PCR2 should be kept to a minimum so as not to change the distribution and representation of the gRNAs in the samples. Over-amplification could introduce a bias if sequences were to be amplified at different rates; this would result in a sample that was no longer representative of the initial cell population. To reduce the risk of overamplification and/or misrepresentation, 20 cycles were performed in PCR2.

4.9.2.4. PCR2: second amplification with barcodes and Illumina adapters

PCR2 is a nested PCR within the PCR1 product. PCR2 could therefore be performed on the crude product from PCR1 since there was no overlap between PCR1 and PCR2 primers (**Fig.3B**). However, PCR2 primers are significantly longer than PCR1 primers because PCR2 was an extra amplification of the sample. PCR2 also allowed the addition of the Illumina adapters and the barcodes to the sequences; PCR2 primers hence contained complementary sequences to bind the fragments flanked by Illumina adapters, which enabled the sequencing. A barcode was also attached on the reverse primer to allow the identification of different samples submitted together as a mix for sequencing.

A PCR mix was prepared with 20µL Herculase Buffer, 1µL dNTPs (mix with 25mM each), 58µL distilled water, and 1µL of Herculase. To this, 10µL of PCR1 product and 5µL of each PCR2 primer at a concentration of 10µM were added to make up a 100µL reaction.

PCR2 conditions were very similar to PCR1, since samples were put in the block at 95°C under the following cycling conditions: initial DNA denaturation and polymerase activation for 1min at 95°C followed by cyclical DNA denaturation (95°C, 30s), primer annealing (53°C, 30s), and extension (72°C, 30s). These cycles were repeated 17 times before a final extension period of 10 min at 72°C and cooling to 4°C.

Samples which were treated once with Lipofectamine2000 only ('- cells') or submitted to three rounds of enrichment ('3+ cells') were tested with their specific primer pairs (reverse primers contained distinct barcodes to allow segregation of the different cell batches during data analysis).

PCR2 products were then loaded on a 2% low melting point agarose gel complemented with SYBR Safe DNA gel stain (**Fig.5**). Samples were run in TBE buffer at 90V for 1h on ice. Bands of around 360 nucleotides were extracted and purified using the QIAquick Gel Extraction Kit (Qiagen) following manufacturer's instructions. The purified PCR2 products (**Fig.3C**) were then precisely quantified before submission to sequencing analysis.

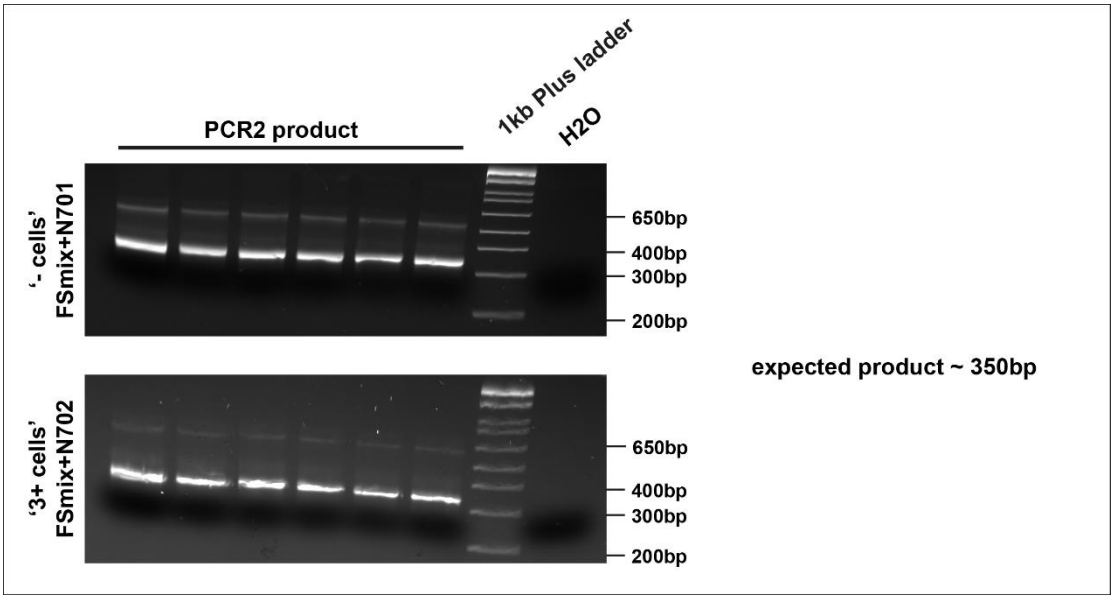

Figure 5: Isolation of PCR2 samples

1.5% low melting point agarose gels were used to purify PCR2 products before gel extraction. Gels for both '- cells' and '3+ cells' samples are shown. Forward primer (FS mix) mix was used for both samples, whereas N701 and N702 were used as reverse primers, respectively.

4.9.3 Quantification and submission for sequencing

4.9.3.1. qPCR

Sample concentration was determined by qPCR. The KAPA SYBR Fast Kit was used, mixing 12.4µL of pre-mix containing Master Mix, primer mix and ROX, 3.6µL of water, and 4µL of either the samples or the standards or water, to make up a 20µL reaction.

The ViiA 7 Real-Time PCR System (ThermoFisher Scientific) was set on Comparative and Fast Analysis using SYBR Green Standard Reagents and including a Melt Curve. Wells were assigned based on which primer sets (Target) and the sample type (Sample) they were. Conditions were as follows: the initial denaturation (95°C, 5min), was followed by 35 cycles of denaturation (95°C, 30s), and extension (60°C, 45s). The Melt Curve analysis was performed between 65°C and 95°C.

The melt curve plot (**Fig.6A**) showed that, as expected, the sample melting temperature was distinct from that of the standards. Furthermore, melt curves exhibited a single peak, indicating that the amplified samples contained sequences of the same length as was required. Standards were samples of known concentrations and their amplification (**Fig.6B**) was fairly robust because the triplicates always overlapped and the differences in the Ct values (cycle number for which the amplification overcome a certain threshold: red line) between the constant dilutions remained identical. A standard curve (**Fig.6C**) was built with the Ct values of the standard samples, to determine the concentrations of the amplified samples yet to be sequenced.

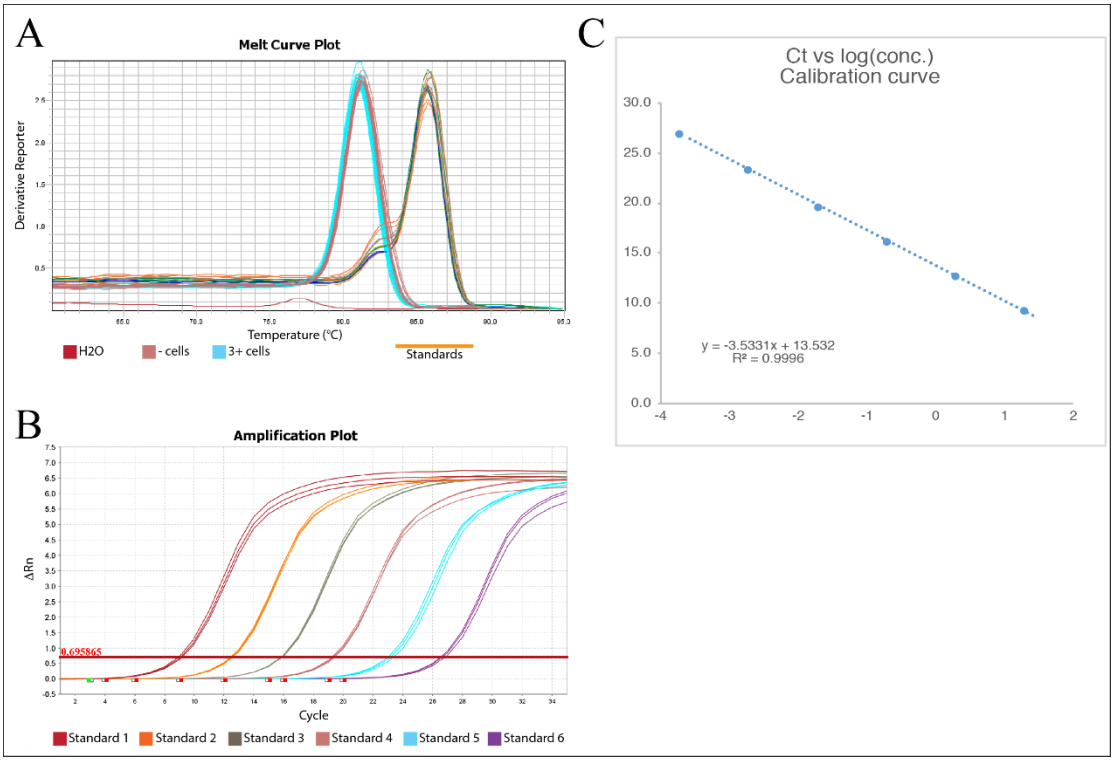

Figure 6: Precise quantification of samples by qPCR

The melt curve (A) shows the two batches of amplified sequences (in blue and pink) compared to the Standards. Amplification curves (B) were plotted for each standard with their triplicates, and Ct values were used to make a calibration curve (C) to determine DNA concentrations in the samples.

NanoDrop (Thermo) and Qubit Fluorometric Quantitation could be used as additional methods but these were not as reliable or precise as qPCR.

4.9.3.2. Preparation of the sample for sequencing

Samples were mixed together, taking into account their individual concentrations, to achieve 50/50 mix in terms of amount – quantity of DNA sequences. Complying to the Genomics Core (CIGC) Illumina sequencing service requirements, samples were diluted to a final concentration of 30nM in 200µL.

4.10 Cell culture

Apart from HFF cells, all cells were cultured in Iscove's Modified Dulbecco's Medium (IMDM, Gibco) supplemented with 10% (v/v) FCS and 30μg/ml gentamycin (Sigma). This medium is commonly referred as G30 medium in the laboratory. HFF cells were cultured in Dulbecco's Modified Eagle's Medium (DMEM, Gibco) supplemented with 10% (v/v) FCS and 10μg/ml gentamycin (Sigma). Cell lines were kept in incubators maintaining constant growth conditions (37°C and 5% CO_2). All cells in the culture room were regularly tested for Mycoplasma. Cells were never passaged for longer than 6 months.

4.10.1 IFN-γ treatment

Human and mouse cell lines were incubated with IFN-γ overnight before the experiment:

*HeLa cells were treated with 2ng/mL human IFN-γ (R&D systems)

*MEF cells were treated with 10ng/mL murine IFN-γ.

4.10.2 Transfection

Control samples were always prepared, irrespective of which agent was transfected. The transfection reagent was added in the same amount but with only Opti-MEM (Gibco) instead of the Opti-MEM mix containing LPS or siRNA.

4.10.2.1. LPS transfection

In a 96-well plate, 1.10^3 HeLa cells were seeded per well while in a 24-well plate they were seeded to be 70-80% confluent on the following day. HeLa cells were grown overnight in G30 medium with half the wells primed with human IFN-γ. *S.* Typhimurium LPS (Sigma) was diluted in water to a concentration of 1mg/mL, aliquoted, and frozen before use. LPS and Lipofectamine2000 (Invitrogen) were separately mixed in Opti-MEM (Gibco) before combining them and the mix was incubated 5-10 min at room temperature before being added to the wells.

Proportions (in µL), for both types of plates are detailed in the table below:

Plate format	**Lipo. 2000**	**Opti-MEM**	**LPS**	**OptiMEM**	**Total**	**added to the well containing**
96-well	0.2	10	1.5	10	20	100
24-well	1.0	50	3.0	50	100	500

Unless otherwise stated, the medium was replaced with fresh medium in all the wells, 5h post-transfection. Cells were analysed the day following the transfection.

4.10.2.2. Bacterial lysates

Bacterial lysates (prepared as described in paragraph 4.11.1.2 “Bacterial lysates”) were transfected into cells using the same protocol as for LPS.

4.10.2.3. siRNAs

siRNAs were transfected into cells to knock down genes of interest, to deplete the encoded proteins and thereby study their role in the context of different assays. HeLa or MEF cells were seeded in 24- or 6-well plates to be confluent at either 72h or 48h post siRNA transfection, respectively. The siRNAs (Dharmacon pools or Silencer Select) were resuspended and diluted in distilled water at a working concentration of 6µM. The transfection reagent RNAiMax and the siRNA were mixed separately in Opti-MEM and, after 5min incubation at room temperature, both preparations were combined. The mixture was then incubated at room temperature for 15min before being added to the wells.

Proportions (in µL) for both types of plates are indicated in the table below:

Plate format	**RNAiMax**	**Opti-MEM**	**siRNA**	**OptiMEM**	**Total**	**added to the well containing**
24-well	1.0	25	1.0	25	50	500
6-well	4.0	100	4.0	100	200	2000

For the 24-well plates, assays were performed directly in the same plate 72h following siRNA transfection. Cells cultured in 6-well plates were trypsinised and seeded in the desired plates at 48h post transfection to perform the assay also 72h after siRNA transfection.

4.10.3 Viral work

Viruses were used as a means to eventually express genes of interest into cell lines. Two different types of viruses were used, depending on whether the parental backbone encoding the gene of interest was a retrovirus or a lentivirus.

Protocols for lentiviral production and transduction were determined after several steps of optimisation (**Fig.7**). To produce lentiviral particles, two packaging plasmids (namely R8.2 and psPAX) were tested and the transfection of 293ET cells was optimised by comparing three different transfection reagents: PEI, Lipofectamine2000, and TransIT-LT1. Batches of lentiviral supernatant were compared by transducing HeLa cells in the same conditions but using lentiviruses produced with one of the three transfection reagents mentioned and either of the two packaging plasmids. Using the packaging plasmid R8.2 gave significantly higher titers than using the psPAX packaging plasmid (**Fig.7A**). In the case of R8.2, Trans-IT gave the best titer, reaching 100% GFP-positive cells with a 1:10 virus dilution while, for the same dilution, Lipofectamine2000 and PEI successfully transduced 85% and 65% of the cells, respectively.

The transduction method was optimised by transducing HeLa cells with lentiviral particles expressing GFP. Cells were centrifuged for 2h either in the presence or absence of polybrene – a chemical agent that neutralises the charge repulsion between virions and sialic acid on the cell surface. Transduction efficiency was assessed by

flow cytometry, where the percentage of GFP-positive cells in the population was measured. The addition of polybrene helped increasing the transduction efficiency from 55% for a 1:10 dilution of virus to 100% (**Fig.7B**).

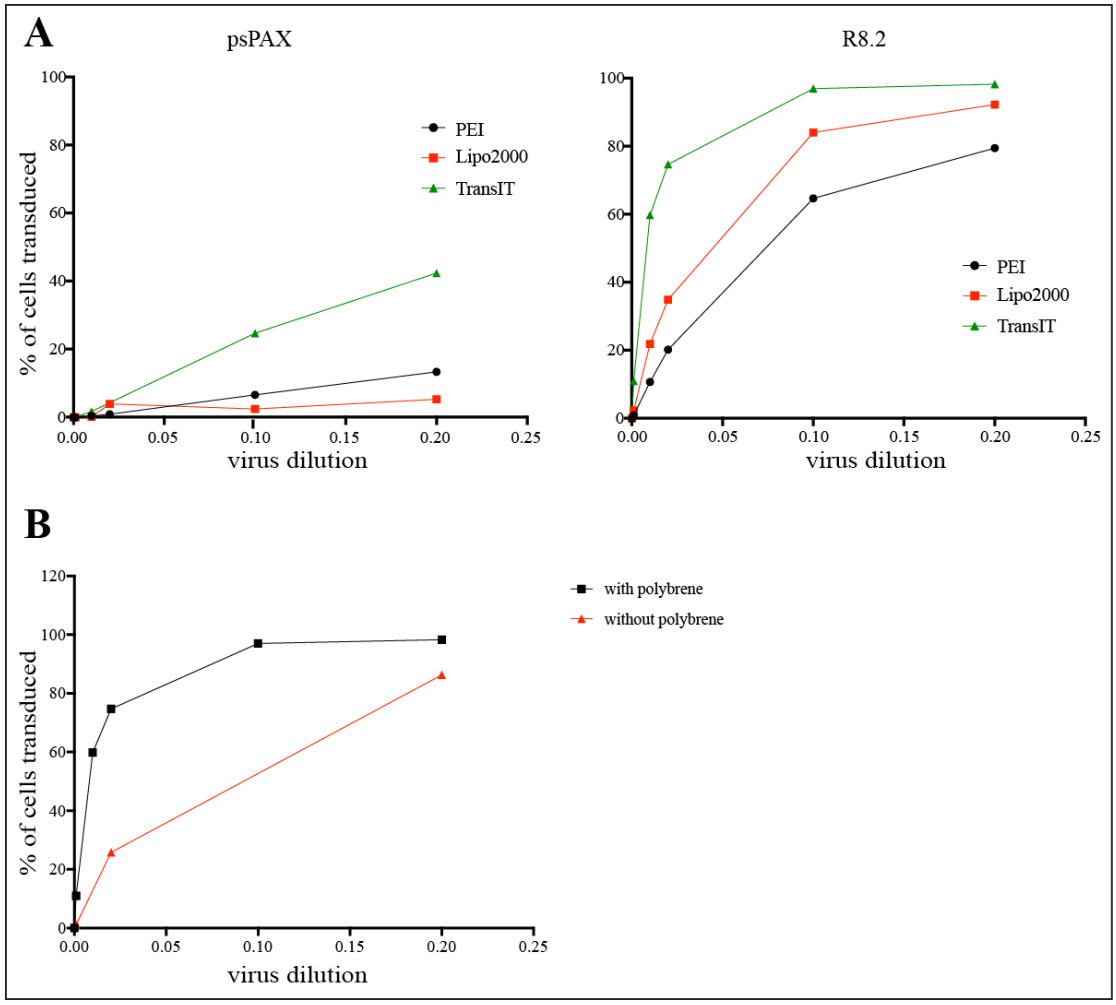

Figure 7: Viral supernatants are produced with R8.2 and transduced with polybrene

(A) 293ET were transfected to produce viruses using psPAX (left) or R8.2 (right) as packaging plasmids. In both cases, three transfection reagents: PEI, Lipofectamine 2000 and TransIT-LT1 were tested. (B) Viruses obtained with R8.2 and TransIT-LT1 were transduced into HeLa cells testing the requirement of polybrene. Viruses produced expressed GFP and so percentages of transduced cells were assessed by flow cytometry.

Based on these preliminary experiments, TransIT was chosen as the transfection reagent for lentiviral production, R8.2 was used as the packaging plasmid, and polybrene was added for the transduction step.

The final protocols used in all experiments were as follows:

4.10.3.1. Viral production

i. Retroviral production

Retroviruses were produced using HEK293-ET cells seeded at about 50% confluency in 6-well plates in 2mL of medium the day before their transfection. The transfection mix contained (for a 6-well format): 1.4µg of retroviral gag/pol plasmid (pMD-OGP), 140ng of viral capsid protein plasmid (pMD-VSVG), 1.4µg of proviral M6P plasmid encoding for the gene of interest and 9µL of TransIT-LT1 transfection reagent (Mirus, MIR2300) in 200µL of Opti-MEM (Gibco). The transfection mix was incubated at room temperature for 10-15min before adding it to the well.

At 16-18h post-transfection, 1mL of medium supplemented with 3% BSA was added to each well. Retroviruses were harvested by collecting the supernatants at 48h post-transfection, aliquoted, and either used directly to transduce cells or stored at -20°C.

ii. Lentiviral production

Lentiviruses were produced using HEK293-ET cells seeded at about 50% confluency in 6-well plates in 2mL of medium the day before their transfection. The transfection mix contained (for a 6-well format): 1.4µg of lentiviral gag/pol/tat/rev packaging plasmid (pCMV-ΔR8.2), 140ng of envelope plasmid (pMD-VSVG), 1.4µg of plasmid encoding for the gene of interest and 9µL of TransIT-LT1 transfection reagent (Mirus, MIR2300) in 200µL of Opti-MEM (Gibco). The transfection mix was incubated at room temperature for 10-15min before adding it to the well.

At 16-18h post-transfection, 1mL of medium supplemented with 3% BSA was added to each well. Lentiviruses were harvested by collecting the supernatants at 48h post-transfection, aliquoted and either used directly to transduce cells or frozen at -20°C.

4.10.3.2. Viral transduction

Transduction enabled the generation of cell lines stably expressing the proteins of interest. HeLa or MEF cells were seeded at approximately 60% confluency in 24-well plates in 500µL of medium the day before transduction. Retroviral or lentiviral

supernatants were either thawed or used directly upon collection after centrifugation at 18000g for 2min in order to pellet cell debris. Appropriate volumes of virus-containing supernatants, determined by preliminary titration, were diluted in 500µL IMDM complemented with 10% FCS, 30µg/ml gentamycin, and 1µg/mL polybrene (SantaCruz) before being added to the wells. Cells were centrifuged at 1800rpm for 2h at room temperature before incubation at 37°C, 5% CO_2. At either 48h or 72h following transduction, transduced cells were expanded and selected with the appropriate antibiotics: puromycin (1µg/mL), blasticidin (5µg/mL), or hygromycin (250µg/mL) depending on the resistance present on the plasmid. Selected cells were then expanded further, used in experiments, and/or frozen down for further use.

4.11 Pathogenic strains

4.11.1 Bacteria

4.11.1.1. *Salmonella enterica* serovar Typhimurium (strain 12023)

Single colony cultures were grown overnight at 37°C in a shaking incubator in LB medium supplemented with 50µg/ml ampicillin for strains constitutively expressing fluorescent markers (mCherry and BFP). Overnight *S.*Typhimurium cultures were sub-cultured (1:33 – 150µL of culture in 5mL fresh medium) in fresh LB plus appropriate antibiotics, for an additional 3.5h before infection.

Cells were grown in an antibiotic-free IMDM medium complemented with 10% FCS (G0 medium) for at least 2h prior to infection. In 24-well plates, cells were infected with 20µL of bacterial sub-culture per well for 15-20min at 37°C. After the initial infection period, cells were washed twice with warm PBS and the medium was replaced with IMDM medium plus 10% FCS containing 100µg/ml gentamycin (G100 medium).

4.11.1.2. Bacterial lysates

Experiments were done transfecting lysates from different mutants of *S.* Typhimurium, presenting various lengths of LPS chains. Single colony cultures of

Salmonella enterica serovar Typhimurium (strain 12023 – WT, ΔrfaL, ΔrfaI, ΔrfaF, ΔrfaG/Q) were grown overnight at 37°C in a shaking incubator in LB medium. OD was measured and adjusted to 1 by adding PBS to reach a final volume of approximately 8mL. Samples were centrifuged at 44krpm for 4min. Bacterial pellets were resuspended in 1mL PBS. Samples of 500µL were boiled at 90°C on the heat-block for either 10min or 20min and were thoroughly vortexed. Boiled samples were then spun down at 13krpm for 15min in order to pellet down denatured proteins. Supernatants were collected, aliquoted and either used directly to transfect cells or frozen at -20°C.

4.11.2 *Toxoplasma gondii*

Toxoplasma gondii was grown using HFF cells. Both strains (RH and PRU) were passaged into new flasks every 2-3days to keep them alive and growing. *T.gondii*-containing HFF cells were scraped in their growth medium, harvested and cells were lysed through a 10mL syringe equipped with a needle. The type I strain (RH) replicates faster than the type II (PRU), and PRU parasites do not survive outside cells contrary to RH. That is why for passaging them every 2 days, 200µL of PRU and 175µL of RH were usually added to the fresh flasks of confluent HFF cells.
To infect MEF cells, 1mL of *T.gondii* was transferred into a new HFF flask 24h before the scheduled infection to have enough parasites for either killing or microscopy assays. On the day of infection, T.*gondii*-containing HFF cells were scraped in their growth medium, harvested, and cells were lysed through a 10mL syringe equipped with a needle. *T.gondii* were counted and pelleted down at 1700rpm for 7min before being re-suspended at the correct concentration in G10 DMEM. 50µL were added in 24-well plates, whereas only 10µL were added in 96-well plates. Infected plates were spun down at 1500rpm for 5min to synchronise infection.

For looking at recruitment by microscopy, coverslips in 24-well plates were infected for 1h at a ratio T.*gondii* to cell number of 4:1 for type II strain (PRU) or 2:1 for type I strain (RH). For killing experiments, cells seeded in 24-well plates were infected with a ratio of 1:1 *T.gondii* to cells for 1h before being washed with PBS and cells were then fixed at different time points (2h, 24h and 48h).

For quantification of variations in mRNA levels of various cytokines upon *T.gondii* infection, cells were seeded in 24-well plates, primed with IFN-γ overnight and infected with a ratio of 1:1 *T.gondii* (PRU) to cells for 1h. Cells were then washed with PBS and lysed at 24h post-infection. mRNA was extracted and purified before reverse transcription and analysis by qPCR using primers designed against several cytokines (see paragraph **4.7.1.1** "Analysis of mRNA levels").

4.12 Detection methods

4.12.1 Protein detection and analysis

4.12.1.1. Sample preparation

A lysis buffer containing 150mM NaCl, 20mM Tris pH 7.4, 0.5% (v/v) Triton-X 100, and protease inhibitors, was prepared on ice. Cells from a confluent 6-well were lysed with the lysis buffer and scraped from the well on ice. The mixture was then centrifuged at 13krpm for 10min at 4°C in order to pellet cell debris. Protein amounts in supernatants were quantified by using Pierce 660nm Protein Assay (ThermoFisher) and protein concentrations were calculated comparing absorbances against samples containing known concentrations of BSA in buffer. Sample protein concentrations were then equalised with lysis buffer before adding 4X Laemmli buffer (40mM Tris pH 6.8, 8% (w/v) SDS, 40% (v/v) glycerol, 0.15% (v/v) bromophenol blue, 5% (v/v) β-mercaptoethanol) and incubated for 5min at 95°C.

4.12.1.2. SDS PolyAcrylamide Gel Electrophoresis (SDS-PAGE)

Samples were loaded into SDS-PAGE NuPAGE Novex 4-12% Bis-Tris pre-cast gels (Life Technologies) along with a sample from the Precision Plus Protein Prestained Standard (Bio-Rad), which provides a protein size ladder for reference. Gels were run in MES buffer (Formedium) at 165V, 300mA for 45min. Gels were then analysed either by Coomassie staining or by western-blotting.

4.12.1.3. Coomassie blue staining

Directly after electrophoresis, gels were immersed in Instant Blue (Expedion) protein stain. They were heated up for 20s in the microwave to accelerate the chemical reaction and enable prompt revelation of the proteins. They were then incubated for 30min at room temperature on an orbital shaker before being extensively washed with water to remove background staining.

4.12.1.4. Western-blotting

Samples were transferred from gels onto PVDF membranes using the Trans-Blot® Turbo™ transfer system (BioRad) for 7min at 1.3A. Membranes were washed with TBS-T (100mM Tris-HCl pH 7.4, 150mM NaCl, 0.1% (v/v) Tween-20) and then blocked in 5% (w/v) dried milk powder (Marvel) in TBS-T for at least 1h at room temperature on the orbital shaker. After washing the membranes several times with TBS-T to remove the milk, membranes were incubated in an appropriate primary antibody solution – dilution made in 2% (w/v) BSA in TBS-T supplemented with 0.1% (w/v) of azide – for either 1-3h at room temperature on the orbital shaker or overnight at 4°C on the rotator depending on the antibody. Membranes were subsequently washed 3-4 times with TBS-T before incubation with secondary HRP-conjugated antibody – diluted in 5% (w/v) dried milk powder (Marvel) in TBS-T – for 1h at room temperature on the shaker. Following the final incubation, membranes were washed 3-4 times in TBS-T. To visualise the proteins, the membranes were incubated for 1min in Amersham Enhanced Chemiluminescence (ECL) detection reagent (GE Healthcare), which was used according to the manufacturer's instructions.

4.12.1.5. Imaging

Coomassie-stained gels were imaged using a ChemiDoc™ MP imaging system (BioRad).

After incubation with ECL detection reagent, membranes were either transferred to an X-ray cassette and exposed to X-ray film (FUJI or Wolflabs) or visualised using a ChemiDoc^{TM} MP imaging system (BioRad). In both cases, exposure time was adjusted according to signal intensity.

4.12.2 Plate reader

4.12.2.1. Luminescence

The cell viability assay CellTiter Glo (CellTiter-Glo® 2.0 Cell Viability Assay, Promega) was used to measure and quantify the proportion of cells still alive after LPS transfection. Assays were performed in 96-well plate (Corning® 96 Well TC-Treated Microplates, Sigma) where 1.10^3 cells were seeded per well (unless otherwise stated). Cells were grown in G30 medium overnight, and on the next day, they were transfected with LPS (see paragraph **4.10.2.1** "LPS transfection"). At 5h post-transfection, the medium in the wells was aspirated and replaced with fresh medium. Cells were only analysed on the following day (i.e. 24h post-transfection).

The CellTiter Glo reagent was added in equal volume to the volume of medium already present in the well (usually 50+50µL). It reacted with ATP; the luminescence signal was therefore proportional to the number of cells still alive in each well. Plates were incubated at room temperature on the shaker for 15-20min. 90µL of the mix were then transferred into an opaque white 96-well plate (Nunc™ F96 MicroWell™ White Polystyrene Plate, ThermoFisher Scientific) to be run on a PHERAstar FS plate reader (BMG LabTech) in order to measure luminescence intensities in the wells. The reader settings were as followed: focal height of 9.7mm, 1 multichromatic, the gain of the optic module LUM plus was set at 2400; measurements were taken every second using a top optic.

Luminescence signals were then compared between conditions but no absolute quantification was performed, since a calibration – measure of the luminescence signal for several known cell numbers – would have been necessary.

4.12.2.2. Absorbance

During the sample preparation for protein analysis, cells were first lysed (see paragraph **4.12.1.1** "Sample preparation"). Then the protein levels were quantified adding 150µL of the Pierce 660nm Protein Assay (ThermoFisher) reagent to 3µL of the unknown sample in a 96-well plate (Corning® 96 Well TC-Treated Microplates, Sigma). The calibration curve was built by adding 150µL of the Pierce reagent to 6µL of BSA solutions at known concentrations. All samples were done in duplicates. The absorbance of each well was measured on a PHERAstar FS plate reader (BMG LabTech) set-up for detection, at the discrete wavelength of 600nm. Settling time was 0.5s and 22 flashes were performed per well. These absorbance values were used for the calculation of protein amounts in the process of making samples for western-blotting.

4.12.3 Flow cytometry

All data acquired on the various flow cytometers were transferred and analysed using the FlowJo software (see paragraph **4.12.3** "Flow cytometry").

4.12.3.1. Isolation of individual clones

Some experiments required cells that were derived from a single mother cell. In order to grow these populations, cells were sorted through a cell sorter (Beckman Coulter MoFlo High Speed Cell Sorter) in a 96-well plate containing G30 medium, complemented with penicillin and streptomycin in order to minimise the risk of contamination. Cell colonies were grown in the 96-well plate until it became visible for selection and expansion.

4.12.3.2. PI staining for assessing cell survival

Cells were seeded in 24-well plates for the experiments. The day after LPS transfection, cells were washed with PBS, trypsinised, centrifuged and re-suspended in 200µL of 100µg/mL of PI (ThermoFisher) in PBS. Samples were transferred into a

flat-bottom 96-well plate which was run on the Eclipse flow cytometer (Sony Biotechnology) for detection at 700nm of unstained (red-negative) cells; that is, alive cells, in a given volume of 150µL. Aspirating and hence analysing the same volume for all samples allowed cells numbers to be compared between different conditions.

4.12.3.3. Staining for MHC Class I receptor to check Cas9 activity

Cells stably expressing Cas9 were transduced with lentiviruses encoding for a gRNA targeting the beta-2 microglobulin (β2M) gene. β2M is a major component of the MHC class I receptor and efficient knockout of the β2M gene should therefore result in a decrease (and eventually an absence) of MHC class I receptors on the outer membrane of transduced cells. To check whether Cas9 was efficient, the transduction of the β2M gRNA was used as an indicator. Several days (clearly stated in **Fig.14** of Chapter 2) after β2M-gRNA transduction, cells were stained by incubating them first with a primary murine antibody against MHC class I receptor and then with a secondary antibody fluorescently labelled (Alexa 488) recognising mouse IgG. Cells expressing only Cas9 should be stained while cells transduced with both Cas9 and the guide should not.

Cells were trypsinised and resuspended in 1%BSA in PBS, incubated with primary antibody (1:50) for 30min, washed and then incubated with secondary antibody (1:500) for 20min. Cells were washed again and resuspended in 1% BSA in PBS for the analysis on the Eclipse flow cytometer (Sony Biotechnology). The secondary antibody was equipped with an Alexa488 fluorophore and the detection was performed at 525nm.

4.12.3.4. *T.gondii* assays

Flow cytometry was used to determine relative rates of *T.gondii* entry (both strains) in different MEF-derived cell lines. These assays also showed whether those cells had the ability to restrict replication of the parasites and provided a relative estimate of cell death upon infection. Prior to analysis, cells (see paragraph **4.11.2** "*Toxoplasma gondii*") were trypsinised and fixed in 4% (w/v) paraformaldehyde (PFA) in PBS for

15 minutes in FACS tubes (Corning™ Cluster Tub, Fisher Scientific) before the reaction was quenched by diluting in FACS buffer (2% BSA (w/v) in PBS). Samples were centrifuged and were all re-suspended in 400µL of FACS buffer. 200µL of the re-suspension were loaded into U-bottom 96-well plates and run on an LSRII SORP flow cytometer (BD BioScience). The following settings were used for the analysis of cells infected with Td-tomato-expressing *T.gondii*: FSC=150V; SSC=270V, YG-582=380V. The plate was run, mixing samples three times at 180µL/sec and aspirating 150µL of sample with a flow rate of 2.5µL/sec, before washing with 200-400µL of sheath (Millipore water with a splash of PBS).

4.12.4 Microscopy

For microscopy analysis, cells were seeded and grown on glass coverslips within 24-well plates or in specific 96-well plates with transparent bottom and black walls. After the experiment (usually infection), cells were washed with PBS and then fixed with 4% (w/v) paraformaldehyde (PFA) for 15min at room temperature. Fixed cells were then washed twice with PBS before overnight incubation in 1M glycine in PBS at 4°C to quench the PFA. Coverslips could be stored in these conditions before being either stained or directly mounted. In the latter case, coverslips were washed in PBS and then in water before mounting them on glass slides using ProLong Gold Antifade Mountant (Sigma). Quantitative analyses (counting) were performed on a Zeiss AxioPlan upright fluorescence microscope (100x 1.3 numerical aperture oil objective), with at least 100 events being counted per coverslip.

Pictures were taken on a Zeiss 780 inverted confocal microscope (63x 1.4 numerical aperture oil objective).

4.12.4.1. Immunostaining

Coverslips of fixed cells stored at 4°C in 1M glycine in PBS were washed with PBS. An immunofluorescence buffer (IF Buffer) containing 2% BSA and 0.1% saponin in PBS was prepared. Coverslips were incubated for 30min at room temperature in the

dark with 300µL of IF Buffer in order to permeabilise and block the cells. Cells were washed with PBS and were incubated with the primary antibody diluted appropriately (see table **4.1.2.1** "Primary antibodies") in IF Buffer, for 1-2h in the dark at room temperature. Cells were then washed in IF Buffer, incubated with secondary antibody and Hoechst, also diluted at the required concentrations (see table **4.1.2.2** "Secondary antibodies") in IF Buffer, for 1h in the dark at room temperature. For antibody incubations, coverslips were transferred onto a Parafilm® M (Sigma) sheet where 20µL drops of the antibody mix were set up. The parafilm sheet displaying the coverslips was incubated on a wet paper towel in a dark box. Dilutions of antibodies were made in IF Buffer as saponin permeabilise the cells in a reversible fashion.

Following the two incubations, coverslips were washed with IF Buffer, then PBS, and finally water before being mounted on glass slides using ProLong Gold Antifade Mountant (Sigma). Slides were left to set at 4°C in the dark, at least overnight before any analysis.

4.12.4.2. High content p65 translocation assay (kindly performed by Dr. Claudio Pathe)

NF-κB signalling is triggered in response to bacterial infection. Its activation results in the nuclear translocation of the protein p65, one of the complex subunits. TNF-α (1:2000, final concentration) was used as positive control for the activation of the NF-κB signalling pathway and hence the translocation of p65.

Fixed cells were stained with p65 antibody. An immunofluorescence buffer (IF Buffer) containing 2% BSA and 0.5% Triton in PBS was prepared. Coverslips were incubated for 10min at room temperature in the dark with 300µL of IF Buffer in order to permeabilise and block the cells. Triton permanently permeabilises the cells. Antibody staining could then be done in PBS supplemented with 2% BSA. After permeabilisation and blocking, cells were washed with PBS and incubated with the rabbit polyclonal p65 antibody diluted 1:1000 in buffer for 1-2h in the dark at room temperature. Cells were then washed in buffer, incubated with secondary antibody

and Hoechst both diluted at the required concentrations in buffer (see table **4.1.2.2** “Secondary antibodies”), for 1h in the dark at room temperature.
Images were acquired in high content manner using a wide-field Nikon HCA (20x/0.75numerical aperture air objective) equipped with a sCMOS camera and supplemented with an automated stage.

4.13 Analysis methods

4.13.1 Sequencing data

4.13.1.1. Sequencher

This software was used to generate a consensus sequence for fragments submitted to GATC sequencing with several primers. It was possible to revert to experimental data, therefore the sequences were processed and trimmed as desired. Chromatograms were also available and allowed systematic analysis if needed.

4.13.1.2. MacVector

This software was used to compare sequenced fragments with references, which could be either DNA or protein sequences. It was primarily used to check plasmids and single-point mutations in genes of interest. MacVector also allowed annotations of various features such as genes, promoters, tags on plasmids, and/or sequences.

4.13.1.3. Algorithms

Sequencing data of the gRNA library (MiSeq) or samples from the screen (HiSeq) were demultiplexed, meaning that the sequences originating from either the three sub-libraries or the two samples submitted in the same line could be respectively segregated according to the barcode they carried. Sequences were trimmed to remove extra base pairs on either side of the actual gRNA sequence. These gRNA sequences were aligned to the list of gRNAs provided as a reference to be identified, counted and related to a gene.

In the case of the gRNA library, the representation was assessed by looking at the number of distinct gRNA sequences present in the sample and the distribution of their frequency.

Concerning the samples from the screen, each sgRNA received a number corresponding to its occurrences in each sample to calculate their enrichment ratio. These numbers were used by all the algorithms to rank the genes and first consider the results in a sgRNA-based manner. Several ranking methods were explored to analyse the results from the screen and are presented below:

i. MaGECK

The model-based analysis of genome-wide CRISPR/Cas9 knockout (MaGECK; Li et al., 2014) first normalises data to correct for differences due to library size and read count distribution. sgRNAs are individually ranked based on their p-value. The p-value is generated by the calculation of the enrichment of each guide in terms of counts over the number of counts in the control condition (reference). Genes are finally ranked based on sgRNA rankings considering the skew to the uniform null model.

Unlike MaGECK, redundant siRNA activity (RSA) was first designed to accommodate and analyse data from siRNA screen.

ii. RSA

The RSA method (König et al., 2007; Birmingham et al., 2009) ranks and calculates p-value for genes based on their guides' distribution of enrichment compared to results obtained by chance.

iii. "5th guide" and Fisher's and Wilcoxon tests

This method takes all sgRNAs and rank them based on their enrichment value, which is defined as the ratio of read counts between the condition tested and the control. Since the genome-wide gRNA library targeted each gene with ten guides, it was decided that the 5th guide (median) would be a good indicator of the gene's participation in the phenotype. Genes were therefore ranked according to their 5th guide rank.

Fisher's and Wilcoxon tests (Prabhakaran, 2016-2017) were used to calculate p-values – representation of the dispersion of the 10 sgRNAs for each gene – on this ranking and to generate volcano plots of the genes overall enriched (blue) or depleted (dark green) in the screen.

4.13.2 Flow cytometry

FlowJO was used to generate dot plots, histograms, and tables from the analysed samples. Gates were drawn first segregating out the debris from the cells and then according to several fluorescent markers. Tables could feature numbers or percentages of cells in those different sub-populations, as well as either the total, average or median intensity of a given population.

4.13.3 Blots and gels

4.13.3.1. Blue light transilluminator

In cases where gels were prepared with 1.5% or 2% (low-melting point) agarose, the mixture was complemented with SYBR Safe (Life Technologies), a DNA gel stain to enable visualisation of the DNA products with this light. It was of great help to extract desired bands out (see paragraph **4.6.4.1** "DNA digestion") or to check whether products were formed during PCRs.

4.13.3.2. ChemiDoc imaging system (Bio-Rad)

Pictures of SYBR Safe-complemented gels could be taken using the Molecular Imager ChemiDoc^{TM} XRS+ Imaging System (Bio-Rad). Default settings for SYBR Safe stain could be used and gels were loaded and illuminated to allow their visualisation. The software allowed brightness, contrast, and exposure to be modified prior to printing.

The ChemiDoc™ MP imaging system (BioRad) could image Coomassie-stained gels and ECL-treated PVDF membranes, changing the detection modes according to the samples and adjusting the exposure time according to signal intensity.

4.13.3.3. Image Lab software

For precast gels, gels were visualised following double incubation with antibodies, using ECL Prime on ChemiDoc™ MP Imaging System (Bio-Rad). Settings used were 'colorimetric' for the ladder and 'chemiluminescence' for the proteins. Images were taken either for a particular exposure time or series of pictures could be defined for a longer exposure time. Images were transferred in Image Lab to be processed, cropped, and exported to create figures.

4.13.4 Microscopy

4.13.4.1. High-content analysis and counting

Wells were imaged on a HCA (high content assay) system consisting of a wide-field Nikon eclipse Ti with a 20x objective and a fluorescent light source, supplemented with an automated stage and plate loader by Prior Scientific. The system was configured to take 12 pictures per well. NIS Elements (4.40) was used as acquisition and analysis software.

The analysis pipeline was designed to identify cells infected with *T.gondii* (Td-tomato) and/or exhibiting p65 nuclear translocation. Cell nuclei were first recognised by Hoechst33342 staining via an intensity threshold. Identified nuclei were then used as the origin of each cell. Cell outlines were drawn base on the p65 staining using Alexa488. *T.gondii* was detected by expression of Td-tomato red and only pathogens within the cell outlines were defined as intracellular. Finally, p65 localisation to the nucleus was determined by using two separate parameters: an intensity threshold was set for Alexa488 signal (p65) within the mask of each nucleus and additionally Hoechst and Alexa488 signals needed to show positive co-localisation scores (Pearson correlation coefficient) for the cell to be considered as positive for p65 translocation (read for NF-κB activation).

4.13.4.2. ImageJ and Photoshop

Pictures taken on the microscope were transferred to ImageJ (Schindelin et al., 2012) as .lsm files for processing. Individual channels could be split and brightness, intensity, and/or contrast were harmonised between samples in order to compare them. Layouts were created displaying the merged image along with the constitutive channels.

Adobe Photoshop was used to resize pictures without losing in definition. Windows could be drawn as well as zoom-ins of desired areas in the pictures. It was also convenient to split the channels and displaying them individually to make figures.

4.13.5 Statistical analysis

GraphPad Prism (version 8.00 for Mac OS X, GraphPad Software, La Jolla California USA, www.graphpad.com) was used to handle a great number of analyses with large amounts of data. It gave the opportunity to visualise data by creating various types of graphs and helped normalise some sets of data or run statistical analyses on certain results such as percentages of surviving cells in different knock-down or knockout cell lines.

To quantify the significance of the difference between two distinct conditions, a two-tailed Student’s t-test was used. One-way ANOVAs with Dunnett multiple comparisons test were used to perform multiple comparisons. Gaussian distribution and equal variance were assumed. Significances are represented on plots and graphs by * and their values are specified in each figure legend.

Conclusion

The purpose of this thesis was to investigate the role of interferon-gamma (IFN-γ) in cell-autonomous immune defence mechanisms against pathogenic infection through the study of its involvement in the response against *Salmonella enterica* serovar Typhimurium (Chapter 2) and *Toxoplasma gondii* (Chapter 3).

Although IFN-γ has a weak antiviral effect, it has demonstrated to be effective in prompting defensive responses to eliminate infectious agents through phagocytosis and promoting intracellular killing. Furthermore, it can act upon most cell types in various body tissues as IFNGR is ubiquitously expressed (Hu & Ivashkiv, 2009). Thanks to this, IFN-γ acts on local tissue cells by inducing the expression of ISGs that mediate host defence and immune responses. In addition to this, it has important effects on the tissue-specific functions of non-immune cells. It also plays an important role in tissue homeostasis and pathobiology through its combined effects on tissue cells and infiltrating immune cells.
To emphasise the important role of IFN-γ in antimicrobial defence, it has been noted that IFNGR deficiencies lead to increased susceptibility to weakly virulent Mycobacteria and to *Listeria* infections (Roesler et al., 1999). These deficiencies can be due to recessive mutations either in the IFGR1 or IFGR2 genes, which respectively prevent either the surface expression of the receptor or the expression of the signalling chain (Casanova & Ochs, 1999). Research was done to understand the tight regulation of its expression considering genetic and epigenetic mechanisms (Aune et al., 2013).

As a result of said research, a number of endogenous and manmade components were found to play a part in the regulation of the IFN-γ signalling. For example, in unstimulated human CD4+ and CD8+ T lymphocytes, the long noncoding RNA (lncRNA) Tmevpg1 is expressed and its pattern of expression during stimulation mirrors that of IFN-γ (Vigneau et al., 2003). That lead to the identification of Tmevpg1 as a candidate target for treatment of infections or autoinflammatory disorders.

Similarly, the antibody Fontolizumab (HuZAF) was developed to bind IFN-γ and inhibit the expression of IFN-γ-regulated genes. This called for an investigation on its viability as a treatment for autoimmune diseases such as Crohn's disease, lupus, rheumatoid arthritis and multiple sclerosis (Skurkovich, 2003).
By contrast, some other strategies aiming to stimulate the host immune system (immunotherapies) have been considered and are used to treat cancer, autoimmune diseases and infections. In addition to vaccines, they include immunomodulators (e.g. Thalidomide), interferons, monoclonal antibodies (e.g. Daratumumab, Elotuzumab); for instance, recombinant IFN-γ was developed as a treatment for a wide variety of clinical indications including cancer, T cell leukemia, tuberculosis (Miller et al., 2009).

Considering these findings, it is reasonable to suggest that understanding the IFN-γ-dependent immune pathways is crucial for the development of new drugs against microbial infections. This last application is especially important in light of the current issue of antibiotic resistance and the severe lack of recent breakthroughs in the field. Similarly, pathways targeted for therapeutic intervention in autoimmune diseases can be harnessed during malignancy and infectious disease to counteract the effect that these conditions have on immune responses.

In the context of infection, multiple cellular processes and protein effectors could be targeted. For example, the IFN-inducible GTPase proteins provide host resistance to a variety of viral, bacterial, and protozoan pathogens through the sequestration of microbial proteins, manipulation of vesicle trafficking, regulation of antimicrobial autophagy (xenophagy), execution of intracellular membranolytic pathways and the activation of inflammasomes (Pilla-Moffett et al., 2016). More specifically, GBPs are IFN-γ-induced GTPases necessary for CASP4 activation in human epithelial cells and monocytes during infection with *S.*Typhimurium or following LPS transfection. GBP1 targets cytosolic *S.*Typhimurium and LPS and recruits GBP2-4 for the recruitment and activation of CASP4 (Wandel et al., 2020) but they do not induce bacteriolysis (Santos et al., 2020). However, GBP1 also plays a crucial role in vacuolar lysis (Haldar et al., 2013; 2015; Fisch et al., 2019a). Deletion of GBP1 compromises the control of *T. gondii* in IFN-γ-treated cells in vitro and increases the susceptibility of mice to infection (Selleck et al., 2013).

The destruction of the SCV or the PV removes the replicative niche for the pathogens, exposing them in the cytosol to further mechanisms of defence including inflammasome activation and cell death. In conclusion, GBP1 expression could be activated to help the host cope with microbial infections.

Rationale for the two projects

The two projects presented in this thesis were motivated by the potential of IFN-γ-regulated pathways to lead to new antimicrobial therapies. They considered the role of IFN-γ, first in the cell death pathway triggered by the presence of cytosolic LPS and second, in the involvement of autophagy and the release of cytokines during *T.gondii* infection.

This section states the knowledge in the fields relevant to the two biological questions asked in the thesis. The two projects are thereby justified by showing the lack of understanding in some areas or the need for identification of new components required in signalling cascades.

The project described in **Chapter 2** investigated the possibility of binding partners for cytosolic LPS that would be involved in the IFN-γ-dependent and LPS-triggered cell death pathway.

It is accepted that the detection of lipopolysaccharide (LPS) is central to host defence against Gram-negative bacterial infections and to the pathogenesis of sepsis. Extracellular LPS is sensed by Toll-like receptor 4 (TLR4), which induces the production of cytokines via the MyD88 and TRIF signalling pathways (Takeuchi & Akira, 2010). Cytosolic LPS is detected by the non-canonical inflammasome, which controls the activation of CASP-4/−5 in humans and Casp11 in mice (Hagar et al., 2013; Kayagaki et al., 2013; 2015; Shi et al., 2014; 2015). These caspases cleave the cell death effector GSDMD to induce pyroptosis and cytokine release by formation of pores in the plasma membrane. In contrast to the activation of other caspases that requires their recruitment to multiprotein platforms formed by dedicated sensor and adaptor proteins (e.g. DISC, apoptosome and canonical inflammasome), no comparable platform has yet been reported for caspase-4/−5 or −11. Instead, their

activation appears to involve a new mode of pattern recognition in which caspase-4/−11 act both as sensor and executor without the need for additional adaptor proteins or co-factors (Shi et al., 2014). This model was proposed based on the observation that caspases-4/−11 binds the highly hydrophobic lipid A moiety of LPS through their CARD (caspase recruitment domain), resulting in their oligomerization and activation (Shi et al., 2014). However, since LPS is hydrophobic and normally present within bacterial membranes, it is conceivable that cytosolic LPS sensing could require accessory factors in analogy to LPS-binding protein (LBP) or cluster of differentiation 14 (CD14) that are required for TLR4 signalling. LBP binds to LPS-containing outer membrane of bacteria and promotes the transfer of LPS onto CD14, which then delivers LPS to the MD-2/TLR4 complex (Gioannini et al., 2004; Park et al., 2009). Moreover, the presence of cytosolic LPS in IFN-γ-primed human monocytic and non-monocytic cells leads to the activation by cleavage of GSDMD proteins, followed by accumulation of GSDMD pores on the plasma membrane, eventually resulting in cell death by pyroptosis (Rathinam et al., 2019).

Experimentation described in **Chapter 2** showed that IFN-γ-dependent cell death triggered by cytosolic *S.*Typhimurium can be recapitulated in HeLa cells by transfection of LPS. Using this model, a human genome-wide CRISPR screen was performed to identify new players in the pathway.

Chapter 3 investigated multiple IFN-γ-dependent cell-autonomous immune responses against the parasite *T.gondii*. They included autophagy and the production of inflammatory cytokines.

The mechanisms of cell death (e.g. apoptosis or pyroptosis) and autophagy (self-eating) are interwoven and have been implicated in microbial infections (Nonaka et al., 1999; Zychlinsky et al., 1992) and autoimmunity. The recently discovered function of autophagy in ATP-dependent generation of engulfment signals and heterophagic removal of apoptotic corpses (Qu et al., 2007) hints at a potential role for autophagy in the prevention of inflammation and autoimmunity. Said rapid removal of apoptotic corpses is critical for the prevention of tissue inflammation (Grossmayer et al., 2005) as there is evidence that autophagy-deficient ($atg5^{-/-}$)

embryos exhibit increased inflammation in tissues due to impaired clearance of apoptotic cells (Qu et al., 2007). Moreover, the lack of efficient apoptotic cell clearance may overcome tolerance to self-antigens and lead to autoimmune diseases such as systemic lupus erythematosis (SLE) (Grossmayer et al., 2005). It is therefore possible that defective autophagy may contribute to the pathogenesis of SLE or other autoimmune diseases.

Autophagy is a conserved cellular degradation process involved in maintaining homeostasis and preventing nutritional, metabolic, and infection-mediated stresses. It plays a beneficial role during infection by simultaneously degrading pathogens, killing infectious agents directly and activating the host's immune system (Levine et al., 2011). Previous work demonstrated that autophagy provides an excellent intracellular defence system against bacterial pathogens, including *Salmonella enterica* serovar Typhimurium (Birmingham et al., 2006), *Listeria monocytogenes* (Yoshikawa et al., 2009), and *Shigella flexneri* (Mostowy et al., 2011).
Further studies on the process of autophagy in different microbial infections (Levine & Kroemer, 2008) could help design and develop novel therapeutic strategies against important pathogenic microbes such as *Toxoplasma gondii*. It can also be argued that understanding the host defence mechanisms along with the avoidance strategies elaborated by *T.gondii* could assist the investigation of new treatment and vaccines (Liu et al., 2012; Scorza et al., 2003).

The autophagy machinery is composed of and regulated by several cellular, membrane-associated or cytoplasmic moieties. The ubiquitinylation cascade, for example, plays an important role in signalling and recruiting proteins such as cargo receptors that are fundamental for the formation of the autophagosome. LUBAC is instrumental to such cascade, as it acts as an E3 ligase and specifically synthesises linear Ub chains. Cells that present a LUBAC deficiency are unable to carry out autophagy adequately and, as a result, exhibit higher rates of infection.
For each of the LUBAC subunits (HOIP, HOIL-1 and Sharpin), inherited deficiencies have been reported and they all participate to autoinflammation and higher susceptibility to infections because it negatively impacts the NF-κB signalling pathway. For example, homozygous mutation in the PUB domain of HOIP, the catalytic subunit of LUBAC, impairs its expression and destabilises the whole

complex (Boisson et al., 2015). Furthermore, loss-of-function and loss-of-expression mutations in HOIL-1 cause hereditary disorders, phenotypically characterised by auto-inflammation, invasive bacterial infections and muscular amylopectinosis. On another note, mice lacking Sharpin (*cpdm*) develop a spontaneous inflammatory syndrome; their cells exhibit decreased NF-κB activation and are more sensitive to TNF-induced cell death (Gerlach et al., 2011; Ikeda et al., 2011; Tokunaga et al., 2011).

Given the importance of LUBAC in antibacterial response and its role in the pathogenesis of multiple inflammatory disorders, its recruitment to *T.gondii* was investigated in **Chapter 3**. By synthesising linear Ub chains, it drives the autophagy machinery; that is why the recruitment of autophagy cargo receptors was also studied.

It should also be noted that impairment of LUBAC stability results differently in various cell types: IL-1β-dependent NF-κB activation is compromised in human fibroblasts but monocytes are hyperresponsive to IL-1β (Boisson et al., 2012). This shows that mutations in the activation pathways of NF-κB can result in aberrant cytokine production. The link between LUBAC and the expression and regulation of certain cytokines and signalling molecules was therefore further investigated in the context of *T.gondii* infection. When infected with a low-virulence form of this protozoan, normal mice are able to control infection, but develop chronic toxoplasmosis. However, IFN-γR1 (-/-) mice are unable to control infection, developing a necrotizing hepatitis, and ultimately succumbing to the pathogen. Hepatic macrophages in infected IFN-γR1 (-/-) mice produced lower levels of TNF-α, iNOS, and IL-1β (Deckert-Schluter et al., 1996).
IFN-γ also induces autophagy through the IRF-1 signalling pathway. Overexpression of IRF-1 enhances autophagosome formation and turnover of LC3 protein in human liver cancer cells whereas silencing IRF-1 expression blocks IFN-γ-induced autophagy (Li et al., 2012).

In addition to the role of LUBAC and autophagy in the immune response against *T.gondii*, the production of cytokines and the requirement for IFN-γ were considered in **Chapter 3**.

New avenues of investigation

The conclusion that can be inferred from **Chapter 2** is that even though there is no definitive proof that binding partners of cytosolic LPS could be involved in the IFN-γ-dependent and LPS-triggered cell death pathway, there is enough evidence to suggest said involvement. Further study on the matter is therefore merited.

Chapter 3 demonstrated the IFN-γ-dependent recruitment of LUBAC and three autophagy cargo receptors (NDP52, p62 and Optn) on type II *T.gondii* in MEF cells. However, the precise binding mechanisms have not been established and require additional experimentation. Moreover, IFN-γ-induced cytokine production was noticed following infection with *T.gondii*. The activation of proinflammatory signalling pathways and the potential role of autophagy during *T.gondii* infection could be investigated further.

Reconsidering the experimental strategy and the models used

The investigation of the IFN-γ-dependent, LPS-triggered cell death mechanism used a human genome-wide CRISPR screen and was carried out in HeLa cells. Although the methodology failed to discover any new players, it was successful in identifying known genes in the pathway and generated a list of genes enriched during the selection process.

The identification of transcription factors within this list could lead to the study of their targets as potential players in the IFN-γ, LPS-triggered cell death mechanism. Some of the transcription factors might be indirectly involved in the pathway by either stimulating or repressing genes. For example, LPS activates the expression of the transcription factor LPS-induced TNF-α factor (LITAF) that regulates TNF-α transcription and STAT6(B). Together, they form a complex that upregulates the production of cytokines, such as TNF-α, IL-1α and IFN-γ (Tang et al., 2005).

Researching these newly identified transcription factors and their target(s) could advance the understanding in the field and potentially serve as a platform for the discovery of new drugs and therapies.

The results from **Chapter 2** also revealed some limitations about the strategy and the model used. Transcriptomics could be used to investigate the discrepancies in the cell

death percentages observed between not only the different cell lines (see Chapter 2, **Figure 4**) but also within a population of HeLa cells (see Chapter 2, **Figure 5**). A significant differential number of mRNAs from certain genes would identify them as actors in the IFN-γ-dependent, LPS-triggered cell death pathway. These genes could either inhibit the pathway or be required for it to operate, depending on whether they are respectively present or absent in cell lines that do not display the cell death phenotype (e.g. 293ET). Performing the screen on a population of HeLa cells constitutes a substantial approximation considering that they can be very heterogenous (Landry et al., 2013). Transcriptomic analysis comparing the surviving cells (see Chapter 2, **Figure 5**) to the rest of the population might also help identifying the genetic reasons for the resistance.

The choice of model organisms also infers a set of constraints. For example, *S.*Typhimurium has been widely used as a model organism to study cell-autonomous immunity pathways such as autophagy. However, experiments carried out in **Chapter 3** established new findings in the case of *T.gondii* infection. These results, complemented with data from the literature, demonstrated that ubiquitylation and recognition of the pathogens or of the vacuolar membrane were shared characteristics during infections with *S.*Typhimurium or non-virulent type II *T.gondii* strains in IFN-γ-primed cells. The mechanisms underlying *T. gondii* detection depend on the virulence of the strains and also on the presence of IFN-γ, reinforcing its essential role in cell-autonomous immunity. IFN-γ is indeed required for the LPS-triggered cell death pathway and the recruitment of LUBAC and autophagy cargo receptors on type II *T.gondii*.

On another note, the reason(s) for the recruitment of LUBAC and autophagy cargo receptors to *T.gondii* needs to be discovered. These recruitment events might be linked to the ATG5-dependent restriction of replication and/or might cause the elevated expression of IL-1α or IL-6 in infected cells. To investigate this further, autophagy- and LUBAC-deficient cells could be primed with IFN-γ and infected with *T.gondii*. The monitoring of *T.gondii* replication using plaque assays (Pfefferkorn & Guyre, 1984) and the levels of cytokine production measured by ELISA would give indications on their requirement.

Localisation and time-sequence of (recruitment) events following infection

Results obtained in **Chapter 3** were limited and some of them deserve to be followed-up in future experiments. The use of high-resolution microscopy would be instrumental to differentiate extracellular from cytosolic *T.gondii*. It would also allow the identification of the particular targets and binding partners of the LUBAC subunits and the three autophagy cargo receptors and their specific localisation (either on the PVM or the parasite itself).

In addition to localisation of the recruited protein, the timing of events in the signalling cascades seems to be an important issue to address. For example, GAL8 is recruited to vacuolar membrane remnants before any LUBAC subunits can access the cytosol-invading *S.*Typhimurium. Moreover, HOIP requires the presence of endogenous HOIL-1 to accumulate on cytosolic *S.*Typhimurium and then recruits HOIL-1 and Sharpin (Noad et al., 2017).

Time-lapse-based microscopy (Velasquez et al., 2019) could be employed to investigate the order of recruitments of LUBAC and its constitutive subunits, autophagy cargo receptors and GBPs, during *T.gondii* infections.

In the case of LPS-triggered cell death in IFN-γ-primed cells, multiple cell death mechanisms might be triggered, and their sequence could be resolved by specifically inhibiting apoptosis, pyroptosis or necrosis when appropriate.

Investigation beyond redundancy: exploring the multiple layers of immune responses

In both chapters, many new questions about redundancy and cross-talk between multiple immune pathways were raised and could be addressed in further experiments.

Multiple complementary strategies could be implemented to identify redundant IFN-γ-dependent cell death mechanisms triggered by cytosolic LPS. GSDMD- or ATG5-deficient cells would respectively provide a cellular background devoid of pyroptosis or autophagy; these cells could be submitted to LPS transfection after priming with IFN-γ. Measure of cell death at different time points could give indications on whether pyroptosis and autophagy are both occurring and their respective timings. To

investigate potential redundancy with other cell death pathways, the simultaneous inhibition of multiple caspases (inflammatory or effector caspases) would disable chosen cell death pathways and allow identification of those that are in play.

From an inflammasome-related perspective, it has been demonstrated that rupture of the PVM followed by release of *T.gondii* DNA triggers the AIM2-ASC-CASP8 inflammasome and results in cell death (Saeij & Frickel, 2017; Fisch et al., 2019b). It might be interesting to consider other inflammasomes or study different cell death mechanisms such as GSDMD-driven pyroptosis in the case of *T.gondii* infection. Such experimentation would provide additional material to compare host immune responses against *T.gondii* and *S.*Typhimurium.

The role of microbial effectors

A more in-depth analysis and comparison of *S.*Typhimurium and *T.gondii* effectors and their impact on the host immunity and the establishment of the infection would be appropriate.

Following *S.*Typhimurium infection, the SCV gets coated by host Rab proteins and is maintained by the effector SopB that also renders the SCV non-fusogenic (Srikanth et al., 2011). Similarly, the *T.gondii* rhoptries ROP18, ROP5 and ROP17 are discharged into the host cytosol and form a complex involved in the formation of the PV (Taylor et al., 2006).

Some other effectors play an important role in virulence. *S.*Typhimurium produce SifA, SSe proteins, SopD2 and PipB2, which are essential for intracellular survival (Srikanth et al., 2011). The pseudokinase ROP5 enhances the kinase activity of ROP18 (Behnke et al., 2012) making the type 1 *T.gondii* strain more virulent, because ROP18 is highly expressed in these parasites. Strains of *T.gondii* are differentially susceptible to destruction by IRGs (Zhao et al., 2009) and GBPs (Selleck et al., 2013), due to active mechanisms of avoidance. Similarly to the mouse system, in IFN-γ-treated HeLa cells, type 2 and 3 strain parasites are susceptible to ubiquitination, the accumulation of the adaptors NDP52 and p62, and the recruitment of LC3 (Selleck et al., 2015), a canonical early marker for autophagosomes. Type 1 strain parasites avoid this ubiquitination-autophagy recruitment pathway by an unknown mechanism. The

accumulation of autophagy adaptors and LC3 leads to engulfment of the PV in host membranes and restricted growth of type 2 parasites, although the compartment does not fuse with lysosomes (Selleck et al., 2015).

T.gondii modulates its host cell on numerous functional levels. *T.gondii* was previously reported to influence host cellular cell cycle and to dampen host cell division. The transmembrane protein GRA7 binds to IRGs and promotes their degradation, protecting the parasites against murine immune defence (Alaganan et al., 2013). ROP16 hijacks the host gene transcription machinery by inducing STAT3 and STAT6 via their phosphorylation (Saeij et al., 2007). Likewise, *S.*Typhimurium have evolved effectors to either harm or fool the host and establish infection. SopA mimics a human protein and undergoes post-translational modifications. It is then cleaved by human CASP3, thereby triggering inflammation. SseL on the other hand acts as a deubiquitinase and inhibits the degradation of IkBα, thereby downregulating the inflammatory response from the NF-κB signalling pathway.

In summary, investigating the roles of IFN-γ and IFN-γ-regulated pathways in the context of microbial infections will help gain further understanding about specific mechanisms of defence. However, proteins can play several roles in different pathways that could be competitive, synergistic or redundant. It is therefore important to put the results into perspective and to integrate new discoveries into the wider picture of the entire immune system, considering both the innate and the adaptive.
Finally, such work is also necessary for the development of new treatments that would be more efficient and targeted, limiting side effects.

Bibliography

Aachoui, Y., Leaf, I. A., Hagar, J. A., Fontana, M. F., Campos, C. G., Zak, D. E., … Miao, E. A. (2013a). Caspase-11 protects against bacteria that escape the vacuole. Science (New York, N.Y.), 339(6122), 975–978. https://doi.org/10.1126/science.1230751

Aachoui, Y., Sagulenko, V., Miao, E. A., & Stacey, K. J. (2013b). Inflammasome-mediated pyroptotic and apoptotic cell death, and defense against infection. Current Opinion in Microbiology, Vol. 16, pp. 319–326. https://doi.org/10.1016/j.mib.2013.04.004

Adamczak, S. E., De Rivero Vaccari, J. P., Dale, G., Brand, F. J., Nonner, D., Bullock, M., … Keane, R. W. (2014). Pyroptotic neuronal cell death mediated by the AIM2 inflammasome. Journal of Cerebral Blood Flow and Metabolism, 34(4), 621–629. https://doi.org/10.1038/jcbfm.2013.236

Adams, L. B., Hibbs, J. B., Taintor, R. R., & Krahenbuhl, J. L. (1990). Microbiostatic effect of murine-activated macrophages for Toxoplasma gondii: Role for synthesis of inorganic nitrogen oxides from L-arginine. . Retrieved from http://www.jimmunol.org/content/144/7/2725

Aglietti, R. A., Estevez, A., Gupta, A., Ramirez, M. G., Liu, P. S., Kayagaki, N., … Dueber, E. C. (2016). GsdmD p30 elicited by caspase-11 during pyroptosis forms pores in membranes. Proceedings of the National Academy of Sciences of the United States of America, 113(28), 7858–7863. https://doi.org/10.1073/pnas.1607769113

Agrotis, A., & Ketteler, R. (2015, September 24). A new age in functional genomics using CRISPR/Cas9 in arrayed library screening. Frontiers in Genetics, Vol. 6, p. 300. https://doi.org/10.3389/fgene.2015.00300

Aguirre, A. J., Meyers, R. M., Weir, B. A., Vazquez, F., Zhang, C. Z., Ben-David, U., … Hahn, W. C. (2016). Genomic copy number dictates a gene-independent cell response to CRISPR/Cas9 targeting. Cancer Discovery, 6(8), 914–929. https://doi.org/10.1158/2159-8290.CD-16-0154

Ainscow, E. K., & Brand, M. D. (1999). Internal regulation of ATP turnover, glycolysis and oxidative phosphorylation in rat hepatocytes. European Journal of Biochemistry, 266(3), 737–749. https://doi.org/10.1046/j.1432-1327.1999.00856.x

Aird, D., Ross, M. G., Chen, W. S., Danielsson, M., Fennell, T., Russ, C., … Gnirke, A. (2011). Analyzing and minimizing PCR amplification bias in Illumina sequencing libraries. Genome Biology, 12(2), R18. https://doi.org/10.1186/gb-2011-12-2-r18

Alaganan, A., Fentress, S.J., Tang, K., Wang, Q., Sibley, L.D. (2013). Toxoplasma GRA7 effector increases turnover of immunity-related GTPases and contributes to acute virulence in the mouse. Proceedings of the National Academy of Sciences USA, 111, 1126–1131. https://doi.org/10.1073/pnas.1313501111

Alix, E., Mukherjee, S., & Roy, C. R. (2011, December 12). Subversion of membrane transport pathways by vacuolar pathogens. Journal of Cell Biology, Vol. 195, pp. 943–952. https://doi.org/10.1083/jcb.201105019

Allam, R., Lawlor, K. E., Yu, E. C., Mildenhall, A. L., Moujalled, D. M., Lewis, R. S., … Vince, J. E. (2014). Mitochondrial apoptosis is dispensable for NLRP 3 inflammasome activation but non-apoptotic caspase-8 is required for inflammasome priming . EMBO Reports, 15(9), 982–990. https://doi.org/10.15252/embr.201438463

Andrade, W. A., Souza, M. D. C., Ramos-Martinez, E., Nagpal, K., Dutra, M. S., Melo, M. B., … Gazzinelli, R. T. (2013). Combined action of nucleic acid-sensing toll-like receptors and TLR11/TLR12 heterodimers imparts resistance to toxoplasma gondii in mice. Cell Host and Microbe, 13(1), 42–53. https://doi.org/10.1016/j.chom.2012.12.003

Ankeny, R. A. (2001). The natural history of Caenorhabditis elegans research. Nature Reviews Genetics, Vol. 2, pp. 474–479. https://doi.org/10.1038/35076538

Aregger, M., Chandrashekhar, M., Tong, A. H. Y., Chan, K., & Moffat, J. (2019). Pooled Lentiviral CRISPR-Cas9 Screens for Functional Genomics in Mammalian Cells. In Methods in Molecular Biology (Vol. 1869, pp. 169–188). https://doi.org/10.1007/978-1-4939-8805-1_15

Aubrey, B. J., Kelly, G. L., Kueh, A. J., Brennan, M. S., O'Connor, L., Milla, L., … Herold, M. J. (2015). An Inducible Lentiviral Guide RNA Platform Enables the Identification of Tumor-Essential Genes and Tumor-Promoting Mutations InVivo. Cell Reports, 10(8), 1422–1432. https://doi.org/10.1016/j.celrep.2015.02.002

Aune, T., Collins, P., Collier, S., Henderson, M., Chang, S. (2013). Epigenetic Activation and Silencing of the Gene that Encodes IFN-γ. Frontiers in Immunology, 4, 112. https://doi.org/10.3389/fimmu.2013.00112

Aviles, H., Stiles, J., O'Donnell, P., Orshal, J., Leid, J., Sonnenfeld, G., & Monroy, F. (2008). Kinetics of Systemic Cytokine and Brain Chemokine Gene Expression in Murine Toxoplasma Infection. Journal of Parasitology, 94(6), 1282–1288. https://doi.org/10.1645/ge-1309.1

Axe, E. L., Walker, S. A., Manifava, M., Chandra, P., Roderick, H. L., Habermann, A., … Ktistakis, N. T. (2008). Autophagosome formation from membrane compartments enriched in phosphatidylinositol 3-phosphate and dynamically connected to the endoplasmic reticulum. Journal of Cell Biology, 182(4), 685–701. https://doi.org/10.1083/jcb.200803137

Baker, P. J., Boucher, D., Bierschenk, D., Tebartz, C., Whitney, P. G., D'Silva, D. B., … Masters, S. L. (2015). NLRP3 inflammasome activation downstream of cytoplasmic LPS recognition by both caspase-4 and caspase-5. European Journal of Immunology, 45(10), 2918–2926. https://doi.org/10.1002/eji.201545655

Barrangou, R., Fremaux, C., Deveau, H., Richards, M., Boyaval, P., Moineau, S., … Horvath, P. (2007). CRISPR provides acquired resistance against viruses in prokaryotes. Science, 315(5819), 1709–1712. https://doi.org/10.1126/science.1138140

Bartha, I., Di Iulio, J., Venter, J. C., & Telenti, A. (2018). Human gene essentiality. Nature Reviews Genetics, 19(1), 51–62. https://doi.org/10.1038/nrg.2017.75

Behnke, M.S., Fentress, S.J., Mashayekhi, M., Li, L.L., Taylor, G.A., Sibley, L.D. (2012). The polymorphic pseudokinase ROP5 controls virulence in Toxoplasma gondii by regulating the active kinase ROP18. PLoS Pathogens, 8:e1002992. https://doi.org/10.1371/journal.ppat.1002992

Bell, B. D., Leverrier, S., Weist, B. M., Newton, R. H., Arechiga, A. F., Luhrs, K. A., … Walsh, C. M. (2008). FADD and caspase-8 control the outcome of autophagic signaling in proliferating T cells. Proceedings of the National Academy of Sciences of the United States of America, 105(43), 16677–16682. https://doi.org/10.1073/pnas.0808597105

Bergsbaken, T., Fink, S. L., & Cookson, B. T. (2009). Pyroptosis: host cell death and inflammation. Nature Reviews Microbiology, 7(2), 99–109. https://doi.org/10.1038/nrmicro2070.Pyroptosis

Berns, K., Hijmans, E. M., Mullenders, J., Brummelkamp, T. R., Velds, A., Heimerikx, M., … Bernards, R. (2004). A large-scale RNAi screen in human cells identifies new components of the p53 pathway. Nature, 428(6981), 431–437. https://doi.org/10.1038/nature02371

Besse, A., Lamothe, B., Campos, A. D., Webster, W. K., Maddineni, U., Lin, S. C., … Darnay, B. G. (2007). TAK1-dependent signaling requires functional interaction with TAB2/TAB3. Journal of Biological Chemistry, 282(6), 3918–3928. https://doi.org/10.1074/jbc.M608867200

Besteiro, S., Dubremetz, J.-F., & Lebrun, M. (2011). The moving junction of apicomplexan parasites: a key structure for invasion. Cellular Microbiology, 13(6), 797–805. https://doi.org/10.1111/j.1462-5822.2011.01597.x

Bettelli, E., Carrier, Y., Gao, W., Korn, T., Strom, T. B., Oukka, M., … Kuchroo, V. K. (2006). Reciprocal developmental pathways for the generation of pathogenic effector TH17 and regulatory T cells. Nature, 441(7090), 235–238. https://doi.org/10.1038/nature04753

Bevan, I. S., Rapley, R., & Walker, M. R. (1992). Sequencing of PCR-amplified DNA. Genome Research, 1, 222–228. https://doi.org/10.1101/gr.1.4.222

Bhavsar, A. P., Brown, N. F., Stoepel, J., Wiermer, M., Martin, D. D. O., Hsu, K. J., … Finlay, B. B. (2013). The Salmonella Type III Effector SspH2 Specifically Exploits the NLR Co-chaperone Activity of SGT1 to Subvert Immunity. PLoS Pathogens, 9(7). https://doi.org/10.1371/journal.ppat.1003518

Bierne, H., Milohanic, E., Kortebi, M. (2018). To Be Cytosolic or Vacuolar: The Double Life of Listeria monocytogenes. Frontiers in Cellular and Infection Microbiology, Vol. 8, p.136. https://doi.org/10.3389/fcimb.2018.00136

Birgisdottir, Å. B., Lamark, T., & Johansen, T. (2013). The LIR motif - crucial for selective autophagy. Journal of Cell Science, Vol. 126, pp. 3237–3247. https://doi.org/10.1242/jcs.126128

Birmingham, A., Selfors, L. M., Forster, T., Wrobel, D., Kennedy, C. J., Shanks, E., … Shamu, C. E. (2009). Statistical methods for analysis of high-throughput RNA interference screens. Nature Methods, 6(8), 569–575. https://doi.org/10.1038/nmeth.1351

Birmingham, C. L., Smith, A. C., Bakowski, M. A., Yoshimori, T., & Brumell, J. H. (2006). Autophagy controls Salmonella infection in response to damage to the Salmonella-containing vacuole. Journal of Biological Chemistry, 281(16), 11374–11383. https://doi.org/10.1074/jbc.M509157200

Biswas, A., Bruder, D., Wolf, S. A., Jeron, A., Mack, M., Heimesaat, M. M., & Dunay, I. R. (2015). Ly6C high Monocytes Control Cerebral Toxoplasmosis . The Journal of Immunology, 194(7), 3223–3235. https://doi.org/10.4049/jimmunol.1402037

Blader, I. J., Manger, I. D., & Boothroyd, J. C. (2001). Microarray Analysis Reveals Previously Unknown Changes in Toxoplasma gondii-infected Human Cells. Journal of Biological Chemistry, 276(26), 24223–24231. https://doi.org/10.1074/jbc.M100951200

Boehm, T. (2012, September 11). Evolution of vertebrate immunity. Current Biology, Vol. 22. https://doi.org/10.1016/j.cub.2012.07.003

Boisson, B., Laplantine, E., Dobbs, K., Cobat, A., Tarantino, N., Hazen, M., … Notarangelo, L. D. (2015). Human HOIP and LUBAC deficiency underlies autoinflammation, immunodeficiency, amylopectinosis, and lymphangiectasia. Journal of Experimental Medicine, 212(6), 939–951. https://doi.org/10.1084/jem.20141130

Boisson, B., Laplantine, E., Prando, C., Giliani, S., Israelsson, E., Xu, Z., … Picard, C. (2012). Immunodeficiency, autoinflammation and amylopectinosis in humans with inherited HOIL-1 and LUBAC deficiency. Nature immunology, 13(12), 1178–1186. https://doi.org/10.1038/ni.2457

Bonnington, K. E., & Kuehn, M. J. (2014). Protein selection and export via outer membrane vesicles. Biochimica et Biophysica Acta - Molecular Cell Research, 1843, 1612–1619. https://doi.org/10.1016/j.bbamcr.2013.12.011

Bordon, Y. (2012, June). Mucosal immunology: Inflammasomes induce sepsis following community breakdown. Nature Reviews Immunology, Vol. 12, pp. 400–401. https://doi.org/10.1038/nri3235

Boutros, M., & Ahringer, J. (2008, July). The art and design of genetic screens: RNA interference. Nature Reviews Genetics, Vol. 9, pp. 554–566. https://doi.org/10.1038/nrg2364

Bouwmeester, T., Bauch, A., Ruffner, H., Angrand, P. O., Bergamini, G., Croughton, K., … Superti-Furga, G. (2004). A physical and functional map of the human TNF-α/NF-κB signal transduction pathway. Nature Cell Biology, 6(2), 97–105. https://doi.org/10.1038/ncb1086

Boyle, J. P., & Radke, J. R. (2009). A history of studies that examine the interactions of Toxoplasma with its host cell: Emphasis on in vitro models. International Journal for Parasitology, 39(8), 903–914. https://doi.org/10.1016/J.IJPARA.2009.01.008

Boyle, K. B., & Randow, F. (2013). The role of "eat-me" signals and autophagy cargo receptors in innate immunity. Current Opinion in Microbiology, Vol. 16, pp. 339–348. https://doi.org/10.1016/j.mib.2013.03.010

Bradley, P. J., Hsieh, C. L., & Boothroyd, J. C. (2002). Unprocessed Toxoplasma ROP1 is effectively targeted and secreted into the nascent parasitophorous vacuole. Molecular and Biochemical Parasitology, 125(1–2), 189–193. https://doi.org/10.1016/S0166-6851(02)00162-7

Brasier, A. R. (2008). Perspective: Expanding role of cyclin dependent kinases in cytokine inducible gene expression. Cell Cycle, 7(17), 2661–2666. https://doi.org/10.4161/cc.7.17.6594

Brazee, P., Dada, L. A., & Sznajder, J. I. (2016). Role of linear ubiquitination in health and disease. American Journal of Respiratory Cell and Molecular Biology, Vol. 54, pp. 761–768. https://doi.org/10.1165/rcmb.2016-0014TR

Brennan, P.J. (2003). Structure, function, and biogenesis of the cell wall of Mycobacterium tuberculosis. Tuberculosis, Vol. 83, pp. 91-97. https://doi.org/10.1016/S1472-9792(02)00089-6

Brenner, S. (1974). The genetics of Caenorhabditis elegans. Genetics, 77(1), pp. 71–94.

Brocker, C., Thompson, D., Matsumoto, A., Nebert, D. W., & Vasiliou, V. (2010). Evolutionary divergence and functions of the human interleukin (IL) gene family. Human Genomics, 5(1), 30–55. https://doi.org/10.1186/1479-7364-5-1-30

Broz, P. (2016). Inflammasomes: Intracellular detection of extracellular bacteria. Cell Research, 26(8), 859–860. https://doi.org/10.1038/cr.2016.67

Broz, P., & Dixit, V. M. (2016). Inflammasomes: mechanism of assembly, regulation and signalling. Nature Reviews Immunology, 16(7), 407–420. https://doi.org/10.1038/nri.2016.58

Broz, P., & Monack, D. M. (2011). Molecular mechanisms of inflammasome activation during microbial infections. Immunological Reviews, Vol. 243, pp. 174–190. https://doi.org/10.1111/j.1600-065X.2011.01041.x

Brubaker, S. W., Bonham, K. S., Zanoni, I., & Kagan, J. C. (2015). Innate immune pattern recognition: a cell biological perspective. Annual Review of Immunology, 33, 257–290. https://doi.org/10.1146/annurev-immunol-032414-112240

Brummelkamp, T. R., Nijman, S. M. B., Dirac, A. M. G., & Bernards, R. (2003). Loss of the cylindromatosis tumour suppressor inhibits apoptosis by activating NF-κB. Nature, 424(6950), 797–801. https://doi.org/10.1038/nature01811

Brunton, L., Chabner, B., Knollman, B. C. (2011-12th edition). Goodman & Gilman's The Pharmacological Basis of Therapeutics. New York(USA): The McGraw-Hill Companies, Inc. ISBN 978-0-07-162442-8. 2084 pp

Bryant, C. E., Gay, N. J., Heymans, S., Sacre, S., Schaefer, L., & Midwood, K. S. (2015). Advances in Toll-like receptor biology: Modes of activation by diverse stimuli. Critical Reviews in Biochemistry and Molecular Biology, Vol. 50, pp. 359–379. https://doi.org/10.3109/10409238.2015.1033511

Bultmann, S., Morbitzer, R., Schmidt, C. S., Thanisch, K., Spada, F., Elsaesser, J., … Leonhardt, H. (2012). Targeted transcriptional activation of silent oct4 pluripotency gene by combining designer TALEs and inhibition of epigenetic modifiers. Nucleic Acids Research, 40(12), 5368–5377. https://doi.org/10.1093/nar/gks199

Cardarelli, F., Digiacomo, L., Marchini, C., Amici, A., Salomone, F., Fiume, G., … Caracciolo, G. (2016). The intracellular trafficking mechanism of Lipofectamine-based transfection reagents and its implication for gene delivery. *Scientific Reports*, *6*. https://doi.org/10.1038/srep25879

Carman, C. V., & Springer, T. A. (2004). A transmigratory cup in leukocyte diapedesis both through individual vascular endothelial cells and between them. Journal of Cell Biology, 167(2), 377–388. https://doi.org/10.1083/jcb.200404129

Carnaud, C., Lee, D., Donnars, O., Park, S.-H., Beavis, A., Koezuka, Y., & Bendelac, A. (1999). Cutting Edge: Cross-Talk Between Cells of the Innate Immune System: NKT Cells Rapidly Activate NK Cells. The Journal of Immunology, 163(9).

Carruthers, V.B. (1999). Armed and dangerous: Toxoplasma gondii uses an arsenal of secretory proteins to infect host cells. Parasitology International, 48(1), 1-10. https://doi.org/10.1016/s1383-5769(98)00042-7

Carswell, E. A., Old, L. J., Kassel, R. L., Green, S., Fiore, N., & Williamson, B. (1975). An endotoxin induced serum factor that cuases necrosis of tumors. Proceedings of the National Academy of Sciences of the United States of America, 72(9), 3666–3670. https://doi.org/10.1073/pnas.72.9.3666

Casanova, JL & Ochs, H.D. (1999). Interferon-γ receptor deficiency: An expanding clinical phenotype?. The Journal of Pediatrics, 135(5), 543-545. https://doi.org/10.1016/S0022-3476(99)70050-8.

Casson, C. N., Yu, J., Reyes, V. M., Taschuk, F. O., Yadav, A., Copenhaver, A. M., … Shin, S. (2015). Human caspase-4 mediates noncanonical inflammasome activation against gram-negative bacterial pathogens. Proceedings of the National Academy of Sciences of the United States of America, 112(21), 6688–6693. https://doi.org/10.1073/pnas.1421699112

Cemma, M., Kim, P. K., & Brumell, J. H. (2011). The ubiquitin-binding adaptor proteins p62/SQSTM1 and NDP52 are recruited independently to bacteria-associated microdomains to target Salmonella to the autophagy pathway. Autophagy, 7(3), 341–345. https://doi.org/10.4161/auto.7.3.14046

Chamaillard, M., Hashimoto, M., Horie, Y., Masumoto, J., Qiu, S., Saab, L., … Inohara, N. (2003). An essential role for NOD1 in host recognition of bacterial peptidoglycan containing diaminopimelic acid. Nature Immunology, 4(7), 702–707. https://doi.org/10.1038/ni945

Chandrasekaran, A. P., Song, M., Kim, K. S., & Ramakrishna, S. (2018). Different Methods of Delivering CRISPR/Cas9 Into Cells. In Progress in Molecular Biology and Translational Science (Vol. 159, pp. 157–176). https://doi.org/10.1016/bs.pmbts.2018.05.001

Chang, H. Y., & Yang, X. (2000). Proteases for Cell Suicide: Functions and Regulation of Caspases. Microbiology and Molecular Biology Reviews, 64(4), 821–846. https://doi.org/10.1128/mmbr.64.4.821-846.2000

Chaplin, D. D. (2010). Overview of the immune response. The Journal of Allergy and Clinical Immunology, 125(2 Suppl 2), S3-23. https://doi.org/10.1016/j.jaci.2009.12.980

Charron, A. J., & Sibley, L. D. (2004). Molecular partitioning during host cell penetration by Toxoplasma gondii. Traffic, 5(11), 855–867. https://doi.org/10.1111/j.1600-0854.2004.00228.x

Chavarría-Smith, J., & Vance, R. E. (2013). Direct Proteolytic Cleavage of NLRP1B Is Necessary and Sufficient for Inflammasome Activation by Anthrax Lethal Factor. PLoS Pathogens, 9(6). https://doi.org/10.1371/journal.ppat.1003452

Chen, D., Fan, W., Lu, Y., Ding, X., Chen, S., & Zhong, Q. (2012). A Mammalian Autophagosome Maturation Mechanism Mediated by TECPR1 and the Atg12-Atg5 Conjugate. Molecular Cell, 45(5), 629–641. https://doi.org/10.1016/j.molcel.2011.12.036

Chen, K. W., Demarco, B., Heilig, R., Shkarina, K., Boettcher, A., Farady, C. J., … Broz, P. (2019). Extrinsic and intrinsic apoptosis activate pannexin-1 to drive NLRP3 inflammasome assembly. The EMBO Journal, 38(10). https://doi.org/10.15252/embj.2019101638

Chen, X., He, W.-T., Hu, L., Li, J., Fang, Y., Wang, X., … Han, J. (2016). Pyroptosis is driven by non-selective gasdermin-D pore and its morphology is different from MLKL channel-mediated necroptosis. Cell Research, 26(9), 1007–1020. https://doi.org/10.1038/cr.2016.100

Cheng, K. T., Xiong, S., Ye, Z., Hong, Z., Di, A., Tsang, K. M., … Malik, A. B. (2017). Caspase-11-mediated endothelial pyroptosis underlies endotoxemia-induced lung injury. Journal of Clinical Investigation, 127(11), 4124–4135. https://doi.org/10.1172/JCI94495

Chipuk, J. E., Moldoveanu, T., Llambi, F., Parsons, M. J., & Green, D. R. (2010). The BCL-2 Family Reunion. Molecular Cell, Vol. 37, pp. 299–310. https://doi.org/10.1016/j.molcel.2010.01.025

Cho, S. W., Kim, S., Kim, J. M., & Kim, J. S. (2013). Targeted genome engineering in human cells with the Cas9 RNA-guided endonuclease. *Nature Biotechnology*, *31*(3), 230–232. https://doi.org/10.1038/nbt.2507

Cho, S. W., Kim, S., Kim, Y., Kweon, J., Kim, H. S., Bae, S., & Kim, J. S. (2014). Analysis of off-target effects of CRISPR/Cas-derived RNA-guided endonucleases and nickases. Genome Research, 24(1), 132–141. https://doi.org/10.1101/gr.162339.113

Choi, J., Park, S., Biering, S. B., Selleck, E., Liu, C. Y., Zhang, X., … Virgin, H. W. (2014). The Parasitophorous Vacuole Membrane of Toxoplasma gondii Is Targeted for Disruption by Ubiquitin-like Conjugation Systems of Autophagy. Immunity, 40(6), 924–935. https://doi.org/10.1016/J.IMMUNI.2014.05.006

Chu, G., Hayakawa, H., & Berg, P. (1987). Electroporation for the efficient transfection of mammalian cells with DNA. In Nucleic Acids Research (Vol. 15).

Ciechanover, A. (2005). Proteolysis: From the lysosome to ubiquitin and the proteasome. Nature Reviews Molecular Cell Biology, Vol. 6, pp. 79–86. https://doi.org/10.1038/nrm1552

Clough, B., & Frickel, E.-M. (2017). The Toxoplasma Parasitophorous Vacuole: An Evolving Host–Parasite Frontier. Trends in Parasitology, 33(6), 473–488. https://doi.org/10.1016/J.PT.2017.02.007

Clough, B., Wright, J. D., Pereira, P. M., Hirst, E. M., Johnston, A. C., Henriques, R., & Frickel, E.-M. (2016). K63-Linked Ubiquitination Targets Toxoplasma gondii for Endo-lysosomal Destruction in IFNγ-Stimulated Human Cells. PLoS Pathogens, 12(11), e1006027. https://doi.org/10.1371/journal.ppat.1006027

Coburn, B., Grassl, G. A., & Finlay, B. B. (2007). Salmonella, the host and disease: a brief review. Immunology and Cell Biology, 85(2), 112–118. https://doi.org/10.1038/sj.icb.7100007

Coers, J., & Haldar, A. K. (2015). Ubiquitination of pathogen-containing vacuoles promotes host defense to Chlamydia trachomatis and Toxoplasma gondii. Communicative & Integrative Biology, 8(6), e1115163. https://doi.org/10.1080/19420889.2015.1115163

Cohen, G. M. (1997, August 15). Caspases: The executioners of apoptosis. Biochemical Journal, Vol. 326, pp. 1–16. https://doi.org/10.1042/bj3260001

Commins, S. P., Borish, L., & Steinke, J. W. (2010). Immunologic messenger molecules: Cytokines, interferons, and chemokines. Journal of Allergy and Clinical Immunology, 125(2 SUPPL. 2). https://doi.org/10.1016/j.jaci.2009.07.008

Cong, L., Ran, F. A., Cox, D., Lin, S., Barretto, R., Habib, N., … Zhang, F. (2013). Multiplex genome engineering using CRISPR/Cas systems. Science, 339(6121), 819–823. https://doi.org/10.1126/science.1231143

Cookson, B. T., & Brennan, M. A. (2001). Pro-inflammatory programmed cell death. Trends in Microbiology, 9(3), 113–114. https://doi.org/10.1016/s0966-842x(00)01936-3

Cooney, R., Baker, J., Brain, O., Danis, B., Pichulik, T., Allan, P., … Simmons, A. (2010). NOD2 stimulation induces autophagy in dendritic cells influencing bacterial handling and antigen presentation. Nature Medicine, 16(1), 90–97. https://doi.org/10.1038/nm.2069

Coppens, I. (2017, December 1). How Toxoplasma and malaria parasites defy first, then exploit host autophagic and endocytic pathways for growth. Current Opinion in Microbiology, Vol. 40, pp. 32–39. https://doi.org/10.1016/j.mib.2017.10.009

Cui, S., Zhang, S., Chen, H., Wang, B., Zhao, Y., & Zhi, D. (2012). The Mechanism of Lipofectamine 2000 Mediated Transmembrane Gene Delivery. *Engineering*, *05*, 172–175. https://doi.org/10.4236/eng.2012.410b045

Cui, Y., Xu, J., Cheng, M., Liao, X., & Peng, S. (2018). Review of CRISPR/Cas9 sgRNA Design Tools. Interdisciplinary Sciences: Computational Life Sciences, Vol. 10, pp. 455–465. https://doi.org/10.1007/s12539-018-0298-z

Damgaard, R. B., Walker, J. A., Marco-Casanova, P., Maher, E. R., Mckenzie, A. N. J., & Komander, D. (2016). The Deubiquitinase OTULIN Is an Essential Negative Regulator of Inflammation and Autoimmunity. Cell, 166, 1230. https://doi.org/10.1016/j.cell.2016.07.019

Davies, C.P., Woods, G., Niesel, D., (1996-4th edition). Introduction to Bacteriology. Medical Microbiology. Galveston (TX): University of Texas Medical Branch at Galveston. PMID 21413299

Davis, B. M., Fensterl, V., Lawrence, T. M., Hudacek, A. W., Sen, G. C., & Schnell, M. J. (2017). Ifit2 Is a Restriction Factor in Rabies Virus Pathogenicity. Journal of Virology, 91(17). https://doi.org/10.1128/jvi.00889-17

de Vasconcelos, N. M., Van Opdenbosch, N., Van Gorp, H., Parthoens, E., & Lamkanfi, M. (2019). Single-cell analysis of pyroptosis dynamics reveals conserved GSDMD-mediated subcellular events that precede plasma membrane rupture. Cell Death and Differentiation, 26(1), 146–161. https://doi.org/10.1038/s41418-018-0106-7

di Russo Case, E., Samuel, J.E. (2016). Contrasting Lifestyles Within the Host Cell. Microbiology spectrum, 4(1). https://doi.org/10.1128/microbiolspec.VMBF-0014-2015

Decker, T., Kovarik, P., & Meinke, A. (1997). GAS elements: A few nucleotides with a major impact on cytokine-induced gene expression. Journal of Interferon and Cytokine Research, 17(3), 121–134. https://doi.org/10.1089/jir.1997.17.121

Deckert-Schlüter, M., Albrecht, S., Hof, H., Wiestler, O. D., & Schlüter, D. (1995). Dynamics of the intracerebral and splenic cytokine mRNA production in Toxoplasma gondii-resistant and -susceptible congenic strains of mice. Immunology, 85(3), 408–418. Retrieved from http://www.ncbi.nlm.nih.gov/pubmed/7558129

Deckert-Schlüter, M., Rang, A., Weiner, D., Huang S, Wiestler, O.D., Hof, H., Schlüter, D. (1996). Interferon‐gamma receptor‐deficiency renders mice highly susceptible to toxoplasmosis by decreased macrophage activation. Laboratory Investigation, 75 (6), 827 841

Degterev, A., Boyce, M., & Yuan, J. (2003, November 24). A decade of caspases. Oncogene, Vol. 22, pp. 8543–8567. https://doi.org/10.1038/sj.onc.1207107

Demon, D., Vande Walle, L., & Lamkanfi, M. (2014). Sensing the enemy within: how macrophages detect intracellular Gram-negative bacteria. Trends in Biochemical Sciences, 39(12), 574–576. https://doi.org/10.1016/j.tibs.2014.10.006

Deng, M., Tang, Y., Li, W., Wang, X., Zhang, R., Zhang, X., … Lu, B. (2018). The Endotoxin Delivery Protein HMGB1 Mediates Caspase-11-Dependent Lethality in Sepsis. Immunity, 49(4), 740-753.e7. https://doi.org/10.1016/j.immuni.2018.08.016

Denkers, E. Y. (2003). From cells to signaling cascades: Manipulation of innate immunity by Toxoplasma gondii. FEMS Immunology and Medical Microbiology, Vol. 39, pp. 193–203. https://doi.org/10.1016/S0928-8244(03)00279-7

Denkers, E. Y., Butcher, B. A., Del Rio, L., & Kim, L. (2004). Manipulation of mitogen-activated protein kinase/nuclear factor-kappaB-signaling cascades during intracellular Toxoplasma gondii infection. Immunological Reviews, 201(1), 191–205. https://doi.org/10.1111/j.0105-2896.2004.00180.x

Denkers, E. Y., & Gazzinelli, R. T. (1998). Regulation and function of T-cell-mediated immunity during Toxoplasma gondii infection. Clinical Microbiology Reviews, Vol. 11, pp. 569–588. https://doi.org/10.1128/cmr.11.4.569

Der, S. D., Zhou, A., Williams, B. R. G., & Silverman, R. H. (1998). Identification of genes differentially regulated by interferon alpha, beta, or gamma using oligonucleotide arrays. Proc. Natl. Acad. Sci. USA, 95, 15623–15628. Retrieved from http://www.pnas.org/content/95/26/15623.full.pdf

Diamond, C. E., Khameneh, H. J., Brough, D., & Mortellaro, A. (2015). Novel perspectives on non-canonical inflammasome activation. ImmunoTargets and Therapy, 4, 131–141. https://doi.org/10.2147/ITT.S57976

Dikic, I., & Dötsch, V. (2009). Ubiquitin linkages make a difference. Nature Structural and Molecular Biology, Vol. 16, pp. 1209–1210. https://doi.org/10.1038/nsmb1209-1209

Dikic, I., Wakatsuki, S., & Walters, K. J. (2009). Ubiquitin-binding domains from structures to functions. Nature Reviews Molecular Cell Biology, Vol. 10, pp. 659–671. https://doi.org/10.1038/nrm2767

Ding, J., Wang, K., Liu, W., She, Y., Sun, Q., Shi, J., … Shao, F. (2016). Pore-forming activity and structural autoinhibition of the gasdermin family. Nature, 535(7610), 111–116. https://doi.org/10.1038/nature18590

Dolasia, K., Bisht, M. K., Pradhan, G., Udgata, A., & Mukhopadhyay, S. (2018, January 2). TLRs/NLRs: Shaping the landscape of host immunity. International Reviews of Immunology, Vol. 37, pp. 3–19. https://doi.org/10.1080/08830185.2017.1397656

Dooley, H. C., Razi, M., Polson, H. E. J., Girardin, S. E., Wilson, M. I., & Tooze, S. A. (2014). WIPI2 Links LC3 Conjugation with PI3P, Autophagosome Formation, and Pathogen Clearance by Recruiting Atg12-5-16L1. Molecular Cell, 55(2), 238–252. https://doi.org/10.1016/j.molcel.2014.05.021

Dubey, J. P., Lindsay, D. S., & Speer, C. A. (1998, April). Structures of Toxoplasma gondii tachyzoites, bradyzoites, and sporozoites and biology and development of tissue cysts. Clinical Microbiology Reviews, Vol. 11, pp. 267–299. https://doi.org/10.1128/cmr.11.2.267

Dupont, N., Lacas-Gervais, S., Bertout, J., Paz, I., Freche, B., Van Nhieu, G. T., … Lafont, F. (2009). Shigella Phagocytic Vacuolar Membrane Remnants Participate in the Cellular Response to Pathogen Invasion and Are Regulated by Autophagy. Cell Host and Microbe, 6(2), 137–149. https://doi.org/10.1016/j.chom.2009.07.005

Ea, C. K., Deng, L., Xia, Z. P., Pineda, G., & Chen, Z. J. (2006). Activation of IKK by TNFα Requires Site-Specific Ubiquitination of RIP1 and Polyubiquitin Binding by NEMO. Molecular Cell, 22(2), 245–257. https://doi.org/10.1016/j.molcel.2006.03.026

Echeverri, C. J., Beachy, P. A., Baum, B., Boutros, M., Buchholz, F., Chanda, S. K., … Bernards, R. (2006). Minimizing the risk of reporting false positives in large-scale RNAi screens. Nature Methods, 3(10), 777–779. https://doi.org/10.1038/nmeth1006-777

Elliott, P. R., Nielsen, S. V, Marco-Casanova, P., Fiil, B. K., Keusekotten, K., Mailand, N., … Komander, D. (2014). Molecular basis and regulation of OTULIN-LUBAC interaction. Molecular Cell, 54(3), 335–348. https://doi.org/10.1016/j.molcel.2014.03.018

Elton, L., Carpentier, I., Verhelst, K., Staal, J., & Beyaert, R. (2015). The multifaceted role of the E3 ubiquitin ligase HOIL-1: beyond linear ubiquitination. Immunological Reviews, 266(1), 208–221. https://doi.org/10.1111/imr.12307

Eren, E., Planès, R., Buyck, J., Bordignon, P.-J., Colom, A., Cunrath, O., … Meunier, E. (2019). Type-3 Secretion System–induced pyroptosis protects Pseudomonas against cell-autonomous immunity. BioRxiv. https://doi.org/10.1101/650333

Ermolaeva, M. A., Michallet, M. C., Papadopoulou, N., Utermöhlen, O., Kranidioti, K., Kollias, G., … Pasparakis, M. (2008). Function of TRADD in tumor necrosis factor receptor 1 signaling and in TRIF-dependent inflammatory responses. Nature Immunology, 9(9), 1037–1046. https://doi.org/10.1038/ni.1638

Fabbi, M., Carbotti, G., & Ferrini, S. (2014). Context-dependent role of IL-18 in cancer biology and counter-regulation by IL-18BP. Journal of Leukocyte Biology, 97(4), 665–675. https://doi.org/10.1189/jlb.5ru0714-360rr

Farkas, T., Daugaard, M., & Jäättelä, M. (2011). Identification of small molecule inhibitors of phosphatidylinositol 3-kinase and autophagy. Journal of Biological Chemistry, 286(45), 38904–38912. https://doi.org/10.1074/jbc.M111.269134

Farrar, M. A., & Schreiber, R. D. (1993). The Molecular Cell Biology of Interferon-gamma and its Receptor. Annual Review of Immunology, 11(1), 571–611. https://doi.org/10.1146/annurev.iy.11.040193.003035

Feasey, N. A., Dougan, G., Kingsley, R. A., Heyderman, R. S., & Gordon, M. A. (2012). Invasive non-typhoidal salmonella disease: An emerging and neglected tropical disease in Africa. The Lancet, Vol. 379, pp. 2489–2499. https://doi.org/10.1016/S0140-6736(11)61752-2

Feng, S., Fox, D., & Man, S. M. (2018). Mechanisms of Gasdermin Family Members in Inflammasome Signaling and Cell Death. Journal of Molecular Biology, 430(18), 3068–3080. https://doi.org/10.1016/J.JMB.2018.07.002

Fenton, M. J., & Golenbock, D. T. (1998). LPS-binding proteins and receptors. Journal of Leukocyte Biology, 64(1), 25–32. https://doi.org/10.1002/jlb.64.1.25

Fentress, S. J., Behnke, M. S., Dunay, I. R., Mashayekhi, M., Rommereim, L. M., Fox, B. A., … Sibley, L. D. (2010). Phosphorylation of immunity-related GTPases by a toxoplasma gondii-secreted kinase promotes macrophage survival and virulence. Cell Host and Microbe, 8(6), 484–495. https://doi.org/10.1016/j.chom.2010.11.005

Ferguson, D. J. P., & Hutchison, W. M. (1987). An ultrastructural study of the early development and tissue cyst formation of Toxoplasma gondii in the brains of mice. Parasitology Research, 73(6), 483–491. https://doi.org/10.1007/BF00535321

Fernandes-Alnemri, T., Yu, J. W., Datta, P., Wu, J., & Alnemri, E. S. (2009). AIM2 activates the inflammasome and cell death in response to cytoplasmic DNA. Nature, 458(7237), 509–513. https://doi.org/10.1038/nature07710

Fiil, B. K., Damgaard, R. B., Wagner, S. A., Keusekotten, K., Fritsch, M., Bekker-Jensen, S., … Gyrd-Hansen, M. (2013). OTULIN Restricts Met1-Linked Ubiquitination to Control Innate Immune Signaling. Molecular Cell, 50(6), 818–830. https://doi.org/10.1016/j.molcel.2013.06.004

Finethy, R., Luoma, S., Orench-Rivera, N., Feeley, E. M., Haldar, A. K., Yamamoto, M., … Coers, J. (2017). Inflammasome Activation by Bacterial Outer Membrane Vesicles Requires Guanylate Binding Proteins. American Society for Microbiology, 8(5), 1–11. Retrieved from https://www.ncbi.nlm.nih.gov/pmc/articles/PMC5626967/pdf/mBio.01188-17.pdf

Fink, S. L., Cookson, B. T., Fink, S. L., & Cookson, B. T. (2005). Eukaryotic Cells MINIREVIEW Apoptosis , Pyroptosis , and Necrosis : Mechanistic Description of Dead and Dying Eukaryotic Cells. 73(4), 1907–1916. https://doi.org/10.1128/IAI.73.4.1907

Fisch, D., Bando, H., Clough, B., Hornung, V., Yamamoto, M., Shenoy, A. R., & Frickel, E. (2019a). Human GBP 1 is a microbe-specific gatekeeper of macrophage apoptosis and pyroptosis . The EMBO Journal, 38(13). https://doi.org/10.15252/embj.2018100926

Fisch, D., Clough, B., Domart, M.-C., Bando, H., Masonou, T., Collinson, L. M., … Frickel, E.-M. (2019b). Differential spatiotemporal targeting of Toxoplasma and Salmonella by GBP1 assembles caspase signalling platforms. BioRxiv, 792804. https://doi.org/10.1101/792804

Fisch, D., Yakimovich, A., Clough, B., Wright, J., Bunyan, M., Howell, M., … Frickel, E. (2019c). Defining host–pathogen interactions employing an artificial intelligence workflow. ELife, 8. https://doi.org/10.7554/eLife.40560

Fiskin, E., Bhogaraju, S., Herhaus, L., Kalayil, S., Hahn, M., & Dikic, I. (2017). Structural basis for the recognition and degradation of host TRIM proteins by Salmonella effector SopA. Nature Communications, 8. https://doi.org/10.1038/ncomms14004

Fitzgerald, K. A., McWhirter, S. M., Faia, K. L., Rowe, D. C., Latz, E., Golenbock, D. T., … Maniatis, T. (2003). IKKepsilon and TBK1 are essential components of the IRF3 signaling pathway. Nature Immunology, 4(5), 491–496. https://doi.org/10.1038/ni921

Foltz, C., Napolitano, A., Khan, R., Clough, B., Hirst, E. M., & Frickel, E.-M. (2017). TRIM21 is critical for survival of Toxoplasma gondii infection and localises to GBP-positive parasite vacuoles. Scientific Reports, 7(1), 5209. https://doi.org/10.1038/s41598-017-05487-7

Forsburg, S. L. (1999). The best yeast? Trends in Genetics, Vol. 15, pp. 340–344. https://doi.org/10.1016/S0168-9525(99)01798-9

Fountoulakis, M., Zulauf, M., Lustig, A., & Garotta, G. (1992). Stoichiometry of interaction between interferon gamma and its receptor. European Journal of Biochemistry, 208(3), 781–787. https://doi.org/10.1111/j.1432-1033.1992.tb17248.x

Frehel, C., Ryter, A., Rastogi, N., & David, H. (n.d.). The electron-transparent zone in phagocytized Mycobacterium avium and other mycobacteria: formation, persistence and role in bacterial survival. Annales de l'Institut Pasteur. Microbiology, 137B(3), 239–257. https://doi.org/10.1016/s0769-2609(86)80115-6

Frenkel, J. K. (1973). Toxoplasma in and around Us. BioScience, 23(6), 343–352. https://doi.org/10.2307/1296513

Frucht, D. M., Fukao, T., Bogdan, C., Schindler, H., O'Shea, J. J., & Koyasu, S. (2001, October 1). IFN-γ production by antigen-presenting cells: Mechanisms emerge. Trends in Immunology, Vol. 22, pp. 556–560. https://doi.org/10.1016/S1471-4906(01)02005-1

Fu, Y., Foden, J. A., Khayter, C., Maeder, M. L., Reyon, D., Joung, J. K., & Sander, J. D. (2013). High-frequency off-target mutagenesis induced by CRISPR-Cas nucleases in human cells. Nature Biotechnology, 31(9), 822–826. https://doi.org/10.1038/nbt.2623

Fuchs, Y., & Steller, H. (2011, November 11). Programmed cell death in animal development and disease. Cell, Vol. 147, pp. 742–758. https://doi.org/10.1016/j.cell.2011.10.033

Fuglewicz, A. J., Piotrowski, P., & Stodolak, A. (2017, September 1). Relationship between toxoplasmosis and schizophrenia: A review. Advances in Clinical and Experimental Medicine, Vol. 26, pp. 1033–1038. https://doi.org/10.17219/acem/61435

Fujita, H., Rahighi, S., Akita, M., Kato, R., Sasaki, Y., Wakatsuki, S., & Iwai, K. (2014). Mechanism Underlying I B Kinase Activation Mediated by the Linear Ubiquitin Chain Assembly Complex. Molecular and Cellular Biology, 34(7), 1322–1335. https://doi.org/10.1128/mcb.01538-13

Fukao, T., Matsuda, S., & Koyasu, S. (2000). Synergistic effects of IL-4 and IL-18 on IL-12-dependent IFN-gamma production by dendritic cells. Journal of Immunology (Baltimore, Md. : 1950), 164(1), 64–71. https://doi.org/10.4049/jimmunol.164.1.64

Furtado, J. M., Smith, J. R., Belfort, R., Gattey, D., & Winthrop, K. L. (2011). Toxoplasmosis: A global threat. Journal of Global Infectious Diseases, 3(3), 281–284. https://doi.org/10.4103/0974-777X.83536

Gaidt, M. M., Ebert, T. S., Chauhan, D., Schmidt, T., Schmid-Burgk, J. L., Rapino, F., … Hornung, V. (2016). Human Monocytes Engage an Alternative Inflammasome Pathway. Immunity, 44(4), 833–846. https://doi.org/10.1016/j.immuni.2016.01.012

Garcia-Del Portillo, F., & Finlay, B. B. (1995). Targeting of Salmonella typhimurium to vesicles containing lysosomal membrane glycoproteins bypasses compartments with mannose 6-phosphate receptors. Journal of Cell Biology, 129(1), 81–97. https://doi.org/10.1083/jcb.129.1.81

Gatica, D., Lahiri, V., & Klionsky, D. J. (2018). Cargo recognition and degradation by selective autophagy. Nature Cell Biology, Vol. 20, pp. 233–242. https://doi.org/10.1038/s41556-018-0037-z

Gazzinelli, R. T., Wysocka, M., Hieny, S., Scharton-Kersten, T., Cheever, A., Kühn, R., … Sher, A. (1996). In the absence of endogenous IL-10, mice acutely infected with Toxoplasma gondii succumb to a lethal immune response dependent on CD4+ T cells and accompanied by overproduction of IL-12, IFN-gamma and TNF-alpha. Journal of Immunology, 157(2), 798–805. Retrieved from http://www.ncbi.nlm.nih.gov/pubmed/8752931

Gazzinelli, R. T., Hieny, S., Wynn, T. A., Wolf, S., & Sher, A. (1993). Interleukin 12 is required for the T-lymphocyte-independent induction of interferon γ by an intracellular parasite and induces resistance in T-cell- deficient hosts. Proceedings of the National Academy of Sciences of the United States of America, 90(13), 6115–6119. https://doi.org/10.1073/pnas.90.13.6115

Gerlach, B., Cordier, S. M., Schmukle, A. C., Emmerich, C. H., Rieser, E., Haas, T. L., … Walczak, H. (2011). Linear ubiquitination prevents inflammation and regulates immune signalling. Nature, 471(7340), 591–596. https://doi.org/10.1038/nature09816

Gessani, S., & Belardelli, F. (1998, May 1). IFN-γ expression in macrophages and its possible biological significance. Cytokine and Growth Factor Reviews, Vol. 9, pp. 117–123. https://doi.org/10.1016/S1359-6101(98)00007-0

Gioannini, T.L., Teghanemt, A., Zhang, D., Coussens, N.P., Dockstader, W., Ramaswamy, S., Weiss, JP. (2004). Isolation of an endotoxin-MD-2 complex that produces Toll-like receptor 4-dependent cell activation at picomolar concentrations. Proceedings of the National Academy of Science USA, 101(12), 4186-91. https://doi.org/10.1073/pnas.0306906101

Girardin, S. E., Boneca, I. G., Carneiro, L. A. M., Antignac, A., Jéhanno, M., Viala, J., … Philpott, D. J. (2003a). Nod1 detects a unique muropeptide from gram-negative bacterial peptidoglycan. Science, 300(5625), 1584–1587. https://doi.org/10.1126/science.1084677

Girardin, S. E., Boneca, I. G., Viala, J., Chamaillard, M., Labigne, A., Thomas, G., … Sansonetti, P. J. (2003b). Nod2 is a general sensor of peptidoglycan through muramyl dipeptide (MDP) detection. Journal of Biological Chemistry, 278(11), 8869–8872. https://doi.org/10.1074/jbc.C200651200

Goffeau, A., Barrell, G., Bussey, H., Davis, R. W., Dujon, B., Feldmann, H., … Oliver, S. G. (1996). Life with 6000 genes. Science, 274(5287), 546–567. https://doi.org/10.1126/science.274.5287.546

Golic, K. G., & Lindquist, S. (1989). The FLP recombinase of yeast catalyzes site-specific recombination in the drosophila genome. Cell, 59(3), 499–509. https://doi.org/10.1016/0092-8674(89)90033-0

Goren, M. B. (1977). Phagocyte Lysosomes: Interactions with Infectious Agents, Phagosomes, and Experimental Perturbations in Function. Annual Review of Microbiology, 31(1), 507–533. https://doi.org/10.1146/annurev.mi.31.100177.002451

Goto, E., & Tokunaga, F. (2017). Decreased linear ubiquitination of NEMO and FADD on apoptosis with caspase-mediated cleavage of HOIP. Biochemical and Biophysical Research Communications, 485(1), 152–159. https://doi.org/10.1016/j.bbrc.2017.02.040

Gram, A. M., Booty, L. M., & Bryant, C. E. (2019). Chopping GSDMD: caspase-8 has joined the team of pyroptosis-mediating caspases. The EMBO Journal, 38(10), e102065. https://doi.org/10.15252/embj.2019102065

Grimm, S. (2004, March). The art and design of genetic screens: Mammalian culture cells. Nature Reviews Genetics, Vol. 5, pp. 179–189. https://doi.org/10.1038/nrg1291

Grissa, I., Vergnaud, G., & Pourcel, C. (2007). The CRISPRdb database and tools to display CRISPRs and to generate dictionaries of spacers and repeats. BMC Bioinformatics, 8(1), 172. https://doi.org/10.1186/1471-2105-8-172

Grossmayer, G.E., Munoz, L.E., Gaipl, U.S., Franz, S., Sheriff, A., Voll, R.E., Kalden, J.R., Hermann, M. (2005). Removal of dying cells and systemic lupus erythematous. Modern Rheumatology, 15, 383–390. https://doi.org./10.1007/s10165-005-0430-x

Guo, H., Callaway, J. B., & Ting, J. P.-Y. (2015). Inflammasomes: mechanism of action, role in disease, and therapeutics. Nature Medicine, 21(7), 677–687. https://doi.org/10.1038/nm.3893

Gurung, P., Anand, P. K., Malireddi, R. K. S., Vande Walle, L., Van Opdenbosch, N., Dillon, C. P., … Kanneganti, T.-D. (2014). FADD and Caspase-8 Mediate Priming and Activation of the Canonical and Noncanonical Nlrp3 Inflammasomes. The Journal of Immunology, 192(4), 1835–1846. https://doi.org/10.4049/jimmunol.1302839

Haas, T. L., Emmerich, C. H., Gerlach, B., Schmukle, A. C., Cordier, S. M., Rieser, E., … Walczak, H. (2009). Recruitment of the Linear Ubiquitin Chain Assembly Complex Stabilizes the TNF-R1 Signaling Complex and Is Required for TNF-Mediated Gene Induction. Molecular Cell, 36(5), 831–844. https://doi.org/10.1016/j.molcel.2009.10.013

Hackstadt, T., Fischer, E. R., Scidmore, M. A., Rockey, D. D., & Heinzen, R. A. (1997, July). Origins and functions of the chlamydial inclusion. Trends in Microbiology, Vol. 5, pp. 288–293. https://doi.org/10.1016/S0966-842X(97)01061-5

Hagar, J. A., Powell, D. A., Aachoui, Y., Ernst, R. K., & Miao, E. A. (2013). Cytoplasmic LPS activates caspase-11: implications in TLR4- independent endotoxic shock. Science, 341(6151), 1250–1253. https://doi.org/10.1126/science.1240988

Hailey, D. W., Rambold, A. S., Satpute-Krishnan, P., Mitra, K., Sougrat, R., Kim, P. K., & Lippincott-Schwartz, J. (2010). Mitochondria Supply Membranes for Autophagosome Biogenesis during Starvation. Cell, 141(4), 656–667. https://doi.org/10.1016/j.cell.2010.04.009

Haldar, A. K., Foltz, C., Finethy, R., Piro, A. S., Feeley, E. M., Pilla-Moffett, D. M., … Coers, J. (2015). Ubiquitin systems mark pathogen-containing vacuoles as targets for host defense by guanylate binding proteins. Proceedings of the National Academy of Sciences, 112(41), E5628–E5637. https://doi.org/10.1073/PNAS.1515966112

Haldar, A. K., Saka, H. A., Piro, A. S., Dunn, J. D., Henry, S. C., Taylor, G. A., … Coers, J. (2013). IRG and GBP Host Resistance Factors Target Aberrant, "Non-self" Vacuoles Characterized by the Missing of "Self" IRGM Proteins. PLoS Pathogens, 9(6), e1003414. https://doi.org/10.1371/journal.ppat.1003414

Halonen, S. K., & Weidner, E. (1994). Overcoating of Toxoplasma Parasitophorous Vacuoles with Host Cell Vimentin Type Intermediate Filaments. Journal of Eukaryotic Microbiology, 41(1), 65–71. https://doi.org/10.1111/j.1550-7408.1994.tb05936.x

Hansen-Wester, I., & Hensel, M. (2001). Salmonella pathogenicity islands encoding type III secretion systems. Microbes and Infection, Vol. 3, pp. 549–559. https://doi.org/10.1016/S1286-4579(01)01411-3

Hansen, G. H., Rasmussen, K., Niels-Christiansen, L. L., & Danielsen, E. M. (2009). Lipopolysaccharide-binding protein: Localization in secretory granules of Paneth cells in the mouse small intestine. Histochemistry and Cell Biology, 131(6), 727–732. https://doi.org/10.1007/s00418-009-0572-6

Haraga, A., & Miller, S. I. (2006). A Salmonella type III secretion effector interacts with the mammalian serine/threonine protein kinase PKN1. Cellular Microbiology, 8(5), 837–846. https://doi.org/10.1111/j.1462-5822.2005.00670.x

Haraga, A., Ohlson, M. B., & Miller, S. I. (2008). Salmonellae interplay with host cells. Nature Reviews Microbiology, Vol. 6, pp. 53–66. https://doi.org/10.1038/nrmicro1788

Hargrave, K. E., Woods, S., Millington, O., Chalmers, S., Westrop, G. D., & Roberts, C. W. (2019). Multi-Omics Studies Demonstrate Toxoplasma gondii-Induced Metabolic Reprogramming of Murine Dendritic Cells. Frontiers in Cellular and Infection Microbiology, 9. https://doi.org/10.3389/fcimb.2019.00309

Hart, T., Chandrashekhar, M., Aregger, M., Steinhart, Z., Brown, K. R., MacLeod, G., … Moffat, J. (2015). High-Resolution CRISPR Screens Reveal Fitness Genes and Genotype-Specific Cancer Liabilities. Cell, 163(6), 1515–1526. https://doi.org/10.1016/j.cell.2015.11.015

Hart, T., Tong, A. H. Y., Chan, K., Van Leeuwen, J., Seetharaman, A., Aregger, M., … Moffat, J. (2017). Evaluation and design of genome-wide CRISPR/SpCas9 knockout screens. G3: Genes, Genomes, Genetics, 7(8), 2719–2727. https://doi.org/10.1534/g3.117.041277

Hayden, M. S., & Ghosh, S. (2014). Regulation of NF-κB by TNF family cytokines. Seminars in Immunology, Vol. 26, pp. 253–266. https://doi.org/10.1016/j.smim.2014.05.004

Hayden, M. S., & Ghosh, S. (2012). NF-κB, the first quarter-century: Remarkable progress and outstanding questions. Genes and Development, 26(3), 203–234. https://doi.org/10.1101/gad.183434.111

Hayward, J. A., Mathur, A., Ngo, C., & Man, S. M. (2018). Cytosolic Recognition of Microbes and Pathogens: Inflammasomes in Action. Microbiology and Molecular Biology Reviews, 82(4). https://doi.org/10.1128/mmbr.00015-18

He, W., Wan, H., Hu, L., Chen, P., Wang, X., Huang, Z., … Han, J. (2015). Gasdermin D is an executor of pyroptosis and required for interleukin-1β secretion. Cell Research, 25(12), 1285–1298. https://doi.org/10.1038/cr.2015.139

Heilig, R., Dick, M. S., Sborgi, L., Meunier, E., Hiller, S., & Broz, P. (2018). The Gasdermin-D pore acts as a conduit for IL-1β secretion in mice. European Journal of Immunology, 48(4), 584–592. https://doi.org/10.1002/eji.201747404

Heintzelman, M. B. (2015, October 1). Gliding motility in apicomplexan parasites. Seminars in Cell and Developmental Biology, Vol. 46, pp. 135–142. https://doi.org/10.1016/j.semcdb.2015.09.020

Hellmich, K. A., Levinsohn, J. L., Fattah, R., Newman, Z. L., Maier, N., Sastalla, I., … Moayeri, M. (2012). Anthrax Lethal Factor Cleaves Mouse Nlrp1b in Both Toxin-Sensitive and Toxin-Resistant Macrophages. PLoS ONE, 7(11). https://doi.org/10.1371/journal.pone.0049741

Hengartner, M. O. (2000, October 12). The biochemistry of apoptosis. Nature, Vol. 407, pp. 770–776. https://doi.org/10.1038/35037710

Hersh, D., Monack, D. M., Smith, M. R., Ghori, N., Falkow, S., & Zychlinsky, A. (1999). The Salmonella invasin SipB induces macrophage apoptosis by binding to caspase-1. Proceedings of

the National Academy of Sciences of the United States of America, 96(5), 2396–2401. https://doi.org/10.1073/pnas.96.5.2396

Hershko, A., & Ciechanover, A. (1992). The Ubiquitin System for Protein Degradation. Annual Review of Biochemistry, 61(1), 761–807. https://doi.org/10.1146/annurev.bi.61.070192.003553

Hershko, A., & Ciechanover, A. (1998). THE UBIQUITIN SYSTEM. Annual Review of Biochemistry, 67(1), 425–479. https://doi.org/10.1146/annurev.biochem.67.1.425

Hibbs, J. B., Lambert, L. H., & Remington, J. S. (1972). Control of Carcinogenesis: A Possible Role for the Activated Macrophage. Science, 177(4053), 998–1000. https://doi.org/10.1126/science.177.4053.998

Hill, D., & Dubey, J. P. (2002). Toxoplasma gondii: Transmission, diagnosis, and prevention. Clinical Microbiology and Infection, 8(10), 634–640. https://doi.org/10.1046/j.1469-0691.2002.00485.x

Hippe, D., Gais, A., Gross, U., & Lüder, C. G. K. (2009). Modulation of caspase activation by Toxoplasma gondii. Methods in Molecular Biology (Clifton, N.J.), 470, 275–288. https://doi.org/10.1007/978-1-59745-204-5_19

Hoffmann, S., Batz, M. B., & Morris, J. G. (2012). Annual cost of illness and quality-adjusted life year losses in the United States due to 14 foodborne pathogens. Journal of Food Protection, 75(7), 1292–1302. https://doi.org/10.4315/0362-028X.JFP-11-417

Honda, K., & Taniguchi, T. (2006, September). IRFs: Master regulators of signalling by Toll-like receptors and cytosolic pattern-recognition receptors. Nature Reviews Immunology, Vol. 6, pp. 644–658. https://doi.org/10.1038/nri1900

Hong, E. A., Gautrey, H. L., Elliott, D. J., & Tyson-Capper, A. J. (2012). SAFB1- and SAFB2-mediated transcriptional repression: Relevance to cancer. Biochemical Society Transactions, 40(4), 826–830. https://doi.org/10.1042/BST20120030

Hook, B. & Landreman, A. Choosing the Right Transfection Reagent for Optimal Efficiency. [Internet] November 2018. Available from: http://www.promega.co.uk/resources/pubhub/tpub-205-choosing-the-right-transfection-reagent-for-optimal-efficiency/

Hornef, M. W., Frisan, T., Vandewalle, A., Normark, S., & Richter-Dahlfors, A. (2002). Toll-like Receptor 4 Resides in the Golgi Apparatus and Colocalizes with Internalized Lipopolysaccharide in Intestinal Epithelial Cells. J. Exp. Med, 035591200(5), 559–570. https://doi.org/10.1084/jem.20011788

Hornung, V., Ablasser, A., Charrel-Dennis, M., Bauernfeind, F., Horvath, G., Caffrey, D. R., … Fitzgerald, K. A. (2009). AIM2 recognizes cytosolic dsDNA and forms a caspase-1-activating inflammasome with ASC. Nature, 458(7237), 514–518. https://doi.org/10.1038/nature07725

Hou, T., Ray, S., & Brasier, A. R. (2007). The functional role of an interleukin 6-inducible CDK9·STAT3 complex in human γ-fibrinogen gene expression. Journal of Biological Chemistry, 282(51), 37091–37102. https://doi.org/10.1074/jbc.M706458200

Hsu, P. D., Scott, D. A., Weinstein, J. A., Ran, F. A., Konermann, S., Agarwala, V., … Zhang, F. (2013). DNA targeting specificity of RNA-guided Cas9 nucleases. Nature Biotechnology, 31(9), 827–832. https://doi.org/10.1038/nbt.2647

Hu, X., Ivashkiv, L.B. (2009). Cross-regulation of signaling pathways by interferon-gamma: implications for immune responses and autoimmune diseases. Immunity, 31(4), 539-50. https://doi.org/10.1016/j.immuni.2009.09.002

Hung, V., Udeshi, N. D., Lam, S. S., Loh, K. H., Cox, K. J., Pedram, K., … Ting, A. Y. (2016). Spatially resolved proteomic mapping in living cells with the engineered peroxidase APEX2. Nature Protocols, 11(3), 456–475. https://doi.org/10.1038/nprot.2016.018

Hunn, J. P., Koenen-Waisman, S., Papic, N., Schroeder, N., Pawlowski, N., Lange, R., … Howard, J. C. (2008). Regulatory interactions between IRG resistance GTPases in the cellular response to Toxoplasma gondii. EMBO Journal, 27(19), 2495–2509. https://doi.org/10.1038/emboj.2008.176

Hunter, C. A., Chizzonite, R., & Remington, J. S. (1995). IL-1 beta is required for IL-12 to induce production of IFN-gamma by NK cells. A role for IL-1 beta in the T cell-independent mechanism of resistance against intracellular pathogens. Journal of Immunology (Baltimore, Md. : 1950), 155(9), 4347–4354. Retrieved from http://www.ncbi.nlm.nih.gov/pubmed/7594594

Hunter, C. A., Subauste, C. S., Van Cleave, V. H., & Remington, J. S. (1994). Production of gamma interferon by natural killer cells from Toxoplasma gondii-infected SCID mice: Regulation by interleukin-10, interleukin-12, and tumor necrosis factor alpha. Infection and Immunity, 62(7), 2818–2824.

Hunter, C. A., & Sibley, L. D. (2012). Modulation of innate immunity by Toxoplasma gondii virulence effectors. Nature Reviews. Microbiology, 10(11), 766–778. https://doi.org/10.1038/nrmicro2858

Hwang, W. Y., Fu, Y., Reyon, D., Maeder, M. L., Tsai, S. Q., Sander, J. D., Peterson, R. T., Yeh, J. R. J., & Joung, J. K. (2013). Efficient genome editing in zebrafish using a CRISPR-Cas system. *Nature Biotechnology*, *31*(3), 227–229. https://doi.org/10.1038/nbt.2501

Ikeda, F., Deribe, Y. L., Skånland, S. S., Stieglitz, B., Grabbe, C., Franz-Wachtel, M., … Dikic, I. (2011). SHARPIN forms a linear ubiquitin ligase complex regulating NF-κB activity and apoptosis. Nature, 471(7340), 637–641. https://doi.org/10.1038/nature09814

Iwasaki, H., Takeuchi, O., Teraguchi, S., Matsushita, K., Uehata, T., Kuniyoshi, K., … Akira, S. (2011). The IκB kinase complex regulates the stability of cytokine-encoding mRNA induced by TLR-IL-1R by controlling degradation of regnase-1. Nature Immunology, 12(12), 1167–1175. https://doi.org/10.1038/ni.2137

Jackson, S. P., & Bartek, J. (2009). The DNA-damage response in human biology and disease. Nature, Vol. 461, pp. 1071–1078. https://doi.org/10.1038/nature08467

Janeway, C. A. (1989). Approaching the asymptote? Evolution and revolution in immunology. Cold Spring Harbor Symposia on Quantitative Biology, 54(1), 1–13. https://doi.org/10.1101/sqb.1989.054.01.003

Ji, C. H., & Kwon, Y. T. (2017, January 1). Crosstalk and interplay between the ubiquitin-proteasome system and autophagy. Molecules and Cells, Vol. 40, pp. 441–449. https://doi.org/10.14348/molcells.2017.0115

Jiang, D., Weidner, J. M., Qing, M., Pan, X.-B., Guo, H., Xu, C., … Guo, J.-T. (2010). Identification of five interferon-induced cellular proteins that inhibit west nile virus and dengue virus infections. Journal of Virology, 84(16), 8332–8341. https://doi.org/10.1128/JVI.02199-09

Jiang, W., Bikard, D., Cox, D., Zhang, F., & Marraffini, L. A. (2013). RNA-guided editing of bacterial genomes using CRISPR-Cas systems. *Nature Biotechnology*, *31*(3), 233–239. https://doi.org/10.1038/nbt.2508

Jiang, W., Brueggeman, A. J., Horken, K. M., Plucinak, T. M., & Weeks, D. P. (2014). Successful transient expression of Cas9 and single guide RNA genes in Chlamydomonas reinhardtii. Eukaryotic Cell, 13(11), 1465–1469. https://doi.org/10.1128/EC.00213-14

Jimenez, A. J., Maiuri, P., Lafaurie-Janvore, J., Divoux, S., Piel, M., & Perez, F. (2014). ESCRT machinery is required for plasma membrane repair. Science, 343(6174). https://doi.org/10.1126/science.1247136

Jinek, M., Chylinski, K., Fonfara, I., Hauer, M., Doudna, J. A., & Charpentier, E. (2012). A Programmable Dual-RNA–Guided DNA Endonuclease in Adaptive Bacterial Immunity. Science, 337(6096), 816–821. https://doi.org/10.1126/science.1138140

Jingjing, W., Peng, H., Ming, Y., Chunhui, W., Choi, W., Jianguo, S., … Yun, Z. (2019). Association between tnfrsf11a and tnfrsf11b gene polymorphisms and the outcome of hepatitis c virus infection. Chinese Journal of Endemiology, 40(10), 1291–1295. https://doi.org/10.3760/cma.j.issn.0254-6450.2019.10.022

Jones, B. D., Ghori, N., & Falkow, S. (1994). Salmonella typhlrnurium initiates murine infection by penetrating and destroying the specialized epithelial M cells of the peyer's patches. Journal of Experimental Medicine, 180(1), 15–23. https://doi.org/10.1084/jem.180.1.15

Jones, E. J., Korcsmaros, T., & Carding, S. R. (2017). Mechanisms and pathways of Toxoplasma gondii transepithelial migration. Tissue Barriers, Vol. 5. https://doi.org/10.1080/21688370.2016.1273865

Jones, T. C., & Hirsch, J. G. (1972). The interaction between toxoplasma gondii and mammalian cells: II. The absence of lysosomal fusion with phagocytic vacuoles containing living parasites. Journal of Experimental Medicine, 136(5), 1173–1194. https://doi.org/10.1084/jem.136.5.1173

Joo, D., Tang, Y., Blonska, M., Jin, J., Zhao, X., & Lin, X. (2016). Regulation of Linear Ubiquitin Chain Assembly Complex by Caspase-Mediated Cleavage of RNF31. Molecular and Cellular Biology, 36(24), 3010–3018. https://doi.org/10.1128/mcb.00474-16

Jorgensen, I., Rayamajhi, M., & Miao, E. A. (2017). Programmed cell death as a defence against infection. Nature Reviews Immunology, 17(3), 151–164. https://doi.org/10.1038/nri.2016.147

Jorgensen, I., Zhang, Y., Krantz, B. A., & Miao, E. A. (2016). Pyroptosis triggers pore-induced intracellular traps (PITs) that capture bacteria and lead to their clearance by efferocytosis. The Journal of Experimental Medicine, 213(10), 2113–2128. https://doi.org/10.1084/jem.20151613

Joshi, A. D., & Swanson, M. S. (2011). Secrets of a successful pathogen: Legionella resistance to progression along the autophagic pathway. Frontiers in Microbiology, 2(JUNE). https://doi.org/10.3389/fmicb.2011.00138

Joung, J., Konermann, S., Gootenberg, J. S., Abudayyeh, O. O., Platt, R. J., Brigham, M. D., … Zhang, F. (2017). Genome-scale CRISPR-Cas9 Knockout and Transcriptional Activation Screening. Nature Protocols, 12(4), 828–863. https://doi.org/10.1101/059626

Kabeya, Y., Mizushima, N., Ueno, T., Yamamoto, A., Kirisako, T., Noda, T., … Yoshimori, T. (2000). LC3, a mammalian homologue of yeast Apg8p, is localized in autophagosome membranes after processing. The EMBO Journal, 19(21), 5720–5728. https://doi.org/10.1093/emboj/19.21.5720

Kagan, J. C., & Medzhitov, R. (2006). Phosphoinositide-Mediated Adaptor Recruitment Controls Toll-like Receptor Signaling. Cell, 125(5), 943–955. https://doi.org/10.1016/j.cell.2006.03.047

Kagan, J. C., & Roy, C. R. (2002). Legionella phagosomes intercept vesicular traffic from endoplasmic reticulum exit sites. Nature Cell Biology, 4(12), 945–954. https://doi.org/10.1038/ncb883

Kageyama, S., Omori, H., Saitoh, T., Sone, T., Guan, J. L., Akira, S., … Yoshimori, T. (2011). The LC3 recruitment mechanism is separate from Atg9L1-dependent membrane formation in the

autophagic response against Salmonella. Molecular Biology of the Cell, 22(13), 2290–2300. https://doi.org/10.1091/mbc.E10-11-0893

Kamanova, J., Sun, H., Lara-Tejero, M., & Galán, J. E. (2016). The Salmonella Effector Protein SopA Modulates Innate Immune Responses by Targeting TRIM E3 Ligase Family Members. PLOS Pathogens, 12(4), e1005552. https://doi.org/10.1371/journal.ppat.1005552

Kanayama, A., Seth, R. B., Sun, L., Ea, C. K., Hong, M., Shaito, A., … Chen, Z. J. (2004). TAB2 and TAB3 activate the NF-κB pathway through binding to polyubiquitin chains. Molecular Cell, 15(4), 535–548. https://doi.org/10.1016/j.molcel.2004.08.008

Kaney, A. R., & Speare, V. J. (1992). A Genetic Screen for Vegetative Gene Expression in the Micronucleus of Tetrahymena thermophila. The Journal of Protozoology, 39(2), 323–328. https://doi.org/10.1111/j.1550-7408.1992.tb01323.x

Karin, M., & Delhase, M. (2000). The IκB kinase (IKK) and NF-κB: Key elements of proinflammatory signalling. Seminars in Immunology, 12(1), 85–98. https://doi.org/10.1006/smim.2000.0210

Karin, M., & Ben-Neriah, Y. (2000). Phosphorylation Meets Ubiquitination: The Control of NF-κB Activity. Annual Review of Immunology, 18(1), 621–663. https://doi.org/10.1146/annurev.immunol.18.1.621

Kasper, L. H., & Buzoni-Gatel, D. (1998, April 1). Some opportunistic parasitic infections in AIDS: Candidiasis, Pneumocystosis, Cryptosporidiosis, Toxoplasmosis. Parasitology Today, Vol. 14, pp. 150–156. https://doi.org/10.1016/S0169-4758(97)01212-X

Kawai, T., & Akira, S. (2007, November). Signaling to NF-κB by Toll-like receptors. Trends in Molecular Medicine, Vol. 13, pp. 460–469. https://doi.org/10.1016/j.molmed.2007.09.002

Kayagaki, N., Stowe, I. B., Lee, B. L., O'Rourke, K., Anderson, K., Warming, S., … Dixit, V. M. (2015). Caspase-11 cleaves gasdermin D for non-canonical inflammasome signalling. Nature, 526(7575), 666–671. https://doi.org/10.1038/nature15541

Kayagaki, N., Warming, S., Lamkanfi, M., Walle, L. Vande, Louie, S., Dong, J., … Dixit, V. M. (2011). Non-canonical inflammasome activation targets caspase-11. Nature, 479(7371), 117–121. https://doi.org/10.1038/nature10558

Kayagaki, N., Wong, M. T., Stowe, I. B., Ramani, S. R., Gonzalez, L. C., Akashi-Takamura, S., … Dixit, V. M. (2013). Noncanonical Inflammasome Activation by Intracellular LPS Independent of TLR4. Science, 341, 1246–1249. Retrieved from http://science.sciencemag.org/content/sci/341/6151/1246.full.pdf

Kebschull, J. M., & Zador, A. M. (2015). Sources of PCR-induced distortions in high-throughput sequencing data sets. Nucleic Acids Research, 43(21), e143. https://doi.org/10.1093/nar/gkv717

Keller, M., Rüegg, A., Werner, S., & Beer, H. D. (2008). Active Caspase-1 Is a Regulator of Unconventional Protein Secretion. Cell, 132(5), 818–831. https://doi.org/10.1016/j.cell.2007.12.040

Kemp, C. J., Sun, S., & Gurley, K. E. (2001). p53 induction and apoptosis in response to radio- and chemotherapy in vivo is tumor-type-dependent. Cancer Research, 61(1), 327–332. Retrieved from http://www.ncbi.nlm.nih.gov/pubmed/11196181

Keusekotten, K., Elliott, P. R., Glockner, L., Fiil, B. K., Damgaard, R. B., Kulathu, Y., … Komander, D. (2013). OTULIN antagonizes LUBAC signaling by specifically hydrolyzing met1-linked polyubiquitin. Cell, 153(6), 1326. https://doi.org/10.1016/j.cell.2013.05.014

Khan, A., & Grigg, M. E. (2017). Toxoplasma gondii: Laboratory Maintenance and Growth. Current Protocols in Microbiology, 44, 20C.1.1-20C.1.17. https://doi.org/10.1002/cpmc.26

Kim, H. S., Lee, K., Kim, S. J., Cho, S., Shin, H. J., Kim, C., & Kim, J. S. (2018). Arrayed CRISPR screen with image-based assay reliably uncovers host genes required for coxsackievirus infection. Genome Research, 28(6), 859–868. https://doi.org/10.1101/gr.230250.117

Kim, H., & Kim, J. S. (2014). A guide to genome engineering with programmable nucleases. Nature Reviews Genetics, 15(5), 321–334. https://doi.org/10.1038/nrg3686

Kim, S.-K., Fouts, A. E., & Boothroyd, J. C. (2007). Toxoplasma gondii Dysregulates IFN-γ-Inducible Gene Expression in Human Fibroblasts: Insights from a Genome-Wide Transcriptional Profiling . The Journal of Immunology, 178(8), 5154–5165. https://doi.org/10.4049/jimmunol.178.8.5154

Kim, Y. G., Cha, J., & Chandrasegaran, S. (1996). Hybrid restriction enzymes: Zinc finger fusions to Fok I cleavage domain. Proceedings of the National Academy of Sciences of the United States of America, 93(3), 1156–1160. https://doi.org/10.1073/pnas.93.3.1156

Kim, Y., Kweon, J., Kim, A., Chon, J. K., Yoo, J. Y., Kim, H. J., … Kim, J. S. (2013). A library of TAL effector nucleases spanning the human genome. Nature Biotechnology, 31(3), 251–258. https://doi.org/10.1038/nbt.2517

Kimata, I., & Tanabe, K. (1987). Secretion by Toxoplasma gondii of an antigen that appears to become associated with the parasitophorous vacuole membrane upon invasion of the host cell. Journal of Cell Science, 88, 231–239.

Kirisako, T., Kamei, K., Murata, S., Kato, M., Fukumoto, H., Kanie, M., … Iwai, K. (2006). A ubiquitin ligase complex assembles linear polyubiquitin chains. EMBO Journal, 25(20), 4877–4887. https://doi.org/10.1038/sj.emboj.7601360

Knodler, L. A., Crowley, S. M., Sham, H. P., Yang, H., Wrande, M., Ma, C., … Vallance, B. A. (2014a). Noncanonical Inflammasome Activation of Caspase-4/Caspase-11 Mediates Epithelial Defenses against Enteric Bacterial Pathogens. Cell Host & Microbe, 16, 249–256. https://doi.org/10.1016/j.chom.2014.07.002

Knodler, L. A., Nair, V., & Steele-Mortimer, O. (2014b). Quantitative assessment of cytosolic Salmonella in epithelial cells. PLoS ONE, 9(1). https://doi.org/10.1371/journal.pone.0084681

Kobayashi, T., Ogawa, M., Sanada, T., Mimuro, H., Kim, M., Ashida, H., … Sasakawa, C. (2013). The Shigella OspC3 effector inhibits caspase-4, antagonizes inflammatory cell death, and promotes epithelial infection. Cell Host and Microbe, 13(5), 570–583. https://doi.org/10.1016/j.chom.2013.04.012

Kofoed, E. M., & Vance, R. E. (2011). Innate immune recognition of bacterial ligands by NAIPs determines inflammasome specificity. Nature, 477(7366), 592–597. https://doi.org/10.1038/nature10394

Koike-Yusa, H., Li, Y., Tan, E.-P., Velasco-Herrera, M. D. C., & Yusa, K. (2014). Genome-wide recessive genetic screening in mammalian cells with a lentiviral CRISPR-guide RNA library. Nature Biotechnology, 32(3), 267–273. https://doi.org/10.1038/nbt.2800

Komander, D., & Rape, M. (2012). The Ubiquitin Code. Annual Review of Biochemistry, 81(1), 203–229. https://doi.org/10.1146/annurev-biochem-060310-170328

König, R., Chiang, C., Tu, B. P., Yan, S. F., DeJesus, P. D., Romero, A., … Chanda, S. K. (2007). A probability-based approach for the analysis of large-scale RNAi screens. Nature Methods, 4, 847–849. https://doi.org/10.1038/nmeth1089

Krakauer, T. (2019). Inflammasomes, autophagy, and cell death: The trinity of innate host defense against intracellular bacteria. Mediators of Inflammation, Vol. 2019. https://doi.org/10.1155/2019/2471215

Krishnamurthy, S., Konstantinou, E.K., Young, L.H., Gold, D.A., Saeij, J.P. (2017). The human immune response to Toxoplasma: Autophagy versus cell death. PLoS Pathogens, 13(3), e1006176. https://doi.org/10.1371/journal.ppat.1006176

Kubori, T., Matsushima, Y., Nakamura, D., Uralil, J., Lara-Tejero, M., Sukhan, A., … Aizawa, S. I. (1998). Supramolecular structure of the salmonella typhimurium type III protein secretion system. Science, 280(5363), 602–605. https://doi.org/10.1126/science.280.5363.602

Kuhle, V., Abrahams, G. L., & Hensel, M. (2006). Intracellular Salmonella enterica Redirect Exocytic Transport Processes in a Salmonella Pathogenicity Island 2-Dependent Manner. Traffic, 7(6), 716–730. https://doi.org/10.1111/j.1600-0854.2006.00422.x

Kulathu, Y., & Komander, D. (2012, August). Atypical ubiquitylation-the unexplored world of polyubiquitin beyond Lys48 and Lys63 linkages. Nature Reviews Molecular Cell Biology, Vol. 13, pp. 508–523. https://doi.org/10.1038/nrm3394

Kuscu, C., Arslan, S., Singh, R., Thorpe, J., & Adli, M. (2014). Genome-wide analysis reveals characteristics of off-target sites bound by the Cas9 endonuclease. Nature Biotechnology, 32(7), 677–683. https://doi.org/10.1038/nbt.2916

Lagrange, B., Benaoudia, S., Wallet, P., Magnotti, F., Provost, A., Michal, F., … Henry, T. (2018). Human caspase-4 detects tetra-acylated LPS and cytosolic Francisella and functions differently from murine caspase-11. Nature Communications, 9(242). https://doi.org/10.1038/s41467-017-02682-y

Lam, S. S., Martell, J. D., Kamer, K. J., Deerinck, T. J., Ellisman, M. H., Mootha, V. K., & Ting, A. Y. (2014). Directed evolution of APEX2 for electron microscopy and proximity labeling. Nature Methods, 12(1), 51–54. https://doi.org/10.1038/nmeth.3179

Lamark, T., Perander, M., Outzen, H., Kristiansen, K., Øvervatn, A., Michaelsen, E., … Johansen, T. (2003). Interaction Codes within the Family of Mammalian Phox and Bem1p Domain-containing Proteins. Journal of Biological Chemistry, 278(36), 34568–34581. https://doi.org/10.1074/jbc.M303221200

Lamb, B. M., Mercer, A. C., & Barbas, C. F. (2013). Directed evolution of the TALE N-terminal domain for recognition of all 50 bases. Nucleic Acids Research, 41(21), 9779–9785. https://doi.org/10.1093/nar/gkt754

Lamkanfi, M. (2011). Emerging inflammasome effector mechanisms. Nature Reviews Immunology, Vol. 11, pp. 213–220. https://doi.org/10.1038/nri2936

Lamkanfi, M., & Dixit, V. M. (2014). Mechanisms and functions of inflammasomes. Cell, 157(5), 1013–1022. https://doi.org/10.1016/j.cell.2014.04.007

Landry, J. J., Pyl, P. T., Rausch, T., Zichner, T., Tekkedil, M. M., Stütz, A. M., … Steinmetz, L. M. (2013). The genomic and transcriptomic landscape of a HeLa cell line. G3 (Bethesda, Md.), 3(8), 1213–1224. https://doi.org/10.1534/g3.113.005777

LaRock, C. N., & Cookson, B. T. (2013). Burning Down the House: Cellular Actions during Pyroptosis. PLoS Pathogens, 9(12), 1–3. https://doi.org/10.1371/journal.ppat.1003793

Laughlin, R. C., Knodler, L. A., Barhoumi, R., Ross Payne, H., Wu, J., Gomez, G., … Garry Adamsa, L. (2014). Spatial segregation of virulence gene expression during acute enteric infection with Salmonella enterica serovar typhimurium. MBio, 5(1). https://doi.org/10.1128/mBio.00946-13

Lee, Y., Sasai, M., Ma, J. S., Sakaguchi, N., Ohshima, J., Bando, H., … Yamamoto, M. (2015). P62 Plays a Specific Role in Interferon-γ-Induced Presentation of a Toxoplasma Vacuolar Antigen. Cell Reports, 13(2), 223–233. https://doi.org/10.1016/j.celrep.2015.09.005

Levine, B. & Kroemer, G. (2008). Autophagy in the pathogenesis of disease. Cell, 132(1), 27–42. https://doi.org/10.1016/j.cell.2007.12.018

Levine, B. & Kroemer, G. (2019). Biological Functions of Autophagy Genes: A Disease Perspective. Cell, Vol. 176, pp. 11–42. https://doi.org/10.1016/j.cell.2018.09.048

Levine, B., Mizushima, N., Virgin, H. (2011). Autophagy in immunity and inflammation. Nature, 469, 323–335. https://doi.org/10.1038/nature09782

Levy, J. K., Liang, Y., Ritchey, J. W., Davidson, M. G., Tompkins, W. A., & Tompkins, M. B. (2004). Failure of FIV-infected cats to control Toxoplasma gondii correlates with reduced IL2, IL6, and IL12 and elevated IL10 expression by lymph node T cells. Veterinary Immunology and Immunopathology, 98(1–2), 101–111. https://doi.org/10.1016/j.vetimm.2003.11.002

Li, L.-F., Yu, J., Li, Y., Wang, J., Li, S., Zhang, L., … Qiu, H.-J. (2016). Guanylate-Binding Protein 1, an Interferon-Induced GTPase, Exerts an Antiviral Activity against Classical Swine Fever Virus Depending on Its GTPase Activity. Journal of Virology, 90(9), 4412–4426. https://doi.org/10.1128/jvi.02718-15

Li, P., Nijhawan, D., Budihardjo, I., Srinivasula, S. M., Ahmad, M., Alnemri, E. S., & Wang, X. (1997). Cytochrome c and dATP-dependent formation of Apaf-1/caspase-9 complex initiates an apoptotic protease cascade. Cell, 91(4), 479–489. https://doi.org/10.1016/S0092-8674(00)80434-1

Li, P., Du, Q., Cao, Z., Guo, Z., Evankovich, J., Yan, W., … Geller, D. A. (2012). Interferon-γ induces autophagy with growth inhibition and cell death in human hepatocellular carcinoma (HCC) cells through interferon-regulatory factor-1 (IRF-1). Cancer letters, 314(2), 213–222. https://doi.org/10.1016/j.canlet.2011.09.031

Li, P., Sanz, I., O'Keefe, R. J., & Schwarz, E. M. (2000). NF-κB Regulates VCAM-1 Expression on Fibroblast-Like Synoviocytes. The Journal of Immunology, 164(11), 5990–5997. https://doi.org/10.4049/jimmunol.164.11.5990

Li, S., Wandel, M. P., Li, F., Liu, Z., He, C., Wu, J., … Randow, F. (2013). Sterical hindrance promotes selectivity of the autophagy cargo receptor NDP52 for the danger receptor galectin-8 in antibacterial autophagy. Science Signaling, 6(261). https://doi.org/10.1126/scisignal.2003730

Li, W., Xu, H., Xiao, T., Cong, L., Love, M. I., Zhang, F., … Liu, X. S. (2014). MAGeCK enables robust identification of essential genes from genome-scale CRISPR/Cas9 knockout screens. Genome Biology, 15(554). https://doi.org/10.1186/s13059-014-0554-4

Ling, Y. M., Shaw, M. H., Ayala, C., Coppens, I., Taylor, G. A., Ferguson, D. J. P., & Yap, G. S. (2006). Vacuolar and plasma membrane stripping and autophagic elimination of Toxoplasma gondii in primed effector macrophages. Journal of Experimental Medicine, 203(9), 2063–2071. https://doi.org/10.1084/jem.20061318

Lippincott's Illustrated Reviews: Immunology. Paperback: 384 pages. Publisher: Lippincott Williams & Wilkins; (July 1, 2007). Language: English. ISBN 0-7817-9543-5. ISBN 978-0-7817-9543-2. Page 68

Liu, F., Pouponnot, C., & Massagué, J. (1997). Dual role of the Smad4/DPC4 tumor suppressor in TGFβ-inducible transcriptional complexes. Genes and Development, 11(23), 3157–3167. https://doi.org/10.1101/gad.11.23.3157

Liu, Q., Das Singla, L., & Zhou, H. (2012). Vaccines against Toxoplasma gondii: Status, challenges and future directions. Human Vaccines and Immunotherapeutics, Vol. 8, pp. 1305–1308. https://doi.org/10.4161/hv.21006

Liu, Q., Wang, Z.-D., Huang, S.-Y., & Zhu, X.-Q. (2015). Diagnosis of toxoplasmosis and typing of Toxoplasma gondii. Parasites & Vectors, 8(1), 292. https://doi.org/10.1186/s13071-015-0902-6

Liu, T., Zhang, L., Joo, D., & Sun, S.-C. (2017). NF-κB signaling in inflammation. Signal Transduction and Targeted Therapy, 2, e17023. https://doi.org/10.1038/sigtrans.2017.23

Liu, X., Zhang, Z., Ruan, J., Pan, Y., Magupalli, V. G., Wu, H., & Lieberman, J. (2016). Inflammasome-activated gasdermin D causes pyroptosis by forming membrane pores. Nature, 535(7610), 153–158. https://doi.org/10.1038/nature18629

Liu, Z., Wang, C., Rathkey, J. K., Yang, J., Dubyak, G. R., Abbott, D. W., & Xiao, T. S. (2018). Structures of the Gasdermin D C-Terminal Domains Reveal Mechanisms of Autoinhibition. Structure Cell Press, 26(5), 778–784. https://doi.org/10.1016/j.str.2018.03.002

Lycke, E., Carlberg, K., & Norrby, R. (1975). Interactions between Toxoplasma gondii and its host cells: function of the penetration enhancing factor of toxoplasma. Infection and Immunity, 11(4), 853–861. https://doi.org/10.1128/iai.11.4.853-861.1975

Ma, H., Su, L., He, X., & Miao, J. (2019). Loss of HMBOX1 promotes LPS-induced apoptosis and inhibits LPS-induced autophagy of vascular endothelial cells in mouse. Apoptosis. https://doi.org/10.1007/s10495-019-01572-6

MacDuff, D. A., Reese, T. A., Kimmey, J. M., Weiss, L. A., Song, C., Zhang, X., … Virgin, H. W. (2015). Phenotypic complementation of genetic immunodeficiency by chronic herpesvirus infection. ELife, 4, e04494. https://doi.org/10.7554/eLife.04494

MacMicking, J. D. (2012, May). Interferon-inducible effector mechanisms in cell-autonomous immunity. Nature Reviews Immunology, Vol. 12, pp. 367–382. https://doi.org/10.1038/nri3210

Madan, R., Rastogi, R., Parashuraman, S., & Mukhopadhyay, A. (2012). Salmonella acquires lysosome-associated membrane protein 1 (LAMP1) on phagosomes from golgi via SipC protein-mediated recruitment of host syntaxin6. Journal of Biological Chemistry, 287(8), 5574–5587. https://doi.org/10.1074/jbc.M111.286120

Madara, J. L., & Stafford, J. (1989). Interferon-γ directly affects barrier function of cultured intestinal epithelial monolayers. Journal of Clinical Investigation, 83(2), 724–727. https://doi.org/10.1172/JCI113938

Mahoney, D. J., Cheung, H. H., Lejmi Mrad, R., Plenchette, S., Simard, C., Enwere, E., … Korneluk, R. G. (2008). Both cIAP1 and cIAP2 regulate TNFα-mediated NF-κB activation. Proceedings of the National Academy of Sciences of the United States of America, 105(33), 11778–11783. https://doi.org/10.1073/pnas.0711122105

Maine, E. M. (2001). RNAi as a tool for understanding germline development in Caenorhabditis elegans: Uses and cautions. Developmental Biology, Vol. 239, pp. 177–189. https://doi.org/10.1006/dbio.2001.0394

Majowicz, S. E., Musto, J., Scallan, E., Angulo, F. J., Kirk, M., O'Brien, S. J., … Hoekstra, R. M. (2010). The Global Burden of Nontyphoidal Salmonella Gastroenteritis. Clinical Infectious Diseases, 50(6), 882–889. https://doi.org/10.1086/650733

Mali, P., Yang, L., Esvelt, K. M., Aach, J., Guell, M., DiCarlo, J. E., … Church, G. M. (2013). RNA-guided human genome engineering via Cas9. Science, 339(6121), 823–826. https://doi.org/10.1126/science.1232033

Mallo, G. V, Espina, M., Smith, A. C., Terebiznik, M. R., Alemán, A., Finlay, B. B., … Brumell, J. H. (2008). SopB promotes phosphatidylinositol 3-phosphate formation on Salmonella vacuoles by recruiting Rab5 and Vps34. The Journal of Cell Biology, 182(4), 741–752. https://doi.org/10.1083/jcb.200804131

Man, S. M., & Kanneganti, T.-D. (2015a). Gasdermin D: the long-awaited executioner of pyroptosis. Cell Research, 25(11), 1183–1184. https://doi.org/10.1038/cr.2015.124

Man, S. M., & Kanneganti, T.-D. (2015b). Converging roles of caspases in inflammasome activation, cell death and innate immunity. Nature Reviews Immunology, 16(1), 7–21. https://doi.org/10.1038/nri.2015.7

Man, S. M., Karki, R., Malireddi, R. K. S., Neale, G., Vogel, P., Yamamoto, M., … Kanneganti, T.-D. (2015). The transcription factor IRF1 and guanylate-binding proteins target activation of the AIM2 inflammasome by Francisella infection. Nature Immunology, 16(5), 467–475. https://doi.org/10.1038/ni.3118

Man, S. M., Karki, R., Sasai, M., Place, D. E., Kesavardhana, S., Temirov, J., … Kanneganti, T. D. (2016). IRGB10 Liberates Bacterial Ligands for Sensing by the AIM2 and Caspase-11-NLRP3 Inflammasomes. Cell, 167(2), 382-396.e17. https://doi.org/10.1016/j.cell.2016.09.012

Man, S. M., Place, D. E., Kuriakose, T., & Kanneganti, T.-D. (2017). Interferon-inducible guanylate-binding proteins at the interface of cell-autonomous immunity and inflammasome activation. Journal of Leukocyte Biology, 101(1), 143–150. https://doi.org/10.1189/jlb.4MR0516-223R

Mandal, P., Feng, Y., Lyons, J. D., Berger, S. B., Otani, S., DeLaney, A., … Mocarski, E. S. (2018). Caspase-8 Collaborates with Caspase-11 to Drive Tissue Damage and Execution of Endotoxic Shock. Immunity, 49(1), 42–55. https://doi.org/10.1016/j.immuni.2018.06.011

Martens, S., & Howard, J. (2006). The Interferon-Inducible GTPases. Annual Review of Cell and Developmental Biology, 22(1), 559–589. https://doi.org/10.1146/annurev.cellbio.22.010305.104619

Martin-Sanchez, F., Diamond, C., Zeitler, M., Gomez, A. I., Baroja-Mazo, A., Bagnall, J., … Pelegrin, P. (2016). Inflammasome-dependent IL-1β release depends upon membrane permeabilisation. Cell Death and Differentiation, 23(7), 1219–1231. https://doi.org/10.1038/cdd.2015.176

Martin, C. J., Booty, M. G., Rosebrock, T. R., Nunes-Alves, C., Desjardins, D. M., Keren, I., … Behar, S. M. (2012). Efferocytosis is an innate antibacterial mechanism. Cell Host and Microbe, 12(3), 289–300. https://doi.org/10.1016/j.chom.2012.06.010

Martinon, F., Burns, K., & Tschopp, J. (2002). The inflammasome: a molecular platform triggering activation of inflammatory caspases and processing of proIL-beta. Molecular Cell, 10(2), 417–426. https://doi.org/10.1016/S1097-2765(02)00599-3

Maruyama, H., Morino, H., Ito, H., Izumi, Y., Kato, H., Watanabe, Y., … Kawakami, H. (2010). Mutations of optineurin in amyotrophic lateral sclerosis. Nature, 465(7295), 223–226. https://doi.org/10.1038/nature08971

Mascarenhas, D. P. A., Cerqueira, D. M., Pereira, M. S. F., Castanheira, F. V. S., Fernandes, T. D., Manin, G. Z., … Zamboni, D. S. (2017). Inhibition of caspase-1 or gasdermin-D enable caspase-8 activation in the Naip5/NLRC4/ASC inflammasome. PLOS Pathogens, 13(8), e1006502. https://doi.org/10.1371/journal.ppat.1006502

Matzinger, P. (1994). Tolerance, Danger, and the Extended Family. Annual Review of Immunology, 12(1), 991–1045. https://doi.org/10.1146/annurev.iy.12.040194.005015

McCusker, C., & Warrington, R. (2011). Primary immunodeficiency. Allergy, Asthma & Clinical Immunology, 7(S1). https://doi.org/10.1186/1710-1492-7-s1-s11

McNeil, P. L., & Kirchhausen, T. (2005). An emergency response team for membrane repair. Nature Reviews. Molecular Cell Biology, 6(6), 499–505. https://doi.org/10.1038/nrm1665

Mei, K., & Guo, W. (2018). The exocyst complex. Current Biology, 28(17), R922–R925. https://doi.org/10.1016/j.cub.2018.06.042

Meissner, F., Scheltema, R. A., Mollenkopf, H.-J., & Mann, M. (2013). Direct Proteomic Quantification of the Secretome of Activated Immune Cells. Science, 340(6131), 475–478. https://doi.org/10.1126/science.1183021

Melo, E. J., Carvalho, T. M., & De Souza, W. (2001). Behaviour of microtubules in cells infected with Toxoplasma gondii. Biocell : Official Journal of the Sociedades Latinoamericanas de Microscopia Electronica ... et. Al, 25(1), 53–59. Retrieved from http://www.ncbi.nlm.nih.gov/pubmed/11387877

Méresse, S., Steele-Mortimer, O., Finlay, B. B., & Gorvel, J. P. (1999). The rab7 GTPase controls the maturation of Salmonella typhimurium-containing vacuoles in HeLa cells. EMBO Journal, 18(16), 4394–4403. https://doi.org/10.1093/emboj/18.16.4394

Merline, R., Moreth, K., Beckmann, J., Nastase, M. V., Zeng-Brouwers, J., Tralhão, J. G., … Schaefer, L. (2011). Signaling by the matrix proteoglycan decorin controls inflammation and cancer through PDCD4 and microRNA-21. Science Signaling, 4(199). https://doi.org/10.1126/scisignal.2001868

Meunier, E., Dick, M. S., Dreier, R. F., Schürmann, N., Broz, D. K., Warming, S., … Broz, P. (2014). Caspase-11 activation requires lysis of pathogen-containing vacuoles by IFN-induced GTPases. Nature, 509, 366–370. https://doi.org/10.1038/nature13157

Miao, E. A., Alpuche-Aranda, C. M., Dors, M., Clark, A. E., Bader, M. W., Miller, S. I., & Aderem, A. (2006). Cytoplasmic flagellin activates caspase-1 and secretion of interleukin 1β via Ipaf. Nature Immunology, 7(6), 569–575. https://doi.org/10.1038/ni1344

Miao, E. A., Mao, D. P., Yudkovsky, N., Bonneau, R., Lorang, C. G., Warren, S. E., … Aderem, A. (2010). Innate immune detection of the type III secretion apparatus through the NLRC4 inflammasome. Proceedings of the National Academy of Sciences of the United States of America, 107(7), 3076–3080. https://doi.org/10.1073/pnas.0913087107

Miles, L. A., Garippa, R. J., & Poirier, J. T. (2016). Design, execution, and analysis of pooled in-vitro CRISPR/Cas9 screens. FEBS Journal, 283, 3170–3180. https://doi.org/10.1111/febs.13770

Miller, C. H., Maher, S. G., Young, H. A. (2009). Clinical Use of Interferon-gamma. Annals of the New York Academy of Sciences, 1182, 69–79. https://doi.org/10.1111/j.1749-6632.2009.05069.x

Miller, J. C., Tan, S., Qiao, G., Barlow, K. A., Wang, J., Xia, D. F., … Rebar, E. J. (2011). A TALE nuclease architecture for efficient genome editing. Nature Biotechnology, 29(2), 143–150. https://doi.org/10.1038/nbt.1755

Miyake, K. (2006). Roles for accessory molecules in microbial recognition by Toll-like receptors. Journal of Endotoxin Research, 12(4), 195–204. https://doi.org/10.1179/096805106X118807

Mizushima, N., & Komatsu, M. (2011). Autophagy: Renovation of cells and tissues. Cell, Vol. 147, pp. 728–741. https://doi.org/10.1016/j.cell.2011.10.026

Mizushima, N., Yoshimori, T., & Ohsumi, Y. (2011). The role of Atg proteins in autophagosome formation. Annual Review of Cell and Developmental Biology, 27, 107–132. https://doi.org/10.1146/annurev-cellbio-092910-154005

Mochizuki, D. Y., Eisenman, J. R., Conlon, P. J., Larsen, A. D., & Tushinski, R. J. (1987). Interleukin 1 regulates hematopoietic activity, a role previously ascribed to hemopoietin 1. Proceedings of the National Academy of Sciences of the United States of America, 84(15), 5267–5271. https://doi.org/10.1073/pnas.84.15.5267

Mogensen, T. H. (2009, April). Pathogen recognition and inflammatory signaling in innate immune defenses. Clinical Microbiology Reviews, Vol. 22, pp. 240–273. https://doi.org/10.1128/CMR.00046-08

Mohr, S. E., Hu, Y., Ewen-Campen, B., Housden, B. E., Viswanatha, R., & Perrimon, N. (2016, September 1). CRISPR guide RNA design for research applications. FEBS Journal, pp. 3232–3238. https://doi.org/10.1111/febs.13777

Mojica, F. J. M., Díez-Villaseñor, C., García-Martínez, J., & Almendros, C. (2009). Short motif sequences determine the targets of the prokaryotic CRISPR defence system. Microbiology, 155(3), 733–740. https://doi.org/10.1099/mic.0.023960-0

Monis, P. T., Giglio, S., & Saint, C. P. (2005). Comparison of SYTO9 and SYBR Green I for real-time polymerase chain reaction and investigation of the effect of dye concentration on amplification and DNA melting curve analysis. Analytical Biochemistry, 340(1), 24–34. https://doi.org/10.1016/j.ab.2005.01.046

Moon, S. Bin, Kim, D. Y., Ko, J. H., Kim, J. S., & Kim, Y. S. (2019). Improving CRISPR Genome Editing by Engineering Guide RNAs. Trends in Biotechnology, Vol. 37, pp. 870–881. https://doi.org/10.1016/j.tibtech.2019.01.009

Mordue, D. G., Desai, N., Dustin, M., & Sibley, L. D. (1999). Invasion by Toxoplasma gondii establishes a moving junction that selectively excludes host cell plasma membrane proteins on the basis of their membrane anchoring. Journal of Experimental Medicine, 190(12), 1783–1792. https://doi.org/10.1084/jem.190.12.1783

Moretti, J., & Blander, J. M. (2017). Cell-autonomous stress responses in innate immunity. Journal of Leukocyte Biology, 101(1), 77–86. https://doi.org/10.1189/jlb.2mr0416-201r

Moscat, J., & Diaz-Meco, M. T. (2000). The atypical protein kinase Cs: Functional specificity mediated by specific protein adapters. EMBO Reports, 1(5), 399–403. https://doi.org/10.1093/embo-reports/kvd098

Mostowy, S., Sancho-Shimizu, V., Hamon, M. A., Simeone, R., Brosch, R., Johansen, T., & Cossart, P. (2011). p62 and NDP52 proteins target intracytosolic Shigella and Listeria to different autophagy pathways. Journal of Biological Chemistry, 286(30), 26987–26995. https://doi.org/10.1074/jbc.M111.223610

Müller, A. J., Kaiser, P., Dittmar, K. E. J., Weber, T. C., Haueter, S., Endt, K., … Hardt, W. D. (2012). Salmonella gut invasion involves TTSS-2-dependent epithelial traversal, basolateral exit, and uptake by epithelium-sampling lamina propria phagocytes. Cell Host and Microbe, 11(1), 19–32. https://doi.org/10.1016/j.chom.2011.11.013

Müller, U., Steinhoff, U., Reis, L. F. L., Hemmi, S., Pavlovic, J., Zinkernagel, R. M., & Aguet, M. (1994). Functional role of type I and type II interferons in antiviral defense. Science, 264(5167), 1918–1921. https://doi.org/10.1126/science.8009221

Mulvihill, E., Sborgi, L., Mari, S. A., Pfreundschuh, M., Hiller, S., & Müller, D. J. (2018). Mechanism of membrane pore formation by human gasdermin-D. The EMBO Journal, 37(14), e98321. https://doi.org/10.15252/embj.201798321

Muñoz-Planillo, R., Kuffa, P., Martínez-Colón, G., Smith, B. L., Rajendiran, T. M., & Núñez, G. (2013). K+ Efflux Is the Common Trigger of NLRP3 Inflammasome Activation by Bacterial Toxins and Particulate Matter. Immunity, 38(6), 1142–1153. https://doi.org/10.1016/j.immuni.2013.05.016

Mussolino, C., Morbitzer, R., Lütge, F., Dannemann, N., Lahaye, T., & Cathomen, T. (2011). A novel TALE nuclease scaffold enables high genome editing activity in combination with low toxicity. Nucleic

Nakamura, K., Okamura, H., Wada, M., Nagata, K., & Tamura, T. (1989). Endotoxin-induced serum factor that stimulates gamma interferon production. Infection and Immunity, 57(2), 590–595.

Nathan, C. F., Murray, H. W., Wlebe, I. E., & Rubin, B. Y. (1983). Identification of interferon-γ, as the lymphokine that activates human macrophage oxidative metabolism and antimicrobial activity. Journal of Experimental Medicine, 158(3), 670–689. https://doi.org/10.1084/jem.158.3.670

Nelms, K. A., & Goodnow, C. C. (2001). Genome-Wide ENU Mutagenesis to Reveal Immune Regulators. Immunity, 15(3), 409–418. https://doi.org/10.1016/S1074-7613(01)00199-6

Nelson, M. M., Jones, A. R., Carmen, J. C., Sinai, A. P., Burchmore, R., & Wastling, J. M. (2008). Modulation of the host cell proteome by the intracellular apicomplexan parasite Toxoplasma gondii. Infection and Immunity, 76(2), 828–844. https://doi.org/10.1128/IAI.01115-07

Ngo, C. C., & Man, S. M. (2017). Mechanisms and functions of guanylate-binding proteins and related interferon-inducible GTPases: Roles in intracellular lysis of pathogens. Cellular Microbiology, 19(12), e12791. https://doi.org/10.1111/cmi.12791

Ngo, V. N., Davis, R. E., Lamy, L., Yu, X., Zhao, H., Lenz, G., … Staudt, L. M. (2006). A loss-of-function RNA interference screen for molecular targets in cancer. Nature, 441(1), 106–110. https://doi.org/10.1038/nature04687

Niedelman, W., Sprokholt, J. K., Clough, B., Frickel, E.-M., & Saeij, J. P. J. (2013). Cell death of gamma interferon-stimulated human fibroblasts upon Toxoplasma gondii infection induces early parasite egress and limits parasite replication. Infection and Immunity, 81(12), 4341–4349. https://doi.org/10.1128/IAI.00416-13

Nishikawa, Y., Ibrahim, H. M., Kameyama, K., Shiga, I., Hiasa, J., & Xuan, X. (2011). Host Cholesterol Synthesis Contributes to Growth of Intracellular Toxoplasma gondii in Macrophages. In J. Vet. Med. Sci (Vol. 73). Retrieved from www.toxodb.org

Nishiyama, M., Oshikawa, K., Tsukada, Y. I., Nakagawa, T., Iemura, S. I., Natsume, T., … Nakayama, K. I. (2009). CHD8 suppresses p53-mediated apoptosis through histone H1 recruitment during early embryogenesis. Nature Cell Biology, 11(2), 172–182. https://doi.org/10.1038/ncb1831

Noad, J., Von Der Malsburg, A., Pathe, C., Michel, M. A., Komander, D., & Randow, F. (2017). LUBAC-synthesized linear ubiquitin chains restrict cytosol-invading bacteria by activating autophagy and NF-κB. Nature Microbiology, 2. https://doi.org/10.1038/nmicrobiol.2017.63

Nolan, P. M., Peters, J., Strivens, M., Rogers, D., Hagan, J., Spurr, N., … Hunter, J. (2000). A systematic, genome-wide, phenotype-driven mutagenesis programme for gene function studies in the mouse. Nature Genetics, 25(4), 440–443. https://doi.org/10.1038/78140

Nonaka, T., Kuwae, A., Sasakawa, C., & Imajoh-Ohmi, S. (1999). Shigella flexneri YSH6000 induces two types of cell death, apoptosis and oncosis, in the differentiated human monoblastic cell line U937. FEMS Microbiology Letters, 174(1), 89–95. https://doi.org/10.1111/j.1574-6968.1999.tb13553.x

Norman, M., Rivers, C., Lee, Y. B., Idris, J., & Uney, J. (2016). The increasing diversity of functions attributed to the SAFB family of RNA-/DNA-binding proteins. Biochemical Journal, Vol. 473, pp. 4271–4288. https://doi.org/10.1042/BCJ20160649

Nowak, D. E., Tian, B., Jamaluddin, M., Boldogh, I., Vergara, L. A., Choudhary, S., & Brasier, A. R. (2008). RelA Ser276 Phosphorylation Is Required for Activation of a Subset of NF- B-Dependent Genes by Recruiting Cyclin-Dependent Kinase 9/Cyclin T1 Complexes. Molecular and Cellular Biology, 28(11), 3623–3638. https://doi.org/10.1128/mcb.01152-07

O'Connell, R. M., Saha, S. K., Vaidya, S. A., Bruhn, K. W., Miranda, G. A., Zarnegar, B., … Cheng, G. (2004). Type I interferon production enhances susceptibility to Listeria monocytogenes infection. Journal of Experimental Medicine, 200(4), 437–445. https://doi.org/10.1084/jem.20040712

O'Neill, L. A. J., Kishton, R. J., & Rathmell, J. (2016). A guide to immunometabolism for immunologists. Nature Reviews. Immunology, 16(9), 553–565. https://doi.org/10.1038/nri.2016.70

Obara, K., & Ohsumi, Y. (2008). Dynamics and function of PtdIns(3)P in autophagy. Autophagy, 4(7), 952–954. https://doi.org/10.4161/auto.6790

Ochman, H., & Groisman, E. A. (1996). Distribution of Pathogenicity Islands in. Microbiology, 64(12), 5410–5412.

Ogawa, M., Yoshimori, T., Suzuki, T., Sagara, H., Mizushima, N., & Sasakawa, C. (2005). Escape of intracellular Shigella from autophagy. Science, 307(5710), 727–731. https://doi.org/10.1126/science.1106036

Ohshima, J., Lee, Y., Sasai, M., Saitoh, T., Ma, J. S., Kamiyama, N., … Yamamoto, M. (2014). Role of Mouse and Human Autophagy Proteins in IFN-γ–Induced Cell-Autonomous Responses against Toxoplasma gondii. The Journal of Immunology, 192(7), 3328–3335. https://doi.org/10.4049/JIMMUNOL.1302822

Ong, Y. C., Reese, M. L., & Boothroyd, J. C. (2010). Toxoplasma Rhoptry Protein 16 (ROP16) subverts host function by direct tyrosine phosphorylation of STAT6. Journal of Biological Chemistry, 285(37), 28731–28740. https://doi.org/10.1074/jbc.M110.112359

Orning, P., Weng, D., Starheim, K., Ratner, D., Best, Z., Lee, B., … Lien, E. (2018). Pathogen blockade of TAK1 triggers caspase-8–dependent cleavage of gasdermin D and cell death. Science, eaau2818. https://doi.org/10.1126/science.aau2818

Palladino, M. A., Bahjat, F. R., Theodorakis, E. A., & Moldawer, L. L. (2003). Anti-TNF-α therapies: The next generation. Nature Reviews Drug Discovery, Vol. 2, pp. 736–746. https://doi.org/10.1038/nrd1175

Pankiv, S., Clausen, T. H., Lamark, T., Brech, A., Bruun, J.-A. A., Outzen, H., … Johansen, T. (2007). p62/SQSTM1 binds directly to Atg8/LC3 to facilitate degradation of ubiquitinated protein aggregates by autophagy. Journal of Biological Chemistry, 282(33), 24131–24145. https://doi.org/10.1074/jbc.M702824200

Parham, P., Barnstable, C. J., & Bodmer, W. F. (1979). Use of a monoclonal antibody (W6/32) in structural studies of HLA-A,B,C, antigens. Journal of Immunology (Baltimore, Md. : 1950), 123(1), 349. Retrieved from http://www.ncbi.nlm.nih.gov/pubmed/87477

Park, B.S., Song, D.H., Kim, H.M., Choi, B.S., Lee, H., Lee, J.O. (2009). The structural basis of lipopolysaccharide recognition by the TLR4-MD-2 complex. Nature, 458(7242), pp.1191-5. https://doi.org/10.1038/nature07830

Park, R. J., Wang, T., Koundakjian, D., Hultquist, J. F., Lamothe-Molina, P., Monel, B., … Walker, B. D. (2016). A genome-wide CRISPR screen identifies a restricted set of HIV host dependency factors. Nature Genetics, 49(2), 193–203. https://doi.org/10.1038/ng.3741

Parnas, O., Jovanovic, M., Eisenhaure, T. M., Herbst, R. H., Dixit, A., Ye, C. J., … Regev, A. (2015). A Genome-wide CRISPR Screen in Primary Immune Cells to Dissect Regulatory Networks. Cell, 162(3), 675–686. https://doi.org/10.1016/j.cell.2015.06.059

Pastre, M. J., Casagrande, L., Gois, M. B., Pereira-Severi, L. S., Miqueloto, C. A., Garcia, J. L., … de Mello Gonçales Sant'Ana, D. (2019). Toxoplasma gondii causes increased ICAM-1 and serotonin expression in the jejunum of rats 12 h after infection. Biomedicine and Pharmacotherapy, 114. https://doi.org/10.1016/j.biopha.2019.108797

Pattanayak, V., Ramirez, C. L., Joung, J. K., & Liu, D. R. (2011). Revealing off-target cleavage specificities of zinc-finger nucleases by in vitro selection. Nature Methods, 8(9), 765–772. https://doi.org/10.1038/nmeth.1670

Paz, I., Sachse, M., Dupont, N., Mounier, J., Cederfur, C., Enninga, J., … Sansonetti, P. (2010). Galectin-3, a marker for vacuole lysis by invasive pathogens. Cellular Microbiology, 12(4), 530–544. https://doi.org/10.1111/j.1462-5822.2009.01415.x

Pelloux, H., Ricard, J., Bracchi, V., Markowicz, Y., Verna, J. M., & Ambroise-Thomas, P. (1994). Tumor necrosis factor alpha, interleukin 1 alpha, and interleukin 6 mRNA expressed by human astrocytoma cells after infection by three different strains of Toxoplasma gondii. Parasitology Research, 80(4), 276. https://doi.org/10.1007/bf02351866

Pfefferkorn, E. R. (1984). Interferon gamma blocks the growth of Toxoplasma gondii in human fibroblasts by inducing the host cells to degrade tryptophan. Proceedings of the National Academy of Sciences of the United States of America, 81(3), 908–912. https://doi.org/10.1073/pnas.81.3.908

Pfefferkorn, E. R., & Guyre, P. M. (1984). Inhibition of growth of Toxoplasma gondii in cultured fibroblasts by human recombinant gamma interferon. Infection and Immunity, 44(2), 211–216. Retrieved from http://www.ncbi.nlm.nih.gov/pubmed/6425215

Piccioni, F., Younger, S. T., & Root, D. E. (2018). Pooled lentiviral-delivery genetic screens. Current Protocols in Molecular Biology, 2018, 32.1.1-32.1.21. https://doi.org/10.1002/cpmb.52

Pierini, R., Juruj, C., Perret, M., Jones, C. L., Mangeot, P., Weiss, D. S., & Henry, T. (2012). AIM2/ASC triggers caspase-8-dependent apoptosis in Francisella-infected caspase-1-deficient macrophages. Cell Death and Differentiation, 19(10), 1709–1721. https://doi.org/10.1038/cdd.2012.51

Pilla, D. M., Hagar, J. A., Haldar, A. K., Mason, A. K., Degrandi, D., Pfeffer, K., … Coers, J. (2014). Guanylate binding proteins promote caspase-11-dependent pyroptosis in response to cytoplasmic LPS. Proceedings of the National Academy of Sciences, 111(16), 6046–6051. https://doi.org/10.1073/pnas.1321700111

Pilla-Moffett, D., Barber, M.F., Taylor, G.A., Coers, J. (2016). Interferon-Inducible GTPases in Host Resistance, Inflammation and Disease. Journal of Molecular Biology, 428(17), 3495-513. https://doi.org/10.1016/j.jmb.2016.04.032

Platanias, L. C. (2005). MECHANISMS OF TYPE-I AND TYPE-II-INTERFERON-MEDIATED SIGNALLING. 375–385. https://doi.org/10.1038/nri1604

Pobezinskaya, Y. L., Kim, Y. S., Choksi, S., Morgan, M. J., Li, T., Liu, C., & Liu, Z. (2008). The function of TRADD in signaling through tumor necrosis factor receptor 1 and TRIF-dependent Toll-like receptors. Nature Immunology, 9(9), 1047–1054. https://doi.org/10.1038/ni.1639

Poon, I. K. H., Hulett, M. D., & Parish, C. R. (2010, March). Molecular mechanisms of late apoptotic/necrotic cell clearance. Cell Death and Differentiation, Vol. 17, pp. 381–397. https://doi.org/10.1038/cdd.2009.195

Prevosto, C., Usmani, M. F., McDonald, S., Gumienny, A. M., Key, T., Goodman, R. S., … Busch, R. (2016). Allele-independent turnover of human leukocyte antigen (HLA) class Ia molecules. PLoS ONE, 11(8). https://doi.org/10.1371/journal.pone.0161011

Price, J. V., & Vance, R. E. (2014, November 20). The Macrophage Paradox. Immunity, Vol. 41, pp. 685–693. https://doi.org/10.1016/j.immuni.2014.10.015

Qiu, S., Liu, J., & Xing, F. (2017). 'Hints' in the killer protein gasdermin D: unveiling the secrets of gasdermins driving cell death. Cell Death and Differentiation, 24(4), 588–596. https://doi.org/10.1038/cdd.2017.24

Qu, X., Zou, Z., Sun, Q., Luby-Phelps, K., Cheng, P., Hogan, R.N., Gilpin, C., Levine, B. (2007). Autophagy gene-dependent clearance of apoptotic cells during embryonic development. Cell, 128, 931–946. https://doi.org/10.1016/j.cell.2006.12.044

Quezada, C. M., Hicks, S. W., Galán, J. E., & Erec Stebbins, C. (2009). A family of Salmonella virulence factors functions as a distinct class of autoregulated E3 ubiquitin ligases. Proceedings of the National Academy of Sciences of the United States of America, 106(12), 4864–4869. https://doi.org/10.1073/pnas.0811058106

Rabinowitz, J. D., & White, E. (2010, December 3). Autophagy and metabolism. Science, Vol. 330, pp. 1344–1348. https://doi.org/10.1126/science.1193497

Radke, J. R., Guerini, M. N., Jerome, M., & White, M. W. (2003). A change in the premitotic period of the cell cycle is associated with bradyzoite differentiation in Toxoplasma gondii. Molecular and Biochemical Parasitology, 131(2), 119–127. https://doi.org/10.1016/S0166-6851(03)00198-1

Radke, J. R., Striepen, B., Guerini, M. N., Jerome, M. E., Roos, D. S., & White, M. W. (2001). Defining the cell cycle for the tachyzoite stage of Toxoplasma gondii. Molecular and Biochemical Parasitology, 115(2), 165–175. https://doi.org/10.1016/S0166-6851(01)00284-5

Rahighi, S., Ikeda, F., Kawasaki, M., Akutsu, M., Suzuki, N., Kato, R., … Dikic, I. (2009). Specific recognition of linear ubiquitin chains by NEMO is important for NF-kappaB activation. Cell, 136(6), 1098–1109. https://doi.org/10.1016/j.cell.2009.03.007

Rahimi, P., Iranpur Mobarakeh, V., Kamalzare, S., SajadianFard, F., Vahabpour, R., & Zabihollahi, R. (2018). Comparison of transfection efficiency of polymer-based and lipid-based transfection reagents. Bratisl Med J, 119(11), 701–705. https://doi.org/10.4149/BLL_2018_125

Ramirez-Solis, R., Liu, P., & Bradley, A. (1995). Chromosome engineering in mice. Nature, 378(6558), 720–724. https://doi.org/10.1038/378720a0

Ramirez, M. L. G., & Salvesen, G. S. (2018, October 1). A primer on caspase mechanisms. Seminars in Cell and Developmental Biology, Vol. 82, pp. 79–85. https://doi.org/10.1016/j.semcdb.2018.01.002

Randow, F., MacMicking, J. D., & James, L. C. (2013). Cellular self-defense: how cell-autonomous immunity protects against pathogens. Science (New York, N.Y.), 340(6133), 701–706. https://doi.org/10.1126/science.1233028

Randow, F., & Youle, R. J. (2014). Self and Nonself: How Autophagy Targets Mitochondria and Bacteria. Cell Host & Microbe, 15(4), 403–411. https://doi.org/10.1016/J.CHOM.2014.03.012

Rathinam, V. A. K., Zhao, Y., & Shao, F. (2019). Innate immunity to intracellular LPS. Nature Immunology, 20(5), 527–533. https://doi.org/10.1038/s41590-019-0368-3

Rathinam, V. A. K. K., Vanaja, S. K., & Fitzgerald, K. A. (2012). Regulation of inflammasome signaling. Nature Immunology, 13(4), 333–342. https://doi.org/10.1038/ni.2237

Rathinam, V. A. K., Jiang, Z., Waggoner, S. N., Sharma, S., Cole, L. E., Waggoner, L., … Fitzgerald, K. A. (2010). The AIM2 inflammasome is essential for host defense against cytosolic bacteria and DNA viruses. Nature Immunology, 11(5), 395–402. https://doi.org/10.1038/ni.1864

Rauch, I., Deets, K. A., Ji, D. X., von Moltke, J., Tenthorey, J. L., Lee, A. Y., … Vance, R. E. (2017). NAIP-NLRC4 Inflammasomes Coordinate Intestinal Epithelial Cell Expulsion with Eicosanoid and IL-18 Release via Activation of Caspase-1 and -8. Immunity, 46(4), 649–659. https://doi.org/10.1016/j.immuni.2017.03.016

Ravenhill, B. J., Boyle, K. B., von Muhlinen, N., Ellison, C. J., Masson, G. R., Otten, E. G., … Randow, F. (2019). The Cargo Receptor NDP52 Initiates Selective Autophagy by Recruiting the ULK Complex to Cytosol-Invading Bacteria. Molecular Cell, 74(2), 320-329.e6. https://doi.org/10.1016/j.molcel.2019.01.041

Rawet Slobodkin, M., & Elazar, Z. (2013). The Atg8 family: Multifunctional ubiquitin-like key regulators of autophagy. Essays in Biochemistry, 55(1), 51–64. https://doi.org/10.1042/BSE0550051

Reijerkerk, A., Kooij, G., van der Pol, S. M. A., Khazen, S., Dijkstra, C. D., & de Vries, H. E. (2006). Diapedesis of monocytes is associated with MMP-mediated occludin disappearance in brain endothelial cells. The FASEB Journal, 20(14), 2550–2552. https://doi.org/10.1096/fj.06-6099fje

Reljic, R. (2007, May). IFN-γ therapy of tuberculosis and related infections. Journal of Interferon and Cytokine Research, Vol. 27, pp. 353–363. https://doi.org/10.1089/jir.2006.0103

Rezaei, F., Sharif, M., Sarvi, S., Hejazi, S. H., Aghayan, S., Pagheh, A. S., … Daryani, A. (2019, October 1). A systematic review on the role of GRA proteins of Toxoplasma gondii in host immunization. Journal of Microbiological Methods, Vol. 165. https://doi.org/10.1016/j.mimet.2019.105696

Rhee, H. W., Zou, P., Udeshi, N. D., Martell, J. D., Mootha, V. K., Carr, S. A., & Ting, A. Y. (2013). Proteomic mapping of mitochondria in living cells via spatially restricted enzymatic tagging. Science, 339(6125), 1328–1331. https://doi.org/10.1126/science.1230593

Riedl, S. J., & Salvesen, G. S. (2007). The apoptosome: Signalling platform of cell death. Nature Reviews Molecular Cell Biology, 8(5), 405–413. https://doi.org/10.1038/nrm2153

Roesler, J., Kofink, B., Wendisch, J., Heyden, S., Paul, D., … Rösen-Wolff, A. (1999). Listeria monocytogenes and recurrent mycobacterial infections in a child with complete interferon-gamma-receptor (IFNgammaR1) deficiency: mutational analysis and evaluation of therapeutic options. Experimental Hematology, 27(9), 1368-74. https://doi.org/10.1016/s0301-472x(99)00077-6

Rogov, V. V., Suzuki, H., Fiskin, E., Wild, P., Kniss, A., Rozenknop, A., … Dötsch, V. (2013). Structural basis for phosphorylation-triggered autophagic clearance of Salmonella. Biochemical Journal, 454(3), 459–466. https://doi.org/10.1042/BJ20121907

Rohde, J. R., Breitkreutz, A., Chenal, A., Sansonetti, P. J., & Parsot, C. (2007). Type III Secretion Effectors of the IpaH Family Are E3 Ubiquitin Ligases. Cell Host and Microbe, 1(1), 77–83. https://doi.org/10.1016/j.chom.2007.02.002

Rook, G. A. W. (2012). Hygiene hypothesis and autoimmune diseases. Clinical Reviews in Allergy and Immunology, 42(1), 5–15. https://doi.org/10.1007/s12016-011-8285-8

Rottenberg, M. E., Gigliotti-Rothfuchs, A., & Wigzell, H. (2002). The role of IFN-gamma in the outcome of chlamydial infection. Current Opinion in Immunology, 14(4), 444–451. https://doi.org/10.1016/s0952-7915(02)00361-8

Rouet, P., Smih, F., & Jasin, M. (1994). Introduction of double-strand breaks into the genome of mouse cells by expression of a rare-cutting endonuclease. Molecular and Cellular Biology, 14(12), 8096–8106. https://doi.org/10.1128/mcb.14.12.8096

Rubin, G. M., & Lewis, E. B. (2000). A brief history of Drosophila's contributions to genome research. Science, Vol. 287, pp. 2216–2218. https://doi.org/10.1126/science.287.5461.2216

Rühl, S., & Broz, P. (2015). Caspase-11 activates a canonical NLRP3 inflammasome by promoting K+ efflux. European Journal of Immunology, 45(10), 2927–2936. https://doi.org/10.1002/eji.201545772

Rühl, S., & Broz, P. (2016). The gasdermin-D pore: Executor of pyroptotic cell death. Oncotarget, 7(36), 57481–57482. https://doi.org/10.18632/oncotarget.11421

Rühl, S., Shkarina, K., Demarco, B., Heilig, R., Santos, J. C., & Broz, P. (2018). ESCRT-dependent membrane repair negatively regulates pyroptosis downstream of GSDMD activation. Science, 362(6417), 956–960. https://doi.org/10.1126/SCIENCE.AAR7607

Russo, A. J., Behl, B., Banerjee, I., & Rathinam, V. A. K. (2018). Emerging Insights into Noncanonical Inflammasome Recognition of Microbes. Journal of Molecular Biology, 430(2), 207–216. https://doi.org/10.1016/J.JMB.2017.10.003

Rüter, C., Lubos, M. L., Norkowski, S., & Schmidt, M. A. (2018, October 1). All in—Multiple parallel strategies for intracellular delivery by bacterial pathogens. International Journal of Medical Microbiology, Vol. 308, pp. 872–881. https://doi.org/10.1016/j.ijmm.2018.06.007

Ryu, J. K., Kim, S. J., Rah, S. H., Kang, J. I., Jung, H. E., Lee, D., … Kim, H. M. (2017). Reconstruction of LPS Transfer Cascade Reveals Structural Determinants within LBP, CD14, and TLR4-MD2 for Efficient LPS Recognition and Transfer. Immunity, 46(1), 38–50. https://doi.org/10.1016/j.immuni.2016.11.007

Sadler, A. J., & Williams, B. R. G. (2008, July). Interferon-inducible antiviral effectors. Nature Reviews Immunology, Vol. 8, pp. 559–568. https://doi.org/10.1038/nri2314

Saeij, J. P. J., Boyle, J. P., & Boothroyd, J. C. (2005). Differences among the three major strains of Toxoplasma gondii and their specific interactions with the infected host. Trends in Parasitology, 21(10), 476–481. https://doi.org/10.1016/j.pt.2005.08.001

Saeij, J.P.J., Coller, S., Boyle, J.P., Jerome, M.E., White, M.W., Boothroyd, J.C. (2007). Toxoplasma co-opts host gene expression by injection of a polymorphic kinase homologue. Nature, 445, 324–327. https://doi.org/10.1038/nature05395

Saeij, J. P., & Frickel, E.-M. (2017). Exposing Toxoplasma gondii hiding inside the vacuole: a role for GBPs, autophagy and host cell death. Current Opinion in Microbiology, 40, 72–80. https://doi.org/10.1016/J.MIB.2017.10.021

Salcedo, S. P., & Holden, D. W. (2003). SseG, a virulence protein that targets Salmonella to the Golgi network. EMBO Journal, 22(19), 5003–5014. https://doi.org/10.1093/emboj/cdg517

Salvesen, G. S., & Dixit, V. M. (1999). Caspase activation: The induced-proximity model. Proceedings of the National Academy of Sciences, 96(20), 10964–10967. https://doi.org/10.1073/PNAS.96.20.10964

Samarajiwa, S. A., Forster, S., Auchettl, K., & Hertzog, P. J. (2009). INTERFEROME: the database of interferon regulated genes. Nucleic Acids Research, 37. https://doi.org/10.1093/nar/gkn732

Sangaré, L. O., Yang, N., Konstantinou, E. K., Lu, D., Mukhopadhyay, D., Young, L. H., & Saeij, J. P. J. (2019). Toxoplasma GRA15 activates the NF-Kb pathway through interactions with TNF receptor-associated factors. MBio, 10(4). https://doi.org/10.1128/mbio.00808-19

Sanjuan, M., Dillon, C., Tait, S. et al. (2007). Toll-like receptor signalling in macrophages links the autophagy pathway to phagocytosis. Nature 450, 1253–1257. https://doi.org/10.1038/nature06421

Santos, J. C., Boucher, D., Schneider, L. K., Demarco, B., Dilucca, M., Shkarina, K., … Broz, P. (2020). Human GBP1 binds LPS to initiate assembly of a caspase-4 activating platform on cytosolic bacteria. Nature Communications, 11(1), 3276. https://doi.org/10.1038/s41467-020-16889-z

Santos, J. C., & Broz, P. (2018). Sensing of invading pathogens by GBPs: At the crossroads between cell-autonomous and innate immunity. Journal of Leukocyte Biology. https://doi.org/10.1002/JLB.4MR0118-038R

Santos, J. C., Dick, M. S., Lagrange, B., Degrandi, D., Pfeffer, K., Yamamoto, M., … Broz, P. (2018). LPS targets host guanylate-binding proteins to the bacterial outer membrane for non-canonical inflammasome activation. The EMBO Journal, 37(4). https://doi.org/10.15252/embj.201798089

Sanz, L., Diaz–Meco, M. T., Nakano, H., & Moscat, J. (2000). The atypical PKC-interacting protein p62 channels NF-kappa B activation by the IL-1-TRAF6 pathway. The EMBO Journal, 19(7), 1576–1586. https://doi.org/10.1093/emboj/19.7.1576

Sarasin-Filipowicz, M., Oakeley, E. J., Duong, F. H. T., Christen, V., Terracciano, L., Filipowicz, W., & Heim, M. H. (2008). Interferon signaling and treatment outcome in chronic hepatitis C. Proceedings of the National Academy of Sciences of the United States of America, 105(19), 7034–7039. https://doi.org/10.1073/pnas.0707882105

Sasai, M., Pradipta, A., & Yamamoto, M. (2018). Host immune responses to Toxoplasma gondii. International Immunology, 30(3), 113–119. https://doi.org/10.1093/intimm/dxy004

Scanga, C. A., Aliberti, J., Jankovic, D., Tilloy, F., Bennouna, S., Denkers, E. Y., … Sher, A. (2002). MyD88 Is Required for Resistance to Toxoplasma gondii Infection and Regulates Parasite-

Induced IL-12 Production by Dendritic Cells . The Journal of Immunology, 168(12), 5997–6001. https://doi.org/10.4049/jimmunol.168.12.5997

Schaeffer, V., Akutsu, M., Olma, M. H., Gomes, L. C., Kawasaki, M., & Dikic, I. (2014). Binding of OTULIN to the PUB Domain of HOIP Controls NF-kB Signaling. 349–361. https://doi.org/10.1016/j.molcel.2014.03.016

Schatz, D. G., & Ji, Y. (2011, April). Recombination centres and the orchestration of V(D)J recombination. Nature Reviews Immunology, Vol. 11, pp. 251–263. https://doi.org/10.1038/nri2941

Schauvliege, R., Vanrobaeys, J., Schotte, P., & Beyaert, R. (2002). Caspase-11 gene expression in response to lipopolysaccharide and interferon-γ requires nuclear factor-κB and signal transducer and activator of transcription (STAT) 1. Journal of Biological Chemistry, 277(44), 41624–41630. https://doi.org/10.1074/jbc.M207852200

Schindelin, J., Arganda-Carreras, I., Frise, E., Kaynig, V., Longair, M., Pietzsch, T., … Cardona, A. (2012). Fiji: An open-source platform for biological-image analysis. Nature Methods, Vol. 9, pp. 676–682. https://doi.org/10.1038/nmeth.2019

Schoggins, J. W., & Rice, C. M. (2011). Interferon-stimulated genes and their antiviral effector functions. Current Opinion in Virology, Vol. 1, pp. 519–525. https://doi.org/10.1016/j.coviro.2011.10.008

Schuster, A., Erasimus, H., Fritah, S., Nazarov, P. V., van Dyck, E., Niclou, S. P., & Golebiewska, A. (2019, January 1). RNAi/CRISPR Screens: from a Pool to a Valid 'Hit'. Trends in Biotechnology, Vol. 37, pp. 38-55Schuster. https://doi.org/10.1016/j.tibtech.2018.08.002

Scorza, T., D'Souza, S., Laloup, M., Dewit, J., De Braekeleer, J., Verschueren, H., … Jongert, E. (2003). A GRA1 DNA vaccine primes cytolytic CD8+ T cells to control acute Toxoplasma gondii infection. Infection and Immunity, 71(1), 309–316. https://doi.org/10.1128/IAI.71.1.309-316.2003

Selleck, E.M., Fentress, S.J., Beatty, W.L., Degrandi, D., Pfeffer, K., Virgin, H.W., Macmicking, J.D., Sibley, L.D. (2013). Guanylate-binding protein 1 (Gbp1) contributes to cell-autonomous immunity against Toxoplasma gondii. PLoS Pathogens, 9:e1003320. https://doi.org/10.1371/journal.ppat.1003320

Selleck, E. M., Orchard, R. C., Lassen, K. G., Beatty, W. L., Xavier, R. J., Levine, B., … David Sibley, L. (2015). A noncanonical autophagy pathway restricts toxoplasma gondii growth in a strain-specific manner in IFN-γ-activated human cells. MBio, 6(5). https://doi.org/10.1128/mBio.01157-15

Sellin, M. E., Müller, A. A., Felmy, B., Dolowschiak, T., Diard, M., Tardivel, A., … Hardt, W. D. (2014). Epithelium-intrinsic NAIP/NLRC4 inflammasome drives infected enterocyte expulsion to restrict salmonella replication in the intestinal mucosa. Cell Host and Microbe, 16(2), 237–248. https://doi.org/10.1016/j.chom.2014.07.001

Seong, H. A., Jung, H., Kim, K. T., & Ha, H. (2007). 3-Phosphoinositide-dependent PDK1 negatively regulates transforming growth factor-β-induced signaling in a kinase-dependent manner through physical interaction with Smad proteins. Journal of Biological Chemistry, 282(16), 12272–12289. https://doi.org/10.1074/jbc.M609279200

Shalem, O., Sanjana, N. E., Hartenian, E., Shi, X., Scott, D. A., Mikkelsen, T. S., … Zhang, F. (2014). Genome-scale CRISPR-Cas9 knockout screening in human cells. Science (New York, N.Y.), 343(6166), 84–87. https://doi.org/10.1126/science.1247005

Sharma, S., TenOever, B. R., Grandvaux, N., Zhou, G. P., Lin, R., & Hiscott, J. (2003). Triggering the interferon antiviral response through an IKK-related pathway. Science, 300(5622), 1148–1151. https://doi.org/10.1126/science.1081315

Shea, J. E., Hensel, M., Gleeson, C., & Holden, D. W. (1996). Identification of a virulence locus encoding a second type III secretion system in Salmonella typhimurium. Proceedings of the National Academy of Sciences of the United States of America, 93(6), 2593–2597. https://doi.org/10.1073/pnas.93.6.2593

Shemesh, K., Iijima, Y., & Fridman, E. (2007). Targeted and non-targeted mutagenesis of metabolic pathways in medicinal plants and herbs. Israel Journal of Plant Sciences, Vol. 55, pp. 115–123. https://doi.org/10.1560/IJPS.55.2.115

Shenoy, A. R., Wellington, D. A., Kumar, P., Kassa, H., Booth, C. J., Cresswell, P., & MacMicking, J. D. (2012). GBP5 Promotes NLRP3 inflammasome assembly and immunity in mammals. Science, 336(6080), 481–485. https://doi.org/10.1126/science.1217141

Shi, J., Zhao, Y., Wang, K., Shi, X., Wang, Y., Huang, H., … Shao, F. (2015). Cleavage of GSDMD by inflammatory caspases determines pyroptotic cell death. Nature, 526(7575), 660–665. https://doi.org/10.1038/nature15514

Shi, J., Zhao, Y., Wang, Y., Gao, W., Ding, J., Li, P., … Shao, F. (2014). Inflammatory caspases are innate immune receptors for intracellular LPS. Nature, 514, 187–192. https://doi.org/10.1038/nature13683

Shu, H. D., Takeuchi, M., & Goeddel, D. V. (1996). The tumor necrosis factor receptor 2 signal transducers TRAF2 and c-IAP1 are components of the tumor necrosis factor receptor 1 signaling complex. Proceedings of the National Academy of Sciences of the United States of America, 93(24), 13973–13978. https://doi.org/10.1073/pnas.93.24.13973

Sibley, D. L. (2011). Invasion and intracellular survival by protozoan parasites. Immunological Reviews, Vol. 240, pp. 72–91. https://doi.org/10.1111/j.1600-065X.2010.00990.x

Sibley, L. D. (2004). Intracellular Parasite Invasion Strategies. Science, Vol. 304, pp. 248–253. https://doi.org/10.1126/science.1094717

Silva, N. M., Manzan, R. M., Carneiro, W. P., Milanezi, C. M., Silva, J. S., Ferro, E. A. V., & Mineo, J. R. (2010). Toxoplasma gondii: The severity of toxoplasmic encephalitis in C57BL/6 mice is associated with increased ALCAM and VCAM-1 expression in the central nervous system and higher blood-brain barrier permeability. Experimental Parasitology, 126(2), 167–177. https://doi.org/10.1016/j.exppara.2010.04.019

Simon, M. M., Moresco, E. M. Y., Bull, K. R., Kumar, S., Mallon, A. M., Beutler, B., & Potter, P. K. (2015). Current strategies for mutation detection in phenotype-driven screens utilising next generation sequencing. Mammalian Genome, Vol. 26, pp. 486–500. https://doi.org/10.1007/s00335-015-9603-x

Simonsen, A., & Tooze, S. A. (2009, September 21). Coordination of membrane events during autophagy by multiple class III PI3-kinase complexes. Journal of Cell Biology, Vol. 186, pp. 773–782. https://doi.org/10.1083/jcb.200907014

Sims, J. E., March, C. J., Cosman, D., Widmer, M. B., Macdonald, H. R., Mcmahan, C. J., … Dower, S. K. (1988). cDNA expression cloning of the IL-1 receptor, a member of the immunoglobulin superfamily. Science, 241(4865), 585–589. https://doi.org/10.1126/science.2969618

Singer, A. U., Rohde, J. R., Lam, R., Skarina, T., Kagan, O., DiLeo, R., … Savchenko, A. (2008). Structure of the Shigella T3SS effector IpaH defines a new class of E3 ubiquitin ligases. Nature Structural and Molecular Biology, 15(12), 1293–1301. https://doi.org/10.1038/nsmb.1511

Singh, R. P., Waldron, R. T., & Hahn, B. H. (2012). Genes, tolerance and systemic autoimmunity. Autoimmunity Reviews, Vol. 11, pp. 664–669. https://doi.org/10.1016/j.autrev.2011.11.017

Skurkovich, B. & Skurkovich, S. (2003). Anti-interferon-gamma antibodies in the treatment of autoimmune diseases. Current Opinion in Molecular Therapeutics, 5(1), 52-57

Slowicka, K., Vereecke, L., Mc Guire, C., Sze, M., Maelfait, J., Kolpe, A., … van Loo, G. (2016). Optineurin deficiency in mice is associated with increased sensitivity to Salmonella but does not affect proinflammatory NF-κB signaling. European Journal of Immunology, 46(4), 971–980. https://doi.org/10.1002/eji.201545863

Smit, J. J., Monteferrario, D., Noordermeer, S. M., Van Dijk, W. J., Van Der Reijden, B. A., & Sixma, T. K. (2012). The E3 ligase HOIP specifies linear ubiquitin chain assembly through its RING-IBR-RING domain and the unique LDD extension. EMBO Journal, 31(19), 3833–3844. https://doi.org/10.1038/emboj.2012.217

Smith, K. C., Neu, J. C., & Krassowska, W. (2004). Model of Creation and Evolution of Stable Electropores for DNA Delivery. *Biophysical Journal*, *86*, 2813–2826. https://doi.org/0006-3495/04/05/2813/14

Soldati, D., Dubremetz, J.F., Lebrun, M. (2001). Microneme proteins: structural and functional requirements to promote adhesion and invasion by the apicomplexan parasite Toxoplasma gondii. International Journal for Parasitology, 31(12),1293-302. https://doi.org/10.1016/s0020-7519(01)00257-0

Sollberger, G., Strittmatter, G. E., Kistowska, M., French, L. E., & Beer, H.-D. (2012). Caspase-4 Is Required for Activation of Inflammasomes. The Journal of Immunology, 188(4), 1992–2000. https://doi.org/10.4049/jimmunol.1101620

Sonda, S., Ting, L.-M., Novak, S., Kim, K., Maher, J. J., Farese, R. V, & Ernst, J. D. (2001). Cholesterol Esterification by Host and Parasite Is Essential for Optimal Proliferation of Toxoplasma gondii. THE JOURNAL OF BIOLOGICAL CHEMISTRY, 276(37), 34434–34440. https://doi.org/10.1074/jbc.M105025200

Srikanth, C. V., Mercado-Lubo, R., Hallstrom, K., McCormick, B. A. (2011). Salmonella effector proteins and host-cell responses. Cellular and molecular life sciences : CMLS, 68(22), 3687–3697. https://doi.org/10.1007/s00018-011-0841-0

Steele-Mortimer, O. (2008, February). The Salmonella-containing vacuole-Moving with the times. Current Opinion in Microbiology, Vol. 11, pp. 38–45. https://doi.org/10.1016/j.mib.2008.01.002

Steimle, A., Autenrieth, I. B., & Frick, J. S. (2016, August 1). Structure and function: Lipid A modifications in commensals and pathogens. International Journal of Medical Microbiology, Vol. 306, pp. 290–301. https://doi.org/10.1016/j.ijmm.2016.03.001

Steinfeldt, T., Könen-Waisman, S., Tong, L., Pawlowski, N., Lamkemeyer, T., Sibley, L. D., … Howard, J. C. (2010). Phosphorylation of Mouse Immunity-Related GTPase (IRG) Resistance Proteins Is an Evasion Strategy for Virulent Toxoplasma gondii. PLoS Biology, 8(12), e1000576. https://doi.org/10.1371/journal.pbio.1000576

Stelzer, S., Basso, W., Benavides Silván, J., Ortega-Mora, L.M., Maksimov, P., Gethmann, J., Conraths, F.J., Schares, G., (2019). Toxoplasma gondii infection and toxoplasmosis in farm

animals: Risk factors and economic impact. Food and Waterborne Parasitology, Vol. 15, e00037. https://doi.org/10.1016/j.fawpar.2019.e00037

Stolz, A., Ernst, A., & Dikic, I. (2014). Cargo recognition and trafficking in selective autophagy. Nature Cell Biology, 16(6), 495–501. https://doi.org/10.1038/ncb2979

Strezoska, Ž., Licon, A., Haimes, J., Spayd, K. J., Patel, K. M., Sullivan, K., … Vermeulen, A. (2012). Optimized PCR Conditions and Increased shRNA Fold Representation Improve Reproducibility of Pooled shRNA Screens. PLoS ONE, 7(8), e42341. https://doi.org/10.1371/journal.pone.0042341

Strowig, T., Henao-Mejia, J., Elinav, E., & Flavell, R. (2012, January 19). Inflammasomes in health and disease. Nature, Vol. 481, pp. 278–286. https://doi.org/10.1038/nature10759

Stuart, L. M., Paquette, N., & Boyer, L. (2013, March). Effector-triggered versus pattern-triggered immunity: How animals sense pathogens. Nature Reviews Immunology, Vol. 13, pp. 199–206. https://doi.org/10.1038/nri3398

Sugawara, K., Suzuki, N. N., Fujioka, Y., Mizushima, N., Ohsumi, Y., & Inagaki, F. (2004). The crystal structure of microtubule-associated protein light chain 3, a mammalian homologue of Saccharomyces cerevisiae Atg8. Genes to Cells : Devoted to Molecular & Cellular Mechanisms, 9(7), 611–618. https://doi.org/10.1111/j.1356-9597.2004.00750.x

Sukharev, S. 1, Klenchin, V. A., Serov, S. M., Chernomordik, L. V, & Chizmadzhev, Y. A. (1992). Electroporation and electrophoretic DNA transfer into cells The effect of DNA interaction with electropores. *Biophysical Journal*, *63*, 1320–1327. https://doi.org/0006-3495/92/11/1320/08

Sukhumavasi, W., Egan, C. E., Warren, A. L., Taylor, G. A., Fox, B. A., Bzik, D. J., & Denkers, E. Y. (2008). TLR Adaptor MyD88 Is Essential for Pathogen Control during Oral Toxoplasma gondii Infection but Not Adaptive Immunity Induced by a Vaccine Strain of the Parasite . The Journal of Immunology, 181(5), 3464–3473. https://doi.org/10.4049/jimmunol.181.5.3464

Suzuki, M., Hisamatsu, T., & Podolsky, D. K. (2003). Gamma interferon augments the intracellular pathway for lipopolysaccharide (LPS) recognition in human intestinal epithelial cells through coordinated up-regulation of LPS uptake and expression of the intracellular Toll-like receptor 4-MD-2 complex. Infection and Immunity, 71(6), 3503–3511. https://doi.org/10.1128/IAI.71.6.3503-3511.2003

Suzuki, Y., Orellana, M. A., Schreiber, R. D., & Remington, J. S. (1988). Interferon-γ: The major mediator of resistance against Toxoplasma gondii. Science, 240(4851), 516–518. https://doi.org/10.1126/science.3128869

Suzuki, Y., Sa, Q., Gehman, M., & Ochiai, E. (2011). Interferon-gamma- and perforin-mediated immune responses for resistance against Toxoplasma gondii in the brain. Expert Reviews in Molecular Medicine, 13. https://doi.org/10.1017/s1462399411002018

Takeuchi, A. (1967). Electron microscope studies of experimental Salmonella infection. I. Penetration into the intestinal epithelium by Salmonella typhimurium. American Journal of Pathology, 50(1), 109–136.

Takeuchi, O., & Akira, S. (2010). Pattern recognition receptors and inflammation. Cell, 140(6), 805–820. https://doi.org/10.1016/j.cell.2010.01.022

Takiuchi, T., Nakagawa, T., Tamiya, H., Fujita, H., Sasaki, Y., Saeki, Y., … Iwai, K. (2014). Suppression of LUBAC-mediated linear ubiquitination by a specific interaction between LUBAC and the deubiquitinases CYLD and OTULIN. Genes to Cells, 19(3), 254–272. https://doi.org/10.1111/gtc.12128

Tanaka, T., Narazaki, M., & Kishimoto, T. (2014). Il-6 in inflammation, Immunity, And disease. Cold Spring Harbor Perspectives in Biology, 6(10). https://doi.org/10.1101/cshperspect.a016295

Tang, X., Marciano, D. L., Leeman, S. E., Amar, S. (2005). LPS induces the interaction of a transcription factor, LPS-induced TNF-alpha factor, and STAT6(B) with effects on multiple cytokines. Proceedings of the National Academy of Sciences of the USA, 102(14), 5132-7. https://doi.org/10.1073/pnas.0501159102

Tanida, I. (2011). Autophagosome formation and molecular mechanism of autophagy. Antioxidants and Redox Signaling, Vol. 14, pp. 2201–2214. https://doi.org/10.1089/ars.2010.3482

Tanida, I., Ueno, T., & Kominami, E. (2004). LC3 conjugation system in mammalian autophagy. International Journal of Biochemistry and Cell Biology, Vol. 36, pp. 2503–2518. https://doi.org/10.1016/j.biocel.2004.05.009

Taylor, S., Barragan, A., Su, C., Fux, B., Fentress, S.J., Tang, K., … Sibley, L.D. (2006). A secreted serine-threonine kinase determines virulence in the eukaryotic pathogen Toxoplasma gondii. Science, 314, 1776–1780. https://doi.org/10.1126/science.1133643

Thomas, K. R., & Capecchi, M. R. (1986). Introduction of homologous DNA sequences into mammalian cells induces mutations in the cognate gene. Nature, 324(6092), 34–38. https://doi.org/10.1038/324034a0

Thomas, K. R., Folger, K. R., & Capecchi, M. R. (1986). High frequency targeting of genes to specific sites in the mammalian genome. Cell, 44(3), 419–428. https://doi.org/10.1016/0092-8674(86)90463-0

Thompson, B. A., Tremblay, V., Lin, G., & Bochar, D. A. (2008). CHD8 Is an ATP-Dependent Chromatin Remodeling Factor That Regulates -Catenin Target Genes. Molecular and Cellular Biology, 28(12), 3894–3904. https://doi.org/10.1128/mcb.00322-08

Thurston, T. L. M., Ryzhakov, G., Bloor, S., von Muhlinen, N., & Randow, F. (2009). The TBK1 adaptor and autophagy receptor NDP52 restricts the proliferation of ubiquitin-coated bacteria. Nature Immunology, 10(11), 1221. https://doi.org/10.1038/ni.1800

Thurston, T. L. M., Wandel, M. P., Von Muhlinen, N., Foeglein, Á., & Randow, F. (2012). Galectin 8 targets damaged vesicles for autophagy to defend cells against bacterial invasion. Nature, 482(7385), 414–418. https://doi.org/10.1038/nature10744

Tieleman, D. P. (2004). The molecular basis of electroporation. *BMC Biochemistry*, *5*, 1–12. https://doi.org/10.1186/1471-2091-5-10

Tokunaga, F., & Iwai, K. (2012). Linear ubiquitination: a novel NF-κB regulatory mechanism for inflammatory and immune responses by the LUBAC ubiquitin ligase complex. Endocrine Journal, 59(8), 641–652. https://doi.org/10.1507/endocrj.ej12-0148

Tokunaga, F., Nakagawa, T., Nakahara, M., Saeki, Y., Taniguchi, M., Sakata, S. I., … Iwai, K. (2011). SHARPIN is a component of the NF-κB-activating linear ubiquitin chain assembly complex. Nature, 471(7340), 633–636. https://doi.org/10.1038/nature09815

Triantafilou, K., Triantafilou, M., & Dedrick, R. L. (2001). A CD14-independent LPS receptor cluster. Nature Immunology, 2(4), 338–345. https://doi.org/10.1038/86342

Tsuda, E., Goto, M., Mochizuki, S. I., Yano, K., Kobayashi, F., Morinaga, T., & Higashio, K. (1997). Isolation of a novel cytokine from human fibroblasts that specifically inhibits osteoclastogenesis. Biochemical and Biophysical Research Communications, 234(1), 137–142. https://doi.org/10.1006/bbrc.1997.6603

Uhlen, M., Fagerberg, L., Hallstrom, B. M., Lindskog, C., Oksvold, P., Mardinoglu, A., … Ponten, F. (2015). Tissue-based map of the human proteome. Science, 347(6220), 1260419–1260419. https://doi.org/10.1126/science.1260419

Valente, G., Ozmen, L., Novelli, F., Geuna, M., Palestro, G., Forni, G., & Garotta, G. (1992). Distribution of interferon-γ receptor in human tissues. European Journal of Immunology, 22(9), 2403–2412. https://doi.org/10.1002/eji.1830220933

Van Dyke, K. (2011). Primary immunodeficiencies. XPharm: The Comprehensive Pharmacology Reference, 125(2), 1–8. https://doi.org/10.1002/jcop.21613

Van Opdenbosch, N., & Lamkanfi, M. (2019). Caspases in Cell Death, Inflammation, and Disease. Immunity, Vol. 50, pp. 1352–1364. https://doi.org/10.1016/j.immuni.2019.05.020

van Wijk, S. J. L., Fricke, F., Herhaus, L., Gupta, J., Hötte, K., Pampaloni, F., … Dikic, I. (2017). Linear ubiquitination of cytosolic Salmonella Typhimurium activates NF-κB and restricts bacterial proliferation. Nature Microbiology, 2, 17066. https://doi.org/10.1038/nmicrobiol.2017.66

Vanaja, S. K., Russo, A. J., Behl, B., Banerjee, I., Yankova, M., Deshmukh, S. D., & Rathinam, V. A. K. (2016). Bacterial Outer Membrane Vesicles Mediate Cytosolic Localization of LPS and Caspase-11 Activation. Cell, 165(5), 1106–1119. https://doi.org/10.1016/j.cell.2016.04.015

Vande Walle, L., & Lamkanfi, M. (2016, July 11). Pyroptosis. Current Biology, Vol. 26, pp. R568–R572. https://doi.org/10.1016/j.cub.2016.02.019

Varfolomeev, E., Goncharov, T., Fedorova, A. V., Dynek, J. N., Zobel, K., Deshayes, K., … Vucic, D. (2008). c-IAP1 and c-IAP2 are critical mediators of tumor necrosis factor α (TNFα)-induced NF-κB activation. Journal of Biological Chemistry, 283(36), 24295–24299. https://doi.org/10.1074/jbc.C800128200

Vaure, C., & Liu, Y. (2014). A comparative review of toll-like receptor 4 expression and functionality in different animal species. Frontiers in Immunology, 5, 316. https://doi.org/10.3389/fimmu.2014.00316

Velásquez, Z.D., Conejeros, I., Larrazabal, C., Kerner, K., Hermosilla, C., Taubert, A. (2019). Toxoplasma gondii-induced host cellular cell cycle dysregulation is linked to chromosome missegregation and cytokinesis failure in primary endothelial host cells. Scientific Reports, 9, 12496. https://doi.org/10.1038/s41598-019-48961-0

Viganò, E., Diamond, C. E., Spreafico, R., Balachander, A., Sobota, R. M., & Mortellaro, A. (2015). Human caspase-4 and caspase-5 regulate the one-step non-canonical inflammasome activation in monocytes. *Nature Communications*, *6*(1). https://doi.org/10.1038/ncomms9761

Vigneau, S., Rohrlich, P. S., Brahic, M., Bureau, J. F. (2003). Tmevpg1, a candidate gene for the control of Theiler's virus persistence, could be implicated in the regulation of gamma interferon. Journal of virology, 77(10), 5632–5638. https://doi.org/10.1128/jvi.77.10.5632-5638.2003

Vince, J. E., & Silke, J. (2016, June 1). The intersection of cell death and inflammasome activation. Cellular and Molecular Life Sciences, Vol. 73, pp. 2349–2367. https://doi.org/10.1007/s00018-016-2205-2

von Muhlinen, N., Akutsu, M., Ravenhill, B. J., Foeglein, Á., Bloor, S., Rutherford, T. J., … Randow, F. (2012). LC3C, Bound Selectively by a Noncanonical LIR Motif in NDP52, Is Required for Antibacterial Autophagy. Molecular Cell, 48(3), 329–342. https://doi.org/10.1016/j.molcel.2012.08.024

Vreugdenhil, A. C. E., Snoek, A. M. P., Greve, J. W. M., & Buurman, W. A. (2000). Lipopolysaccharide-Binding Protein Is Vectorially Secreted and Transported by Cultured Intestinal Epithelial Cells and Is Present in the Intestinal Mucus of Mice. The Journal of Immunology, 165(8), 4561–4566. https://doi.org/10.4049/jimmunol.165.8.4561

Wack, A., Terczyńska-Dyla, E., & Hartmann, R. (2015). Guarding the frontiers: the biology of type III interferons. Nature Immunology, 16(8), 802–809. https://doi.org/10.1038/ni.3212

Wagner, S., Carpentier, I., Rogov, V., Kreike, M., Ikeda, F., Löhr, F., … Beyaert, R. (2008). Ubiquitin binding mediates the NF-κB inhibitory potential of ABIN proteins. Oncogene, 27(26), 3739–3745. https://doi.org/10.1038/sj.onc.1211042

Walczak, H., & Krammer, P. H. (2000). The CD95 (APO-1/Fas) and the TRAIL (APO-2L) apoptosis systems. Experimental Cell Research, 256(1), 58–66. https://doi.org/10.1006/excr.2000.4840

Wandel, M.P., Kim, B.H., Park, E.S., Boyle, K.B., Nayak, K., Lagrange, B., … Randow, F. (2020) Guanylate-binding proteins convert cytosolic bacteria into caspase-4 signaling platforms. Nature Immunology, 21(8), 880-891. https://doi.org/10.1038/s41590-020-0697-2

Wandel, M. P., Pathe, C., Werner, E. I., Ellison, C. J., Boyle, K. B., von der Malsburg, A., … Randow, F. (2017). GBPs Inhibit Motility of Shigella flexneri but Are Targeted for Degradation by the Bacterial Ubiquitin Ligase IpaH9.8. Cell Host & Microbe, 22(4), 507-518.e5. https://doi.org/10.1016/j.chom.2017.09.007

Wang. (2006). Chapter 1: Introduction. https://doi.org/10.1271/nogeikagaku1924.76.48

Wang, L., Yan, J., Niu, H., Huang, R., & Wu, S. (2018a). Autophagy and Ubiquitination in Salmonella Infection and the Related Inflammatory Responses. Frontiers in Cellular and Infection Microbiology, 8(78). https://doi.org/10.3389/fcimb.2018.00078

Wang, S., & Fischer, P. M. (2008). Cyclin-dependent kinase 9: a key transcriptional regulator and potential drug target in oncology, virology and cardiology. Trends in Pharmacological Sciences, Vol. 29, pp. 302–313. https://doi.org/10.1016/j.tips.2008.03.003

Wang, S., Yuan, Y. H., Chen, N. H., & Wang, H. B. (2019). The mechanisms of NLRP3 inflammasome/pyroptosis activation and their role in Parkinson's disease. International Immunopharmacology, Vol. 67, pp. 458–464. https://doi.org/10.1016/j.intimp.2018.12.019

Wang, T., Larcher, L. M., Ma, L., & Veedu, R. N. (2018b). Systematic screening of commonly used commercial transfection reagents towards efficient transfection of single-stranded oligonucleotides. Molecules, 23(2564). https://doi.org/10.3390/molecules23102564

Wang, T., Birsoy, K., Hughes, N. W., Krupczak, K. M., Post, Y., Wei, J. J., … Bushman, F. D. (2015). Identification and characterization of essential genes in the human genome. Science (New York, N.Y.), 350(6264), 1096–1101. https://doi.org/10.1126/science.aac7041

Wang, T., Wei, J. J., Sabatini, D. M., & Lander, E. S. (2014). Genetic screens in human cells using the CRISPR/Cas9 system. Science, 343(6166), 80–84. https://doi.org/10.1126/science.1246981

Wang, Y., Gao, W., Shi, X., Ding, J., Liu, W., He, H., … Shao, F. (2017). Chemotherapy drugs induce pyroptosis through caspase-3 cleavage of a gasdermin. Nature Publishing Group, 547. https://doi.org/10.1038/nature22393

Watts, E., Zhao, Y., Dhara, A., Eller, B., Patwardhan, A., & Sinai, A. P. (2015). Novel approaches reveal that toxoplasma gondii bradyzoites within tissue cysts are dynamic and replicating entities in vivo. MBio, 6(5). https://doi.org/10.1128/mBio.01155-15

Wei, S., Nandi, S., Chitu, V., Yeung, Y.G., Yu, W., Huang, M., … Stanley, E.R. (2010). Functional overlap but differential expression of CSF-1 and IL-34 in their CSF-1 receptor-mediated regulation of myeloid cells. Journal of Leukocyte Biology, 88(3), 495-505. https://doi.org/10.1189/jlb.1209822

Weidel, W., Pelzer, H. (1964). Bagshaped macromolecules − a new outlook on bacterial cell walls. Advances in Enzymology, Vol.26, pp.193-232

Weilhammer, D. R., & Rasley, A. (2011). Genetic approaches for understanding virulence in Toxoplasma gondii. Briefings in Functional Genomics, 10(6), 365–373. https://doi.org/10.1093/bfgp/elr028

Wertz, I. E., & Dixit, V. M. (2010). Signaling to NF-kappaB: regulation by ubiquitination. Cold Spring Harbor Perspectives in Biology, Vol. 2. https://doi.org/10.1101/cshperspect.a003350

Whitfield, C., & Trent, M. S. (2014). Biosynthesis and Export of Bacterial Lipopolysaccharides. Annual Review of Biochemistry, 83(1), 99–128. https://doi.org/10.1146/annurev-biochem-060713-035600

Wiedenheft, B., Sternberg, S. H., & Doudna, J. A. (2012). RNA-guided genetic silencing systems in bacteria and archaea. *Nature*, *482*, 331–338. https://doi.org/10.1038/nature10886

Wild, P., Farhan, H., McEwan, D. G., Wagner, S., Rogov, V. V., Brady, N. R., … Dikic, I. (2011). Phosphorylation of the autophagy receptor optineurin restricts Salmonella growth. Science, 333(6039), 228–233. https://doi.org/10.1126/science.1205405

Winters, B. D., Eberlein, M., Leung, J., Needham, D. M., Pronovost, P. J., & Sevransky, J. E. (2010). Long-term mortality and quality of life in sepsis: A systematic review. Critical Care Medicine, 38(5), 1276–1283. https://doi.org/10.1097/CCM.0b013e3181d8cc1d

Wolfe, S. A., Nekludova, L., & Pabo, C. O. (2000). DNA Recognition by Cys2His2 Zinc Finger Proteins. Annual Review of Biophysics and Biomolecular Structure, 29(1), 183–212. https://doi.org/10.1146/annurev.biophys.29.1.183

Wu, B., & Guo, W. (2015). The exocyst at a glance. Journal of Cell Science, 128(15), 2957–2964. https://doi.org/10.1242/jcs.156398

Wujcicka, W., Wilczyński, J., Śpiewak, E., & Nowakowska, D. (2018). Genetic modifications of cytokine genes and Toxoplasma gondii infections in pregnant women. Microbial Pathogenesis, 121, 283–292. https://doi.org/10.1016/j.micpath.2018.05.048

Wullaert, A., Bonnet, M. C., & Pasparakis, M. (2011, January). NF-κB in the regulation of epithelial homeostasis and inflammation. Cell Research, Vol. 21, pp. 146–158. https://doi.org/10.1038/cr.2010.175

Xie, X., Li, F., Wang, Y., Wang, Y., Lin, Z., Cheng, X., … Pan, L. (2015). Molecular basis of ubiquitin recognition by the autophagy receptor CALCOCO2. Autophagy, 11(10), 1775–1789. https://doi.org/10.1080/15548627.2015.1082025

Yamaguchi, Y., Kurita-Ochiai, T., Kobayashi, R., Suzuki, T., & Ando, T. (2017). Regulation of the NLRP3 inflammasome in Porphyromonas gingivalis-accelerated periodontal disease. Inflammation Research, 66(1), 59–65. https://doi.org/10.1007/s00011-016-0992-4

Yamamoto, M., Standley, D. M., Takashima, S., Saiga, H., Okuyama, M., Kayama, H., … Takeda, K. (2009). A single polymorphic amino acid on Toxoplasma gondii kinase ROP16 determines the direct and strain-specific activation of Stat3. Journal of Experimental Medicine, 206(12), 2747–2760. https://doi.org/10.1084/jem.20091703

Yamamoto, M., Yamazaki, S., Uematsu, S., Sato, S., Hemmmi, H., Hoshino, K., … Akira, S. (2004). Regulation of Toll/IL-1-receptor-mediated gene expression by the inducible nuclear protein IκBζ. Nature, 430(6996), 218–222. https://doi.org/10.1038/nature02738

Yamano, S., Dai, J., & Moursi, A. M. (2010). Comparison of transfection efficiency of nonviral gene transfer reagents. Molecular Biotechnology, 46(3), 287–300. https://doi.org/10.1007/s12033-010-9302-5

Yang, J., Zhao, Y., & Shao, F. (2015). Non-canonical activation of inflammatory caspases by cytosolic LPS in innate immunity. Current Opinion in Immunology, 32, 78–83. https://doi.org/10.1016/j.coi.2015.01.007

Yang, Y., Cui, J., Xue, F., Zhang, C., Mei, Z., Wang, Y., … Xu, Z. Q. D. (2015). Pokemon (FBI-1) interacts with Smad4 to repress TGF-β-induced transcriptional responses. Biochimica et Biophysica Acta - Gene Regulatory Mechanisms, 1849(3), 270–281. https://doi.org/10.1016/j.bbagrm.2014.12.008

Yarovinsky, F., Zhang, D., Andersen, J. F., Bannenberg, G. L., Serhan, C. N., Hayden, M. S., … Sher, A. (2005). TLR11 activation of dendritic cells by a protozoan profilin-like protein. Science, 308(5728), 1626–1629. https://doi.org/10.1126/science.1109893

Yasuda, K., Nakanishi, K., & Tsutsui, H. (2019, February 1). Interleukin-18 in health and disease. International Journal of Molecular Sciences, Vol. 20. https://doi.org/10.3390/ijms20030649

Yi, Y.-S. (2017). Caspase-11 non-canonical inflammasome: a critical sensor of intracellular lipopolysaccharide in macrophage-mediated inflammatory responses. Immunology, 152, 207–217. https://doi.org/10.1111/imm.12787

Yoon, H. (2016). Bacterial Outer Membrane Vesicles as a Delivery System for Virulence Regulation. Journal of Microbiology and Biotechnology, 26(8), 1343–1347.

Yoshikawa, Y., Ogawa, M., Hain, T., Yoshida, M., Fukumatsu, M., Kim, M., … Sasakawa, C. (2009). Listeria monocytogenes ActA-mediated escape from autophagic recognition. Nature Cell Biology, 11(10), 1233–1240. https://doi.org/10.1038/ncb1967

Yoshimoto, T., Takeda, K., Tanaka, T., Ohkusu, K., Kashiwamura, S., Okamura, H., … Nakanishi, K. (1998). IL-12 up-regulates IL-18 receptor expression on T cells, Th1 cells, and B cells: synergism with IL-18 for IFN-gamma production. Journal of Immunology (Baltimore, Md. : 1950), 161(7), 3400–3407. Retrieved from http://www.ncbi.nlm.nih.gov/pubmed/9759857

Zajdenweber, M. E., Marshall, J. C., Logan, P., Bakalian, S., Belfort Neto, R., Belfort Jr., R., & Burnier, M. N. (2007). Type 1 and Type 2 Toxoplasma Gondii Strains: Differences in Growth and Invasive Abilities. Investigative Ophthalmology & Visual Science, 48(13).

Zanoni, I., Ostuni, R., Marek, L. R., Barresi, S., Barbalat, R., Barton, G. M., … Kagan, J. C. (2011). CD14 controls the LPS-induced endocytosis of toll-like receptor 4. Cell, 147(4), 868–880. https://doi.org/10.1016/j.cell.2011.09.051

Zhang, S. Y., Boisson-Dupuis, S., Chapgier, A., Yang, K., Bustamante, J., Puel, A., … Casanova, J. L. (2008). Inborn errors of interferon (IFN)-mediated immunity in humans: Insights into the respective roles of IFN-α/β, IFN-γ, and IFN-λ in host defense. Immunological Reviews, Vol. 226, pp. 29–40. https://doi.org/10.1111/j.1600-065X.2008.00698.x

Zhang, Y., Higashide, W. M., McCormick, B. A., Chen, J., & Zhou, D. (2006). The inflammation-associated Salmonella SopA is a HECT-like E3 ubiquitin ligase. Molecular Microbiology, 62(3), 786–793. https://doi.org/10.1111/j.1365-2958.2006.05407.x

Zhao, H., Han, Q., Lu, N., Xu, D., Tian, Z., & Zhang, J. (2018). HMBOX1 in hepatocytes attenuates LPS/D-GalN-induced liver injury by inhibiting macrophage infiltration and activation. Molecular Immunology, 101, 303–311. https://doi.org/10.1016/j.molimm.2018.07.021

Zhao, Y., Ferguson, D. J. P., Wilson, D. C., Howard, J. C., Sibley, L. D., & Yap, G. S. (2009). Virulent Toxoplasma gondii Evade Immunity-Related GTPase-Mediated Parasite Vacuole Disruption within Primed Macrophages . The Journal of Immunology, 182(6), 3775–3781. https://doi.org/10.4049/jimmunol.0804190

Zhao, Z., Fux, B., Goodwin, M., Dunay, I. R., Strong, D., Miller, B. C., … Virgin, H. W. (2008). Autophagosome-Independent Essential Function for the Autophagy Protein Atg5 in Cellular Immunity to Intracellular Pathogens. Cell Host and Microbe, 4(5), 458–469. https://doi.org/10.1016/j.chom.2008.10.003

Zheng, B., Sage, M., Cai, W. W., Thompson, D. M., Tavsanli, B. C., Cheah, Y. C., & Bradley, A. (1999). Engineering a mouse balancer chromosome. Nature Genetics, 22(4), 375–378. https://doi.org/10.1038/11949

Zheng, Y. T., Shahnazari, S., Brech, A., Lamark, T., Johansen, T., & Brumell, J. H. (2009). The Adaptor Protein p62/SQSTM1 Targets Invading Bacteria to the Autophagy Pathway. The Journal of Immunology, 183(9), 5909–5916. https://doi.org/10.4049/jimmunol.0900441

Zhou, R., Yazdi, A. S., Menu, P., & Tschopp, J. (2011). A role for mitochondria in NLRP3 inflammasome activation. Nature, 469(7329), 221–226. https://doi.org/10.1038/nature09663

Zhu, Y., Li, H., Hu, L., Wang, J., Zhou, Y., Pang, Z., … Shao, F. (2008). Structure of a Shigella effector reveals a new class of ubiquitin ligases. Nature Structural and Molecular Biology, 15(12), 1302–1308. https://doi.org/10.1038/nsmb.1517

Zuber, J., Shi, J., Wang, E., Rappaport, A. R., Herrmann, H., Sison, E. A., … Vakoc, C. R. (2011). RNAi screen identifies Brd4 as a therapeutic target in acute myeloid leukaemia. Nature, 478(7370), 524–528. https://doi.org/10.1038/nature10334

Zychlinsky, A., Prevost, M. C., & Sansonetti, P. J. (1992). Shigella flexneri induces apoptosis in infected macrophages. Nature, 358(6382), 167–169. https://doi.org/10.1038/358167a0